The origin, nature and tectonic significance of the Hällinmäki Cu-deposit, Virtasalmi District, South-central Finland

Kenneth Campbell Lawrie

Thesis submitted for the degree of Doctor of Philosophy

Department of Geology, University of Glasgow

July 1987

Acknowledgements

This research was carried out during the tenureship of a Glasgow University Postgraduate Scholarship Award from 1981-1984, the receipt of which is gratefully acknowledged. Outokumpu Oy. of Finland provided considerable and invaluable logistical support during my field seasons, for which I thank them. I am particularly grateful for the fullest cooperation I was afforded by the staff at Hällinmäki Mine, who went out of their way to make me feel at home. Heikki Saarnio, geologist at Kotalahti Mine is also thanked for his hospitality.

The field staff of Outokumpu's Exploration Division, who were based in Virtasalmi, particularly Marti Tumanto and Jorma Suvanto and their wives as well as Heikki Pustijarvi, Jukka Jokela, Timo Heino and Helena Viita are thanked for their friendship and making my stay in Finland so enjoyable. Dr. Tapio Koistinen is similarly thanked for his hospitality and comments in the field.

I wish to express my appreciation to my supervisor, Professor D. R. Bowes, for his support, encouragement and critical comments in the field and on this manuscript.

The technical staff at the Geology Department in Glasgow University, and in particular Mr Roddy Morrison and Mrs Betty Mackenzie are thanked for their friendly, willing and capable assistance. I am indebted to Douglas McLean for his help in preparation of all photographic material.

Drs. A. F. Park, P. Ward and K. A. S. Davidson and Mr G. Waller are thanked for useful discussions, and, together with Drs. C. J. Burton, D. S. Weedon and Janey MacDougall, are thanked for their help and friendship.

I particularly want to thank my parents for their unstinting support and encouragement, for which no words here are adequate.

To my wife Helen, who from both near and afar has had to put up with the rocks of the Virtasalmi District for so long, who has helped discuss my ideas before I put them to paper, and then retyped them several times, and who has never questioned my need to complete this work, I offer my deepest thanks.

CONTENTS

ABSTRACT

The Hällinmäki Cu-deposit is a polyphase deformed and metamorphosed orebody located within the Early Proterozoic Svecofennides of South-Central Finland. The lithological assemblage within which the orebody is situated dominantly comprises amphibolites, with minor marbles, calc-silicate skarn lithologies and gneisses, together with syn-kinematic intrusions dominantly of tonalitic composition.

Fold and fabric elements of seven deformational phases (D_1-D_7) have been recognised in the study area. The first deformational phase, D_1, is expressed principally as a penetrative S_1 fabric axial planar to F_1 folds. However, evidence for both these structural elements has been largely destroyed by subsequent overprinting during D_2 and D_3.

The major structural features recognised are folds developed during D_2 and D_3. The study area lies in the hinge zone of a large tight, reclined F_3 fold with a NW-SE-trending axis and which closes to the SE. This structure refolds large tight-isoclinal plunging inclined asymmetrical F_2 folds, to which a variably penetrative S_2 fabric is axial planar. Post-D_3 structures are expressed as more localised fold and fabric elements.

Peak dynamothermal metamorphism representing recrystallisation under conditions of the upper amphibolite-granulite facies transition zone (750-800^{o}C; 3.5-5.5 kb) was attained during D_1-M_1. There was subsequent pervasive recrystallisation of the D_1-M_1 assemblage during D_2-M_2 to

conditions of the lower amphibolite facies (450-550°C; 2-3.5 kb).

The syn-kinematic intrusions which constitute approximately 60% of the lithological assemblage are a gabbro-diorite-quartzdiorite-tonalite-trondhjemite suite, with I-type characteristics. There is apparently no systematic change in the composition of these intrusions with respect to their emplacement throughout the deformational history.

The earliest-emplaced intrusions recorded at Hällinmäki Mine (early syn-D_1) were observed to post-date Cu-mineralisation which was found to be essentially strata-bound, but with evidence of remobilisation. This mineralisation occurs both as small lenses and as disseminated chalcopyrite ore within amphibolites, thinly interlayered with largely ore-free calc-silicate skarn lithologies. A lateral gradation in ore composition from Cu-dominated to Fe-dominated silicate facies iron formation was recorded towards the south-east. At Hällinmäki Mine the ore-bearing layers were observed to be truncated by non-mineralised amphibolites along a pre-D_1 surface interpreted as a local unconformity. The evidence points to a pre-D_1 syn-volcanic, hydrothermal exhalative origin for this mineralisation.

A calc-silicate skarn lithology subjacent to the mineralised layers is considered to have formed by interaction of a basaltic protolith with a metasomatic fluid under conditions of a high water : rock ratio, during a period of extensive syn-volcanic hydrothermal alteration. This skarn, which is mineralised in places, is interpreted as a stockwork zone to the ore deposit.

Amphibolites interpreted as underlying the ore deposit show effects of spilitisation and silicification.

This alteration is most intense in haloes around calc-silicate skarn patches interpreted as conduits for pre-kinematic hydrothermal fluid flow. Many of the elements leached from the amphibolites in these alteration haloes show corresponding increases in the calc-silicate skarn stockwork zone at Hällinmäki Mine; a genetic link is proposed. Leaching of the Cu from the amphibolites is seen as a possible source of the Cu at Hallinmaki Mine.

There are three chemically distinct groups of amphibolites: these originally constituted a suite of basaltic volcanic rocks some of which show evidence for submarine extrusion. From geochemical characteristics the three groups are interpreted as having evolved separately, and to have originated from different sources. They are most closely analogous to Phanerozoic E-type MORBs (Groups I and III) and island arc tholeiites (Group II). The close spatial association of these chemical types corresponds to that found in Phanerozoic back-arc basins.

The demonstrated history of polyphase deformation and metamorphism and the sequence of emplacement and chemistry of igneous intrusions are considered to represent the progressive accretion of a back-arc basin terrane onto the margin of the Archaean Sarmatian craton during the Early Proterozoic Sveco-karelian Orogeny.

Despite complex structural and metamorphic over-printing and abundant igneous emplacement, representing activity at mid-crustal levels, it has been possible to establish the origin and nature of the Hällinmäki Cu-deposit.

SECTION 1

Introduction and rock types

PART 1

Introduction

1.1.1 Regional geological setting

The Hällinmäki Cu deposit is located within the Virtasalmi District of South-Central Finland, approximately 300 km north of Helsinki (Fig. 1.1.1a). The lithologies in this study area form part of the Early Proterozoic Svecokarelides (Eskola, 1963; Simonen, 1980) (Fig. 1.1.1b). The Svecokarelides consist of two roughly coeval and juxtaposed parts (Kouvo, 1958), the Svecofennian complex (Svecofennides), within which the Virtasalmi District is located, and the Karelian schist belt (Karelides) (Hietanen, 1975; Laajoki, 1986) (Fig. 1.1.1b). These two units differ fundamentally in lithological assemblages, tectonic styles and basement-cover relationships (reviewed in Simonen, 1980).

Svecofennides

The Svecofennides consist of a series of predominantly E-W trending linear metavolcanic and metasedimentary belts which have been intruded by syn-kinematic plutonic rocks (Simonen, 1980). The metasedimentary belts mainly comprise turbiditic sediments and their highly metamorphosed migmatitic mica schist or gneiss equivalents. Within the metavolcanic belts the volcanism is predominantly basaltic in composition with tholeiitic (Mäkelä, 1980;

Kousa, 1985) and calc-alkaline (Latvalahti, 1979; Kähkönen & Laitakari, 1983) types identified. Komatiites (Kousa, 1985) and intermediate-acidic volcanic assemblages have also been recorded (Kähkönen, 1987; Koistinen, pers. comm.). Kähkönen (1987) noted that calc-alkaline-intermediate rocks dominate in the Tampere Schist Belt. However in the Virtasalmi-Mikkeli Volcanic Belt as a whole, intermediate-acidic compositions appear to constitute <20% of the total supracrustal assemblage.

Pillow lavas are frequently observed in the Svecofennides, indicating that submarine volcanism was common. The occurrence of limestones and iron formations (often in association with the volcanic rocks) has generally been taken as an indicator of relatively shallow marine conditions (Simonen, 1953).

Granitoids make up a significant proportion of the lithological assemblage, with regional estimates of 70% for the Svecokarelides as a whole commonly accepted (Huhma, 1986). The syn-kinematic plutonism and volcanism in the Svecofennides took place between about 1.9 and 1.87 Ga in Finland (Neuvonen et al., 1981; Front & Nurmi, 1987), 1.91-1.86 Ga in northern Sweden (Skiöld & Cliff, 1984; Skiöld, 1987) and between 1.89 and 1.86 Ga in central Sweden (Åberg, 1978; Welin et al., 1980; Aberg et al., 1984). A U-Pb zircon date of c. 1.89 Ga for granitic pebbles in conglomerates from the Tampere schist belt suggests that sedimentation in the Svecofennides was roughly contemporaneous with igneous activity (Kouvo & Tilton, 1966). Sm-Nd isotopic studies of Svecofennian metasediments also indicate that the bulk of the sediments were eroded from newly formed crust (Huhma, 1987), most probably syn-orogenic material.

Karelides

The Karelides occur to the north-east of the Svecofennides, and preservation of original stratigraphic relationships (Pekkarinen, 1979; Park & Bowes, 1983) reveals that they rest unconformably on the pre-Svecokarelian granite-gneiss and greenstone belt complexes which constitute the Archaean Sarmatian craton of central and northern Finland. This is despite the fact that a significant proportion of the Karelides is preserved predominantly as an allochthonous nappe terrane (Koistinen, 1981).

The supracrustal formations within the Karelides (i.e. Karelian) are subdivided into a lower (Sariolan and Jatulian) and upper (Kalevian) part (Simonen, 1980). Ward (1985, 1987) has recognised that this subdivision corresponds to deposition within two distinct provinces, now separated by a major Svecokarelian thrust zone. The earlier and more easterly of the two provinces (the Hoytiainen Province) is characterised by deposition of early chemogenic and pelitic sediments associated with sporadic tholeiitic volcanism followed by input of coarse clastic detritus. This is considered to represent deposition in a transtensional en echelon system of basins developed either in an intracratonic or cratonic margin setting (Ward, 1987). Modal Pb ages indicate ages of c. 2.1 Ga (Kuovo & Kulp, 1961; Rickard, 1978; Vaasjoki, 1981) and U-Pb zircon ages of c. 1.97 Ga (Koistinen, 1981) for this sequence.

The Savo Province comprises a largely allochthonous nappe sequence (Ward, 1987). It includes the distinctive Outokumpu assemblage which has been interpreted as remnants of 'typical' oceanic crust (Koistinen, 1981) or a more marginal

sea crust e.g. back-arc basin (Park, 1983, 1985) and a monotonous sequence of Kalevian metasediments which are predominantly marine flysch-type sediments. This sequence was deposited at the margin of the Archaean craton between 2.05 and 1.9 Ga ago (Koistinen, 1981; Bowes et al., 1984).

Svecofennian-Karelian relationships

Ward (1987) has suggested that exposure of the oldest (1.92 ga: Helovuori, 1979; Korsman et al., 1984) Svecofennian rocks, may have contributed source material for the Kalevian. However, Huhma (1987) has pointed out that at least locally, a variety of components was required and that the Svecofennian terrane could not have been the only 'younger' source. Instead, a mixture of 2.1 Ga Jatulian rocks, the 2.0 Ga Granulite Belt (Fig. 1.1.1b) in northern Finland, with a possible Svecofennian component, as well as Archaean-derived material, is suggested as a more probable combination of sources. This interpretation implies a northerly derivation for the components, and it may be supported by evidence of a major uplift of Archaean rocks in Lapland at 2.0 to 1.9 Ga (Barbey et al., 1984).

In general, however, the isotopic evidence indicates that formation of the Svecofennides largely post-dates formation of the Karelides, at least in southern Finland (Huhma, 1986). The relationships become more complex north of Kuopio (Fig. 1.1.1b) as illustrated by coeval development of Kalevian flysch and a Svecofennian volcanic belt in the Skellefteå District of Northern Sweden (Lundquist, 1980; Park, 1985). Also, in northern Sweden, subaerial volcanism appears to have been more common (Welin, 1987).

The two-fold subdivision of the Svecokarelides is further supported by isotopic evidence from the granitoids. εNd(T) values for syn-kinematic granitoids emplaced in the Karelian domain suggest a contribution of recycled Archaean crustal material was significant in their genesis, but that those in the Svecofennian domain consist largely of newly mantle-derived material with only minor admixture of older continental crust (Huhma, 1985, 1986).

This suggests that the boundary zone between the two domains is roughly coincident with the western edge of the Archaean craton. No basement complex to the Svecofennian supracrustal rocks has been demonstrated. Other tectonic models which propose an Archaean basement to the Svecofennian (Welin, 1987) are not consistent with the isotopic data (Huhma, 1986) including Nd isotopic studies (Patchett & Kuovo, 1986; Patchett et al., 1987). Also, it has been suggested that the shear-net pattern in the Svecokarelides is controlled by pre-existing basement block structures (Tuominen et al., 1973) and that the similarity between the shear zones within the Svecofennides with those in the exposed Archaean craton is evidence for an Archaean basement to the Svecofennides (Welin, 1987). This not only assumes that all the shear zones within the Archaean craton area are of Archaean age, which they are not (Park & Bowes, 1983), but is also inconsistent with regional kinematic and palaeostress interpretations of orientation and timing of these shear zones (Bowes et al., 1984; Berthelsen & Marker, 1986) during the Svecokarelian orogeny.

The Svecofennides are separated form the Karelides along an approximately NW-SE trending lineament zone from the

Gulf of Bothnia to Lake Ladoga (Figs. 1.1.1b and 1.1.2) (Gaál, 1972). This zone has been termed the Main Sulphide Ore Belt (Kahma, 1973) or the Raahe-Ladoga lineament or shear belt (Gaál et al., 1978). It is marked by the occurrence of a number of Ni-Cu sulphide-bearing basic-ultrabasic intrusions aligned within the zone and coincident with a positive gravity anomaly and a deep-seated fracture zone (Luosto et al., 1983; Korsmann et al., 1984). The zone is also characterised by the distinct Pb-isotopic composition of galenas (Kuovo & Kulp, 1961; Vaasjoki, 1981).

Svecokarelian orogeny

The Svecokarelian orogeny is a major crustal event which is expressed mainly in southern and central Finland, northern and eastern Sweden and Soviet Karelia (Bowes, 1976). It is characterised by the development of low pressure/high temperature metamorphic facies (e.g. Hietanen, 1975; Campbell, 1980; Korsmann et al., 1984), by the abundance of syn-kinematic granitoids and migmatites (e.g. Sederholm, 1926) and by polyphase deformational tectonic histories (Bowes et al., 1984). There are important regional variations both in the timing of peak metamorphic conditions and in the climactic grade of metamorphism achieved (Campbell et al., 1979; Halden, 1982; Halden & Bowes, 1984).

Deformation within the Svecokarelides also appears to have been diachronous. Development of the earliest phases in Karelia appears to have occurred at 1.9 Ga, at the same time as the earliest magmatic activity in the Tampere and Skaldø belts

(Huhma, 1986) (Fig. 1.1.1b). The main orogenic stage seems to have occurred between 1.9 and 1.87 Ga (Huhma, 1986) although neosome emplacement continued in some parts until c. 1.8 Ga (Hopgood et al., 1983). A late thermal event c. 1.8 Ga is suggested by Rb-Sr whole rock and U-Pb monazite and sphene ages of syn-kinematic granitoids (Aho, 1979; Welin et al., 1980; Patchett & Kouvo, 1986), and by the emplacement of late kinematic granites in a W-SW to E-NE belt in southernmost Finland. Patchett et al. (1987) subdivide the granitoids within the Svecofennides into two main suites (see Fig. 1.1.1b). Between 1.9 and 1.86 Ga, differentiated I-type plutonic and volcanic rocks were formed and between 1.82 and 1.78 Ga a suite of little differentiated S-type granitic rocks were emplaced.

It has been suggested that the first deformational events which can be correlated between the Svecofennides and Karelides across the Raahe-Ladoga lineament are conjugate sets of wrench faults which predominantly trend NW-SE (Bowes et al., 1984; Ward, 1987). In places these wrench systems controlled neosome emplacement, dated at 1786 ± 80 m.y. in the Savonranta area within the Karelides (Halden, 1982) (Fig. 1.1.2).

A number of models have been proposed to explain the development of the Svecokarelides in terms of modern plate tectonic hypotheses (Hietanen, 1975; Berthelsen, 1980; Bowes, 1980; Gaál, 1982; Park, 1985). Most workers consider that the Svecofennides are the product of subduction and formation of island arcs (Hietanen, 1975; Front & Nurmi, 1987) and that the Svecofennides and Karelides represent a tectonic collage which was partially accreted onto the margin of the Sarmatian craton (Park, 1985; Ward, 1987).

There are however a number of important differences between the Svecokarelian terrane and possible Phanerozoic analogues, most notably the apparent rapidity of crustal growth in the Svecokarelian and the lack of a geographical age or chemical zonation, particularly in the granitoids (Huhma, 1986; Front & Nurmi, 1987). Also, Ehlers et al (1986) have noted that the chemistry of some metavolcanic rocks in the south-western Svecofennides is dissimilar to that of Phanerozoic island arcs. While a collage model intrinsically allows for juxtaposition of a number of different or exotic tectonic terranes, very few detailed geochemical studies of the volcanic assemblages have been carried out in the Svecofennides and a great deal more work is required to characterise the nature of this Early Proterozoic terrane before more definite analogies can be drawn with Phanerozoic environments.

1.1.2 Previous work in the study area and initial aims of this project

The study area is located 50km west of the Raahe-Ladoga lineament which is considered to mark the eastern extremity of the Svecofennides (see Fig. 1.1.2).

The first mention of the Virtasalmi District on a geological map was on the (1:400,000) sheet produced by Frosterus (1903), but the area was not studied in any detail. The first detailed map was produced as a consequence of mineral exploration in the southern part of this study area by the Geological Survey of Finland in the 1960's. This map (1:20,000) was compiled from outcrop observations, drill core analysis and

geophysical measurements (Siikarla, 1967) and was published along with a geological description of the Hällinmäki ore prospect and the surrounding area by Hyvärinen (1969). A 1:20,000 map covering the northern half of the area was published in 1971 by the Geological Survey of Finland.

On the basis of gross lithological features and few geochemical analyses Hyvärinen suggested that the rocks of the Virtasalmi District were originally of intermixed volcanic and sedimentary origin. He proposed that there had been subsequent regional metamorphism at conditions of the amphibolite facies but below those conditions necessary for partial melting to occur, and that there had been deformation in the form of a single phase of isoclinal folding which also affected a series of syn-orogenic plutonic rocks. These intrusions were classified mainly on the basis of petrography, and only a few incomplete geochemical analyses were presented.

Hyvärinen tentatively ascribed the origin of the Hällinmäki ore deposit to a contact pneumatolitic origin on the basis of the classification by Schneiderhohn (1949). He also applied the classification of Cussarz (1965) to further suggest that the mineralisation took place in the late orogenic stage, being genetically related to the emplacement of syn-orogenic quartz diorites.

However, one particularly notable inconsistency in Hyvärinen's model for generation of the ore deposit is his assertion that the skarn formation pre-dates the mineralisation and that the skarns are regionally developed and not of contact metasomatic origin. In addition this model does not take into account the polyphase nature of deformation and metamorphism

regionally expressed in the Svecokarelides (Bowes et al., 1984), nor does it attempt to determine the relative ages of emplacement of the intrusions. In comparison, Gaál & Rauhamaki (1971) have demonstrated that in an adjacent part of the Svecofennides (25 km due east of Virtasalmi) a similar initial lithological assemblage had been subjected to three major phases of deformation, spatially variable peak metamorphism of amphibolite-granulite facies and that a suite of peridotitic-gabbroic-tonalitic-mangeritic and trondhjemitic intrusions had been emplaced throughout the deformational sequence.

Hence the initial aims of this project were to resolve the conflicting evidence regarding the origin of the Hällinmäki Cu deposit and host lithologies, to determine its three-dimensional structure and elucidate the polyphase deformational and metamorphic history of the area.

1.1.3 Scope and organisation of the thesis

A description of the general lithology distribution based on the geological map which was constructed as a result of this project is given in Section 1, Part 2.1. This outlines the distribution of principal lithologies and the major structural features. It should be noted that some data has had to be omitted for reasons of commercial confidentiality. In Section 1, Part 2.2, the field relations and petrographic descriptions of the pre-tectonic lithologies which were encountered are also described.

Section 2 deals with the tectonic and metamorphic development of the study area. The major structural features and polyphase deformational history are elucidated in Part 1.

The polyphase metamorphic history and the nature of coexisting mineral assemblages are described in Part 4. Brief petrographic descriptions and the sequence of emplacement of the syn-kinematic intrusive suite that was identified is outlined in Part 2. The relative sequence of emplacement for a series of syn-kinematic veins and pegmatites is given in Part 3. A summary and discussion of the tectonic development of the Virtasalmi District is presented in Section 2, Part 5.

As a direct consequence of the detailed fabric and structural relationships which were ascertained, it became clear that the Hällinmäki ore deposit was pre-tectonic in origin and intimately related with the host amphibolites and calc-silicate skarn lithologies. The geochemistry of these skarns and amphibolites was investigated in order to determine their original nature and the effects of subsequent chemical modification. The results of this study are presented in Section 3, Part 1.

The three-dimensional structure, original stratigraphy, distribution and relative timing of mineralisation and associated alteration, and a model in which the origin of the Hällinmäki Cu-deposit is proposed, are outlined in Section 3, Part 2. The implications of this model for other Cu-deposits and exploration policy in the study area are also discussed.

In Section 4, a brief analysis of the chemistry, nature and origin of the syn-kinematic intrusive suite which constitutes a volumetrically significant proportion of the lithological assemblage, is presented.

Finally, a summary of the findings of this thesis, the regional and general implications, and suggestions for future work resulting from this study, are contained in Section 5.

1.1.4 Terrain

The total area covered in this study is approximately 125 km^2. However, over a significant proportion of this area the exposure is poor due to surficial glacial deposits and lakes. This distribution of exposure is indicated in Map 1. There is negligible exposure on the margins of the lakes. Topographic relief over the area is negligible, varying from a base level on lake shores of 100 m up to 170 m.

Most of the exposures are flat and glaciated and often have to be cleared by rolling back a thin mossy covering. Sampling from such exposures was greatly facilitated by provision of a portable drill capable of taking 30 cm long, 3 cm diameter cores. Much of the rock was weathered to a depth of 2-3 cm.

Full access was afforded to underground workings and open pit exposures at Hällinmäki Mine. Drill core and drill core records were examined in the core store at Kotalahti Mine.

Grid references used for sample locations are taken from the 1:20,000 topographic series of the Finnish Cartographic Series. The base maps used for fieldwork are 1:4,000 enlargements with numbered exposures which were supplied by Outokumpu Oy. A great deal more exposure was marked on these maps than is immediately obvious from the 1:20,000 series maps.

Fig. 1.1.1 Figure 1.1.1a is a geographical map showing the location of the study area (Virtasalmi District) in Finland.

Figure 1.1.1b is a simplified geological map showing the major Precambrian features of the Baltic Shield.

KEY:

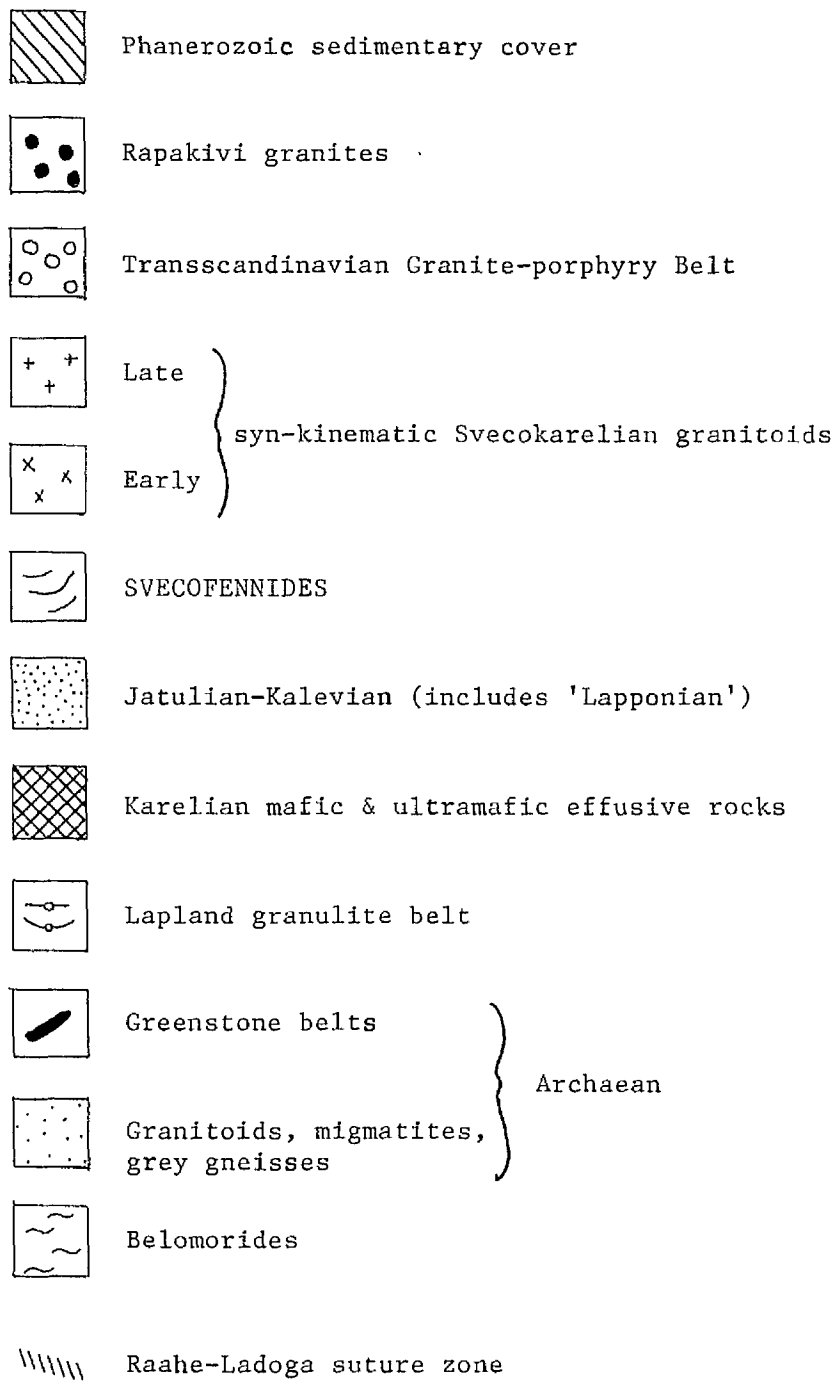

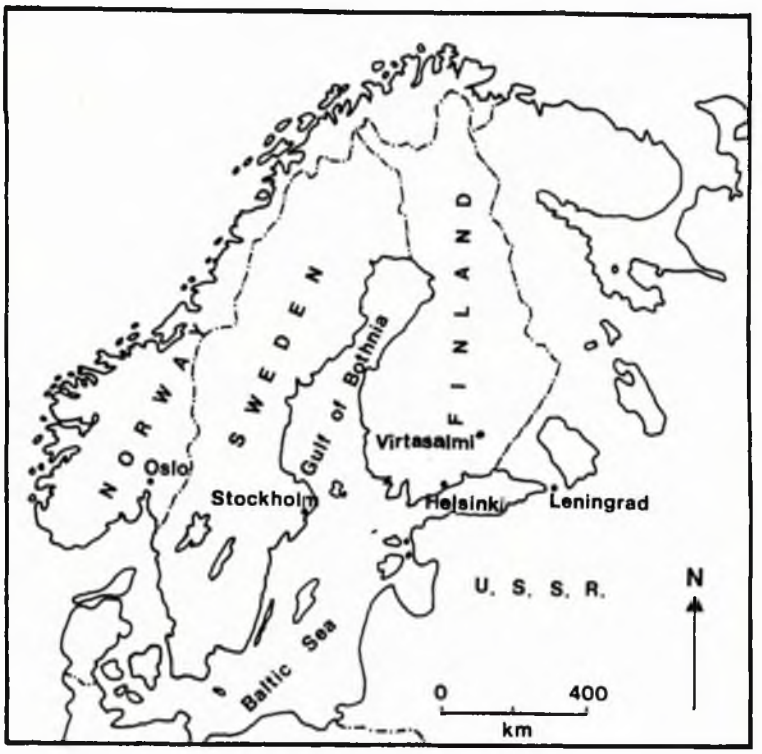

Figure 1.1.1a

Figure 1.1.1b

Fig. 1.1.2 Geological map of South-central-eastern Finland (including unpublished information of Outokumpu Oy.). Adapted from Bowes et al. (1984).

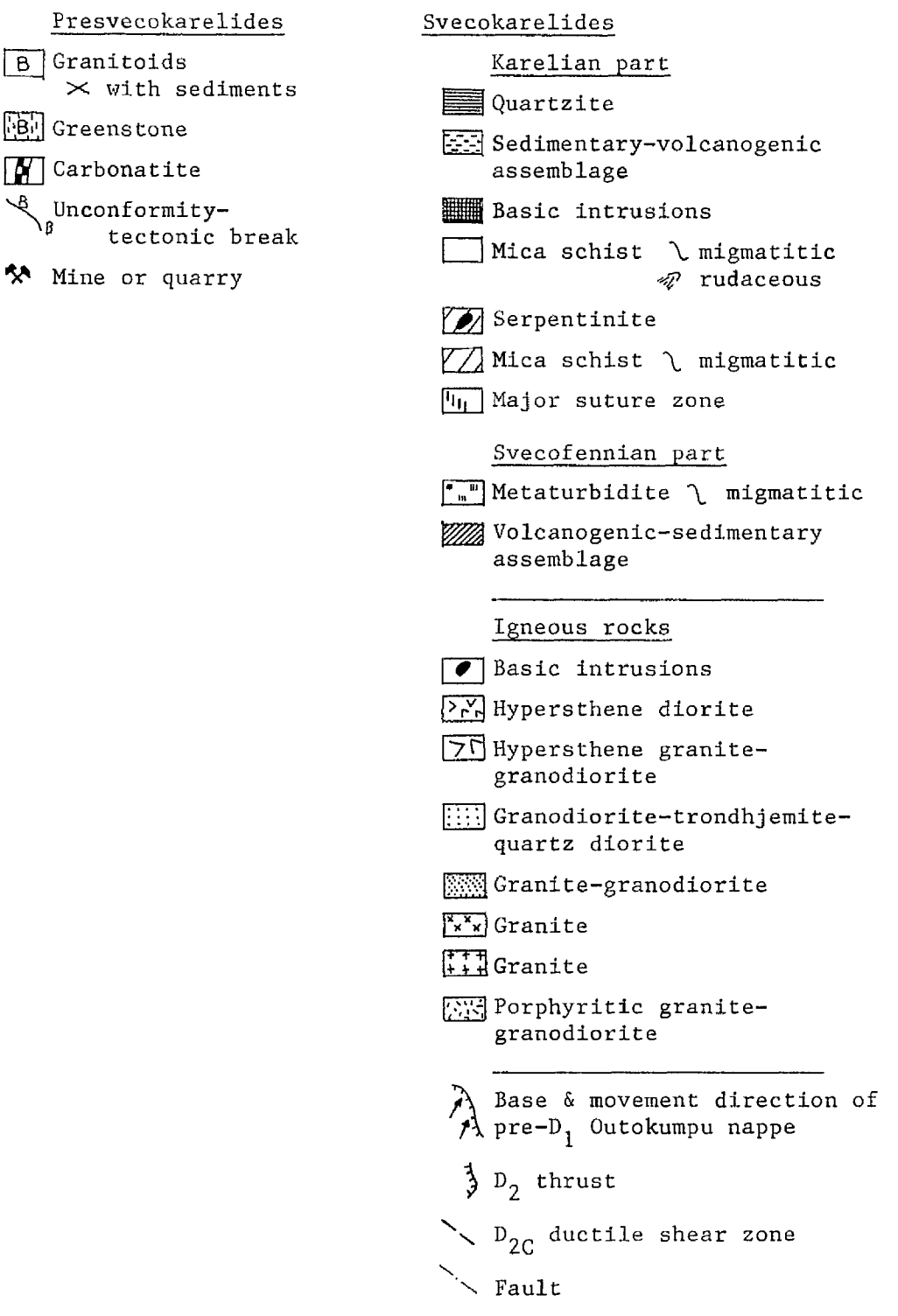

Figure 1.1.2

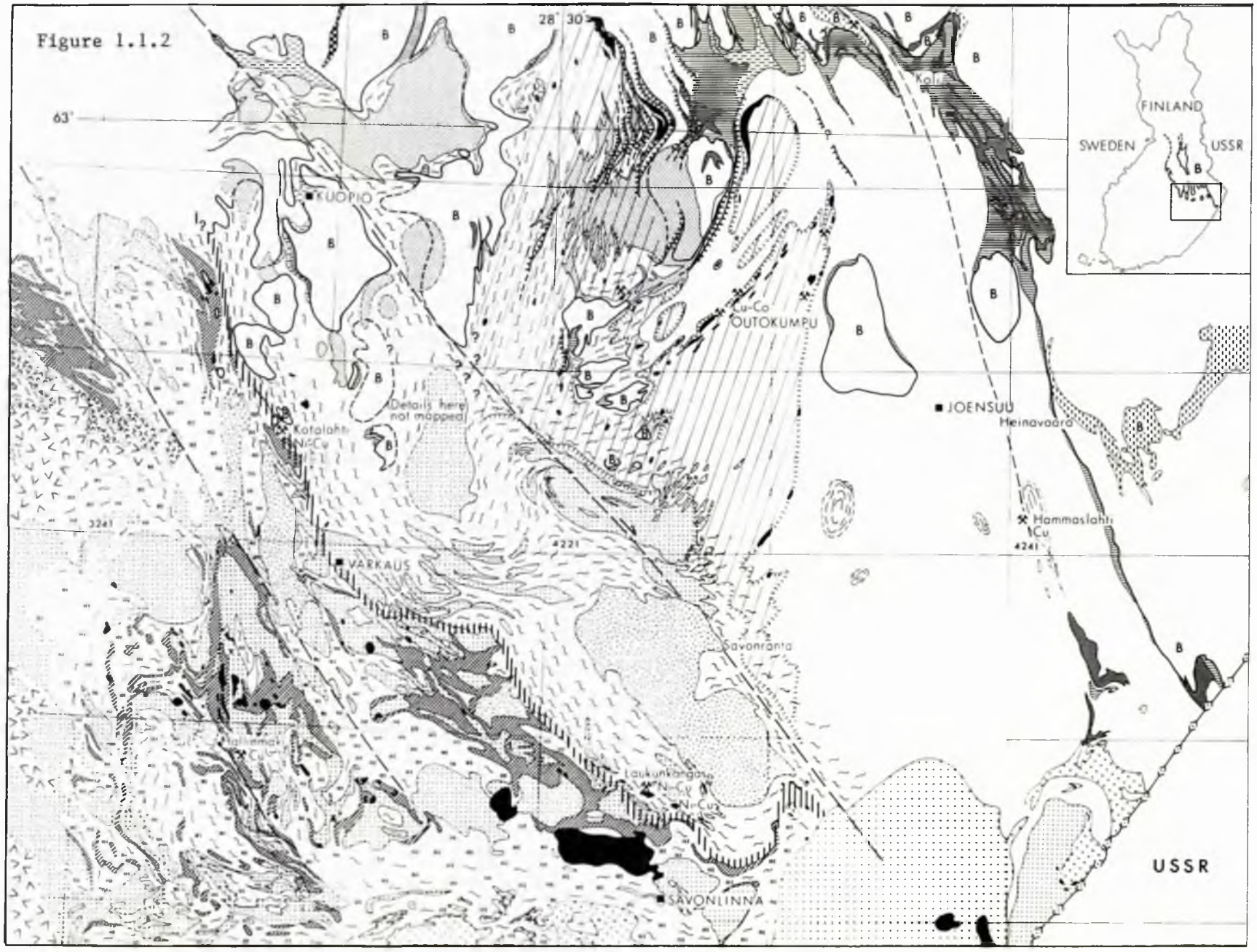
28°
30°
63°
FINLAND
SWEDEN
USSR
KUOPIO
Cu-Co
OUTOKUMPU
Details here not mapped
Kotalahti
Ni-Cu
JOENSUU
Heinavaara
Hammaslahti
Cu
3241
4221
4241
VARKAUS
Savonranta
Laukunkangas
Ni-Cu
SAVONLINNA
USSR

SECTION 1

PART 2

Lithologies

1.2.1 General lithology distribution

Map 1 is a lithological and structural map of the study area. Approximately 60% of the lithologies in the area are syn-kinematic intrusions and these are emplaced unevenly throughout the area. The intrusions cause the pre-existing country rock to be largely dissected, providing a further obstacle in attempts to correlate the pre-tectonic lithological assemblage. In the study area the latter dominantly comprises amphibolites, with various calc-silicate skarn lithologies and thin marbles.

In Map 1 it can be seen that on a regional scale this predominantly amphibolitic belt is largely set amongst gneisses and schists which are similarly extensively dissected by syn-kinematic intrusions. It was possible to establish boundaries between petrographically and geochemically distinct amphibolite groups only in the southern half of the area (see Section 3, Part 1) (Map 1). The distribution of these amphibolites and some of the other distinctive lithologies mapped delimit major fold structures which are described in Section 2, Part 1. In general however, there is a lack of distinctive, continuous lithological units which can be used to delimit these major strucures, hence structural criteria such as vergence changes in minor asymmetrical folds are relied

upon to indicate the presence of larger than outcrop scale folds.

Within the area there are large tracts solely comprising syn-kinematic intrusions. These intrusions most commonly occur as poorly defined by apparently irregularly-shaped masses, ranging from common vein networks and dykes to larger bodies a few hundred metres across. However there are very few instances where examples of the latter are not extensively truncated by a variety of subsequently injected intrusions. Similarly virtually all exposures of the pre-kinematic lithological assemblage are dissected by successively injected vein neosomes and intrusions ranging in composition from gabbro to trondhjemite (Section 2, Part 2 and Section 4).

Hence any regional scale map which attempts to show the distribution of lithologies (e.g. Map 1) must be a simplified representation. The basis for the construction of Map 1 therefore is that where the proportion of pre-kinematic lithologies in individual exposures is < 40%, then the pre-kinematic assemblage is most likely to form narrow screens and detached blocks within intrusions, and hence the former are marked with a 'schlieren' symbol within the predominant intrusive type. As over most of the area the predominant intrusions are gabbros and diorites, and since very few individual, discrete intrusions can be recognised, the bulk of these intrusions are represented on Map 1 by one symbol. Also, due to the fact that compositionally and petrographically similar intrusions were emplaced throughout the syn-kinematic sequence (Section 2, Part 2; Section 4) and for the reasons of complexity outlined above, then it has not been possible

to indicate the relative age of emplacement of many of the intrusions on Map 1. A few of the larger, more petrographically distinct intrusions are delineated separately. The presence of minor intrusive types is signified by the 'schlieren' symbol.

The construction of Map 1 was also greatly aided by extensive drill core information provided by Outokumpu Oy. However, for reasons of confidentiality this information, and the location of other ore occurrences, have been omitted. Where previously published drill core results (Hyvärinen, 1969) have been utilised, however, then the location of the drill holes is marked on Map 1.

The distribution of the lithologies with respect to the major structures is described in Section 2, Part 1. In the remainder of this section the petrography and field relations of the pre-kinematic lithological assemblage are described. The petrography and field relations of the intrusions is described in Section 2, Part 2.

1.2.2 Pre-D_1 lithological assemblage: petrography and field relationships

1.2.2(i) Amphibolites

1.2.2(i)(a) Amphibolites comprise 70% of the pre-tectonic assemblage in the study area. Due to the combined effects of considerable tectonic modification (Section 2, Part 1) and widespread emplacement of syn-tectonic intrusions (Section 2, Part 2) it was not possible to work out the volcanic stratigraphy except in very local domains. Nor was

it possible, for the same reasons, to arrive at a reliable estimate for the original thicknesses of units in the volcanic pile, which itself can only be crudely estimated at between 2 and 5 km thick.

Macroscopically identifiable units of amphibolite consist of interlayered massive, banded and striped lithologies with rare evidence for original volcanic features. All of these lithology types are described below.

1.2.2(i)(b) Petrography

The amphibolites can be subdivided into three major groups on the basis of petrography: magnetite-rich, hornblende-rich, clinopyroxene and sphene-poor lithologies (Group I); medium-grained to coarse-grained hornblendites and hornblende metagabbros (Group II); and fine to medium-grained ilmenite and sphene-bearing salitic clinopyroxene-rich lithologies (Group III). The mineral assemblages are not only a function of the intensity of M_2 retrogression of higher grade M_1 assemblages (Section 2, Part 4), but can also be broadly correlated with chemically distinctive groups (Section 3, Part 1). Group I and II amphibolites are not spatially associated (see Map 1). The medium to coarse-grained hornblendites of Group II are observed to be enclosed within Group III amphibolites, mostly in the northern half of the area.

Grain size variations within the amphibolites are largely controlled by metamorphic recrystallisation: M_1 assemblages are typically coarser-grained than those developed

in M_2 within the same unit (Section 2, Part 4),(reflecting a decrease in overall P-T conditions) and this difference is most marked where penetrative S_2 foliations are developed in narrow D_2 high strain zones (Fig. 1.2.1).

The textures developed are also largely dependent on the local intensity of deformation, and vary from granoblastic polygonal textures which occur in low strain zones to those which are intensely foliated with higher strain zones (Section 2, Part 1).

Due to the preservation of polymetamorphic assemblages (Section 2, Part 4) and the development of sub-millimetre-scale banding (Section 2, Part 1) modal mineral abundances are observed to be highly variable often even on this very small scale. For example, in one finely banded amphibolite from Narila (Fig. 2.4.7), the following modal abundance variations were noted between bands : plagioclase 0-70%, amphibole 2-90%, orthopyroxene 0-30%, clinopyroxene 0-20%. This degree of variation is reflected in modal abundances of amphibolites throughout the area: amphibole varies from 10-80%, clinopyroxene 0-50%, plagioclase 20-60%, orthopyroxene 0-10% (based on whole thin section analyses). Other minerals such as epidote, scapolite, magnetite, ilmenite and sphene tend to be associated with lithologies with specific ranges in chemical composition, notably those amphibolites that are variably 'skarned' (see next section).

The plagioclase in general is fresh and tends to be altered only adjacent to late vein-filled fracture cleavages. Approximate plagioclase compositions were determined optically using the Michel-Levy method and rarely the extinction

of combined Carlsbad-Albite twins. As the former method relies on statistical analysis (Battey, 1972), no sample with less than 6 appropriate sections cut perpendicular to (010) was considered to give a reliable estimate of composition.

Much of the plagioclase is normally zoned, as indicated by a variably distinct outer rim. This is interpreted as the result of re-equilibration during D_2-M_2 (Section 2, Part 4), and the interpreted reduction in An content towards plagioclase rims is consistent with thermal decline from M_1 to M_2 (Section 2, Part 4). Plagioclase within D_2 high strain zones and in thin bands where there has been extensive 'amphibolitisation' of D_1-M_1 assemblages during D_2-M_2, tends to occur as smaller, often more intensely zoned and less commonly twinned crystals.

The plagioclase compositions (determined optically) from a representative sample of the amphibolites are presented in Table 1.2.1 together with their respective chemical compositions. The An content refers to measurements made on crystal centres in zoned crystals and from crystals considered to be in textural equilibrium with other minerals in the M_1 assemblage. They are therefore considered to reflect compositions during D_1-M_1 only.

This data indicates that there is a rough correlation observed between the An content of plagioclase and the CaO content of the rock. This is in agreement with findings from amphibolite facies meta-basites elsewhere (e.g. Weaver et al., 1982). However, similar ranges in plagioclase composition within interbanded amphibolites are not generally recognised in other metamorphic belts and has

not been taken into account in the construction of metamorphic zones where subdivision is at least in part dependent on the An content of plagioclase from meta-basites (see Turner, 1980).

1.2.2(i)(c) Pillow lavas-lava tubes

Thin (up to 2 cm thick) dark-coloured bands define ovoid and more elongate tube-like features in exposures at Kiviniemi and Narila (Fig. 1.2.2a, b). Discrete ovoid pillow forms from 10 cm to 1.5 m in cross-sectional width were observed in only a few isolated 2-dimensional glaciated exposures. It was nowhere possible to establish whether these examples formed discrete pillows in 3-dimensions, or whether they form interconnected pillows, or are cross-sections through lava tubes.

The elongate tube-like features vary in length from 1 m to over 7 m, with thicknesses up to 50 cm. They are interpreted as oblique cross-sections through lava tubes and pillow lavas. Many of them do not have either tachylite or palagonitised zones developed at several points of contact and this has resulted in the formation of an interconnected network of lava tubes-pillows, similar to those described from Archaean greenstone belt sequences (Jones, 1969; Hargreaves & Ayers, 1979; Barager, 1983). Although all these features were noted in the study area (e.g. Fig. 1.2.2), they were best demonstrated at Pallionmaki, just outwith the mapped area (Fig. 1.2.3). These lava tubes-pillows probably formed by digital advance in a similar fashion to subaerial pahoehoe lava toes (Swanson, 1973). While this lack of chilling and

alteration points to an apparent exclusion of seawater at several points of contact, the rims of adjacent tubes have mineralogical compositions consistent with considerable palagonitisation (described below) and traverses across individual tubes indicate considerable alteration has occurred (see Section 3, Part 1). Diagrammatic sections, adapted from Jones (1969) and Hargreaves & Ayers (1979) show possible views through interconnected lava tubes in order to illustrate the range of above interpretations (Fig. 1.2.4).

The preponderance of interconnected lava tubes over discrete pillows (while noting the possibility of bias due to the limited preservation and recognition of these features) in the study area, is consistent with observations in other volcanic sequences. Studies of both Recent pillow lava flows (Moore et al., 1973; Ballard & Moore, 1979) and Phanerozoic (Jones, 1968) and Archaean (Hargreaves & Ayers, 1979) pillow lavas have demonstrated that most pillows are interconnected, having formed by budding from often similarly interconnected sub-aqueous lava tubes (Moore, 1975). Units comprising discrete pillows are less common (Arndt, 1973; Dimroth et al., 1978, 1979).

Also in common with many Archaean sequences (Dimroth et al., 1979), the pillowed-tube units, where recognised, are commonly observed to be interlayered with homogeneous amphibolites interpreted as aphyric massive flows (Fig. 1.2.5). As well as forming discrete flows, more complex flows similar to those also identified in some Archaean sequences (Dimroth et al., 1978; Hargreaves & Ayers, 1979) were also observed. In a low strain zone at Kiviniemi for example, a complex flow

unit was observed to comprise a thin pillowed base overlain by a massive homogeneous flow unit at least 5 m thick (Fig. 1.2.6). This vertical transition probably resulted from a combination of factors such as increasing volume and flow rate, decreasing viscosity and slopes. At the base of this unit, and observed in other tubes-pillows at Narila, a light-coloured, largely concentric but sometimes discontinuous zone 3-5 cm thick occurs a few centimetres in from the pillow margins (Fig. 1.2.6). This zone now consists of an (M_2) epidote + quartz assemblage, as distinct from the (M_2) hornblende in the adjacent pillow-tube interior. This zone is considered to have resulted from concentration of calcium-rich fluids in the form of amygdales, as described from some modern pillows (Scott & Hajash, 1976), although no individual amygdales now remain. The apparent vesicularity of the 'pillows' in this and several other examples (together with the presence of flow top breccias in underlying units) also seems to indicate that eruption took place in relatively shallow water depths (Jones, 1968), with the possibility of emergence.

In common with (many) Archaean pillows (e.g. Hargreaves & Ayers, 1979) most of the rims to the pillow- and tube-like forms comprise two distinct zones. There is normally an outer dark green zone, between 2 mm and 1 cm thick and an inner black zone of similar width (Fig. 1.2.6). The outer zone is characterised by a mineralogy of (M_1) diopside and plagioclase (zoned) which is variably retrogressed to an (M_2) assemblage of hornblende and/or epidote. The inner zone dominantly comprises dark green hornblende. In modern pillows (e.g. Scott & Hajash, 1976) the selvedges usually

comprise an outer, commonly palagonitised sideromelane zone, to which the outer dark green rims of pillows-tubes in this study are compared, and an inner black tachylite zone with which the black hornblende-rich zones are considered analogous. Similar comparisons have been drawn in previous studies of Archaean pillows (Barager, 1983).

At Narila, in particular, there is often no outer dark green selvedge to the pillows and tubes and the rim is marked by a single black zone comprising equal amounts of biotite and hornblende with minor plagioclase, muscovite, sphene, pyrite and magnetite. This mineralogy apparently indicates a marked increase in K_2O (and FeO) in rim compositions, and is consistent in particular with observed alkali enrichment in both modern and Archaean pillow rims, which is considered to be the result of palagonitisation (Barager et al., 1979). The differences observed in pillow-tube margin structures and compositions, as reflected in the present mineralogy, are therefore interpreted in this study to be the result of varying intensities of alteration, and in particular the intensity of palagonitisation which is apparently most marked in lava tubes from Narila.

Both pillow lavas and lava tubes have been recognised in areas immediately outwith the study area (Koistinen, pers. comm.) while pillow lavas have been reported from other metavolcanic belts within the Svecofennides (Gaál & Rauhamaki, 1971; Gaál, 1980; Mäkelä, 1980; Ehlers et al, 1986).

1.2.2(i)(d) Banded amphibolites

This section deals with the many amphibolites in the area which frequently are compositionally banded, i.e. with morphologically distinct bands normally between 0.2 cm and 10 cm thick.

Compositional layering (S_0) on a scale from less than 0.5 mm to several centimetres across is a common occurrence in Virtasalmi amphibolites. In one example in the vicinity of Virtasalmi Village, amphibolites banded on a scale of 0.5 mm to 1 cm across were noted to be cross-cut at a low angle by a more homogeneous amphibolite (Fig. 1.2.7). The S_1 fabric is continuous across this lithological contact, which is an irregular surface. On the basis of this evidence, the contact between the two sets of amphibolites is interpreted as pre-tectonic, pre-dating as it does the earliest recognisable deformational event.

The banding in the truncated amphibolite is shown predominantly by varying proportions of diopside and plagioclase in the M_1 assemblage, now largely retrogressed to hornblende and epidote or plagioclase, and most probably reflects original chemical differences. In view of the fine-scale of this pre-tectonic layering the banded amphibolites are interpreted as meta-volcanic tuffs, while the later amphibolite is considered to have been a massive homogeneous lava flow or sill.

Similar fine-scale pre-tectonic layering was observed at Hållinmäki Mine and at Narila, and this points to the probable presence of tuffs in several parts of the volcanic pile.

Also, in another example, near Virtasalmi Village, a diopside-rich band less than 0.5 mm wide was observed to occur within an otherwise relatively homogeneous amphibolite. This band could be traced around several isoclinal F_2 folds, and in the hinge of one of these it was observed to have a thickness of up to 10 cm and consist of several distinct compositional bands (Fig. 1.2.8). Hence in this particular instance it is possible to demonstrate that a very thin diopside-rich stripe is the tectonically-thinned equivalent (in F_3 fold limb zones) of several originally distinct compositional bands which are evident in the F_3 hinge. Many other similar occurrences like this were recorded throughout the area. These bands are almost certainly thin tuffaceous layers between more massive volcanogenic units.

Fine-scale (c. 0.5 mm to 1 cm) compositional layering was noted to form discordantly to S_0 at many localities. Nowhere was the relationship between this S_1 banding and F_1 folds directly observed, but it is considered to have developed axial planar to larger F_1 structures (Section 2, Part 1). By contrast S_2 compositional layering is often observed to be axial planar to minor F_2 folds (Fig. 1.2.9). Mapping vergence changes of the minor F_2 folds reveals that the S_2 layering is also axial planar to major F_2 folds.

In most instances the S_1 and S_2 layering is defined by varying proportions of plagioclase and mafic minerals (diopside or hornblende). This layering is interpreted to have formed as a result of metamorphic differentiation (Leake, 1964; Bowes & Park, 1966).

Within compositionally distinct amphibolites interlayered on a scale of 10s of cm, it was observed that plagioclase-rich stripes were restricted to particular bands (Fig. 1.2.10), now dominantly comprising varying proportions of hornblende (M_1 and M_2) and plagioclase with little relict diopside. In adjacent bands there is markedly less abundant hornblende, although both S_1 and S_2 foliations are outlined principally by varying proportions of diopside and plagioclase with hornblende. These variations seem to indicate that in some instances the form which the tectono-metamorphic fabric has taken may be controlled by original protolith compositions.

In addition to the penetrative compositional layering noted above, leucocratic stripes consisting mainly of plagioclase, minor quartz and with trace diopside or hornblende, and between 0.5 and 2 mm in width, are observed to occur sub-parallel to both S_1 and S_2 axial planar mineral foliations in many amphibolites (Fig. 1.2.11). Stripes formed in both D_1 and D_2 are of similar character: individual stripes formed during the same deformational event are usually sub-parallel on outcrop scale but are rarely observed to be continuous for more than 1 m. They are often irregularly spaced on a scale of a few millimetres to several centimetres. Those stripes occurring axial planar to F_2 folds (Section 2, Part 1), which may themselves be outlined by pre-existing stripes sub-parallel to the S_1 foliation (Fig. 1.2.11), tend to be concentrated within the limb zones of the F_2 folds, although smaller less continuous stripes are also occasionally present in fold hinges. Formation of these stripes is considered to have been by more localised

metamorphic segregation-differentiation, possibly reflecting less homogeneous strain distribution.

At Narila a gradual transition is observed from lava tubes containing weakly expressed tectonic mineral foliations, through a zone several metres wide marked by an increase in the amount of flattening and attenuation of the lava tubes, together with development of a penetrative (S_2) mineral foliation, to a banded rock with only rarely preserved pillow-tube closures (Fig. 1.2.12). Myers (1978) and Park & Bowes (1981) have described similar features from highly deformed terranes. Within the Virtasalmi District, recognition of original pillow lava and lava tube forms is usually only possible within similar low-strain zones, and recognition of banded amphibolites as pillow lavas or lava tubes is only possible where low-high strain zone transitions are preserved.

Hence the fine banding-striping noted in amphibolites in the Virtasalmi District is the result either of original lithological layering (tuffaceous), metamorphic differentiation in D_1 and/or D_2, or flattening and attenuation in higher strain zones without significant metamorphic recrystallisation-segregation.

1.2.2(ii) Marbles and calc-silicate (skarn) lithologies

1.2.2(ii)(a) Marbles

Marbles are a comparatively minor component of the lithological assemblage in the Virtasalmi District. Within the area mapped they commonly occur as narrow interbeds,

from 1 cm to 2 m thick, within the sequence of amphibolites. It was only rarely possible to trace individual marble bands for more than a few 10s of metres due to the poor exposure. They are normally consistent in width along one horizon within a sequence of interbanded marble layers but typically form lensoid masses in 3-dimensions which is attributed to boudinage particularly during D_2 and D_3 (Section 2, Part 1). Hence, as with all other lithologies, there has been considerable tectonic modification of original thicknesses. In two instances, at Hällinmäki Mine and at Maaninsaari Island, thicker marbles were identified. At Hällinmäki Mine, drill core records were used to illustrate the three-dimensional lensoid shape of a unit of marble which has dimensions of approximately 400 m X 300 m X 200 m. At Maaninsaari Island a marble unit is 30 m thick but can only be traced for 100 m due to poor exposure.

In the very west of the mapping area and extending outwith it, there is a particularly thick marble horizon which is 300-400 m wide and can be traced for 10 km between Narila and Ankele. Due to poor exposure its continuance over this area has largely been proven by a combination of geophysical information (Siikarla, 1967) and boreholes (Hyvärinen, 1969). As a result of the poor exposure within the study area, the unit was not studied in detail so it is unclear how much tectonic modification it has undergone. Nevertheless, it would seem to represent considerable carbonate deposition. At its northern end, the limestone is bounded principally by gneisses, with increasingly abundant amphibolites present towards the south. At Ankele quarry, just outwith the study area, the only amphibolites observed within the thick marble

sequence displayed discordant relationships to the composite S_0-S_1 foliation, suggesting a syn-tectonic intrusive origin.

The marbles throughout the Virtasalmi District appear fairly uniform, being white to pink in colour, and with the carbonate comprising almost pure calcite (MgO 0.1-1.76%; Hyvärinen, 1969), with only rare amounts of dolomite as myrmekite-like inclusions in calcite grains (Hyvärinen, 1969). The marbles typically contain up to 10% calc-silicate minerals, with diopside being most abundant, but with calcic garnet, hornblende, tremolite, epidote, plagioclase, microcline, quartz, sphene, scapolite, biotite, muscovite, serpentine (after olivine) and minor chalcopyrite, pyrite and magnetite noted in this study, and with wollastonite and olivine found in areas just outwith the mapped area, both minerals previously having been recorded in the study area (Hyvärinen, 1969). The calc-silicate minerals vary in size from 0.1-3 mm, averaging 0.2 mm, and are typically much finer grained than the re-crystallised calcite plates which have a typical grain size of 5 mm-1 cm. Calcite twin lamellae are frequently kinked as a result of late deformation.

1.2.2(ii)(b) Calc-silicate skarns

The calc-silicate minerals occur not only as grains disseminated throughout the marble but also as continuous bands which range from <1 mm to 20 cm thick. These are parallel to S_0 in the marble, as marked by thin alternating layers of pink and rarer grey calcite.

Within the study area all lithologies comprising calc-silicate minerals have previously been called 'skarns'

(Hyvärinen, 1969). This term is widely used, particularly in Fennoscandia to describe calc-silicate-bearing lithologies (Hiltunen, 1982) within metamorphosed sequences. Originally the word 'skarn' was introduced into the literature as a collective term for the silicate gangue in certain Swedish ore deposits (Tornebohm, 1875). However, various workers have since expanded the use of this term so that to many workers it has specific genetic connotations.

The most commonly held interpretation is that the mineralogy and composition of skarns is the result of the replacement of carbonates (limestones or dolomites) principally by the metasomatic introduction of Si, Fe, Mg and volatiles emanating from a magmatic source usually at intrusive contacts (Lindgren, 1905; Kemp, 1907; Goldschmidt, 1911; Eskola, 1914; Zharikov, 1970; Brock, 1972; Smirnov, 1976). This process has been called skarnification (Sangster, 1969; Boyle, 1970). Other workers however recognise that skarns may have formed in additional or alternative ways. For example it has been suggested that some skarns may result from the metamorphism of impure limestones (Geijer & Magnusson, 1944, 1952; Watanabe, 1960), or from metamorphism of shaley limestones or metal-rich silica carbonates involving no metasomatism (Zharikov, 1979).

Geijer & Magnusson (1944) also recognise that other skarns may form from metamorphism of pre-metamorphic hydrothermic-metasomatic lithologies. The possibility of formation as a result of bimetasomatic reaction between unlike lithologies has also been proposed (Magnusson, 1930; Eskola, 1939; Magnusson, 1960), and it is thought to occur by diffusion of components (Korzhinskii,1964, 1965; Vidale, 1969; Vidale &

Hewitt, 1973). In addition it has been recognised that the metamorphism of certain volcanogenic-sedimentary assemblages associated with stratabound exhalative metal enrichments can also result in formation of skarn mineral assemblages (Magnusson, 1960; Peters et al., 1977; Einaudi et al., 1981).

Since, from this evidence there appears to be no single genetic process responsible for the formation of skarns, the definition of a skarn as a 'metasedimentary or metavolcanic rock whose main components are calcium-rich silicates' (Verkaeren & Bartolome, 1979), is favoured here. A more complete review of the historical background to the use and development of the term 'skarns' is provided in Einaudi et al. (1981) or Hiltunen (1982).

In this study lithologies with a calc-silicate mineralogy were observed to occur in many forms which display different relationships to adjacent or enclosing lithologies. These are subdivided into types based on this morphological evidence and are described below. The origin of the skarns is discussed in Section 3, Part 1.

(1) Type I : The calc-silicate bands found within marbles are usually multicomponent, and comprise varying proportions of andradite-grossular garnet, diopside-hedenbergite clinopyroxene ± scapolite ± quartz. The contacts between these bands and the enclosing marble are invariably sharp, with no mineralogical or chemical gradations observed. Where M_1 assemblages have not been retrogressed, textures are seen to be polygonal granoblastic, with the calcic garnet often being idioblastic. Epidote + quartz typically form a secondary retrogressive assemblage. Calc-silicate bands with similar

mineralogy, petrography, chemical composition and field relations have been described from other Proterozoic terranes (Jaques et al., 1982).

(2) Type II : In contrast to the skarn-marble contact described above, all contacts between amphibolites identified as pre-D_1 in origin, and marbles are characterised by gradational relationships. In one example from 0.5 km west of Hällinmäki Mine, a few thin marble bands up to 10 cm thick were observed within a sequence of amphibolites. In Figure 1.2.13 the changes in mineralogy which characterise amphibolite-marble contacts are clearly visible. In this example the 1 cm thick marble comprises 95% calcite and 5% diopside as small scattered grains. Bordering the marble is a 2 mm wide monomineralic zone comprising calcic garnet (andradite) which in turn is separated from the plagioclase-diopside-magnetite amphibolite by a monomineralic zone of hedenbergitic clinopyroxene, also approximately 2 mm wide. These zones are symmetrically developed and in this case are observed to envelope the marble where it is terminated at a boudin neck (as in Fig. 1.2.13). Within the amphibolite, plagioclase compositions were observed to become more calcic towards the marble. All plagioclase compositions were determined optically. At 30 cm from the contact with marble the plagioclase is typically An_{42}; 10 cm from the contact it is An_{54-69}; and < 1 cm from the contact it is An_{68-69}. Within the marble, rare plagioclase gives an estimated composition of An_{80}. The width of the skarn zone (or zones) at marble-amphibolite contacts is apparently roughly proportional to the width of the marble band, typically being only 5% of the width of the latter.

(3) Type III : Within several pillow lava-lava tube units at both Narila and Kiviniemi, ovoid or more irregular patches with a calc-silicate mineralogy and between 2 and 20 cm wide are developed (Figs. 1.2.2b, 1.2.6, 1.2.14). The patches either occur singly (Figs. 1.2.6, 1.2.14) or may form several different patches within individual pillows (Fig. 1.2.2b). Their mineralogy consists predominantly of diopside, scapolite ± calcic plagioclase and calcic (andradite) garnet in M_1-D_1, largely retrogressed to an M_2 assemblage of hornblende, actinolite, epidote or zoisite, with quartz and sphene. In some oblique sections through lava tubes, calc-silicate skarn alteration was observed to be elongate parallel to the margins of the tubes but was contained within individual lava tubes (Fig. 1.2.15). Patches up to 1 m in diameter but with relatively sharply defined margins are also developed in otherwise homogeneous amphibolites.

Calc-silicate patches with a similar mode of occurrence have been described from several metavolcanic sequences. They have been described from greenschist facies metavolcanic rocks in the Archaean (Harrigan & McLean, 1976; MacGeehan & McLean, 1980), in the Proterozoic (Reed & Morgan, 1971; Wilson & Leake, 1972) and in the Ordovician and Cretaceous (Stephens, 1982; Lydon & Jamieson, 1984), respectively, as well as from present day mid-ocean-ridge environments (Humphris & Thomson, 1978) and from prehnite-pumpellyite facies metavolcanics in the Ordovician (Smith, 1968; Jolly & Smith, 1972; Bevins, 1985), where the patches have been termed calc-silicate or calcium-rich 'metadomains'.

(4) Type IV : A similar calc-silicate mineralogy was noted in zones 1-5 cm thick which typically occur a few centimetres within the interior of and parallel to the margins of pillows and lava tubes (Figs. 1.2.6, 1.2.16). These zones are usually fairly continuous around individual pillow forms. They are considered most likely to have resulted from recrystallisation of Ca-rich amygdale layers.

(5) Type V : Within a few amphibolite units at Narila, Hallinmaki Mine, and at Kiviniemi, a gradation from 'unaltered' amphibolite to massive calc-silicate skarn, marked by an often spatially irregular increase in the proportion of calc-silicate minerals, is observed.

In one example at Kiviniemi a complex lava flow with a pillowed base is seen to truncate an underlying 'skarned' amphibolite unit, the upper part of which consists of a flow-top breccia. In this underlying unit there is an irregular increase in the proportion of calc-silicate minerals (now retrogressed mainly to an epidote-quartz assemblage) towards its top, with the upper 5-30 cm altered entirely to a calc-silicate mineral assemblage (Fig. 1.2.6). The base of the overlying unit is unaltered.

The other examples distributed throughout the area show similar gradational relationships with sharp planar 'tops' which, when combined with corroboratory evidence such as truncation of the 'underlying' skarned units, as occurs at Hällinmäki Mine (see Map 4), is taken as evidence for way-up of the sequence.

In all the examples at Hällinmäki Mine the transition from unaltered amphibolite-skarn is marked firstly

by the appearance and very gradual increase in the proportion of calcic (andradite) garnet at the expense principally of plagioclase, together with a rapid change in the pyroxene composition as indicated by a change in its colour from pale to dark green. This is interpreted as an increase in the hedenbergite component at the expense of diopside (Deer et al., 1966).

Plagioclase compositions are also observed to change: as the proportion of calc-silicate minerals increases (in tandem with the CaO content of the rock) the plagioclase becomes more calcic, having a composition of An_{44-47} in least altered amphibolite to An_{78-82} in massive skarn (Table 1.2.2). Calcic andradite garnet forms up to 90% of the rock in places. Scapolite occasionally occurs instead of plagioclase.

These transitions were observed to occur over zones between 2 cm and 10 m wide. In the mine area it was possible to demonstrate that while some of the bands were repeated by folding, several distinct amphibolite units had been altered in a similar way.

At Hällinmäki Mine the gradation within the amphibolite to the skarn was occasionally observed to be more in the form of a vein-like network. A similar feature was observed at Kurrikamaki (Fig. 1.2.17). In this example the host amphibolite is more breccia-like in appearance.

In the Hällinmäki Mine example, there is Cu-mineralisation associated with these Type V skarns.

(6) Type VI : At Huutoniemi a distinctive unit interbedded within the amphibolites and approximately 200 m thick and traceable for 600 m is exposed. It consists of

angular fragments of amphibolite, variably flattened and attenuated and between 5 mm and 15 cm square, set within a calc-silicate skarn matrix (Fig. 1.2.18).

(7) Type VII : A superficially similar lithology to that at Huutoniemi was noted at Karankalahti (Fig. 1.2.19). However in this example similar sized 'blocks' were recorded to consist predominantly of epidote while the 'matrix' was noted to mainly comprise abundant magnetite and finer-grained epidote. Spatially associated with this 'skarn' is a lithology consisting of angular fragments up to 3 cm in size. This 'breccia' also has a calc-silicate petrography, with epidote, chlorite and serpentine in the centre of the fragments, a rim of diopside in an andradite matrix (Suvanto, 1983).

The relationship of these skarns to the other country rocks was not readily discernible due to the abundance of syn-kinematic intrusions nearby. However, drill core results show that they occur in close proximity to a Cu-rich horizon (Koistinen, pers. comm.).

(8) Type VIII : At a few localities, e.g. Hällinmäki Mine and at Kiviniemi, calc-silicate skarn layers varying from < 1 cm thick up to 3 m thick and comprising andradite + minor hedenbergite and scapolite were observed to occur as relatively continuous layers parallel to S_0 within amphibolites (Fig. 2.2.6). At Hällinmäki Mine these skarn bands were observed to be interlayered with both chalcopyrite-rich and magnetite-rich 'skarned' amphibolite bands (see Map 4). There is no internal zoning within the bands and they are not apparently associated with any marble layers.

Hence, from the descriptions given above it is clear that rocks with a 'skarn' petrography in the Virtasalmi District exist as morphologically diverse lithologies. This diversity is reflected in the mode(s) of origin discussed in Section 3, Part 1.

1.2.2(iii) Quartzofeldspathic schists and gneisses

Pre-tectonic quartzofeldspathic schists and gneisses are a rare constituent of the lithological assemblage in the study area, only occurring as relatively thin interbeds within amphibolites in the Narila area. Many outcrops of 'gneiss' indicated in previous work (Hyvärinen, 1969) were found to be syn-tectonic gabbros and diorites in which truly gneissose textures were developed only in localised thin high strain zones. Pre-tectonic quartzofeldspathic gneisses are the dominant lithology immediately outwith the study area.

The polymetamorphic mineral assemblages of the gneisses and schists are elucidated in Section 2, Part 4. They consist of varying proportions of quartz, plagioclase, biotite, almandine, cordierite, sillimanite and cummingtonite as the major constituents. There is considerable variation in the abundance of mica, and hence in the development of schistose or gneissose foliations. In exposures 1 km north of Narila, gneissose banding is only weakly developed, the rock being fairly massive in character and < 20 m thick. Weak later foliations are defined by the realignment of mica in particular. This unit is unusual in containing a high percentage

of sulphides (pyrrhotite), and containing thin bands with a more mafic character (cummingtonite-quartz-feldspar bands).

In exposures around the south of Lake Virmasjarvi at Virmaanpaa the rocks are more schistose and comprise > 50% mica.

Quartzofeldspathic segregations or blebs up to 10 cm long and with diffuse margins occur sub-parallel to the composite foliation in some outcrops of gneiss. The blebs are coarse-grained and consist of quartz, plagioclase with myrmekite and microcline.

1.2.2(iv) Other lithologies

Limited descriptions of the petrography and field relationships of the intrusions and veins are provided in Section 2, Part 2, and Section 2, Part 3 respectively.

Table 1.2.1

Group A			
Analysis No.	170	257	260
Plagioclase (An content)	An_{52-58}	An_{54-58}	An_{48-54}
Rock CaO content	9.52%	9.28%	9.67%

Group B					
Analysis No.	29	182	262	199	184
Plagioclase (An content)	An_{44-47}	An_{50-68}	An_{65-72}	An_{59-64}	An_{43-49}
Rock CaO content	10.31%	22.55%	18.80%	15.90%	15.58%
Analysis No.	185	4	259	21	222
Plagioclase (An content)	An_{60-69}	An_{59-69}	An_{65-80}	An_{38-43}	An_{43-45}
Rock CaO content	24.15%	23.31%	18.71%	9.44%	13.70%

Group C			
Analysis No.	96	102	97
Plagioclase (An content)	An_{40-42}	An_{40-44}	An_{42-46}
Rock CaO content	7.53%	6.88%	6.61%

Table 1.2.1 shows the apparent relationship between plagioclase composition and CaO content of the rock, and the variation that is apparent between the three main amphibolite groups that are distinguished petrographically. All plagioclase compositions were determined optically.

Table 1.2.2

Analysis No.	9	4	10	14	29
Plagioclase (An content)	An_{68-76}	An_{59-69}	An_{50-69}	An_{44-50}	An_{44-47}
Rock CaO content	26.08%	23.31%	25.09%	12.80%	10.31%

Table 1.2.2 shows changes in plagioclase composition which correspond roughly with increases in CaO content. The samples were collected in a traverse across a transition from amphibolite (Analysis No. 14) to Type V calc-silicate skarn, T370m, Hällinmäki Mine. All plagioclase compositions were determined optically.

Fig. 1.2.1 Narrow discrete D_2 high strain zone developed obliquely to a pre-existing penetrative S_1 fabric. Outwith the high strain zone, where S_2 is only weakly developed, the S_1 fabric is coarse-grained. In the high strain zone, S_1 is destroyed and S_2 is finer-grained. Within hornblende gabbro, Kiviniemi.

Fig. 1.2.2(A) Thin dark coloured hornblende-rich bands define ovoid pillow forms in amphibolites, Kiviniemi.


1.2.1
S_2
S_1
F_3


1.2.2
A

Fig. 1.2.2(B) Thin dark coloured hornblende-rich bands outline elongate tube-like features, in amphibolites Narila.

Fig. 1.2.3 Interconnected pillow lavas-lava tubes at Pallionmaki, just outwith the mapped area. These are considered to represent a less highly strained and less altered example with which to compare similar features in the study area (e.g. see Fig. 1.2.2(B) for comparison).

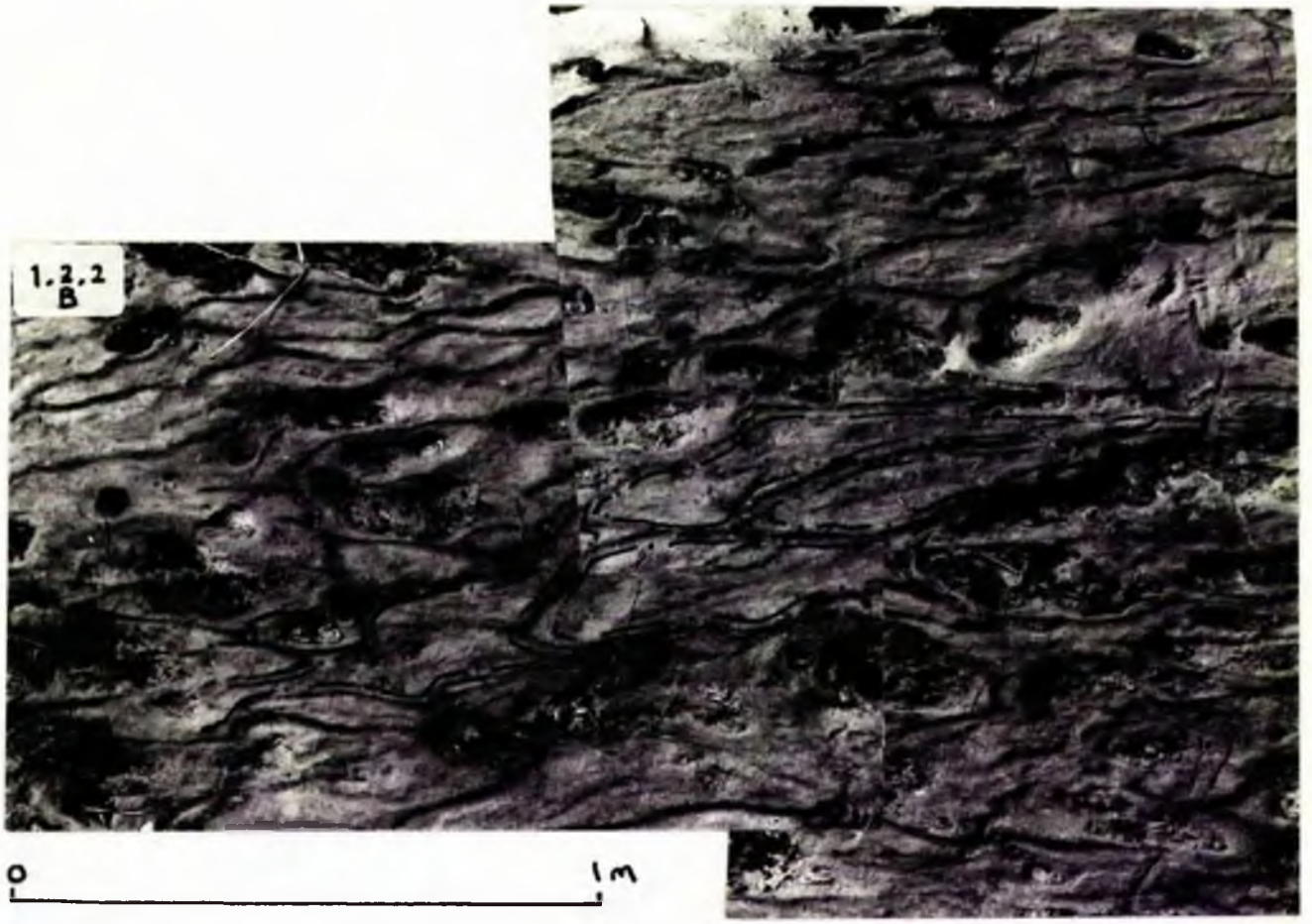
1.2.2
B
0
1m


1.2.3

Fig. 1.2.4 Diagramatic sections showing possible views through interconnected lava tubes. Adapted from Hargreaves & Ayers (1979) and Jones (1969).

Fig. 1.2.5 Highly strained pillow lavas-lava tubes (see Section 2, Part 1) interlayered with more homogeneous amphibolite interpreted as an aphyric lava flow. Near Narila.

Fig. 1.2.4

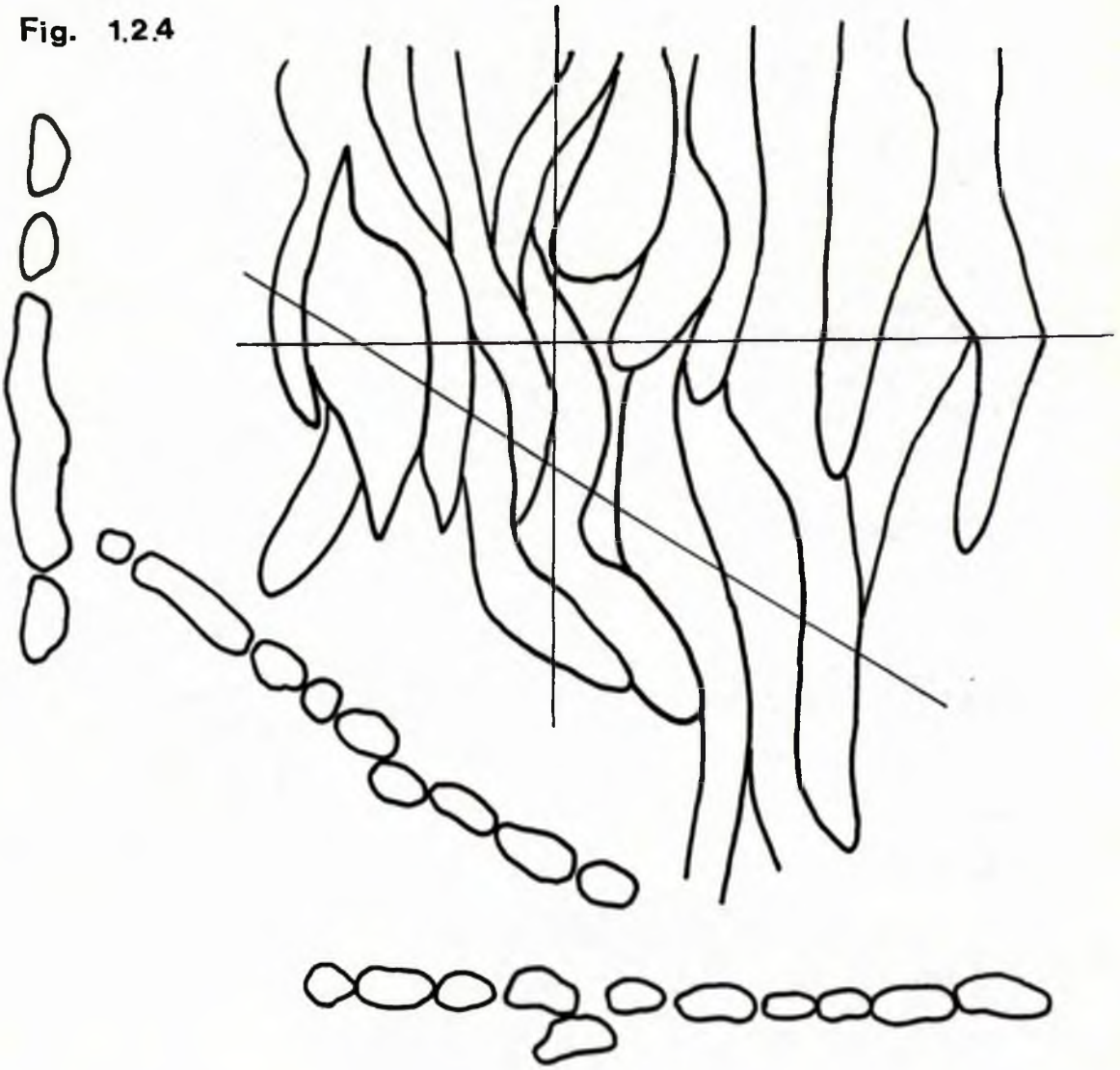

Fig. 1.2.6 Complex lava flow with pillowed base unconformably overlies a massive lava with a calc-silicate skarned flow top breccia. Within the 'pillows' there are ovoid Type III skarn patches, in addition to less well developed Type IV skarn zones concentric with the pillow rims.

Key to tracing overlay

A Type III skarn patch

B Alteration halo around A

C Recrystallised Ca-amygdale-rich zone

D 'Skarned' flow top breccia

E Massive lava (gradational contact to 'D')

F Pillowed base to complex lava flow

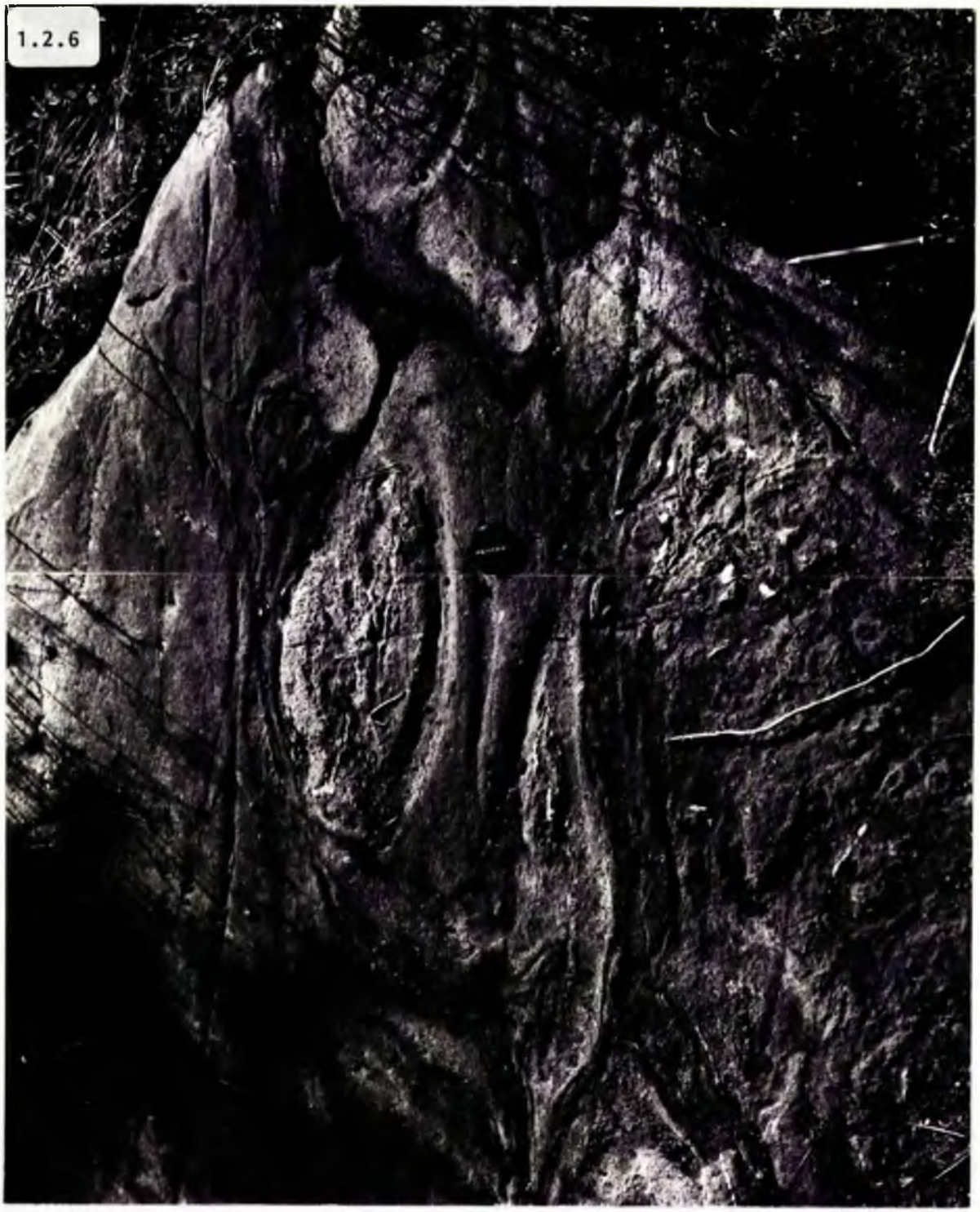
1.2.6


1.2.6
A
B
C
B
A
A
C
BASE of PILLOW LAVAS
D
E
F

Fig. 1.2.7 Thinly banded amphibolites are cross-cut at a low angle by a more homogeneous amphibolite. The S_1 fabric is continuous across the lithological contact, which is irregular. Taking this evidence into account and as the two amphibolite units are apparently cogenetic (Section 3, Part 1), then the contact between the two units is considered to be pre-tectonic. The banded amphibolites are interpreted as tuffs. Virtasalmi Village.

Fig. 1.2.8 A thin diopside-rich stripe ← in otherwise homogeneous amphibolite is observed to be the tectonically thinned equivalent of several distinct compositional bands. Virtasalmi Village.


1.2.7
S_0
S_1
0 10 cm

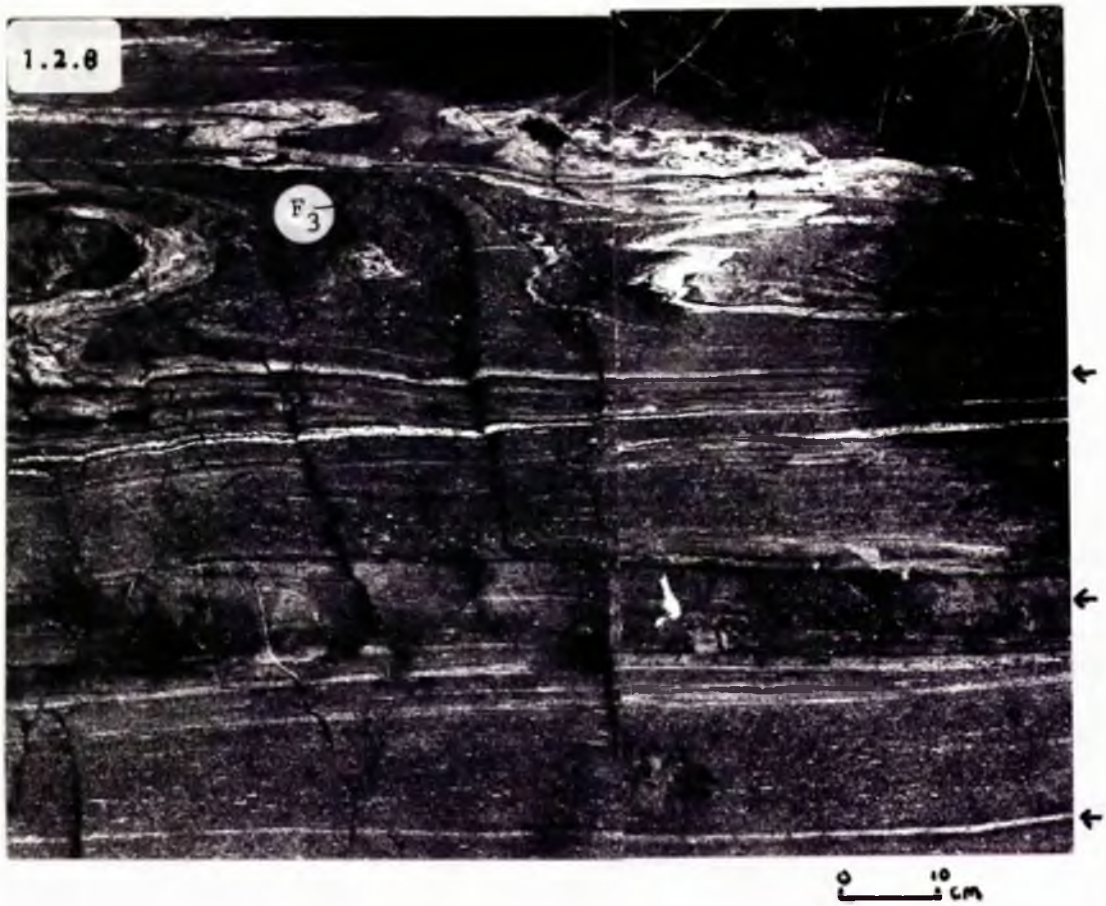
1.2.8
F_3
0 10 cm

Fig. 1.2.9 S_2 metamorphic differentiation banding axial planar to F_2 folds. Amphibolites, west of Hällinmäki Mine.

Fig. 1.2.10 In a sequence of thinly interlayered amphibolites, plagioclase-rich stripes interpreted to have formed by metamorphic differentiation are restricted to petrographically (and compositionally) distinct bands. The latter contain less clinopyroxene than adjacent layers. South-west of Hällinmäki Mine.


1.2.9
S_{0-1}
F_2
S_2


1.2.10
S_C
F'_6

Fig. 1.2.11 Leucocratic stripes interpreted to have formed as a consequence of metamorphic differentiation are observed to have formed sub-parallel to both S_1 and S_2. Amphibolites, Virtasalmi Village.

Fig. 1.2.12 In the field, the locality for Figure A occurs approximately 5 m to the left of that for Figure B (viewed from the same orientation). A gradual transition from easily recognisable lava tubes containing weakly expressed tectonic fabrics (Fig. 1.2.12A), through a zone of increased flattening and attenuation of the lava tubes accompanied by development of a more intensely penetrative S_2 fabric, to a banded rock with only rarely preserved pillow-tube closures (Fig. 1.2.12B) is observed. Amphibolites, Narila.


1.2.11
S_2
S_1


1.2.12
A


1.2.12
B

Fig. 1.2.13 Type II skarn. Symmetrical development of mono-mineralic zones at marble-amphibolite contact. A 2 mm wide zone comprising andradite garnet borders the 1 cm thick marble, and a rim of hedenbergitic clinopyroxene occurs between the andradite zone and the plagioclase-diopside-magnetite amphibolite. West of Hällinmäki Mine. (×30 mag.)

Fig. 1.2.14 Ovoid Type III skarn patch within lava tubes, in amphibolites, Narila.

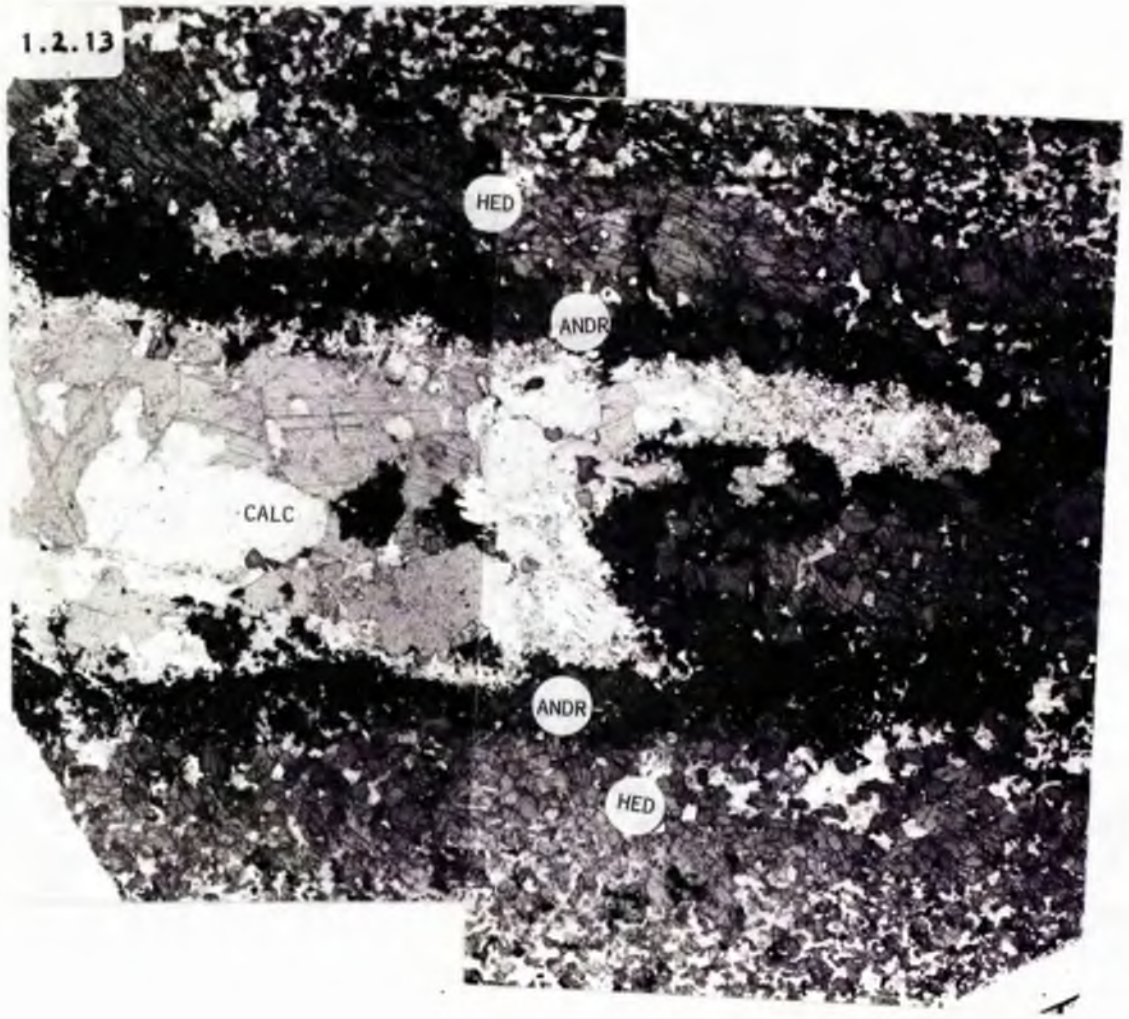
1.2.13
HED
ANDR
CALC
ANDR
HED


1.2.14

Fig. 1.2.15 Skarn alteration within and elongate parallel to lava tube margins. Probably an oblique cross-section of the Type III alteration patches which are ovoid in cross-sectional views (see Fig. 1.2.14). Compare Figs. 1.2.14 and 1.2.15 with reference to the possible sectional views indicated in Fig. 1.2.4.

Fig. 1.2.16 Type IV calc-silicate alteration zones from fairly continuous bands concentric with lava tube-pillow margins, Narila.

Fig. 1.2.17 Slabbed block of skarn breccia, Kurrikamaki. Petrography mostly comprises andradite, hedenbergite and scapolite. Leucocratic rims around some fragments are the result of D_2-M_2 epidotisation. Smaller fragments often completely retrogressed. Scale bar is 2 cm long.


1.2.15
0
10 cm


1.2.16


1.2.17

Fig. 1.2.18 Angular blocks of amphibolite in calc-silicate skarn matrix. Type VI skarn, Huutoniemi.

Fig. 1.2.19A Blocks with a calc-silicate petrography (epidotised) set within a finer-grained matrix containing abundant magnetite. Type VII skarn, Karrankalahti.

Fig. 1.2.19B Spatially associated with the lithology illustrated in Fig. 1.2.19A is a breccia comprising smaller angular fragments. Suvanto, 1984, noted that the fragments were zoned as follows:

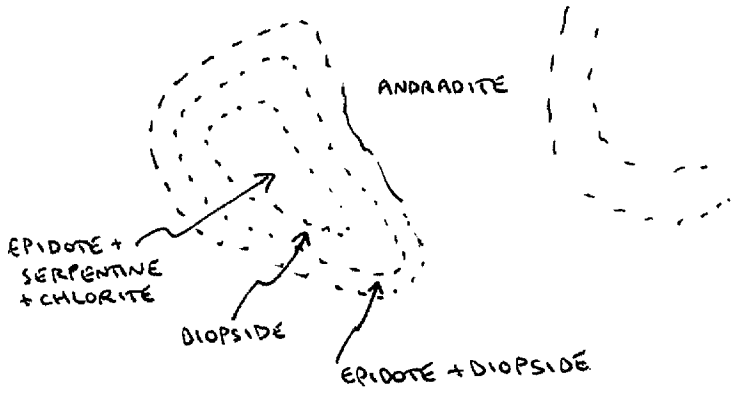

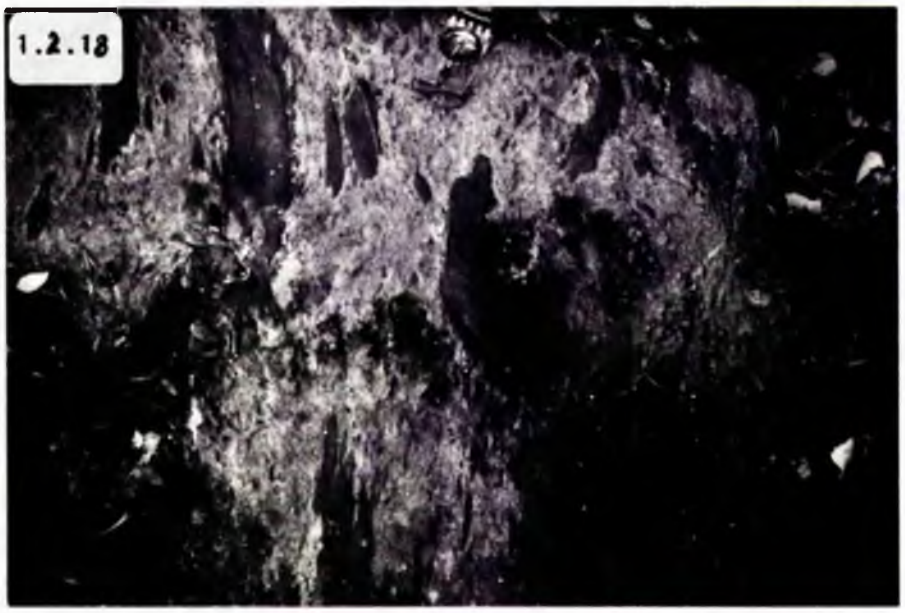
1.2.18

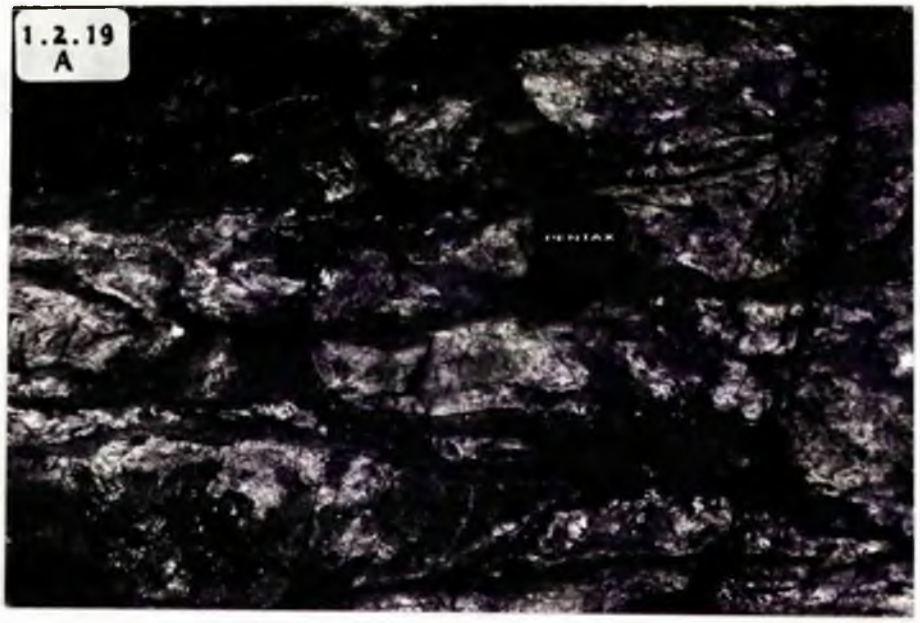
1.2.19
A


1.2.19
B

SECTION 2

Structural, igneous and metamorphic features

PART 1

Structural development of the Virtasalmi District

2.1.1 Introduction

A detailed study of fold and fabric elements together with lithology has revealed a complex structural pattern in the Virtasalmi District (see Fig. 2.1.1) which is interpreted as having resulted from polyphase deformation. The resulting widely varying attitudes of folds was recorded by Hyvärinen (1969) but not interpreted by him as the result of the presence of folds of different generations. In addition previous work has not recognised all of the major folds identified in the present study. Consequently a reinterpretation of the structural development of the area is necessary.

Despite the many studies in the Karelides where the polyphase nature of deformation and metamorphism and the relationship of igneous intrusions to structural sequence has been elucidated over wide areas (Bowes et al., 1984), there have been few similar studies in the Svecofennides, especially adjacent to the Karelides. An important exception to this is the study by Gaál & Rauhamaki (1971) in the Rantasalmi-Haukivesi area 40 km east of Virtasalmi which showed that a generally corresponding lithological assemblage had undergone polyphase deformation and emplacement of pre- and syn-tectonic intrusions not unlike those at Virtasalmi.

2.1.2 Major structural features

Throughout the area there is a lack of distinctive lithologies that are continuous for any considerable distance. Hence delineation of major structures depends largely on observation of the geometries and vergence of minor folds and attitude of metamorphic mineral fabrics.

In the northern half of the study area the distribution of lithological units, the orientation of the prominent planar metamorphic foliations and vergence changes in minor folds outline the shape of a NW-trending steeply plunging major reclined fold which closes towards the SE (Fig. 2.1.1). The western limb of this structure is not well exposed and as the closure extends well outwith the area mapped, the overall shape of the fold is best demonstrated on an aeromagnetic map of the area (Map 2).

It should be noted here that in the course of this study it was found that great caution had to be exercised in using an aeromagnetic map for interpretation of structural features due to the emplacement of syn-tectonic intrusions and the resultant complexities posed for contouring the data. Nevertheless they were found to be of use where lithological and structural data constrained the interpretation.

Vergence changes of minor folds which have orientations consistent with their being parasitic to this major structure indicate that this is an F_3 structure. In the hinge zone of the structure to the SW of Virtasalmi Village, 'M' folds have amplitudes of up to several hundred metres.

At outcrop scale two distinct sets of folds (F_1 & F_2) and associated axial planar fabrics (S_1 & S_2) are seen to be affected by folds of the same generation as these NW-trending F_3 folds. Throughout the study area the occasional angular relationship between lithological layering and a fabric (S_1) axial planar to minor F_1 folds indicated the existence of larger F_1 folds, although no F_1 closures larger than outcrop scale could be identified.

The existence of major second generation structures however has been established on the basis of changes of vergence on minor asymmetrical F_2 folds and the relationship of the metamorphic fabric (S_2) developed axial planar to F_2 folds, to earlier fabrics. In the northern half of the area it was impossible to delimit major F_2 closures due to the intensity of overprinting by F_3 structures, although major F_2 structures were recognised in the southern half of the area. The geometry of minor F_2 folds varies markedly over the area due to later refolding, particularly within major F_3 hinge zones (e.g. at Narila). Over most of the area, however, minor F_2 folds were observed to be tight with gently plunging axes and inclined axial planes.

At Hällinmäki Mine it was possible to establish younging directions in the amphibolites sequence. These observations were used to establish that the northerly plunging large 'sinistral' F_2 structure noted in the mine is an anticline. From this evidence it is concluded that the larger F_2 structure, which from vergence changes and S_0-S_1-S_2 relationships is recorded to close to the NW, is at least antiformal if not anticlinal. The amplitude of this F_2 structure is c. 1 km.

A larger F_2 synform has been delineated to the west of the latter antiform. Its western limb is defined by a thick marble unit largely proven from a combination of borehole and geophysical data (see Map 2). This unit can be traced from Ankele in the west to near Narila in the south-east. The south-easterly closure of the synform is also mapped mainly by changes in vergence and S_{0-1}-S_2 relationships, although differences in the amphibolites help to delimit it. The fold axes of both these major F_2 structures are refolded by large F_3 and F_6 folds in particular (e.g. F_3 fold at Narila) (see Fig. 2.1.2a,b).

Although less well defined, the hinge zone of the major F_3 fold identified in the northern half of the area can be traced in a south-easterly direction through the southern half of the area. However, its axis is largely obliterated by syn-kinematic intrusions.

The amount and direction of plunge of the minor folds defining the larger F_3 structures vary markedly but systematically. Around Kiviniemi, Hällinmäki and Narila F_3 folds plunge 45-70° SE, while in the vicinity of Virtasalmi Village and Kurrikamaki it is 40-65° NW. These variations are related to refolding about large steeply plunging open-tight folds (F_6) with NE-trending axes and amplitudes of 300-500 m.

Few structures of considerable size which can be attributed to other phases of deformation on the basis of overprinting and refolding criteria are developed throughout the area. One example however is at Karankalahti where a WNW-trending F_4 fold causes reorientation of F_3 and

earlier structures.

The interpretation of the pattern of major structures is dependant upon an understanding of the polyphase deformational sequence. The dominant pattern results from the combination and interference of major D_2 and D_3 structures. However it is not possible to demonstrate the form of the major F_2 structures in the northern half of the area due to the intensity of overprinting. Major F_1 folds may also exist but it is not possible to establish their geometries. Post D_3 deformation is not pervasive on a large scale and is patchily expressed.

2.1.3 Structural sequence

Observation of relationships of structural features has revealed the products of seven phases of deformation, excluding later faulting in the Virtasalmi District. Successive phases are labelled D_1, D_2....D_7, with corresponding folds, axial planar fabrics and lineations referred to as F_1, F_2....F_7, S_1, S_2....S_7 and L_1, L_2....L_7 respectively. Surfaces interpreted as original lithological layering are referred to as S_0.

Demonstration of a structural sequence in such highly deformed terrane depends primarily on recognition of overprinting and refolding relationships (see Hopgood, 1980). Evidence for each phase of deformation is rarely seen within one outcrop, and the expression of a particular deformational phase may vary due to local competence contrasts or due to changes in the stress system, with the result that fold sets

may be expected to vary in style or be of limited expression.

However, despite the possible variations of expression, correlation of structural sequences established locally can be made with considerable confidence provided there are sufficient parameters available for correlation and provided the local "subareas" for which correlation is made are not too large or too widely spaced. In this study outcrop to outcrop correlation was made and structural sequences were established in 4 subareas (see Map 1). In each subarea the structural sequence was the same, so that the following sections describe features, and their sequential development, for the entire area with variations of expression of individual features from place to place indicated.

2.1.4 Lithological layering (S_0)

In rare instances both S_1 and S_2 were observed to be discordant to lithological layering (S_0). For example, in low strain zones characterised by the concurrence of weakly expressed tectonic (S_1 and S_2) fabrics, notably at Kiviniemi and at Hällinmäki Mine, pre-tectonic angular discordances were recorded in amphibolite-skarn lithologies (e.g. Fig. 1.2.6 and Map 4). These examples provide useful way-up indicators and are described in more detail in Section 3. Lithological layering (S_0) was seen to be discordant to other S_0 surfaces and to S_1 in exposures of pillow lavas/lava tubes.

2.1.5 First phase of deformation (D_1)

The earliest expressions of deformation in the Virtasalmi District are small-scale tight to isoclinal folds (F_1) which deform lithological layering (S_0) (Figs. 2.1.3 & 2.1.4). These F_1 folds show marked thinning of S_0 on fold limbs and have amplitude : wavelength ratios > 10:1. Fold noses are commonly angular but are sometimes arcuate especially in more competent lithologies such as marbles and calc-silicate rocks. Restricted occurrence on flat, glaciated exposures precluded measurement of fold plunge and attitude of axial plane.

Commonly there is an axial planar metamorphic fabric (S_1) developed (Fig. 2.1.4). This is variably expressed as a schistosity or metamorphic segregation-differentiation banding (Fig. 2.1.5) or a foliation defined by an oriented mineral growth but without formation of banding by a segregation process. Hence in some units there is a linear fabric rather than a planar fabric resulting from the dimensional alignment particularly of pyroxenes and amphiboles. The expression of the oriented fabric is interpreted as being dependent on lithology, local stress conditions and the distribution and movement of fluids.

Over much of the area S_0 and S_1 were observed to be coplanar, or nearly so. However in a few places, for example near Kiviniemi and at Narila, non-coplanar relationships between S_0 and S_1 were recorded (Figs. 2.1.5 and 2.2.1) that suggest the existence of F_1 folds larger than observed at outcrop scale. It was only possible to map small isolated

limb segments of these structures due to the combined effects of poor exposure, the lack of distinctive lithological marker horizons, and later tectonic and metamorphic overprinting. Because of these factors it was not possible to establish the three-dimensional shape of F_1 folds.

S_1 planar features range from a penetrative schistosity (1 mm scale) to a spaced cleavage (2 mm scale) in the amphibolites and gneisses. In the amphibolites S_1 comprises varying proportions of diopside, hornblende, plagioclase, biotite, cummingtonite and rare hypersthene, while in the gneisses S_1 mainly comprises alternating biotite-rich and quartzofeldspathic layers. Marble, calc-silicate and 'skarn' lithologies display no penetrative S_1 fabric development either macroscopically or microscopically. The granoblastic textures they show are the products of static recrystallisation. In several of the pre-D_1-early syn-D_1 intrusions, xenoliths ranging from relatively undeformed, irregularly-shaped blocks to long, narrow discontinuous bands were observed (Fig. 2.1.6). These bands are interpreted as having resulted from flattening, attenuation and rotation of these xenoliths (c.f. Fig. 4.11) into alignment with S_1.

Penetrative D_1 fabrics are retained solely in zones of relatively low D_2 strain (Fig. 2.1.5). They are destroyed in D_2 high strain zones where S_1 minerals either have been completely recrystallised or, more commonly, have undergone a combination of (1) mechanical rotation into a position perpendicular to the D_2 maximum stress orientation together with (2) a grain size reduction and incomplete resorbtion, leaving only the mineral cores with compositions

corresponding to equilibrium D_1 conditions. Retention of D_1 fabrics in D_2 low strain zones is probably due both to absence of a penetrative D_2 strain component and to more limited retrogression of D_1 assemblages which implies enhanced movement of retrogressive fluids within D_2 high strain zones.

2.1.6 Second phase of deformation (D_2)

During D_2, S_0, F_1 folds and S_1 fabrics were refolded by tight to isoclinal folds, with localised formation of Type 3 F_2-F_1 interference structures (Ramsay, 1967) (Fig. 2.1.3). Fold styles vary markedly due to local competence contrasts. An axial planar foliation (S_2) (Fig. 2.1.7a-c) is commonly developed, however there is a marked variation in intensity of development of this fabric (e.g. Fig. 2.1.8a,b) indicating that there were variations in the distribution of strain during D_2.

Most F_2 folds approximate to the similar fold model (Class II, Ramsay, 1967) and have angular fold noses often with fold hinges thicker than limbs (Figs. 2.1.3 and 2.1.9) probably as a result of greater attenuation on the limbs. This feature is particularly striking where there are large competence contrasts between lithologies, and where isoclinal folds are developed in zones of intense flattening interpreted as higher strain zones (FIg. 2.1.10). In other instances there is no marked thinning on limbs relative to hinge zones (Figs. 2.1.11 and 2.1.12).

Minor F_2 folds were observed to have tighter inter-limb angles where they were noted to occur in the limb zones of F_3 fold structures. This is considered to be due

to attenuation on the limb zones of the latter folds. The amount and direction of plunge of F_2 folds is also observed to vary even over short distances. This is also considered to be the result of refolding, primarily during D_3. This can also be demonstrated on a regional scale, for example between Hällinmäki and Narila. To the west of Hällinmäki Mine F_2 folds were noted to plunge about subhorizontal axes with axial planes dipping eastwards, but in the Narila area they plunge about subvertical axes with axial planes dipping northwards. The change in F_2 fold attitude across the F_3 fold is illustrated schematically in Fig. 2.1.2. Over most of the area however, F_2 folds are gently plunging with steeply inclined axial planes. Examination of the S_2 foliation in F_2 suggests that there was an axial planar slip component involved in F_2 development. In most instances the shear planes are separated by infinitely small amounts, producing continuously curving marker surfaces (folds). However, step-like discontinuities, with sinistral or dextral displacements depending on the limb involved, were recorded in some fold hinges. These features are marked by particularly intense S_2 foliation development (see Fig. 2.1.13). In contrast, discrete shear zones which are in effect planar discontinuities not marked by an intense foliation development, were observed to occur axial planar to F_2 folds (Figs. 2.1.3 and 2.1.9). Formation of these surfaces has apparently resulted in segmentation of pre-existing marker surfaces and re-alignment of S_0-S_1 features parallel to F_2 axial planes. One result is to make the appearance of F_1 folds more complex (Fig. 2.1.3); another is the development of ovoid or rectangular lithons within anastomosing planar

discontinuities. These are most commonly developed where there are large competence contrasts between lithologies (Fig. 2.1.3).

Boudins were observed to have formed where there were large competence contrasts between lithologies, however in a couple of examples boudin-shapes were observed within relatively homogeneous amphibolite masses (Fig. 2.1.14). The boudin shapes are variable depending on the particular lithologies involved, with ovoid or rectangular boudins (Figs. 2.1.15a, b) recorded as well as more irregular forms (Fig. 2.1.16). Whereas the lithons associated with transposition structures probably formed initially by tectonic segmentation followed by mechanical rotation, these boudins almost certainly resulted merely from ductile flow in response to extension in one or more directions as a result of bedding normal compression (Ramberg, 1955; Patterson & Weiss, 1968; Lloyd et al., 1982).

Scar folds, formed by flowage of less competent material into boudin necks (c.f. Hobbs, Means & Williams, 1976), are a common occurrence with boudins in the area (Fig. 2.1.16). The development of D_2 scars is frequently associated with quartz segregations. The latter are considered to have developed by migration of quartz (Fig. 2.1.15b) or, where present, chalcopyrite ore, into the low pressure zones in the boudin necks. Within the Hällinmäki area, the boudins tend to have near chocolate-block form (c.f. Wegmann, 1932; Sylvester & Christie, 1968), with the principle extension direction parallel to the plunge of F_2 hinges and maximum shortening perpendicular to the axial planes. The presence

of fairly equidimensional boudins is interpreted as an indication that all directions within the boudinaged layer were in extension for part of their history (Hobbs, Means & Williams, 1976).

It is typical for the more competent units to be calc-silicate assemblages or marbles, with the less competent material being amphibolite (Figs. 2.1.15, 2.1.17 and 2.1.18). There is a great range in size of the boudins observed, from those within layers < 1 cm thick, to those up to 50 m wide and several hundred metres in length. An example of this occurs at Hällinmäki Mine, where a lensoid sequence of marble and calc-silicate skarn layers was recorded from drill core.

In the vicinity of Narila, the principal extension direction of the boudins is also parallel to the F_2 fold plunge. These boudins are more elongate, probably as a result of smaller amount of extension parallel to the intermediate axis. Evidence to support this interpretation lies in the presence of a strong rodding and mineral lineation (L_2), which also was observed to plunge parallel to the F_2 fold hinges (Figs. 2.1.19a, b). The rodding appears to be confined to areas such as this where one main extension direction seems to have predominated. Elsewhere, L_2 mineral growth in S_2 has two components, with some minerals aligned normal to the fold hinge and others parallel to the hinge. Where foliation development is most penetrative and flattening is extreme, the 001 axes of minerals (0001 axes in micas) are typically aligned normal to fold hinges. This indicates that the orientation of stress conditions for mineral growth in these zones was essentially the same as that involved in producing the shear offsets often present in minor F_2 folds. In many parts of the study area however

the attitude of L_2 is difficult to measure because of the lack of three-dimensional exposure.

The axial planar foliation S_2 is variably expressed, and, like S_1, it can be unequivocally demonstrated to form a metamorphic differentiation banding. In some of the amphibolites near Virtasalmi Village the S_2 fabric is developed as a metamorphic differentiation fabric in zones 10-20 cm wide where it is also seen to cross-cut the earlier S_1 banding (Fig. 2.1.20a). Individual leucocratic segregations are 0.5-5 mm wide and are of constant thickness over several metres. In certain diopside amphibolites an interference pattern (Fig. 2.1.20b) between S_1 and S_2 is produced where there is a measurable angle between the two fabrics and where S_2 only partially overprints S_1. In many amphibolites however, S_2 is developed as a relatively homogeneous mineral foliation with no segregation banding visible (Figs. 2.1.12b and 2.1.21).

In the gneisses, S_2 commonly forms an axial planar segregation banding defined by biotite and quartzo-feldspathic layers (Fig. 2.1.5). Over much of the area, however, S_0, S_1 and S_2 are subparallel, with S_2 merely enhancing the earlier fabrics.

In calc-silicate, skarn or marble boudins there is commonly no penetrative S_2 fabric developed, probably because these lithologies form more competent boudins. Similarly, there is a weakly penetrative S_2 fabric developed near the margins of some late-D_2 metagabbro intrusions (Section 2, Part 2) but a blasto-hypidiomorphic texture in the centre resulting from static recrystallisation.

In addition to the narrow planar high strain zones formed in response to axial planar shear movements in some F_2 hinge zones, there are other zones typified by intense foliation development, flattening and attenuation of pre-existing features, and variable ductile shear displacement. These zones are apparently unrelated to any obvious F_2 fold structures and in that sense are similar to structures described by Myers (1978). They range from a few cm to 100 m wide, but due to lack of exposure could only be traced for up to 200 m. Interpretation of these zones as a consequence of strain variation is greatly assisted by the preservation of relatively narrow transition zones within which the intensity of development of the S_2 fabric is seen to grade from a non-penetrative or weakly lineated fabric to an intensely penetrative new mineral foliation.

Approaching these zones, S_0 and S_1 become increasingly flattened and attenuated and show features consistent with a gradual rotation into parallelism with S_2 planar features. On the microscopic scale this is accompanied by a grain size reduction, extensive recrystallisation of the D_1 assemblage, and development of a new intensely penetrative S_2 fabric resulting in the formation of a new metamorphic banding. Features interpreted as having resulted from such processes occur within pre-tectonic intrusions in the vicinity of Hällinmäki Mine and Kiviniemi. In one metagabbro near Hällinmäki Mine abundant coarse-grained xenoliths and aplitic veins become thinner, streaked out, and reoriented into a zone less that 5 m across (Figs. 2.1.22a-c). This has resulted in formation of gneissose layering, with alternating hornblende-rich and

quartzofeldspathic bands where deformation is most extreme. Similarly at Kiviniemi xenoliths are flattened, attenuated and reorientated into parallelism with the margin of the intrusion (Fig. 2.1.6).

In the area south of Kiviniemi there are other narrow zones characterised by intense flattening. However, these show a more clearly illustrated grain size reduction within the zones which have sharp margins. These zones are 10-50 cm wide, and three zones were noted spaced at c. 2 m apart (Figs. 2.1.23a, b). Within them there is a strongly penetrative S_2 fabric shown by small, intensely zoned aggregates of plagioclase and fine-grained hornblende and sphene. As noted above the margins of these zones are sharp with a discordance of up to 30° with the earlier fabric (Fig. 2.1.23b). In this respect they differ from continuous ductile shear zones (Ramsay & Graham, 1970) and similar features have been termed discontinuous (Burg & Laurent, 1978) or discrete (Vauchez, 1987) ductile shear zones. There is some bifurcation of the zones with the distribution fo pre-existing fabrics in intervening blocks suggesting that the blocks themselves have undergone some rotation (Fig. 2.1.24). The marked retrogression (epidotisation) concentrated within one such block suggests that these high strain zones could have acted as foci for increased fluid movement during D_2.

Vauchez (1987) considered similar discrete shear zones to have evolved by increases in strain, stress and strain-rate magnitudes, and deformation mechanism form continuous shear zones. The petrofabrics developed in the zones observed in this study, and in particular the reduced

grain size of feldspar and its grain shape, point to dynamic recrystallisation of the feldspars to form a continuous banding.

2.1.7 Third phase of deformation (D_3)

F_2 folds, S_2, D_1 fabric elements and any remnant S_0 were refolded about NW-trending axes during the third phase of deformation (D_3). Where F_2 hinge zones are folded, both Types 2 and 3 interference structures were formed (Figs. 2.1.25 and 2.1.11a).

F_3 folds are consistently tight, have round to angular hinge zones, and are mostly flexural slip folds with slightly to moderately attenuated limb zones (Figs. 2.1.26, 2.1.27 and 2.1.28). Their amplitude : wavelength ratios vary form 2:1 to 5:1, and minor F_3 folds with amplitudes of 1-5 m are ubiquitously developed. The three-dimensional orientation of F_3 folds is variable over the area (Section 3.2). Mostly, F_3 folds vary in attitude from reclined to steeply plunging inclined.

Disharmonic folds sometimes develop where there are marked competence contrasts in thinly layered sequences, this being particularly notable where there are interlayered skarn or calc-silicate rocks and amphibolites (Fig. 2.1.29). The disharmonic appearance of certain F_3 folds is sometimes accentuated by the discontinuous nature of certain layers frequently due to boudin formation during D_2.

In the vicinity of Hällinmäki Mine many assymetrical minor F_3 folds have attenuated long limbs which pass into narrow zones of extreme attenuation and brittle

discontinuity. These zones, which are interpreted as high strain zones, are commonly less than 30 cm across and are discontinuous over distances less than 15 m. Within them there is no new mineral growth and rare recrystallisation of pre-existing assemblages. However a spaced fracture cleavage (S_3), commonly developed axial planar to F_3 folds, becomes more penetrative and closely spaced as these zones are approached. Where the zones are less intensely developed they are observed to have formed in the hinge zones of small, tight synforms (Fig. 2.1.30). They alternate with zones of intense S_3 development which occupy the positions of intervening short limbs. In the well-developed D_3 high strain zones at Hällinmäki Mine, pre-existing S_0, S_1 and S_2 surfaces are truncated against axial planar tectonic discontinuities (Fig. 2.1.30a - c). The F_3 folds with which they are associated vary in size and shape along profile and die out in more competent units.

In a few examples individual shear zones not only replace the short limbs of tight synforms but also continue out of a specific hinge zone and cut across other F_3 folds. This and their deformation by F_4 folds constrains their temporal development.

An interpretation of the development of D_3 high strain zones is that a strong ductile shear component became predominant over the compressive stress responsible for F_3 fold formation, and that this resulted, initially, in marked attenuation and led to brittle failure.

Other evidence for brittle failure late in D_3 occurs in the same area where small NW-trending subvertical

wrench-faults not associated with any minor F_3 folds, and with displacements of < 1 m, are seen. Also, in the vicinity of Virtasalmi Village and at Kiviniemi small faults with a sinistral displacement of a few centimetres were observed to be axial planar to F_3 folds but offset the short limbs (Fig. 2.1.31).

There is no evidence of a general recrystallisation of the D_2 mineral assemblage during D_3; the axial planar S_3 fabric varies from a closely-spaced to weakly developed fracture cleavage (Figs. 2.1.32, 2.1.31 and 2.1.25). There is only localised new mineral growth in fractures where any retrogressive fluid appears to have been concentrated. The mineral paragenesis is retrogressive and the fluid could be related to igneous emplacement (see Section 2, Part 2).

A mineral lineation (L_3) is only very rarely expressed, mostly in gneisses and occasionally in amphibolites where there is oriented growth of biotite in S_3 (Fig. 2.1.7). In the biotite-rich amphibolites and gneisses S_3 is expressed as a crenulation cleavage (Fig. 2.1.33).

2.1.8 Fourth phase of deformation (D_4)

Locally F_3 folds, S_3 fabrics and earlier fabric elements are refolded by minor folds (F_4) which represent the fourth deformational phase (D_4) (Fig. 2.1.34). They have only been recognised unequivocally in a few isolated occurrences north of Virtasalmi Village and at Hällinmäki Mine. Amplitudes are less than 1 m, the folds are open to tight, and plunge at 40-70° WNW (290-305°), with upright axial planes (Fig. 2.1.35). F_4 hinge zones are mostly round, and an axial planar fabric (S_4)

is restricted in development to a weakly penetrative spaced fracture cleavage which in calc-silicate skarn lithologies, is occasionally vein filled (by epidote and quartz). In several outcrops a weak to moderately penetrative spaced fracture cleavage with an orientation consistent with that of S_4 is developed. Regionally its expression is generally weak.

2.1.9 Fifth phase of deformation (D_5)

F_4 folds are commonly cross-cut by either a strongly penetrative epidotised fracture cleavage, especially in calc-silicate lithologies, or by a closely-spaced weakly-developed fracture cleavage (Fig. 2.1.35), both of which are expressed regionally. Locally the fabric (S_5) is intensely penetrative and developed axial planar to steeply plunging folds (F_5) with tight to open interlimb angles (30-60°) and round hinge zones, which plunge at 60-80° to 340-360°. Rare unequivocal recognition of F_5 folds in the area precludes the direct observation of refolding relationships between F_5 and F_4 folds, and evidence of relative age relationships between the two phases of deformation is based on the cross-cutting relationship of S_5 to F_4.

F_5 folds are, however, in a couple of instances seen to refold F_3, S_3 and all other earlier fabric elements, particularly in the southern half of the area. However throughout the area F_3 and F_5 folds are virtually coaxial and the presence of distinct sets could only be demonstrated at Kurrikamaki and Kiviniemi and at Hällinmäki Mine. At Hällinmäki

Mine F_5 refolds of F_3 hinge zones take the form of Type 3 interference structures with marked curvature of F_3 axial planes by small-scale open F_5 folds associated with development of an S_5 penetrative fracture cleavage. 'Balloon-shaped' interference structures are similarly formed on refolding of F_3 by F_5 folds but differ in that they appear to have resulted from the combined effects of (1) the marked attenuation and shearing our of limbs of F_3 folds by late D_3 ductile shear zones, and (2) later refolding by F_5 folds (Fig. 2.1.36).

2.1.10 Sixth phase of deformation (D_6)

F_5 folds, S_5, and all previous structural elements are refolded by folds (F_6), with F_6 refolding of F_3 the most common relationship observed (Fig. 2.1.37). Most minor F_6 folds have amplitudes of less than 2 m, commonly less than 50 cm, and they plunge at 50-80° to 205-240° with sub-vertical axial planes. Hinge zones are either round or angular, often seemingly dependent on the competence contrasts between lithologies. Asymmetrical F_6 folds have attenuated limbs and commonly have shear offsets developed with a displacement of a few cm (Fig. 1.2.10). Pre-existing quartzofeldspathic bands or veins are sometimes remobilised into these shear zones.

An axial planar fabric (S_6) is commonly expressed as a weakly penetrative fracture cleavage (Fig. 2.1.36), which is often associated with limited epidotisation especially in the northern half of the area (Fig. 2.1.38).

Small wrench fault structures a few cm to 3 m wide and with displacement of < 2 m cause strong local re-orientation of pre-existing structures. These zones often contain a high proportion of neosome material, the local emplacement of which was probably structurally controlled (see Section 2, Part 3) (Fig. 2.1.39).

There are four sets of fracture cleavages, which in places are clearly axial planar to F_3, F_4, F_5 or F_6 folds, and are often associated with localised retrogression or epidotisation. These fractures are common in most exposures, with gradations between the fracture cleavages and mineral foliations or crenulation cleavages developed in response to lithology and/or local stress variations. However, when some of these upright fracture cleavages are examined in detail, there is occasionally found to be considerable spread in their trends of up to 40°, as well as splaying of fractures, notably where epidotisation accompanies them. Moreover, in well-exposed areas where there has been no refolding or variation in lithology to produce cleavage refraction, individual fractures may curve through 50° over distances of 1-10 m (Fig. 2.1.40). Thus there can occasionally be large variations in trend of these fractures which is indicative of local strain inhomogeneities, and suggests that caution must be exercised in case there is overlap in trend between sets.

2.1.11 Seventh phase of deformation (D_7)

A few small ENE-trending upright open folds (F_7) refold D_6 planar elements. These folds have amplitudes of less than 0.5 m, and do not form any major structures, serving merely to buckle F_6 axial planes. In the hinge zones of F_7 folds, there is a weakly-developed axial planar fracture cleavage with no associated metamorphic recrystallisation, other than some sericitisation of feldspars. In a few examples, pre-existing quartzofeldspathic veins are remobilised concordant to F_7 axial planes. Fold hinges plunge at greater then 75^{o} to 070-085^{o}, and axial planes are sub-vertical.

A late set of sub-horizontal epidotised fractures also occurs in the area north of Virtasalmi. These post-date S_6 fractures.

2.1.12 Late faults

The generally poor exposure does not permit recognition of many faults, but in the continuous sections of the Hällinmäki Mine, several sets of faults and late shear zones can be distinguished, many associated with pegmatite intrusion or the injection of veins with a variety of compositions.

Mapping the 3D exposures around the open pits, and in the underground tunnels, revealed a large number of closely-spaced reverse faults. Displacement varies from a few tens of cm to several m; it is most commonly around 3-4 m. Fault planes dip at c. 40^{o} to NE, and are commonly spaced at about 10 m apart. They are usually associated with the

injection of K-feldspar-rich pegmatites, which may contain chalcopyrite ore, e.g. at the southern end of the open pit, that is incorporated into the veins as they cross-cut mineralised horizons.

Low angle normal faults and crush zones without any significant displacement are also commonly observed. The crush zones are about 15 cm wide, and within these zones there are several planar discontinuities with intense sericitisation of feldspars. Those measured dip at roughly 20^{o} to 080^{o}. The low angle normal faults are commonly associated with vein injection (Section 2, Part 3), and where there has been displacement on the faults, sinusoidal fabrics may be present. More indications of a complex history of movements on these faults is present in the tunnel at 175 m level, where two different compositions of vein material, one cutting the other and containing more than one successively developed fabric are intruded up one of these faults. Cross-cutting relationships indicate a sequence of displacement - vein injection - displacement - vein injection - displacement, or possibly continuous movement with sporadic vein injection.

Those normal faults which could be measured were found to dip at c. 45^{o} to 306^{o}. There is also a component of strike-slip movement, e.g. one fault in the 175 m tunnel has a low-angle displacement of 1 m and a sinistral strike-slip displacement of 40 cm. The vein material intruded along these faults is cut by several sets of very weakly expressed fracture cleavages, but the fault planes themselves are not folded, and indeed cause displacement of F_3 axial planes at the northern end of the main open pit at Hällinmäki. The

fracture cleavages have orientations which are consistent with their having formed in the D_5, D_6 and D_7 stress systems, but there is no other structural evidence to place the timing of these faults any closer than being post-D_3 and probably pre-D_5.

In addition to the sub-vertical wrench faults identified as late D_3 and D_6 in age, there are at least three sets of later faults, two of which can only be seen at Hällinmäki Mine. The faults of one set dip steeply at about 80° to the west, and trend NNW; they also have pegmatite intrusions intruded wholly or partly along them. The pegmatites are variable in composition, being either composite pegmatites or K-feldspar-biotite-rich pegmatites. One of these displaces a crush zone at the southern end of the main open pit. In another example, bisecting the open pit, more than one phase of movement is indicated by pegmatite injection up a sub-vertical fault plane, which was followed by later shearing of large orthoclase phenocrysts.

There is a relatively small amount of displacement (less than 1 m) across sub-vertical NW-trending faults, which are associated with the intrusion of coarse-grained aplitic vein material, and which occur throughout the area. The faults displace F_3 axial surfaces, and although nowhere seen to be folded, the associated aplites are cut by several late fracture cleavage sets (S_5 and later), place their age post-D_3-pre-D_5.

A few of the late syn-D_3 gabbroic dykes seen in the 370 m tunnel have sub-vertical faulted contacts, apparently with a displacement of a few metres. There are also several

faults trending 270-290°, e.g. at the tunnel entrance, which offset pegmatites by an unknown amount of displacement that is certainly greater than 10 m.

Fig. 2.1.1 Schematic structural diagram showing major folds and some of the intrusions in the study area.

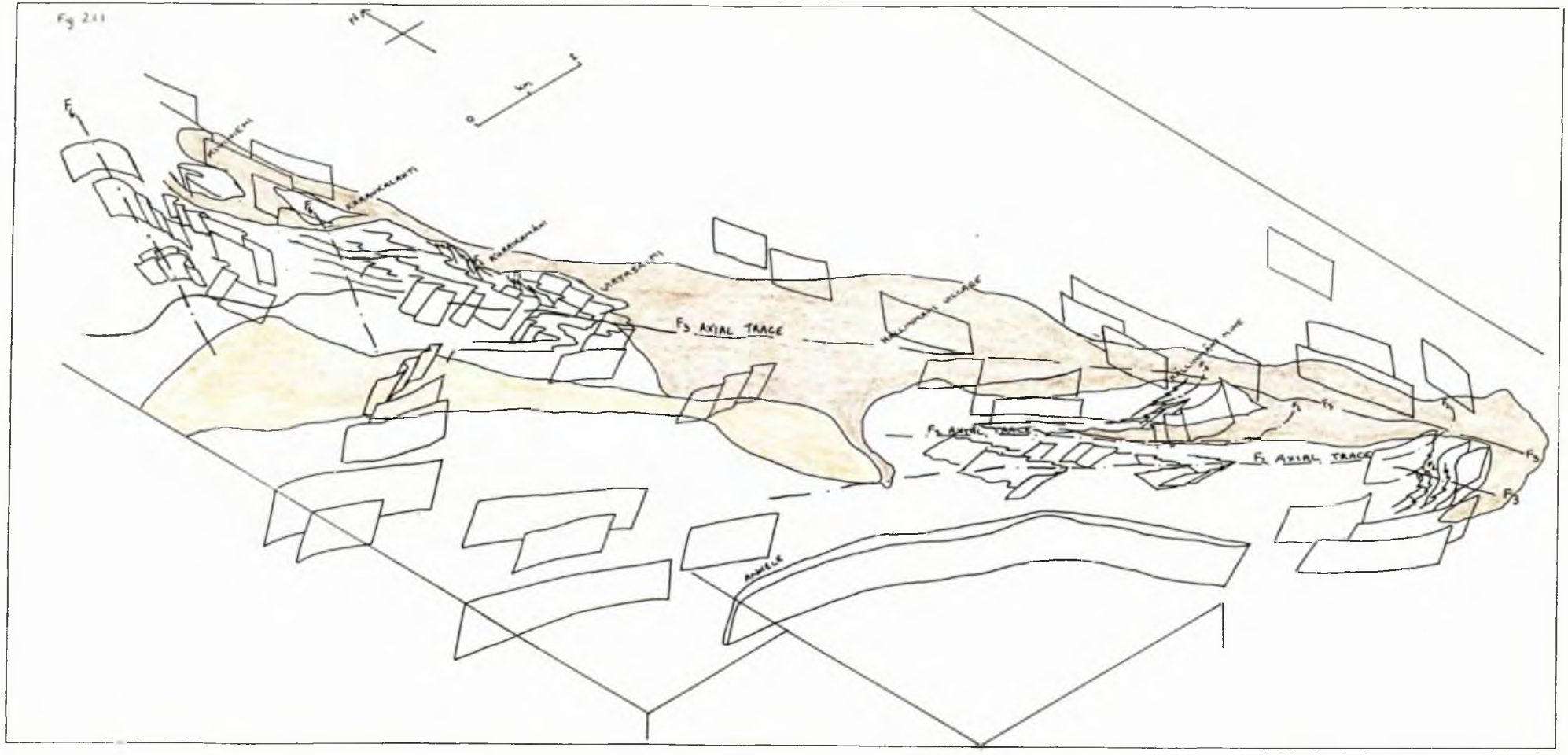
Fig 2.11
N
0
1km
2
F4
F3 AXIAL TRACE
F2 AXIAL TRACE
F2 AXIAL TRACE
F1
F2
F3
F3
F3
F3
ANGELE

Fig. 2.1.2 A schematic block diagram of the southern half of the study area is presented in Figure 2.1.2a. The distribution of the main intrusive masses is also indicated in an overlay.

The insert diagram (Fig. 2.1.2b) which is cut away along section line A-B in Figure 2.1.2a shows the geometry of F_2 folds in the vicinity of Hällinmäki Mine.

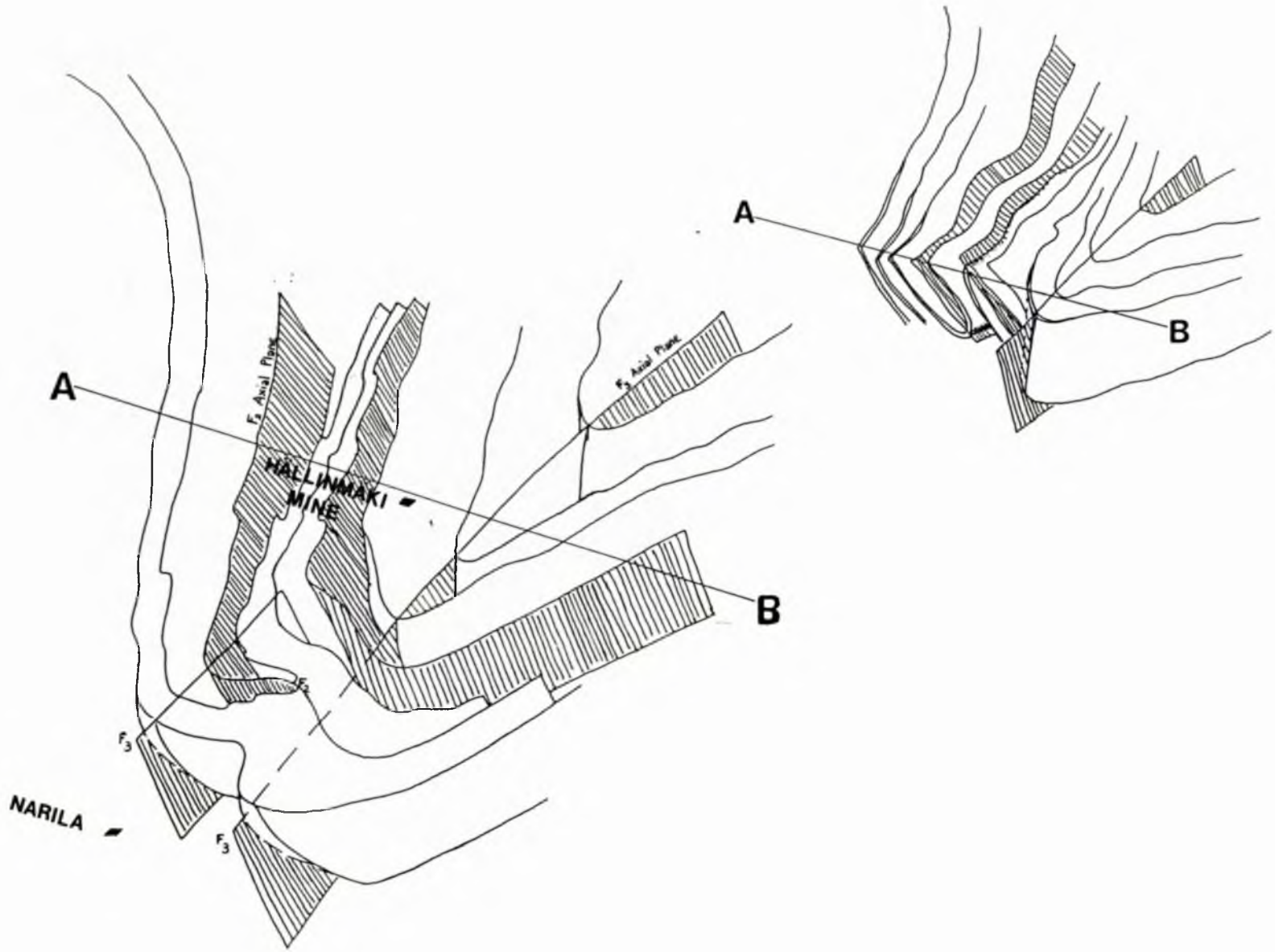
A
B
A
B
F_3 Axial Plane
F_3 Axial Plane
HALLIMAKI MINE
F_2
F_3
F_3
NARILA

Fig. 2.1.3 Sequence of interlayered Type VIII skarns and amphibolites, Kiviniemi. S_0 layering is folded by prominent tight-isoclinal F_2 folds to which a strongly penetrative S_2 foliation is axial planar. There are planar S_2 transposition surfaces (seen to bifurcate in places) in F_2 limb zones. These cause segmentation of S_0.

Insert diagram shows outline of F_1 fold modified by S_2 transposition at top right hand corner of diagram. The S_1 fabric is only preserved within skarn layers in F_2 hinge zones, where it is parallel to S_0.

Figure 2.1.3

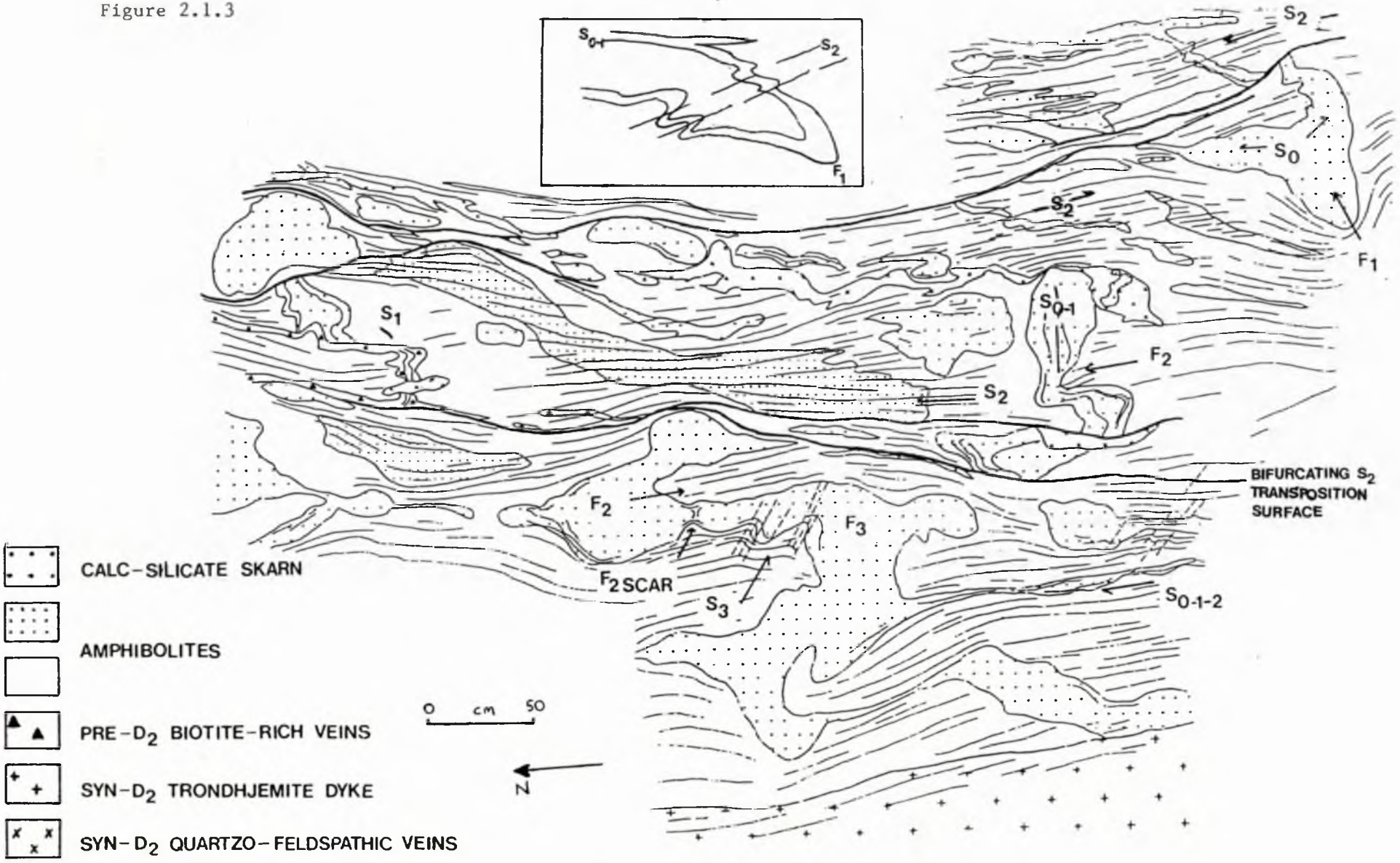
S_{0-1}
S_2
F_1
S_2
S_0
S_2
F_1
S_1
S_{0-1}
F_2
S_2
BIFURCATING S_2 TRANSPOSITION SURFACE
F_2
F_3
F_2 SCAR
S_3
S_{0-1-2}
CALC-SILICATE SKARN
AMPHIBOLITES
0 cm 50
PRE-D_2 BIOTITE-RICH VEINS
SYN-D_2 TRONDHJEMITE DYKE
N
SYN-D_2 QUARTZO-FELDSPATHIC VEINS

Fig. 2.1.4 Penetrative S_1 metamorphic differentiation banding generally sub-parallel to S_0 is seen here to be axial planar to an isoclinal F_1 fold. A less penetrative S_2 metamorphic differentiation banding and mineral foliation cross-cuts S_0-S_1 and F_1 at a low angle and is axial planar to small asymmetric F_2 folds which are also observed to refold F_1. Amphibolites, Narila.

Fig. 2.1.4

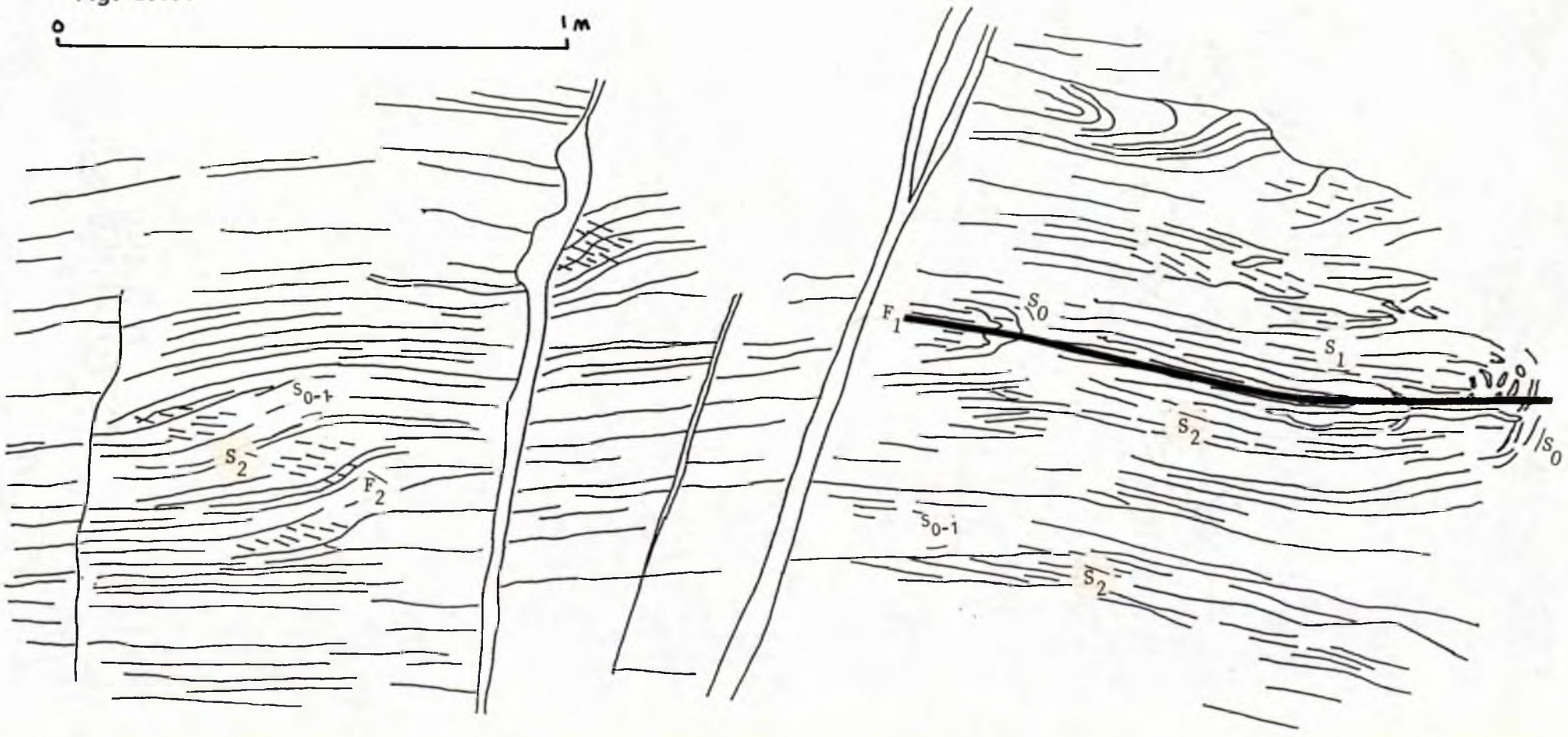

Fig. 2.1.5 Penetrative S_1 and S_2 metamorphic differentiation banding in amphibolites, Kiviniemi. In this instance S_2 is only intensely penetrative within discrete narrow zones and is sub-parallel to S_0. S_1 is discordant to S_0 (and S_2) suggesting the existence of F_1 folds larger than those observed at outcrop scale.

Fig. 2.1.6 Penetrative S_1 and S_2 fabrics developed in a xenolith-rich pre-early syn-D_1 intrusion at Kiviniemi. Thin melanocratic bands considered to represent xenoliths which have been flattened and attenuated sub-parallel to S_1 are observed to be realigned and further attenuated within a D_2 high strain zone marked by an intensely penetrative S_2 fabric. There is a grain size reduction within the D_2 zone. The more uniform banded appearance of the rock in this D_2 high strain zone is a function of the deformation and for geochemical studies in particular, great caution had to be exercised to avoid sampling from such tectonically homogenised lithologies. Figure 2.1.6(B) is an interpreted drawing of Figure 2.1.6(A).

Fig. 2.1.6B

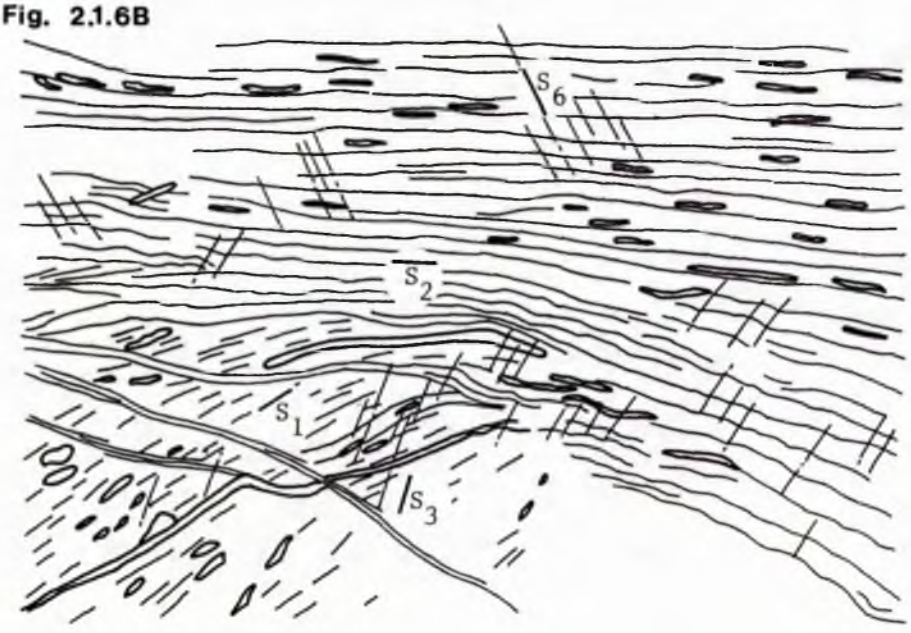

Fig. 2.1.7 Figure 2.1.7(A) shows a minor asymmetric tight F_2 fold in amphibolites near Narila. Figure 2.1.7(B) is a photomicrograph [MAG. X30, PPL] of the F_2 hinge zone outlined in (A). An S_1 fabric is observed to be sub-parallel to S_0, and an intensely penetrative S_2 fabric is clearly developed axial planar to the F_2 fold. A more weakly penetrative S_3 fabric is also discernible. Figure 2.1.7(C) is a close-up of the limb zone of the fold outlined above within the melanocratic biotite-rich layer. The angular discordance between S_1, S_2 and S_3 is clearly demonstrated. [MAG. × 200]


2.1.7
A
F_2


2.1.7
B
S_2
S_3
F_2
S_{0-1}
S_3


2.1.7
C
S_2
S_1
S_3
S_2
S_1

Fig. 2.1.8A Intensely penetrative S_2 fabric is seen to be axial planar to an F_2 fold in a pre-early-syn-D_1 intrusion at Hällinmäki Mine. S_2 foliation development is particularly intense within narrow zones where an S_2 banding is produced.

Fig. 2.1.8B A syn-D_1 trondhjemite dyke is observed to truncate an earlier syn-D_1 metagabbro at Kiviniemi. On the left hand side of the figure, within the dyke, an S_2 segregation banding is developed. On the right hand side of the figure the S_2 fabric is only developed as a weakly expressed mineral foliation.

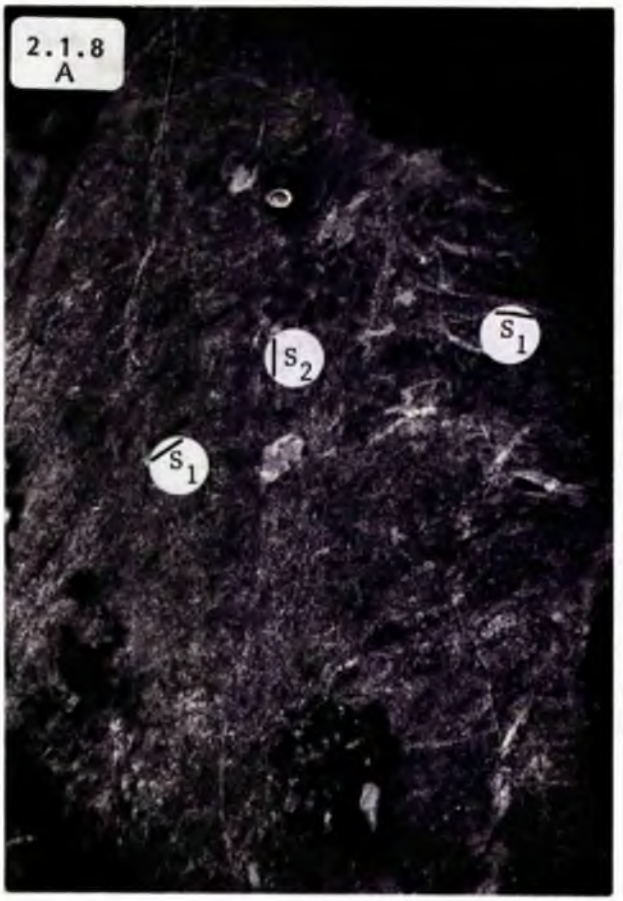
2.1.8
A
S2
S1
S1


2.1.8
B
S2

Fig. 2.1.9 Tight-isoclinal F_2 folds in amphibolites in the small open pit at Hällinmäki Mine. There is marked thinning of lithologies in F_2 fold limbs. F_2 hinge zones are mostly angular and occasionally irregular in shape. This is compounded by the presence of planar surfaces of transposition both in limb zones and in fold hinges.

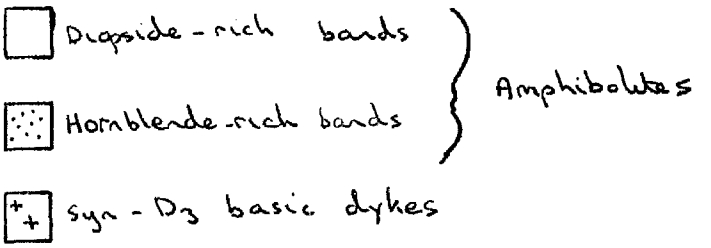

Fig. 2.1.9

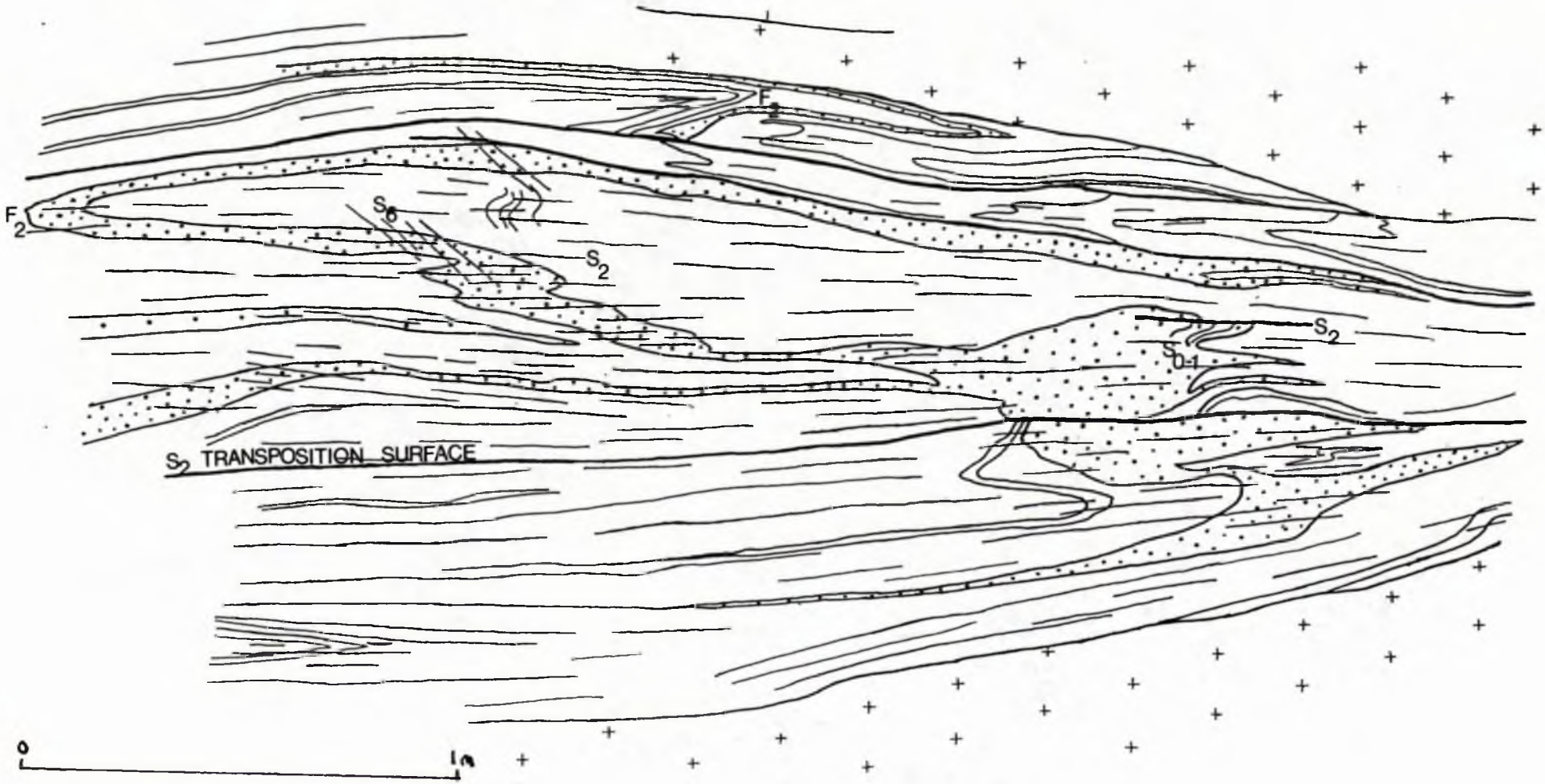

Fig. 2.1.10 Isoclinal F_2 fold with marked attenuation on limbs with D_2 high strain zones in interlayered basic-intermediate composition metavolcanic rocks near Narila.

Fig. 2.1.11 Tight-isoclinal F_2 folds in amphibolites, near Narila. There is little thinning on limb zones relative to hinges (Fig. 2.1.11A). Figure 2.1.11B is a close-up of (A) showing development of an axial planar S_2 fabric, and refolding of the F_2 fold by F_3.

Fig. 2.1.12 Tight-isoclinal F_2 folds in amphibolites, west of Hällinmäki Mine. There is no thinning on limb zones relative to hinges. An S_2 metamorphic differentiation banding is developed axial planar to F_2. (A close-up of this F_2 fold is given in Fig. 1.2.9).


2.1.10
F2
S0-1
S2


2.1.11
A
F2
F3
F2

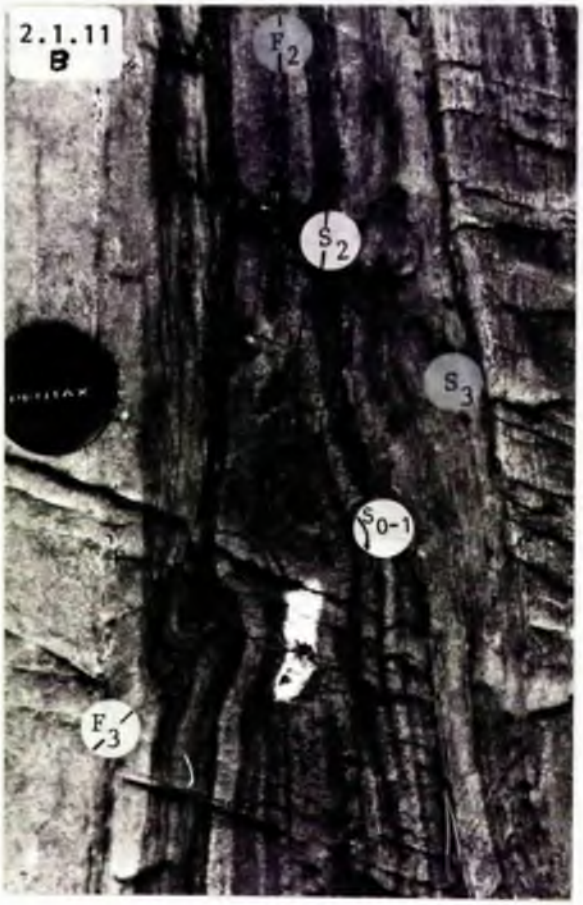
2.1.11
B
F2
S2
S3
S0-1
F3


2.1.12
F2
S2
S0-1
F2

Fig. 2.1.13 Step-like discontinuities marked by particularly intense S_2 foliation development are observed to be associated with sinistral displacement across them on the dextral limb of an F_2 fold within an early intrusion at Hällinmäki Mine. This figure is a close up of Figure 2.1.8(A).

Fig. 2.1.14 D_2 boudin-like structure within banded amphibolites at Hällinmäki Mine.

Fig. 2.1.15 Rectangular D_2 boudins partially reoriented in D_3 stress system and cut by S_3 (Fig. 2.1.15A). Quartz-rich segregations are commonly observed to occur in the low pressure zones of boudin necks both where there is almost complete segmentation of more competent layers (Fig. 2.1.15A) and where there is only minor scar fold development (Fig. 2.1.15B). Kiviniemi.


2.1.13
S_1
S_2
S_1
S_2


2.1.14
S_C
S_C


2.1.15
A
S_C
S_3

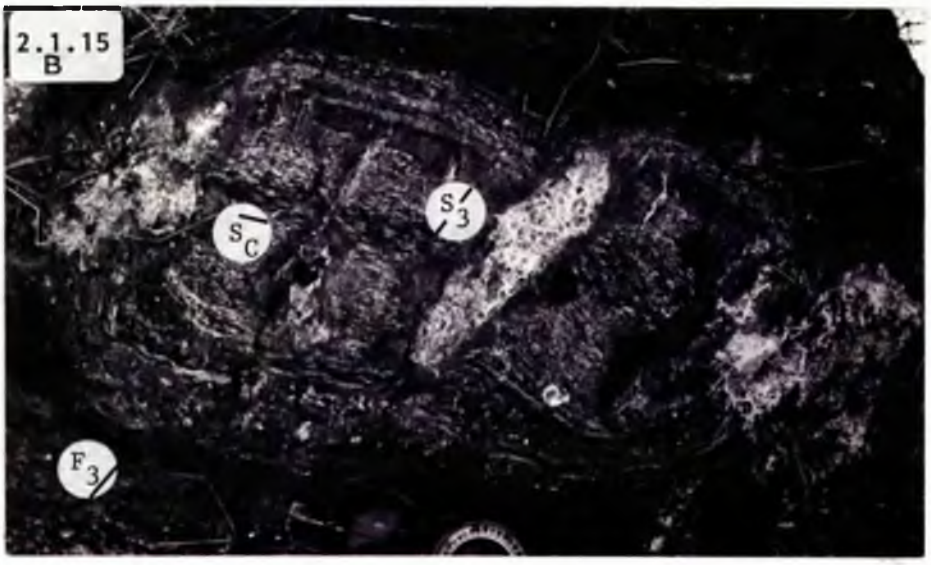
2.1.15
B
S_C
S_3
F_3

Fig. 2.1.16 Both rectangular and less regularly-shaped boudins within interlayered skarn and amphibolite, Narila. Scar folds formed by flowage of less competent material (amphibolite) between boudinaged skarn layers is a common occurrence.

Fig. 2.1.17 Discrete D_2 ovoid boudin comprising a calc-silicate lithology is observed within amphibolite west of Hällinmäki Mine.

Fig. 2.1.18 Discrete D_2 lensoid boudin comprising calc-silicate layers is deformed by minor F_3 folds, west of Hällinmäki Mine.


2.1.16
0 10cm


2.1.17


2.1.18

Fig. 2.1.19 Figure 2.1.19A shows an S_2 foliation developed axial planar to F_2 folds in interlayered calc-silicate and amphibolite bands, near Narila. In Figure 2.1.19B a steeply plunging rodding is observed to have formed by the intersection of S_0-S_1 with S_2. However, M_2 mineral growth (hornblende) is also found to plunge sub-parallel to the rodding.

Fig. 2.1.20 In Figure 2.1.20A the S_2 fabric is observed as a metamorphic differentiation banding in narrow zones axial planar to F_2 folds. The S_1 fabric, which also occurs as a metamorphic differentiation banding is observed only in the intervening low strain D_2 zones. Within amphibolites, Virtasalmi Village. In Figure 2.1.20B an interference pattern produced by the dissection of S_1 by S_2 is observed. Within amphibolites, south-west of Hällinmäki Mine.

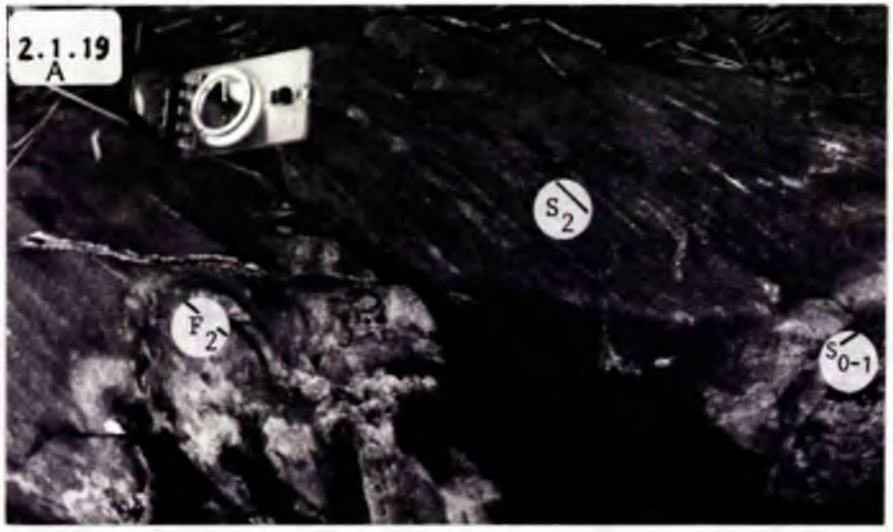
2.1.19
A
S_2
F_2
S_{0-1}


2.1.20
A
S_2
S_1
S_C


2.1.19
B
L_2


2.1.20
B
S_1
S_2
S_{0-1}

Fig. 2.1.21 S_2 is observed to cross-cut S_0-S_1 in the hinge zone of a minor F_2 fold in an early intrusion, Hällinmäki Mine (Fig. 2.1.21A). The S_2 fabric is penetrative, but only occurs as a relatively homogeneous mineral foliation.
In Figure 2.1.21B, an axial planar S_2 foliation is similarly developed as a penetrative mineral foliation rather than as a banding.


2.1.21
A
F_2
S_{0-1}
S_2


2.1.21
B
F_2
S_{0-1}
S_2
S_3

Fig. 2.1.22 Figures 2.1.22A-C are taken in a traverse (over a distance of 5 m across) within an inhomogeneous pre-early-syn-D_1 intrusion at Hällinmäki Mine. In Figures 2.1.22A and B coarse-grained melanocratic xenoliths are observed to be irregularly shaped, and patchily distributed, as are vein networks of cross-cutting aplitic veins. Over the distance of 2 m however, the xenoliths and veins become streaked out sub-parallel to an intensely penetrative S_2 fabric. The resultant rock resembles a fairly homogeneous banded amphibolite.


2.1.22
A


2.1.22
B


2.1.22
C

Fig. 2.1.23 Three sub-parallel discrete ductile shear zones, marked by development of an intensely penetrative fabric and an accompanying grain size reduction, are observed to be spaced at intervals of about 2 m in interlayered pre-kinematic gabbros and amphibolites at Kiviniemi (Fig. 2.1.23A). There is no apparent rotation of the pre-existing S_1 fabric into these shear zones, which have sharply discontinuous boundaries (Fig. 2.1.23B). These shear zones are here observed to be deformed by minor asymmetric F_3 folds.

Fig. 2.1.24 Bifurcation of the shear zones described in Figure 2.1.23 has led in places to increased retrogression (including epidotisation) of lithologies in the intervening blocks.


2.1.23
A

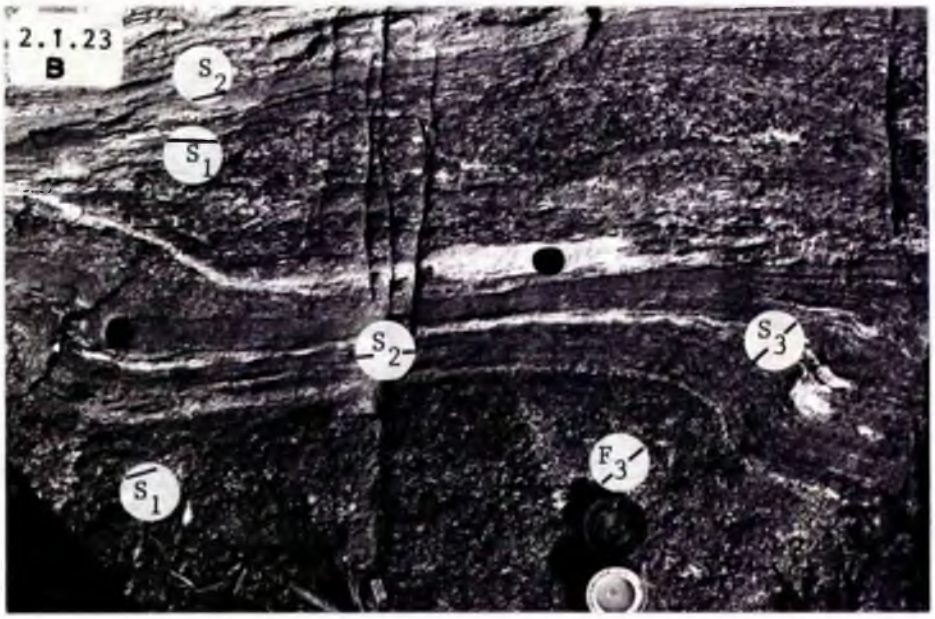
2.1.23
B
S2
S1
S2
S3
S1
F3


2.1.24

Fig. 2.1.25 Type II 'mushroom' interference structure formed by refolding of F_2 folds by F_3. This particular structure is dissected by late D_3 vein neosome material.

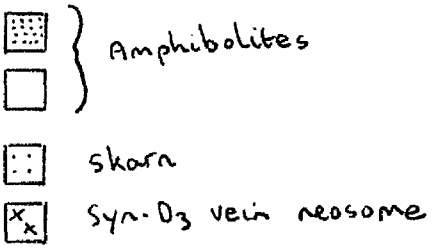

Fig. 2.1.25

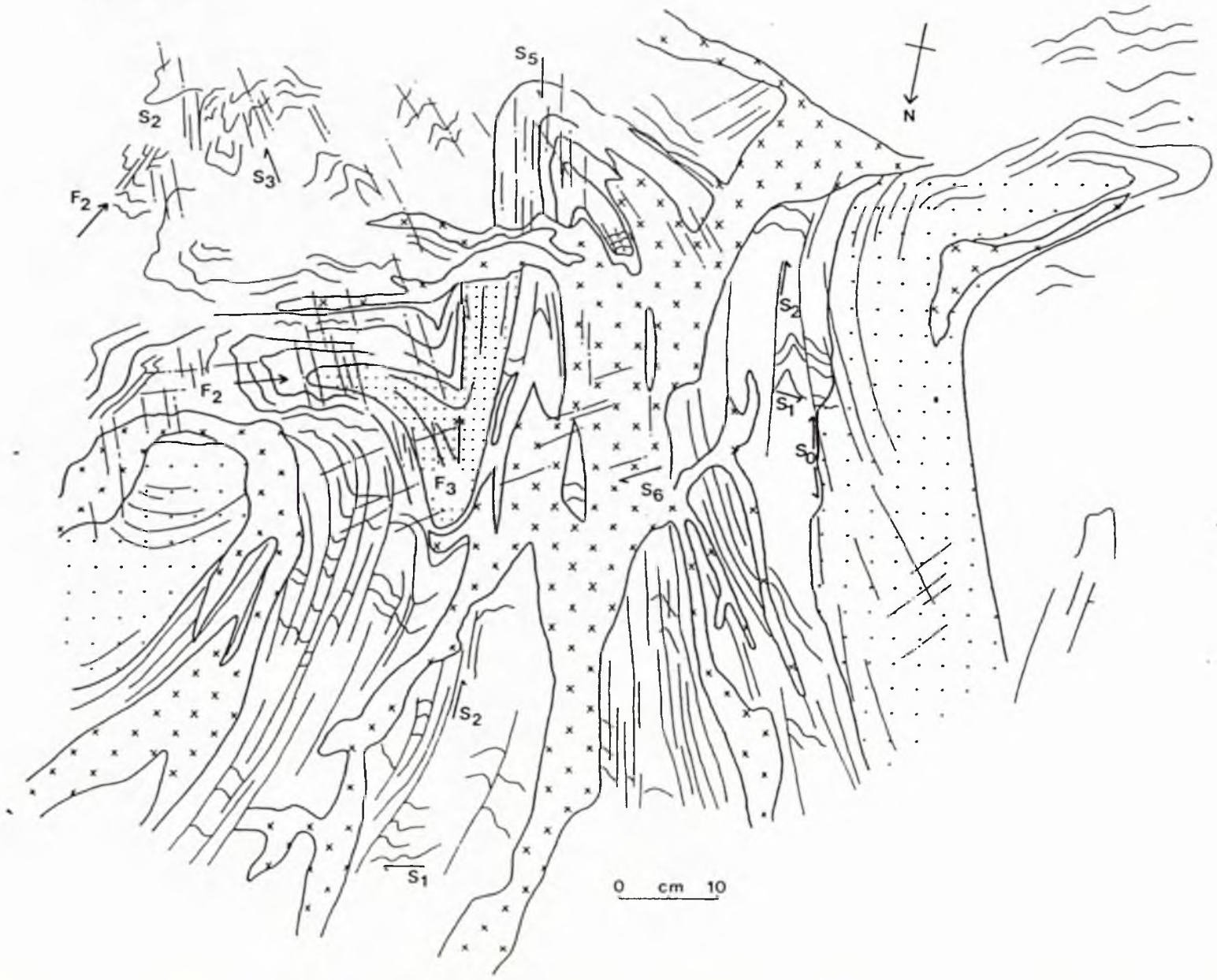

Fig. 2.1.26 Minor asymmetric-al F_3 folds refold S_0-S_2. The F_3 folds are tight and the hinge zones are angular. An axial planar mineral foliation or fracture cleavage is sometimes developed. There is only slight thinning in F_3 limb zones in this figure. Hällinmäki Mine.

Fig. 2.1.27 Minor asymmetric-al F_3 structure refolds S_0-S_2. The hinge zone is angular and the fold tight. There is some thinning in the limb zones, particularly on the short limb. Hällinmäki Mine.

Fig. 2.1.28 Minor asymmetric-al F_3 fold but with an axial planar brittle discontinuity seen to cause offset in the hinge zone. Hällinmäki Mine.

Fig. 2.1.29 F_3 disharmonic folds developed within thinly interlayered amphibolites and skarns in the hinge zone of a larger asymmetric F_3 fold, Hällinmäki Mine.


2.1.26
F3
SC


2.1.27
SC
F3


2.1.28
F3
SC

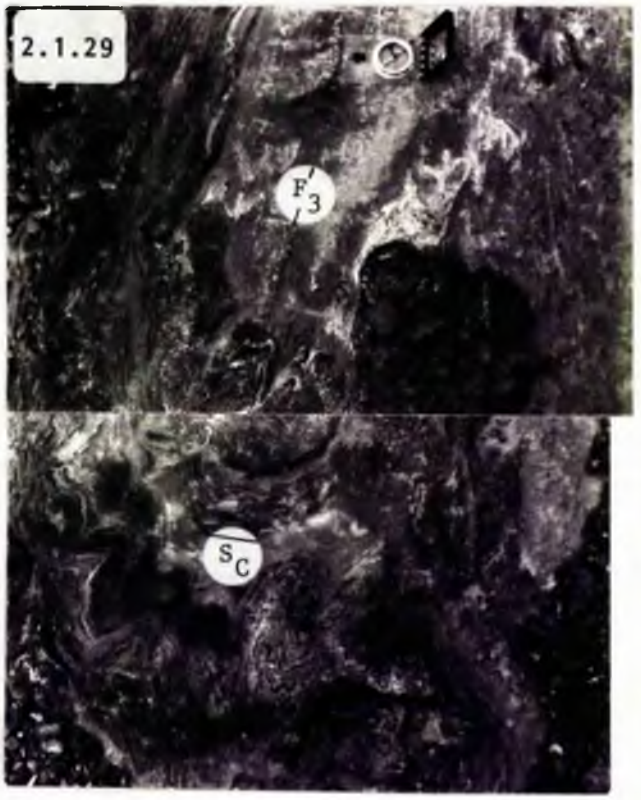
2.1.29
F3
SC

Fig. 2.1.30 Surfaces of discontinuity are observed to have developed in the attenuated limbs of some tight asymmetric F_3 folds in amphibolites at Hällinmäki Mine. These discontinuities tend to occur in the hinge zones of small tight synforms (Fig. 2.1.30A). A penetrative S_3 fracture cleavage is more intensely developed towards these brittle features. Figure 2.1.30B is an interpreted drawing of Figure 2.1.30A. Where these D_3 high strain zones are intensely developed, S_0-S_2 surfaces are observed to be truncated at a high angle to the surface of discontinuity (Fig. 2.1.30C).

Fig. 2.1.31 A small aplite-vein-filled fault with a sinistral displacement is observed to truncate the short limb of a minor asymmetric F_3 fold in amphibolites near Virtasalmi Village. The fault is however concordant with the F_3 axial plane.

Fig. 2.1.30B

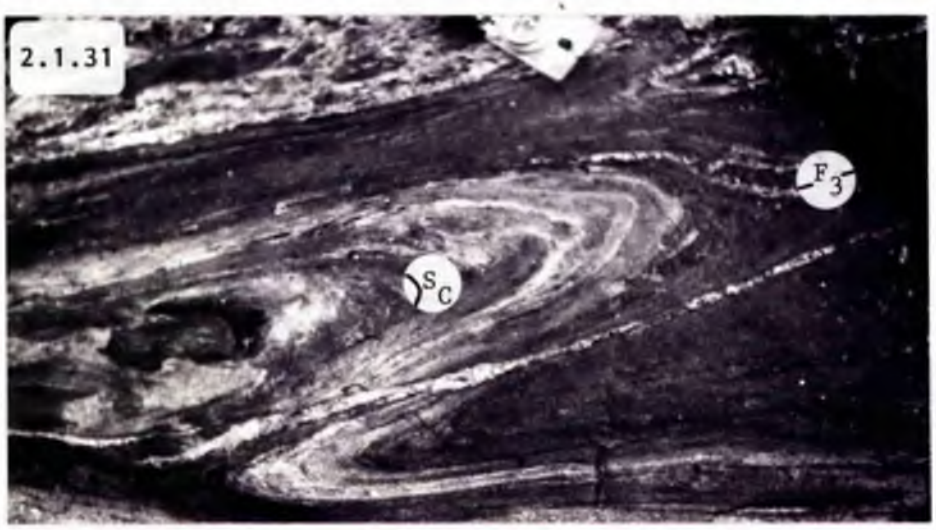

Fig. 2.1.32 S_3 fabric developed axial planar to minor asymmetrical F_3 fold, in amphibolites at Hällinmäki Mine. In this hinge zone the fabric is observed to vary from a weakly developed M_3 mineral foliation (biotite) to a strongly penetrative fracture cleavage.

Fig. 2.1.33 S_3 expressed as a crenulation cleavage in early syn-kinematic intrusion, Hällinmäki Mine.

Fig. 2.1.34 Minor asymmetrical F_4 fold, within the hinge zone of a larger F_4 fold is seen here to have refolded a pre-existing asymmetrical F_3 fold. The axial plane of the latter is observed to have been refolded by the effect of more open F_4 warping. Virtasalmi Village.

Fig. 2.1.35 Minor asymmetrical F_4 fold with small aplitic vein injected in its short limb, sub-parallel to the F_4 fold axis. Virtasalmi Village.


2.1.32
S_3
S_C
F_3


2.1.33
S_C
S_3


2.1.34
F_4
S_4
S_C
F_3


2.1.35
S_C
S_4
F_4

Fig. 2.1.36 'Balloon'-shaped interference structures within amphibolites, Hällinmäki Mine. These structures have formed as a result of the combined effects of marked attenuation and shearing out of F_3 limbs by late D_3 ductile shear zones (in one place a discontinuity is observed to transect an individual F_3 fold), combined with refolding of F_3 folds by almost coaxial F_5 folds. The structural pattern is further complicated by the refolding of F_2 folds by F_3 to produce Type III interference structures in the same outcrop.

Fig. 2.1.36

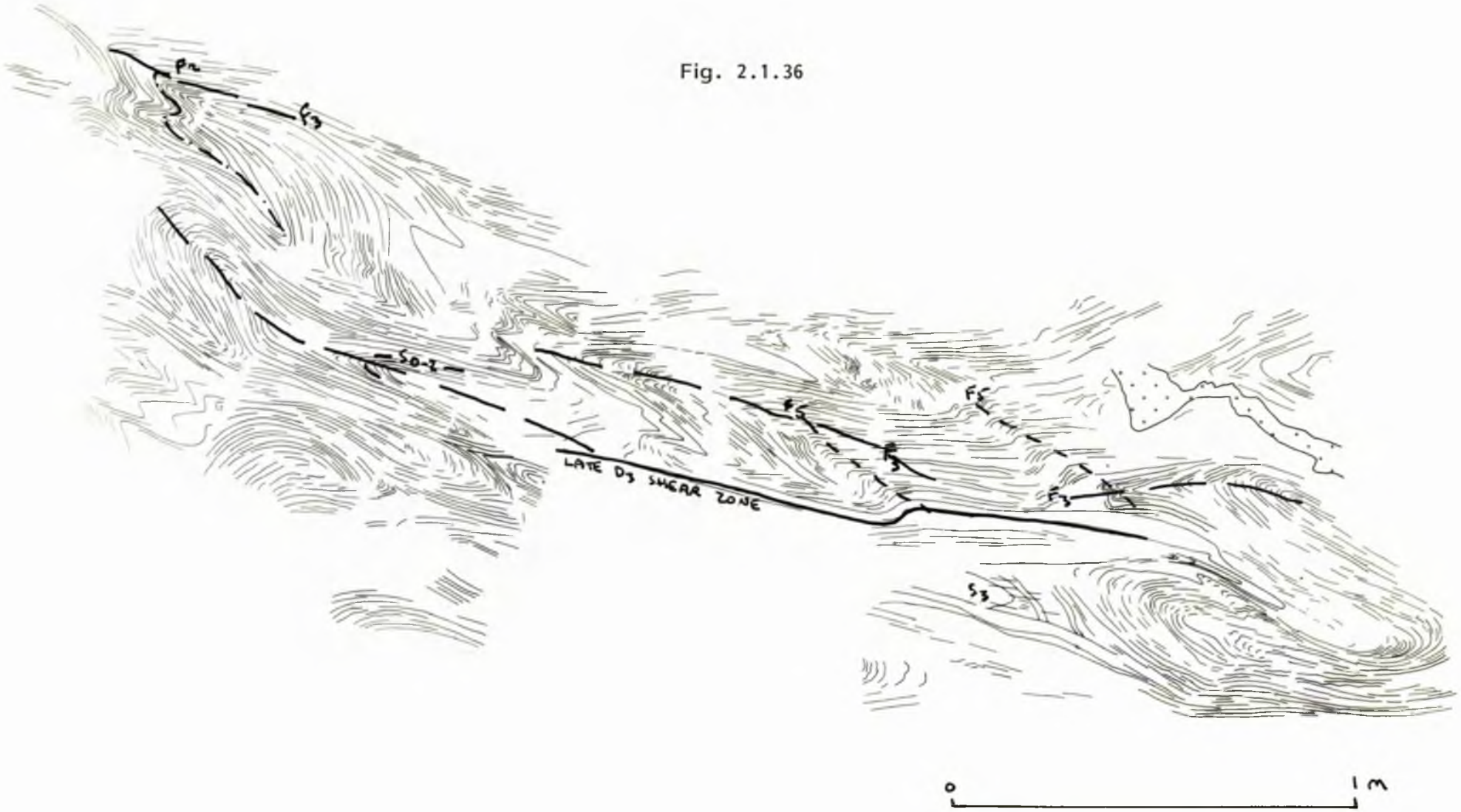

Fig. 2.1.37 Type III interference structure formed by the refolding of tight asymmetric F_3 folds by open-tight F_6 folds (Fig. 2.1.37A). Figure 2.1.37B is a drawing of this outcrop, but is of a different photograph which was taken from a very slightly different angle.
Axial planar S_6 spaced fracture cleavage is observed to transect the pre-existing structures. Insert diagram drawn from the top left hand side of the figure shows refolding of small isoclinal F_2 fold by asymmetric F_3 which is in turn cross-cut by S_6. In amphibolites, Kurrikamaki.

Fig. 2.1.38 F_3 fold cross-cut by S_6 fracture cleavage. Weakly expressed within amphibolite, the S_6 fabric is often vein-filled on cross-cutting skarn lithologies. In this instance it has an epidote + quartz infilling and appears to be strongly penetrative on transecting the skarned lithology.

Fig. 2.1.37B

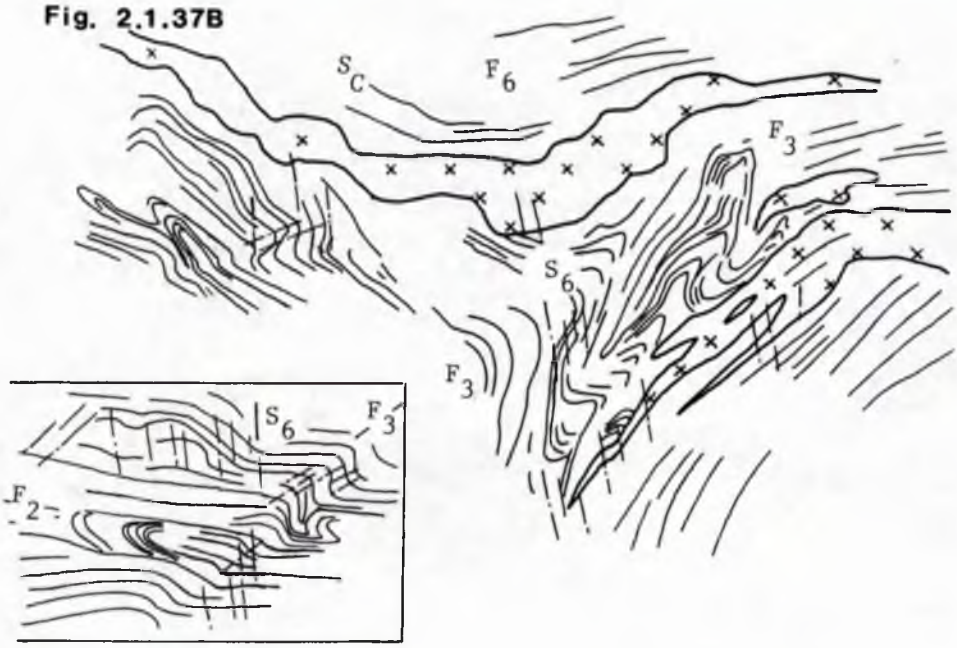

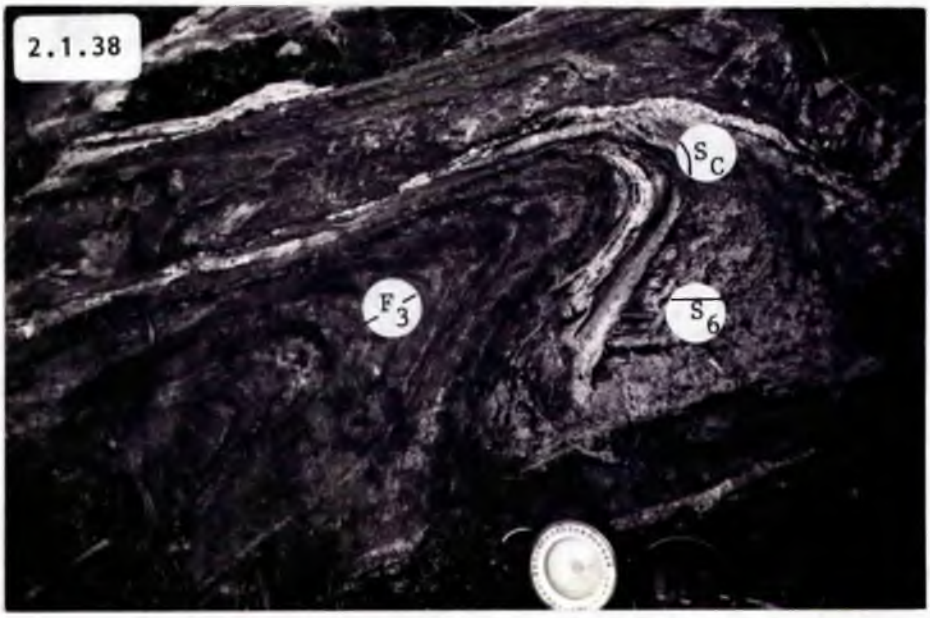

Fig. 2.1.39 Strong reorientation of pre-existing features within small D_6 wrench fault structures in amphibolites, Virtasalmi Village. The margins of the zones are marked by the presence of leucocratic veins sub-parallel to the structure which trends NE-SW. Figure 2.1.39B is an interpreted drawing of 2.1.39A.

Fig. 2.1.40 Epidote + quartz-filled fracture cleavages within amphibolites, Keskikangas. Individual fracture cleavages are observed to curve through 50° in an area of approximately 1 m^2.

Fig. 2.1.39B

SECTION 2

PART 2

Relationship of igneous intrusions to the structural sequence

2.2.1 Introduction

Igneous intrusions are an important member of the lithological assemblage in the Virtasalmi District. Although their distribution is irregular (Fig. 2.1.1 and Map 1), they constitute up to 60% of lithologies in the area. Examination of cross-cutting relationships between intrusions themselves and between intrusions and fold and fabric elements has enabled their timing of emplacement relative to the structural sequence to be established.

Resolution of the relative timing of emplacement of each intrusion was essential in investigating the proposed genetic link (Hyvärinen, 1969) between 'quartz-diorites' and the copper deposit at Hällinmäki Mine, and also provided a framework for understanding the geochemical evolution of the intrusions themselves (Section 4). It was also necessary to map out intrusions in order to ascertain any effects or influence they may have had on pre-existing structures or on the structural development of the area.

The lack of any evidence for thermal aureoles at contacts indicates that the intrusions were emplaced into rocks already undergoing high-grade metamorphism (Watson, 1964). However, the presence of a strongly penetrative S_2 fabric in particular, associated with retrogressive mineral reactions,

commonly causes obliteration of M_1-S_1 fabrics, so that any pre-existing hornfels textures might not be expected to survive. Many intrusions emplaced prior or syn-D_2 have high strain S_2 zones located at the margins and in adjacent country rocks. Even in D_2 lower strain zones, due to the high grade of metamorphism attained during D_1-M_1 (upper amphibolite-granulite facies transition zone) combined with development of a penetrative S_1 fabric any pre-existing contact metamorphic minerals might not be expected to be preserved (even as pseudomorphs). Hence for most intrusions containing an S_1 fabric, and showing no relationship to F_1 folds, it was not possible clearly to establish whether they were intruded syn-D_1 or prior to deformation. In a few instances however, geochemical evidence suggests that certain amphibolitic meta-gabbros and meta-peridotites are cogenetic with the 'host' amphibolites, and these may have been intruded prior to deformation.

The detailed criteria employed to ascertain relative ages of emplacement follow those used in similar studies (e.g. Halden, 1982).

2.2.2(i) Pre-D_1 or early syn-D_1 intrusions

In the area west of Virtasalmi Village there are intimately associated hornblende gabbros and hornblende peridotites. These coarse-grained intrusions are affected by S_1, S_2 and later fabrics, with S_2 only penetrative near the margins of the intrusions. The intrusions are not very well exposed, but drill core and geophysical measurements suggest that one intrusion is 150m thick and can be traced for over 1.5 km (Hyvärinen, 1969; see Map 1).

Gradations from almost pure hornblendite to feldspathic hornblende peridotite occur over several metres. Although the mineralogy is metamorphic it reflects pre-existing compositional variations and layering in these intrusions. In the hornblendites, over 80% of the rock is composed of hornblende, with 15% plagioclase (An_{58}) and 5% ilmenite, which is partially retrogressed to sphene.

Further to the north and on the eastern shores of Langelmaenjärvi, coarse-grained hornblende peridotite and hornblende gabbros showing similar age relationships are intruded in the form of narrow dykes or sills, and larger irregular bodies. The intrusions vary from 1 m to 200 m wide and up to 300 m long, and are locally discordant to S_0 (Fig. 2.1.23). They consist of varying proportions of hornblende, plagioclase, chalcopyrite and ilmenite.

The geochemistry of all these intrusions (see Section 3, Part 1) indicates that they are cogenetic with the host amphibolites and were therefore probably intruded prior to deformation.

In the area around Kiviniemi and to the west of Lake Tiikala, several inhomogeneous hornblende meta-gabbro intrusions, between 50 m and 300 m wide and up to 500 m long, were intruded into the amphibolites. The intrusions cut across S_0 but strongly developed S_1 and S_2 fabrics are penetrative through them, indicating pre-tectonic or early syn-D_1 emplacement.

The inhomogeneity in these intrusions is due to the presence of abundant, predominantly amphibolitic xenoliths of variable petrography which show evidence of assimilation, and which constitute between 30% and 50% of the total volume

of the intrusions. However, near the centres of the largest bodies, xenoliths are smaller and not so numerous, possibly due to greater assimilation.

Most xenoliths are aligned within the S_1 foliation planes (Fig. 2.1.6), frequently at a high angle to the margins. An S_2 fabric is penetrative only in a marginal envelope or in other discrete high strain zones within the intrusions, causing flattening and marked attenuation or streaking out of the xenoliths in association with grain size reduction forming an apparently more homogeneous rock in these zones (Fig. 2.1.6).

A similar meta-gabbroic intrusion occurs near the entrance to Hällinmäki Mine, but with xenoliths solely of hornblende amphibolite. These xenoliths frequently have ill-defined margins, appearing as coarse-grained pegmatoid patches where partially absorbed (Fig. 2.1.22a). The contacts of this intrusion cross-cut S_0 and the presence of the S_1 fabric suggests a pre-tectonic or early syn-D_1 emplacement. The size of the intrusion is unclear due to poor exposure, but it is less than 100 m across. The inhomogeneities within all these intrusions made sampling to derive their initial geochemistry impossible. It is not therefore possible to determine whether these intrusions were emplaced prior to or early syn-D_1.

Adjacent to, but tectonically separated from the aforementioned intrusion at Hällinmäki Mine is another meta-gabbro with a distinct layering developed. The textures and mineralogy of this intrusion are tectono-metamorphic with individual layers now consisting mainly of different proportions of hornblende and plagioclase. The layering is

commonly 1 cm to 3 cm thick, but with almost monomineralic layers of hornblende up to 6 cm thick.

Two penetrative foliations, S_1 and S_2, are present with the S_1 foliation parallel to the prominent layering (Fig. 2.2.1). Metamorphic segregation may have enhanced pre-existing layers but the latter are apparently deformed around a small F_1 fold which suggests they are probably some form of igneous layering. As with the above example, this intrusion is also poorly exposed. However, in an F_2 hinge zone it was seen to be at least 30 m thick, but to have later faulted contacts. This intrusion was also emplaced either prior to or early syn-D_1.

In the immediate vicinity of the ore zone at Hällinmäki Mine, the intrusion interpreted as emplaced earliest in the sequence is a metagabbro which cuts S_0, but has a relict M_1 mineral assemblage and is folded by F_2 folds with a strong axial planar S_2 fabric developed. The intrusion cuts across ore-bearing horizons at a high angle (Map 5), and contains xenolithic blocks and screens of mineralised amphibolites near its margins. The intrusion is not cogenetic with the amphibolites and this together with the field evidence presented above on balance suggests that it was intruded syn-tectonically during D_1 rather that pre-tectonically.

2.2.2(ii) Syn-D_1 trondhjemite dykes

A suite of trondhjemite dykes present throughout the area is seen to cross-cut both S_0 (at high angles), and metagabbroic intrusions interpreted as having been emplaced prior to D_1 or pre peak D_1-M_1 conditions (Fig. 2.2.2a-c). However, these dykes are affected by an S_1 fabric which is mostly

preserved in F_2 hinge zones, and which varies in intensity from a mineral lineation to a strongly developed banding (Fig. 2.2.2b). Leucocratic bands 1-5 cm thick, interpreted as the result of metamorphic segregation sometimes form sub-parallel to S_1 (Fig. 2.2.2a).

The dykes range in width from 30 cm up to 5 m but can only be traced for distances up to 30 m because of poor exposure. No relationship with F_1 folds was observed but they are commonly refolded by F_2 and later sets of folds.

This evidence suggests that these dykes were emplaced prior to peak D_1-M_1 conditions.

2.2.3 Syn-D_2 intrusions

2.2.3(i) Gabbros

Many hornblende gabbro intrusions, present throughout the area, are observed to cross-cut S_0 and S_1 and are mostly emplaced in the limb zones of F_2 folds. They often contain a strongly penetrative S_2 mineral foliation at their margins, may contain xenoliths with discordant S_1 foliations (Fig. 2.2.3), but were nowhere observed to cross-cut F_2 folds, and are refolded by F_3 structures. Green hornblende which defines the S_2 foliation is commonly altered to blue-green hornblende or chlorite at its margins. This evidence suggests emplacement of these hornblende gabbros syn-D_2. The largest of the intrusions, as observed at Narila, Hällinmäki, Sahinjoki and at several locations around and to the north of Virtasalmi Village are up to 500 m long and between 50 and 200 m across (Map 1). Smaller dykes, 4-10 m across, are also numerous, especially in the vicinity of Hällinmäki Mine.

2.2.3(ii) Diorites

Diorite and quartz diorite intrusions cross-cutting S_0 and S_1 but containing only a weak S_2 foliation occur as dykes and larger intrusions, but are not as abundant as gabbros. They are deformed by F_3 folds and are considered to be emplaced late during D_2. Coarser pegmatoid patches are commonly injected into the centre of the dykes. Diorite intrusions are most common between Virtsalmi Village and Hällinmäki Mine. Rare granodiorites show similar age relationships and are present mainly near Hällinmäki Village.

2.2.3(iii) Porphyritic granodiorite

In the north-west of the area, on the western side of Langelmaenjärvi, a large intrusion of porphyritic granodiorite roughly 2 km across at its widest, narrowing to the south-west, is exposed. This intrusion is characterised by the presence of abundant orthoclase phenocrysts, varying from 1 cm to 5 cm in diameter, which define a strong foliation and increase towards the centre. Individual phenocrysts are frequently sheared and rounded where deformation was most intense. Folds with an orientation consistent with F_3 and with wavelengths of between 5 m and 10 m fold the foliation and have a weakly developed axial planar S_3 cleavage. The dominant foliation is considered to be S_2 because no fabric was observed between development of the foliation and S_3-S_6 fabrics, while S_2 is the dominant fabric in adjacent country rocks. These factors suggest that the intrusion was emplaced early during D_2.

2.2.3(iv) Syn-D_2 trondhjemites

In the vicinity of Virtasalmi Village, there are two types of intimately associated leucocratic dykes with trondhjemitic compositions, which either form separate intrusions or show a multiple injection relationship. The dykes are between 50 cm and 2 m wide and are seen to cross-cut S_0 and S_1. However, they contain an S_2 foliation although they are not folded by F_2 folds (Fig. 2.2.4), but are folded by F_3 folds, indicating emplacement post major D_2 shortening but prior to that during D_3. Where the dykes are associated with F_2 folds they are often intruded into their limb zones as subvertical sheets trending sub-parallel to F_2 fold axes, suggesting at least a localised control on their emplacement.

2.2.3(v) Syn-D_2 multiple dykes

A few dykes in the southern half of the area were found to consist of two compositionally distinct halves, one of basaltic composition, the other being either granodioritic or occasionally a more feldspathic basalt, with a small granodiorite dyke in the centre. The dykes cut S_0-S_1 but contain a weak S_2 foliation and are folded by F_3 structures. The basic dykes are medium-grained hornblende amphibolites, while the granodiorite is a quartz-plagioclase-hornblende rock. They show no chilling against one another, and a weakly developed compositional banding in the amphibolites is developed parallel to the margins of the dyke, and is not a continuation of metamorphic segregation in the enclosing amphibolites. Similar dykes showing the same relationships cross-cut the S_1 foliation

in pre-tectonic inhomogeneous gabbros at Kiviniemi (Fig. 2.2.5). This evidence suggests that they were emplaced syn-D_2.

2.2.4(i) Syn-D_3 intrusions

Hornblende gabbros similar to those emplaced during D_2 were observed to cross-cut these earlier intrusions and both F_2 folds and boudins (Fig. 2.2.6). They are observed to be intruded sub-parallel to and within limb and hinge zones of F_3 folds, although they may contain an L_3 mineral lineation and are cross-cut by a penetrative axial planar S_3 fracture cleavage. Where narrow tongues of magma are observed to split off from the larger intrusion, a penetrative igneous foliation is occasionally seen to develop, becoming more intense as the dyke narrows further. These intrusions, as well as diorites and granodiorites showing similar age relationships are considered to be emplaced during D_3. They are particularly common within the southern half of the study area, in the hinge zone of the major F_3 structure, and this, together with their generally NW-SE elongation, suggests that locally this structure may have controlled their emplacement. Within this zone, however, many of the intrusions have a less regular shape, and determination of their size is made very difficult by the large number of cross-cutting relationships observed.

Little variation in attitude of F_3 structures was recorded adjacent to any of these intrusions although screens of country rock are common within them.

North of Virtasalmi Village, on the eastern shore of Langelmaenjärvi, there are a couple of elongate

intrusions which range in size from 10 m to 200 m across, and are continuous for several hundred metres. They have sharply defined contacts and cross-cut S_0-S_1 and S_2, and are emplaced in the limb zones of F_3 folds parallel to their axial planes (Fig. 2.2.7). They contain a weak S_3 fracture cleavage and are deformed by F_4 folds, all of which indicates emplacement late syn-D_3. The bulk of these intrusions comprises feldspathic hornblende gabbro or diorite with only very rare xenoliths. Towards their central portions cross-cutting relationships indicate that a network of successively injected dykes-veins and more irregular patches of biotite granodiorites, then quartz-plagioclase pegmatoids and finally K-feldspar-rich pegmatites were emplaced.

2.2.4(ii) Granites

Intrusions with a granitic composition occur rarely in the area, either as small dyke-like intrusions, 1-3 m wide as at Hällinmäki Mine, or as larger, more irregular intrusions at least 30 m across, as seen west of Hällinmäki Village. Where contacts were observed, the intrusions were often seen to cross-cut previously emplaced gabbros and diorites and the S_0, S_1 and S_2 fabrics. They are cut by S_3 and later fabrics, suggesting emplacement syn-D_3. They have a mineralogy of quartz, plagioclase, biotite and varying amounts orthoclase, with a myrmekitic texture sometimes developed. In two examples a strong foliation was developed within the intrusions parallel to their margins. These intrusions truncated S_0-S_2 at high angles, while S_3 and later

fabrics were clearly distinguished within the intrusion, suggesting that the foliation was wholly the result of viscous magmatic flow.

A larger coarse-grained intrusion, with similar mineralogy was observed near Kiiskilanmaki. This intrusion is at least 200 m long and 100 m across, although no contacts were observed. It is unfoliated, and is cut by several sets of fracture cleavages and joints. However, no associated minor fold structures were observed. The orientation and intensity of the fractures was found to be variable, and the presence of the numerous joint sets made determination of relative emplacement age impossible.

2.2.4(iii) Syn-D_3 multiple dykes

Multiple dykes (Fig. 2.2.8a) forming a suite of intrusions found in the Hällinmäki area are observed to cross-cut S_0-S_1-S_2 (Fig. 2.2.8b) and F_3 folds (Fig. 2.2.8c), but are mostly intruded in the limb zones of F_3 folds. Locally they are associated with small-scale NW-trending wrench faults (D_{3late}). The dykes become thinner in these fault zones, but are not tectonically thinned and have no penetrative fabric imposed on them. A penetrative fracture cleavage, interpreted as S_3, and later fabrics cross-cut the dykes. These factors suggest emplacement of the dykes late syn-tectonic during D_3, late on in the development of F_3 folds but prior to fabric formation.

The dykes comprise a fine-grained amphibolite, or hornblende diorite, and a feldspathic hornblende gabbro

which occur in variable proportions, from 50:50 (amphibolite:gabbro) to 80:20 (amphibolite:gabbro). Neither lithology shows evidence for chilling against the other, but there are sharp mineralogical contacts developed between them. However, the gabbro is always found within the amphibolite, with the former never coming into contact with the country rocks, whether the dykes are in the form of thin irregular veins of roughly 2 cm wide (Fig. 2.2.8d), or larger dykes up to 2 m across (Fig. 2.2.8a).

Amphibolitic dykes and larger feldspathic gabbroic intrusions, with similar chemical compositions to those in the multiple intrusions (Section 4), which show similar relative ages of emplacement, also occur as independent intrusions throughout the Virtasalmi District.

2.2.5 Post-D_3-pre-D_6 intrusions

Several diorite intrusions which cut across S_0-S_1-S_2-S_3 and F_3 folds but are affected by S_5 and/or S_6, and rarely by F_6 folds, occur throughout the Virtasalmi District. Due to poor exposure it is difficult to estimate the size of many of these intrusions. However, the largest demonstrable of these (at Lari) would appear to have dimensions up to 1 km x 500m, while others may be only 10% of this size. The intrusion at Lari is a coarse-grained quartz-diorite observed to cut across F_3 folds but cut by S_5 and S_6 and later neosome interpreted as injected syn-D_6 (Fig. 2.3.4). This, and similar intrusions are not foliated, and have hypidiomorphic textures comprising hornblende, plagioclase and quartz. The margins of the intrusions are irregular, with finger-like tongues and larger dyke-like

offshoots seen to brecciate host amphibolites and 'skarns'. Up to 20 m from the margins of the main intrusion, pre-existing structures become increasingly irregular in orientation, with respect to adjacent areas, and axial surfaces become increasingly contorted. Towards the contacts, increasingly numerous dyke offshoots, typically xenolith-rich, produce screens of host-rock, with blocks eventually being detached, rotated and incorporated into the intrusion with signs of assimilation. Hence, the intrusion at Lari and others showing similar relationships are interpreted to have been emplaced post-D_3, and mainly pre-D_6 or D_5, with limited local reorientation of pre-existing structures and evidence that stoping was an important emplacement mechanism.

2.2.6 Syn-D_6 intrusions

Quartz diorite dykes up to several metres across which cross-cut all folds and fabrics prior to D_6 are observed to be intruded concordant with F_6 axial planes. No cross-cutting relationships were observed with F_6 folds and the only fabric seen to affect the dykes is a weak S_6 fracture cleavage. Also thin quartz diorite dykes were observed to be locally intruded into small wrench faults interpreted to have been emplaced late during D_6.

Similarly, intrusions of trondhjemitic composition form a suite of NE-trending dykes a few of which are locally observed to be axial planar to and within the hinge zones of larger F_6 folds (Fig. 2.2.9). These dykes are seen to cross-cut S_5 and all earlier fabrics but unlike the quartz diorite intrusions mentioned above, they are commonly cut by a penetrative S_6 fracture cleavage. This evidence suggests emplacement syn-D_6.

2.2.7 Basic dykes

Several distinctive suites of basic dykes between 5 cm and 1 m thick are considered to have been emplaced syn-tectonically at various stages in the structural development of the area. In the areas around Kurrikamaki and Narila dykes comprising hornblende-plagioclase cut S_0 and S_1 but contain an S_2 foliation and are emplaced axial planar to F_2 folds (Fig. 2.2.10). They are considered to have been emplaced syn-D_2 and their attitude suggests some structural control on their emplacement.

Mineralogically similar dykes in the Hallinmaki area cross-cut F_2, S_2 and earlier structures, but are intruded into the limb zones of F_3 folds and contain a weak S_3 fabric (Fig. 2.2.11). These are interpreted to have been emplaced syn-D_3, and are similar in composition to the finer grained portions of multiple dykes considered to have formed at the same time.

Biotite amphibolite dykes form a suite in the Hällinmäki area. They cut S_0-S_1 and anastomose F_2 fold hinges to which they are generally intruded axial planar. They contain a strong S_2 foliation and are deformed by F_3 folds. They are interpreted to have formed syn-D_2.

Another set of biotite amphibolite dykes was observed in the southern half of the area. These dykes truncate F_3 folds and S_0-S_3, generally at a high angle and contain a weak foliation interpreted as the result of magmatic flow. S_5 and later fabrics were observed to cross-cut the dykes, which are generally oriented NE-SW. This evidence suggest emplacement post-D_3 and pre- or syn-D_5.

2.2.8 Summary

The evidence that has been presented, primarily based on cross-cutting relationships, demonstrates that igneous intrusions were emplaced both prior to and throughout the progressive deformation of the area. The largest and most abundant syn-tectonic intrusions are feldspathic hornblende gabbros and diorites which show evidence of emplacement commencing early syn-D_1, and with magmas of broadly similar composition continuing to be emplaced syn-D_6.

Many of the intrusions, on all scales, show some evidence of their local emplacement at least being partially controlled by fold structures: many elongate intrusions and dykes are intruded axial planar to contemporaneous fold sets, being controlled by the position of limb and hinge zones. This probably reflects injection of magma under the influence of both regional and more localised stress systems. This is illustrated by the apparent concentration of syn-D_3 intrusions within the hinge zone of the major F_3 structure, and on a smaller scale it is reflected in the orientation of dyke swarms, particularly during the later phases of deformation.

The syn-tectonic intrusions commonly cross-cut earlier fold structures, making it particularly difficult to map F_1 and F_2 major structures. Their emplacement into rocks undergoing ductile deformation might have been expected to have produced localised stress inhomogeneities. However, during D_1 and in particular D_2, the distribution of high and low strain zones is observed to be independent of the emplacement of contemporaneous intrusions. Also, structural mapping has

revealed that while the emplacement of syn-tectonic intrusions may cause local reorientation of pre-existing structures near their margins, and obviously in screens, no systematic change in orientation/attitude of contemporaneous structures towards the largest intrusions was observed.

Fig. 2.2.1

Pre-D_1 or early syn-D_1 metagabbro, Hållinmäki Mine. Two strongly penetrative fabrics, S_1 and S_2, are developed. S_1 is largely subparallel to a compositional layering in the intrusion, marked by some virtually monomineralic hornblende-rich layers up to 6 cm thick. This layering is observed to be folded around a small F_1 fold, demonstrating the pre-kinematic origin of the layering. Both the S_0-S_1 fabric and the F_1 fold are seen to be refolded in the hinge of an F_2 structure, and transected by a penetrative S_2 foliation.

Fig. 2.2.2 Syn-D_1 trondhjemite dyke, Kiviniemi. This dyke is between 2-4 m wide and cross-cuts S_0 in amphibolites in addition to transecting pre-early syn-D_1 intrusions (Fig. 2.2.2 a). The dyke is affected by two prominent fabrics, S_1 and S_2. In Fig. 2.2.2 B the S_2 fabric is observed to transect the margins of the dyke at an angle of c. 20°. The fabric varies in intensity from a mineral lineation to a banding. Within the dyke a number of coarser-grained leucocratic bands 1-5 cm thick and subparallel to the dyke margins are developed. In Fig. 2.2.2 C these can be seen to be folded by minor F_2 structures to which S_2 is axial planar. In the hinge zones of the F_2 folds it is also possible to observe an S_1 foliation to which the coarser leucocratic bands are subparallel.

Fig. 2.2.3 Syn-D_2 gabbro, Sikalanniemi. This intrusion contains many irregularly shaped xenoliths of adjacent country rocks including calc-silicate skarns and melanocratic amphibolite. The latter are observed to contain a penetrative S_1 fabric which is not present in the adjacent intrusion. A more weakly expressed but penetrative S_2 fabric is developed consistently throughout the intrusion and the xenoliths. This evidence is consistent with emplacement syn-D_2. In this figure an irregular leucocratic grano-diorite dyke is seen to cross-cut the syn-D_2 gabbro. This is not foliated and elsewhere at this exposure is seen to be intruded axial planar to F_3 folds.


2.2.2
A
F_2
F_2


2.2.2
B
S_{0-1}
S_2


2.2.2
C
F_2
S_1
S_2


2.2.3
S_{0-1}
S_2

Fig. 2.2.4 Syn-D_2 multiple trondhjemite dykes, Virtasalmi Village. Chemically similar but petrographically distinct (one type contains poikilitic pyroxene) trondhjemite dykes cross-cut S_0-S_1 but contain a weak S_2 foliation. They are not folded by F_2 folds, being intruded concordant with F_2 axial planes), but are seen to be deformed by F_3 folds. This suggests their emplacement syn-D_2.

Fig. 2.2.5 Syn-D_2 multiple dyk, Kiviniemi. This multiple dyke is seen to cross-cut an earlier inhomogeneous gabbro intrusion. The S_1 foliation in the pre-existing intrusion is also truncated by the dyke which is only weakly foliated by an S_2 fabric. This evidence suggests a syn-D_2 emplacement age for the dyke. The dyke consists of two compositionally distinct parts, i.e. basalt and grandiorite. Although no chilled margins are developed, the more acidic dyke offshoots apparently cross-cut the more basic parts of the dyke.

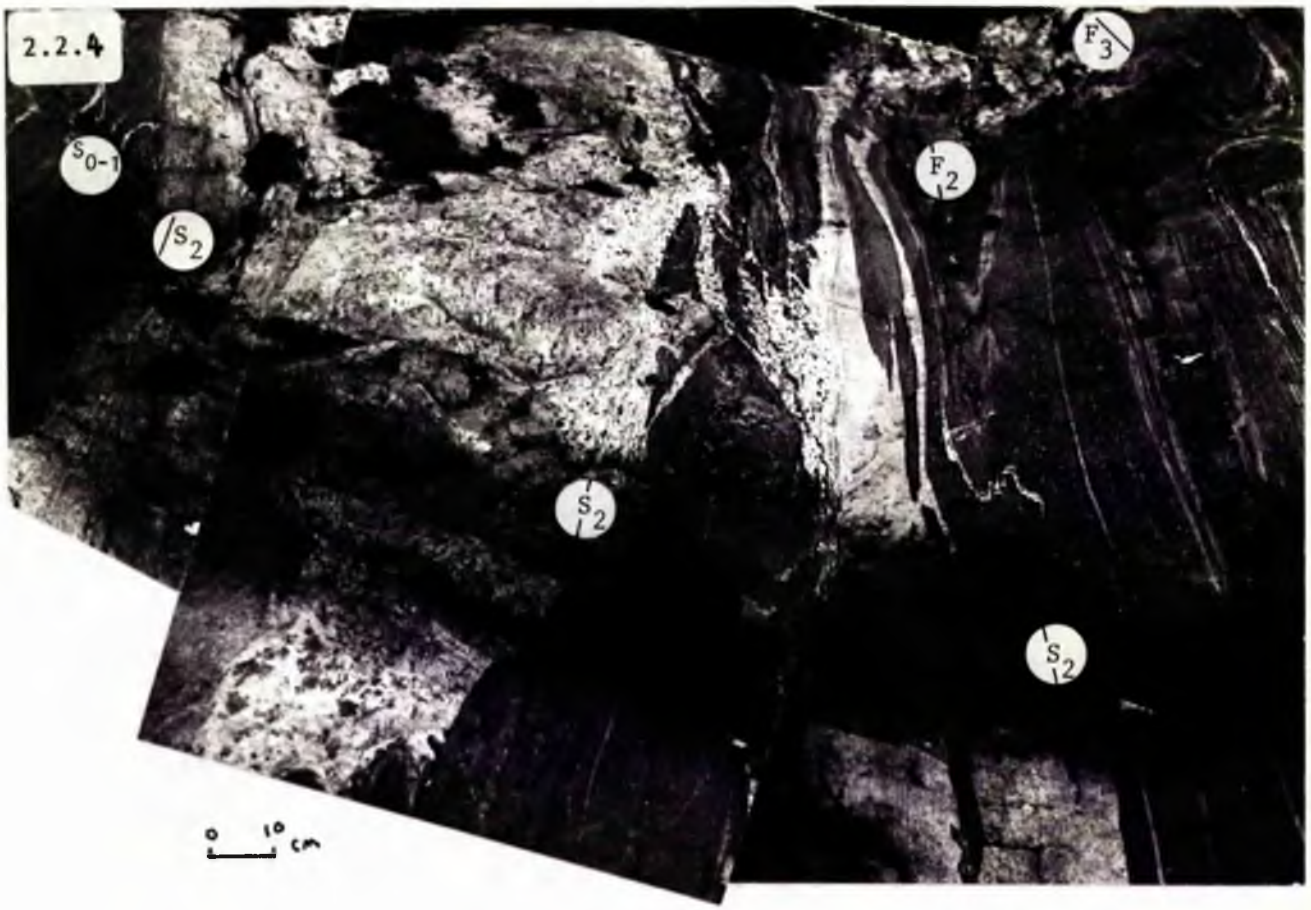
2.2.4
S_{0-1}
S_2
S_2
F_2
F_3
S_2
0 10 cm


2.2.5
S_1
S_2

Fig. 2.2.6 A dyke-like offshoot of a larger coarse-grained hornblende gabbro intrusion is observed to cross-cut S_0-S_1-S_2 in adjacent amphibolites and calc-silicate skarn lithologies. It also truncates D_2 boudins and is cross-cut by S_3, suggesting injection syn-D_3. In this figure however, the intrusion also contains a weak foliation, but only in these narrow dyke offshoots and not where the intrusion becomes wider. This foliation is possibly the result of a component of igneous flow lamination. Elsewhere at this locality (see Map 4) this intrusion cross-cuts S_0-S_1 at high angles, is not foliated and other dyke offshoots are intruded concordant with F_3 axial planes. Hällinmäki Mine.

2.2.6
S_{C_1}
S_3
S_{C_1}

Fig. 2.2.7 Map showing the distribution of a large dyke-like intrusion at Keskigangas. It predominantly comprises feldspathic hornblende gabbro, but towards the centre of this intrusion there are progressively more acidic and coarser-grained dyke and vein networks injected. This intrusion cross-cuts S_0-S_1-S_2, contains a weak S_3 fabric and is folded by a larger F_4 structure, indicating emplacement syn-D_3.

KEY:

Amphibolite

Early-syn-D_1 foliated metagabbro

Syn-D_3 metadiorite

Syn-D_3 biotite granodiorite

Syn-D_3 coarse-grained granite and granitic vein neosome

Syn-D_4 composite pegmatite

Late K-feldspar pegmatites

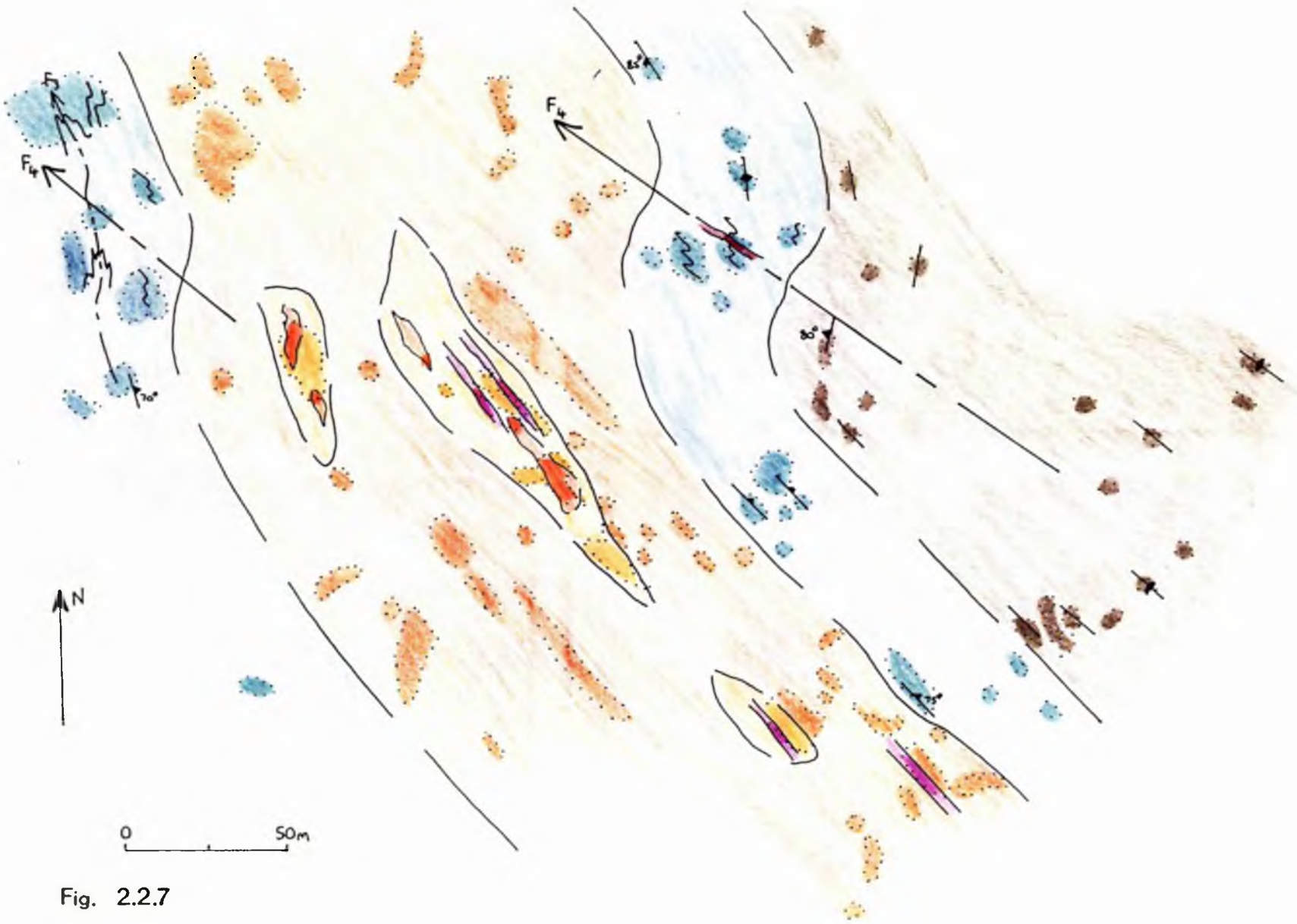

Fig. 2.2.7

Fig. 2.2.8 Syn-D_3 multiple dykes, Hällinmäki Mine. These intrusions comprise finer-grained basalt (amphibolite) and a more leucocratic gabbro part (Fig. 2.2.8 A). They occur as complex (Fig. 2.2.8 A) or simple (Fig. 2.2.8 B) dyke-like forms. From the latter figure it is evident that there are no chilled margins developed. The dykes are emplaced concordant with F_3 axial planes, mostly in the limb zones. They are not deformed by F_3 structures and are seen to truncate S_0-S_1-S_2 particularly in F_3 hinge zones. This points to a syn-D_3 emplacement age. In places there are ptygmatic vein-like offshoots from the larger dykes. In all these intrusions, whether veins or dykes, the coarser-grained gabbro is contained within the finer-grained lithology.

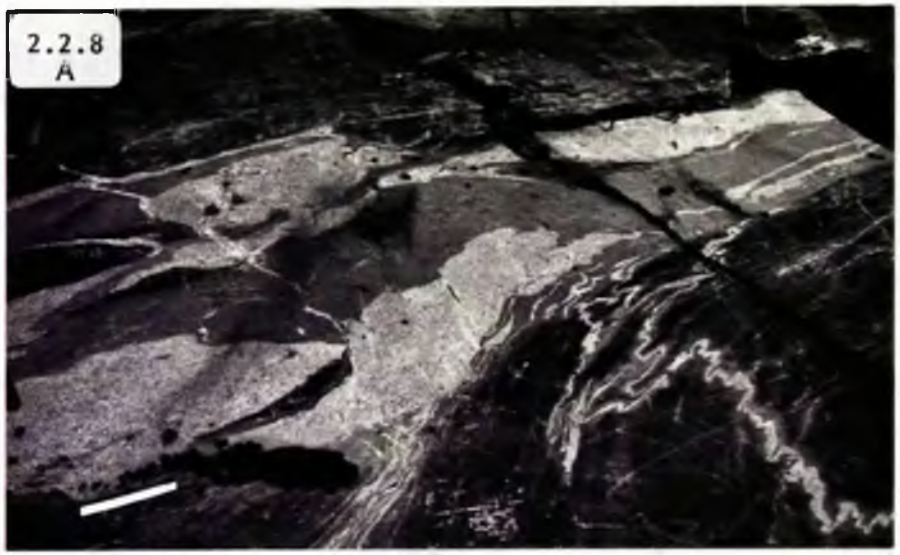
2.2.8
A

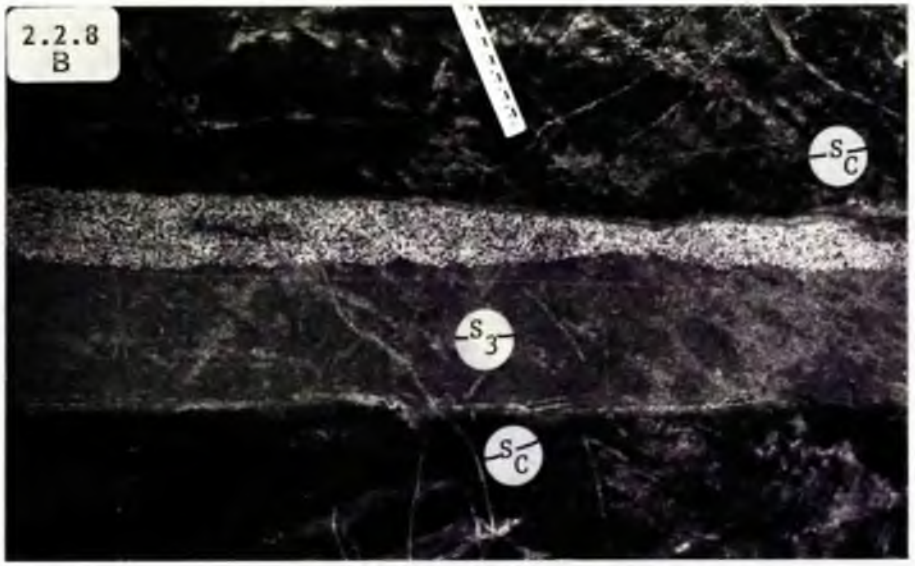
2.2.8
B
S_C
S_3
S_C

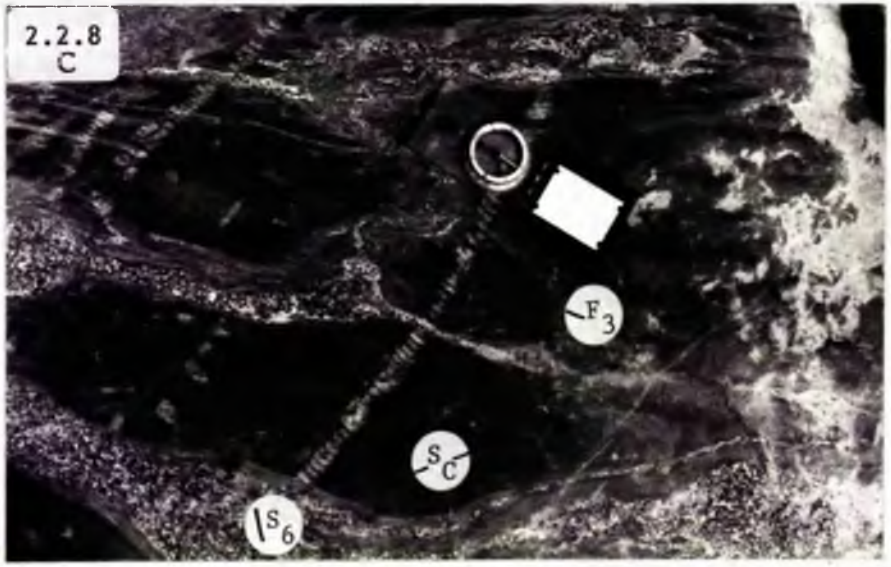
2.2.8
C
F_3
S_C
S_6

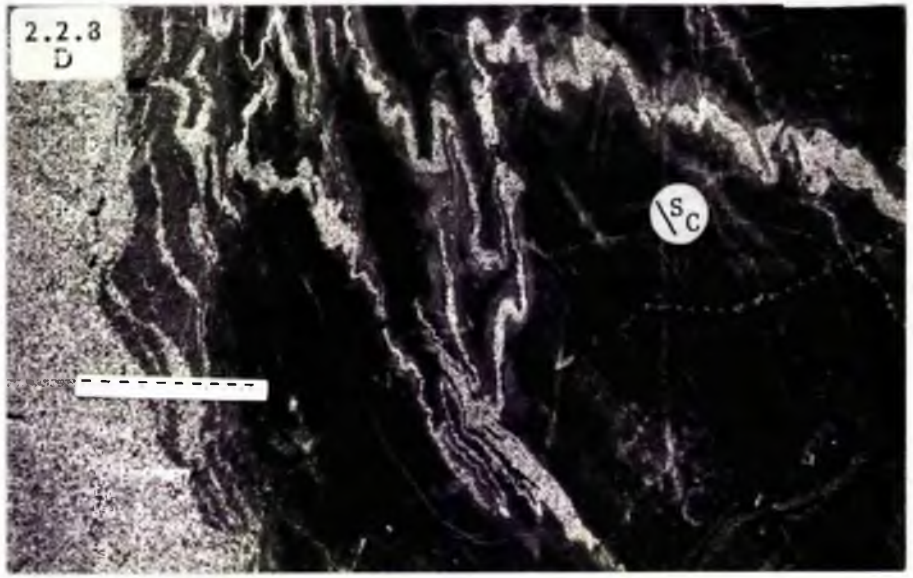
2.2.8
D
S_C

Fig. 2.2.9 Syn-D_6 trondhjemite dyke, Kurrikamaki. Dyke-like intrusions emplaced concordant with the axial plane and in the hinge zone of an F_6 fold. Cross-cuts S_0-S_5 but contains S_6 fabric suggesting injection syn-D_6.

Fig. 2.2.10 Syn-D_2 basic dyke, Kurrikamaki. Cross-cuts S_0-S_1; intruded axial planar to F_2 fold and contains S_2 foliation.

Fig. 2.2.11 Syn-D_3 basic dyke, Hallinmaki Mine. Truncates S_0-S_1-S_2 and F_3 hinge. Emplaced concordant with F_3 axial planes and contains weak S_3 fabric.


2.2.9
F6
S6


2.2.10
S3
S2
S2
S1
S3


2.2.11
S3
F3
SC

SECTION 2

PART 3

The relationship of veins and pegmatites to the structural sequence

2.3.1 Introduction

Throughout the Virtasalmi District vein development is extensive. Aside from small dykes and narrow veins of basic to intermediate composition which are commonly the offshoots of larger, syn-tectonic intrusive igneous bodies, veins of predominantly quartzofeldspathic composition and various pegmatites exhibit cross-cutting relationships with their host rocks, with one another, and with folds and fabric elements. This wealth of cross-cutting data enables the vast majority of vein material to be placed within the structural sequence, permitting its study within the framework of metamorphic and structural development of the area.

Veins constitute from 0-30% of most outcrops, and petrographically similar veins, which display consistent ages of emplacement are developed throughout the study area. Only a few types are restricted to particular lithologies or localised areas. Vein development occurred throughout the progressive deformation of the area.

Criteria used in establishing the relative age of emplacement of intrusive material have previously been discussed (Hopgood, 1980; Campbell, 1980). Recognition of the earliest fabric in quartzofeldspathic veins in particular,

notably those intruded prior to D_4 in this study, was made more difficult by the tectonic overprinting by several minor late deformational events and by post-tectonic recrystallisation. In particular, it was found that attempts to use fracture cleavages in determining relative emplacement ages were only valid where cleavages could be directly linked to fold sets, due to uncertainties caused by observed localised variations in orientation of fracture cleavages. Also there was difficulty in observing fractures in often quite thin veins, especially in quartz-rich veins where fractures were seen in thin section to follow grain boundaries rather than to fracture individual quartz grains, which may only be strained.

Recognition of tectonic remobilisation of pre-existing vein material into low pressure zones such as boudin necks and hinge zones of later fold sets was also important in attempting to understand the overall development of veins. In other studies it has been assumed that where narrow veins are axial planar to fold sets, either occurring in hinge zones or in sheared out short limbs, that these form synchronously with the later stages of the formation of that particular fold. However, in a few instances exposure has permitted demonstration that some veins oriented axial planar to folds were remobilised from pre-existing vein material (Fig. 1.1.10). Sometimes this remobilisation is accompanied by changes in the relative proportions of the constituent minerals in the veins. Remobilised and newly emplaced veins are often cut by the fracture cleavage which developed axial planar to the same fold at a slightly later stage. Also, where there was refolding and rotation of individual folds into coplanar

attitudes with later folds, some veins apparently 'axial planar' to the earlier fold set were demonstrated in places to be discordant and axial planar to the later set.

2.3.2 Syn-D_1 vein neosomes

Within the gneisses of the Narila area there are isolated blebs of quartzofeldspathic composition up to 1 cm in diameter which occasionally merge to form more continuous segregations up to 5 cm in length. They accentuate the S_1 fabric which is itself interpreted as a product of metamorphic segregation: locally they cross-cut the S_1 layering, indicating that they formed after development of the S_1 fabric. The observation that they are partially rotated or stretched out into alignment with the S_2 fabric seems to place their formation as late during D_1. Mineralogically the blebs consist of K-feldspar and a myrmekitic intergrowth of quartz and plagioclase. Their restricted occurrence within the gneiss in a sequence of thinly interbanded gneiss and amphibolite would seem to preclude an intrusive origin and suggests that they were derived by in situ partial melting; this interpretation is supported by their composition and is consistent with metamorphic conditions at their time of formation (Section 2.4) which indicates peak P-T conditions above the granite solidus curve.

Also, in a few localities in the very north of the study area, there is developed a leucocratic neosome with a composition of plagioclase, quartz and diopside ± hornblende. This neosome forms long veins between 0.5 mm and 3 cm thick which are continuous for several metres, are

sub-parallel to S_1 and are folded by F_2 folds (Fig. 2.3.1). In places these veins are interbanded with melanocratic amphibolitic bands and constitute 50% of the rock, giving the impression that they formed by metamorphic differentiation. However, the leucocratic segregations also seem to coalesce to form more irregular patches apparently truncating S_1, yet also folded in D_2. Hence these patches, which are up to 5 cm wide and 20 cm long, may have been formed by the remobilisation of previously formed segregations later during D_1.

In adjacent diopside-cummingtonite amphibolites smaller irregular patches of leucocratic vein material containing a weak S_1 foliation were also probably formed by segregation and subsequent mobilisation. This amphibolite and adjacent gabbroic intrusions that were emplaced prior to D_1 are intruded by a few coarse-grained aplitic veins up to 5 cm across and several metres long. These cross-cut both S_0 and D_1 features but are truncated by S_2 planar features, suggesting emplacement late during D_1.

Biotite-rich veins cross-cutting S_0 but strongly foliated by S_1 and folded by F_2 (Fig. 2.1.3) occur in several places; emplacement early during D_1 is deduced.

2.3.3 Syn-D_2 vein neosomes

A metamorphic segregation-differentiation banding (S_2) was locally observed to form during D_2. This is consistent with the P-T conditions as indicated by M_2 mineral assemblages, as is the lack of any observed features to suggest partial melting in the gneisses. However, remobilisation of quartzo-

feldspathic segregations (except into boudin necks and fold hinge zones) was commonly observed.

In the calc-silicate skarn lithologies there is a large volume of quartzofeldspathic neosome which was interpreted to have formed during D_2. Within the skarns of the northern area in particular, M_1 andradite was retrogressed to an assemblage of epidote + quartz during D_2. In some instances this quartz is observed to coalesce and form large irregular patches or a branching network of veins. There is generally no elongation of these veins and only a weak S_2 fabric is imposed on them due to the fact that most skarn bands are in the form of discontinuous structures with most of the strain taken up in the surrounding less competent amphibolites. This has generally resulted in static recrystallisation within the boudins. Post-D_2 recrystallisation of the vein material may also have obliterated previous fabrics. There is also remobilisation of the vein material into D_2 boudin necks (Fig. 2.1.15).

2.3.4 Syn-D_3 vein neosomes

Aplitic veins developed axial planar to minor F_3 folds (Fig. 2.3.2) are commonly between 5 cm and 50 cm in length and less than 2 cm in width. They occur in hinge zones or sheared-out short limbs of F_3 folds and form in a wide variety of rock types, ranging from amphibolites through diorite to trondhjemite. In many cases, pre-existing neosome was apparently remobilised to form the veins. They cut across S_0-S_1-S_2 fabrics but are cut by an S_3 fracture cleavage, and are hence interpreted as forming syn-D_3.

Quartz-plagioclase veins with minor hornblende are seen to anastomose some F_3 fold hinges (Fig. 2.1.25). Irregular patches of comparable lithology either mimic F_3 fold closures or, in other places, truncate them. This material is found to intrude both amphibolites and skarns, and in some cases at least is derived from remobilisation of D_2 neosome. As with the veins above, they cross-cut S_1-S_2 and are commonly deformed by D_4 structures, and they are interpreted as having developed late during D_3.

Quartz-plagioclase pegmatites, 10-20 cm wide and trending NW-SE, have characteristic quartz-rich centres with quartz-plagioclase margins. They are intruded into F_3 hinge zones, cross-cut S_2, are cut by an S_3 fracture cleavage and are folded by later structures. Hence they are interpreted to have been intruded late syn-D_3.

In the hinge of a major F_3 structure near Hällinmäki, there is a poorly defined intrusion of muscovite-bearing quartz-plagioclase-K-feldspar pegmatoid which is cut by later fabrics, S_5 and S_6, but which itself contains no strong foliation, indicating a possible emplacement syn-D_3.

In Hällinmäki Mine two pegmatoid veins containing abundant apatite phenocrysts up to 1 cm in diameter, plagioclase, K-feldspar and quartz (and locally some chalcopyrite where they cross-cut ore-bearing horizons) are also seen to truncate S_0-S_1-S_2. They are intruded concordant to F_3 axial planes and cut by S_{3-6}, also indicating emplacement syn-D_3.

2.3.5 Syn-D_4 pegmatites and veins

Composite veins, consisting of narrow margins up to 3 cm wide comprising a coarse-grained assemblage of quartz, feldspar and magnetite, and with medium-grained centres of varying width comprising quartz, plagioclase and orthoclase cross-cut S_0-S_1-S_2 and are apparently intruded concordant to the axial planes of F_4 folds. They are cut by S_5 and later sets of fracture cleavages which constrains their development as syn-D_4. These pegmatites can be traced for several metres, but they are not of constant thickness, varying from 10 cm to 30 cm wide, with the margins almost merging in some places.

Also intruded parallel to the axial planes of minor F_4 folds are quartzofeldspathic veins of up to 50 cm in length and 2 cm in width. These tend to form in the hinge zones or in the short limbs of F_4 folds (Fig. 2.1.35), and are seen to truncate S_0, S_1, S_2 and S_3 and to contain later fracture cleavages, including S_4, showing that the latter developed after vein emplacement. This places them after D_3 but syn-D_4.

2.3.6 Syn-D_5 neosomes

In the hinge zones of F_5 folds, quartzofeldspathic veins folded around F_5 hinges are commonly remobilised to form short (up to 30 cm long) elongate veins. Near Hällinmäki small pegmatites of quartz and plagioclase, up to 20 cm wide, cut S_2 and D_2 intrusions as well as D_5 but are intruded concordantly with F_5 axial planes and are cut by S_6. Therefore, they must have been intruded late during D_5.

At Hallinmaki Mine, thin (< 2 cm) veins of quartz, plagioclase and chloritised hornblende are intruded into the hinge zone of small angular F_5 folds. Also intruded into F_5 hinge zones are pegmatoid orthoclase-plagioclase-quartz veins. These are dyke-like veins, 10 cm to 25 cm wide, which cut across S_0, S_1, S_2 and S_3 but contain the S_5 and S_6 fracture cleavages, and are apparently remobilised into F_6 hinge zones (Fig. 2.3.3).

2.3.7 Syn-D_6 vein neosomes

In the hinge zones of asymmetrical F_6 folds, small shear offests were observed. Intruded along some of these small shears, or in the hinge zone of small-scale F_6 folds, are thin (< 2 cm), short (10-50 cm) quartzofeldspathic veins. The relatively restricted occurrences of veins within striped hornblende amphibolites (Fig. 1.2.10), rather than in adjacent diopsidic amphibolites, suggests that in many cases these veins were formed by mobilisation of pre-existing quartzofeldspathic segregations. The composition of these veins, similar to that of the pre-existing segregations, is plagioclase and quartz, with a few hornblende phenocrysts.

At Lari, an anastomosing network of thin quartzofeldspathic veins is seen to coalesce to form a large dyke-like vein intrusion which agmatises previous fold hinges, detaching and rotating amphibolite blocks up to a metre long (Fig. 2.3.4). The vein is on average 1 m wide, and evidence of a small (< 1 m) dextral sense of movement across it suggests that it is associated with small-scale wrench faults, a feature commonly noted and

interpreted as syn-D_6 elsewhere in the area. The vein cuts S_{0-5}, F_3 folds and late syn-D_3 diorites. It is only cut by S_6 and S_7, and this evidence together with its northwest-southeast trend suggests a syn-D_6 origin. In general syn-D_6 veins have a high proportion of feldspar to quartz and are more readily distinguishable from the quartz-rich syn-D_2 neosome which is commonly present in skarn rocks of the northern area. Other more irregular patches of this vein material also occur at Lari where they agmatise blocks of skarn rock.

A few coarse-grained quartz-plagioclase-orthoclase pegmatites, generally c. 20 cm thick, trend approximately 045°, cut across F_3 folds, S_{0-5}, and are cut by S_7; this suggests emplacement during D_6. A large number of other pegmatites showing similar syn-D_6 age relationships, and consisting predominantly of orthoclase with minor quartz and plagioclase, form large branching networks or isolated dyke-like pegmatites throughout the area.

2.3.8 Syn-D_7 and post-D_7 neosomes

Several sets of pegmatites and veins, which are interpreted as post-dating D_6, have been identified. One set of composite pegmatites, 12-20 cm wide, with K-feldspar centres and quartz-K-feldspar-magnetite-plagioclase margins, cut S_6 but contain the S_7 fracture cleabage. These pegmatites trend from 080°-100°, which generally corresponds to the attitude of the axial planes of isolated F_7 folds. Coarse-grained aplitic veins up to 5 cm wide, showing similar age relationships and orientations to these pegmatites, are also interpreted to be syn-D_7 in origin.

In the Mine vicinity, pegmatite dykes and veins associated with three sets of faults were observed, Composite pegmatites with coarse-grained quartz-rich centres and K-feldspar + biotite margins, and K-feldspar-biotite pegmatites are associated with north-south trending normal faults with small amounts of displacement.

Veins associated with low angle 'thrust' faults have compositions of zoned hornblende, plagioclase and sphene. These vary from 2 cm to 10 cm wide and several may occur along the one fault plane, often displaying cross-cutting relationships, indicating that they had been intruded in more than one pulse. Some of these veins are foliated, with the foliation displaying a sinusoidal distribution within the vein which suggests non-brittle movement on the fault while the vein material was still ductile.

Pegmatites and veins which cross-cut S_0-S_6 and F_1-F_6, and are not themselves folded, were intruded post-D_6.

Quartz-filled tension gashes up to 20 cm long and trending 170° and 060°, are found in all lithologies, truncating F_3 and F_6 folds structures, and may be related to D_6 and D_{late} faults. These veins are dilational and the quartz was probably introduced by hydrothermal solutions (Campbell, 1980).

Fig. 2.3.1 Syn-D_1 neosome predominantly comprising plagioclase with quartz and minor diopside-hornblende. This leucocratic neosome appears to have formed initially by metamorphic differentiation which produced an alternating melanocratic and leucocratic S_1 banding. These leucocratic segregations coalesce in places to form thicker bands or more irregular patches of neosome which are folded by F_2 folds, pointing to their development during D_1. In amphibolites, Kiviniemi.

Fig. 2.3.2 Aplitic veins developed axial planar to F_3 folds. In places (X) these veins may have developed by local remobilisation of pre-existing leucocratic segregations. However, in other instances (Y) a link between immediately adjacent pre-existing segregations is less obvious. Amphibolites, Virtasalmi Village.

Fig. 2.3.3 Coarse-grained pegmatoid veins cross-cut S_0-S_3, are intruded subparallel to F_5 axial traces and contain S_5 and S_6 fabrics indicating injection probably syn-D_5. Here seen to be locally remobilised into small F_6 hinge zones. Hällinmäki Mine.


2.3.1
S_{0-1}
S_2
F_2


2.3.2
S_3
S_C
S_C
F_3
F_3


2.3.3
F_6
S_6
S_C
S_6
F_5
S_5

Fig. 2.3.4 An anastomosing network of quartzofeldspathic veins is observed to coalesce and form a NW-SE-trending dyke-like intrusion at Lari. The veins truncate S_0-S_5, F_3 folds and a syn-D_3 diorite intrusion, but are cut by S_6 and S_7 fabrics. This neosome is also seen to agmatise F_3 fold hinges and contains detached and rotated blocks of amphibolite. There appears to be a small (< 1 m) dextral component of displacement across the dyke. All this evidence indicates emplacement of this vein neosome syn-D_6.
The diorite which is truncated by the syn-D_6 neosome truncates S_0-S_2 and also agmatises pre-existing F_3 fold hinges. The intrusion contains large stoped blocks of the adjacent country rock, some of which are partially resorbed. The intrusion is not foliated but is cross-cut by S_3-S_7 fracture cleavages, indicating a late syn-D_3 (post-F_3 formation) emplacement age.

Fig. 2.3.4

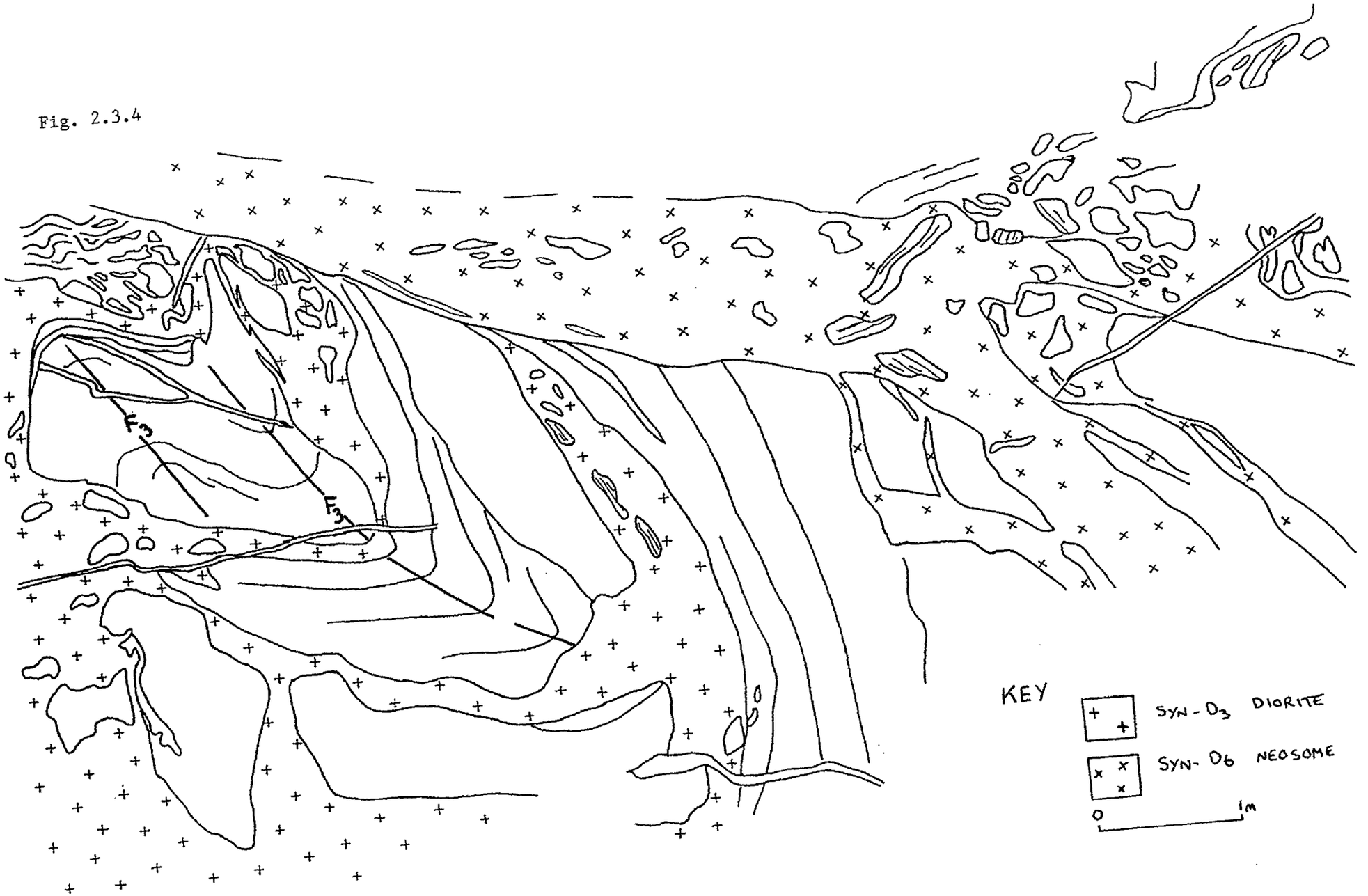

SECTION 2

PART 4

Metamorphic history

2.4.1 Introduction

The syn-kinematic polymetamorphic history of the rocks in the Virtasalmi District has been elucidated on the basis of mineral assemblages, textural relationships and the relationship of mineral growth to structural elements. The methods used follow those used previously by Campbell (1980), Koistinen (1981), Park (1983), Halden & Bowes (1984), and others to determine the tectonothermal history in other parts of the Svecokarelides. The P-T conditions and, to a lesser extent, fluid compositions during successively developed deformational phases, have been estimated from coexisting mineral assemblages in relation to the experimentally determined stability fields of the minerals concerned. The fairly constricted stability fields so determined must be viewed within the limitations of such an approach, e.g. accuracy, consistency and applicability of experimentally derived reaction curves, the effects of substitution of components in solid solution series, and the effects that variations in $X_{CO_2}^{gas}$ and $X_{H_2O}^{gas}$ can have in altering the positioning of equilibrium in natural systems.

Evidence for pre-kinematic metamorphism is discussed in Section 3, Part 1.

2.4.2(i) M_1 mineral assemblages

The observation that whole-rock mineral assemblages in the rocks studied do not represent a single equilibrium assemblage, together with the preservation of reaction textures, provides the basis for elucidating the polyphase metamorphic history. Textural evidence such as the sharing of straight-grain boundaries and the common presence of 120° triple point junctions (Fig. 2.4.1) is used to demonstrate which minerals constitute equilibrium M_1 assemblages. Such relationships are best preserved in calc-silicate marble and skarn lithologies, but in these rocks, and in all others, M_1 minerals occur principally as (1) cores within corona structures (Fig. 2.4.2), (2) cores of markedly zoned minerals such as plagioclase, (3) relict minerals which are variably corroded to form new M_2 aggregates at their margins (Figs. 2.4.3 and 2.4.4), and (4) minerals forming a preferred alignment that can occasionally be unequivocally identified as an S_1 fabric (Fig. 2.4.5). Generally M_2 has largely destroyed textural evidence for M_1 mineral reactions so that the nature of the mineral assemblages themselves have to be used to postulate at least some of the possible reactions. These assemblages (Table 2.4.1) are consistent in defining a higher grade than that operative during subsequent recrystallisation events.

Gneisses

Although the quartzofeldspathic gneisses are not volumetrically significant, they exhibit a large variety of mineral assemblages on account of original compositional

variations preserved as small-scale lithological layering (S_0), combined with or enhanced by metamorphic segregation banding (S_1) (see Fig. 2.4.5).

The mineral assemblages observed are:

(1) garnet + biotite + andesine (+ quartz)

(2) cordierite + biotite + andesine (+ quartz)

(3) garnet + sillimanite + biotite + andesine (+ quartz)

(4) cordierite + sillimanite + K-feldspar (microcline) + andesine + biotite +/- garnet

(5) garnet + cordierite + biotite + andesine (+ quartz)

(6) cummingtonite + biotite + andesine (+ quartz)

(7) biotite + andesine + quartz

(8) K-feldspar (microcline) + andesine + biotite (+ quartz)

(9) sillimanite + biotite + andesine + quartz

(10) cordierite + sillimanite + biotite + andesine + quartz.

M_1 sillimanite coexists with K-feldspar (assemblage 4) and this together with the absence of M_1 muscovite suggests the reaction

muscovite + quartz = K-feldspar + sillimanite + H_2O

(Helgeson et al., 1978).

Where large prismatic sillimanite grains occur as an intergrowth with biotite (9) (Fig. 2.4.4), a possible reaction is

muscovite + garnet = biotite + sillimanite + quartz

(Schreyer, 1965; Tracey et al., 1976).

Although cordierite and almandine were nowhere seen to share a stable grain boundary, textural evidence demonstrates their presence within M_1, with adjacent grains separated by mineral aggregates formed during D_2 (Fig. 2.4.6). Hence the probable coexistence in equilibrium of almandine with cordierite, biotite, plagioclase, quartz and K-feldspar may be represented by the sliding reaction

cordierite + biotite = almandine + K-feldspar + H_2O

(Currie, 1971; Hansen & Green, 1972)

where reactants and products coexist over a narrow range of temperature and pressure. Almandine coexisting with biotite, plagioclase and quartz (1) may have formed by the reaction

chlorite + biotite + quartz = almandine + biotite + H_2O

(Chakraborty & Sen, 1967).

Almandine coexisting with sillimanite, biotite, plagioclase and quartz (3) may have formed by the reaction

Fe-rich chlorite + muscovite + qtz = almandine-rich garnet + biotite + Al_2O_3 + H_2O

(Hirschberg & Winkler, 1968).

Cordierite coexisting with sillimanite, biotite, plagioclase and quartz (10) may have formed by the reaction

chlorite + muscovite + qtz = cordierite + biotite + Al_2O_3 + H_2O

(Hirschberg & Winkler, 1968).

Cordierite coexisting with K-feldspar, sillimanite, biotite, plagioclase and quartz (4), could be the result of the divariant reaction

Mg-biotite + sillimanite + qtz = Fe-biotite + cordierite + K-feldspar + H_2O

(Campbell, 1980).

Amphibolites

The original compositional diversity of the amphibolites is reflected in the development of varied M_1 mineral assemblages often poorly preserved but occasionally seen to occur as a metamorphic differentiation fabric (S_1) (Fig. 2.1.13). Direct evidence demonstrating equilibrium M_1 assemblages is generally poorest in the amphibolites, with grain-grain contacts between minerals interpreted as having formed during D_1-M_1 only rarely present. However, the widespread retrogression of these lithologies, with enclosure of corroded minerals within later M_2 amphiboles, in particular, frequently allows recognition of pre-existing assemblages which are consistent in their P-T constraints. Those assemblages noted are:

(1) hypersthene + andesine

(2) diopside + scapolite + andradite + ilmenite

(3) diopside + cummingtonite + andesine

(4) diopside + andesine + magnetite

(5) cummingtonite + andesine

(6) diopside + green-brown hornblende + andesine-labradorite

(7) green-brown hornblende + cummingtonite + andesine

(8) diopside + biotite + andesine-labradorite + ilmenite

(9) diopside + andradite + labradorite-bytownite

(10) green-brown hornblende + andesine

(11) diopside + andesine +/- scapolite (+ magnetite).

Hypersthene occurs in narrow bands (1) within diopside-bearing amphibolites in the vicinity of Hällinmäki. This suggests that locally, at least, conditions of the amphibolite-granulite transition zone were attained. As Hoshino (1979) has shown, orthopyroxene-bearing assemblages can coexist with orthopyroxene-free assemblages above the second sillimanite isograd in the amphibolite-granulite facies transition zone, with the orthopyroxene forming in lithologies with high FeO/(FeO + MgO). However, it is normally only when hypersthene occurs in rocks of intermediate composition that conditions of full granulite facies are considered to have been attained (Schreurs, 1984). No pre-kinematic intermediate volcanic rocks were mapped during this study. Also, amphibolitisation of hypersthene-diopside-bearing assemblages can apparently take place without extant relict orthopyroxene (Beach, 1974). Therefore hypersthene may have been more widely developed in the amphibolites of the Virtasalmi District than immediately apparent, being preserved only in the less retrogressed bands of restricted compositional range. This is demonstrated in amphibolites from the Narila area where there is textural evidence preserved which indicates almost complete recrystallisation of the hypersthene-bearing D_1-M_1 assemblage in plagioclase-deficient bands (Fig. 2.4.7).

Hypersthene could have formed by the reaction

hornblende + quartz = anorthite + diopside + orthopyroxene + H_2O

(modified from Binns, 1965; Hoshino, 1979).

Diopside is abundant in many lithologies (2,3,4,6,8,9). Bands consisting of apparently unretrogressed M_1 assemblages and comprising varying proportions of diopside and plagioclase with magnetite, ilmenite and quartz are observed in amphibolites throughout the area. Individual mineral grains have straight or slightly curved grain boundaries, with the diopside forming elongate grains or large irregular poikiloblastic plates, while other minerals form more equidimensional grains. Plagioclase zoning, however, indicates some retrogression. Diopside may have formed at the threshold of the amphibolite facies in calcium-rich amphibolites by the reaction

tremolite + calcite + quartz = diopside + CO_2 + H_2O

(Miyashiro, 1973).

Alternatively, in less calcareous assemblages largely devoid of M_1 hornblende (3,4), diopside may have formed at higher temperatures and pressures from the decomposition of hornblende (Binns, 1965). Similarly, cummingtonite (3,5) may have formed from the decomposition of hornblende by the reaction

tschermakite + quartz = cummingtonite + anorthite + H_2O

(Miyashiro, 1973).

Green-brown hornblende is sometimes observed as cores within later (M_2) hornblende in association with either cummingtonite or diopside (6,7). This suggests that

the elimination of the tschermakite component in hornblende during the formation of cummingtonite or diopside may have resulted in the persistence of a green-brown hornblende richer in TiO_2 and in the edenite or pargasite-hastingsite components (Binns, 1965; Miyashiro, 1973).

The presence of scapolite in assemblages both containing and devoid of calcic plagioclase (2,11) suggests that its formation was dependent on the distribution or availability of volatile constituents such as Cl or CO_2 (Jaques et al., 1982). The reaction by which it formed is likely to have been

plagioclase + calcite = scapolite (Deer et al., 1976).

While adjacent diopside grains are mostly rimmed by M_2 hornblende, scapolite is invariably rimmed by epidote, making direct demonstration of coexistence with other M_1 minerals impossible.

The presence of scapolite also suggests that P-T conditions may have reached those of granulite facies (Sivraprakash, 1981; Warren & Hensen, 1983), or of the amphibolite-granulite facies transition zone (Jaques et al., 1982).

Calcic garnet (andradite-grossular) occurs mostly as M_1 porphyroblasts in a few amphibolites (9). Evidence that these garnets grew pre-D_2 is shown by their variable corrosion to form new (M_2) mineral products. In quartz-bearing assemblages it may have formed by the reaction

anorthite + hedenbergite = 1/3 almandine + 2/3 grossular + qtz

(Jaques et al., 1982).

In quartz-deficient assemblages it may be formed either by the reaction

anorthite + quartz + calcite = grossular + CO_2

(Jaques et al., 1982)

or by the reaction

zoisite + quartz = andradite-grossular + anorthite + H_2O

(Jaques et al., 1982).

Plagioclase compositions, from optical determinations only, show a wide range (An_{36-80}). There is a direct correlation between the CaO and Na_2O contents of the rock and the plagioclase composition, and this is examined further in Section 3, Part 1.

Sphene does not occur in the M_1 assemblage in the amphibolites; the stable Ti-bearing phase is ilmenite.

Calc-silicates

As indicated above, samples taken from marbles mostly with less than 10% silicate minerals, from calcareous quartzofeldspathic bands and from various calc-silicate skarn lithologies have preserved within them textural evidence for equilibrium M_1 assemblages (Fig. 2.4.1). The following M_1 assemblages were observed:

(1) andradite-grossular garnet + diopside + scapolite + calcite

(2) diopside + calcite

(3) diopside + forsterite + calcite

(4) wollastonite + calcite + quartz

(5) andradite-grossular + calcite

(6) diopside + scapolite + calcite.

In addition, Hyvärinen (1969) recorded

(7) wollastonite + diopside.

In the thinly banded calc-silicate skarns, assemblages are

(8) hedenbergite + andradite + scapolite + andesine (An_{43-47})

(9) hedenbergite + bytownite

(10) andradite + bytownite

(11) magnetite + hedenbergite + pyrrhotite + chalcopyrite

(12) magnetite + andradite + quartz

(13) magnetite + hedenbergite + quartz

(14) andradite + hedenbergite + magnetite.

In narrow zones 1-30 cm wide which are formed at the contacts between marble and amphibolite (Section 1, Part 2) and interpreted as metasomatic skarns, assemblages are crudely zoned, with those on the amphibolite side being

(17) diopside- and hedenbergite-rich,

and those on the marble side being

(18) andradite-rich.

Other lithologies interpreted as metasomatic skarns but with less obvious zoning have assemblages with a greater mineralogical variety

(19) andradite + scapolite + diopside + calcite + quartz.

In all the calc-silicate lithologies the M_1 assemblages are only partly retrogressed, with many assemblages preserved intact, although no M_1 reaction-forming textures were observed, and these are inferred from the assemblages themselves.

The presence of wollastonite along with calcite and quartz (4) suggests the reaction

calcite + quartz = wollastonite (Greenwood, 1962, 1967; Turner, 1980),

but in some bands this was retrogressed during D_2. Hyvärinen (1969) also described wollastonite and diopside in the same rock; this is presumed to represent an M_1 assemblage.

Diopside is likely to have formed by the reaction

tremolite + calcite + quartz = diopside + CO_2 + H_2O

(Turner, 1980; Jaques et al., 1982)

since reactions involving dolomite and quartz occur over a limited range of temperature and $X_{CO_2}^{gas}$ (Slaughter et al., 1975).

As diopside, forsterite and calcite coexist in the M_1 assemblage (3), forsterite is not likely to have formed by the reaction of diopside + dolomite, and the reaction is likely to have been

tremolite + dolomite = forsterite + calcite (Metz, 1976).

The stable coexistence of $grossular_{SS}$ and diopside would appear to rule out the grossular having formed by the reaction

anorthite + diopside = $grossular_{SS}$ + pyrope + quartz

(Jaques et al., 1982).

A more likely reaction is

zoisite + quartz = grossular + anorthite + H_2O

(Jaques et al., 1982),

or

epidote + quartz = grossular-andradite + anorthite + H_2O

(Winkler, 1979).

Scapolite of almost pure meionite composition (Hyvärinen, 1969) coexisting with andradite-grossular, diopside and calcite (1) is likely to have formed by a similar reaction to that described for scapolite formation in the amphibolites.

The most common assemblage in calc-silicate skarns is that comprising varying proportions of andradite, hedenbergite and scapolite or plagioclase (bytownite) (8). Andradite was shown by White (1959) and Sivraprakash (1981) to form at the expense of hedenbergite by reactions including

hedenbergite + calcite + H_2O = andradite + CO_2 + H_2O

and

hedenbergite + O_2 = andradite + quartz + magnetite

(Liou, 1974; Taylor & Liou, 1978).

In the Virtasalmi lithologies hedenbergite and andradite coexist stably, with straight grain boundaries and minerals forming a granoblastic texture with 120° triple points developed (Fig. 2.4.1). The rim compositions of hedenbergite and andradite may be in equilibrium, but internally marked compositional zoning is developed in the hedenbergite; it has

dark green cores and light green margins, the variation probably corresponding to an increase in the diopsidic component towards the rims. Hence the andradite garnet apparently formed at the expense of the hedenbergitic component of pyroxene, probably with increased f_{O_2} between bands (after Sivraprakash, 1981).

Unlike the assemblages described by White (1959), however, M_1 andradite is not a secondary metasomatic mineral, as texturally it appears in equilibrium with scapolite and rim compositions of pyroxene. However, later growth of garnet or epidote within veins in the Hällinmäki and Kurrikamäki areas is probably linked to limited metasomatism, with the metasomatic fluid phases reponsible possibly being related to the intrusion of gabbros and granodiorites during D_3.

Hedenbergite (8,9,11,13,14,17) probably formed during prograde metamorphism from ferroactinolite which became unstable with rising temperature. The reaction involved is probably

ferroactinolite + calcite + quartz = hedenbergite + CO_2 + H_2O

(Deer et al., 1966).

2.4.2(ii) M_1 metamorphic conditions

The intercalation of calc-silicate, gneiss and amphibolitic units containing several index minerals permits metamorphic conditions developed during D_1 to be ascertained to within a narrow P-T range. A lower limit for temperature can be established because of the absence of muscovite and the presence of coexisting K-feldspar and sillimanite in the

gneisses (4); the second sillimanite isograd defined by the reaction

muscovite + quartz = K-feldspar + sillimanite

(Fig. 2.4.8, curve 3) must be passed and andradite-grossular formed from epidote (Fig. 2.4.8, curve 4). However, the occurrence of wollastonite in calc-silicate bands sets a more closely defined lower temperature limit, even allowing for variations in fluid composition (Fig. 2.4.8, curve 5), while the presence of meionitic scapolite provides a further refinement of temperatures as illustrated by the low temperature end of the meionite stability field (Fig. 2.4.8, curve 6) (Ellis, 1978). An upper temperature limit can be set using the reaction

biotite + garnet + qtz = hypersthene + cordierite + K-feldspar + H_2O

(Hess, 1969; Campbell, 1980)

(Fig. 2.4.8, curve 7), as the assemblage biotite and almandine is stable (1,2) and hypersthene is not found.

The presence within certain gneiss bands of lensoid veins with a composition of K-feldspar (microcline) + plagioclase + quartz + myrmekite is taken to indicate localised partial melting of the gneisses, since the presence of myrmekite implies crystallisation from a melt, and the vein assemblage also corresponds to a possible eutectic melt. The other relevant reaction curves confirm that temperatures exceeded the H_2O-saturated granite melting curve. Hence the granite melting curve (Tuttle & Bowen, 1958; Merrill et al., 1970)

(Fig. 2.4.8, curve 8) also constrains the lower temperature limit, although as pointed out by Campbell (1980), partial melting is unlikely to begin in the presence of mixed CO_2-H_2O fluids until well in excess of the granite solidus. A further complication in some gneisses is the possible presence of a sulphur phase, indicated by the presence of abundant pyrrhotite which is aligned within S_1.

The stable coexistence of garnet, sillimanite and K-feldspar (4) together with garnet-cordierite (4,5) and cordierite-K-feldspar-sillimanite assemblages (4) allows the Fe and Mg end member reaction

sillimanite + biotite + quartz = cordierite + K-feldspar + H_2O

(Holdaway & Lee, 1977)

(Fig. 2.4.8, curve 9), to delimit a maximum pressure of 5.5 kb for the M_1 assemblage. The lower pressure limit of 3.5 kb is determined from the Fe-end member reaction

cordierite = garnet + sillimanite + quartz

(Richardson, 1968)

(Fig. 2.4.8, curve 10).

The narrow temperature range of 750-800°C and the pressure range of 3.5-5.5 kb for M_1 bear a close resemblance to estimates for the peak metamorphism in the Rantasalmi-Sulkava District, 25 km to the east. These recalibrations of original data (Korsmann, 1977) on garnet-cordierite equilibration by Campbell (1980) suggested metamorphic conditions in the range of 4.4-4.8 kb and 750-800°C. The previous estimate of metamorphic conditions in the Virtasalmi District (Hyvärinen, 1969) suggested

temperatures of 650 ± 30°C and pressures of 5 ± 1 kb, but did not recognise the existence of a polymetamorphic history and was therefore based on whole-rock mineral assemblages.

The M_1 conditions for the Virtasalmi District therefore correspond to the transition zone between the amphibolite and granulite facies as denoted by Turner (1980). Minerals usually indicative of the granulite facies, such as hypersthene, which is also known to have formed in the amphibolite-granulite transition zone where metabasites have high FeO/(FeO + MgO) ratios (Hoshino, 1979), and to a lesser extent scapolite, which may form depending on availability of Cl and CO_2 (Jaques et al., 1982), occur locally but were probably not pervasively developed. The estimates of geobarometry and geothermometry suggest that the lithologies were buried to a depth of c. 12-18 km with a thermal gradient of c. 45-70°C/km, which is in accordance with the heat flow determined elsewhere in the Svecokarelides (Campbell, 1980).

2.4.3(i) M_2 mineral assemblages

In the gneisses and amphibolites in particular, the variety of reaction textures preserved indicates that recrystallisation during D_2 was heterogeneous on a small scale. This is expressed as small-scale layering (S_2), or as patchy recrystallisation within compositional bands unrelated to penetrative development of an S_2 fabric. This distribution and intensity of recrystallisation is interpreted as a reflection of the movement of the intergranular fluid, the presence of which is essential in all hydration reactions (Beach, 1974).

There are no large areas where an M_1 assemblage is wholly preserved, with the most intense retrogression seen where a penetrative S_2 tectonic fabric is developed, most noticably in D_2 high strain zones where the M_1 mineralogy is largely destroyed. However, microscopically it is often possible to see a complete range of textures from partially altered M_1 assemblages, indicated most clearly by preservation of corona textures, to almost wholly recrystallised M_2 assemblages.

Gneisses

The following mineral assemblages were developed in M_2

(1) chlorite + andalusite + biotite + muscovite

(2) pinnite + biotite + chlorite + magnetite + muscovite

(3) sillimanite (fibrolite) + magnetite

(4) biotite + chlorite + magnetite + plagioclase + quartz

(5) biotite + quartz + plagioclase.

The juxtaposition of relict M_1 and new M_2 mineral assemblages is shown in the gneisses to even greater extent than in the amphibolites. This results not only from recrystallisation, but as the presence in adjacent bands of M_2 fibrolitic sillimanite (3) and M_2 andalusite (1) suggests, also as the result of heterogeneous fluid movement.

While little altered M_1 cordierite is common within particular bands, in adjacent bands the cordierite may be almost completely retrogressed (compare adjacent bands in Figs. 2.4.4 and 2.4.6). In bands lacking in M_1 sillimanite and

garnet, retrogression was to aggregates of chlorite, andalusite and minor biotite and muscovite (1) (Fig. 2.4.9). The biotite and andalusite are interpreted as the products of the reaction

cordierite + K-feldspar = Fe-biotite + Al_2SiO_5 (andalusite) + qtz (Holdaway & Lee, 1977).

In one band where cordierite is associated with garnet and biotite, plagioclase and quartz, a range of reaction textures is seen, from unaltered cordierite to pinnite developed along fractures, to strongly pinnitised cordierite breaking down to biotite, chlorite, magnetite (+ muscovite) (2), and finally to very small cordierite relics within recrystallised aggregates of biotite, chlorite and muscovite. The interpreted reactions are

cordierite = pinnite

or

cordierite = biotite + chlorite + muscovite.

Bands containing cordierite in association with M_1 sillimanite, garnet, biotite, K-feldspar, plagioclase and quartz may contain large fibrous mats of fibrolitic sillimanite formed during D_2 associated with the breakdown of cordierite, with nucleation on relics of cordierite and adjacent biotite (Fig. 2.4.4). The biotite itself is corroded with small grains of magnetite formed at the breakdown sites (3). The reaction involved may be similar to the cordierite + K-feldspar reaction set out above, but at a slightly higher temperature and pressure.

In one instance where an S_2 segregation banding cross-cuts S_0, M_1 cordierites within the biotite-rich S_2 layering are corroded and reduced in size to small equidimensional, pinnitised grains aligned within the S_2 fabric. The cordierite is not completely retrogressed, possibly due to the almost monomineralic nature of the S_2 band.

M_1 almandine was retrogressed during D_2 to aggregates consisting of varying proportions of biotite, chlorite, magnetite, plagioclase and quartz (4). While a few euhedral margins are occasionally preserved, most grain boundaries are irregular, often with large embayments filled with breakdown products (Fig. 2.4.10). In several instances, parts of the margin and the centre of the garnets may be replaced, giving the impression of atoll garnets, which in this case certainly formed during retrogression from higher P-T conditions, unlike the mode of formation proposed by Smellie (1974) for the atoll garnets in a thermal aureole.

M_1 cummingtonite is corroded and replaced mainly by biotite at its margins and along cleavages (Fig. 2.4.11). Quartz and feldspar also form at the reaction site (5).

Fibrolitic sillimanite forms ubiquitously during D_2. Textures suggest that it formed in two ways. In cordierite-biotite assemblages fibrolite often forms fibrous mats nucleating at the site of cordierite + biotite breakdown as in the reaction set out above. Alternatively, where large, prismatic M_1 sillimanite crystals are intergrown with biotite, M_2 fibrolite nucleates on both sillimanite and biotite (Fig. 2.4.12a, b), with corrosion of the sillimanite at grain boundaries and along cleavages and breakdown of biotite with formation of

small magnetite grains (3). This may be represented by reactions involving biotite as a catalyst (Chinner, 1961), or may actually involve the breakdown and solution of M_1 sillimanite and re-nucleation of Al_2O_3 and SiO_2 components at the reaction sites as fibrolite.

Amphibolites

The following are mineralogical expressions of M_2

(1) hornblende + magnetite (+ quartz)

(2) diopside + hornblende + sphene (+ andesine)

(3) hornblende + andesine + quartz + magnetite

(4) hornblende

(5) actinolite + andesine (+ epidote)

(6) epidote + quartz.

M_2 hornblende occurs not only as rims around individual diopside and hypersthene grains, but also as elongate poikiloblasts which enclose several grains of either of these M_1 minerals (Figs. 2.4.13 and 2.4.14). Where hypersthene is the core mineral, the latter is often fractured, and small subgrains which form along the grain boundary may be detached. Small aggregates of magnetite occur at these boundaries and these coalesce to form larger grains away from the margins of the hypersthene, but enclosed within the hornblende (1) (Fig. 2.4.13). There is little internal replacement of the hypersthene with small amounts of hornblende and magnetite occurring in fractures or cleavages. More complete replacement is accompanied by more intense fracturing of the core mineral.

Grain boundaries are deeply embayed and may link up with retrogression in the fractures. In addition to hornblende and magnetite, quartz appears to form as another reaction product; it occurs as small blebs associated with magnetite and enclosed in hornblende.

Where the M_1 assemblage consisted of green-brown hornblende + diopside, M_2 green hornblende does not form rims around M_1 minerals but tends instead to occur as small, very irregularly-shaped grains. Diopside itself is typically recrystallised to small equi-dimensional grains or more irregular grains characterised by containing many small inclusions, mostly of sphene, which is also abundant as small crystals at grain boundaries (2). This sphene most likely formed on liberation of Ti from higher temperature minerals.

There are bands consisting entirely of green hornblende or hornblende + plagioclase (+ quartz) (+ magnetite) (3). These are interpreted as representing complete retrogression of the M_1 assemblage. The hornblende is generally not zoned and forms elongate grains with straight boundaries. Just prior to complete elimination of hypersthene in the more mafic bands, the latter is observed to occur along with magnetite as small blebs or as thin bands interstitial to green hornblende plates (Fig. 2.4.15) which are free from inclusions and are not zoned.

In Figure 2.4.14 it should be noted that hornblende was observed to form large irregular poikiloblasts enclosing several grains of diopside, magnetite, chalcopyrite and pyrrhotite, and some plagioclase (4) in some of the main chalcopyrite-pyrrhotite-magnetite-bearing diopside amphibolites in Hällinmäki Mine.

There are a number of other less common assemblages developed. M_1 cummingtonite is altered to greenish hornblende along cleavages and around corroded grain boundaries (Fig. 2.4.16). Also, in certain compositional bands, actinolite is formed rather than green hornblende; it occurs in close association with small amounts of epidote (5). The latter also occurs either as rims around M_1 grossular porphyroblasts (Fig. 2.4.17), or as fine-grained aggregates of epidote + quartz (Fig. 2.4.18) where the garnet has been extensively corroded and largely pseudomorphosed (6).

Calc-silicates

As in the gneisses, the retrogression of calc-silicate assemblages in D_2 was only partial and reaction textures are preserved. Mineralogical expressions are

(1) epidote + quartz

(2) zoisite + quartz

(3) antigorite + magnetite

(4) calcite + quartz.

In the impure marbles, and in the zones interpreted as resulting from diffusion metasomatism, $grossular_{SS}$ mineral grains are corroded and rimmed by an intergrowth of either epidote + quartz (1) (Fig. 2.4.2) or zoisite + quartz (2), as illustrated by the reaction

grossular + anorthite + H_2O = zoisite + quartz

(Winkler, 1979).

Large zoned grossular$_{SS}$ porphyroblasts in impure marbles show selective replacement of certain compositional zones by epidote (Fig. 2.4.19). In calc-silicate skarn lithologies, andradite garnet is retrogressed to an assemblage of epidote + quartz with the quartz frequently observed to have coalesced to form veinlets, commonly remobilised into low pressure hinge zones or boudin necks.

The presence of small grains of antigorite + magnetite (3) probably indicates recrystallisation and pseudomorphs of olivine grains. Hyvärinen (1969) also reported olivine breakdown to antigorite, possibly involving the reaction

forsterite + talc + H_2O = antigorite (Turner, 1980).

Wollastonite coexists metastably with calcite and quartz (4), to which it retrogresses via the reaction

wollastonite = calcite + quartz (Turner, 1980).

In all calc-silicate lithologies, scapolite is often rimmed by epidote (Fig. 2.4.20) or zoisite, having formed by the reaction

scapolite + H_2O = zoisite + CO_2 (Sivraprakash, 1981).

2.4.3(ii) M_2 metamorphic conditions

As the preservation of reaction textures shows, the recrystallisation of M_1-D_1 metamorphic assemblages in D_2 took place at lower temperature and pressure conditions, and involved the hydration (retrogression) of relatively anhydrous

amphibolite-granulite facies transition assemblages, and the amphibolitisation of meta-basaltic units. The minerals formed in M_2 are listed in Table 2.4.1.

This retrogression is inhomogeneous on all scales and as a result whole-rock assemblages contain components of both M_2 and M_1 assemblages.

The lower temperature limit of M_2 is best defined by the widespread occurrence of tremolite in tremolite-quartz intergrowths in calc-silicate rocks, the lower temperature stability of which is given by the reaction

dolomite + quartz + H_2O = tremolite + calcite

(Turner, 1980)

(Fig. 2.4.21, curve 2). The tremolite forms from the breakdown of diopside with the reaction

tremolite + calcite + quartz = diopside + CO_2 + H_2O

(Turner, 1980)

(Fig. 2.4.21, curve 3), also placing an upper temperature limit on the stability of tremolite.

Metamorphic conditions can be further refined because of evidence for the formation of epidote + quartz or zoisite + quartz from the breakdown of grossular as shown by the reaction

zoisite + quartz = grossular + anorthite + H_2O

(Winkler, 1979)

(Fig. 2.4.21, curve 4) as well as by the formation of antigorite

from olivine breakdown, possibly by the reaction

antigorite = forsterite + talc + H_2O (Turner, 1980)

(Fig. 2.4.21, curve 5).

While these reactions in the calc-silicate units delimit minimum temperatures to within a narrow range, pressure can be determined approximately by the reactions within the gneisses. The occurrence of the Al_2SiO_5 polymorphs, andalusite and fibrolite, in adjacent bands suggest conditions close to the inversion curve

sillimanite = andalusite (Holdaway, 1971)

(Fig. 2.4.21, curve 6), with the intersection of the inversion curve with the calc-silicate reaction curves providing an upper pressure limit on maximum D_2 retrogression conditions. Hence the maximum effect of retrogression during D_2 was to reduce temperatures to 450-550°C at pressures of 2-3.5 kb (Fig. 2.4.21). This places the assemblage in the lowermost amphibolite facies, which is consistent with the evidence of widespread stability of M_2 green hornblende, andesine, epidote and occasional diopside in the amphibolites. Chlorite does not appear in the metabasites until further limited retrogression in D_3, and its absence from M_2 assemblages in metabasites is taken to indicate temperatures above those marking the upper limit of the greenschist-amphibolite transition zone (Moody et al., 1983). In this study, rare actinolite was noted in certain compositional bands, and abundant sphene was observed which forms new grains as well as rims around ilmenite during D_2. The sphene was noted to

be in equilibrium with green hornblende. While this also suggests that the M_2 assemblage developed in the lowermost amphibolite facies, in some experimental reactions, the presence of both actinolite and sphene has been considered to be characteristic of the greenschist-amphibolite facies transition zone (Moody et al., 1983). The evidence in these rocks would seem to contradict these experiments, particularly with regard to the occurrence of sphene.

The estimated thermal gradient of 50-70°C/km for the M_2-D_2 metamorphic conditions is similar to that ascertained for M_1-D_1 conditions, suggesting continuation of the pre-existing heat flow environment, but with uplift and cooling related to tectonism. The development of hydrated minerals points to the influx of water, possibly connected to syn-tectonic magmatism.

2.4.4 Metamorphism during D_3

The stability and general lack of retrogression of minerals formed in D_2 suggests that there was no pervasive recrystallisation during D_3. However, there is localised recrystallisation often within S_3 fracture cleavages, and also locally within tight synformal F_3 fold hinges where an S_3 foliation is developed in biotite-rich lithologies, as in the closure of the major F_3 synform at Narila. Gabbroic and dioritic intrusions emplaced syn-tectonically late-D_2 and syn-D_3 also show the effects of limited retrogression. The minerals formed in D_3 are summarised in Table 2.4.1. In the gneisses biotite, muscovite and chlorite locally delineate a penetrative S_3 foliation or define a weaker

mineral lineation (Fig. 2.4.5). The S_3 fracture cleavage is commonly filled by epidote + quartz, especially in the vicinity of retrogressed calc-silicate skarn lithologies. M_3 assemblages, particularly the coexistence of blue-green hornblende-actinolite-chlorite locally in the metabasites suggests conditions of the greenschist-amphibolite facies transition zone were attained in restricted zones, with the formation of these minerals probably being dependent on the influx of retrogressive fluids as suggested by their association with sub-vertical fracture cleavages.

The replacement of pyrite porphyroblasts, which formed originally in syn-D_3 breccia ore, by pyrrhotite, is also consistent with increased temperatures late in D_3, suggesting that syn-tectonic intrusions may have been responsible for locally higher temperatures.

2.4.5 Later recrystallisation

Post-D_3 recrystallisation is limited to breakdown of pre-existing minerals in the vicinity of fracture cleavages, with new growth of biotite, muscovite, chlorite or magnetite parallel to S_4, S_5 or S_6 fracture cleavages. However, vein-filled fracture cleavages are common, being filled with epidote + quartz in S_4, S_5 and S_7. S_6 veins commonly consist of plagioclase + quartz + calcite. As in many cases, the veins are characterised by a consistent mineralogy irrespective of the lithology they cross-cut and introduction of Ca-rich fluids is proposed. In addition in several instances epidote + quartz veins are restricted near to retrogressed skarn bands, suggesting

possible mobilisation and re-precipitation of these mineral components.

Alteration of pre-existing minerals in less penetrative fractures, with the possible introduction solely of water occurs widely in S_4, S_5, S_6 and S_7. A late set of sub-horizontal epidote-filled fracture cleavages also occurs in the northern half of the area, adjacent to syn-D_6 intrusions. This may indicate that in this case the origin of the fluids is related to the localised emplacement of intrusions rather than the regionally pervasive introduction of fluids.

2.4.6 Summary

Evidence for pre-tectonic metamorphism related to a syn-volcanic phase of hydrothermal alteration which resulted in calc-silicate skarn formation is discussed in Section 3, Part 1.

Peak syn-kinematic metamorphism corresponding to conditions of the amphibolite-granulite facies transition zone, with temperature 750-800°C and pressure 3.5-5.5 kb, were attained during the first phase of deformation (D_1-M_1). These conditions, and the high geothermal gradient inferred, are consistent with peak metamorphic conditions identified elsewhere in Svecofennide terranes (Gaál & Rauhamaki, 1972; Mattila, 1976; Campbell, 1980; Korsmann et al., 1984; Schreurs, 1984).

Post-D_1 recrystallisation essentially involved the hydration and retrogression of M_1 assemblages under conditions of cooling related to continued deformation and uplift. The

influx of fluids into the lithologies was locally very heterogeneous, with only a limited structural control, and resulted in the juxtaposition of disequilibrium assemblages. Recrystallisation over most of the area terminated during D_2 at conditions of the lower amphibolite facies, with temperature 450-500^{o}C and pressure 2-3.5 kb, which resulted in the widespread amphibolitisation of the metabasalts. There was localised recrystallisation of these assemblages under conditions of the greenschist-amphibolite facies transition zone during D_3, while the presence of upright fracture cleavage fabrics in D_3-D_7 facilitated the movement of H_2O- and CO_2-bearing fluids, which caused late retrogression or veining. The character and composition of these veins may have been influenced by the emplacement of syn-tectonic intrusions.

TABLE 2.4.1 Sequence of mineral growth in relation to structural development

	amphibolites	gneisses	calc-silicate marbles & skarns
D_1 M_1	diopside cummingtonite hornblende (green-brown) (hypersthene) ilmenite scapolite plagioclase (andesine-labradorite) calcic garnet biotite magnetite-chalcopyrite-pyrrhotite rutile (quartz)	cordierite almandine garnet sillimanite biotite K-feldspar (microcline) plagioclase (andesine) cummingtonite quartz pyrrhotite (apatite)	wollastonite forsterite diopside-hedenbergite andradite-grossular scapolite plagioclase (bytownite) calcite
D_2 M_2	diopside hornblende (green) actinolite sphene epidote plagioclase (andesine) quartz	fibrolitic sillimanite andalusite chlorite biotite muscovite plagioclase (andesine but more sodic) magnetite quartz	tremolite epidote quartz antigorite (zoisite) biotite plagioclase (more sodic) calcite
D_3 M_3	metasomatic andradite, epidote blue-green hornblende chlorite biotite magnetite local scapolite local epidote (local tremolite)	biotite muscovite chlorite	metasomatic andradite, epidote
D_{late} M_{late}	Localised chlorite, magnetite and epidote and calcite growth. Saussuritisation of feldspars.	Biotite, muscovite or chlorite. Saussuritisation of feldspars.	calcite

Fig. 2.4.1 Granoblastic texture, with straight grain boundaries and 120° triple point junctions indicative of an equilibrium D_1-M_1 assemblage (hedenbergite + andradite + scapolite) in calc-silicate skarn, Hällinmäki Mine.
[MAG. X30, XPL]

Fig. 2.4.2 Corona texture with M_1 calcic garnet porphyroblast replaced by M_2 intergrowth of epidote + quartz at corroded rims and along fractures.
[MAG. X75, PPL]

Fig. 2.4.3 M_1 cordierite largely replaced by M_2 aggregate of andalusite + biotite + chlorite.
[MAG. X75, PPL]

Fig. 2.4.4 M_2 fibrolite nucleating on M_1 pinnitised cordierite. (B) is close up of (A).
[MAG. X75, PPL (A); X120, PPL (B)]

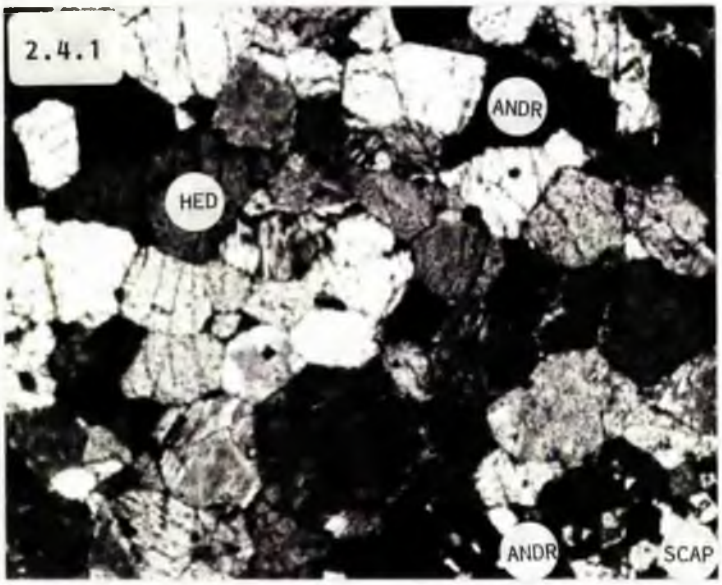
2.4.1
ANDR
HED
ANDR
SCAP

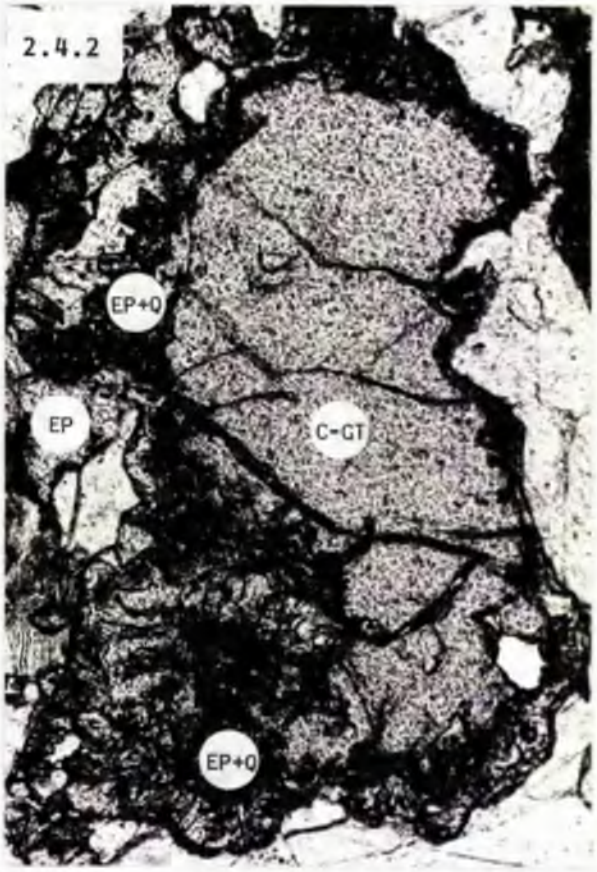
2.4.2
EP+Q
EP
C-GT
EP+Q

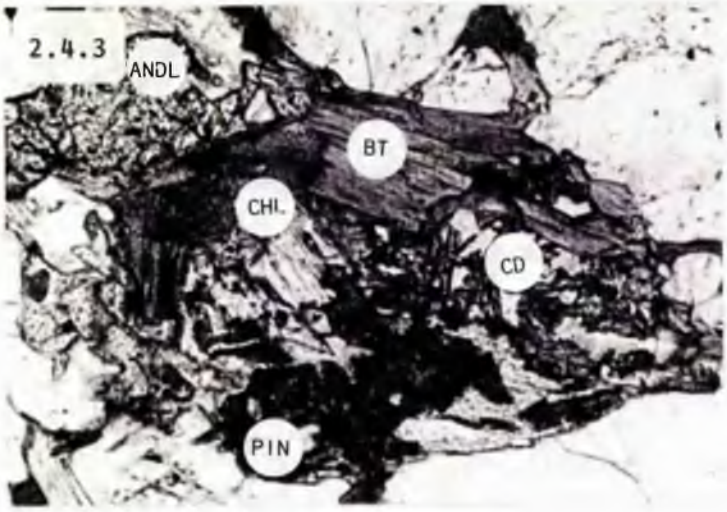
2.4.3
ANDL
BT
CHL.
CD
PIN

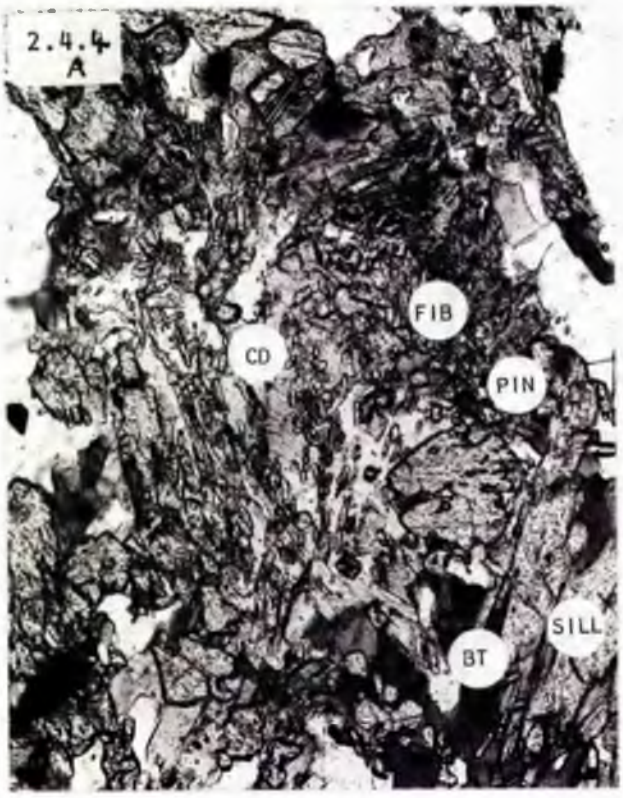
2.4.4
A
FIB
CD
PIN
SILL
BT

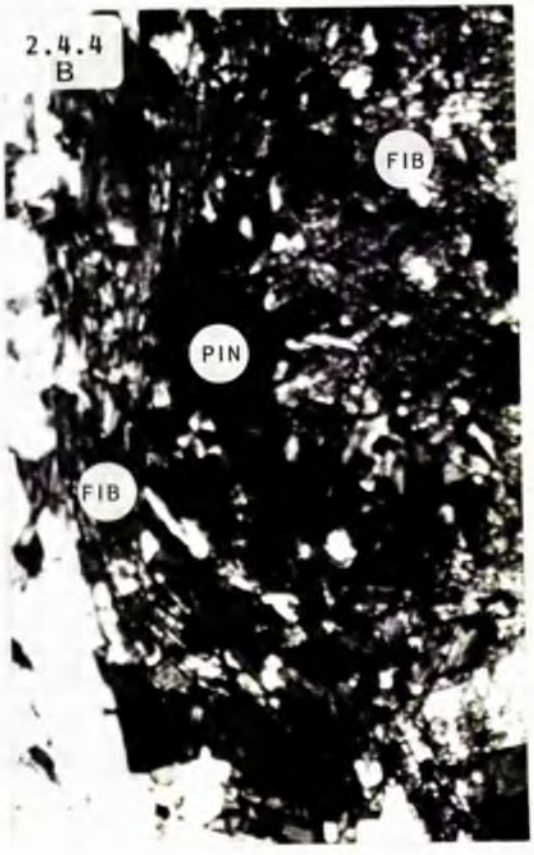
2.4.4
B
FIB
PIN
FIB

Fig. 2.4.5 Penetrative S_1, S_2 and S_3 fabrics developed in mica gneisses, near Narila. S_1 segregation banding, shown principally by alignment of biotite and M_1 sillimanite porphyroblasts enhances S_0. Preferred alignment of biotite marks both S_2 and S_3 fabrics. [MAG. X39 PPL]

Fig. 2.4.6 M_1 almandine garnet and cordierite both extensively corroded and replaced by M_2 aggregates of biotite + chlorite + Al_2SiO_5, particularly at grain rims, hence destroying any pre-existing stable grain boundaries that might have existed between the M_1 index minerals. Mica gneisses, near Narila. [MAG. X75, PPL]

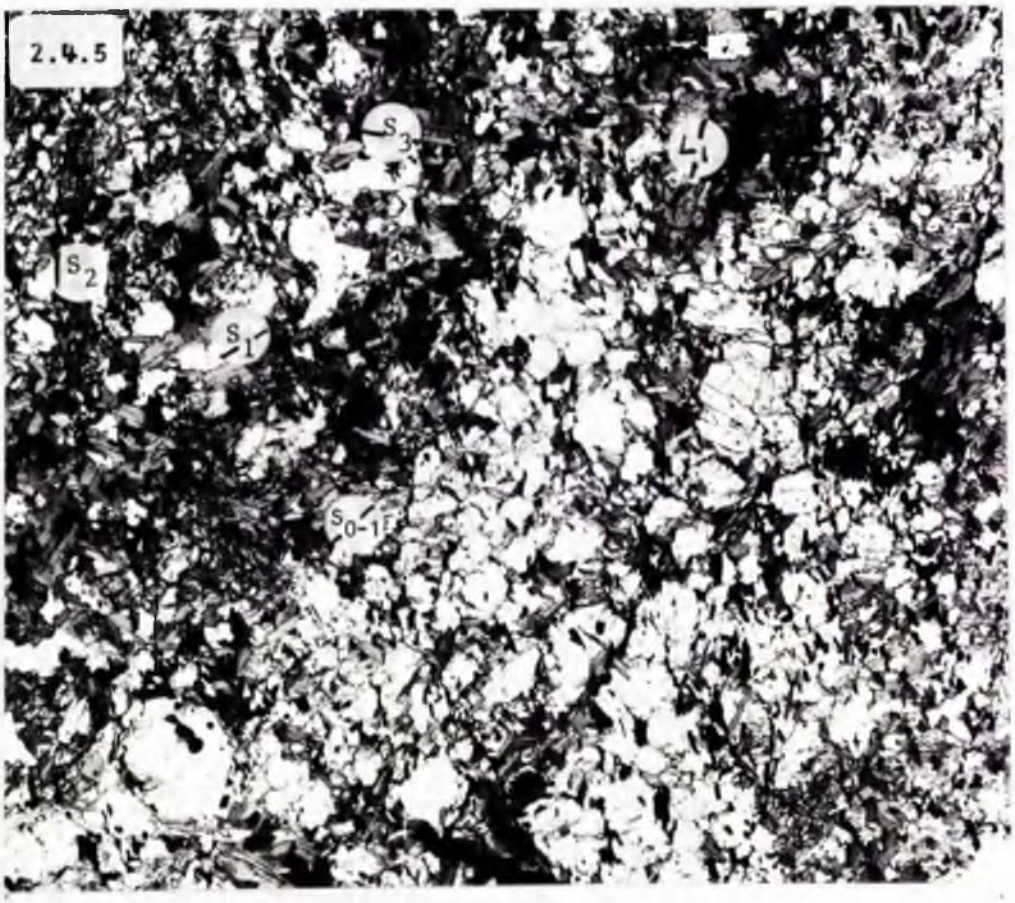
2.4.5
S_3
L_1
S_2
S_1
S_{0-1}

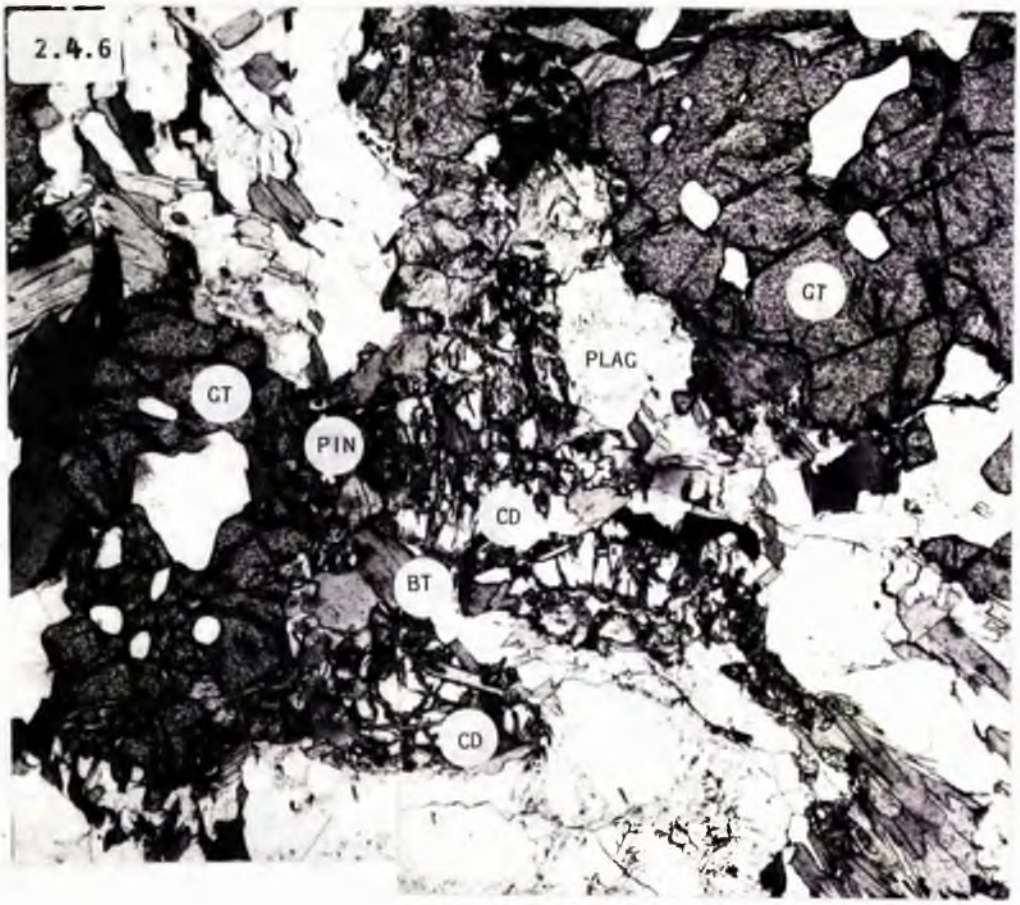
2.4.6
GT
PLAG
GT
PIN
CD
BT
CD

Fig. 2.4.7 Composite S_0-S_1-S_2 foliation in amphibolites near Narila. Almost complete recrystallisation of hypersthene-bearing D_1-M_1 assemblage in plagioclase-deficient bands. Minor hypersthene and magnetite preserved interstitially between M_2 hornblende in retrogressed bands (see Fig. 2.4.15).
[MAG. X30, PPL]

Fig. 2.4.8 Petrogenetic grid illustrating the metamorphic reactions which constrain the range of metamorphic conditions during D_1-M_1. Curves 1-10 are indicative of the following reactions:

1. Aluminosilicate triple point (after Holdaway, 1971).
2. Muscovite + quartz = K-feldspar + sillimanite (after Helgeson et al., 1978).
3. Tremolite + dolomite = forsterite + calcite + CO_2 (Metz, 1976) + H_2O.
4. Epidote + quartz = grossular/andradite + anorthite (Winkler, 1979) + H_2O.
5. Calcite + quartz = wollastonite (Turner, 1980).
6. Low temperature stability curve for meionite formation (Ellis, 1978).
7. Biotite + garnet + quartz = hypersthene + cordierite + K-feldspar + H_2O (Hess, 1969; Campbell, 1980).
8. Granite melting curve (Tuttle & Bowen, 1958; Merrill et al., 1970).
9. (9') Sillimanite + biotite + quartz = cordierite + K-feldspar + H_2O (Holdaway & Lee, 1977).
10. Cordierite = garnet + sillimanite + quartz (Richardson, 1968).

The stability field of D_1-M_1 conditions is marked by the hatched area 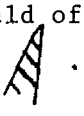 .

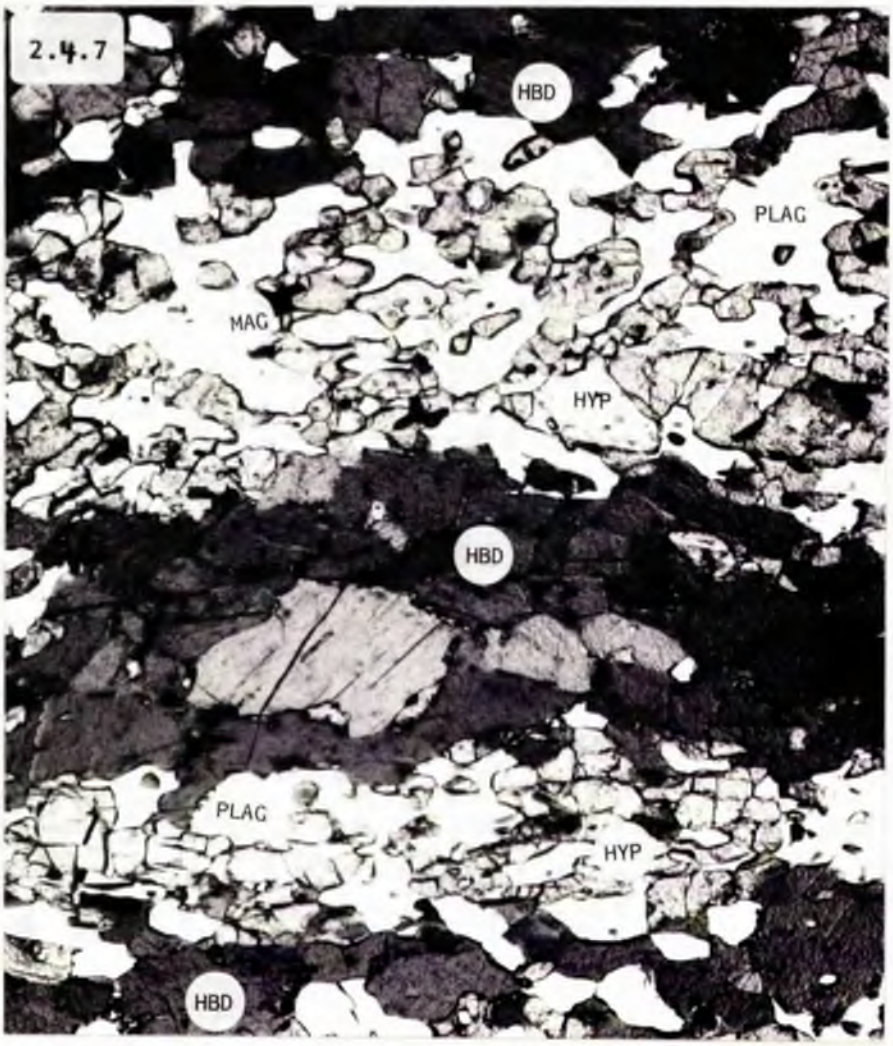
2.4.7
HBD
PLAG
MAG
HYP
HBD
PLAG
HYP
HBD

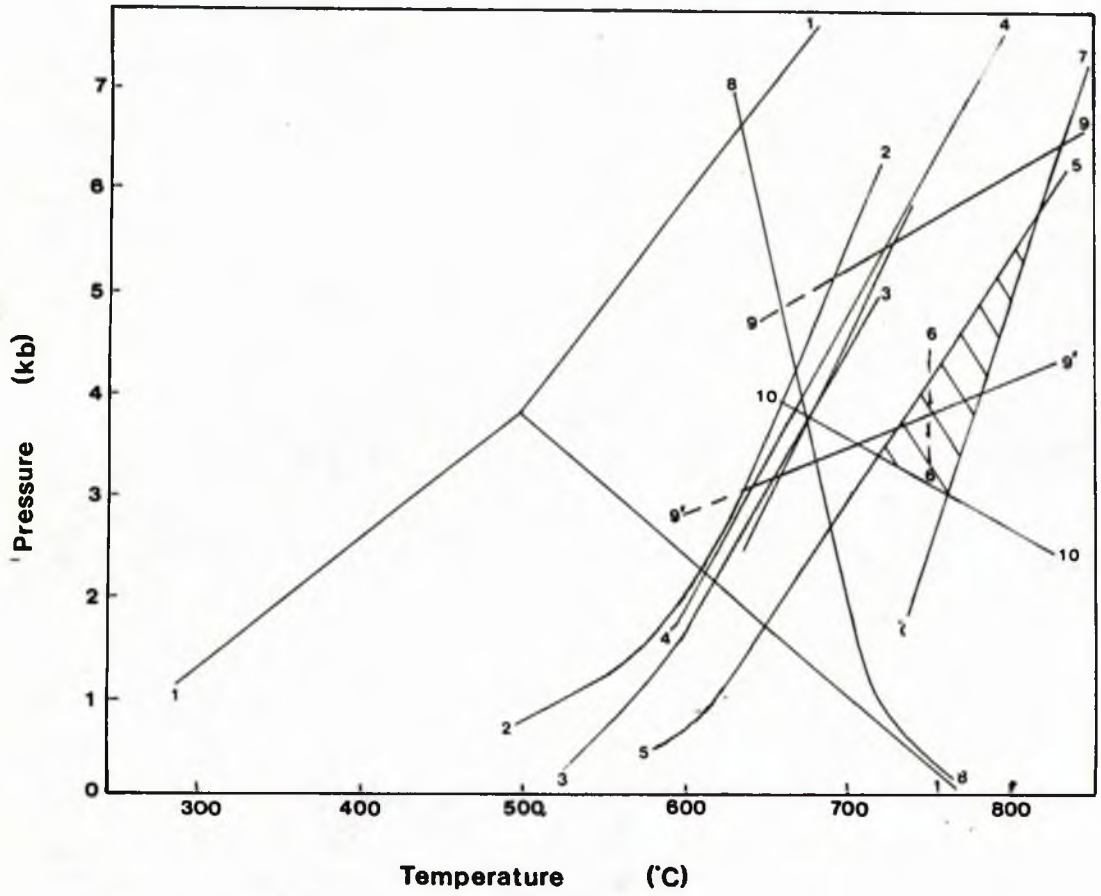
Pressure (kb)
Temperature (°C)
0
1
2
3
4
5
6
7
300
400
500
600
700
800

Fig. 2.4.8

Fig. 2.4.9 Within bands lacking M_1 sillimanite and almandine garnet, cordierite is typically retrogressed to aggregates of andalusite, chlorite, biotite and muscovite. Mica gneiss, Narila.
[MAG. X120, PPL]

Fig. 2.4.10 M_1 almandine garnet corroded and replaced by aggregates of biotite + chlorite + quartz. Mica gneiss, Narila.
[MAG. X30, PPL]

Fig. 2.4.11 M_1 cummingtonite corroded and replaced mainly by biotite at its margins and along cleavages. Mica gneiss, Narila.
[MAG. X75, XPL]

Fig. 2.4.12 Corrosion of M_1 sillimanite at grain boundaries and along cleavages, with nucleation of M_2 fibrolitic sillimanite either as dense mats on adjacent M_1 biotite (A) or, predominantly, on the M_1 sillimanite itself (B). Mica gneiss, Narila.
[MAG. X75, PPL (A); X75, PPL (B)]

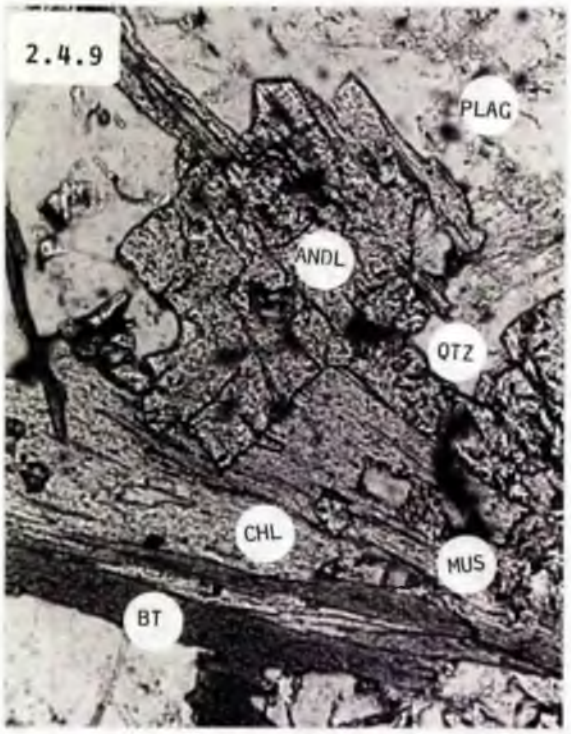
2.4.9
PLAG
ANDL
QTZ
CHL
MUS
BT


2.4.10
BT
GT

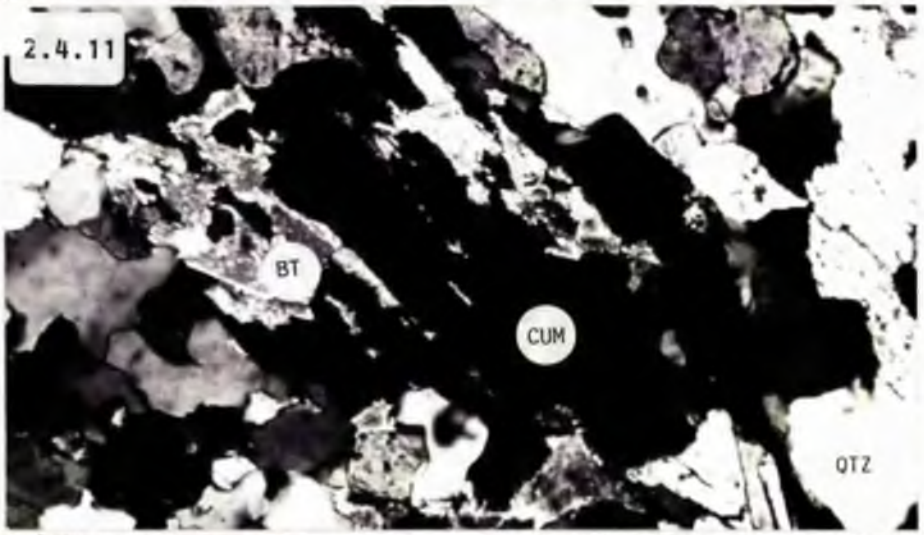
2.4.11
BT
CUM
QTZ


2.4.12
A
SILL
BT
FIB
QTZ

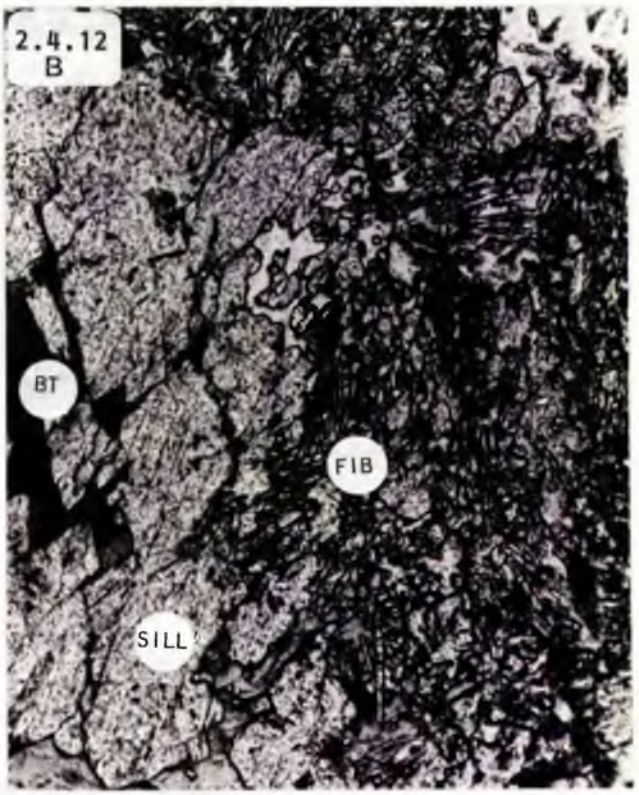
2.4.12
B
BT
FIB
SILL

Fig. 2.4.13 M_1 hypersthene fractures and embayed particularly at grain margins, with several grains enclosed by large poikiloblasts of M_2 hornblende. These are elongate and aligned within the composite S_0-S_1-S_2 foliation. Magnetite occurs as small aggregates at the hypersthene/hornblende contacts. Amphibolites, north of Narila.
[MAG. X7½, PPL]

Fig. 2.4.14 Large, irregularly-shaped poikiloblasts of M_2 hornblende enclose a pre-existing assemblage (M_1) which comprises diopside, plagioclase, chalcopyrite, pyrrhotite and magnetite. The diopside and ore minerals all have rounded, embayed grain boundaries. Individual ore grains delineate the S_0-S_1 fabric. Ore-bearing amphibolites, Hällinmäki Mine.
[MAG. X7½, PPL]

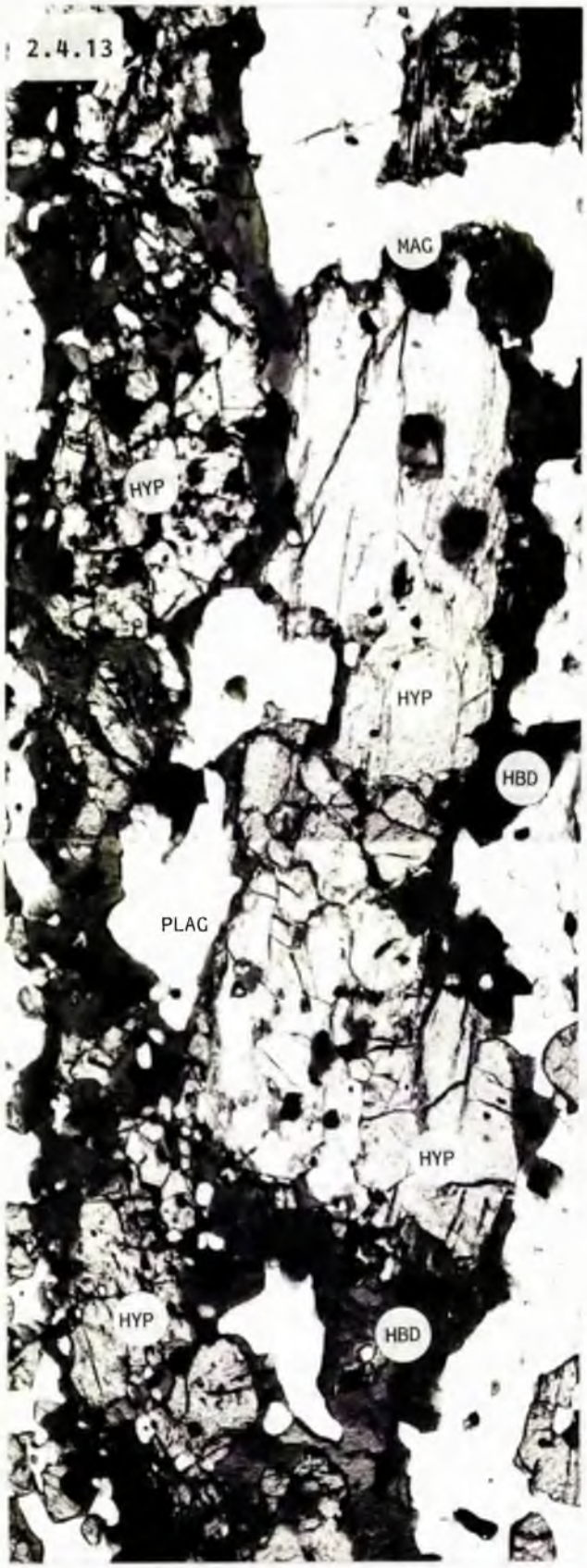
2.4.13
MAG
HYP
HYP
HBD
PLAG
HYP
HYP
HBD


2.4.14
MAG
HBD
DIOP
PYRR
CHAL
DIOP

Fig. 2.4.15 Prior to complete retrogression of the D_1-M_1 assemblage, hypersthene occurs together with magnetite as small interstitial blebs between grains of M_2 hornblende. Amphibolites, Narila. [MAG. X120, PPL]

Fig. 2.4.16 M_1 cummingtonite altered to green M_2 hornblende around grain margins and extensively along cleavages. Amphibolites, Kiviniemi. [MAG. X120, PPL]

Fig. 2.4.17 M_1 calcic garnet embayed and rimmed by a thin mantle of M_2 epidote. Calc-silicate skarn, Karrankalahti. [MAG. X75, PPL]

Fig. 2.4.18 Calcic garnet M_1 porphyroblasts largely replaced by small irregularly shaped grain aggregates of epidote + quartz. Note the mantling zone which consists predominantly of plagioclase + quartz. Amphibolites, Huutoniemi. [MAG. X75, PPL]

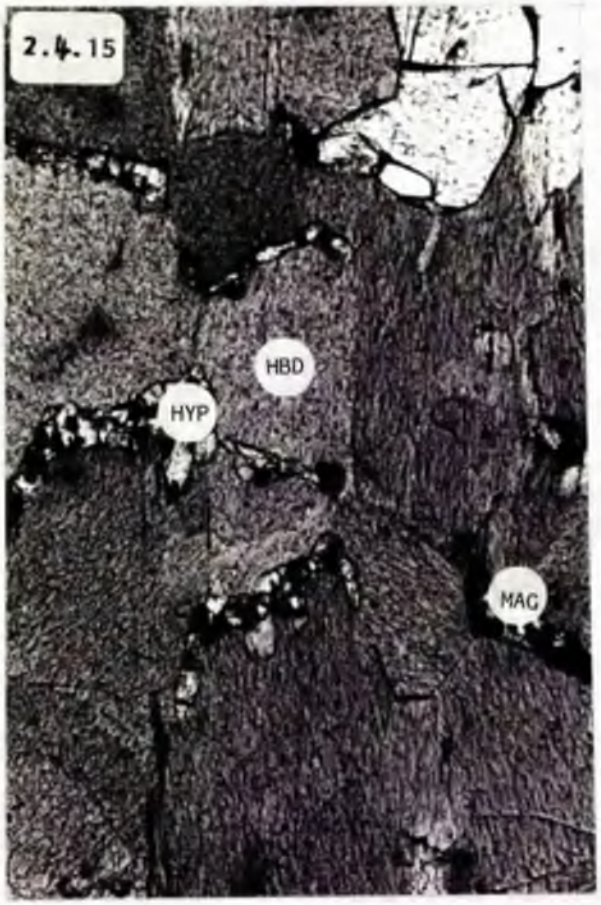
2.4.15
HBD
HYP
MAG


2.4.16

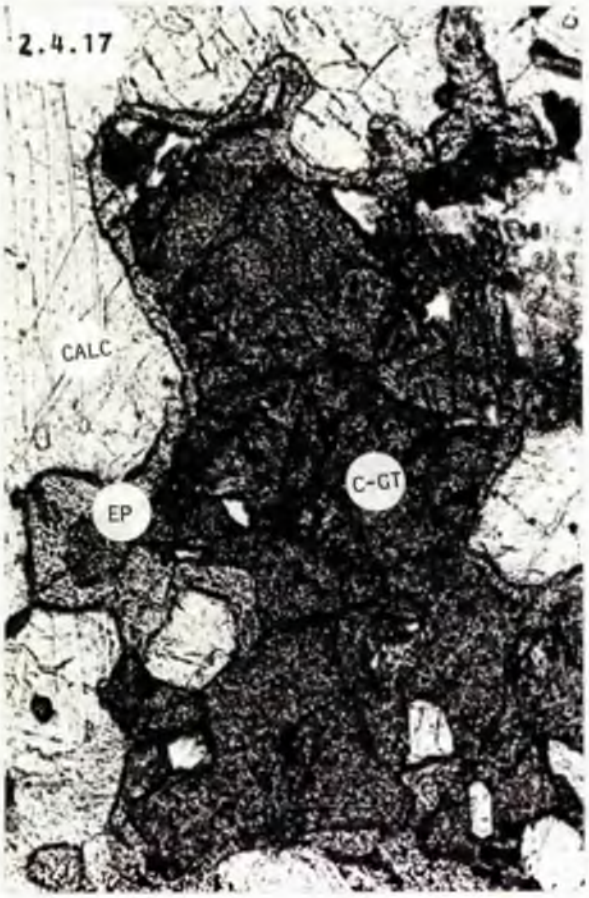
2.4.17
CALC
EP
C-GT


2.4.18
C-GT
PLAG
QTZ

Fig. 2.4.19 Selective replacement of large multiply-zoned M_1 calcic garnet porphyroblast by M_2 epidote. Calc-silicate skarn band within marble, Hällinmäki Mine.
[MAG. X75, PPL]

Fig. 2.4.20 M_1 scapolite rimmed and replaced by M_2 epidote in calc-silicate skarn, Narila.
[MAG. X75, XPL]

Fig. 2.4.21 Petrogenetic grid outlining the metamorphic reactions used to delimit the metamorphic conditions which prevailed during D_2-M_2. Curves 1-9 represent the following reactions:

1. Pyrophyllite = Al_2SiO_5 + quartz (Turner, 1980)
2. Dolomite + quartz + H_2O = tremolite + calcite (Turner, 1980)
3. Tremolite + calcite + quartz = diopside + CO_2 + H_2O (Turner, 1980)
4. Zoisite + quartz = grossular + anorthite + H_2O (Winkler, 1979)
5. Antigorite = forsterite + talc + H_2O (Turner, 1980)
6. Al_2SiO_5 triple point (Holdaway, 1971)
7. Fe-chlorite + quartz = almandine + H_2O (Turner, 1980)
8. Muscovite + quartz = K-feldspar + sillimanite (Helgeson et al., 1978)
9. Sillimanite + biotite + quartz = cordierite + K-feldspar + H_2O (Holdaway & Lee, 1977)

The stability field for D_2-M_2 conditions is marked by the hatched area and an arrow is used to mark the most likely reaction path between D_1-M_1 conditions and those in D_2-M_2.

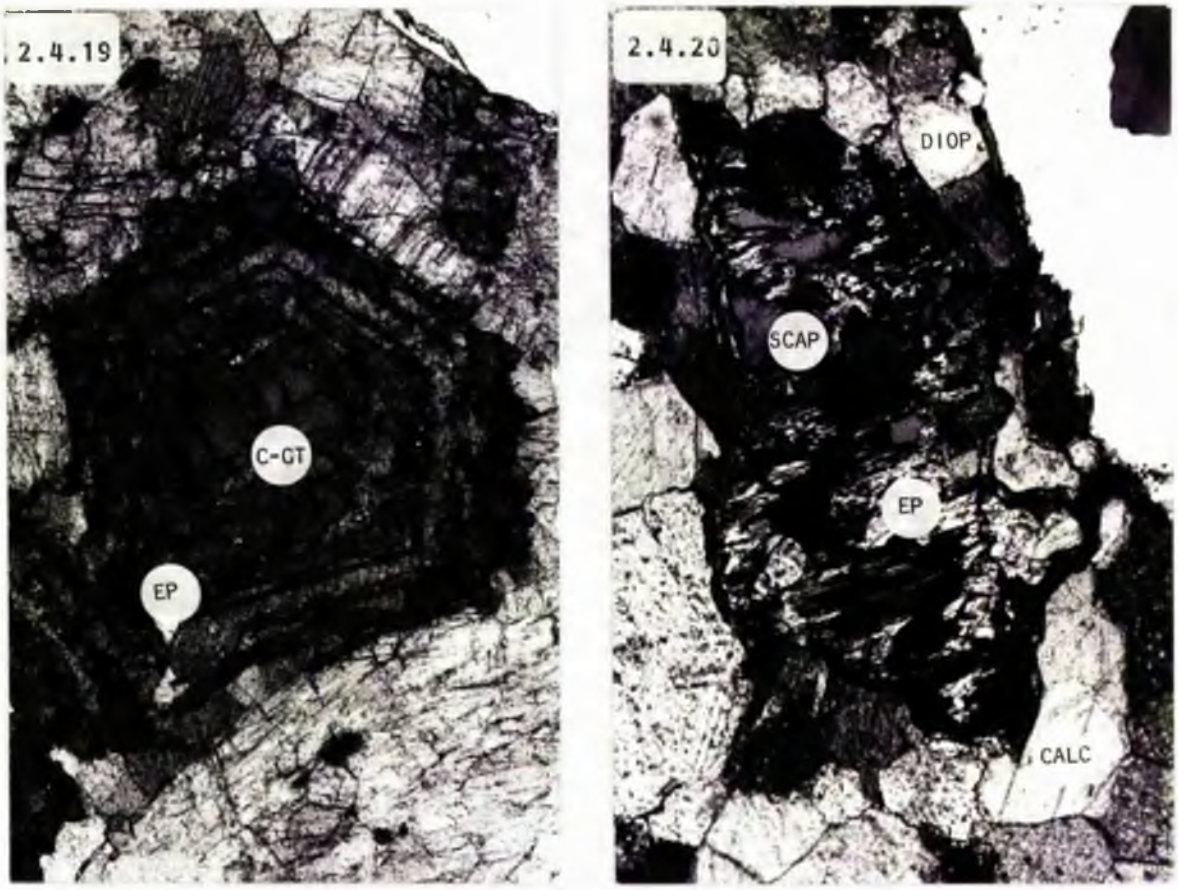
2.4.19
C-GT
EP
2.4.20
DIOP
SCAP
EP
CALC

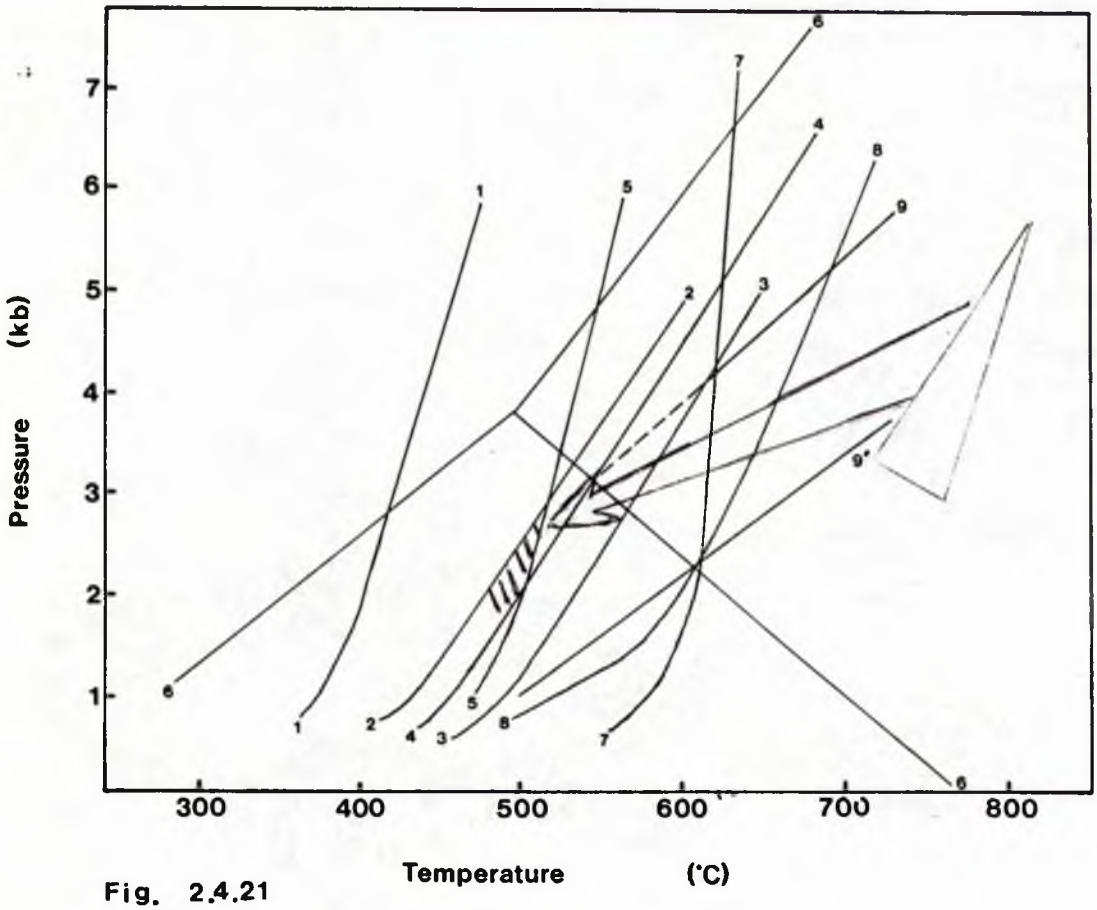
Pressure (kb)
1
2
3
4
5
6
7
300
400
500
600
700
800
Temperature (°C)

Fig. 2.4.21

SECTION 2

PART 5

Summary of the tectono-metamorphic development and syn-kinematic intrusive history of the Virtasalmi District and the kinematic interpretation and regional correlation

A summary of the principal tectono-metamorphic features and the relative sequence of emplacement of the main igneous intrusions and vein neosomes is presented in Table 2.5.1.

The observed sequence of polyphase deformation, the grade of peak metamorphism and the composition and relative age of emplacement of the igneous intrusions established in this study is broadly similar to that recognised in the Rantasalmi-Haukivesi area (Gaál & Rauhamaki, 1971), 25 km east of Virtasalmi (see Fig. 1.1.2). No other comparable studies have been carried out (or are published) in the Svecofennides within a 50 km radius.

Although there is obviously a need for structural studies in the area between Haukivesi and the Virtasalmi District, preliminary observations in the intervening area by the author and staff from the Exploration Department of Outokumpu Oy. would seem to suggest that the deformational sequence is at least consistent with that recorded in the adjacent areas (Gaál & Rauhamaki, 1971; this study).

In the Haukivesi area better exposure, an apparently smaller number of syn-kinematic intrusions, and less intense overprinting by later fabrics, provides more information on

the nature of D_1 structures than can be elucidated in the Virtasalmi District. Within the Haukivesi area, D_1 structures are described as major south-facing recumbent folds with associated thrusts (Gaál & Rauhamaki, 1971), while in the Virtasalmi District, D_1 is only expressed or preserved as a few small isoclinal folds, and as an axial planar S_1 fabric. The discordance of the latter to S_0 in places does however suggest the presence of larger than outcrop scale F_1 folds. However, it was not possible to establish what the principal stress orientations were during D_1 in the Virtasalmi District.

In Section 2, Part 1, it was demonstrated that the dominant structure in the Virtasalmi District is a major NW-SE-trending F_3 fold structure which refolds large tight-isoclinal F_2 folds (Map 1). In order to determine the prevailing principal stress orientations during D_2 it is necessary first to remove the effects of regional D_3 deformation. The available data set means that this can only be done here simplistically, and requires the assumption to be made that pre-D_3 orientations can be restored mainly by removal of the principal E-W shortening component responsible for the formation of the major NW-SE-trending F_3 fold structures. This exercise is valid only if it is recognised as a preliminary investigation, and as long as the limitations of the approach are understood.

Removal of the E-W D_3 principal shortening component over the Virtasalmi District suggest that the main F_2 folds must have had a more E-W trending attitude at the time of their development that their present attitude suggests. This is an important point with respect to attempts to correlate structures regionally as F_2 structures in the Haukivesi area

are tight-isoclinal folds reckoned to have had E-W axial trends (Gaál & Rauhamaki, 1971).

The postulated principal stress orientations for D_2 in the Virtasalmi District at the time of F_2 fold formation are illustrated schematically in Fig. 2.5.1(a). The orientation of σ_3 in Fig. 2.5.1(a) is based upon recognition of an L_2-M_2 mineral lineation which is observed to plunge subparallel to F_2 fold hinges at Narila. This is taken to indicate a stretching direction and it is concluded that the parallelism of L_2-M_2 with F_2 fold hinges is most likely to have resulted from rotation of F_2 fold hinges towards the finite extension direction during progressive D_2 deformation (c.f. Bell, 1978). This interpretation is supported by the concurrence of L_2 parallelism with F_2 hinge zones in areas of particularly high D_2 strain (deduced from intense flattening and attenuation of pillow lavas-tubes in the same area). However this evidence was contradicted at one exposure near Hällinmäki Mine, where L_2 was noted to be virtually orthogonal to the F_2 fold plunge in zones of intense foliation development. Due to the paucity of the data set, however, it was impossible to determine which example is more representative in the study area, or whether marked local variations are common. The decrease in metamorphic conditions from D_1 to D_2 indicated by M_1 and M_2 mineral assemblages suggests that deformation during D_2 occurred at a higher structural level than that during D_1.

In the Haukivesi area, F_2 folds were noted to be subsequently deformed and rotated towards NW-SE by a strong simple shear stress, accompanied by development of subvertically plunging 'right-hand' folds (i.e. with a sinistral sense), together with associated shear zones. While the orientation of D_3 structures

within the Virtasalmi District is similar to that recorded at Haukivesi, there is a difference in that flexural slip folds were developed in the Virtasalmi District, while slip-similar folds were formed in the Haukivesi area. Also, a strong shear component only became predominant late in D_3 (i.e. post most F_3 fold development) within discrete high strain zones in the Virtasalmi District.

The principal stress orientations deduced for D_3 in the Virtasalmi District are presented in Fig. 2.4.1(b). The development of NW-SE-trending shear zones in D_3 and the curvilinear nature of F_3 fold hinges in some D_3 high strain zones suggests that there was an additional shear strain component in D_3. This appears to have become important only late in D_3. It should be noted that the orientations of σ_2 and σ_3 in Fig. 2.5.1(b) may be dependent on resolution of the shear component responsible for producing curvilinear F_3 hinges, and it was not possible to resolve this in 3-dimensions in this study.

D_3 deformation occurred at higher crustal levels than during D_2, suggesting that there was continued uplift from D_1-D_3. It can be seen from comparison of Figure 2.5.1(a) and Figure 2.5.1(b) that between D_2 and D_3 the directions of maximum stress are switched, with the northern component of shortening in D_2 replaced by an E-W component during D_3. Later deformational events, D_4-D_7, are less penetrative regionally and are considered to be related to continued uplift.

Major shear zones and wrench faults (e.g. Halden, 1982) with the same orientation as late D_3 structures in the Virtasalmi District are also observed to affect the Karelian cover sequence to the east. Koistinen (1981) has suggested that these structures may represent the first regionally

correlatable structures common both to the Karelide and Svecofennide terranes. In the Karelides the polyphase deformational sequence can be explained by crustal thickening in response to overthrusting of cover units in nappes and recumbent folds onto basement, followed by more zonal upright structures formed as a result of gravitational and thermal disequilibrium in the overthrust Archaean crust (Ward, 1987). However, there is no Archaean basement to the Svecofennides (Huhma, 1986), and a number of other important dissimilarities exist between the two terranes. These include the intrusion of a considerably greater number of syn-kinematic igneous masses in the Svecofennides, and the fact that in parts of the latter terrane emplacement of these intrusions was apparently contemporaneous with volcanism and sedimentation (Kouvo & Tilton, 1966; Huhma, 1987). Moreover, the earliest phases of deformation in Karelia were contemporaneous with volcanism in the Svecofennides, for example at Tampere and Skaldo (Huhma, 1986). These features point to major differences in styles and timing of deformation in the two terranes.

The observed sequence of deformation, metamorphism and syn-kinematic intrusion is interpreted as the result of progressive accretion of the Svecofennide terranes onto the margin of the Archaean Sarmatian craton (c.f. Park, 1985). The section exposed in the Virtasalmi District is considered to represent syn-kinematic deformation and intrusion at mid-crustal levels.

TABLE 2.5.1 Summary of the geological history of the Virtasalmi District

	STRUCTURES	METAMORPHISM	IGNEOUS MASSES & VEIN NEOSOMES
		Extensive pre-kinematic syn-volcanic hydrothermal alteration. (Greenschist or amphibolite facies)	Predominantly (submarine) basaltic volcanism; emplacement of cogenetic peridotites and gabbros.
D_1	Small isoclinal folds (F_1); segments of larger isoclinal folds; penetrative axial planar fabric (S_1) mostly subparallel to S_0. No measurable mineral lineation (L_1).	Amphibolite facies - granulite facies transition zone assemblages (M_1). Segregation banding in amphibolites and gneisses parallel to S_1 resultant from metamorphic differentiation. Almandine porphyroblasts in gneiss; diopside poikiloblasts in amphibolite - late D_1 static recrystallisation.	K-feldspar-bearing partial melt segregation patches in gneiss. Emplacement of gabbro and diorite intrusions and trondhjemite, basalt, granite and diorite minor intrusions, some strongly foliated.
D_2	Large tight-isoclinal folds (F_2) - similar style; axial planar fabric (S_2); zones of high and low strain; transposition of S_0, S_1 into composite foliation S_0-S_1-S_2; mineral lineation (L_2).	Lower amphibolite facies assemblages (M_2). Pervasive retrogression by infiltration metasomatism. Segregation banding in amphibolites and gneisses.	Quartz-rich veins and patches in skarns derived from retrogression of M_1 andradite. Intrusion of gabbros, diorites, quartz diorites, biotite and porphyritic granodiorites, and dykes of trondhjemite, biotite-amphibolite, dolerite and composite dolerite-granodiorite dykes.
D_3	Large F_3 folds, many parasitic flexural slip folds with curvilinear hinges and attenuated limb zones. Brittle faults on short limbs (late D_3). F_2-F_3 interference structures. Axial planar mineral growth, spaced fracture cleavage and crenulation cleavage (S_3).	Localised greenschist-amphibolite facies transition zone assemblages (M_3).	Small gabbro, diorite, granodiorite and granite plutons. Basic dykes and composite/multiple dykes. Aplitic veins intruded axial planar to F_3 folds. Pegmatite veins.
D_4	Minor open-tight steeply plunging folds (F_4) with axial planes trending WNW-ESE. Subvertical axial planar fracture cleavage (S_4). This deformation only expressed in northern half of area.	Local epidotisation in fracture cleavages.	Aplitic veins intruded concordantly with F_4 axial planes. Composite pegmatites. Amphibolite dykes. Quartz diorite plutons.
D_5	Open-tight steeply plunging folds (F_5) with NNW-SSE-trending axial planes. Subvertical axial planar spaced fracture cleavage (S_5). F_5-F_2 and F_5-F_3 interference structures.	Local retrogression in fracture cleavages.	Remobilisation of pre-existing vein material concordant with F_5 axial planes. Pegmatoid veins.
D_6	Open-tight upright folds (F_6) with NE-SW-trending axial planes. Subvertical axial planar spaced fracture cleavage (S_6). Narrow ductile/brittle wrench shear/fault zones. Interference structures.	Vein-filled fracture cleavages, retrogression in fracture cleavages.	Quartzofeldspathic vein networks emplaced within ductile/brittle shear/fault zones. Pegmatites, some composite. Quartz diorite, trondhjemite minor intrusions.
D_7	Small isolated upright folds (F_7) with ENE-WSW-trending axes. Poorly developed axial planar fracture cleavage (S_7). F_7-F_6 interference structures.	Retrogression in fracture cleavages.	
D_{late}	Several sets of subvertical normal faults; a set of low angle reverse faults; low angle normal faults.		Aplites, pegmatites.

Figure 2.5.1a D_2 Principal stress axes, i.e. assuming removal of D_3 principal stress.

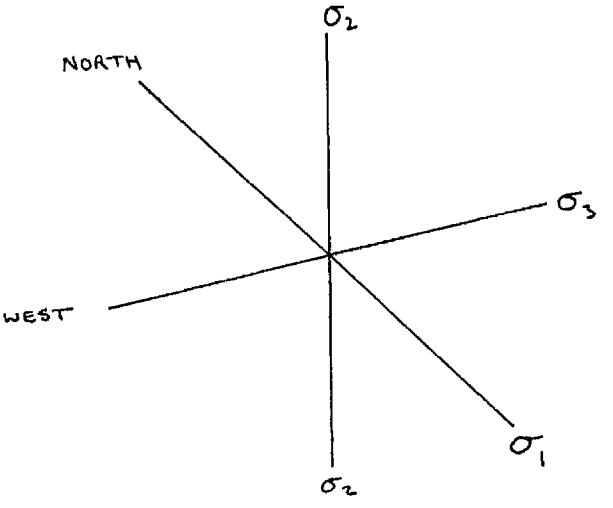

Figure 2.5.1b D_3 Principal stress axes.

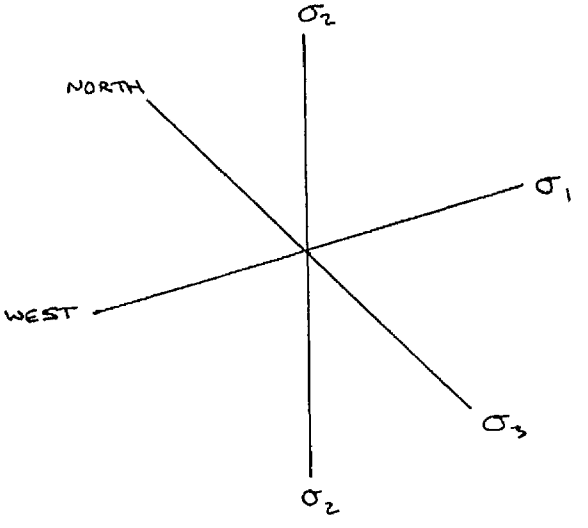

SECTION 3

Amphibolites, skarns and Cu-deposit

PART 1

The geochemistry and origin of the amphibolites and calc-silicate skarns

3.1.1 Introduction

As indicated in Section 1, Part 2, field evidence which clearly demonstrates the original nature of the amphibolites in the Virtasalmi District is generally lacking. However, pillow lavas and/or lava tubes, tuffs, massive lavas and sills and/or dykes have locally been recognised within low strain zones from isolated exposures throughout the study area (Section 2, Part 1,2(i)). While this points to an igneous-volcanic derivation for at least part of the amphibolite sequence, it was considered necessary to carry out a geochemical study on samples reckoned to be representative of all the lithological variations observed in the amphibolites to ascertain their origin(s) and the nature of any chemical variation found in them. This study was considered to be of particular importance to the project in view of the close spatial relationship observed between amphibolites and the ore occurrences at Hällinmäki Mine and elsewhere in the study area (Section 3, Part 2).

Also, as field evidence indicates the presence of calc-silicate skarn lithologies of several different types (Section 1, Part 2) including some which display gradational

contacts with amphibolites, it was decided to study the geochemistry of these skarns both to establish their origins and to examine their relationships with the amphibolites in the study area.

The amphibolites referred to in this Section all pre-date D_1. The geochemistry of syn-tectonic amphibolitic dykes is discussed in Section 4.

3.1.2 Analytical techniques, methodology (and terminology)

A total of 170 samples consisting of 140 amphibolites not visibly skarned and 30 variably skarned (based on petrography) lithologies were collected from localities throughout the study area and analysed for major, trace and LREEs using XRF techniques. These samples/analyses are considered representative of all the lithologies exposed.

The methods of collection, preparation and analysis are presented in Appendix 1. Tabulated geochemical analyses are contained in Appendix 2, while brief petrographic descriptions are provided in Appendix 3. Sample localities are indicated on Map 8.

3.1.3 General chemical characteristics

3.1.3(i) Previous studies (which have attempted to use geochemistry to demonstrate the origin of amphibolites) have found that distinctions between ortho- and para-amphibolites cannot always be made by considering element abundances alone, especially where Cr, Ni and Ti contents are low (Leake, 1964). However, it has been shown to be possible to make this distinction by comparing trends of variation in element abundances with

known igneous and sedimentary trends (Evans & Leake, 1960; Leake, 1964).

In subsequent studies, very few workers (e.g. Muecke et al., 1985; Rock & Waterhouse, 1986) have been able to demonstrate a sedimentary origin (i.e. by admixture of dolomite and pelite) for amphibolites. In most studies an igneous origin has been established by virtue of the nature of systematic changes in certain inter-element ratios which are considered most likely to reflect magmatic differentiation. Either niggli mg (Leake & Evans, 1960; Wilson & Leake, 1972; Clough & Field, 1980); or major element ratios e.g. FeO*/(FeO* + MgO*) (Graham, 1976); or the Solidification Index (S.I.) (Jelínek et al., 1980); or trace elements e.g. Zr (Weaver et al., 1982), have been used in past studies as an index of differentiation.

However, in some metamorphic-metasomatic environments the component elements used to determine values of S.I., FeO*/(FeO* + MgO*), and niggli mg have been shown to be very mobile (Cann, 1970; Pearce & Cann, 1973; Humphris et al., 1978; Mottl & Holland, 1978; Donnelly et al., 1979; Gibson et al., 1983). In contrast, Zr has been found to be relatively immobile under most conditions (Cann, 1970; Pearce & Cann, 1973; Floyd & Winchester, 1975; Weaver & Tarney, 1981; Weaver et al., 1982), although it may be mobile in rocks undergoing CO_2-metasomatism (Hynes, 1980; Murphy & Hynes, 1986), or extreme hydrothermal alteration (McGeehan & MacLean, 1980; Schiffman et al., 1987). In this study Zr was used as the main differentiation index as it was considered to be the element least likely to be affected by any alteration.

3.1.3(ii) Figures 3.1.1a-d are element distribution plots for Virtasalmi amphibolites. Good linear covariation is expressed between Zr, a high field strength (HFS) element, which is considered a reliable indicator of fractionation (Sceal & Weaver, 1971), and Ce, the HFS elements Nb, TiO_2 and P_2O_5 all of which are incompatible in basaltic systems (Wood, et al, 1981). A linear distribution of this kind is usually considered to indicate relative immobility of all these elements (e.g. Weaver et al, 1982). However if there is evidence to suggest that a CO_2-rich fluid phase has at some time interacted with the rocks, then a linear data distribution can be interpreted to result from systematic changes in inter-element ratios during metamorphism and that this can lead to a greater spread in Zr abundances (i.e. the differentiation index) without producing a greater scattering when the latter is plotted against the other HFS elements. As the variable and high CaO content of some of the amphibolites had led Hyvärinen (1969) to suggest that the Virtasalmi amphibolites had possible undergone CO_2 metasomatism, then this possibility had to be investigated.

Murphy & Hynes (1986) considered two main cases where CO_2 metasomatism might occur.

1. Where several different mineral assemblages are developed (at the same P-T conditions) this is considered to indicate ineffective X_{CO_2} buffering, i.e. a range of X_{CO_2} with mobility of the HFS elements controlled by chemical potential differences between the different assemblages.

2. Where uniform assemblages are developed, X_{CO_2} is externally buffered and mobility of HFS elements will be controlled by partition of these elements between the mineral assemblages and the fluid. In this example the authors demonstrated depletion of the HFS elements Zr and Y, with progressive carbonation, which correlates with increasing modal abundance of calcite. Considerable geochemical variation was observed in CO_2-rich lithologies, and an increased but systematic linear spread of data noted on binary scatter diagrams.

In this present study the amphibolites were not analysed for CO_2 hence no direct comparisons can be drawn with the work of Murphy & Hynes (1986). Nevertheless the relative mobility of the HFS elements Zr and Y can be examined in a number of other ways.

Within Virtasalmi amphibolites a banding (S_1 sub-parallel to S_0), defined by different M_1 mineral assemblages, is observed to occur at different scales, from sub-millimetre scale to a few metres wide in individual outcrops, up to the interlayering of petrographically distinct units hundreds of metres thick (Sections 1 & 2). The presence of the finer-scale layering in particular is considered to indicate that equilibrium conditions existed within individual bands and that there was disequilibrium between bands. These differences are reflected in variations in mineral compositions, e.g. variations in Ca content of plagioclase, between layers and units. The presence of this layering is considered indicative of ineffective CO_2 buffering, and it is inferred that any

mobility of the HFS elements, Zr and Y would have been controlled by chemical potential differences between the different mineral assemblages (example 1 above, Murphy & Hynes, 1986). The development of low variance skarn assemblages (Type 2) in very narrow zones at all marble-amphibolite contacts is supportive of this model, and it is also considered evidence for the limited nature of interband diffusion, given that the greatest chemical potential gradient would have existed between marble and amphibolite.

Also, the relative mobility of these elements within discrete units of amphibolite can be examined more rigorously using spidergrams of Rock/MORB or Chondrite-normalised data. Figures 3.1.2a, b are spidergrams for two distinct interlayered amphibolites exposed at Hallinmaki Mine. The units are respectively 3 m and 30 m thick where sampled. It is clear from these diagrams that within each unit, inter-element ratios and absolute element abundances of Zr, Y, Ti, P and Nb are very consistent, despite the variable and high CaO contents observed in these lithologies. These observations appear to rule out any partial equilibration produced in response to chemical potential gradients between layers. A similar consistency in the same inter-element ratios has also been noted in studies involving calcification (often in the form of zeolitisation) of basaltic material in lower grade terranes (e.g Floyd, 1986). Hence these inter-element ratios most probably reflect original processes.

In contrast, Fig. 3.1.3 is a spidergram plot for samples taken across the irregular and gradational contact

from amphibolite to a Type V garnet skarn (Section 1, Part 2) at T370m in Hällinmäki Mine. This skarn is considered to have formed from an amphibolite protolith by alteration including carbonatisation. Its origin and nature are discussed in more detail later in this section. However, it can be seen from Fig. 3.1.3 that the inter-element ratios between the HFS elements, Zr and Y, are all changed and in a non-systematic manner. The same pattern of variation was found in similar skarn types throughout the area (later this section), hence it appears that disruption of these inter-element ratios only occurs with extreme alteration characterised by development of calc-silicate skarn mineral assemblages.

In Fig. 3.1.1c all the calc-silicate skarns sampled are plotted. Although these skarn lithologies plot with a more scattered distribution, a well constrained linear relationship is still evident. As the covariation diagrams used in this section are primarily required to examine the original character of the amphibolites, and as many of the Type V skarn lithologies appear to be replacive in origin (Section 1, Part 2), analyses of skarns are only illustrated here on 2 diagrams (TiO_2 vs Zr (Fig. 3.1.1c) and Y vs Zr (Fig. 3.1.13)) to demonstrate that although the skarns have a more scattered distribution, the linear distributions displayed by amphibolites are not invalidated.

On balance therefore the linear distribution of elements shown by the amphibolites and observed in Figs. 3.1.1a-d is interpreted largely to reflect original processes, with very limited secondary redistribution having occurred. The trends displayed in these figures are considered to be closely

analogous to trends resulting from primary igneous fractionation processes, indicating an igneous-volcanic derivation for the Virtasalmi amphibolites.

In contrast, a scattered distribution results when the large ion lithophile (LIL) elements, i.e. Ba, Sr, Rb, Na and K, are plotted against Zr (Figs. 3.1.4a-e). As Zr was previously demonstrated to be relatively immobile, the observed distribution in the latter plots is considered to indicate mobility of the LIL elements during post-crystallisation alteration processes. Plots of CaO and SiO_2 against Zr also show a scattered distribution (Figs. 3.1.5a, b), and this is similarly interpreted.

Poorly defined trends are developed in plots of MgO, FeO* and La against Zr (Figs. 3.1.6a-c) and in plots of Cr and Ni vs Zr (Figs. 3.1.6d, e respectively). The distribution of analyses in the latter two plots is discussed in more detail later. The observed element distributions are considered to show igneous fractionation trends which have been modified as a result of post-crystallisation mobility of Mg and Fe, but to a lesser extent than for Ba, Sr, Na, K or Ca.

The apparent mobility of FeO*, MgO, Na_2O, K_2O and SiO_2 which is indicated from the above graphs confirms that use of niggli mg, FeO*/(FeO* + MgO), or S.I. as indicators of differentiation in Virtasalmi amphibolites is unwise, being likely to introduce scatter not attributable to the original rock-forming process.

One further point concerning the interpretation of the binary scatter diagrams has been raised by Aitchison (1984a,b) and Butler & Woronow (1986). These workers argue

that it is not possible to tell if the linear trend on co-variation diagrams is due to closure of the data set (i.e. analyses do not sum to 100%) or due to a strong linear association. However as the elements employed here seem to have behaved in a predictive way in accordance with their chemical properties, and as long as the exercise is recognised as being comparative, within the limits of such an approach, then the arguments of these authors are not considered to have any significance for data analysis in this study.

3.1.4 Nature of the chemical mobility

The nature, extent and relative timing of the alteration episodes which have caused the redistribution of elements noted in the aforementioned variation diagrams was investigated using geochemical analyses to back up field and petrographic observations.

3.1.4(i) Pre-D_1-M_1 alteration

(1) Evidence that the amphibolites have undergone pre-tectonic alteration was derived from observations on the nature of their relationship with certain skarn lithologies (Type III and V; see Section 1, Part 2) and this is considered below.

A) Around many of the Type III skarn patches in Virtasalmi amphibolites there is commonly a zone from 1 cm to 15 cm wide in which the amphibolite is bleached a light greenish-grey colour (Figs. 1.2.6, 1.2.2b and 3.1.7), in marked contrast to the surrounding dark greenish-grey-greenish-black

colour of unskarned amphibolite. Similar bleached zones have been described from around calc-silicate patches in Archaean metavolcanic lithologies (MacGeehan & MacLean, 1980). The often widespread extent of this alteration is demonstrated in Fig. 3.1.7.

The chemical changes associated with formation of the bleached zones were investigated by comparing the analyses from these latter zones with those from surrounding darker amphibolite and from the central portion of calc-silicate skarn patches in two examples.

In the first example described, the samples were collected from within an interconnected lava tube at Narila. The analyses are presented in Table 3.1.1a. The bleached zone is observed to have a higher content of SiO_2, Na_2O, Cu and S, and to a lesser extent Zr, Y, Ti and Co as well as a significantly lower content of Fe_2O_3*, CaO, MgO, K_2O, Ni, Zn, Ba, Sr and Rb, in comparison with the unbleached portion of the lava tube.

The second example is from within a massive amphibolite a few hundred metres west of Hallinmaki Mine. The analyses are presented in Table 3.1.1b. In this example the bleached zone has a higher content of SiO_2, TiO_2, Al_2O_3, Na_2O, K_2O, Y, Zr, Ga, Cu, S, Ce, Ba, Sr and Rb, and a lower content of Fe_2O_3*, MnO, MgO, CaO, P_2O_5, Co, Zn and Ni in comparison with the unbleached surrounding amphibolite.

Hence although there are minor differences between the two examples described, there is broad agreement in major changes in chemistry, with an increase in SiO_2, TiO_2, Al_2O_3, Na_2O, Cu, S, Zr and Y and decrease in Fe_2O_3*, MnO, MgO, CaO, P_2O_5, Zn and Ni noted in traverses from 'original'

composition to 'bleached' amphibolite. The significantly higher SiO_2 and Na_2O contents in the bleached zones points to spilitisation and silicification of the original amphibolite protolith, at least in the immediate vicinity of the skarn patches. In the second example the chemical changes resulted in formation of a rock of broadly andesitic composition from a basaltic protolith. Similar chemical transformations have been recorded elsewhere (MacGeehan & MacLean, 1980).

From Table 3.1.1a,b it is also evident that there are marked changes in inter-element ratios associated with development of the bleached zones and that even normally immobile elements, e.g. Zr, have been mobilised. This is generally considered to indicate that metasomatic fluid flow with high water-rock ratios was responsible for development of the altered lithology (Schiffman et al., 1987).

In contrast, consistent inter-element ratios for the Hallinmaki amphibolites (Group I, see Section 3.1.5, Fig. 3.1.8) are taken as further evidence that these samples, which were collected as far as possible from skarn patches, have 'immobile' element values that most probably reflect original igneous values.

B) The observation that Type III skarns have relict M_1 assemblages and are often restricted to within individual lava tubes suggests that they formed pre-D_1. In Section 1.2 it was also noted that although most of these skarns were observed to be ovoid in cross-section, in oblique cross-sections some were noted to be elongate parallel to lava tube margins (Fig. 1.2.15). Similar features were recognised by Barager (1983) who demonstrated that metasomatic fluid flow responsible

for formation of quartz and calc-silicate-rich hydrothermal precipitates, utilised pre-existing intra-pillow or intra-lava tube cavities in Archaean metavolcanic rocks, and that a zone of alteration in the basalt was developed around these vein-filled cavities.

Hence it is possible that some of the Type III skarns, specifically those that occur within lava tube-pillow lava exposures may have originated as cavity-filling hydrothermal precipitates. However the fact that similar skarn patches are also observed within more massive amphibolites suggests that at least in some instances, Type III skarn formation has resulted from replacive metasomatism of amphibolite protoliths. The lack of development of transitional bleached zones around some Type III skarns is attributed to conditions of higher fluid/rock ratios in these zones (see Wilson, 1959; Schiffman et al., 1987).

From other studies in volcanic terranes it seems unlikely that original porosity and permeability distributions in the rocks would be preserved past a very early stage in the development of a volcanic pile due to the likely ubiquitous circulation of H_2O and/or CO_2-rich fluids during cooling and/or burial metamorphism. Hence on balance it seems most likely that Type III skarn patches were formed syn-volcanically or were at least associated with a pre-tectonic phase of hydrothermal alteration.

However, it should be noted that there is some controversy over the mechanism by which calc-silicate patches similar to these Type III skarns have been formed in other metavolcanic sequences (Lydon & Jamieson, 1984). The argument

is essentially whether the patches do represent the conduits to a system of large-scale metasomatic fluid flow under conditions of high water: rock ratios (e.g. MacGeehan & MacLean, 1980) or whether they are indicative of extensive mineral transformations under conditions of low water : rock ratios (Lydon & Jamieson, 1984). Both models have important implications for the overall geochemistry of the amphibolites and in the prediction of ore occurrences.

The model of Lydon & Jamieson (1984) requires that pre-existing calcium- or gypsum-bearing veins were available to react with a chloritic host rock to form calc-silicate (epidote-rich) patches. In this model no large-scale transfer of chemical components is anticipated, while any evidence for the existence of these veins is destroyed during prograde reaction. While such reactions may occur, clear textural evidence showing preservation of primary igneous textures, despite drastic changes in whole rock and mineral chemistry, has been demonstrated to have taken place in the formation of some Archaean calc-silicate patches (MacGeehan & MacLean, 1980). Hence, while Lydon & Jamieson's model may be valid in certain circumstances, it does not invalidate models which postulate large-scale metasomatic fluid-flow. Theoretical models also predict formation of similar calc-silicate patches (epidote-quartz-chlorite assemblages) under conditions of high fluid : rock ratios, i.e. between 10 and 20 (Spooner & Bray, 1977). Furthermore, observations made in active oceanic ridge and geothermal areas suggest that the processes predicted in the latter model may be a common occurrence. In particular these observations counter claims by Lydon &

Jamieson (1984) that the formation of an essentially epidote + quartz assemblage, which requires a large H_2O flux with high Ca/(Mg + Fe), i.e. seawater that has already reacted with basalt, with a need to change pH, PO_2, activity Ca^{2+}, or temperature (equation 1)

$$2.00 \text{ chlorite} + 3.48\ Ca^{2+} + 10.6\ H^{+} + 0.30\ O_2 =$$
$$1.89 \text{ epidote} + 0.78 \text{ quartz} + 5.00\ Mg^{2+} + 3.28\ Fe^{2+} + 10.37\ H_2O$$

in order to form epidote at the expense of chlorite, is unlikely. In fact alteration of basalt by seawater by this mechanism and resulting in epidote-rich assemblages seems to occur at present day oceanic ridges (Humphris & Thomson, 1978).

Also, in considering the economic implications for these conflicting models, and models which link large-scale metasomatic fluid flow to the development of exhalative ore-bodies in particular, Lydon & Jamieson argue that many metals which occur as diadochic substitutions in common rock-forming minerals will be leached mostly under conditions of low bulk water : rock ratios, e.g. during thermal metamorphism (Lydon, 1981). However, in many high heat flow areas, e.g. active ridge or other volcanic geothermal areas, mineralogical transformation of the volcanics usually accompanies large-scale metasomatic fluid flow (Humphris & Thomson, 1978; Kristmansdottir, 1981) i.e. leading to the availability of these metals at the same time as chemical disequilibrium between the hydrothermal solution and the rock-forming minerals, contrary to the conclusions of Lydon & Jamieson (1984).

Recently Schiffman et al. (1987) have also concluded that the paucity of transitional assemblages and sharp margins

to many 'epidosites', including those described by Lydon & Jamieson, indicates that the calc-silicate alteration was strongly controlled by fluid infiltration, with high water : rock ratios suggested. Hence on balance it would appear to be most likely that the Type III skarns observed in this study have formed in a similar way to the calc-silicate or epidosite patches described above by MacGeehan & MacLean (1980) and Schiffman et al. (1987), i.e. that they formed by interaction of the wall rock with metasomatic fluids which infiltrated the rocks under conditions of relatively high water : rock ratios. The formation of transitional bleached zones may have been due to relatively lower water : rock ratios than in zones where sharp skarn-amphibolite contacts were developed. It should be noted that the predominance of epidote + quartz assemblages in Type III skarns in the northern half of the area, rather than andradite-bearing assemblages, is a consequence of more pervasive retrogressive regional metamorphism in that area (Section 2.4).

2) The chemical analyses taken in a profile from 'unaltered' amphibolite to Type V calc-silicate skarns from T370m at Hällinmäki Mine are presented in Figure 3.1.9. The MORB-normalised spidergram for analyses from this profile was presented earlier (Fig. 3.1.3). From these analyses it is apparent that there are some systematic changes in element abundances which parallel the mineralogical variations which are described more fully in Section 1.2.

In tandem with an increase in the proportion of andradite (-hedenbergite) towards the top of the unit (Section 1.2), there is a gradational increase noted in

abundances of FeO, MnO, CaO, La, Y, Zr, Cu, S, Co and Zn. Contents of SiO_2, Al_2O_3, Na_2O, P_2O_5, Cr, K_2O, Ba, Sr and Rb are all observed to decrease towards the top, while TiO_2, MgO, Ni, Ce and Nb show variations but with no obvious trend towards enrichment or depletion.

From this data it is concluded that all the elements that have been analysed for have been mobilised to varying extents during formation of Type V skarns from amphibolite protoliths. As demonstrated in Fig. 3.1.3, inter-element ratios for the HFS elements, Zr and Y, have also been changed in a non-systematic manner.

The observation that in several instances Type V skarns are unconformably overlain by relatively unaltered amphibolites (these relationships are described in more detail in Section 1, Part 2, and in Section 3, Part 2) is considered to indicate that Type V skarns form either at or near basalt-seawater interfaces, and/or at depth at permeability interfaces within the volcanic pile, as observed in Recent hydrothermal volcanic systems (Kristmansdottir, 1981). Therefore it seems most probable that Type V skarns also formed syn-volcanically.

3) The development of monomineralic calc-silicate skarn zones (Type II skarns: Section 1, Part 2) at pre-D_1 amphibolite-marble contacts and their symmetrical development around marble bands points to their formation by diffusive metasomatism between the marble and adjacent amphibolite.

In Figure 3.1.10 the major and trace element geochemistry for three samples collected in a traverse from amphibolite to skarn at the contact with a pure calcite marble,

is plotted. Strongly differential movement is indicated for most components, and the development of low variance assemblages in particular is consistent with a model where the chemical potentials of the more mobile components are buffered outwith the individual skarn bands. This is similar to the model proposed by Vidale (1969) to explain the development of calc-silicate bands at synthetic pelite-calcite contacts. Activity gradients are likely to have been controlled by local changes in equilibrium between the mineral phases and intergranular fluid.

A decrease in $_{a}SiO_2$ and increase in $_{a}CaO$ towards marble is suggested by a decrease in SiO_2 and increase in CaO content respectively and this probably precluded wollastonite formation. A sharp decrease in CaO content within amphibolite away from the contact of a Type II skarn is typically recorded by a change in plagioclase composition (from An_{68-69} to An_{42}) (see Section 1, Part 2).

It is not obvious however whether formation of these Type II skarns was initiated by interaction between a fluid phase associated with penetrative syn-volcanic hydrothermal alteration, with carbonate (and CO_2)-rich fluids derived locally from the marble bands, or whether development was initiated during prograde regional metamorphism.

However, in the formation of Type III and V skarns there is considerable evidence to suggest that there was penetrative and widespread movement of syn-volcanic metasomatic fluids in the volcanic pile. Also, Vidale (1969) demonstrated that development of skarns at synthetic pelite-marble contacts was greatly enhanced by increased pore fluid,

higher salt concentrations in the pore fluid, and higher temperatures. These factors are likely to have been particularly favourable during syn-volcanic hydrothermal alteration, as witnessed by spilitisation of the amphibolites and the fact that porosity and permeability were probably greatest at this stage. Elevated temperatures are also indicated by the extent of interaction between basalt protoliths and fluid to form Type III skarns and bleached zones. Analogous features in less highly metamorphosed terranes have been found to develop at or near the critical point of the fluid phase, e.g. at or above 400°C at 0.75 bars (MacGeehan & MacLean, 1980).

The grade of metamorphism associated with this event cannot be established with any great certainty due to D_1-M_1 overprinting. Determination of conditions is complicated by the fact that the observed peak assemblages have been recorded as a pervasive alteration assemblage at depths just over 1000 m in Recent hydrothermal systems in Iceland (Kristmansdottir, 1981), as well as in response to high grade regional dynamothermal metamorphism (Jaques, 1982). In order to resolve this problem a microprobe study is required to determine the distribution coefficients and composition of co-existing element pairs for the diopside-hedenbergite$_{SS}$ and andradite-grossular$_{SS}$-bearing assemblages in Type II skarns, as any prograde redistribution of components against the background of pre-existing chemical gradients would suggest peak metamorphic re-equilibration of pre-existing gradients. Although there is a marked optical zonation observed in these assemblages it is not clear if this is a prograde feature or whether it is in response to syn-D_2 retrogressive re-equilibration. Considering the evidence for

timing of formation of Type III and V skarns it seems likely that Type II skarn formation was at least initiated during pre-tectonic hydrothermal alteration.

4) Summary of pre-tectonic mobility

Skarn Types III and V both apparently formed through interaction of basaltic protoliths with a metasomatic syn-volcanic hydrothermal fluid phase. Type II skarns were also most probably formed at this stage as a result of interaction between basalt and limestone promoted by the presence of this metasomatic fluid phase.

As there is a close spatial link between many of the skarns and Cu-mineralisation a detailed model which attempts to demonstrate the scale(s) on which pre-tectonic hydrothermal alteration was operative, and the consequences for the overall geochemistry of the amphibolites and for formation of the ore deposits in the area, is left to Section 3, Part 2. However, it is evident from the scale of skarn formation that metasomatism during syn-volcanic hydrothermal alteration must have been a principal contributor to the element mobility reflected in the scatter observed in the covariation diagrams presented in Section 3.1.3.

3.1.4(ii) Syn-D_1-M_1 alteration

In Section 2, Part 4 it was demonstrated that the rocks of the Virtasalmi District have been subjected to peak regional dynamothermal metamorphism corresponding to conditions of the Upper Amphibolite-Granulite Facies Transition

Zone during D_1-M_1. The consistency of variation in the HFS elements Nb, Ti, P and Ce with Zr suggests that these elements remained relatively immobile during prograde metamorphism.

The extent to which the other major and trace elements have been mobilised during prograde metamorphism is not easily demonstrable as these elements were shown to have been mobile during pre-kinematic alteration, while the scatter shown by the LIL elements on variation diagrams of syn-kinematic intrusions (see Section 4) also suggests that dynamothermal metamorphism was not isochemical with respect to these elements.

Comparison with other studies of Upper Amphibolite to Granulite Facies regional dynamothermal metamorphism of metabasaltic sequences also suggests that metamorphism is likely to be virtually isochemical but with a redistribution in the LIL elements in particular, as well as SiO_2 (Muecke et al., 1979; Weaver & Tarney, 1981; Weaver et al., 1982). However, Clough & Field (1980) recorded an overall depletion in the LIL elements and in increase in Na_2O in traverses across an Upper Amphibolite-Granulite Facies Transition Zone in Proterozoic metabasalts.

In this study redistribution of chemical components in some amphibolites during D_1 is indicated by development of striping and compositional banding oblique to S_0 and sub-parallel to S_1. This is attributed, as in many other studies, to the effects of metamorphic differentiation (Section 2, Part 1), which involves the segregation and redistribution of more mobile constituents into lower pressure foliation planes (along which slip probably occurred) with concommitant development of selvedges preferentially

enriched in the less mobile constituents. Where formed, stripes and bands were generally observed to have developed uniformly on a scale of less than 1 mm in width, so for the purposes of geochemical analysis the scale on which mobility is likely to have occurred is considered to have resulted in an essentially isochemical balance.

However, in a few instances leucocratic stripes 2-3 mm wide were observed to be less regularly spaced at up to 1 cm intervals in zones within otherwise homogeneous units. Samples were not generally taken where this occurred. Two samples were taken however in order to examine the extent of redistribution (Analysis nos. 231 and 232). Analysis no. 232 was observed to contain a higher proportion of leucocratic stripes than the adjacent melanocratic sample. There is a significant difference in the SiO_2 content of these two analyses (53.42% in 232, c.f. 44.27% in 231). In order to compare the other elements, by bypassing the statistical problem of proportionality caused by expression of the major elements as percentages, their niggli values were calculated. These are presented in Table 3.1.2. this confirms that there was significant redistribution of SiO_2 and alkalies (niggli si, alk and k), minor redistribution involving al, and no significant mobility recorded in values of fm, c, ti or mg. All the trace elements were found to be relatively depleted within the leucocratic band.

Hence, apart from these rare examples, D_1-M_1 metamorphism is likely to have been isochemical for most elements but with redistribution of LIL elements likely.

3.1.4(iii) Syn-D_2-M_2 alteration

In Section 2, Part 4 it was shown that metamorphic conditions during D_2 were retrogressive from those during D_1-M_1 and that in the metabasalts this primarily resulted in amphibolitisation of pre-existing assemblages. As in D_1-M_1 leucocratic stripes and compositional bands were developed sub-parallel to S_2 in the amphibolites, indicating that metamorphic differentiation processes were still operative. However, in general development of these fabrics was more localised than in D_1-M_1 (Section 2, Part 1).

For the same reasons given in Section 3.1.4(ii) it is difficult to determine what the overall chemical effects of amphibolitisation were in this area, particularly since it was not found to be possible to collect an amphibolitised and pre-amphibolitisation sample from the same layer.

In addition to hydration of D_1-M_1 assemblages, element mobility in syn-kinematic intrusions suggests that there was probably LIL redistribution during D_2-M_2, which is consistent with other observations of amphibolitisation (Weaver & Tarney, 1981), although Beach (1974) demonstrated a slight loss of Ca and Mg and a gain in Na for the amphibolitisation of some pyroxene granulites.

In several previous studies however, the mobility of elements during amphibolitisation has been shown to be largely dependent on the availability and distribution of a fluid phase (Weaver & Tarney, 1981). Amphibolitisation is likely to have been facilitated in the Virtasalmi District during D_2 by the upright nature of the main structures and the

development of sub-vertical axial planes and shear zones at that time. These may have acted as channelways for fluids migrating upwards as a consequence of dehydration reactions in the lower crust (see Section 2, Part 1). The emplacement of a large number of intrusions during D_2 (Section 4) may have contributed to the availability of a H_2O-rich fluid phase.

However, in low strain D_2 zones in particular, both pre-D_2 amphibole-rich and amphibole-deficient bands were observed, and this suggests that there may have been some pre-D_2 lithological-mineral control or differences in fluid composition between bands which hindered amphibolitisation of D_1-M_1 assemblages outwith high strain D_2 zones.

3.1.4(iv) Post-D_2-M_2 alteration

Post-D_2 chemical alteration effects are limited to the retrogression of pre-existing minerals along some fracture cleavages. This has resulted in localised sericitisation of plagioclase and breakdown of hornblende to chlorite + magnetite + biotite aggregates (Section 2.4).

It was noted in Section 2, Part 1 that where some late fracture cleavages were observed to cross-cut skarn lithologies, vein-filling of these cleavages by epidote + quartz extended for a few centimetres into the amphibolite. The fact that re-precipitation of these minerals in the fracture cleavages occurs only a few centimetres into adjacent amphibolite is considered to demonstrate that these fluids were locally derived and do not signify large scale introduction of Ca-bearing fluids.

In Hällinmäki Mine there was some remobilisation of sulphides into late fracture cleavages.

As most vein-filled and other penetrative fracture cleavages could be identified in hand-specimen, samples for geochemical analysis were collected to avoid these features. Many thin sections were also taken to ensure that samples did not contain any significant late alteration effects, hence the effects of post-D_2 alteration in the analyses is likely to be insignificant.

3.1.5 Origin of the calc-silicate skarns : summary

From the foregoing petrographic and field evidence (Section 1, Part 2) and chemical evidence (Section 3, Part 1.4) it is clear that the morphologically different skarn types (I-VIII) recognised in this study formed in different ways.

Type I skarns, which are calc-silicate bands within marbles, probably formed from an admixture of carbonate and silicate material (the latter being possibly tuffaceous in origin) which was probably isochemically recrystallised during dynamothermal metamorphism.

Type II skarns occur at amphibolite-marble contacts and are apparently the result of diffusive metasomatism, initiated probably during syn-kinematic hydrothermal alteration.

Type III skarns almost certainly represent the conduits to pre-kinematic syn-volcanic hydrothermal metasomatic fluid flow. Those with sharp boundaries and no transitional zones developed are considered to represent zones of fluid flow with particularly high water : rock ratios. The bleached zones around these skarns represent alteration haloes.

Type IV skarns occur in pillow lavas-lava tubes, and are often concentrically developed near to the exterior margins. These are interpreted as relict Ca-amygdale-rich zones.

Type V skarns show gradational and irregular contacts with amphibolite. These are considered to have formed by metasomatic alteration of amphibolite protoliths. These zones occasionally display evidence for truncation by overlying relatively unaltered amphibolites, and occur as stockwork zones to overlying stratabound Cu-mineralisation. Hence these skarns are considered to have formed syn-volcanically, during a period of extensive hydrothermal alteration either at or near the surface or at depth at permeability interfaces.

Type VI skarns occur as a distinctive lithology characterised by the presence of amphibolite blocks in a calc-silicate matrix. This lithology may represent a debris flow (with a calc-silicate matrix) or an agglomerate with an altered matrix.

Type VII skarns are similar to VI above, but are characterised by either comprising more highly skarned blocks or smaller breccia-like fragments. They are closely associated with Cu-mineralisation and may represent syn-volcanic hydrothermal breccias.

Type VIII skarns occur as variably thick bands inter-layered with Cu-bearing amphibolite bands at Hallinmaki Mine. Laterally there is a gradation between calc-silicate bands dominated by andradite to those dominated by magnetite. These bands are considered to represent admixtures of chemical precipitates and tuffaceous material and formed at the site

of syn-volcanic ore-rich exhalative discharges. These skarn bands may be classified as silicate facies iron formation.

3.1.6 Chemical subdivisions and petrogenesis of the amphibolites

In Section 3, Part 1.3 an igneous-volcanic origin was demonstrated for the Virtasalmi amphibolites in spite of the effects of considerable post-crystallisation alteration (Section 3, Part 1.4). In this section the chemistry of the amphibolite suite as a whole and that of the recognised sub-divisions is considered, and the petrogenetic implications discussed.

1) The magmatic affinities of the amphibolites cannot be demonstrated here using major element chemistry due to the mobility of many of these elements (Section 3, Part 1.4). Nor could modal or C.I.P.W. normative mineralogy be used for the reasons just cited and also because ferrous/ferric ratios were not determined which would have permitted these calculations to be made. However, it is considered most likely that these ratios would have reflected alteration effects rather than original magmatic ratios anyway (Tarney et al., 1979).

Discrimination diagrams which use incompatible element abundances can however be used to determine the magmatic affinities of most volcanic suites (Floyd & Winchester, 1975, 1976; Ikin, 1983). In this study a plot of Nb/Y vs Zr/P_2O_5 (Fig. 3.1.11) clearly demonstrates that the Virtasalmi amphibolites have a subalkalic tholeiitic character.

2) Within the amphibolites three main groups have been identified on the basis of field evidence and petrography alone (Section 1.2). Using a combination of several element covariation diagrams and MORB-normalised spidergrams it has been possible to distinguish chemically these main groups and to subdivide them into a number of mappable subgroups. This was only possible where exposure permitted resolution of the structure and elucidation of the local volcanic stratigraphy (see Map 1). In the southern half of the study area in particular it was possible to collect samples along fairly well-exposed traverses which enabled individual volcanic units (i.e. possibly individual flow units) to be identified and, despite the complex deformation, place these samples within the context of a (local) vertical chemical stratigraphy. This proved invaluable in understanding the compositional range observed within the amphibolites as a whole, especially in the less well exposed northern area.

For each chemically distinct and mappable subgroup the MORB-normalised spidergrams are displayed in Figs. 3.1.12a-i. The distribution of the various amphibolite subgroups is indicated in Map 1.

(a) Group I

Reference to Map 1 shows that amphibolites identified as belonging to this group are predominantly exposed in the southern half of the area. In this area, apparently non-tectonic inter-layering of Group I and Group III amphibolites was observed.

This has resulted in a two-fold subdivision of Group I amphibolites into subgroups Ia and Ib on the basis of this interlayering.

In Section 1, Part 2 it was noted that most Group I amphibolites are petrographically distinguished by containing magnetite rather than ilmenite or sphene. They are predominantly aphyric but are intruded by a few pre-tectonic sub-concordant sills or dykes which contain abundant leucocratic 'blebs' which are interpreted as recrystallised relict plagioclase phenocrysts. Only one sample (107) of these porphyritic units was collected and its chemistry is more akin to that of Group III amphibolites.

In general, Group I amphibolites are characterised by significantly higher SiO_2, Na_2O, FeO and Y, and lower MgO, CaO, Cr and Ni abundances. In Section 3.1.3 it was demonstrated however that many of these elements have been extensively redistributed and the major elements in particular might not reflect original magmatic values. However in a plot of Y vs Zr (Fig. 3.1.13) Group I and Group III amphibolites are seen to define two separate linear trends which are interpreted here as reflecting differences in original chemistry.

Plots of Cr vs Zr (Fig. 3.1.14a) and Ni vs Zr (Fig. 3.1.14b) for Group I, Group IIc, Group IIIb and Group IIIa amphibolites from a traverse across the main open pit at Hällinmäki Mine, similarly display linear trends which are distinct from the trends shown by the other groups. Comparison of these plots with Figs. 3.1.6d and 3.1.6e, i.e. plots of Cr and Ni vs Zr respectively, for all the amphibolites in the study area, shows the usefulness of considering the chemistry of individual groups and analyses from well constrained traverses.

The trends shown in Figs. 3.1.14a and b are consistent with crystal fractionation of mafic phases. The constancy of the Zr/Y ratio also implies that samples within the group are related by fraction of major phases. However, the constancy of this ratio combined with the systematic increase in Y and Zr precludes crystallisation of CPX (or apatite) as Y would be preferentially incorporated into one of these phases (Floyd, 1986b). Instead, it most probably points to incorporation of Cr into a Cr-spinel. The decrease in Ni with increasing Zr is consistent with olivine crystallisation.

However, from a plot of FeO/MgO vs TiO_2 (Fig. 3.1.15) it appears that within Group I there is greater iron-enrichment than in Group III. This is considered to reflect original magmatic enrichment, as both Fe and Mg were noted to decrease where hydrothermal alteration was recorded to be most intense (Section 3, Part 1.3). Taken with a plot of Sr vs Zr for Group I amphibolites only (Fig. 3.1.16), which despite the effects of later redistribution is interpreted to show a marked decrease in Sr with increasing Zr, this suggests that the dominant crystallising phase was plagioclase and that its fractional crystallisation controlled final magmatic compositions. Low mg numbers, i.e. between 0.35 and 0.55 also indicate that the volcanic rocks of this group have undergone significant crystal fractionation and that they represent a moderately evolved group.

(b) Group II

This group mostly consists of a number of small medium- to coarse-grained hornblende metaperidotite (subgroup IIa),

and hornblende metagabbroic (subgroup IIb) bodies which are found enclosed within Group II amphibolites predominantly in the northern half of the area. They are interpreted to have been emplaced penecontemporaneously within the volcanic pile (Section 1, Part 2). Petrographically their medium-coarse grain size, occasional monomineralic hornblendite layers and coarse-grained aggregates of titanomagnetite (often re-crystallised to sphene aggregates) distinguish them from other groups.

Group II lithologies are chemically distinctive in having lower P_2O_5, Ce and SiO_2 abundances, high TiO_2/Zr and high FeO^{tot}/MgO : Zr ratios. Subunits IIa and IIb have a broadly similar overall chemistry although they plot as discrete units.

The plot of TiO_2 vs Zr (Fig. 3.1.1c) demonstrates the relative TiO_2 enrichment at low Zr content of this group compared to others, and is considered to indicate that titanomagnetite was an important crystallising phase. The fractional crystallisation of olivine is also suggested by a rapid decrease in Ni with increased Zr (Fig. 3.1.14b) while crystallisation of CPX is implied from a similar decrease in Cr with increasing Zr (Fig. 3.1.14a). The overall composition, iron enrichment and the lack of feldspar in some bands, which suggests that these lithologies show some signs of a cumulate mineralogy, supports the interpretation that fractional crystallisation was an important mechanism in this suite. This is consistent with the interpretation of the amphibolites of subgroups IIa and IIb as tectonised relics of high level magma chambers and/or sills emplaced into the (coeval) metavolcanic assemblage.

Two other units show a similar overall chemistry to the Group II amphibolites. This similarity is best illustrated in a comparison of spidergrams (Figs. 3.1.12c-f). The analyses in Fig. 3.1.12c were sampled from a sequence of melanocratic amphibolites comprising complex lava flows including pillow lavas, and outcrop in the extreme north of the study area. The analyses in Fig. 3.1.13e were collected from a fine- to medium-grained amphibolite unit approximately 30 m thick which occurs at Hällinmäki Mine and is interlayered with Group III amphibolites. Within this unit there is a sharp drop noted in Cr and Ni content (generally towards the top of the unit) within a narrow range of Zr content (Figs. 3.1.14a,b) which points to fractional crystallisation of CPX (or Cr spinel) and olivine.

(c) Group III

Those amphibolites without the distinctive field and petrographic features of Groups I and II amphibolites are collectively ascribed to Group III. Although the amphibolites within the group display a range of morphological features, petrographically they are less distinct and possess poly-metamorphic mineralogies which mostly comprise varying proportions of diopside, plagioclase (An_{40-80}), hornblende and ilmenite or sphene (Section 1, Part 2).

However to a much greater extent than Group I amphibolites they are commonly interlayered with or have gradational relationships with Type V calc-silicate skarn lithologies. At several localities amphibolites of this group

host Cu-mineralisation, although their immobile element chemistry is not radically different from the adjacent Cu-free amphibolites.

Several subdivisions are recognised on the basis of a combination of chemistry, petrography and field distribution. In the northern half of the area, i.e. north of Virtasalmi Village, limited, less continuous exposure has led to a poorer understanding of the structure (Section 2, Part 1) and permitted only limited sampling of the volcanic sequence. In view of the importance attached to being able to place samples within the framework of a recognisable stratigraphy (which is possible to a much greater degree in the southern half of the area) and with the added complication of there being much less control on Type V skarn alteration in this northern area, the majority of amphibolites from this latter area are considered as a separate subgroup (IIIc).

In Section 3, Part 1.4 it was demonstrated that mobility of the more 'immobile' elements increased markedly from amphibolite to Type V calc-silicate skarn lithologies resulting in non-systematic changes in inter-element ratios from 'least' to more altered amphibolites (see Fig. 3.1.3). Hence in this study of amphibolite petrogenesis it was necessary to discriminate rigorously between the 'skarned' amphibolites and those least altered.

It was possible to identify 'most altered' amphibolite both petrographically, by the presence of the characteristic alteration assemblage (at M_1) of andradite-hedenbergite-scapolite, and chemically, where sampling permitted study of intra-unit variations. Those amphibolites that have

been significantly 'skarned' were thus identified and are not considered further in this section. Amphibolites from the southern area which have a petrography and chemistry characteristic of Group III amphibolites are collectively ascribed to subgroup IIIa.

A MORB-normalised spidergram of the amphibolites from this subgroup (Fig. 3.1.12g) shows that the inter-element ratios for the HFS elements in particular remain fairly constant and although the LIL elements and Ce show greater variation, as anticipated (Section 3, Part 1.4), they are confined within a fairly narrow range of values.

In Section 3, Part 2 it is shown that the original volcanic stratigraphy in the Mine vicinity can largely be reconstructed but that few individual volcanic units can be correlated throughout the Mine. However, it was possible to sample from an uninterrupted sequence of amphibolites in the main open pit at Hällinmäki Mine. The chemical variation noted in this traverse is shown in Fig. 3.1.17. From the 'sawtooth' pattern in Ni and Cr contents observed in inter-layer variations, this is suggestive of derivation of each unit from a magma chamber that was periodically replenished (open system fractionation). Also, in Figs. 3.1.14a and b there are decreases noted in both Cr and Ni contents, respectively, suggesting that CPX and olivine were crystallising phases. However the amphibolites of Group III do not show Fe-enrichment to the same degree as Group I or II amphibolites (Fig. 3.1.15).

In the extreme south of the area there is a sequence of amphibolites within which interlayered pillow

lava-lava tubes are predominant. This sequence is termed subgroup IIIb. A spidergram plot of these amphibolites is presented in Fig. 3.1.12h. In Figs. 3.1.14a and b, as in other Group III amphibolites, there is a marked decrease in both Cr and Ni contents respectively with increasing Zr, interpreted as the result of CPX and olivine fractionation.

The majority of amphibolites exposed in the northern half of the area (subgroup IIIc) have a petrography and chemistry similar to that of subgroup IIIa amphibolites (see Figs. 3.1.1, 3.1.13, 3.1.15).

3.1.7 Petrogenetic and source variability

In the preceding section fractional crystallisation was demonstrated to be an important mechanism in determining the present compositions of lithologies within each of the three main groups of amphibolites. It was also possible to show that the fractionating phases were different within each group, with minor differences also observed between subgroups. However, it was also considered necessary to try to establish whether fractional crystallisation was the dominant mechanism accounting for the main compositional differences within and between groups and whether all three groups are cogenetic.

Log plots of Zr/Y vs Zr for Group I (subgroups a and b), Group II (subgroups b and c) and Group III (subgroups a and b) are presented in Fig. 3.1.18a, and those for Group III (subgroup c) are presented in Fig. 3.1.18b. Analyses for subgroups IIa and b cannot be plotted on these graphs as units contain evidence for a cumulate mineralogy and the plots are

restricted in use to aphyric lithologies (Pearce & Norry, 1979). This also applies to the small number of amphibolites enclosed primarily within Group III and Group I amphibolites, which are interpreted as containing relict plagioclase phenocrysts.

In Fig. 3.1.18a all three groups show a marked separation. Group I amphibolites are largely parallel to vector $\bar{b}$ and Group III subparallel to vector $\bar{a}$ but with a significant component parallel to $\bar{b}$. These differences in distribution are caused by retention of Y to a greater extent in Group I amphibolites (Fig. 3.1.13). The constancy of the Zr/Y ratio with increasing Zr content for the Group I amphibolites is considered to indicate that their composition is predominantly controlled by the process of crystal fractionation, i.e. of plagioclase, olivine and Cr-spinel (Section 3.1.6), rather than by partial melting processes.

It was demonstrated earlier that CPX was an important phase during fractional crystallisation in Group III amphibolites. As CPX incorporates Y into its structure preferentially with respect to Zr, Y should behave in a more compatible fashion than Zr on crystallisation of CPX (Floyd, 1986b). Although such a variation is observed for Group III amphibolites the magnitude of the variation anticipated from this process alone is considered unlikely to account for the large variation observed in Figs. 3.1.18a and b for Group III amphibolites (Pearce & Norry, 1979). Instead the distribution of Group III amphibolites on these plots is considered more likely to be a function either of a systematic source heterogeneity or partial melting processes which has been modified or enhanced by fractional crystallisation.

Since the variation in Zr/Y ratios for Group III amphibolites is observed to extend over the fields of MORBs and WPBs (see Figs. 3.1.18a,b) it is unlikely that such a large systematic variation, apparently within one volcanic group, can be produced by source heterogeneities. This is also supported by plots of the other more immobile elements (see Section 3, Part 1.3) vs Zr (Fig. 3.1.1a-d) where the good co-linearity suggests an overall similar source chemistry, i.e. similar parental magmas or fractional crystallisation of common parental magmas.

It is considered more likely that this range in Zr/Y ratios in Group III amphibolites is the result of variable but low degrees of partial melting of a homogeneous source with Y being retained in a residual melting phase such as garnet (or to a lesser extent CPX) (see Floyd, 1986). Open system fractional crystallisation, some evidence for which was presented in the preceding section, may also allow Y retention in the residual melting phase (O'Hara, 1977). Overall Group IIIc amphibolites show a similar but more scattered distribution in Fig. 3.1.18b than Group IIIa and b amphibolites in Fig. 3.1.18a. This is considered to be due to the poorer sampling and poorer control on skarn distribution as discussed in Section 3.1.6.

In Fig. 3.1.18a Group II (subgroups c and d) amphibolites plot parallel to vector $\bar{c}$, significantly to the left of vector $\bar{a}$. This distribution suggests derivation by variable degrees of partial melting of a more depleted source than that from which Group III amphibolites were derived. The depleted character of Group II amphibolites is also suggested in spidergram plots (Fig. 3.1.12c-f).

To determine whether Group III and Group I were derived from a common source it is necessary to examine the ratios of elements which remain unaffected by partial melting or fractional crystallisation processes such as La/Nb, P_2O_5/Ce, La/Ce and Zr/Nb (Wood et al., 1979; Bougault et al., 1979). Variations in these ratios most probably reflect heterogeneities in source composition (Tarney et al., 1979).

La/Nb and Zr/Nb ratios for Group IIIa amphibolites were observed to be slightly lower than those for Group I amphibolites and on a plot of La/Nb vs Zr/Nb (Fig. 3.1.19) the lithologies in the two groups apparently plot in separate fields with virtually no overlap (Fig. 3.1.19). However, when the large analytical errors for these elements using XRF techniques are considered (even at one standard deviation), it becomes impossible to discern two distinct groups. Nevertheless the differences in the distribution of analyses from the two groups is non-random and cannot be ascribed to possible bias introduced by analytical techniques (Tilling et al., 1987), suggesting that the separation in their fields of distribution has a statistical validity and reflects real geochemical variations which would seem to indicate that the two groups were derived from different sources or from a heterogeneous source. Group II amphibolites also plot in a distinct field supporting derivation from a separate source.

As the term 'incompatible' has been shown to be generally uninformative in more detailed discussion concerning element behaviour during petrogenesis (Wood et al., 1979) the term hygromagmatophile (HYG) is used here in further discussions of element behaviour during petrogenesis (see

Treuil & Varet, 1973; Wood et al., 1979). Elements with bulk solid/liquid distribution coefficients (D) less than or equal to 0.01 (e.g. Rb, K, U, Th, Nb, Ba, La, Ce, Zr) are termed 'more-HYG' and those with D = 0.01-0.1 (e.g. Sr, P, Ti, Y) are termed 'less-HYG'. Ratios of more-HYG/less-HYG elements can provide information on the relative importance of source heterogeneities, partial melting processes and fractional crystallisation (Wood et al., 1979).

Fig. 3.1.20a is a plot of Ce vs Y (i.e. a plot of a more vs less-HYG element) for Group I and Group II amphibolites. Group I amphibolites fall on a linear trend with approximately chondritic ratios (approximately equivalent to Ce_n/Ho_n)' and $Ce_n:Y_{nMORB} \mp 2$. The trend has an approximate zero intercept. Subgroup IIIa amphibolites (Fig. 3.1.20b) are also characterised by a linear (slightly more scattered) distribution but with much higher Ce/Y ratios, i.e. $Ce_n:Y_{nMORB} \mp 4.5$ and an intercept just slightly greater than zero on the axis for Y. The distribution of Ce vs Y for Group IIIb (Fig. 3.1.20b) and Group IIIc amphibolites (Fig. 3.1.20c) is similar (but more scattered) in comparison with subgroup IIIa amphibolites. Group II amphibolites (Fig. 3.1.20a) have characteristically low values of both Ce and Y and Ce/Y ratios apparently less than or equal to 2.

Ratios of more-HYG/less-HYG elements are generally unaffected by fractional crystallisation processes (Floyd, 1986) however in certain instances ratios such as Ce/Y can be significantly affected by open system crystallisation where small batches of magma might be erupted repeatedly, or by substantial CPX removal. The fact that there are large

variations in certain less-HYG/more-HYH element ratios, e.g. Ce/Y, suggests that it is unlikely that Groups I and III can be related by closed system fractional crystallisation. This is also borne out by the variations in element abundances, e.g. Ni and Cr, previously noted in traverses through the volcanic sequence (Fig. 3.1.17). In this example the saw-tooth pattern is interpreted as indicative of replenishment by a more primitive magma which is insufficient volumetrically to modify the trend towards incompatible element enrichment (Figs. 3.1.1, 3.1.14). This either points to open system fractional crystallisation (O'Hara, 1977) or to the existence of small coexisting magma chambers with different fractional crystallisation histories.

On the plots of Cr vs Zr and Ni vs Zr (Figs. 3.1.14a,b) most primitive compositions in each subgroup have the same Cr or Ni content at markedly different Zr contents (e.g. for IIIb, IIIc, etc.), and hence for example many of the amphibolites in Group IIIa cannot be derived from crystal fractionation from Group IIIb. This is further evidence to suggest that open system fractional crystallisation and batch melting processes were operative.

As mentioned above, the degree of fractionation in Zr/Y ratios, and by analogy Ce/Y ratios, which can be attributed to Y incorporation into a fractionation phase such as CPX or apatite is considered to be negligible compared to that possible during partial melting involving garnet or CPX retention in the residual melting phase (Pearce & Norry, 1979). Also if the separate distributions observed for the different groups in Fig. 3.1.20 were to be attributable to

different degrees of equilibrium partial melting (batch or continuous) of a homogeneous source, then the products should lie along a curved line (Treuil & Varet, 1973) on plots of more vs less-HYG elements. Although this relationship may not hold if there is evidence to suggest that the most primitive compositions have undergone significant crystal fractionation with respect to primary liquids (Wood et al., 1979), in this study the more primitive compositions, e.g. in Group IIIa amphibolites, often have MgO > 8%, have Mg/(Mg + Fe) > 0.6 and intercepts on the Ce/Y plot only slightly > 0, which is considered to indicate that the more primitive compositions are not significantly removed from primary compositions (Wood et al., 1979).

The fact that Group IIIa amphibolites also have substantially higher Ni and Cr content than Group I amphibolites and similar or slightly higher average HYG element abundances (e.g. Nb, La, Zr,TiO) on balance also suggests that it is unlikely that the source for these Group I and III amphibolites was identical.

Hence on consideration of all the available geochemical and field evidence, and despite the absence of HREE data and greater resolution for the LREE and some of the other HYG elements (notably Nb), it is considered most likely that Group I and Group III amphibolites not only evolved separately with partial melting processes the controlling influence in Group III amphibolites and fractional crystallisation processes predominant in Group I amphibolites, but that they were also derived from different initial sources. It would

appear that the chemistry of Group II amphibolites was also controlled by partial melting processes but that there was extensive modification by fractional crystallisation in high level magma chambers, Group II amphibolites were derived from a more depleted source than either Group I or Group III amphibolites.

3.1.8 Tectonic setting

It was considered important to determine, if possible, the likely geological-tectonic setting in which the pre-tectonic rocks of the Virtasalmi district were deposited-extruded, as the Svecofennian terrane in which they are situated has been variably ascribed on the basis of geochemistry to such diverse settings as island arcs (Löfgren, 1979; Loberg, 1980; Latvalahti, 1979; Mäkelä, 1980; Kähkönen, 1987), oceanic 'basement' or marginal basin crust (Pharoah & Pearce, 1984), and crust with a composition most closely analogous to that of ocean island basalts (Ehlers et al., 1986).

In these studies and in other attempts to determine the tectonic setting of Early Proterozoic rocks, great reliance has usually been placed on being able to compare the geochemistry of associated volcanic lithologies with that of relatively unaltered Mesozoic and younger volcanic rocks from known tectonic settings. This approach suffers from a number of fundamental difficulties.

Most important, there is the question of how valid these discrimination diagrams are, given the wealth of geochemical data that has emerged since the compositional fields commonly used to delineate tectonic settings were

established (Pearce & Cann, 1973). This problem is highlighted by Saunders (1987), who points out that there are most probably three or four end-member compositional types of oceanic basalt between which there is a continuum of variation reflecting a heterogeneity in source composition. The fact that seamounts are also recognised to be much more ubiquitous features, e.g. forming up to 20% of the Pacific ocean crust, adds to the problems of identifying unique tectonic settings.

The problem is further complicated as this range in composition has also been found in marginal and back-arc basins (Gill et al., 1984; Saunders & Tarney, 1984). These latter authors demonstrated that in some back-arc basins the basalts are transitional in composition between N-type MORB and island arc basalts or even calc-alkaline basalts. A marked variation in basalt composition, e.g. from N-type MORB to calc-alkaline has also been observed to occur within a single back-arc basin, with the variation occurring not only temporally but with the two types being erupted contemporaneously and in close spatial proximity. This compositional diversity can only be explained by invoking source heterogeneities which are only in part related to subduction processes. In depth discussions of the causes of the observed heterogeneity are provided in Saunders & Tarney (1984) and Saunders (1987).

Pharaoh & Pearce (1984) pointed out that there are added problems when dealing with Early Proterozoic rocks in that the discrimination diagrams in use make no allowance for upper mantle evolution since the Early Precambrian, nor do they take account of the changes in heat flow which would have influenced the depths and degrees of partial melting

of the mantle, the likelihood of crustal contamination and possibly the geometry of subduction and related processes.

Given that there are limitations in the validity of identifying the tectonic setting of modern volcanic rocks when based on geochemistry alone, it is obvious that the discrimination diagrams in common usage (Pharoah & Pearce, 1984) can in themselves serve only as a reference framework with which Early Proterozoic rocks can be compared. An integrated approach which utilises geochemistry, isotopic systems which reflect source character (e.g. Nd^{143}/Nd^{144}), and which considers the character of the lithological assemblage as a whole is required before tectonic setting can be determined with any hope of approaching a unique solution.

In addition to the problems outlined above, there is in this study the additional problem of comparing the Virtasalmi amphibolites which have undergone extensive syn-volcanic hydrothermal alteration and high grade regional metamorphism including amphibolitisation, with relatively unaltered post-Mesozioc rocks. While the problem of mobility of elements was addressed in Section 3, Part 1.3, the importance of rigorously selecting relatively unaltered amphibolites for the purpose of determining tectonic setting cannot be overstated. This is of particular importance in the Virtasalmi amphibolites as in the absence of REE data, the elements Ti, Zr, Y and Cr are most extensively used to determine tectonic setting, and these have all been shown to be locally mobile (in proximity to Type V skarn development) during the period of syn-volcanic hydrothermal alteration.

The use of discrimination diagrams based solely on inter-element ratios of Ti, Zr and Y may also be misleading. Although these ratios do not change significantly with the degree of partial melting when the degree of partial melting is large (Pearce & Norry, 1979), recent theoretical modelling is reported to suggest that the degree of melting required to produce basalts is as low as 1-5% in contrast to the previous estimates of 30% for MORB (Saunders, 1987).

The behaviour of Y may also cause problems, as it has been observed to vary in a more compatible fashion in basalts at some DSDP sites. This is considered to be due to its incorporation either in a refractory partial melting phase (garnet or CPX) (Floyd, 1986b), or in CPX during fractional crystallisation, with the result that highly variable Zr/Y ratios are produced within a single volcanic suite.

It is against this background of uncertainty in the validity of using such diagrams that the analyses of Virtasalmi amphibolites are presented in Figs. 3.1.21a-c. In Fig. 3.1.21a both Group I and Group II amphibolites plot in fairly well constrained groups almost entirely within field B. In contrast however, Group IIIa and b amphibolites are spread mainly across fields B and D (Fig. 3.1.21b) as well as lying outwith the recognised field boundaries towards the Zr apex. Group IIIc amphibolites are scattered across fields A, B and D (Fig. 3.1.21c).

The distribution of Group I amphibolites is comparable to that for a present day tholeiitic island arc, ocean-floor or marginal-back-arc basin environment, with a

calc-alkalic island-arc origin ruled out on account of the degree of Fe-enrichment (Fig. 3.1.15) and low $(Nb/P_2O_5)/(Zr/P_2O_5)$ (Fig. 3.1.11).

Any interpretation of the distribution of Group III analyses must be even more ambiguous covering as it does not only the above settings, but also the intra-plate setting, not to mention the spread of data points outwith the recognised field boundaries. Furthermore, inspection of Fig. 3.1.1c reveals that the two groups have broadly similar Ti/Zr ratios and that the differences in distribution apparent in Fig. 3.1.21 are predominantly due to variations in Y content. As demonstrated in Section 3.1.6, within Group III the amphibolites have variable Zr/Y ratios, and these are considered to be due to partial melting and fractional crystallisation processes. However, the (Ti/100)/Zr/(Y/3) discrimination diagram apparently does not take the effects of these processes fully into account and because of this fails to distinguish magma types and tectonic settings.

It was demonstrated in Section 3.1.6 that the major groups and subgroups could be distinguished on MORB-normalised 'spidergrams' (Figs. 3.1.12). These diagrams can also be used as a basis for comparing rocks from different tectonic settings (Pearce, 1983).

This approach suffers from many of the same constraints outlined above, with the fact that there is probably a continuous range in composition between the two magma types is likely to be reflected in the shape of the geochemical patterns. The fact that a greater number of elements is considered in this type of graph has both the benefit of considering a greater number of elements in one diagram, and drawbacks.

The mobility of the LIL elements in the amphibolites of the Virtasalmi District (Section 3, Part 1.3) presents an obvious problem in determining the validity of the abundances for discrimination of tectonic setting. However, as observed in Figs. 3.1.12 the distribution of the LIL elements within each group defines a broadly consistent pattern even although there is a greater variation than for the HFS elements.

Also, the diagrams take no account of the time-integrated depletion of elements in the mantle which results from crustal growth. For K and Th, 25% is estimated to have been extracted from primordial mantle since 2 Ga (Sun & Nesbitt, 1977; O'Nions et al., 1979) while the amount of Rb, Ba, Ce, Nb, La, Sm, Zr, Y, Yb and Ti extracted is thought to be less than experimental error (Pharaoh & Pearce, 1984). Furthermore, since differences in the degree of fractionation of upper mantle and differences in degree of partial melting will change the level of the patterns, they are not thought to change their shape (Pearce, 1983). Hence, although minor corrections e.g. for K and Th in particular should be made, for practical purposes Early Proterozoic patterns can be directly compared with those for post-Mesozoic volcanics (Pharaoh & Pearce, 1984).

Figures 3.1.22a-d are MORB-normalised spidergrams for basalts from intra-plate, volcanic-arc LIL-enriched continental tholeiite patterns and oceanic calc-alkali basalts respectively (after Pearce, 1983; Pharaoh & Pearce, 1984).

Comparison of spidergrams for Group I and Group III amphibolites with Figs. 3.1.22 shows that neither group shows the characteristic depletion (relative to MORB) from Y to Nb that is typical of tholeiitic island arcs.

Instead they show a 'humped' distribution due to LREE and LIL element enrichment which is characteristic of post-Mesozoic intra-plate tholeiites (Fig. 3.1.21a). Also, although there are similarities with continental calc-alkali basalts, it was demonstrated earlier that the amphibolites have a tholeiitic rather than calc-alkaline affinities (Fig. 3.1.11). As the elements Y, Ti, Zr, P, Ce and Nb were shown earlier to have been affected by limited post-crystallisation mobility, the enrichment relative to MORB shown by the pattern from Nb-Sr is also considered to be real, for the reason cited above. However, the magnitude of the original 'hump' is less certain as it is unclear how much of the LIL element depletion likely to have occurred during syn-volcanic hydrothermal alteration and prograde metamorphism has been nullified, if at all by LIL addition during amphibolitisation-retrogression (Section 3, Part 1.3).

These patterns for Group I and Group III amphibolites are broadly similar to those from the mafic volcanic rocks of the Nagu-Korpo area in the Svecofennian of SW Finland (Ehlers et al., 1986), the only other study in the Finnish Svecofennides with a full range of trace element (and REE) data available.

Group IIIc amphibolites also have LIL and LREE enriched patterns but for the same reasons as given for recognising this as a separate subgroup (Section 3, Part 1.6), this is less well constrained.

However, it has been noted above that although Group I and III amphibolites can be characterised as closely

resembling E-type basalts (Sun et al., 1979), this gives a non-unique solution to tectonic setting.

Vaasjoki (1977), Huhma (1986) and Kuovo & Patchett (1986) have all pointed out that there is no isotopic evidence to suggest the presence of an Archaean basement to the Svecofennides, which seems to rule out formation of the Virtasalmi volcanics in an intra-continental rift basin.

It was demonstrated in Section 3, Part 1.7 that Group II amphibolites are derived from a relatively depleted source. Comparisons of the MORB-normalised spidergrams of Group II amphibolites with Figs. 3.1.22a-d show that these amphibolites are most similar to Phanerozoic island arc tholeiites. Another distinctive feature of Group II amphibolites is that they posses negative Ce anomalies (Fig. 3.1.12c-f). In Phanerozoic volcanics, negative Ce anomalies have been discovered principally in island arcs (Jakeš & Gill, 1970; Thirwall & Graham, 1984; White & Patchett, 1984; Hole et al., 1984) but also in ocean island settings (Clague & Frey, 1983; Roden et al., 1984). From the evidence given, Dickin (1987) has demonstrated that on a broad scale Ce behaves coherently during mantle differentiation and has noted that negative Ce anomalies can be attributed to several possible origins: remelting of Ce-anomalous sediment in subduction zones or from the effect of subducted water on the redox conditions in the mantle melting zone; unusual oxidation states in the mantle source; or assimilation of Ce-anomalous sediment at the base of volcanic edifices.

Hence the occurrence of negative Ce anomalous volcanics by itself cannot provide a unique solution to tectonic setting. However, the association of the volcanics with large

volumes of fine-grained metasediments by and large locally derived with only a minor Archaean source (Huhma, 1986, 1987) is inconsistent with a seamount or ocean island origin.

In conclusion, there is no unequivocally unique tectonic setting evident from the available chemical data in this study, however this fact in itself may be significant. The fact that there was apparently coeval magmatism with derivation from more than one source is most closely analogous with eruption in Phanerozoic back-arc basins.

The common assumption that island arc volcanism predominated in the Svecofennides in Finland in particular has generally been made without regard to rigorous evaluation of chemical data. The few detailed studies that do exist suggest a greater complexity than previously assumed.

It is necessary to establish whether the 'depleted' character of basaltic volcanic rocks represented by Group II amphibolites in this study or the LIL- and LREE-enriched metabasalts of Groups I and III are more representative of Svecofennian volcanism, and whether there are geographical zonations.

Fig. 3.1.20 Plots of Ce vs Y are presented for amphibolite Groups I and II (Fig. 3.1.20a), Group IIIb (Fig. 3.1.20b) and Group IIIc amphibolites (Fig. 3.1.20c). Group I amphibolites in particular display a linear trend with low Ce/Y ratios. More poorly defined trends, but suggestive of Ce/Y ratios greater than for Group I amphibolites are observed for Group III amphibolites.

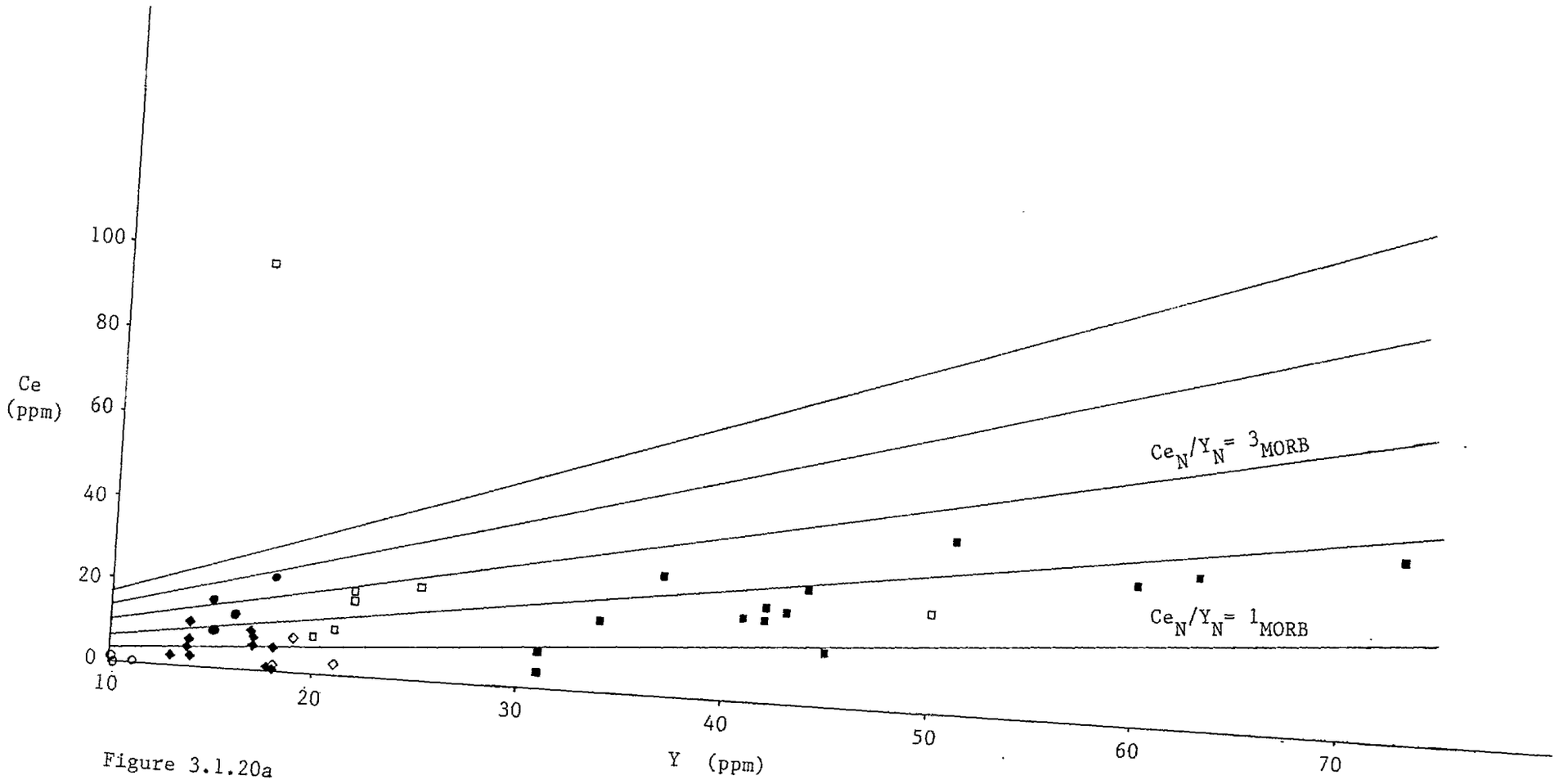

Figure 3.1.20a

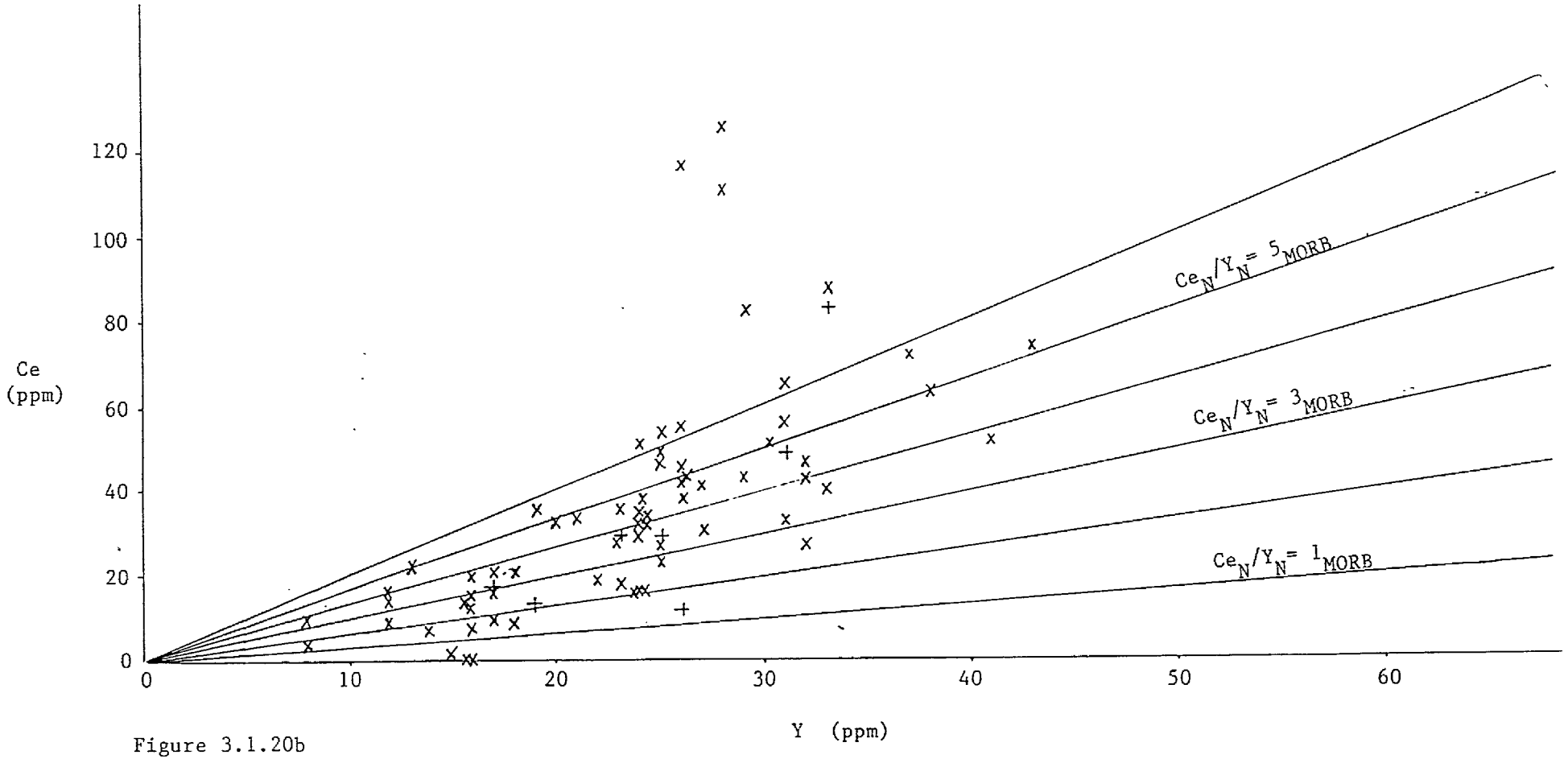

Figure 3.1.20b

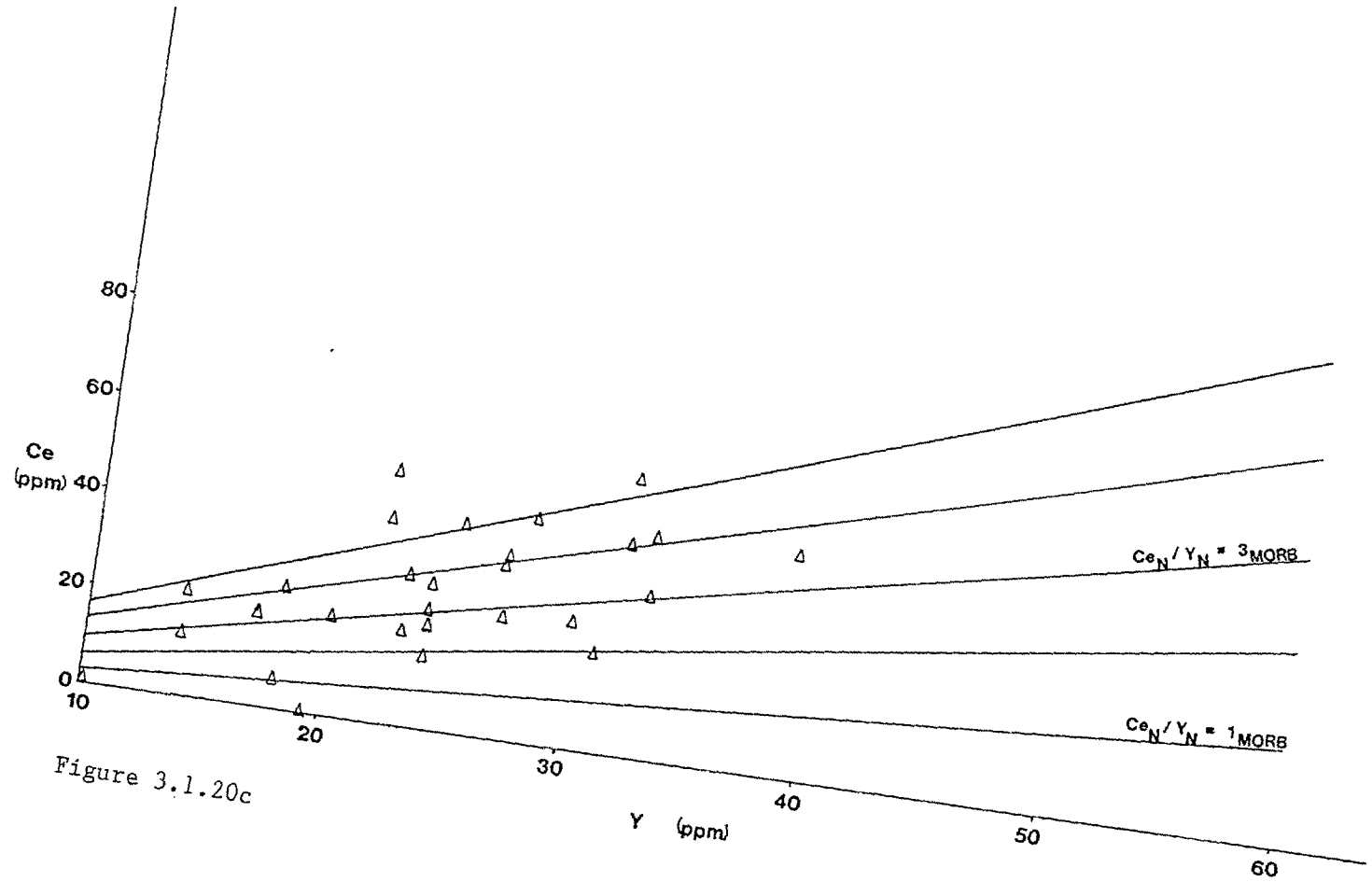

Figure 3.1.20c

Fig. 3.1.21 Figures 3.1.21a-c are Ti/100 vs Zr vs Yx3 plots for Virtasalmi amphibolites. Group I and Group II amphibolites plot within Field B (Fig. 3.1.21a), while Group IIIa and Group IIIb are distributed in a narrow band straddling Fields A, B and D (Fig. 3.1.21b) and Group IIIc amphibolites have a scattered distribution, also over Fields A, B and D. The compositional fields are taken from Pearce & Cann (1973) and correspond with the following tectonic settings:

A Island arc tholeiites (I.A.T.)

B I.A.T.'s, Mid-Ocean Ridge Basalts, and calc-alkalic basalts

C C.A.B.

D Within plate basalts

Figure 3.1.21a

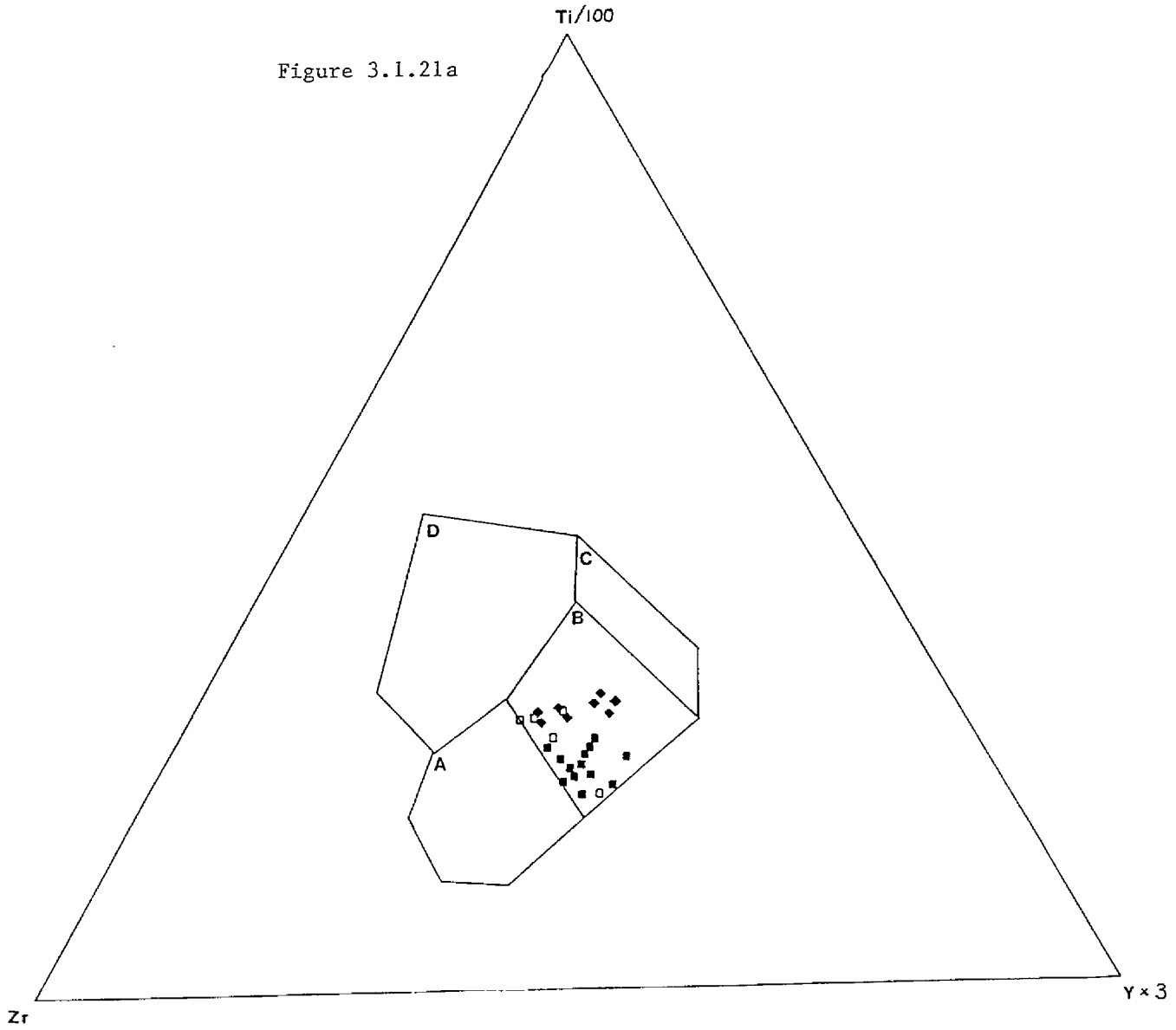

Figure 3.1.21b

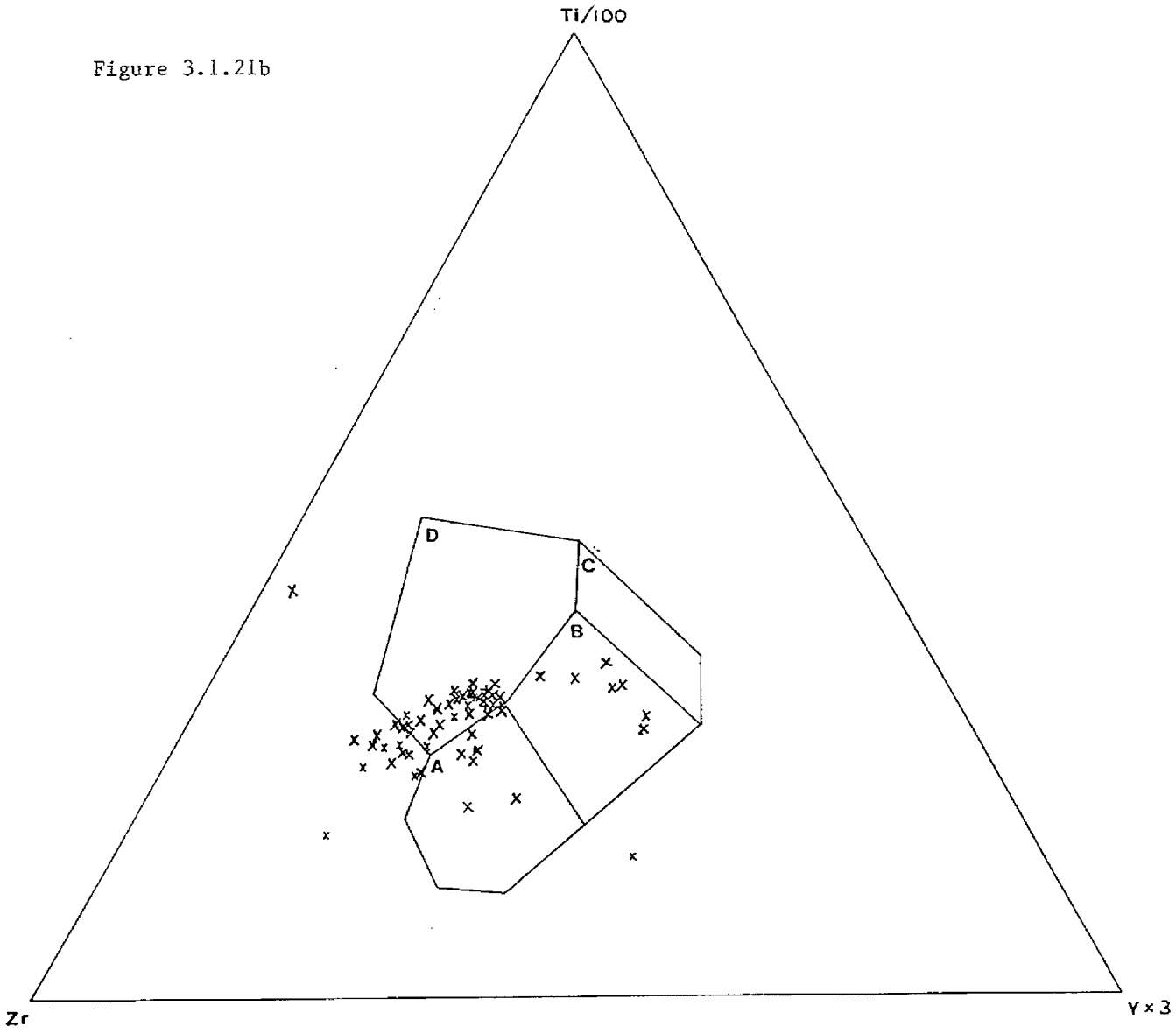

Figure 3.1.21c

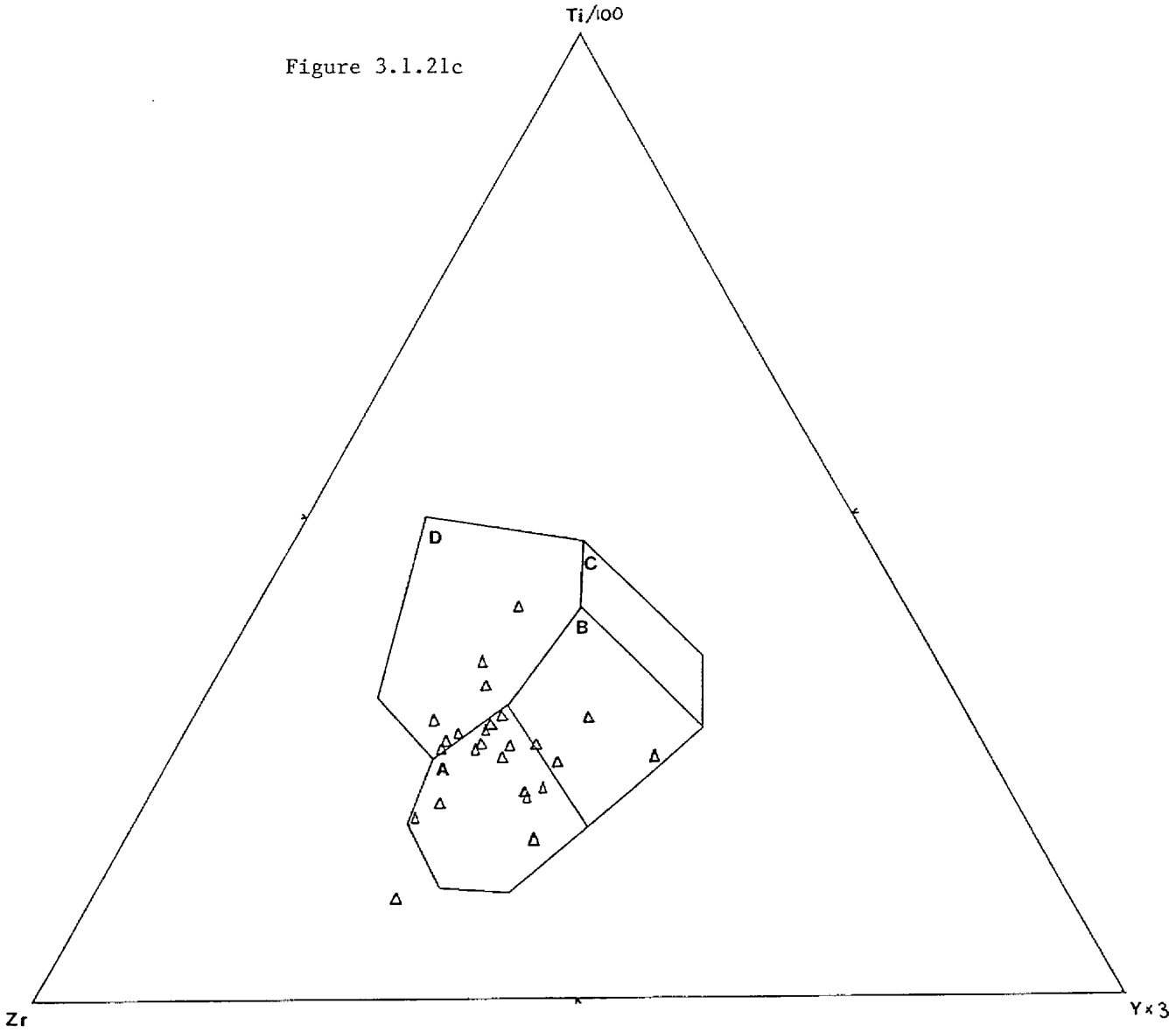

Fig. 3.1.22 Figure 3.1.22a-d are MORB-normalised plots for basaltic rocks from Phanerozoic tectonic settings (after Pearce, 1983). They are as follows:

(a) Island arc tholeiites

(b) Within plate basalts

(c) Oceanic calc-alkaline basalts

(d) Continental calc-alkaline basalts

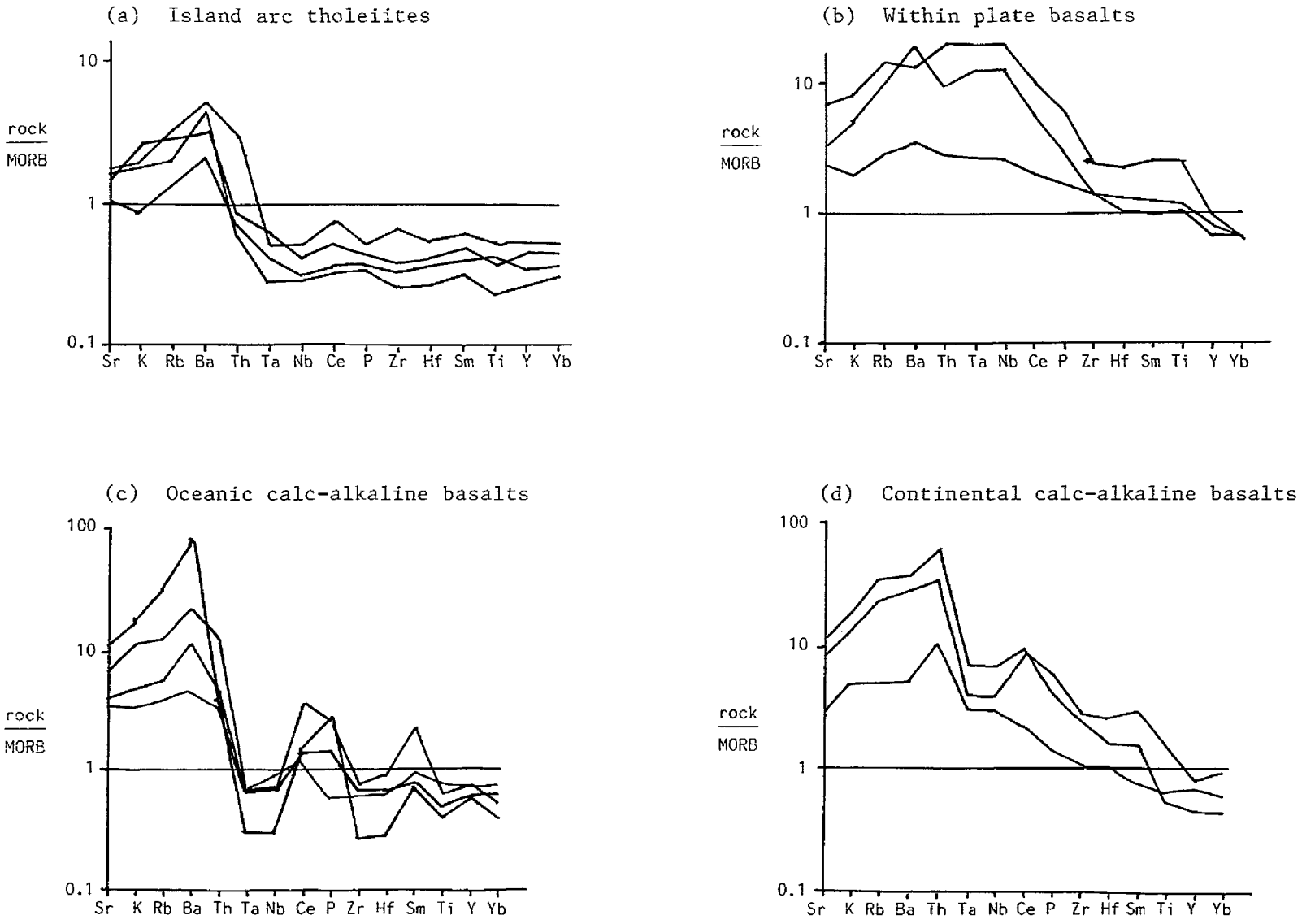
(a) Island arc tholeiites
(b) Within plate basalts
(c) Oceanic calc-alkaline basalts
(d) Continental calc-alkaline basalts
rock
MORB
10
1
0.1
100
Sr K Rb Ba Th Ta Nb Ce P Zr Hf Sm Ti Y Yb

Figure 3.1.22

SECTION 3

PART 2

The origin, nature and structure of the Hällinmäki Cu-deposit

3.2.1 Introduction

The Hällinmäki Cu-deposit is the largest of several small copper ore-bodies which occur in the Virtasalmi District. It was discovered in 1964 by the Geological Survey of Finland and mined by Outokumpu Oy. from 1968-1984. During this period approximately 3.5 million tonnes of Cu-ore was extracted from open pit and underground workings. The mine was closed in 1984 due to exhaustion of reserves.

Just prior to commencement of mining operations, a description of the mineralisation based on surface exposures and drill core results was given by Hyvärinen (1969). The mineralisation was tentatively attributed to a contact pneumatolytic origin, related to the intrusion of quartz diorite intrusions.

In this section evidence relating to the distribution of ore, the relative timing of mineralisation and emplacement of intrusions in the Mine vicinity, and the structure of the ore body is reviewed, and a model for the genesis of the ore deposit presented.

3.2.2 Distribution of lithologies

3.2.2(i) Major structural features

The location of Hällinmäki Mine with respect to the major structures in the Virtasalmi District is indicated on Map 1 and in Figure 2.1.1. From these it is evident that the Mine lies on the eastern limb of a large northerly plunging F_2 antiform. This structure is in turn refolded around the hinge of the major upright F_3 open-tight fold, the axial plane of which trends NW-SE through the study area. Fig. 2.1.2 is a schematic block diagram illustrating these features.

The surface distribution of lithologies and structural data from the vicinity of Hällinmäki Mine is shown in Map 3. However, the main open pit at the Mine had been excavated in the early 1970's and no sufficiently detailed map of the lithologies exposed there was constructed. Hence the distribution of lithologies within the area of the main open pit, and shown in Map 3, is a reconstruction based not only on exposure that was preserved on the surface and around the margins of the main open pit and in its walls, but also on observations of drill core and drill core records. The information gained in mapping a tunnel (T95m) which was located immediately below the bottom of the main open pit was used as a guide to the interpretation of drill core.

3.2.2(ii) Minor structural features in the Mine vicinity

With the exception of D_4 and D_7 structures, evidence for all the phases of deformation outlined in Section 2,

Part 1, was encountered in the vicinity of Hällinmäki Mine. In this section a brief description of the principal minor structural evidence encountered in the Mine vicinity is given.

a) D_1 structures

Only one F_1 fold (within an intrusion) was recorded near to the Mine. The S_1 fabric is preserved mainly in the hinge zones of a few F_2 folds (Fig. 2.2.1) and is often obliterated in F_2 hinges due to development of an intensely penetrative S_2 fabric (see Fig. 2.2.3). As a result, the dominant fabric is the composite foliation S_0-S_1-S_2. Recognition of the S_1fabric is also hindered by the nature of the M_1 mineral assemblage in many of the ore-bearing lithologies, in that few of the M_1 silicate minerals have a pronounced elongation, e.g. diopside-hedenbergite, andradite-grossular, scapolite, with M_1 hornblende or plagioclase rarely preserved.

Due to a combination of their crystal form, later recrystallisation and remobilisation, very little evidence for an S_1 fabric is preserved in the sulphides or ironstones. However, in Figure 3.2.1, which is a thin section of a Cu-ore-rich skarned amphibolite from T175m and taken where chalcopyrite ore grains in hand specimen were observed to occur in bands, a crude alignment of ore grains in S_1 (parallel to S_0) is visible. Chalcopyrite + pyrrhotite ore remobilised parallel to S_2 is seen to be discordant to S_0-S_1 in Fig. 3.2.1. Also, in Fig. 3.2.2 elongate grains of chalcopyrite + pyrrhotite are observed to be sub-parallel to S_0, and are interpreted to be aligned in the S_1 fabric. This sample was collected from near an F_2 hinge zone and the S_2 fabric is clearly discordant to both S_0 and S_1.

b) D_2 structures

Several minor F_2 folds were recorded in the Mine vicinity. Mapping the vergence of these folds permitted recognition of a large F_2 fold with an axis trending NW-SE through the main open pit (Map 3). This large F_2 fold was noted to plunge variably due to later refolding, but in general the information given by parasitic minor folds suggest a northwards plunge at c. 20°. The axial planes of the associated minor folds suggest that the axial plane of the main fold is inclined, dipping east at c. 60°.

c) D_3 structures

F_3 folds are the most abundant minor structures observed in exposures around the Mine. As described in Section 2, Part 1, they are asymmetric, upright and in the open pit axes plunge SE at $50-70^{\circ}$ with steeply dipping ($60-80^{\circ}$E) axial planes. They are variably curvilinear, but are never observed to develop into sheath folds. Several small-scale late D_3 high strain zones were also noted in the Mine vicinity. Small Type III interference structures formed by refolding of F_2 by F_3 were occasionally observed within the Mine.

d) Post-D_3 structures

A few minor F_5 folds, almost coaxial with F_3, were seen to refold F_3 and late D_3 high strain zones in the Mine vicinity. Small F_6 folds are more common but neither F_5 nor F_6 folds form significant structures in the Mine vicinity.

Several late sets of faults do have significant displacements within the Mine. In particular, a number of

reverse faults, often vein-filled by pegmatites, cause significant offsets of the ore-bearing horizons. The largest of these faults has a displacement of 50 m (see Enclosure 9).

3.2.2(iii) Stratigraphy

Despite the structural complexity of the area it is nevertheless possible to establish details of the original stratigraphy in the Mine vicinity. "Way-up" evidence for the sequence was obtained in the small open pit (SOP), and in the tunnels at 175 m (T175m) and 370 m (T370m) levels. This evidence is discussed below.

a) S.O.P. stratigraphy

The location of the small open pit with respect to the Mine complex is indicated in Map 3. Map 4 is a 1 : 100 map of part of this exposure. The only significant minor structures recorded here were asymmetrical isoclinal F_2 folds, which are refolded by asymmetric markedly curvilinear F_3 folds.

A number of petrographically and chemically distinct amphibolite and skarn units can be identified, and in Map 4 these have been labelled units A-E from west-east respectively. Unit A is a fairly massive amphibolite but it is variably skarned (Type V) and also contains disseminated chalcopyrite and pyrrhotite mineralisation. Both the proportion of skarned amphibolite and percentage of ore minerals decrease markedly to the south-east in this exposure.

Unit B consists predominantly of a sequence of sub-parallel interlayered hedenbergite-bearing 'amphibolites' and andradite skarns (Type VIII). Individual layers are up

to 2 m thick but are commonly < 5 cm thick. However there is an angular discordance between units B and C, and this has resulted in progressive truncation of layers within unit B towards the south-east. This has also caused an overall thinning of Unit B to the south-east.

The contact between units B and C is an irregular surface and as such is considered most likely to be a pre-tectonic feature rather than a tectonic slide or thrust. Hence the most likely explanation would seem to be that Unit B is unconformably overlain by Unit C and that there was tilting and erosion of the volcanic assemblage prior to eruption of Unit C. The fact that a thinly banded sequence of amphibolites (Units D and E) above Unit C appear to be conformable with the latter is taken as supportive evidence for this interpretation. It is considered unlikely that units D and E would be sub-parallel to unit C if the latter was intrusive into an otherwise conformable sequence (e.g. as a sill).

Hence it is suggested that the base of the sequence in this exposure lies towards unit A, and the top towards unit E, i.e. that the younging direction is from unit A to unit E. This has important implications for the interpretation of the observed ore distribution.

In the "basal" part of unit B, two lense-shaped bodies of ore were observed. These lenses were noted to be up to 30 cm thick and 5 m in length and formed a discontinuous horizon confined within one band in unit B. The ore consists predominantly of medium-grained recrystallised chalcopyrite with minor pyrrhotite in a hedenbergite-scapolite matrix. Ore grains constitute c. 70% of the lenses. Towards the

south-east in this exposure there were only very thin pockets of ore observed. The disseminated mineralisation and skarn development noted in unit A directly 'underlies' the more massive lenses. During excavation of this pit the ore lenses were directly observed to be continuous for at least 10 m in depth.

There is no Cu-mineralisation in the remaining layers in unit B, in fact the Cu content is abnormally low (i.e. 1 ppm). Instead, however, the layers contain abundant magnetite either as coarse-grained aggregates or small pockets of fine-grained disseminated ore. It should also be noted that Hyvärinen (1969) reported the occurrence of lenses of banded magnetite-skarn rock from the Mine area.

Unit C contains some Cu-sulphide mineralisation, but only in very small pockets locally at its base. As this unit is unconformable on underlying lithologies, including those that are ore-bearing, it seems likely that this minor ore concentration may have been derived by contamination from underlying lithologies.

b) T175m stratigraphy

The location of this tunnel with respect to the other Mine workings is indicated in Fig. 3.2.3, and a 1 : 100 scale map of the lithologies encountered in the tunnel is presented in Map 5.

It should be noted that this tunnel is situated on the short overturned limb of the main F_2 fold. The sequence observed can be subdivided into three distinct units, labelled A, B and C in Map 5.

Unit B comprises an interlayered sequence of massive andradite skarns (Type VIII) and hedenbergite-bearing amphibolites. Disseminated chalcopyrite mineralisation is common throughout the amphibolites, but is only present within the skarn layers where there has been tectonic remobilisation towards boudin necks or minor fold hinges. The layers within unit B are progressively cut out towards the north by unit C, which is a relatively ore-free banded amphibolite. The contact between units B and C is not a flat planar surface, but on close inspection is fairly irregular. Hence it is interpreted in an analogous way to the contact between units B and C in the small open pit, i.e. that it is a pre-tectonic surface, and in T175m gives an indication of younging to the west from unit A to unit C.

Within unit B there are also a couple of thin, < 20 cm thick, massive lenses of chalcopyrite with minor pyrrhotite. At the 'base' of this unit the amphibolite contains a high proportion of fine-grained disseminated chalcopyrite in a band c. 10-15 cm thick. There is a sharp base to this unit which is underlain by Type V skarns within unit A. Within the basal chalcopyrite-rich band the ore percentage is fairly constant for c. 10 cm and then is observed to decrease rapidly upwards from c. 60% to 10%.

Unit A comprises a fairly massive amphibolite within which there is a gradational but marked increase in the proportion of skarn minerals and ore content 'upwards' and laterally (to the north) in this tunnel.

Comparison of the lithologies in Maps 4 and 5 shows that there is a similar stratigraphy on both limbs of the major F_2 fold.

c) T370m stratigraphy

The location of this tunnel with respect to the mine workings is indicated in Fig. 3.2.3. A 1 : 100 scale map of this tunnel is presented in Map 6. Unfortunately there are a greater number of syn-tectonic intrusions in this tunnel than in those exposures described above and an incomplete cross-section of the original stratigraphy remains.

Minor asymmetrical F_2 structures in this tunnel confirm that the exposures here lie on the eastern limb of the large F_2 fold through the Mine.

In Map 6 the pre-intrusion lithologies over the ore-bearing sections are labelled A-E respectively. The contact between unaltered amphibolite and (Type V) skarn within unit A is (irregular and) gradational. It is marked firstly by the replacement of diopside in the amphibolite by hedenbergite, then finally into an andradite-hedenbergite-scapolite skarn containing disseminated chalcopyrite.

By contrast, the contact between units A and B is sharp. Unit B is a banded amphibolite containing fine andradite skarn layers, parallel to the A/B contact. It is evident that the skarn contact within Unit A is discordant both to this layering and the A/B contact. Comparisons with the sections in the other tunnels reveals a marked similarity but that the sequence here in thinner. On the basis of these analogies the sequence in T370m is considered to young from unit A to unit E.

In this tunnel unit B also contains a very high proportion of fine-grained disseminated chalcopyrite, but this proportion is variable (10-70%) between the layering and fairly constant within individual layers.

Unfortunately the contacts between units B and C and between C and D are masked by late intrusions. Unit C contains no ore and is a diopside-hornblende banded amphibolite. Unit D is a variable skarned amphibolite, with a mesh-like network comprising andradite skarn superimposed on an amphibolite host-rock. Directly above this, in unit E, there are two c. 3 cm thick pyrrhotite-rich layers interbanded with ore-free amphibolite.

d) T95m stratigraphy

The position of this tunnel with respect to the Mine is shown in Fig. 3.2.3. A 1 : 100 scale map of the tunnel is given in Map 7. Due to the presence of several late vein-pegmatite filled faults, of uncertain displacement, only portions of the original stratigraphy can be ascertained in this tunnel. There are also no features which can be used as way-up indicators at this locality, except by drawing comparisons with the sequence observed in other tunnels.

The attitude of banding and minor structures indicates that part of the tunnel lies within the hinge zone of the major F_2 fold in the Mine. At the northern end of the tunnel, a sequence of interbanded amphibolites and (Type VIII) andradite skarns was noted. The mineralisation in T95m is primarily concentrated within the amphibolites and the skarns only contain ore where there is evidence for tectonic vein-associated ore remobilisation. Within the amphibolite layers and away from minor fold structures the ore consists of fine-grained disseminated chalcopyrite and pyrrhotite. Magnetite was only rarely observed. The sulphides typically constitute between 20-40% of the rock volume.

As in all the other localities in the Mine the sequence observed here bears a marked similarity to the stratigraphy oulined in all the other localities described from the mine. Hence, by analogy and correlation along strike from the small open pit, these interbanded skarns and ore-bearing amphibolites are considered to correspond with unit B in the other localities. Also similar is the fact that the ore-bearing horizons are overlain by a Cu-ore-free banded amphibolite.

In both T95m and T370m, but not at any of the other localities, there are two thin pyrrhotite-rich layers present approximately 6 m above the base of the 'barren' amphibolite. These pyrrhotite layers are up to 3 cm thick, of consistent width, are continuous along strike and parallel a prominant compositional banding in the amphibolite.

The amphibolite unit immediately 'above' the pyrrhotite layers at this locality has a markedly different chemical composition compared to other amphibolites in the Mine sequence. This unit can be traced from T95m directly to the surface of the main open pit, and also traced across this to the small open pit.

3.2.2(iv) Major structural and stratigraphic synthesis

It is clear from the evidence given above that a consistent stratigraphy is recognisable throughout the Mine area. A schematic diagram which attempts to summarise the structural- stratigraphic relationships observed in the Mine vicinity, is presented in Fig. 3.2.4. The main ore-bearing

horizon (unit B) comprises interlayered amphibolites and skarns (Type VIII). Throughout most of the Mine, the mineralisation in this unit comprises abundant fine-grained chalcopyrite (c. 25%) with some pyrrhotite (c. 5%) and minor magnetite. In places this mineralisation occurs in thin lenses comprising more massive ore. Towards the south-east, Cu-ore mineralisation is restricted to ore-lenses in pockets at the base of the unit. However there is a marked increase in the proportion of magnetite in these upper layers. In places a banded magnetite-hedenbergite skarn lithology, with minor chalcopyrite in some bands was observed (Fig. 3.2.5).

Underlying this main ore horizon is a variably skarned amphibolite (unit A). There is an increase in the degree to which this unit is skarned, together with an increase in Cu-ore (fine-grained disseminated chalcopyrite), coincident with the increase in Cu-mineralisation in the above unit B.

An E-W cross-section across the Mine is presented in Enclosure 9. The 3-dimensional structure of the deposit could only be elucidated where control was provided by detailed mapping of tunnel exposures. The lack of lithologies which could be readily identified and correlated in drill core, and the recognition only of 'skarn zones' in Mine records together with the truncation of the original stratigraphic units by syn-kinematic intrusions and late faults has made it impossible to demonstrate the complete three dimensional structure of the ore deposit.

3.2.3 Timing of mineralisation

3.2.3(i) Introduction

From the preceding section it is evident that ore mineralisation in Hällinmäki Mine is stratigraphically confined. Although this suggests a pre-tectonic and hence probably a syn-volcanic-exhalative origin for the deposit, it does not strictly preclude an epigenetic origin for the mineralisation related to the emplacement of intrusions. The contacts between the latter and ore horizons at Hällinmäki were well exposed and the relationships could be readily ascertained. In this section the petrofabric evidence which indicates the relative timing of mineralisation and the relative timing of emplacement of intrusions is discussed.

3.2.3(ii) Petrofabric evidence

Within the Mine complex many of the hornblende-bearing chalcopyrite-rich amphibolites were observed to contain M_2 hornblende poikiloblasts which enclose the M_1 mineral assemblage. In particular hornblende was observed to enclose diopside-hedenbergite and chalcopyrite-pyrrhotite-magnetite assemblages (Fig. 2.4.14). This is considered to demonstrate that the ore recrystallised in the M_1 assemblage, although from this evidence it is not clear whether the ore is pre- or syn-D_1 in origin.

Unfortunately, while S_0, S_1, S_2 relationships were readily demonstrable in the silicates, later recrystallisation and extensive small scale remobilisation have caused

these relationships to be less readily ascertainable in the sulphides and skarn mineral assemblages (Fig. 3.2.1). The apparent ease with which the chalcopyrite and pyrrhotite ore recrystallise and change their grain shape makes is very difficult to demonstrate S_1-S_2 relationships in the ore-bearing horizons except in isolated localities. In Figure 3.2.1 the interpretation is further complicated by the presence of a sub-vertical S_3 fracture cleavage zone. The sulphides appear to show some further grain realignment into parallelism with this fabric.

3.2.3(iii) Relationship to intrusions

In addition to numerous syn-kinematic basic dykes and late kinematic pegmatites, two main plutonic intrusive bodies were recorded within Hällinmäki Mine. These igneous masses consist of leucogabbros-diorites and diorites-tonalites, and these two types display different relationships to the structural sequence (Section 2, Part 2). All of the intrusions are irregularly shaped, with the diorites-tonalites in particular noted to form numerous dyke-like masses which appear to become more numerous with depth.

The relationship of the leucogabbros-diorites to the ore was best demonstrated in T175m (Map 5). At this locality the intrusion was observed to cross-cut S_0 and the ore-bearing horizons at a high angle. At the margins of the intrusion the country rock was observed to be split into several narrow screens. A few blocks of amphibolite appear to be detached within the intrusion although S_1 was continuous through the xenoliths and the intrusion. However, the S_1 fabric was

observed to be strongly penetrative (an S_1 differentiation banding) within the amphibolite xenoliths, and only weakly expressed in the intrusion.

In addition to this it was noted that the xenoliths and the adjacent country rock contain abundant chalcopyrite, whereas the intrusion contains no significant Cu-sulphides. Hence on the basis of the observed cross-cutting relationship of the intrusion contact and the barren nature of the stock in comparison with the Cu-bearing nature of the country rock and xenoliths, the mineralisation is interpreted to pre-date emplacement of the earliest syn-kinematic intrusion within the Mine.

The diorite-tonalites, which are volumetrically the most abundant intrusive type in the Mine complex, contain only very weak metamorphic fabrics, and were observed to truncate D_2 boudins (Fig. 2.2.6), and cut across ore-bearing lithologies at a high angle. Neither S_1 or S_2 are developed in these intrusions, although a weak S_3 fabric was noted, hence they can readily be demonstrated to post-date mineralisation.

3.2.3(iv) Timing of mineralisation : summary

From the evidence given above, it is clear that the ore assemblages at Hällinmäki Mine have been recrystallised during D_1 and subsequent tectono-metamorphic events. The mineralisation and skarn formation apparently pre-dates all syn-kinematic intrusive replacement, and hence the ore deposit cannot have formed as a result of contact pneumatolytic processes, as proposed earlier by Hyvärinen (1969).

There are instead a number of features which, when considered together, point to a pre-tectonic origin for the mineralisation. First , there is evidence which indicates that most of the mineralisation is stratabound within unit B and that there is also a lateral gradation in ore composition within this unit. Second, beneath the Cu-mineralised part of unit B, i.e. within unit A, there is a Type V calc-silicate skarn alteration zoned developed. This contains Cu-ore where it directly underlies the Cu-ore-bearing portion of unit B, and the skarn itself is replacive of a pre-existing basaltic protolith and is discordant at a high angle to S_0. This skarn is interpreted as an alteration stockwork to the overlying stratabound mineralisation. The apparently close spatial and genetic links between this skarn and the ore deposit also provide evidence for the timing of mineralisation. In Section 3, Part 1, and in Section 1, Part 2, evidence was presented which demonstrates that these skarns are pre-D_1 and probably syn-volcanic in origin.

In Section 3, Part 2.5 the probable link between the ore deposit and skarn formation is discussed further and a model to explain the ore occurrence is presented.

3.2.4 Nature and extent of syn-kinematic ore remobilisation

3.2.4(i) Syn-D_1 mobilisation

Within the S_0-S_1 composite foliation the two most common ore minerals, chalcopyrite and pyrrhotite, occur predominantly as fine-grained aggregates (0.1-0.4 mm), with individual

grains typically displaying an elongation parallel to the foliation (Fig. 3.2.2). Occasionally thin bands (< 0.5 mm) up to 10 cm long and comprising grains of chalcopyrite and pyrrhotite were observed within the disseminated ore (Fig. 3.2.1). These bands were found to be generally sub-parallel to S_0, however in Figure 3.2.1 there is a slight discordance between the ore-rich band and S_0 and this evidence is considered to indicate that there has been some sulphide remobilisation sub-parallel to the S_1 foliation. The ore-rich band in this figure shows a higher discordance to S_2 and S_3. However, the only significant large-scale within-unit variation in ore-composition noted is the aforementioned increase in magnetite to the south-east, and this is almost certainly a pre-tectonic feature related to the original ore distribution.

The thicker elongate lenses of ore which were noted earlier, e.g. in the S.O.P., were generally observed to be sub-parallel to S_0-S_1-S_2 and it is not usually possible to distinguish S_1-S_2 features within them. However, in one small example in T95m it was possible to demonstrate the presence of a compositional banding within part of the lense (which is 1 m wide and comprises fine-grained chalcopyrite) (Fig. 3.2.6). This banding is discordant to the margins of the lense, and therefore suggests that the present lense shape is the result of boudinage in D_1. However, in most instances it was not possible to ascertain to what extent syn-D_1 mobilisation has contributed to formation of these lenses.

In view of the preservation of much of the ore as fine-grained disseminated aggregates, and the paucity of evidence for D_1 structures in the Mine vicinity, it is considered

most likely that during D_1-M_1 the ore deposit underwent mainly static recrystallisation during prograde metamorphism. Limited dynamic recrystallisation and solid state diffusion under low stress and low strain rates is indicated by mineral elongation, but large-scale mobilisation appears to have been negligible, apart from the limited evidence for tectonic segmentation of ore layers by boudinage.

Despite the high grade metamorphic conditions which prevailed during D_1, there is no evidence either for partial melting of the sulphides (Vokes, 1971) or for the consequential development of sulphide metapegmatites (Lawrence, 1967). Whether partial melting occurs or not may be critically dependent on sulphur fugacities (Plimer, 1984).

3.2.4(ii) Syn-D_2 mobilisation

Where it is possible to distinguish between S_1 and S_2 within the fine-grained disseminated ore, sulphide grains are often observed to be reoriented in the S_2 fabric (Fig. 3.2.1).

In the ore lense observed at T95m (Fig. 3.2.6) it is possible to distinguish between the S_0-S_1 and S_2 fabrics within the ore. The S_2 fabric is characterised by the development of numerous sub-parallel discontinuous 'stringers', up to 25 cm long and 5 cm wide, which are aligned within the S_2 axial planar fabric. Within these 'stringers' the ore is coarser grained than in the matrix and consists mostly of chalcopyrite.

In both T95m and T175m tunnels there is evidence for mobilisation of ore into boudin necks. The ore in these instances is also predominantly coarser grained and mostly chalcopyrite with very minor pyrrhotite.

Ore was also observed to have been remobilised into veins which were emplaced mainly in the hinge zones of F_2 folds. The veins truncate S_0-S_1 at a high angle but are observed to contain a strong foliation (S_2). The ore is primarily concentrated at the vein margins and in one such vein a fine-banding, which is probably a combination of flow banding and tectonic foliation development, was developed.

3.2.4(iii) Syn-D_3 mobilisation

There is evidence for extensive remobilisation of sulphides during D_3, particularly where minor F_3 fold structures refold ore-bearing lithologies. Two examples are described here, one from the small open pit where a pre-existing ore lense is refolded, and an example from T95m where disseminated ore within amphibolites is refolded.

In the small open pit the ore within the pre-existing lense was observed to be remobilised to form a cigar-shaped body oriented sub-parallel to the F_3 fold axis (Map 4). Within the body the ore is recrystallised into coarser grained aggregates (up to 5 cm across) consisting principally of chalcopyrite. This remobilised ore truncates adjacent S_0 layering, with clasts of these skarn and amphibolite layers caught up and rotated within the ore to form a breccia. During mining operations it was possible to observe that this breccia

ore-body plunges at c. 60° south-east, i.e. sub-parallel to the axis of the F_3 fold, and within its hinge zone.

Another example occurs in the tunnel at 95 m level (Fig. 3.2.7), where F_3 folds were observed to deform disseminated Cu-bearing skarned amphibolites which are interlayered with Type VIII skarn lithologies. In Fig. 3.2.7 it can be seen that as the hinge zone is approached, the ore (chalcopyrite with minor pyrrhotite) changes in the nature of its occurrence from fine grained disseminated ore to elongate blebs which in turn coalesce to form microbreccia ore in the limb zone. In the hinge zone itself the microbreccia ore gives way to massive recrystallised coarse-grained chalcopyrite ore, which also contains minor cubic recrystallised pyrrhotite 'porphyroblasts'. At some distance (in this case > 5 m) from these minor F_3 hinge zones the ore is clearly preferentially concentrated within the amphibolite layers. However, towards these structures the ore is remobilised across S_0, resulting in mineralisation of the Type VIII skarn layers. As with the previous example, the massive ore in the hinge zone was observed to plunge parallel to the F_3 fold axis.

Hence there is clear evidence to show that during D_3 there was extensive differential remobilisation of sulphides in Hällinmäki Mine. The remobilisation from limb zones of F_3 folds and its concentration within hinge zones demonstrates that the mobilisation was largely in response to stress-induced diffusion during folding. Similar features have been observed in studies of other polyphase deformed ore-bodies (e.g. McDonald, 1970; Pederson, 1980; Koistinen, 1981). The observed increase in grain size towards the hinge zones is consistent with this

interpretation and also with theoretical thermodynamic studies which predict that larger grains would be expected to grow in low stress areas such as fold hinges or boudin necks (Stephansson, 1974).

There are three possible mechanisms by which this remobilisation can take place: partial melting (Lawrence, 1967); solid state diffusion involving diffusion creep (Graf & Skinner, 1970; Mookherjee, 1971; Atkinson, 1975) or dislocation creep (Atkinson, 1974); or fluid state remobilisation (Gresens, 1966; Durney, 1972; Stephansson, 1974). The silicate mineral assemblages developed in the country rocks however indicate that during D_3 there was little metamorphic re-equilibration of pre-existing assemblages, that there was only localised M_3 mineral growth, and that greenschist facies conditions prevailed (Section 2, Part 4). These P-T conditions are well below what is required for sulphide partial melts to form (i.e. 500-700^{o}C in presence of high f_{S_2}).

Experimental work on sulphides has demonstrated that solid state diffusion is likely to be an important deformation mechanism in sulphide deposits in medium to high grade terranes (Roscoe, 1975). Atkinson (1974) suggested that chalcopyrite deforms plastically by dislocation and/or glide and twinning, while pyrrhotite is likely to deform by a combination of dislocation glide, twinning and kinking. However, these features are likely to be modified or obliterated by subsequent recrystallisation (Roscoe, 1975). No attempt was made in this study to examine the ore textures in detail.

In recent studies of naturally-occurring ore deposits deformed at similar P-T conditions to those prevailing

in the Virtasalmi District during D_3, remobilisation of chalcopyrite into open-tight folds has been attributed to a combination of solid state diffusion and fluid state remobilisation (Pederson, 1981; Plimer, 1984). Ductile flow of sulphides is suggested at Hällinmäki by the thinning of the sequence on F_3 limbs and thickening in the hinge zones. However, many of the silicate minerals (principally plagioclase and hedenbergite) immediately ahead of the microbreccia stringers (assuming that there was remobilisation of ore towards the F_3 hinge zones) are intensely fractured, and some grains are split into two parts with the fractures infilled by chalcopyrite. This is considered as evidence for mechanical fracturing of the silicates followed by injection of sulphide. Hence while remobilisation by solid state diffusion may have been the initial response of the sulphides during D_3, it is considered most likely that the fracturing of silicates and injection of sulphides involves fluid state diffusion, aided by the presence of a vapour of fluid phase (e.g. Atkinson, 1974; Plimer, 1984). This may have become the dominant process in the later stages of D_3 remobilisation.

It was also noted that contacts between plagioclase and sulphide grains which were not remobilised during D_3 are sharp with no mineral reaction observed between them. In marked contrast grain contacts between D_3 remobilised chalcopyrite-pyrrhotite and plagioclase are characterised by development of narrow reaction rims (Fig. 3.2.8). Scapolite is observed to form a discontinuous zone (or occasionally two zones) in contact with the ore. This inner scapolite rim only rarely occurs in direct contact with plagioclase (Hyvärinen, 1969).

Between the ore and plagioclase or between the scapolite and plagioclase there is normally a continuous rim of epidote (Fig. 3.2.8). Occasionally another zone is developed which comprises highly altered scapolite and the contact between this and plagioclase is highly irregular.

The formation of these reaction zones indicates local chemical disequilibrium and solid-state diffusion of components between the silicate wall rock and the ore minerals. The precise timing of formation of these rims with respect to syn-D_3 ore mobilisation and the degree to which back-reaction annealing has modified the initial reaction zones is not clear.

3.2.4(iv) Post-D_3 mobilisation

There is limited remobilisation, principally of chalcopyrite into cleavages and even some late joints which cross-cut the main ore horizons. Similarly, many of the late veins and pegmatites were observed locally to contain some chalcopyrite on contact with ore-bearing lithologies.

3.2.5 Model for formation of Hallinmaki Cu-deposit

In Section 3, Part 1 it was demonstrated that calc-silicate skarn Types III and V were formed through interaction of a metasomatic fluid phase with basaltic protoliths during a period of widespread syn-volcanic hydrothermal alteration. Evidence was also presented which points to the formation of some Type V skarns either at or near the basalt-seawater interface or at subsurface permeability interfaces (see Fig. 1.2.6).

Also, earlier in this section, the presence of a Type V skarn zone beneath the main Cu-bearing lithologies (i.e. in 'Unit A') was demonstrated. The close spatial relationship between this replacive skarn lithology and overlying stratabound mineralisation, the high angle of discordance which this skarn shows to overlying units, the presence of disseminated and breccia ore (predominantly chalcopyrite) within the skarn, and the fact that large fluid fluxes with high water : rock ratios appear to be involved in formation of this lithology (Section 3, Part 1.4), all point to the interpretation of this Type V skarn as part of a stockwork zone which developed beneath the Hällinmäki ore deposit.

Recognition of such a stockwork zone subjacent to the ore deposit together with the elucidation of the stratbound nature of the bulk of the ore (in unit B) (Section 3, Part 2.2(iii)), and the lateral within unit gradation from Cu-mineralisation to banded iron formation are features which point to a volcanogenic-exhalative origin for the mineralisation (Franklin et al., 1981). Hence from this evidence, and from the field and geochemical evidence summarised in Section 3, Part 1, there appears to have been a period of extensive hydrothermal alteration of the volcanic pile which was roughly coeval with exhalative mineralisation at Hällinmäki Mine.

In recent years, lithological, geochemical and isotopic investigations have shown that there is a genetic link between large-scale syn-volcanic metasomatic alteration of basaltic crust at presently active oceanic ridges and the formation of exhalative sulphide deposits (e.g. Spooner & Fyfe, 1973; Parmentier & Spooner, 1978; Edmond et al., 1982;

Skirrow & Coleman, 1982). Parallel studies have shown that similar processes were responsible for formation of sulphide deposits in Phanerozoic ophiolites (Constantinou & Govett, 1972; Spooner, 1977; Fleet & Robertson, 1980). In addition geochemical studies have identified both sub-vertical tabular or cone-shaped alteration stockworks and semi-conformable alteration areas below sulphide ore horizons in some Archaean greenstone belts (MacGeehan & MacLean, 1980), Proterozoic successions (Scott & Taylor, 1982) and Early Phanerozoic volcanic belts (Zachrisson, 1982; Stephens, 1982). Franklin et al. (1981) have concluded that similar alteration zones may be 'virtually ubiquitous' in massive sulphide districts, and that the presence of these zones is indicative of a genetic link between alteration of the volcanics and development of stratiform sulphide ore-bodies, in an analogous way to the processes observed at present day oceanic ridges.

In the Virtasalmi District it was noted in Section 2, Part 1, that it is not generally possible to work out 'way-up' directions except in isolated exposures, due mainly to the lack of such indicators. However, it was demonstrated earlier in this section that the 'way-up' direction can locally be established in Hällinmäki Mine. On the basis of these observations and taking into consideration the limited exposure and structural data, it is suggested here that the ore deposit at Hällinmäki may originally have overlain amphibolite Unit Ia (Section 3, Part 1). The latter unit is both highly altered and contains many of the Type II skarn patches that have been interpeted as the conduits for hydrothermal metasomatic fluid flow.

In Figure 3.2.9 the geochemical changes which were noted to accompany skarn formation in the stockwork zone subjacent to the Cu-deposit at Hällinmäki Mine and in development of skarn patches in the 'underlying' units are summarised.

As indicated in Section 3, Part 1, the compositions of the central portions of Type III calc-silicate skarn patches can be attributed in different instances to the modification of basaltic protolith compositions by interaction with metasomatic fluids, or by the infilling of cavities by hydrothermal precipitates. In both cases, the present composition of the skarn is unlikely to provide much information on the nature of overall element addition or depletion with respect to protolith compositions, as these are likely to have been so extensively modified and the compositions probably now result from precipitation of elements supersaturated with respect to the fluid.

By contrast, the compositions observed in alteration haloes around the skarn patches are likely to represent a zone of interchange between the fluid and protolith in a zone of lower H_2O/rock ratios (Schiffman *et al.*, 1987), and possibly lower permeabilities and hence may be indicative of the broad changes in chemistry characteristic of the main hydrothermal alteration stage (MacGeehan & MacLean, 1980). The observed increases in Na and Si within the bleached zones around Type III skarns are considered evidence for spilitisation and silicification of the protoliths as a result of interaction with the hydrothermal fluid. In places the bleaching of the rock is not limited to discrete haloes, but is pervasive, with few enclaves of less altered protolith preserved (Fig. 3.1.7).

It was also noted that many of the elements depleted in these alteration haloes show a concommitant increase in the Type V skarn stockwork subjacent to the Hällinmäki ore deposit, including Cu. Hence there appears to be evidence to suggest that the elements which show marked increases in the stockwork were leached from the amphibolites underlying the ore deposit. Both Cu and S values are variable in the skarn centres and the alteration haloes. However, samples collected up to 5 m distant from the skarn patches had consistently very low values (e.g. Cu < 20ppm) suggesting that Cu, which is readily re-distributed during low temperature alteration of seafloor basalts (Gitlin, 1985), may have been leached from these amphibolites at distances greater than suggested for other elements in the distinctive alteration haloes.

However, it is almost certainly unrealistic to attempt a more quantitative (mass balance) analysis of this relationship as the precipitation of elements in the stockwork is likely to be dependent on a number of factors including original wall-rock composition, and the wall-rock mineralogy which is likely to change through time in response to changes in fluid chemistry, temperature and other properties (notably Eh and pH). It is also very unlikely that a realistic account of elements not precipitated in the stockwork can be taken, as in any exhalative system some elements are likely to be dispersed and not precipitated locally (often depending on local topography). Moreover, components which are interpreted to have re-precipitated locally, e.g. as sulphides, iron formation and chert-carbonate layers, in the form of exhalite layers, appear to have only been partially preserved as a

result of truncation and probably erosion of the sequence (see Map 4).

From comparisons of the chemistry of Group Ia and Group IIIa amphibolites, it is clear that in general Group IIIa has anomolously high CaO (c. 17%) values, in particular, for basalts. In comparison Group Ia has quite low average CaO values (c. 7%), high Na_2O and SiO_2. Clearly the marked differences in CaO content between interlayered amphibolite groups rule out pervasive calcification of the volcanic pile as witnessed at some present day volcanic centres (Kristmansdottir, 1981). Also, while Groups Ia and IIIa are apparently sourced from slightly different magmas and evolved differently (Section 3, Part 1), the very high average CaO values (c. 17%) in both this group and in Group IIc amphibolites at the Mine, points to post-crystallisation metasomatic redistribution being responsible for this enrichment. Coupled with the evidence for low CaO values in the underlying unit, and the evidence for Ca-supersaturation in syn-volcanic hydrothermal conduits (Type III skarns) then this seems further evidence for large-scale hydrothermal alteration. However, recent theoretical and experimental and field studies suggest that fluid flow convection cells are likely to be complex rather than simple (Cathles, 1981) and that fluid temperatures, composition and water:rock ratios are all likely to change through time (Cathles, 1978).

The occurrence of a banded iron formation at Karhuniemi, apparently at approximately the same stratigraphic horizon (Map 1) as that anticipated for an extension of the main Hällinmäki ore deposit suggests that there may have been an exhalative horizon developed regionally at the contact between amphibolite units Ia and IIIa.

For reasons of data confidentiality, descriptions of a number of other ore occurrences in the study area are omitted.

3.2.6 Conclusions

The Hällinmäki Cu-deposit is a polyphase deformed (exhalative) orebody. Mineralisation is stratabound except in a subjacent calc-silicate stockwork zone, and where there has been syn-kinematic remobilisation. There is a lateral gradation from disseminated chalcopyrite and pyrrhotite with some more massive ore lenses to silicate facies iron formation.

The ore is mainly hosted within thin amphibolite layers which are probably tuffaceous in origin. This points to contemporaneous volcanism and mineralisation. Faulting contemporaneous with this volcanism and mineralisation is suggested by tilting of the ore horizons and their truncation by the overlying volcanic assemblage.

Both the ore and calc-silicate gangue components were probably sourced from underlying volcanic rocks which were subjected to large-scale hydrothermal alteration through interaction with seawater. The preservation of pillow lavas in the underlying units and the distribution of ore primarily within tuffs points to development of the orebody in a relatively shallow submarine environment.

In many respects the Hällinmäki ore deposit is similar to other predominantly Cu-bearing exhalative orebodies described from present day (Skirrow & Coleman, 1982), Phanerozoic (Schiffman et al., 1987) and Archaean (Appel, 1977, 1979) examples.

The principal differences in associated gangue minerals are attributed to variations in post-mineralisation metamorphism. Hence the calc-silicate 'epidosites' noted by Schiffman et al. (1987) and MacGeehan & MacLean (1980), both from terranes where peak metamorphism was greenschist-lower amphibolite facies, are considered to be analogous here to some of the andradite-bearing skarns, metamorphosed to conditions of Upper Amphibolite-Granulite Facies metamorphism (Section 2, Part 4).

The major structure in the Mine is a large tight-isoclinal F_2 fold with an easterly-dipping axial plane and a variably plunging axis (generally gently dipping northwards). There is evidence for some syn-kinematic ore mobilisation. During D_1 and D_2 mobilisation was principally related to boudinage. There was also significant refolding during D_3 and development of breccia orebodies on refolding of the Cu-ore-bearing horizons. These breccias plunge steeply, parallel to F_3 fold hinges. Syn-D_3 remobilisation was an important mechanism responsible for enhancing the grade of ore for the purposes of economic extraction.

It was not possible to resolve completely the three-dimensional structure of the ore deposit or reconstruct the original ore distribution in anything but a schematic way due principally to truncation of original lithologies by syn-kinematic intrusions and the lack of a distinctive original stratigraphy that can readily be identified in drill core.

Fig. 3.2.1 Chalcopyrite-pyrrhotite-bearing skarned (ie. hedenbergite-bearing) amphibolite, T175m at Hällinmäki Mine. There is crude alignment of ore grains sub-parallel to a mesoscopic banding (S_0-S_1). Both ore mineral phases are remobilised to form 'stringers' of ore aligned in the S_2 fabric. There is also limited reorientation of the ore grains into parallelism with an S_3 fabric, which is expressed as a penetrative fracture cleavage in adjacent ore-free lithologies.

Fig. 3.2.2 Chalcopyrite-pyrrhotite ore is observed to occur as disseminated grains and as thin bands in amphibolite, T95m at Hällinmäki Mine. In places these bands are discordant to the S_0-S_1 layering in the silicates, and is considered evidence for syn-D_1 remobilisation of the ore. A penetrative S_2 fabric is observed to be highly discordant to S_0-S_1 in the silicates and the syn-D_1 mobilised ore. However, there is evidence for further remobilisation of ore into parallelism with S_2.

3.2.1

3.2.2

Fig. 3.2.3 Sectional plan of Mine workings at Hällinmäki Mine. Section is oriented N-S. Locations of the tunnels mapped in this study are given.

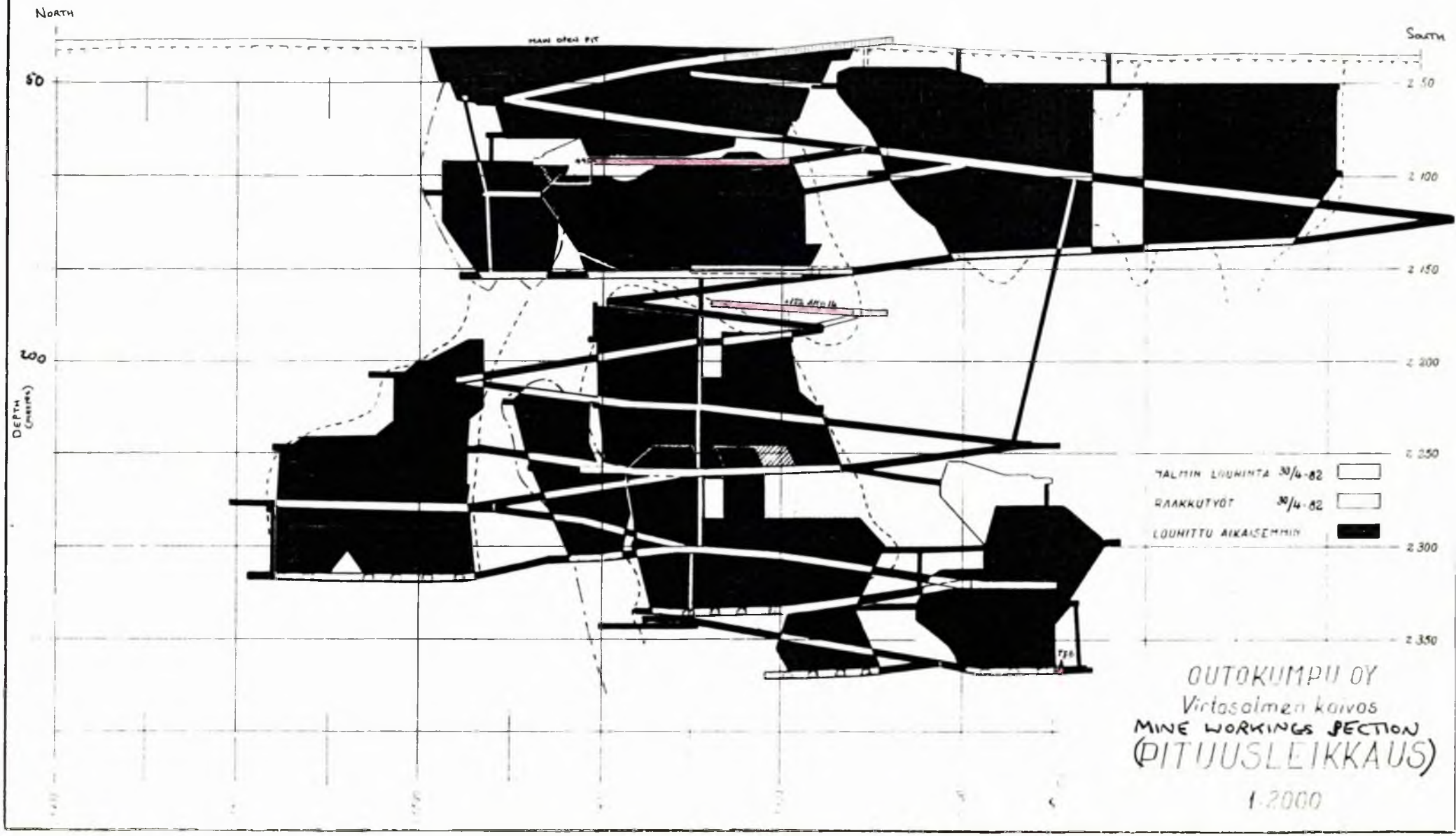
NORTH
SOUTH
MAIN OPEN PIT
50
100
DEPTH (METRES)
2 50
2 100
2 150
2 200
2 250
2 300
2 350
TALMIN LOUHINTA 30/4-82
RAAKKUTYÖT 30/4-82
LOUHITTU AIKAISEMMIN
OUTOKUMPU OY
Virtasalmen kaivos
MINE WORKINGS SECTION
(PITUUSLEIKKAUS)
1:2000

Fig. 3.2.4 Schematic diagram (not drawn to scale) showing the relationship of lithologies mapped in the small open pit exposure to those in the tunnels at T95m, T175m, T370m and around the Mine entrance.

FIGURE 3.2.4.

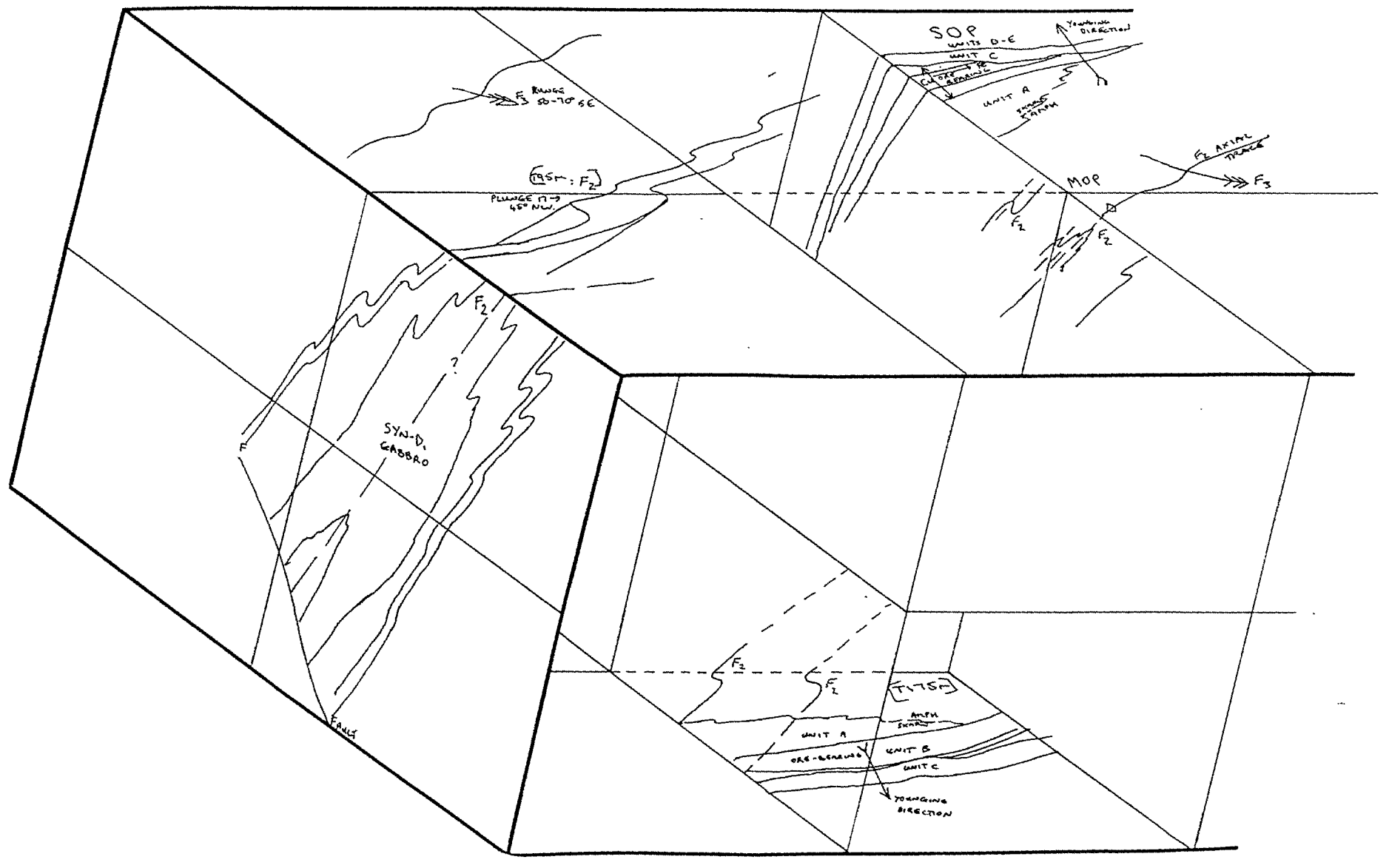
SOP
UNITS D-E
UNIT C
UNIT A
MOP
F_2 AXIAL TRACE
F_3
F_2
F_1
SYN-D_1 GABBRO
FAULT
UNIT A
UNIT B
UNIT C
YOUNGING DIRECTION

Fig. 3.2.5 Slice through hand specimen of compositionally banded magnetite-hedenbergite skarn lithology interpreted as silicate facies iron formation. There is also disseminated chalcopyrite and pyrrhotite mineralisation restricted to within certain compositional bands. The banding is composite S_0-S_1-S_2, and is observed to be folded by a minor F_3 fold. There is some remobilisation of ore, principally chalcopyrite, into small low pressure F_3 hinge zones. Sample collection from small open pit. Scale bar is 2 cm long.

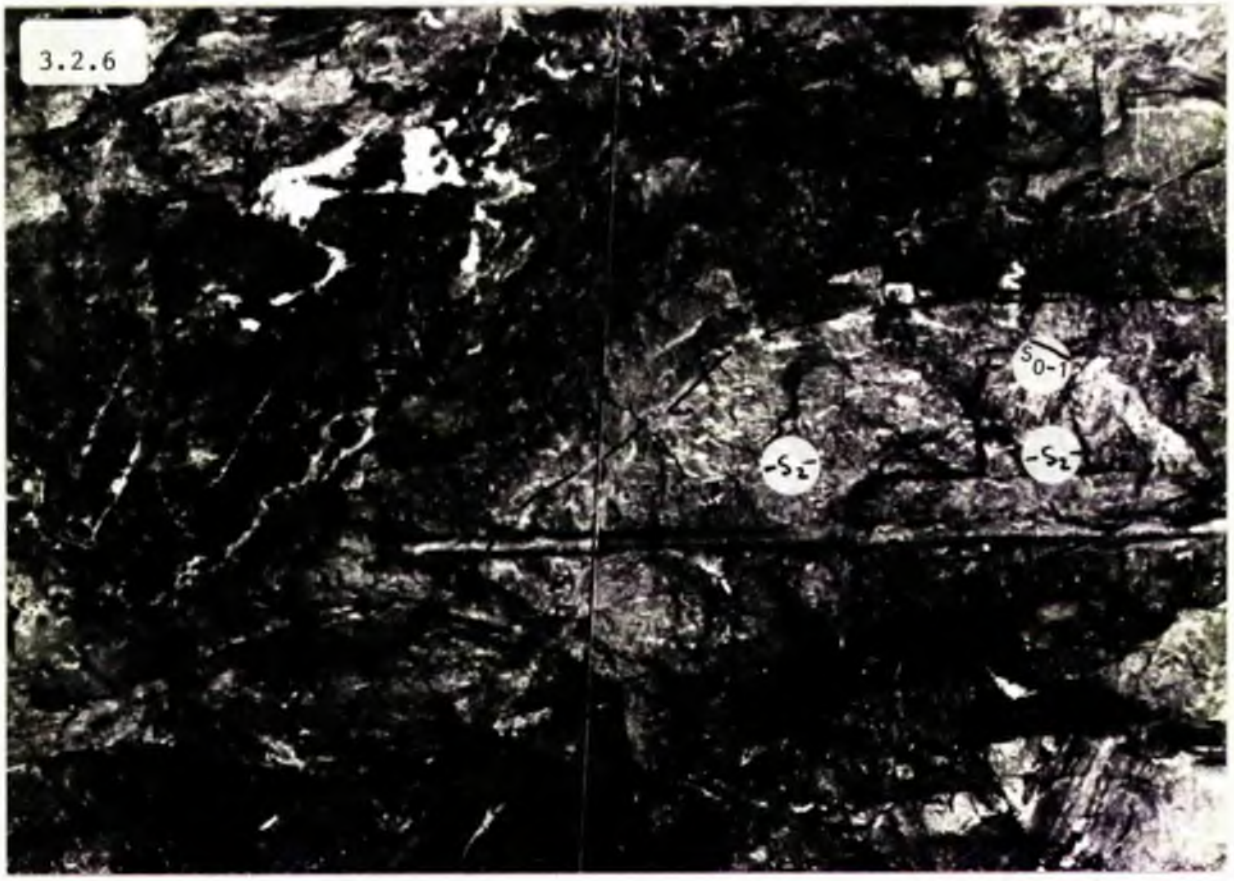

Fig. 3.2.6 Cu-ore-bearing lense within interlayered amphibolites and calc-silicate skarns, T95m. This is a photograph of a tunnel wall, oblique to strike. Vertical view is c. 2 m. A compositional banding (shown by varying ore (chalcopyrite & pyrrhotite) percentages and calc-silicate minerals) is discordant to the margins of the lense. The latter is interpreted as a D_1 boudin. Thin chalcopyrite-pyrrhotite ore stringers which are observed to be discordant to both S_0-S_1 features in the lense and the lense margins are considered to have resulted from syn-D_2 remobilisation.

Fig. 3.2.7 F_3 folds observed to deform Cu-ore-bearing amphibolites interlayered with calc-silicate skarns. Syn-D_3 remobilisation is indicated by change in nature of ore occurrence from disseminated ore (see A on Fig. 3.2.7) in F_3 limb zones, to microbreccia ore (B) nearer the hinge zone, and a massive breccia-ore (C) in the F_3 hinge zone itself.
This is a photograph of a tunnel wall in T95m. The F_3 plunges obliquely to the right and steeply (c. 60°) as viewed. Vertical view is c. 2.5 m.

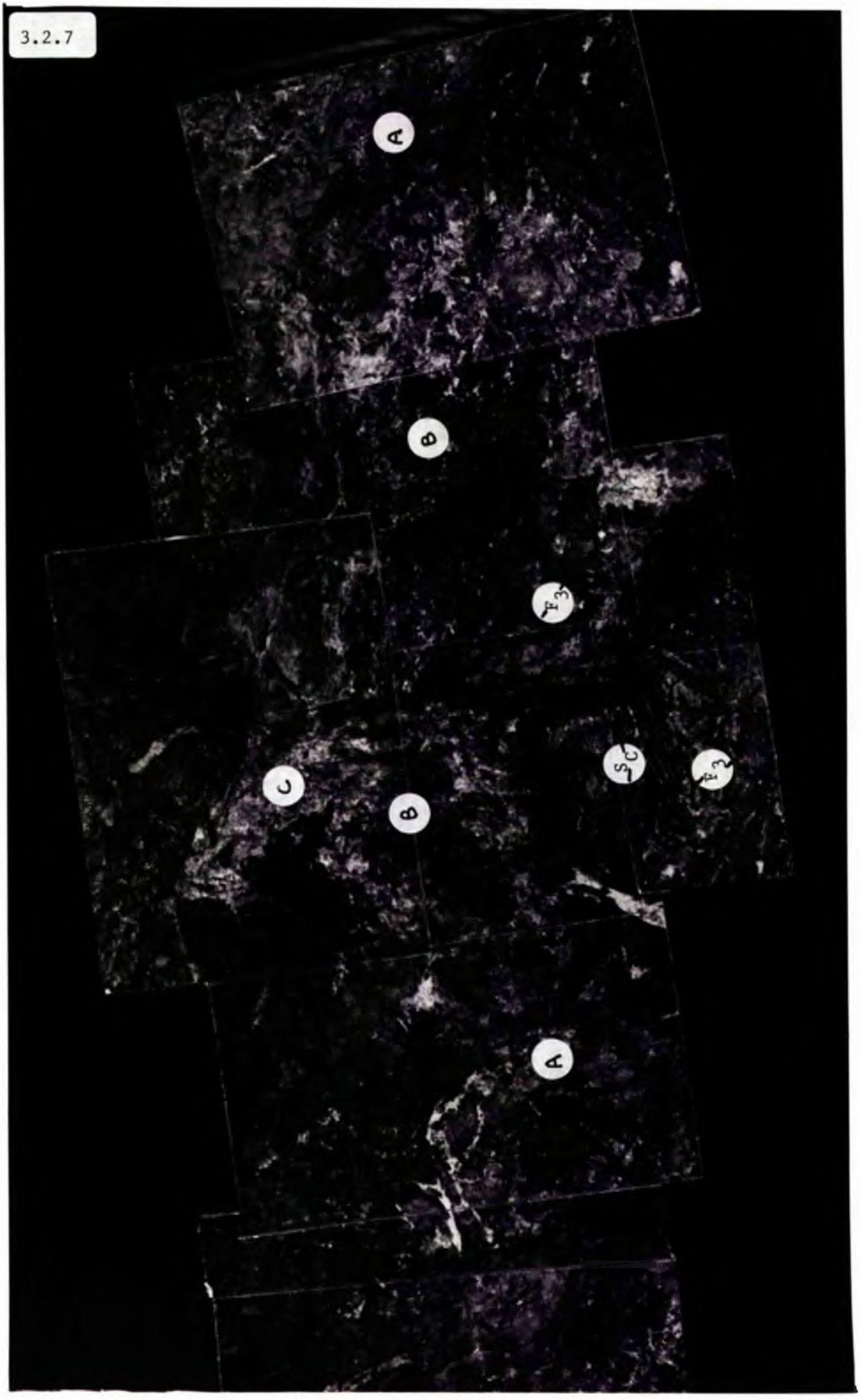
3.2.7
A
B
F3
C
B
SC
F3
A

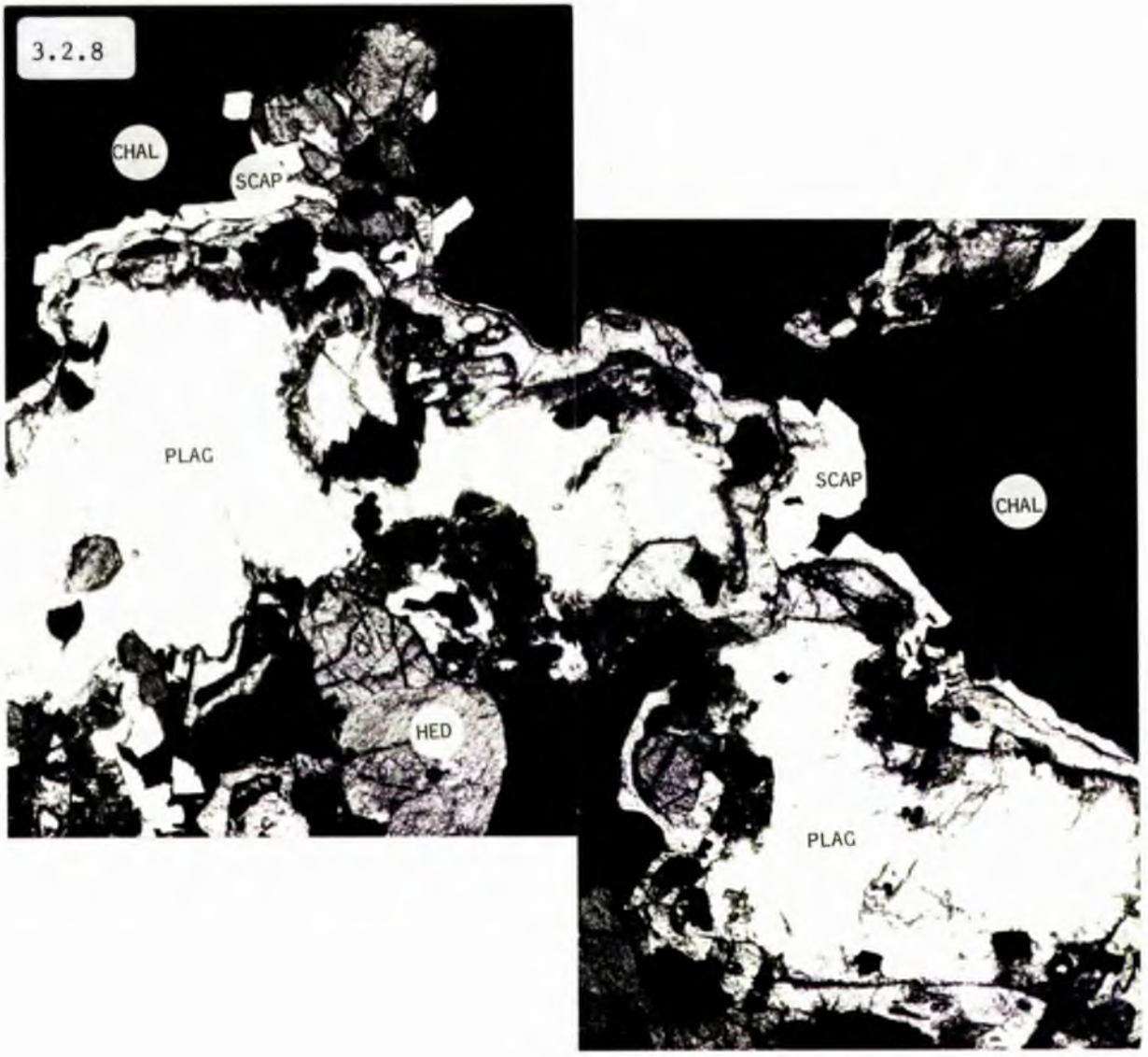

Fig. 3.2.8 Grain contacts between chalcopyrite ore remobilised during D_3 and plagioclase of the D_1-M_1-D_2-M_2 assemblage in host amphibolites are marked by reaction rims. In Figure 3.2.8 an inner discontinuous rim of scapolite is observed, and an outer apparantly continuous rim of epidote. Sample from T95m (see Fig. 3.2.7).

Fig. 3.2.9 Figure 3.2.9 is a schematic diagram which shows the geochemical changes accompanying the formation of alteration haloes around Type III skarns, and noted to accompany the formation of Type III skarns and Type V skarns subjacent to the Hällinmäki Cu-deposit.

Figure 3.2.9

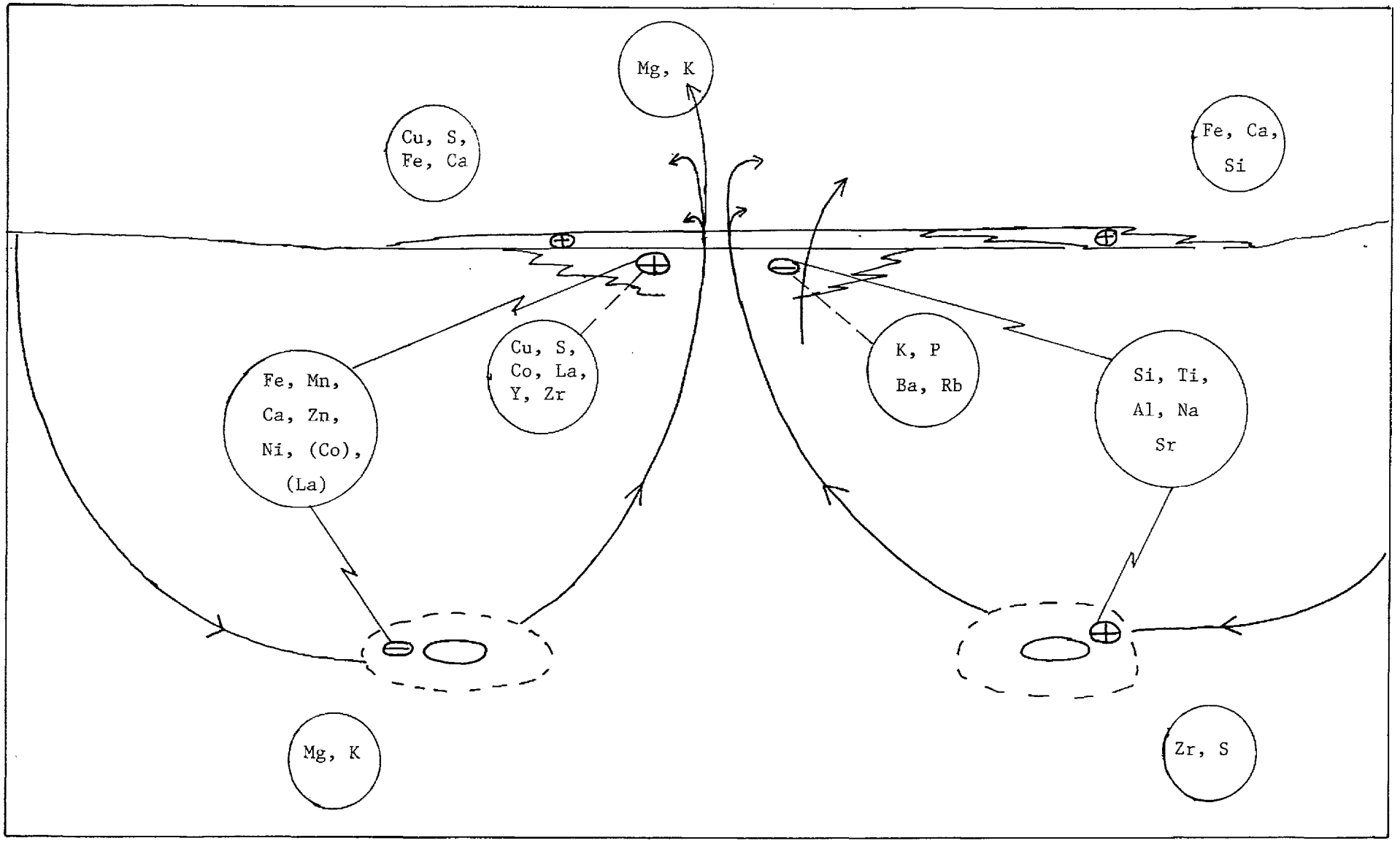
Mg, K
Cu, S,
Fe, Ca
Fe, Ca,
Si
Cu, S,
Co, La,
Y, Zr
Fe, Mn,
Ca, Zn,
Ni, (Co),
(La)
K, P
Ba, Rb
Si, Ti,
Al, Na
Sr
Mg, K
Zr, S

SECTION 4

Chemistry, petrogenesis and origin of syn-tectonic intrusions

4.1 Introduction

In Section 1 it was noted that syn-tectonic intrusions were observed to constitute around 60% of the lithological assemblage in the Virtasalmi District. Hence a study of their chemistry was considered important in attempting to understand the geological evolution of the area.

Approximately 50 samples, considered to be representative of the lithological diversity encountered, were collected and analysed for major and trace elements as described in Appendix 1. The results must be viewed as those of a preliminary investigation, as there have been only limited attempts here to examine the possibility both of chemical variation within individual intrusions, and variations between petrographically similar intrusions, which may be spatially separated or may have been emplaced at different times.

The combined field and petrofabric evidence used to determine the relative ages of emplacement of the intrusions was presented in Section 2. Brief petrographic descriptions of the main types were also given.

4.2 Sampling constraints

In Section 2 it was demonstrated that intrusions were emplaced throughout the sequence of deformation. One consequence of this is that the intrusions exposed at the

present level of erosion must have been emplaced at different crustal levels, as indicated by the decrease in metamorphic (P-T) conditions recorded in the mineral assemblages of the country rocks from D_1 to D_6.

Intrusions emplaced during D_1 were trapped at the deepest level, within amphibolites that were undergoing metamorphic differentiation and segregation of leucocratic material, and adjacent to gneisses which were being partially melted (Section 2, Part 4). Many of the intrusions emplaced at this time contain abundant xenoliths. The similarity of many of these with the country rocks indicates that some xenoliths are almost certainly stoped blocks (of amphibolite and skarn), derived locally. However, some particularly melanocratic xenoliths may be fragments of entrained and incompletely resorbed restite material. In most of the hornblende gabbro and hornblende diorite intrusions the xenoliths are variably resorbed. The resulting inhomogeneity of these intrusions makes them very difficult to sample in order to chemically characterise the magma type.

A further problem is posed by the effects of inhomogeneous strain. As demonstrated in Section 2, extreme flattening and attenuation of veins and xenoliths in high strain zones can result in formation of apparently homogeneous lithologies and the original relationships can only be demonstrated if the transition from low-high strain zones is both gradational and exposed.

4.3 Classification

The classification scheme which proved to be the most practical in assigning rock names to the various intrusions was based primarily on field observations, i.e. on petrographic, textural and structural criteria. This method of subdividing successively emplaced syn-tectonic neosomes has been described and applied successfully in several previous studies (c.f. Brown, 1978; Hopgood & Bowes, 1978; Halden, 1982). Hence this is the basis for the terms applied in Section 2, Part 2.

However, for discussion on the geochemistry of the intrusions a more rigorous quantitative approach is required. Due to the fact that a high proportion of the intrusions have a mineralogy which is the result of metamorphic recrystallisation (Section 2, Part 4), classification schemes which are based on petrographic modal analysis (e.g. Streckeisen, 1975) were considered inappropriate for this study. Instead, a scheme based on chemistry, such as that utilising normative Ab:An:Or ratios on ternary diagrams (e.g. Hietanen, 1975) is favoured in classifying the suite quantitatively. Use of this method also has an advantage as it has been employed in studies of other intrusive suites emplaced during the Svecokarelian Orogeny in Finland (e.g. Hietanen, 1975; Halden, 1982; Fergusson, 1982), facilitating comparisons.

Figure 4.1 is a normative An-Ab-Or plot for the Virtasalmi intrusions. Under this classification it is apparent the analyses form a continuous series ranging across the fields delineated for gabbros, quartz diorites, tonalites, monzo-tonalites,

and granitic trondhjemites. Hence in general the rock names applied in Section 2, Part 2, were found to be consistent with the terms suggested from the fields of composition outlined in Figure 4.1. However there are a number of differences, notably the fact that most 'granodiorites' identified in the field fall within the tonalite or monzo-tonalite fields and some leucogabbros (i.e. SiO_2 = 45-52%) fall within the diorite field. Also it should be noted that the fine- to medium-grained basic dykes plot within the gabbro field.

Another refinement considered necessary is a stricter chemical definition for trondhjemites than that implied in Figure 1, in view of the wide variations in use of this term (summary in Barker, 1979). The definition of Barker (1979), which is based principally on chemistry, is preferred here. Hence analysis nos. 142, 162 and 179 which fall within the monzo-tonalite field in Figure 1 are termed trondhjemites in this study. It should be noted however that the subdivision of trondhjemites into low-Al_2O_3 and high-Al_2O_3 types (Barker et al., 1976; Barker, 1979) is unwarranted, as the best fit line for the Virtasalmi intrusions passes through, or is at least within one standard deviation of the point at which the separation is made on a plot of Al_2O_3 vs SiO_2 (Fig. 4.2). One last amendment required to the classification indicated in Figure 4.1 is the subdivision of quartz diorites into diorites and quartz diorites, as many of the diorites were observed to be petrographically devoid of free quartz. This is also demonstrated on a plot of K_2O vs CaO (Fig. 4.3), where a large number of the 'diorites' are observed to lie within the field

of no free quartz. In Appendix 3, both the field term applied in Section 2, and the terminology established in this section (in brackets) is given.

A close similarity between the range of compositions encountered in the Virtasalmi intrusive suite and that from south-west Finland (Hietanen, 1975) is observed (Fig. 4.1). The most significant difference appears to be the lower average K_2O content of the Virtasalmi intrusive suite. Nevertheless on an A:F:M plot (Fig. 4.4) Virtasalmi intrusions show a distinct calc-alkaline trend similar to that observed in other studies of syn-kinematic intrusions elsewhere in the Svecofennides (Hietanen, 1975; Arth et al., 1978; Fergusson, 1982).

In summary, the syn-kinematic intrusions in the Virtasalmi District constitute a gabbro-diorite(-quartz diorite)-tonalite-trondhjemite suite broadly similar to those described throughout the Svecokarelides (Arth et al., 1978; Front & Nurmi, 1987).

4.4 Major and trace element geochemistry

Plots of $Fe_2O_3^{tot}$, CaO, MgO, TiO_2, MnO, P_2O_5, Cr, Ni, Co and Zn vs SiO_2 (Fig. 4.5a-j) show relatively consistent linear covariation. This, together with the close spatial association shown by the suite, suggests that despite the temporal variation in relative age of emplacement, the majority of intrusions are co-genetic. The relatively limited amount of scatter from the best fit lines indicated in Figure 4.5a-j suggests that SiO_2 is a useful indicator of differentiation in these rocks and that neither SiO_2 nor any of

the aforementioned elements have undergone significant post-crystallisation mobilisation.

However there are a few important analyses which form groups distinct from the trends displayed by the majority of intrusions. In the plots of MgO, Cr and Ni vs SiO_2 (Fig. 4.5a, 5b and 5c respectively), three distinct small subgroups can be identified. Sub-group I intrusions consist of syn-D_1 leuco-gabbros from Hällinmäki Mine which are the earliest emplaced intrusions in the mine vicinity, and within which compositional layering in the form of up to 6 cm thick hornblende-rich layers (Fig.2.2.1)was identified. This is considered evidence for crystal settling and formation of cumulate layering in the intrusions. Sub-group II intrusions comprise a suite of syn-D_2 diorites in the Kiviniemi area and sub-group IIIa,b intrusions were sampled from biotite amphibolite dykes intruded syn-D_1 to D_4. The fact that in these groups Ni, Cr and Mg contents are similar for variable SiO_2 makes it unlikely that the magma responsible for the main intrusive suite could have produced these abundances. Hence different source compositions are indicated. The relative similarity in other elements vs SiO_2 in Fig. 4.5, however, suggests that these differences reflect relatively minor variations in source chemistry.

In contrast to the distribution of elements observed in Fig. 4.5, plots of K_2O, Na_2O, Rb, Ba, Sr, Zr and to a lesser extent Ce and La vs SiO_2 (Fig. 4.6a-h) are characterised by a more scattered distribution. This is considered most likely to be due to post-crystallisation alteration although in the plot of K_2O vs SiO_2, fractional crystallisation of a biotite-rich (or at least K_2O-rich) magma is suggested by the presence

of a suite of biotite amphibolite dykes. In sample 228 (porphyritic granodiorite) K_2O is higher due to concentration of orthoclase phenocrysts. Hence in some instances a component of the scattering is the result of fractional crystallisation, and not solely metasomatic redistribution. This is similarly demonstrated in a plot of $(K_2O + Na_2O)$ vs SiO_2 (Fig. 4.7). In this plot most intrusions plot in the subalkaline field, but others plot in the alkaline field, including the biotite amphibolite dykes. However not all of the scatter can be explained by the precipitation of phenocryst phases.

The fact that there is LIL redistribution is particularly important towards studies of the pre-tectonic amphibolites, as from this study a component of the LIL element redistribution is very probably syn-deformational in origin. Equally, the lack of mobility shown by the other elements is further evidence for re-distribution of these elements in the amphibolites to be of pre-tectonic origin.

Plots of Al_2O_3 and Ga vs SiO_2 (Fig. 4.2 and Fig. 4.8 respectively) show initial increases in both Al_2O_3 and Ga followed by systematic decreases from intermediate to acidic compositions. These elements also show very little effect of post-crystallisation redistribution.

As mentioned above, there are a number of high-K_2O (now biotite-rich amphibolite) dykes (sub-group III intrusions), although the absence of evidence for biotite-rich cumulates suggests that there was a relatively small degree of biotite removal from melts. Biotite fractional crystallisation is supported by higher Ba content (Fig. 4.6d) in these biotite-rich amphibolites.

Plots of Y_N vs Y_N/La_N and Y_N vs Y_N/Ce_N are presented in Figure 4.9 a,b. In the absence of a full set of REE data these diagrams can be used to predict the rough shape of REE patterns (Halden, 1982). In Figure 4.9 a,b the slopes are negative and this suggests LREE enrichment. This is most likely to have resulted by removal of hornblende from basic-intermediate magmas.

Hence there is evidence to suggest that development of the Virtasalmi syn-tectonic intrusive suite involved fractional crystallisation processes and in particular the removal of hornblende and biotite from the melt. This is consistent with modelling which predicts that the formation of trondhjemitic magmas is strongly controlled by fractionation of these two minerals (Barker, 1979).

4.5 Origin of the syn-kinematic intrusive suite - a summary and discussion

From the available field, petrographic and geochemical evidence presented in Section 2, Part 2, and earlier in this section it seems likely that different processes were operative to varying extents in producing the range of composition encountered in the syn-kinematic intrusive suite. In addition to providing a summary of the evidence, an attempt is made in this section to determine which process, if any, was dominant in the evolution of this suite, while the implications for the initial source is also discussed.

4.5(i) Stoping and assimilation

There is field evidence for stoping and assimilation of xenoliths (by mechanical breakdown followed by dissolution) (Fig. 4.10) though only in magmas of gabbroic-dioritic composition and particularly during D_1, i.e. at the deepest level-highest grade metamorphic conditions to which these rocks were subjected. However, there is also evidence to indicate assimilation during emplacement of syn-D_6 intrusions (Fig. 2.3.4) and it is not clear to what extent these later intrusions, and those of gabbroic-dioritic composition in particular, have assimilated country rock at deeper levels.

4.5 (ii) Partial melting

In some of the metavolcanic amphibolites around Kiviniemi, there is limited evidence which indicates that leucocratic segregations, formed as a result of metamorphic differentiation during D_1, were tectonically remobilised over distances of a few centimetres during late-D_1. These segregations were observed to coalesce to form small amounts of aplitic or trondhjemitic neosome discordant to S_1 (Fig. 2.3.1). No similar features were recorded elsewhere in the study area. However, in some of the syn-D_1 basic intrusions, particularly melanocratic coarse-grained hornblende-rich xenoliths were noted (Fig. 4.11). These are dissimilar to adjacent country rock and are interpreted as entrained restite material or as disrupted cumulate layers.

4.5 (iii) Fractional crystallisation

The wide range in rock compositions through time and the lack of compositional gaps in the magma series, together with their close spatial association, development of apparently cogenetic trondhjemitic magmas, and evidence for LREE enrichment all point to fractional crystallisation involving hornblende, biotite, sphene/ilmenite (+ plagioclase?) as an important mechanism in the formation of these rocks. This interpretation is supported by the common occurrence of relatively small but compositionally zoned large dyke-like intrusions which display a wide range in compositions, e.g. from diorite-granodiorite-complex granitic pegmatites within one body. This association is considered to have resulted from fractional crystallisation in a partially closed system which underwent episodes of pressure release and consequential resurgent boiling in the melt, as summarised in Park & MacDiarmid (1975).

4.5 (iv) Discussion

In the absence of isotopic data, consideration of the geochemistry, mineralogy and the overall geology can be used to provide pointers to the likely classification of the granitoid suite in terms of S, I or A types (Pitcher, 1983), although this must be a less certain technique outwith the Phanerozoic.

The dominance of tonalitic magmas, diversity of compositional types, calc-alkaline nature of the suite and the presence of sphene as a crystallising phase (c.f. White & Chappell, 1977) all suggest I-type affinities for this intrusive

suite. This is consistent with the interpretations of similar syn-kinematic intrusive suites emplaced in the Svecokarelides (Patchett et al., 1987; Front & Nurmi, 1987).

This I-type character implies that the granitoids were derived by partial melting of igneous material, either involving fractional crystallisation of basaltic magmas derived directly from amphibolite or eclogite in the sub-lithospheric mantle, or by variable degrees of partial melting of basaltic source rocks in the lower crust (Arth et al., 1978; Gromet & Silver, 1987). In the absence of REE and isotopic data, field and geochemical evidence is used here to try to elucidate some of the processes responsible for formation of the syn-kinematic intrusive suite.

From the geochemical evidence outlined above (e.g. Cr, Ni and MgO vs SiO_2) it would appear that some of the more basic intrusions are not co-magmatic with the rest of the suite. This probably points to different sources for these magmas. Also, intrusion of some of the more basic members of the suite does appear to have resulted in some re-working of the pre-existing (largely meta-volcanic) crust by stoping and assimilation. Reworking of this crust (at greater depths) is further supported by the direct observation of limited partial melting within the supracrustal sequence at the D_1-M_1 crustal level. Extrapolation of the syn-kinematic geothermal gradients suggested from the D_1-M_1 and D_2-M_2 metamorphic assemblages in the study area also indicates that granitoid melts may be derived by partial melting of basaltic source rocks in deeper parts of the crust (Section 2, Part 5).

When considered along with the evidence for fractional crystallisation, it is clear that the syn-kinematic intrusions have had a complex history which may have included hybridisation of crustal and mantle magmas. Front & Nurmi (1987) have suggested that intrusion of mafic plutons into the lower crust would have provided additional localised heat sources which may have caused remelting to produce granitoid magmas.

Without major, trace and REE modelling however, in addition to greater sampling and isotopic data, it is not possible to throw further light on the origin of the syn-kinematic suite in this study. It should be noted, however, that there appear to be some important differences between the intrusions in the Virtasalmi District and those in the Uusikaupunki-Kalanti area in Southern Finland where (1) the trondhjemites appear to be 20 m.y. older than the gabbros and diorites-tonalites, (2) have lower ε_{Nd} values than the rest of the suite (Patchett & Kouvo, 1986), and (3) the mafic rocks occur only as small inclusions within homogeneous tonalites and trondhjemites. This is taken to imply that partial melting processes controlled the composition of the suite (Front & Nurmi, 1987) rather than fractional crystallisation (Arth et al., 1978).

However, in contrast to this, trondhjemites in the Virtasalmi District were emplaced throughout the structural sequence, together with basic rocks (Section 2.2). Also, many of the tonalitic intrusions are inhomogeneous or compositionally zoned.

It is not clear whether these variations reflect fundamental differences in the two suites, or whether there may be some sampling bias. Fergusson (1982) noted in a study of syn-tectonic intrusions in south-west Finland that felsic minor intrusions, which were emplaced at a late syn-kinematic stage, were compositionally related to earlier emplaced diorites, etc.. Hence great care has to be taken to ensure that the timing of intrusion relative to the structural sequence is ascertained, and that the isotope systematics of intrusions from the same suite are compared, before generalised conclusions can be drawn on the origin of and dominant processes operative in formation of the syn-kinematic intrusive suites of the Svecokarelides.

Fig. 4.1 Figure 4.1 is an An-Ab-Or plot for the Virtasalmi syn-kinematic intrusions (after Hietanen, 1975) (Field A). For comparison, the field of composition for syn-kinematic intrusions from SW Finland is plotted (Field B).
From Figure 4.1 it can be seen that there are marked differences between the syn-kinematic intrusions in the Virtasalmi District (and SW Finland) in comparison with syn-kinematic intrusions in the Savonranta area (after Halden, 1982) (Fields C and D).

The numbered areas correspond to the following lithologies

1. gabbro
2. quartz diorite
3. granodiorite
4. tonalite
5. monzotonalite
6. quartz monzonite
7. granite-trondhjemite
8. granite
9. alkali granite

KEY TO SYMBOLS USED FOR VIRTASALMI INTRUSIONS:

× DIORITES, TONALITES
\+ BASIC INTRUSIONS
□ BIOTITE AMPHIBOLITE DYKES
● GRANODIORITES – TRONDHJEMITES

Figure 4.1

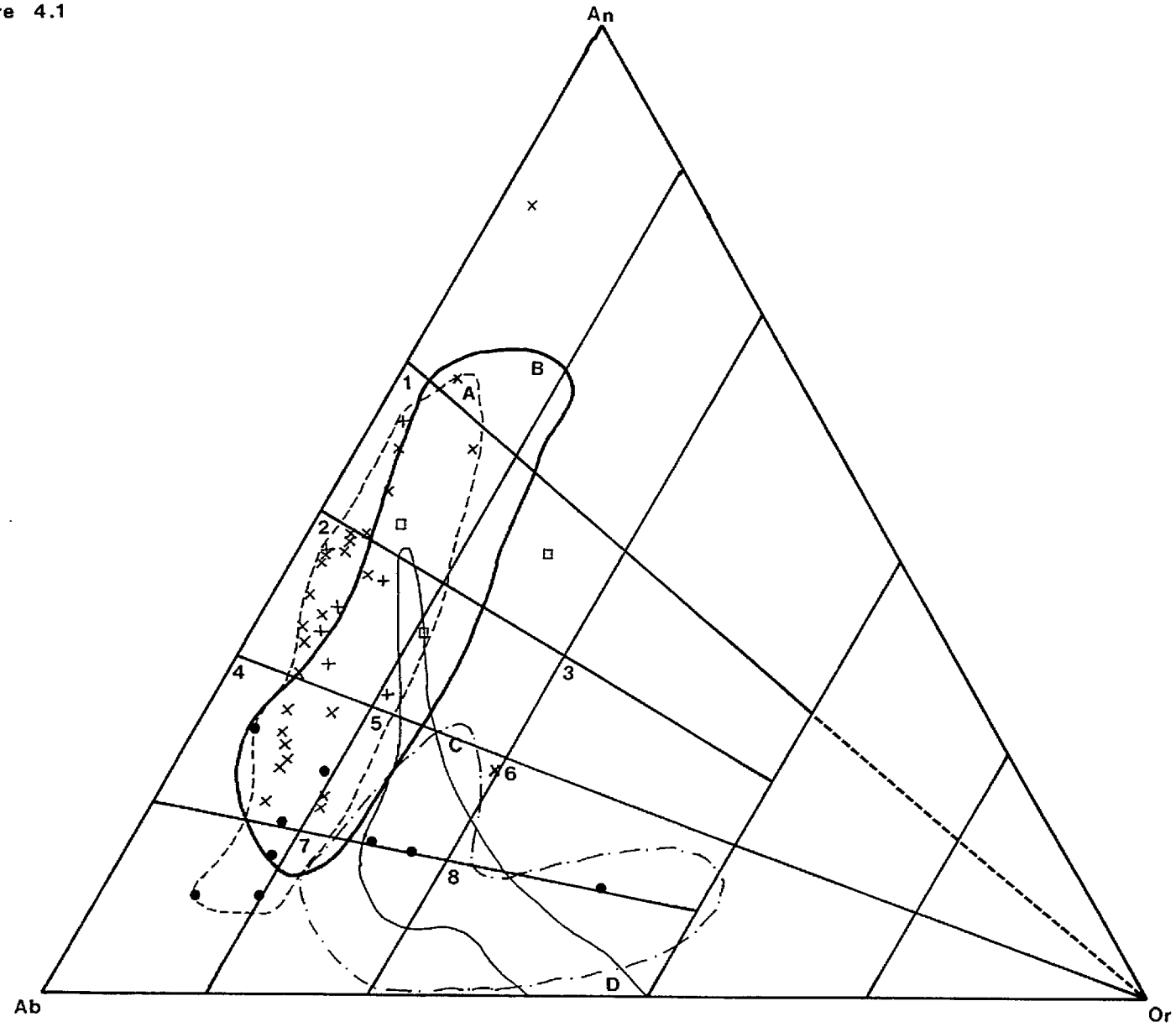

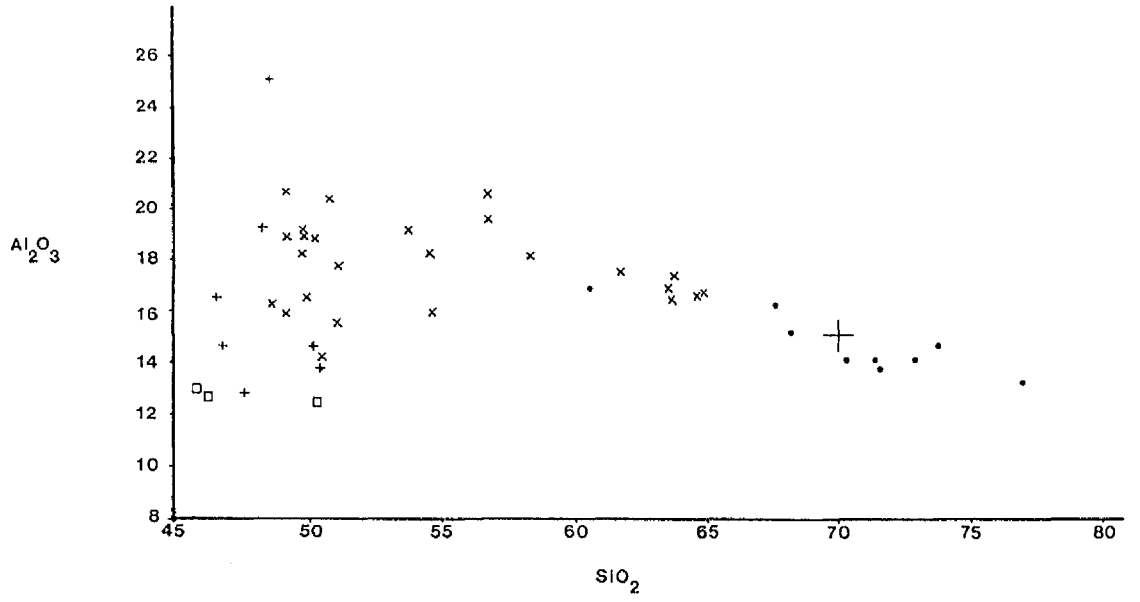

Fig. 4.2 Figure 4.2 is a plot of Al_2O_3 vs SiO_2 for Virtasalmi intrusions. The large plus sign denotes the point above or below which the high-low alumina subdivision of Barker (1979) is made.

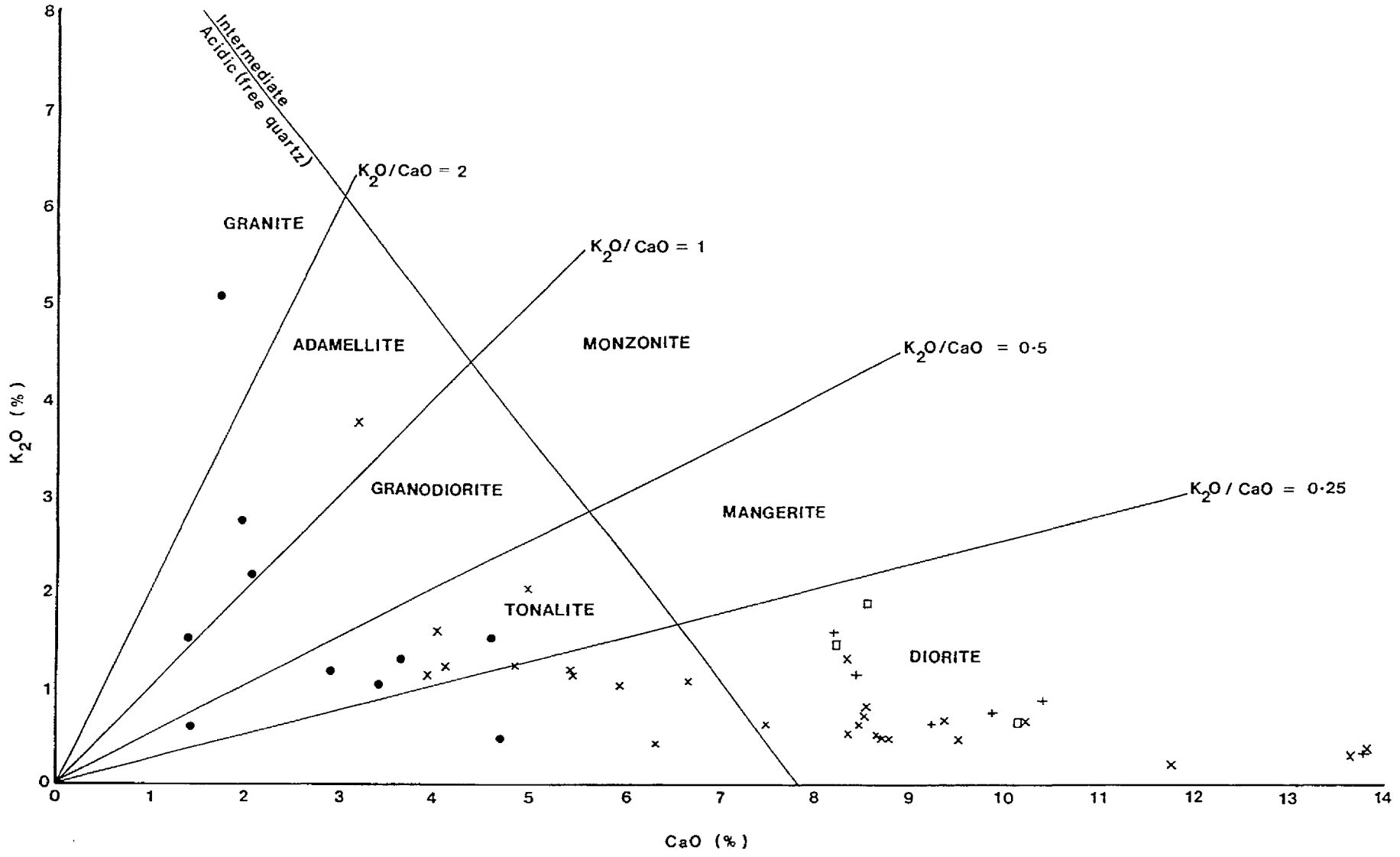

Fig. 4.3 A plot of K_2O vs CaO for Virtasalmi intrusions. The compositional fields delineated are from Harpum (1963)

Figure 4.4

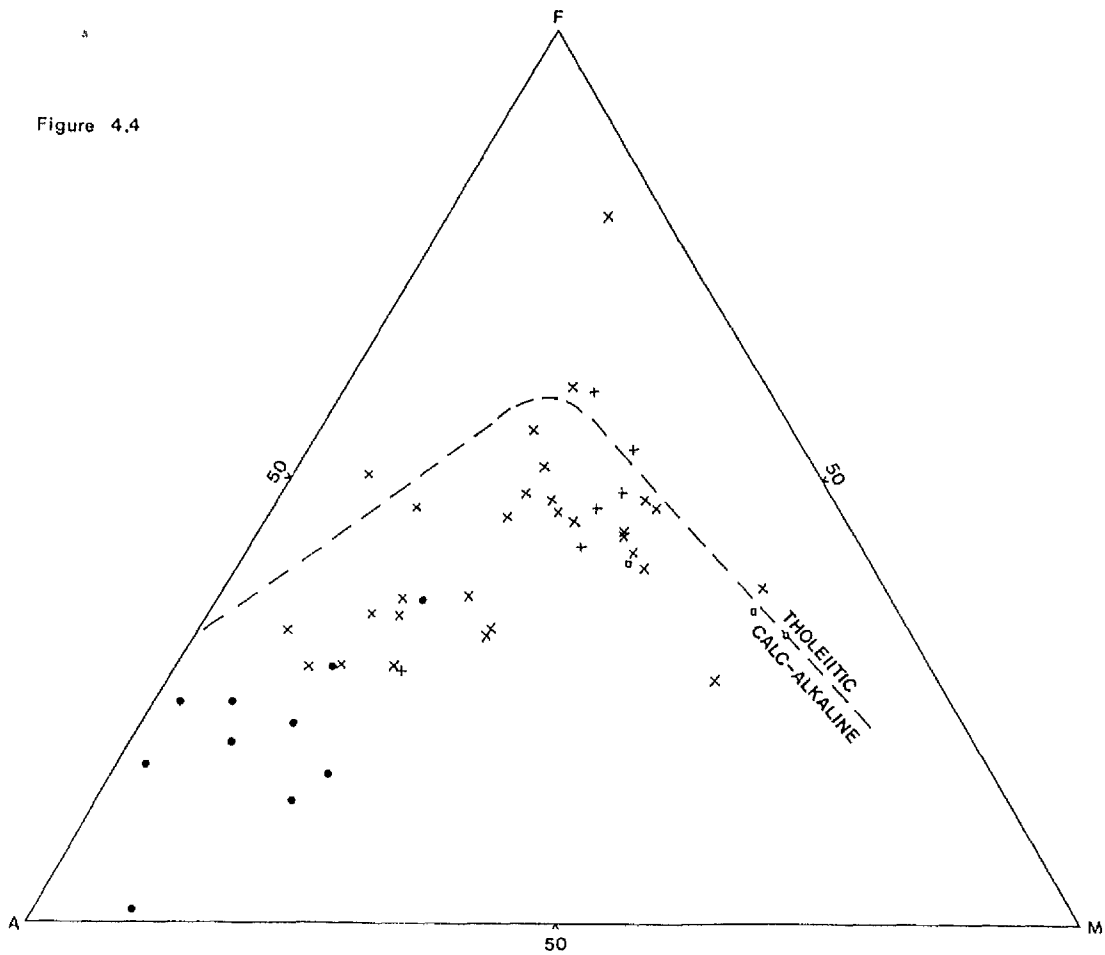

Fig. 4.4 A calc-alkaline trend is shown by Virtasalmi intrusions on an AFM diagram.

Fig. 4.5a-j Plots of Fe_2O_3, CaO, MgO, TiO_2, MnO, P_2O_5, Cr, Ni, Co and Zn vs SiO_2 for Virtasalmi intrusions are presented in Figures 4.5a-j respectively. Fairly linear distributions are seen on all these figures.

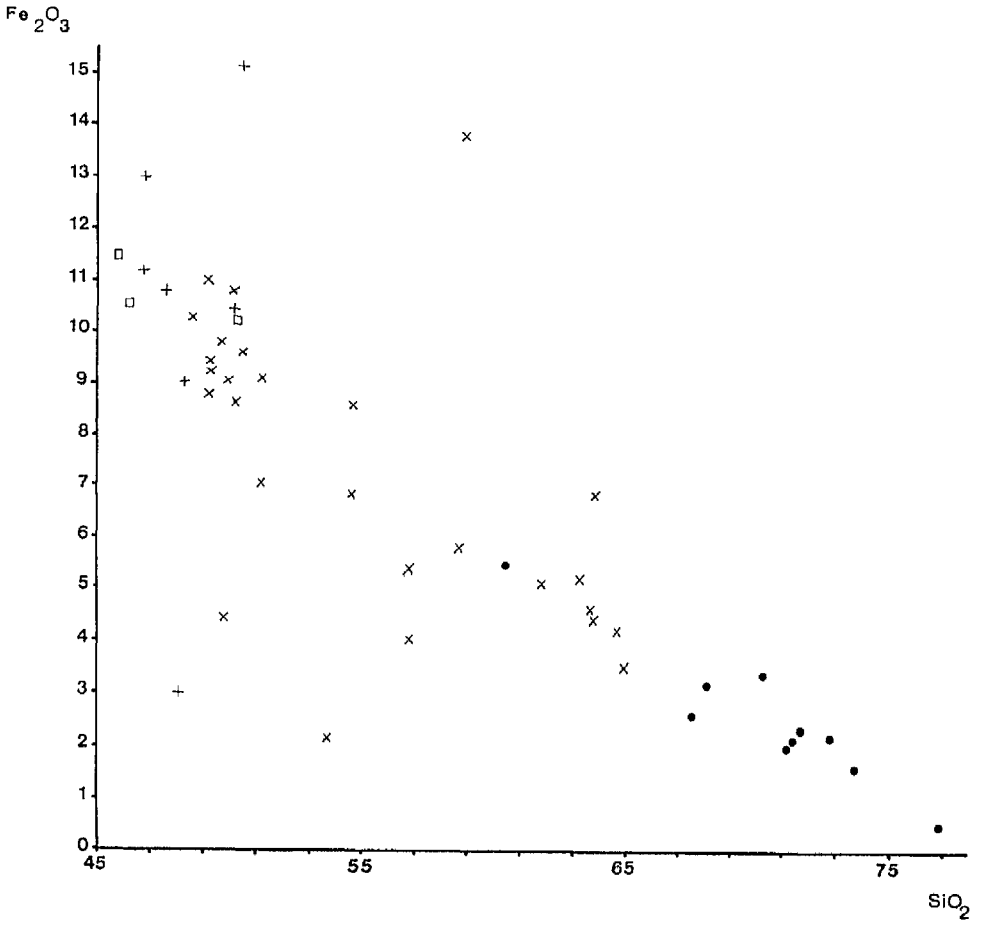

Figure 4.5a

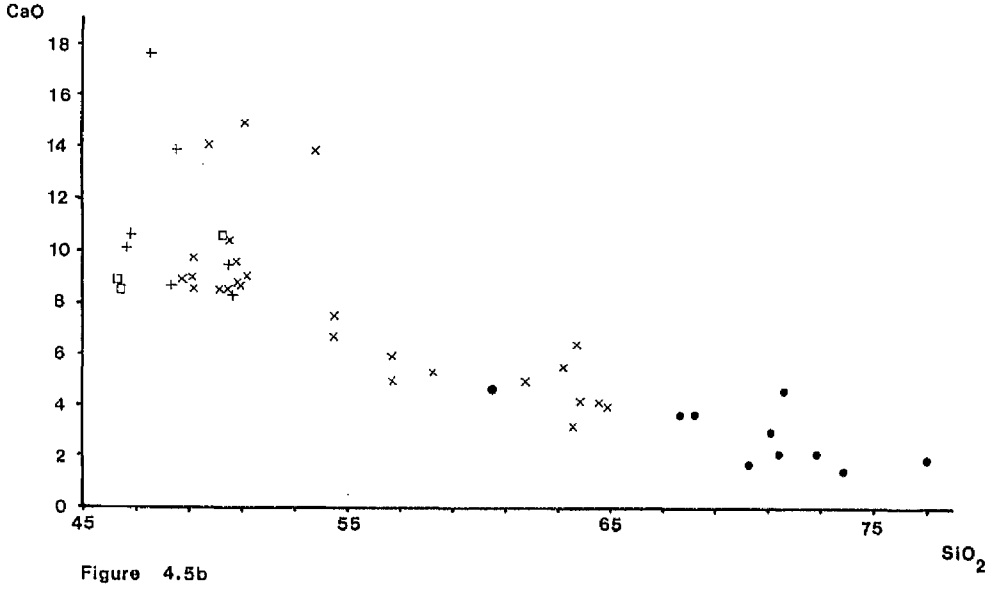

Figure 4.5b

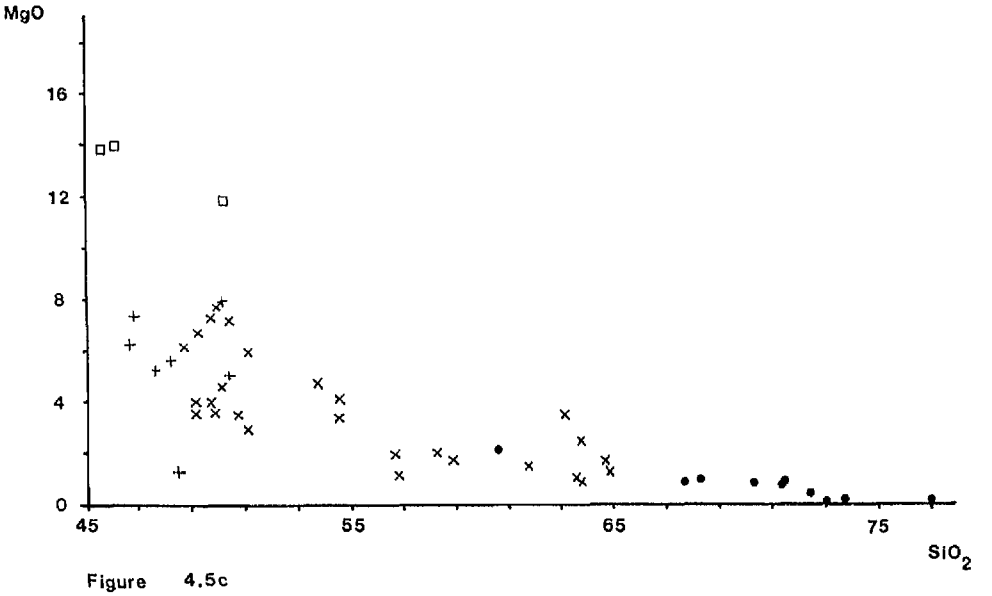

Figure 4.5c

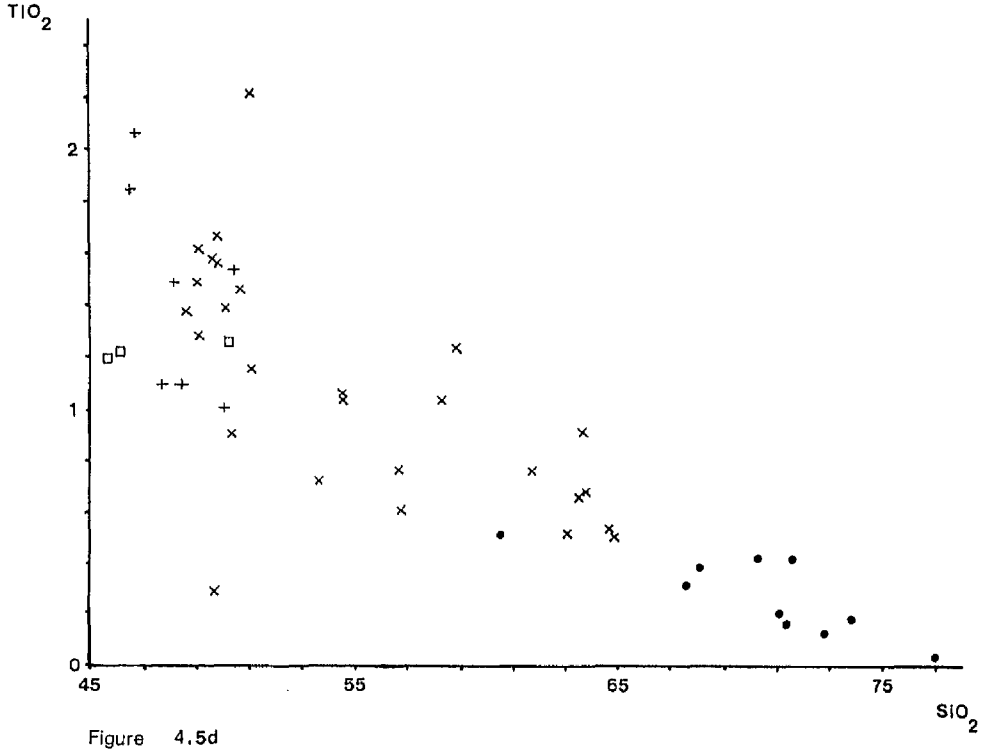

Figure 4.5d

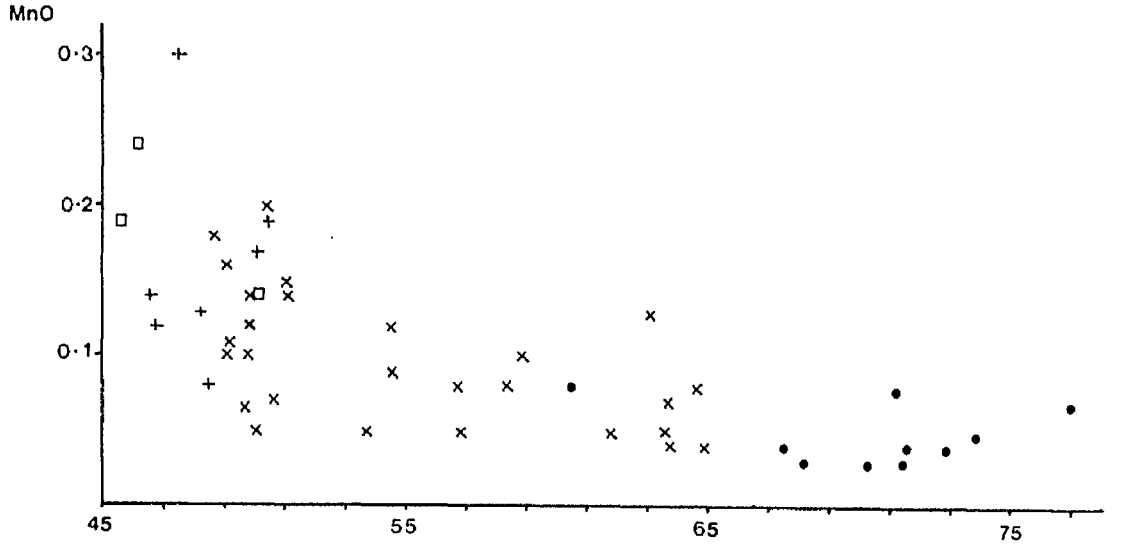

Figure 4.5e

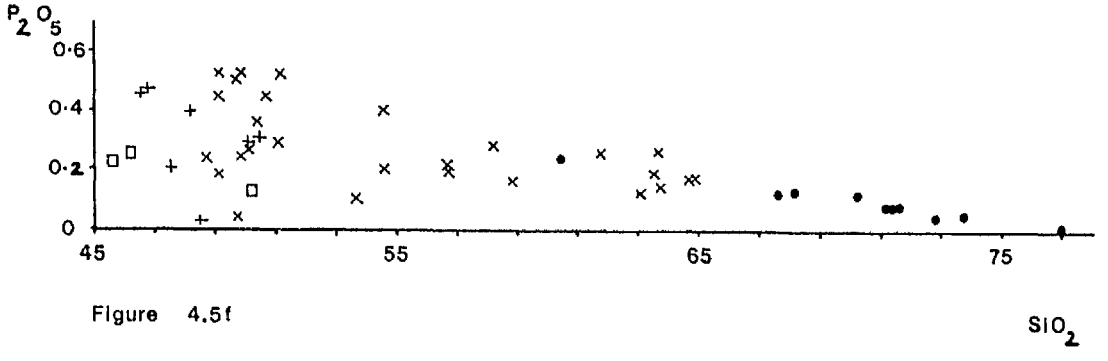

Figure 4.5f

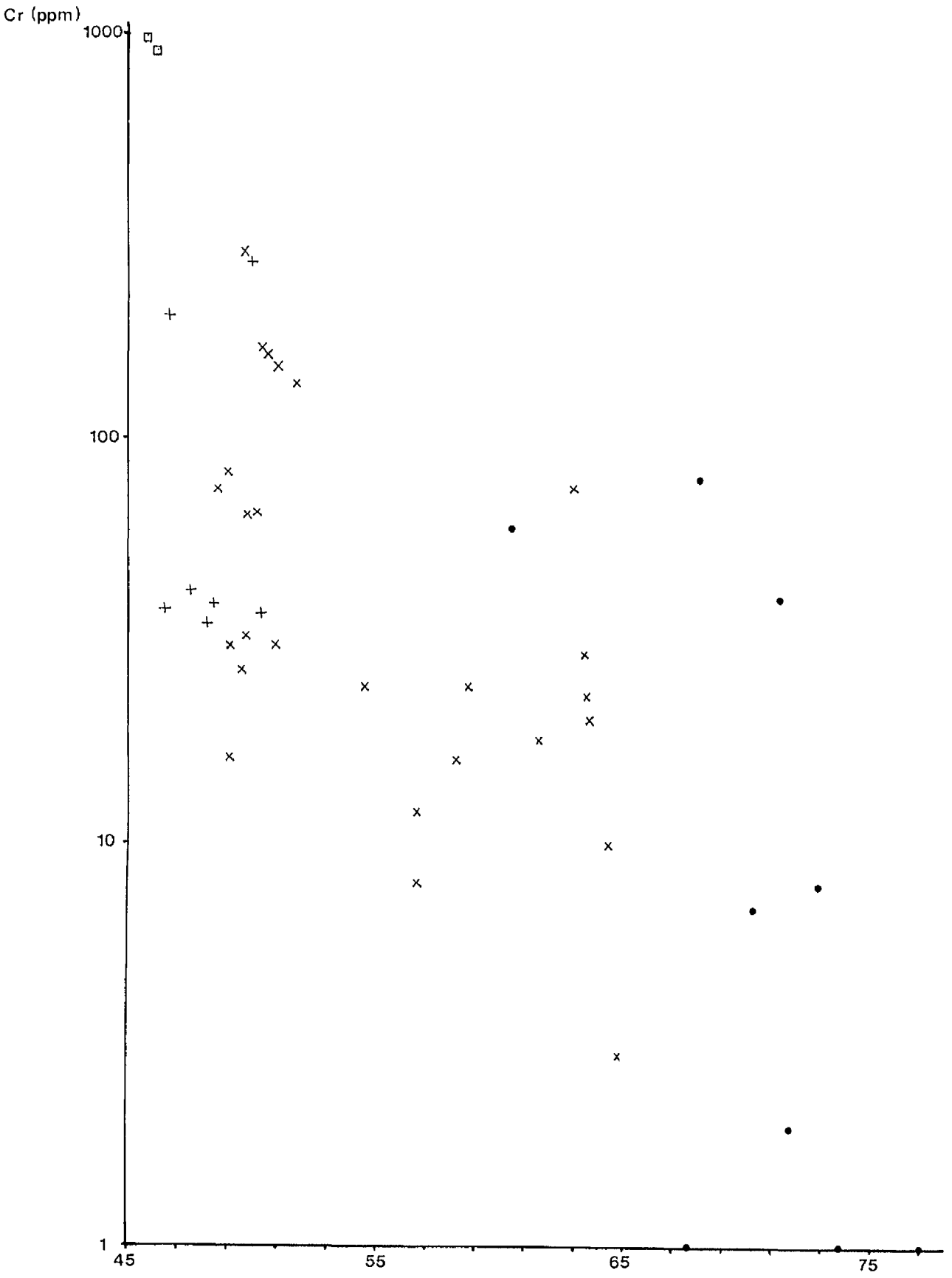

Figure 4.5g

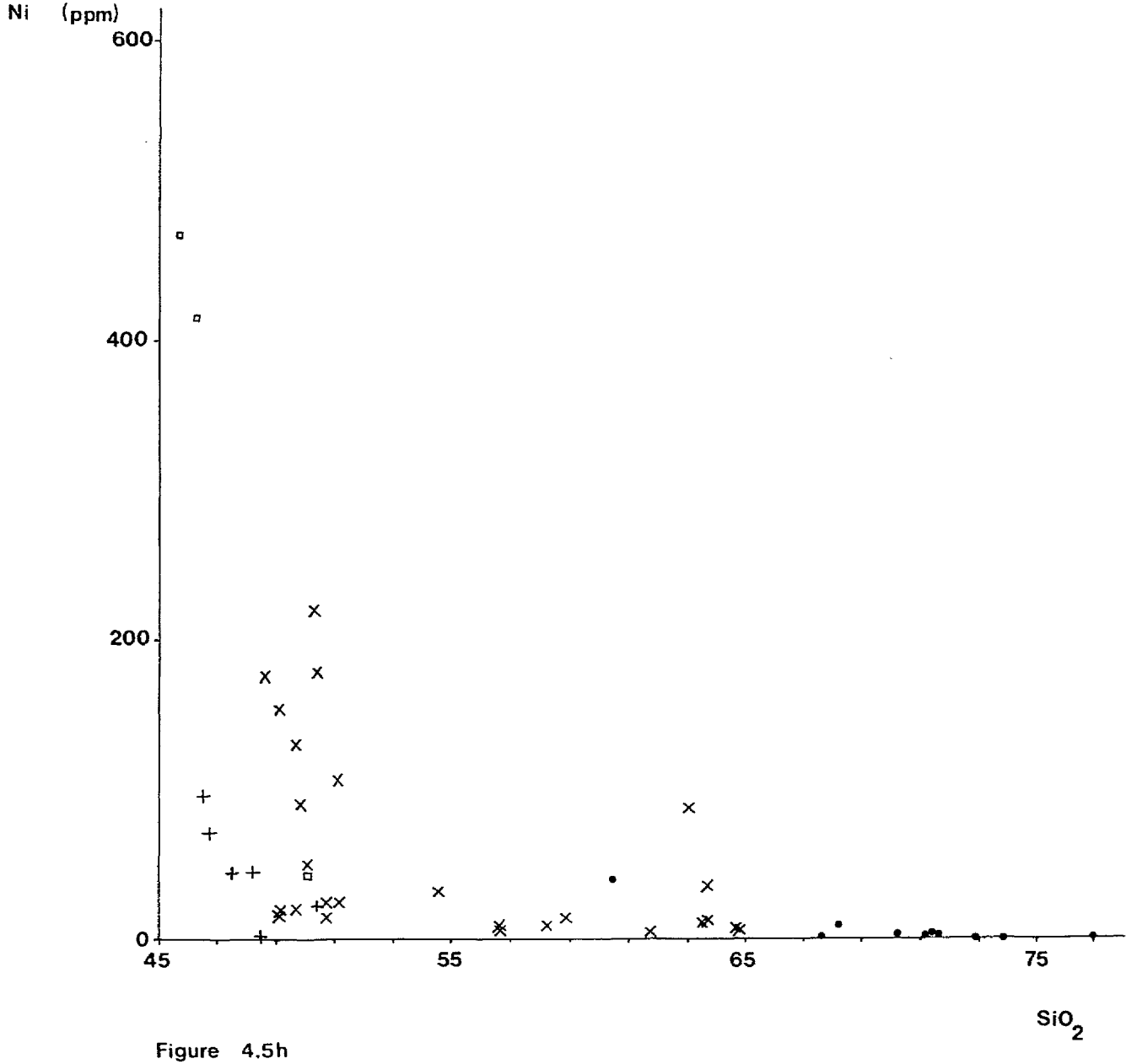

Figure 4.5h

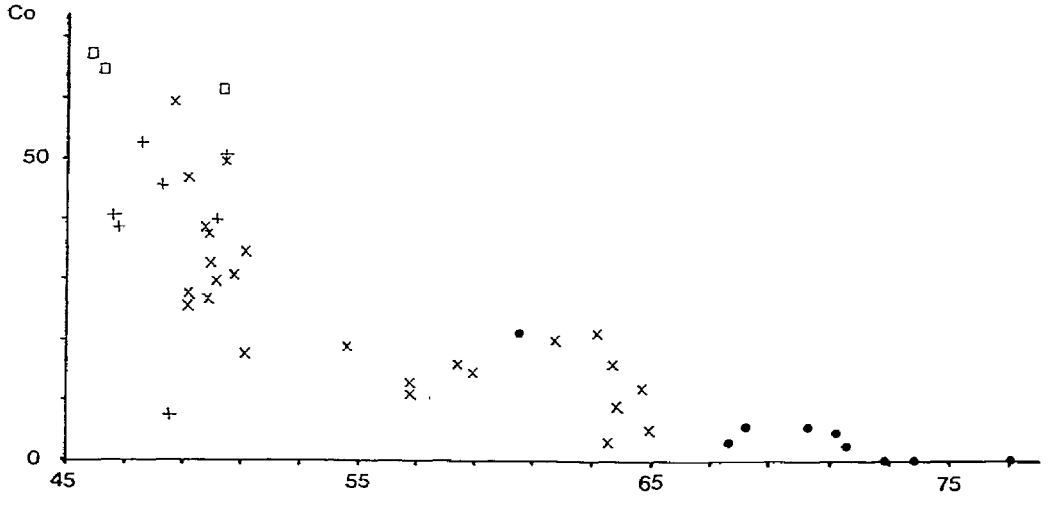

Figure 4.5i

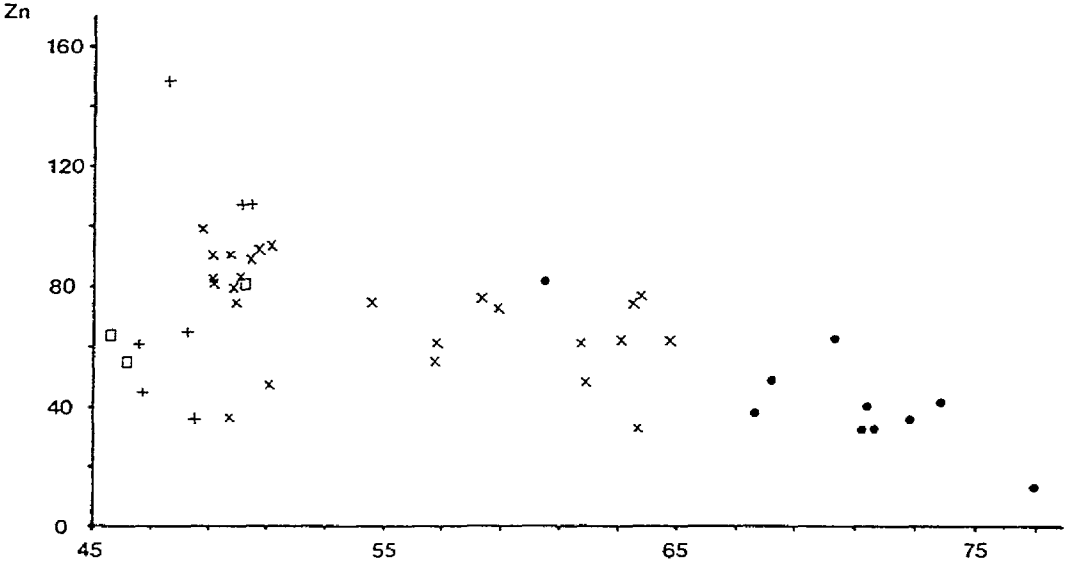

Figure 4.5j

Figs. 4.6a-h Plots of K_2O, Na_2O, Rb, Ba, Sr, Zr, Ce and La vs SiO_2 for Virtasalmi intrusions are presented in Figures 4.6a-h respectively. A more scattered distribution than in Figure 4.5a-j is noted.

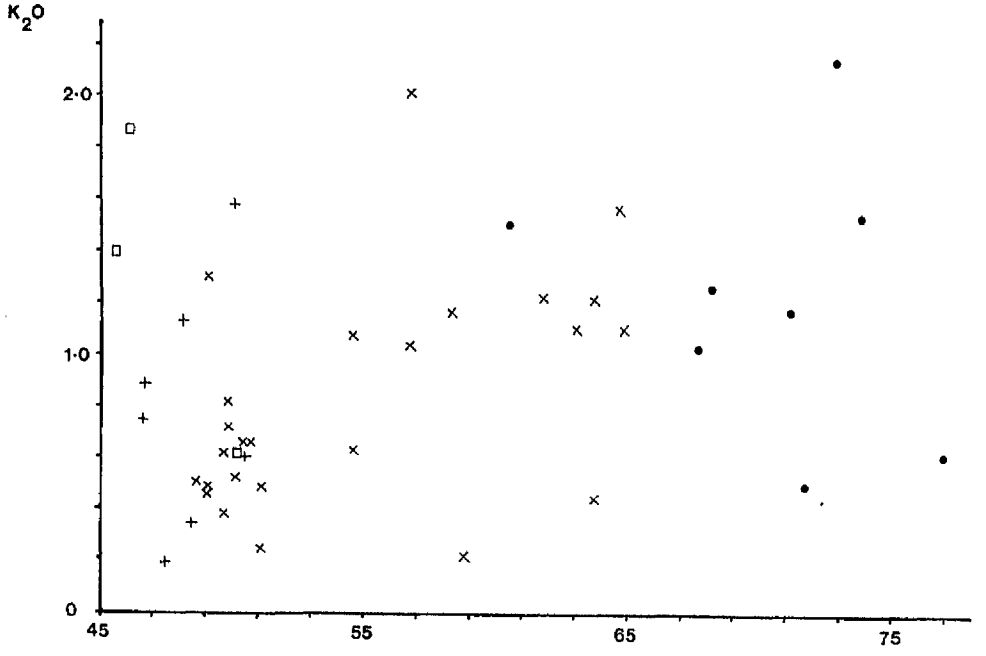

Figure 4.6a

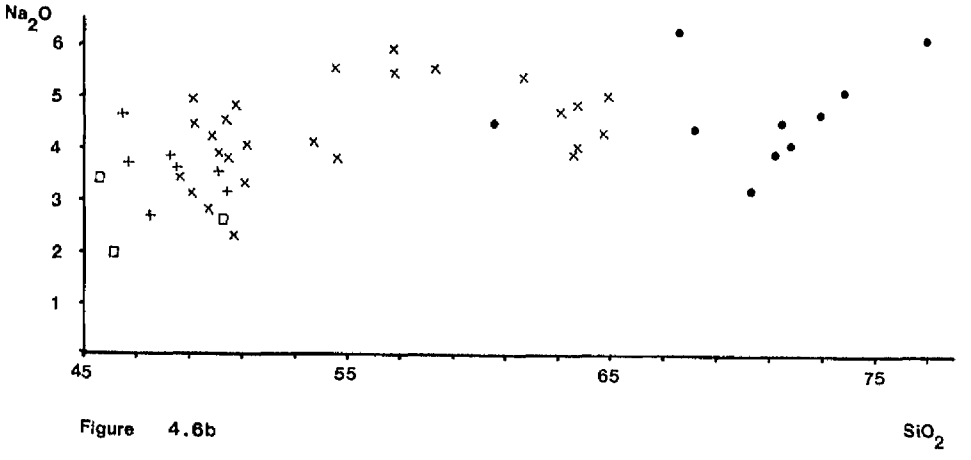

Figure 4.6b

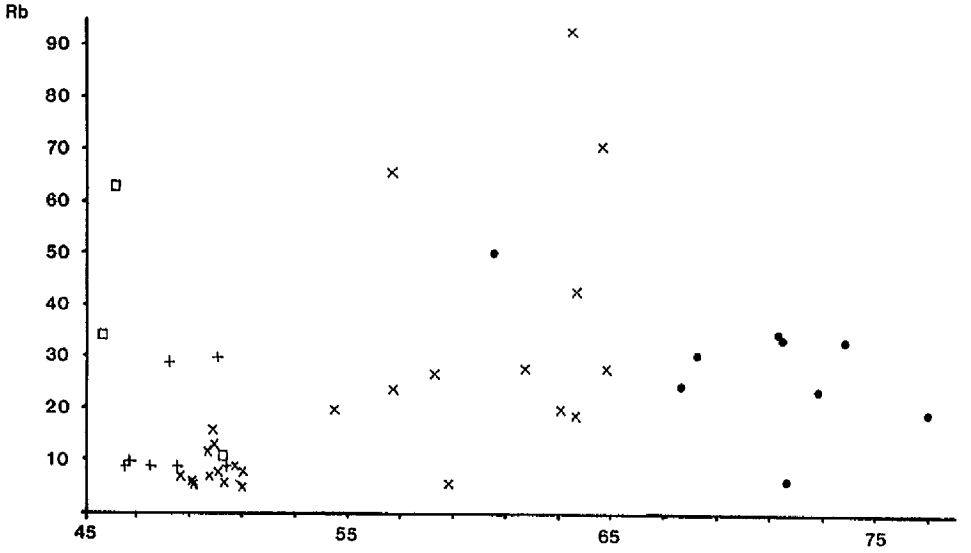

Figure 4.6c

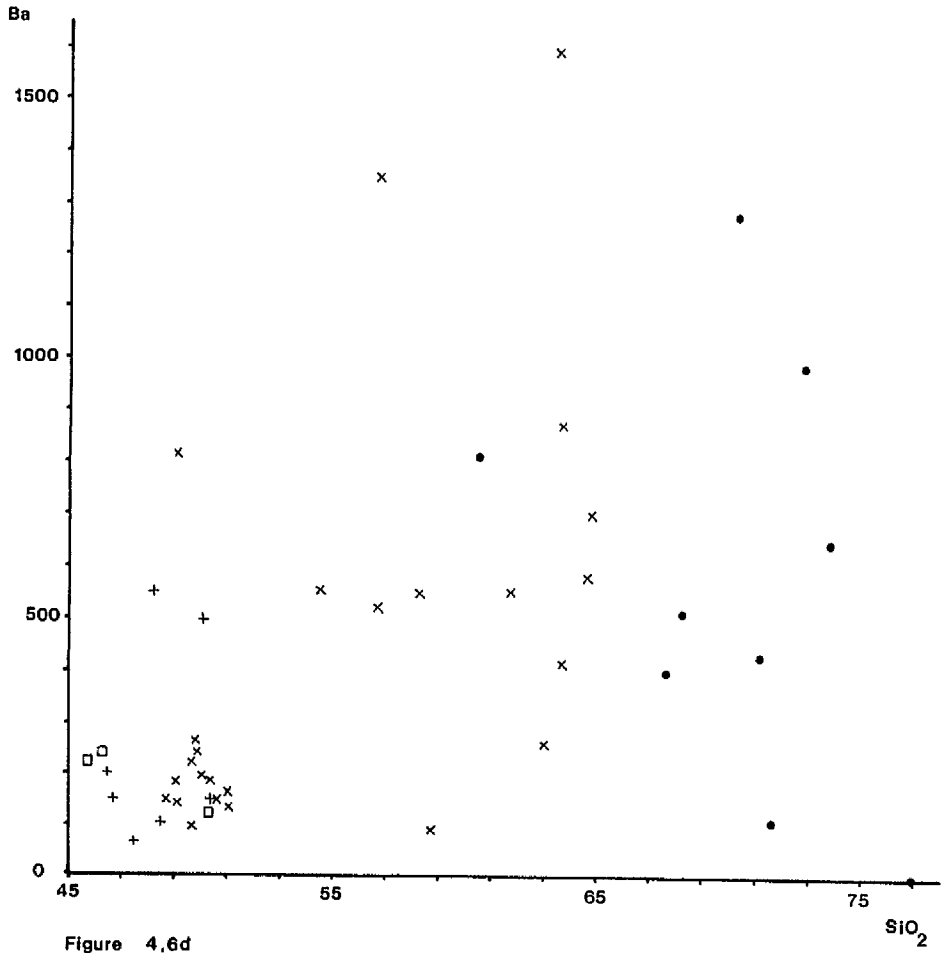

Figure 4.6d

Figure 4.6e

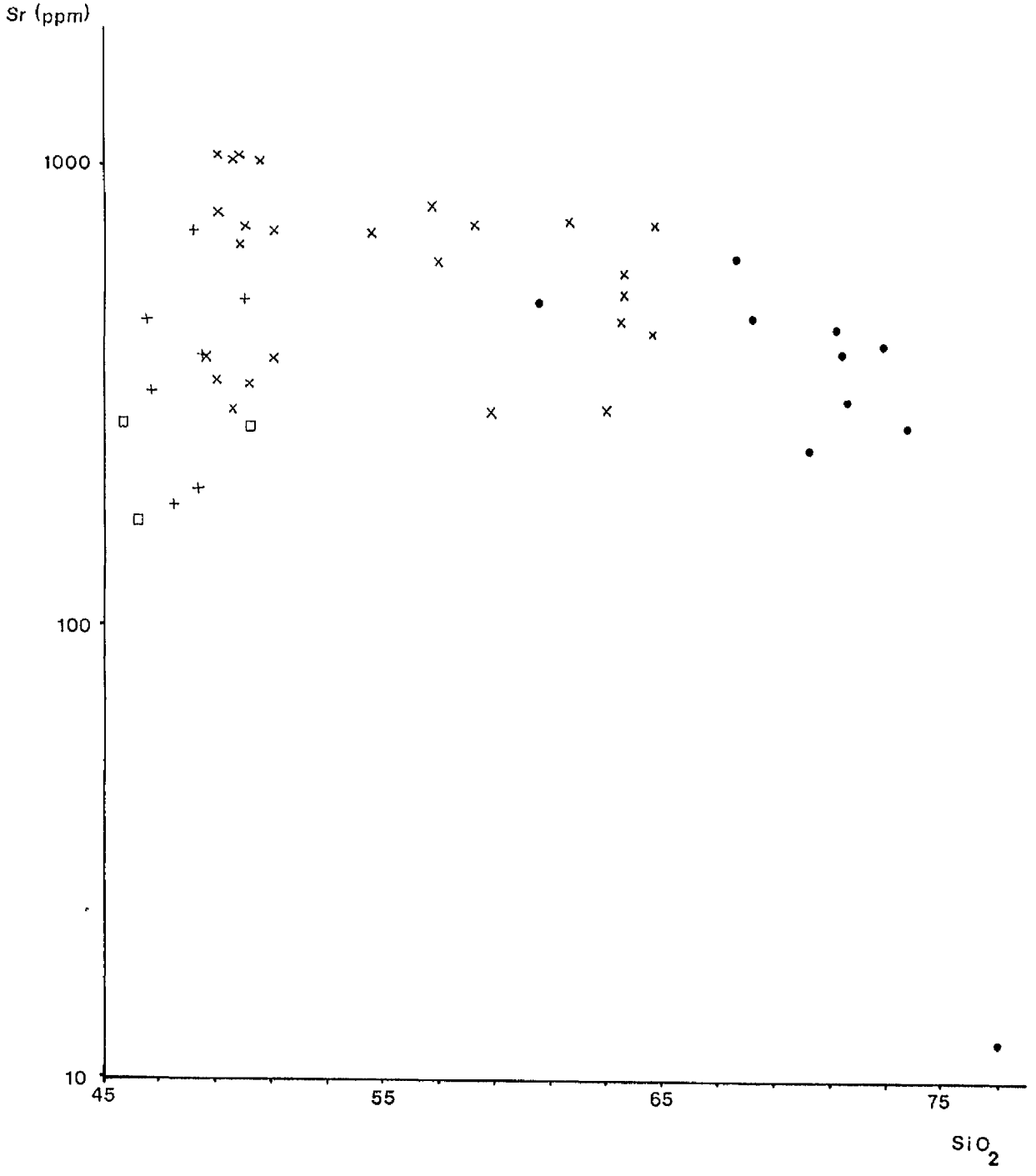

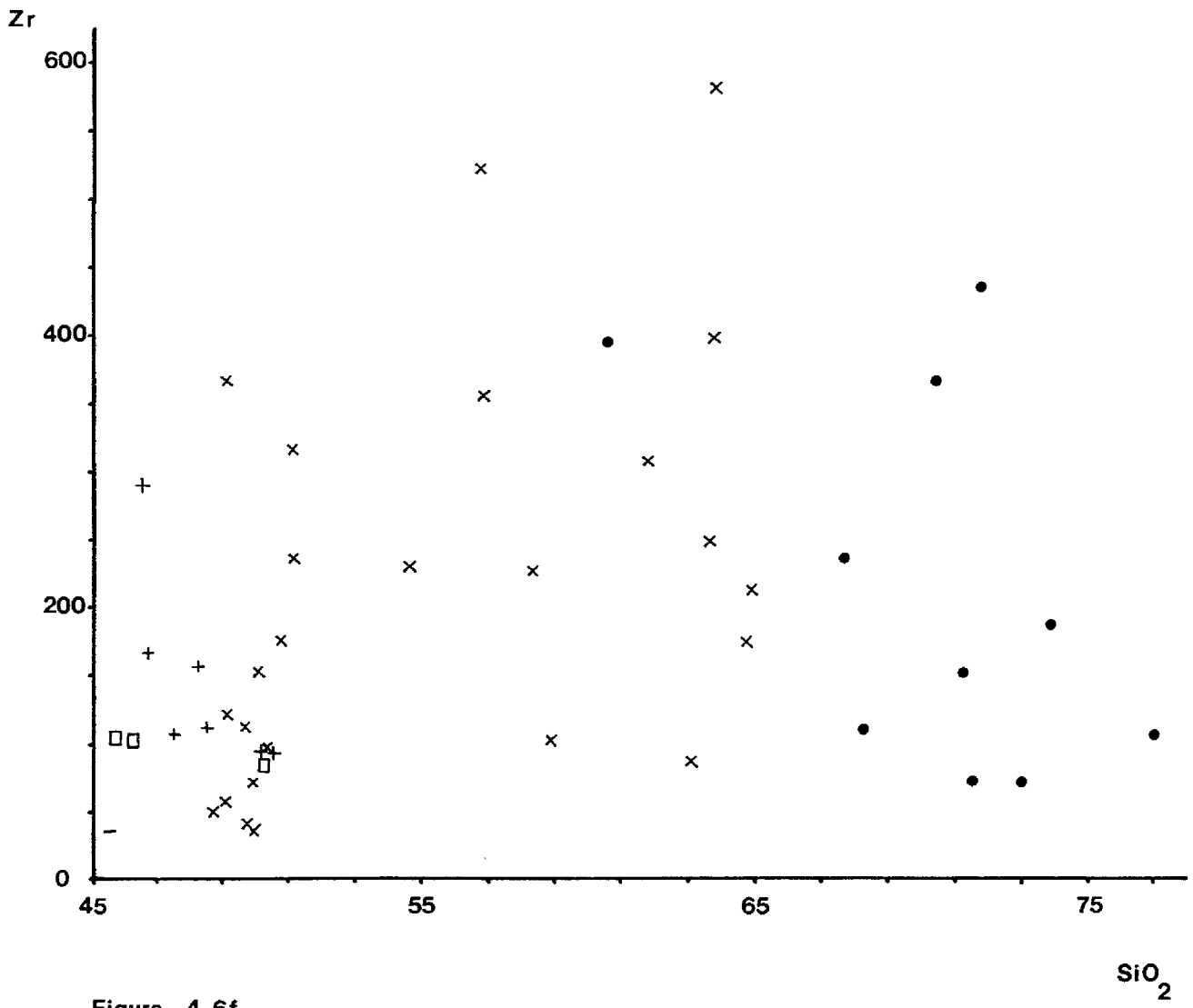

Figure 4.6f

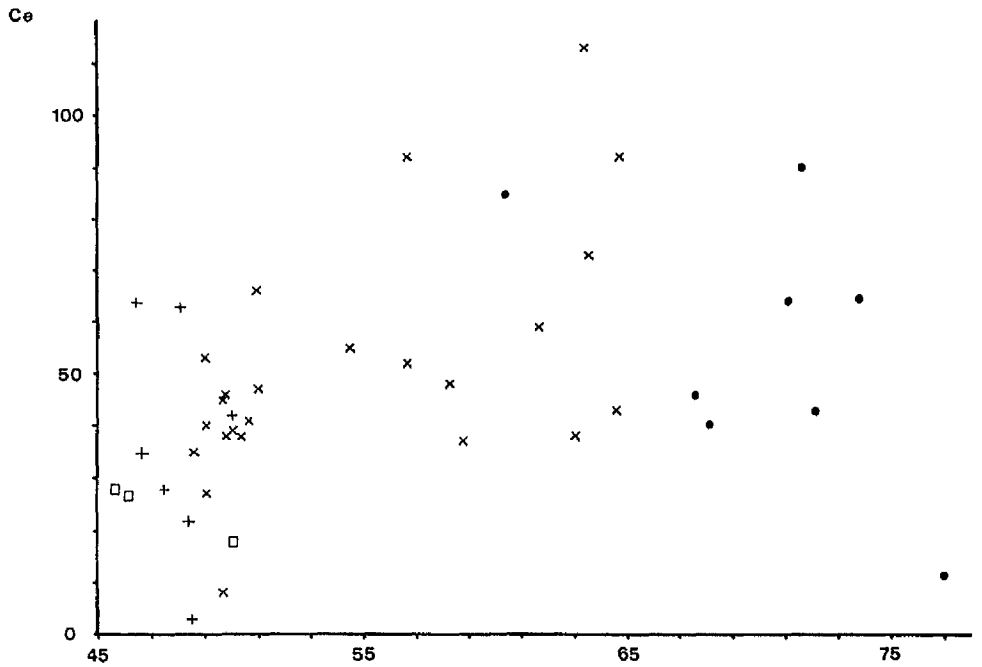

Figure 4.6g

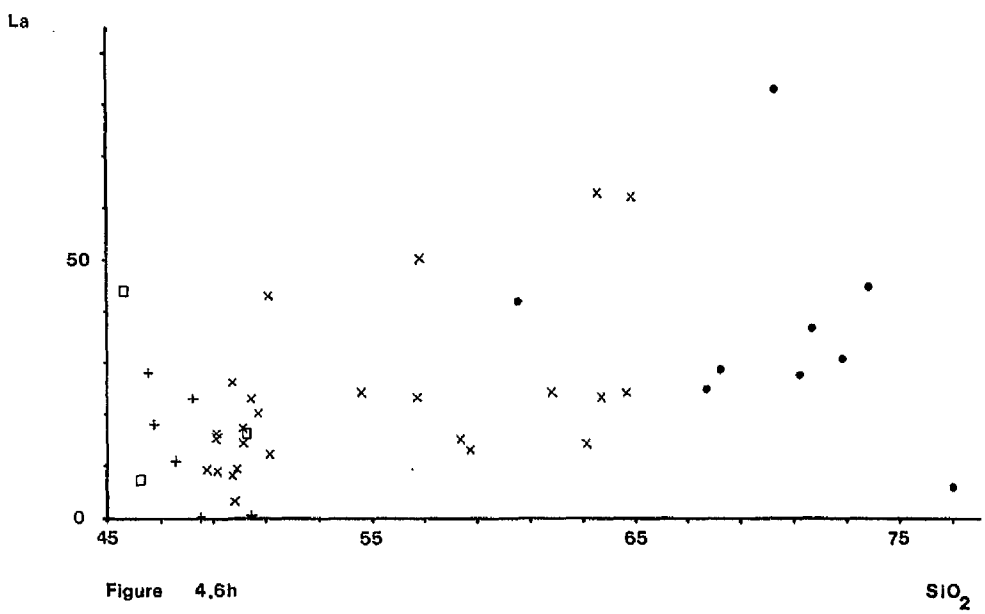

Figure 4.6h

Fig. 4.7 Figure 4.7 is a plot of $Na_2O + K_2O$ vs SiO_2 for Virtasalmi intrusions. The data is seen to plot across the Alkali-subalkali subdivision (after Irvine & Barager, 1971).

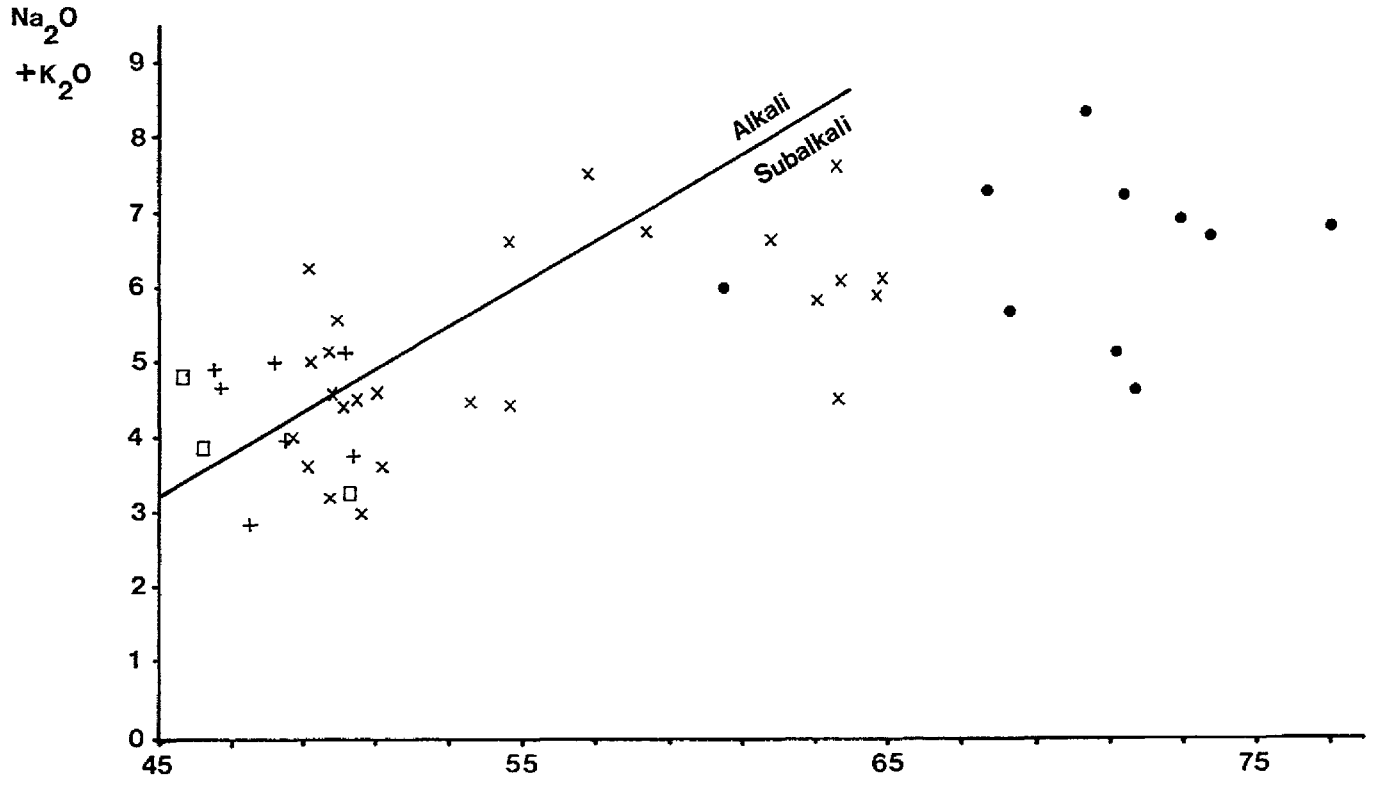

Figure 4.7

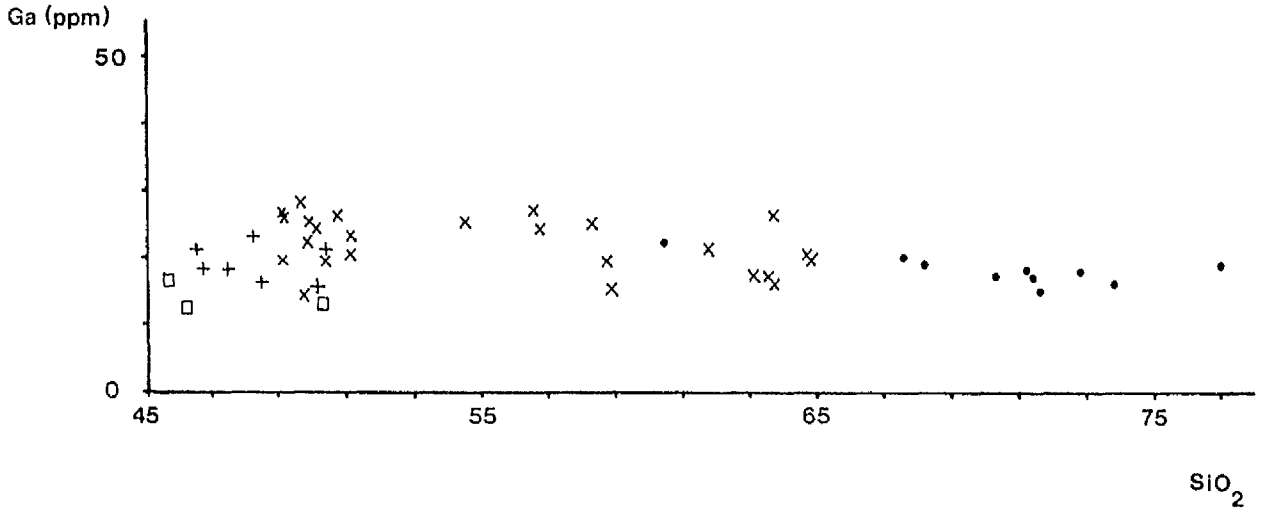

Figure 4.8

Fig. 4.8 Figure 4.8 is a plot of Ga vs SiO_2,

Fig. 4.9a,b Chondrite-normalised plots of Y* vs Y*/La* and Y*/Ce* are presented in Figures 4.9a and 4.9b respectively. Positive slopes suggest LREE enrichment.

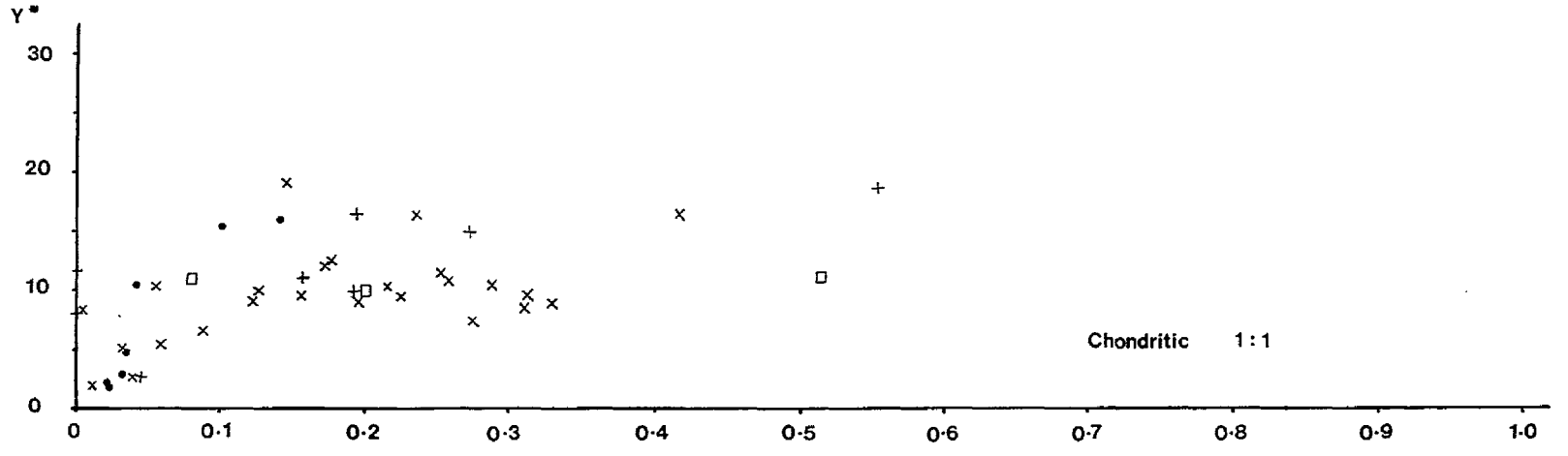

Figure 4.9a

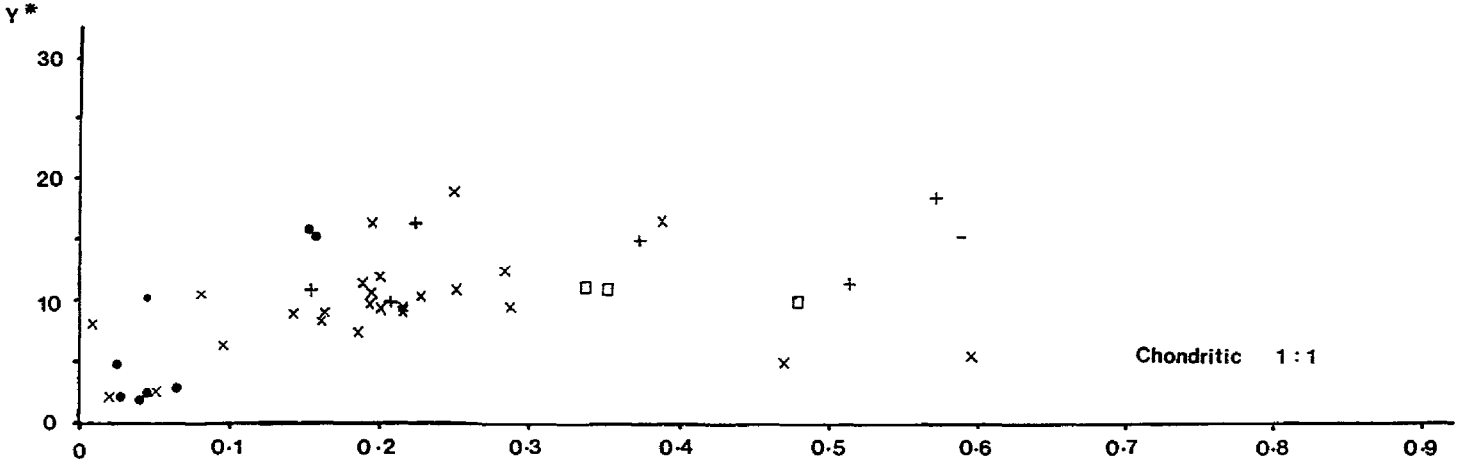

Figure 4.9b

Fig. 4.10 Partially assimilated xenolith in early syn-D_1 xenolith-rich medium-grained gabbro, Kiviniemi.

Fig. 4.11 Irregularly-shaped, melanocratic hornblende-rich xenoliths observed in a pre-early syn-D_1 intrusion near Kiviniemi. Some late retrogression adjacent to late fractures has resulted in epidote replacement of hornblende.

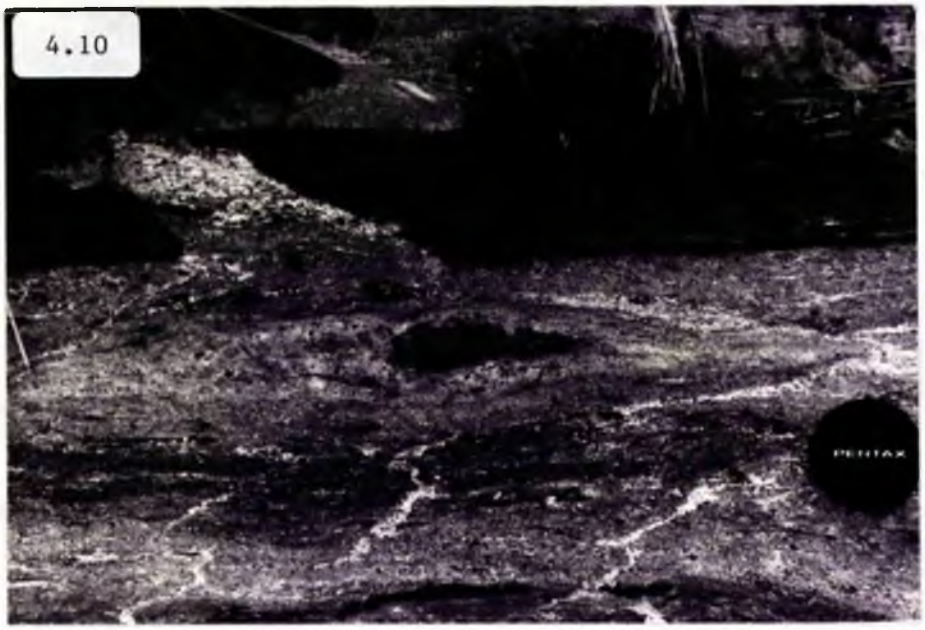
4.10


4.11

SECTION 5

Conclusions

The following points are the major conclusions of this study. They are presented along with suggestions for future work in the order with which they are dealt in the preceding sections.

A) Listed below are the major conclusions of Section 1.

1. The pre-kinematic lithological assemblage in the study area comprises a sequence of amphibolites with minor marbles, calc-silicate skarns and rare gneisses. These lithologies lie within a belt up to 5 km across which is enclosed by thick sequences of gneisses.
2. Approximately 60% of the whole lithological assemblage comprises syn-kinematic intrusions which range in composition from gabbros to trondhjemites. Syn-kinematic vein neosomes constitute on average about 10% of each outcrop.
3. Within the amphibolites a number of distinctive morphological features were recognised which indicate the presence of pillow lavas-lava tubes, tuffs, complex lava flows and flow top breccias. These point to a submarine volcanic origin for some of the amphibolites.
5. Petrographically similar calc-silicate skarns were observed to show different relationships to adjacent lithologies. A summary of the different types observed is included later.

6. It is only possible to establish the 'way-up' of the lithological assemblage in a few localities, including Hällinmäki Mine.
7. A great deal more lithological-structural mapping is required to establish the relationship of the amphibolite-dominated belt to the thick sequences of gneisses and marbles in adjacent areas.

B) A summary of the conclusions of Section 2 are presented below.

1. The pre-kinematic lithological assemblage has been polyphase deformed, with three main deformational phases (D_1-D_3) and four later phases (D_4-D_7), whose expression is of smaller magnitude and restricted in development, are recognised.
2. Evidence for D_1 structures has been largely destroyed by later overprinting events, however the presence of large fold structures is suggested by discordances between S_0 and S_1.
3. The dominant major structures in the area are steeply plunging large tight F_3 refolds of variably plunging tight-isoclinal F_2 folds. The NW-SE trend of structural elements in the study area is largely a result of reorientation in D_3.
4. Syn-kinematic dynamothermal metamorphism resulted in peak metamorphic conditions of the Upper Amphibolite to Granulite Facies Transition Zone during D_1-M_1.
5. An estimate of P-T conditions based on mineral assemblages and reactions suggests peak temperatures

were in the range 750-800°C, and that pressures were in the range of 3.5-5.5 kb.

6. The estimates of geobarometry and geothermometry suggest burial depths of 12-18 km with a geothermal gradient of 45-70°C/km.

7. During D_2-M_2 there was pervasive retrogressive recrystallisation of D_1-M_1 assemblages to conditions of the Lower Amphibolite Facies.

8. In the amphibolites retrogression involved hydration (by infiltration metasomatism) of the pre-existing relatively anhydrous D_1-M_1 assemblages, and this resulted in widespread amphibolitisation.

9. An estimate of D_2-M_2 P-T conditions (using the same basis as for D_1-M_1 estimates) suggests temperatures in the range of 450-550°C at pressures of 2-3.5 kb.

10. There was no post-D_2 pervasive recrystallisation of metamorphic assemblages, only localised retrogression during D_3 to conditions of the Greenschist-Lower Amphibolite Facies Transition Zone.

11. Estimates of geothermal gradient and the low pressure nature of deformation is consistent with other studies in the Svecofennides.

12. Cross-cutting relationships were used to establish the sequence of emplacement of the syn-kinematic intrusive suite. Intrusions were emplaced throughout most of the sequence, from D_1-D_6.

13. Many of the intrusions show some evidence for at least localised structural control on their emplacement: many intrusions are axial planar to contemporaneous

fold sets, probably reflecting injection of magma under the influence of both regional and more localised stress systems.

14. Emplacement of the intrusions has apparently only had a local effect on the orientation of pre-existing fold structures, while no systematic change in orientation-attitude of contemporaneous structures towards the largest intrusions was observed.

15. There is no systematic change in the composition of syn-kinematic intrusions relative to the structural evolution of the area.

16. Quartzofeldspathic vein neosomes were also emplaced throughout the structural sequence. They range in origin from derivation by partial melting of gneisses, to remobilisation of pre-existing leucocratic segregations formed by metamorphic differentiation, vein offshoots of larger intrusions, and late pegmatites.

17. There is a dearth of structural information in the adjacent areas in particular as well as regionally. Many more studies are required before regional structural correlations within the Svecofennides can be attempted.

C) (i) The main conclusions regarding the geochemistry and origin of the amphibolites and calc-silicate skarns, discussed in Section 3, Part 1, are as follows.

1. The amphibolites are all ortho-amphibolites, i.e. volcanic in origin.

2. They have undergone extensive syn-volcanic hydrothermal alteration in addition to syn-kinematic metamorphism and infiltration metasomatism.

3. TiO_2, Y, Nb, P_2O_5, Cr, Ni, Zr and to a lesser extent Ce remained relatively immobile in the amphibolites generally except in zones of high water : rock ratios during syn-volcanic hydrothermal alteration.

4. All the other elements analysed for were variably mobile principally as a consequence of redistribution during syn-volcanic hydrothermal alteration and infiltration metasomatism (amphibolitisation) during D_2.

5. Calc-silicate skarn lithologies in the Virtasalmi District are deduced to have formed in a number of different ways including admixture of carbonate and silicate (tuffaceous) material; diffusive metasomatism at amphibolite-marble contacts; and by interaction of amphibolite protoliths with syn-volcanic hydrothermal metasomatic fluids.

6. Three main groups can be petrographically and chemically distinguished in the Virtasalmi amphibolites. A number of subdivisions can be recognised on the basis of geographical distribution and minor variations in petrography and chemistry.

7. Fractional crystallisation was an important mechanism in determining final compositions within each group. However, the fractionating phases were different in each group and were of varying overall importance in determining group chemistry.

8. However, while the composition of Group I amphibolites is mainly controlled by fractional crystallisation processes, the chemistry of Group III amphibolites is controlled by variable degrees of partial melting, and only modified slightly by fractional crystallisation processes.

Group II amphibolites are derived from a depleted source relative to amphibolites of Groups I and III, and their composition was controlled by variable degrees of partial melting of that source.

9. There is some evidence to indicate that Group I and Group III amphibolites were derived from different sources. However REE data is required to substantiate this. Group II amphibolites were derived from a separate source.

10. Open system fractional crystallisation and batch melting processes were operative.

11. Chemically, Groups I and III amphibolites most closely resemble E-type basalts, while Group II amphibolites, which have negative Ce anomalies, most closely resemble Phanerozoic island are tholeiites.

12. Considering the range of magma types found in the study area and taking into consideration the association of the metavolcanic assemblage with large volumes of fine-grained metasediments, and the recognition of tuffs together with pillow lavas-tubes then the tectonic setting of the Virtasalmi amphibolites is considered most closely analogous to Phanerozoic back-arc basins.

13. Most recent plate tectonic reconstructions of Sveco-karelian geology suggest that the metavolcanic belts of the Svecofennides represent island arcs, which were accreted onto the margin of the Archaean craton (now located to the NE). However, the chemistry of the volcanic rocks in this study, which suggests a closer analogy may be Phanerozoic back-arc basins, would seem to indicate that this widely held view that the

Svecofennides represent island arcs is simplistic.

14. Many more geochemical studies (utilising REE data in particular) would appear to be required before the original nature of the Svecofennide terrane can be discussed in terms of modern plate tectonic models.

15. The manner in which it has been possible to unravel the complexities of regional dynamothermal deformation and metamorphism as well as syn-kinematic intrusion emplacement to determine the existence of extensive pre-kinematic syn-volcanic alteration, and yet also be able to determine the original chemistry and tectonic setting of the amphibolites, has important applications to studies elsewhere in the Svecofennides in particular, but also to other terranes.

C) (ii) The following are the main conclusions regarding the Hällinmäki Cu-deposit described in Section 3, Part 2.

1. Cu-mineralisation in the Hällinmäki ore deposit is mostly stratabound.

2. It is primarily hosted within thin Ca-rich amphibolite layers interpreted as altered tuffaceous layers.

3. These ore-bearing layers are interlayered with essentially ore-free calc-silicate (Type VIII) skarn layers which are mostly ore-free except where ore is syn-kinematically remobilised into them.

4. The ore occurs mainly as fine-grained disseminated chalcopyrite + pyrrhotite + minor pyrite, but occasionally occurs as more massive lenses.

5. There is a lateral gradation in ore composition with a marked increase in magnetite to the SE, where silicate

facies banded iron formation is found at the same horizon as Cu-mineralisation within the Mine. This suggests that the mineralisation is exhalative in origin.

6. In the S.O.P. and in T175m the aforementioned interlayered sequence of Cu-bearing amphibolites and barren Type VIII skarns is progressively truncated by barren amphibolites. This is a pre-D_1 surface, and together with the evidence outlined in points 1-5 above, is considered proof for the syn-volcanic timing and exhalative nature of Cu-mineralisation at Hällinmäki Mine. The latter point is also evidence for way-up in the Mine vicinity.

7. The interlayered ore-bearing amphibolites and barren Type VIII skarns are underlain by a Type V skarn which can be shown to be discordant to S_0 in the overlying ore-bearing amphibolites. It can also be demonstrated to have formed by metasomatic transformation of an original amphibolite protolith.

8. This Type V skarn is mineralised (disseminated Cu mineralisation and occasional chalcopyrite microbreccia), but only where subjacent to the overlying ore-rich layers.

9. Together with evidence from Section 3, Part 1, which suggests that the Type V skarns are formed through interaction of basalt with synvolcanic hydrothermal fluids under conditions of high water : rock ratios then this is considered to indicate that the Type V skarn, subjacent to the main ore-rich layers in the Mine, is the stockwork zone to the overlying strata-bound ore deposit.

10. The source of the Cu is probably underlying volcanic rocks which have undergone extensive synvolcanic hydrothermal alteration.

11. Type III skarns probably represent the conduits for the hydrothermal fluids.

12. The ore deposit is polyphase deformed.

13. The major structure in the Mine is a large tight-isoclinal F_2 fold which plunges gently northwards with an easterly-dipping axial plane.

14. There was significant refolding of F_2 structures by steeply plunging reclined F_3 folds.

15. There is significant ore remobilisation during D_3, with formation of breccia orebodies which plunge steeply, sub-parallel to F_3 fold axes. These are important features in the economic concentration of ore at Hällinmäki Mine.

16. The ore deposit is truncated by several syn-kinematic intrusions, principally by early-syn-D_1 leucogabbros and syn-D_3 diorites. These truncate ore-bearing lithologies and were emplaced post-mineralisation.

17. Determination of the stratabound nature of mineralisation at Hällinmäki has important implications for the understanding of other deposits in the area.

18. Determination of different origins for petrographically similar calc-silicate skarn lithologies may be of regional importance in particular, due to the occurrence of petrographically similar lithologies in many places throughout the Svecofennides. The recognition that some skarns are highly metamorphosed conduits to ore-bearing solutions or are stockwork zones to ore deposits

has implications for mineral exploration in high grade terranes.

D) The main conclusions regarding the chemistry of the syn-kinematic intrusive suite are as follows:

1. Chemically the syn-kinematic intrusions can be classified as a gabbro-diorite-quartz-diorite-tonalite -trondhjemite suite.
2. The intrusions are calc-alkaline and bear a close similarity in their range of composition to the syn-kinematic intrusions of SW Finland, although the latter have higher K_2O values. Tonalites are predominant.
3. Fractional crystallisation involving hornblende, biotite, sphene or ilmenite + plagioclase is an important mechanism in determining the composition of this suite. However, hybridisation of crustal material in particular is suggested by evidence for stoping and assimilation of xenoliths mainly in syn-D_1 basic intrusions. Some early intrusions also contain particularly melanocratic hornblende-rich xenoliths dissimilar to the country rock. These xenoliths are interpreted as entrained restite material or disrupted cumulate layers, and may be evidence for partial melting of the pre-kinematic lithological assemblage at greater depths.
4. Overall the suite has I-type characteristics.
5. Greater sampling, major, trace and REE modelling and isotopic data are required however if further light is to be thrown upon the origins of and relative dominance of processes in this intrusive suite.

6. It would also be interesting to compare the character of this intrusive suite with syn-kinematic intrusions within adjacent gneiss belts, particularly to establish the distribution of I- and S-type granitoids.

REFERENCES

ÅBERG, G., 1978. Precambrian geochronology of south-eastern Sweden. GEOL. FÖREN. STOCKHOLM FÖRH., 100, 125-154.

ÅBERG, G., LEVI, B. & FREDERIKSSON, G., 1984. Zircon ages of metavolcanic and synorogenic granitic rocks from the Svardsjo and Yxsjorberg areas, south central Sweden. GEOL. FÖREN. STOCKHOLM FÖRH., 105, 199-203.

AHO, L., 1979. Petrogenetic and geochronological studies of metavolcanic rocks and associated granitoids in the Pihtipudas area, Central Finland. GEOL. SURV. FINL., BULL., 300, 22pp.

AITCHISON, J. A., 1984a. The statistical analysis of geochemical compositions. MATH. GEOL., 16, 525-540.

AITCHISON, J. A., 1984b. Reducing the dimensionality of compositional data. MATH. GEOL., 16, 617-650.

APPEL, P. W. U., 1977. Aeolian differentiation of basaltic tuffs in the Early Precambrian Isua supracrustal belt, West Greenland. N. JAHRB. MINER. MH., 11, 521-528.

APPEL, P. W. U., 1979. Stratabound Copper Sulphides in a Banded Iron Formation and in Basaltic Tuffs in the Early Precambrian Isua Supracrustal Belt, West Greenland. ECON. GEOL., 74, 45-52.

ARNDT, N. T., 1973. Pillows and lava toes in modern and ancient lavas. GEOL. SOC. AM. ABSTR. WITH PROGS., 5, p536.

ARTH, J. G., 1976. Behaviour of trace elements during magmatic processes - a summary of theoretical models and their applications. J. RES., U.S. GEOL. SURV., 4, 41-47.

ARTH, J. G., BARKER, F., PETERMAN, Z. E. & FRIEDMAN, I., 1978. Geochemistry of the gabbro-diorite-tonalite-trondhjemite suite of southwest Finland and its implications for the origin of tonalitic and trondhjemitic magmas. J. PETROL., 19, 289-316.

ATKINSON, B. K., 1974. Experimental deformation of polycrystalline galena, chalcopyrite and pyrrhotite. TRANS. INST. MIN. METAL. BULL. (SECT. B), 83, B19-29.

ATKINSON, B. K., 1975. Experimental deformation of polycrystalline pyrite : effects of temperature, confining pressure, strain rate and porosity. ECON. GEOL., 70, 473-488.

BARAGER, W. R. A., PLANT, A. G., PRINGLE, G. J. & SCHAU, M., 1979. Diagenetic and postdiagenetic changes in the composition of an Archaean pillow. CAN. J. EARTH SCI., 16, 2102-2121.

BARAGER, W. R. A., 1983. Pillow formation and layered flows in the Circum-Superior Belt of eastern Hudson Bay. CAN. J. EARTH SCI., 21, 781-792.

BARBEY, P., COUVERT, J., MOREAU, B. & CAPDEVILA, R., 1984. Petrogenesis and evolution of an Early Proterozoic collisional orogenic belt : the Granulite belt of Lapland and the Belomorides (Fennoscandia). BULL. GEOL. SOC. FINLAND, 56(2), 161-168.

BARKER, F., ARTH, J. G., PETERMAN, Z. E. & FRIEDMAN, I., 1976. The 1.7-1.8 b.y. old trondhjemites of southwestern Colorado and northern New Mexico: Geochemistry and depths of genesis. GEOL. SOC. AM. BULL., 87, 189-198.

BARKER, F., 1979. Trondhjemite : definition, environment and hypotheses of origin. In 'Trondhjemites, dacites and related rocks', Ed. F. Barker. Developments in Petrology, 6, ppl-11.

BATTEY, M. H., 1972. Mineralogy for students. Oliver & Boyd; Edinburgh. 323pp.

BEACH, A., 1974. Amphibolitisation of Scourian granulites. SCOTT. J. GEOL., 10, 35-43.

BELL, T. H., 1978. Progressive deformation and reorientation of fold axes in a ductile mylonite zone : the Woodroffe thrust. TECTONOPHYS., 128, 163-181.

BERTHELSEN, A., 1980. Towards a palinspastic tectonic analysis of the Baltic Shield. 26TH INT. GEOL. CONGR., SECTION 6, 6-21.

BERTHELSEN, A. & MARKER, M., 1986. 1.9-1.8 Ga old strike-slip mega-shears in the Baltic Shield, and their plate tectonic implications. TECTONOPHYS., 128, 163-181.

BEVINS, R. E., 1985. Pumpellyite-dominated metadomain alteration at Builth Wells, Wales - evidence for a fossil submarine hydrothermal system? MINER. MAG., 49, 451-457.

BINNS, R. A., 1965. The mineralogy of metamorphosed basic rocks from the Willyama Complex. Broken Hill district, New South Wales, Parts 1 & 2. MINER. MAG., 35, 306-326, 561-587.

BOUGAULT, H., CAMBON, P., CORRE, T., JORON, J. L. & TREUIL, M., 1979. Evidence for variability of magmatic processes and upper mantle heterogeneity in the axial region of the Mid-Atlantic Ridge near 22°N and 36°N. TECTONOPHYS., 55, 11-34.

BOWES, D. R. & PARK, R. G., 1966. Metamorphic segregation banding in the Loch Kerry basite sheet from the Lewisian of Gairloch, Ross-shire, Scotland. J. PETROL., 7, 306-330.

BOWES, D. R., 1976. Tectonics in the Baltic Shield in the period 2000-1500 million years ago. ACTA GEOL. POL., 26, 355-376.

BOWES, D. R., 1980. Structural sequence in the gneissose complex of Eastern Finland as a basis for correlation in the Presvecokarelides. ACTA GEOL. POL., 30(1), 15-26.

BOWES, D. R., HALDEN, N. M., KOISTINEN, T. J. & PARK, A. F., 1984. Structural features of basement and cover rocks in the Eastern Svecokarelides, Finland. pp 157-171 in 'Precambrian Tectonics Illustrated', eds. A. Kroner and R. Greiling, Schweizerbatische Verlagsbuchhandlung, Stuttgart.

BOYLE, R. W., 1970. The source of metals and gangue elements in hydrothermal deposits. In 'Problems of hydrothermal ore deposition, the origin, evolution, and control of ore-forming fluids'. Internat. Union Geol. Sci. A2. Stuttgart, 3-6.

BROCK, K. J., 1972. Genesis of Garnet Hill skarn, Calaveras County, California. GEOL. SOC. AM. BULL., 83, 3391-3404.

BROWN, M., 1978. The tectonic evolution of the Precambrian rocks of the St. Malo region, Armorican Massif, France. PRECAMB. RES., 6, 1-21.

BURG, J. P. & LAURENT, P., 1978. Strain analysis of a shear zone in a granodiorite. TECTONOPHYS., 47, 15-42.

BUTLER, J. C. & WORONOW, A., 1986. Discrimination among tectonic settings using trace element abundances of basalts. J. GEOPHYS. RES., 91, B10, 10289-10300.

CAMPBELL, D. S., TRELOAR, P. J. & BOWES, D. R., 1979. Metamorphic history of staurolite-bearing schist from the Svecokarelides, near Heinavaara, Eastern Finland. GEOL. FOREN. STOCKHOLM. FORH., 101, 105-118.

CAMPBELL, D. S., 1980. Structural and metamorphic development of migmatites in the Svecokarelides, near Tampere, Finland. TRANS. ROY. SOC. EDIN., 71, 185-200.

CANN, J. R., 1970. Rb, Sr, Y, Zr and Nb in some ocean floor basalt rocks. EARTH PLANET. SCI. LETT., 10, 7-

CATHLES, L. M., 1978. Hydrodynamic constraints on the formation of Kuroko deposits. MINING GEOL. (JAPAN), 18, 257-265.

CHAKRABORTY, K. R. & SEN, S. K., 1967. Regional metamorphism of pelitic rocks around Kandra, Singhbkum, Bihar. CONTRIB. MINERAL. PETROL., 16, 210-232.

CHINNER, G. A., 1961. The origin of sillimanite in Glen Clova, Angus. J. PETROL., 2, 312-323.

CLAGUE, D. A. & FREY, F. A., 1983. Rare earth element and Sr isotopic evidence for the origin of the East Molokai Volcanics, Hawaii. EOS, 64, 902.

CLOUGH, P. W. L. & FIELD, D., 1980. Chemical variation in metabasalts from a Proterozoic amphibolite-granulite transition zone, S. Norway. CONTRIB. MINERAL. PETROL., 73, 277-286.

CONSTANTINOU, G. & GOVETT, G. J. S., 1972. Genesis of sulphide deposits, ochre and umber of Cyprus. INST. MINING METALL. (SECT. B), 8, B34-46.

CURRIE, K. L., 1971. The reaction 3 cordierite = 2 garnet + 4 sillimanite + 5 quartz as a geological thermometer in the Openicon Lake region, Ontario. CONTRIB. MINERAL. PETROL., 33, 215-226.

CUSSARZ, A., 1965. Einfurung in die allgemene und systematische Lagerstattenlehre. Stuttgart.

DEER, W. A., HOWIE, R. A. & ZUSSMAN, J., 1966. An introduction to the rock-forming minerals. New York, Wiley.

DE JONGH, W. K., 1973. X-ray fluorescence analysis applying theoretical matrix corrections; Stainless steel. X-RAY SPECTROMETRY, 2, 151-158.

DICKIN, A. P., 1987. Cerium isotope geochemistry of ocean island basalts. NATURE, 326, 283-

DIMROTH, E., COUSINEAU, P., LEDUC, M. & SANSCHAGRIN, Y., 1978. Structure and organization of Archaean subaqueous basalt flows, Rouyn-Noranda area, Quebec, Canada. CAN. J. EARTH SCI., 15, 902-918.

DIMROTH, E., COUSINEAU, P., LEDUC, M., SANSCHAGRIN, Y. & PROVOST, G., 1979. Flow mechanisms of Archaean subaqueous basalt and rhyolite flows. CURRENT RESEARCH, GEOL. SURV. CAN., PAPER 79-1A, 207-211.

DONNELLY, T., FRANCHETEAU, J., BRYAN, W., ROBINSON, P., FLOWER, M., SALISBURY, M., et al., 1979. The chemistry of altered basalts at Site 417, Deep Sea Drilling Project, Leg 51. INIT. RPTS. DSDP, 51, 52, 53, PART II, US Govt Printing Office.

DURNEY, D. W., 1972. Solution-transfer, an important geological deformation mechanism. NATURE, 235, 315-316.

EDMOND, J. M., VON DAMM, K. L., MCDUFF, R. E. & MEASURES, C. I., 1982. Chemistry of hot springs on the East Pacific Rise and their effluent dispersal. NATURE, 297, 187-191.

EHLERS, C., LINDROOS, A. & JAANUS-JARKKALA, M., 1986. Stratigraphy and geochemistry in the Proterozoic mafic volcanic rocks of the Nagu-Korpo area, SW Finland. PRECAMB. RES., 32, 297-317.

EINAUDI, M. T., MEINERT, L. D. & NEWBERRY, R. J., 1981. Skarn Deposits. ECON. GEOL., 75th Anniversary Volume, 317-391.

ELLIS, D. E., 1978. Stability and phase equilibria of the chloride and carbonate-bearing scapolites at 750°C and 4000 bar. GEOCHIM. ET COSMOCHIM. ACTA, 42, 1271-1281.

ESKOLA, P., 1914. On the petrology of the Orijärvi District in South-western Finland. BULL. COMM. GEOL. FINLANDE, 40, 252-263.

ESKOLA, P., 1939. Die metamorphen Gesteine. In Barth, T. F. W., Correns, c. w. and Eskola, P. 'Die Entstehung der Gesteine': Berlin, Springer-Verlag. pp263-407.

ESKOLA, P., 1963. The Precambrian of Finland. In 'The Precambrian Vol. 1', ed. by K. Rankana. John Wiley, New York, pp 145-263.

EVANS, B. W. & LEAKE, B. E., 1960. The composition and origin of the striped amphibolites of Connemara, Ireland. J. PETROL., 1, 337-363.

FERGUSSON, I. W., 1982. Geochemistry of amphibolites and related rocks in the Svecokarelides, Ekenas archipelago, SW Finland. Unpublished PhD Thesis. Glasgow University.

FLEET, A. J. & ROBERTSON, A. H. F., 1980. Ocean-ridge metalliferous and pelagic sediments of the Semail Nappe, Oman. J. GEOL. SOC. LOND., 137, 403-

FLOYD, P. A. & WINCHESTER, J. A., 1975. Magma type and tectonic setting discrimination using immobile elements. EARTH PLANET. SCI. LETT., 27, 211-218.

FLOYD, P. A., 1986. Geochemistry and provenance of basaltic clasts within volcaniclastic debris flows, East Mariana Basin, DSDP site 585. In 'Init. Repts. DSDP, 89': Washington (U.S. Govt. Printing Office), ed. Orlofsky, S. pp 449-470.

FLOYD, P. A., 1986b. Petrology and geochemistry of oceanic intraplate sheet-flow basalts, Nairn Basin, DSDP Project, leg 69. In 'Init. Rpts. DSDP, 89': Washington (U.S. Govt. Printing Office), ed. Orlofsky, S.

FRANKLIN, J. M., LYDON, J. W. & SANGSTER, D. F., 1981. Volcanic-associated massive sulfide deposits. ECON. GEOL., 75th ANNIVERSARY VOLUME, 485-627.

FRONT, K. & NURMI, P. A., 1987. Characteristics and geological setting of synkinematic Svecokarelian granitoids in Southern Finland. PRECAMB. RES., 35, 207-224.

FROSTERUS, B., 1903. Vourilajikartan seltys C2, Mikkeli (General geological map of Finland) 1:400000, 102p.

GAÁL, G. & RAUHAMAKI, E., 1971. Petrological and structural analysis of the Haukivesi area between Varkaus and Savonlinna, Finland. BULL. GEOL. SOC. FINLAND, 43, 265-337.

GAÁL, G., 1972. Tectonic control of some Ni-Cu deposits in Finland. 24TH INT. GEOL. CONGR., SECTION 4, 215-224.

GAÁL, G., MIKKOLA, A. & SODERHOLM, B., 1978. Evolution of the Archaean crust in Finland. PRECAMB. RES., 6, 199-215.

GAÁL, G., 1980. Geological setting and intrusion tectonics of the Kotalahti nickel-copper deposit, Finland. BULL. GEOL. SOC. FINLAND, 52, 101-128.

GAÁL, G., 1982. Proterozoic tectonic evolution and late Svecokarelian plate deformation of the Central Baltic Shield. GEOL. RUNDSCH., 71, 158-170.

GEIJER, P. & MAGNUSSON, N. H., 1944. De mellansvenska jarnmalmernas geologi. SVERIGES GEOL. UNDERS., 35.

GEIJER, P. & MAGNUSSON, N. H., 1952. The iron ores of Sweden. XIX CONGR. GEOL. INT. ALGER 1952, SYMP. GISEM. FER MONDE, 2, 477-499.

GIBSON, H. L., WATKINSON, D. H. & COMBA, C. D. A., 1983. Silicification: Hydrothermal alteration in an Archaean geothermal system within the Amulet Rhyolite Formation, Noranda, Quebec. ECON. GEOL., 83, 954-971.

GILL, J. B., STORK, A. L. & WHELAN, P. W., 1984. Volcanism accompanying backarc basin development in the south-west Pacific. TECTONOPHYS., 102, 207-224.

GITLIN, E., 1985. Sulfide remobilisation during low temperature alteration of seafloor basalt. GEOCHIM. COSMOCHIM. ACTA, 49, 1567-1579.

GOLDSCHMIDT, V. M., 1911. Die Kontaktmetamorphose im Kristianiagebiet Videnskabsselsk. SKRIFTER I, KRISTIANA, 483pp.

GRAF, J. L. & SKINNER, B. J., 1970 Strength and deformation of pyrite and pyrrhotite. ECON. GEOL., 65, 206-215.

GRAHAM, C. M., 1976. Petrochemistry and tectonic setting of Dalradian metabasaltic rocks of the SW Scottish Highlands. J. GEOL. SOC., 132, 61-84.

GREENWOOD, H. J., 1962. Metamorphic systems involving two volatile components. CARNEGIE INST. WASH. YEARBOOK, No. 61, 82-85.

GREENWOOD, H. J., 1967. Mineral equilibria in the system MgO-SiO_2-H_2O-CO_2. In 'Researches in Geochemistry II', ed. Abelson, P.H. Wiley, New York. pp 542-547.

GRESENS, R. L., 1966. The effects of structurally produced pressure gradients on diffusion in rocks. J. GEOL., 74, 307-312.

GROMET, L. P. & SILVER, L. T., 1987. Variations across the Peninsular Ranges Batholith: Implications for batholithic petrogenesis and crustal growth in magmatic arcs. J. PETROL., 28, 75-127.

HALDEN, N. M., 1982. Structural, metamorphic and igneous history of migmatites in the deep levels of a wrench-fault regime, Savonranta, Eastern Finland. TRANS. R. SOC. EDIN. EARTH SCI., 73, 17-30.

HALDEN, N. M. & BOWES, D. R., 1984. Metamorphic development of cordierite-bearing layered schist and mica schist in the vicinity of Savonranta, eastern Finland. BULL. GEOL. SOC. FINLAND, 56, 3-23.

HANSEN, B. J. & GREEN, D. H., 1972. Experimental study of the stability of cordierite and garnet in pelite compositions at high pressures and temperatures. II. Compositions without excess alumino silicate. CONTRIB. MINERAL. PETROL., 35, 331-354.

HARGREAVES, R. & AYRES, L. D., 1979. Morphology of Archaean metabasalt flows, Utik Lake, Manitoba. CAN. J. EARTH SCI., 16, 1452-1466.

HARRIGAN, D. B. & MACLEAN, W. H., 1976. Petrography and geochemistry of epidote alteration patches in gabbro dykes at Matagami, Quebec. CAN. J. EARTH SCI., 13, 500-511.

HARVEY, P. K., TAYLOR, D. M., HENDRY, R. D. & BANCROFT, F., 1973. An accurate fusion method for the analysis of rocks and chemically related materials by X-ray fluorescence spectrometry. X-RAY SPECTROMETRY, 2, 33-44.

HARVEY, P. K. & ATKIN, B. P., 1981. The rapid determination of Rb, Sr and their ratios in geological materials by X-ray fluorescence spectrometry using a Rhodium X-ray tube. CHEM. GEOL., 32, 291-301.

HARVEY, P. K. & ATKIN, B. P., 1982. The estimation of mass absorption coefficients by compton scattering - extensions to the use of Rh Ka Compton radiation and intensity ratios. AMER. MINER., 67, 534-537.

HELGESON, H. C., DELANY, J. M., NESBITT, H. W. & BIRD, D. K., 1978. Summary and critique of the thermodynamic properties of rock-forming minerals. AM. J. SCI., 278, 229pp.

HELOVUORI, O., 1979. Geology of the Pyhasalmi ore deposit, Finland. ECON. GEOL., 1084-1101.

HESS, P. C., 1969. The metamorphic paragenesis of cordierite in pelitic rocks. CONTRIB. MINERAL. PETROL., 24, 191-207.

HIETANEN, A., 1975. Generation of potassium-poor magmas in the northern Sierra Nevada and the Svecofennian in Finland. JOUR. RES. U.S. GEOL. SURV., 3, 631-645.

HILTUNEN, A., 1982. The Precambrian geology and skarn iron ores of the Rautuvaara area, N. Finland. GEOL. SURV. FINLAND BULL., 318, 133p.

HIRSCHBERG, A. & WINKLER, H. G. F., 1968. Stabilitatbeziehungen zwischen Chlorit, Cordierit und Almadin bei der Metamorphose. CONTRIB. MINER. PETROL., 18, 17-42.

HOBBS, B. E., MEANS, W. & WILLIAMS, P. F., 1976. An outline of structural geology. Wiley, New York, 571pp.

HOLDAWAY, M. J., 1971. Stability of andalusite and the aluminium silicate phase diagram. AM. J. SCI., 271, 97-131.

HOLDAWAY, M. J. & LEE, S. M., 1977. Fe-Mg cordierite stability in high-grade pelitic rocks based on experimental, theoretical and natural observations. CONTRIB. MINERAL. PETROL., 63, 175-198.

HOLE, M. J., SAUNDERS, A. D., MARRINER, G. F. & TARNEY, J., 1984. Subduction of pelagic sediments : implications for the origin of Ce-anomolous basalts from the Mariana islands. J. GEOL. SOC. LOND., 141, 453-472.

HOPGOOD, A. M. & BOWES, D. R., 1978. Neosomes of polyphase agmatites as time markers in complexly deformed migmatites. GEOL. RUNDSCH., 67, 313-330.

HOPGOOD, A. M., 1980. Polyphase fold analysis of gneisses and migmatites. TRANS. R. SOC. EDIN. EARTH SCI., 71, 55-68.

HOPGOOD, A. M., BOWES, D. R., KOUVO, O. & HALLIDAY, A. N., 1983. U-Pb and Rb-Sr isotopic study of polyphase deformed migmatites in the Svecokarelides, Southern Finland. In 'Migmatites, Melting and Metamorphism', ed. by Atherton, M. P. & Gribble, C. D.. Shiva Publishing Ltd., 80-92.

HOSHINO, M., 1979. Two-pyroxene amphibolites in Dogo, Oki Islands, Shumane-ken, Japan. JAP. ASSOC. MINERAL., PETROL. ECON. GEOL. J., 74(3), 87-99.

HUHMA, H., 1985. Provenance of some Finnish sediments. GEOLOGI, 37, 23-35.

HUHMA, H., 1986. Sm-Nd, U-Pb and Pb-Pb isotopic evidence for the origin of the Early Proterozoic Svecokarelian crust in Finland. GEOL. SURV. FINLAND BULL., 337, 48pp.

HUHMA, H., 1987. Provenance of Early Proterozoic and Archaean metasediments in Finland: a Sm-Nd Isotopic Study. PRECAMB. RES., 35, 127-143.

HUMPHRIS, S. E. & THOMPSON, G., 1978. Hydrothermal alteration of oceanic basalts. GEOCHIM. ET COSMOCHIM. ACTA, 42, 107-125.

HUMPHRIS, S. E., MORRISON, M. A. & THOMPSON, R. N., 1978. Influence of rock crystallisation upon subsequent lanthanide mobility during hydrothermal alteration of basalts. CHEM. GEOL., 23, 125-137.

HYNES, A. J., 1980. Carbonatization and mobility of Ti, Y and Zr in Ascot Formation metabasalts. SE Quebec. CONTRIB. MINERAL. PETROL., 75, 79-87.

HYVÄRINEN, L., 1969. On the geology of the copper ore field in the Virtasalmi area, eastern Finland. BULL. COMM. GEOL. FINLANDE, 240, 82pp.

IKIN, N. P., 1983. Petrochemistry and tectonic significance of the Highland Border Suite mafic rocks. J. GEOL. SOC. LOND., 140, 267-278.

IRVINE, T. N. & BARAGER, W. R. A., 1971. A guide to the chemical classification of the common volcanic rocks. CAN. J. EARTH SCI., 8, 523-548.

JAKEŠ, P. & GILL, J., 1970. Rare earth elements and the island arc tholeiite series. EARTH PLANET. SCI. LETT., 9, 17-28.

JAQUES, A. L., BLAKE, D. H. & DONCHAK, P. J. T., 1982. Regional metamorphism in the Selwyn Range area, Northwest Queensland. BMR J. AUSTR. GEOL. GEOPHYS., 181-196.

JELÍNEK, E., SOUCEK, J., BLUCK, B. J., BOWES, D. R. & TRELOAR, P. J., 1980. Nature and significance of beerbachites in the Ballantrae ophiolite, SW Scotland. TRANS. R. SOC. EDIN., 71, 159-179.

JENKINS, R. & DEVRIES, J. L., 1967. Practical X-ray spectrometry.

JOLLY, W. T. & SMITH, R. E., 1972. Degradation and metamorphic differentiation of the Keweenawan tholeiitic lavas of northern Michigan, U.S.A. J. PETROL., 13, 273-309.

JONES, J. G., 1968. Pillow lava and pahoehoe. J. GEOL., 76, 485-488.

JONES, J. G., 1969. Pillow lavas as depth indicators. AM. J. SCI., 267, 181-195.

KÄHKÖNEN, Y. & LAITAKARI, I., 1983. Metavolcanics and metasediments of the Proterozoic Tampere schist belt. In 'Exogenic processes and related metallogeny in the Svecokarelian geosynclinal complex', ed. by Laajoki, K. & Paakola, S. Geol. Surv. Finland, Guide 11, 110-134.

KÄHKÖNEN, Y., 1987. Geochemistry and tectonomagmatic affinities of the metavolcanic rocks of the Early Proterozoic Tampere Schist Belt, Southern Finland. PRECAMB. RES., 35, 295-311.

KAHMA, A., 1973. The main metallogenic features of Finland. GEOL. SURV. FINLAND BULL., 265, 28pp.

KEMP, J. F., 1907. Ore deposits at the contacts of intrusive rocks and limestones; and their significance as regards the general formation of veins. ECON. GEOL., II, 1-14.

KOISTINEN, T., 1981. Structural evolution of an early Proterozoic strata-bound Cu-Co-Zn deposit, Outokumpu, Finland. TRANS. R. SOC. EDIN., EARTH SCI, 72, 115-158.

KONTINEN, A., 1987. An Early Proterozoic ophiolite - the Jormua mafic-ultramafic complex, northeastern Finland. PRECAMB. RES. 35, 313-341.

KORSMANN, K., 1977. Progressive metamorphism of the metapelites in the Rantasalmi-Sulkava area, southeastern Finland. BULL. GEOL. SURV. FINLAND, 290, 82pp.

KORSMANN, K., HOLTTA, P., HAUTALA, T. & WASENUS, P., 1984. Metamorphism as an indicator of evolution and structure of the crust in Eastern Finland. GEOL SURV. FINLAND BULL., 328, 40pp.

KORZHINSKII,D. S., 1964. An outline of metasomatic processes. INTERNAT. GEOL. REV. 6, 1713-1734; 1920-1952; 2169-2198.

KORZHINSKII,D. S., 1965. The theory of systems with perfectly mobile components and processes of mineral formation. AM. J. SCI., 263, 193-205.

KOUSA, J., 1985. The tholeiitic and komatiitic metavolcanics in Rantasalmi, southeastern Finland. GEOLOGI, 37, 17-22.

KOUVO, O., 1958. Radioactive age of some Finnish pre-Cambrian minerals. BULL. COMM. GEOL. FINLANDE 182, 70pp.

KOUVO, O. & KULP, J. L., 1961. Isotopic composition of Finnish galenas. ANN. N.Y. ACAD. SCI. 91, 476-491.

KOUVO, O. & TILTON, G. R., 1966. Mineral ages from the Finnish Precambrian. J. GEOL., 74, 421-442.

KRISTMANSDOTTIR, H., 1981. Wollastonite from hydrothermally altered basaltic rocks in Iceland. MINER. MAG., 44, 95-99.

LAAJOKI, K., 1986. The Precambrian supracrustal rocks of Finland and their tectonic-exogenic evolution. PRECAMB. RES., 33, 67-86.

LATVALAHTI, U., 1979. Cu-Zn-Pb ores in the Ayala-Orijarvi area, southwest Finland. ECON. GEOL. 74, 1035-1059.

LAWRENCE, L. J., 1967. Sulphide neomagmas and highly metamorphosed sulphide ore deposits. MINER. DEPOSITA, 2, 5-10.

LEAKE, B. E., 1964. The chemical distinction between ortho- and para-amphibolites. J. PETROL., 5, 238-254.

LEAKE, B. E., HENDRY, G. L., KEMP, A., PLANT, A. G., HARVEY, P. K., WILSON, J. R., COATES, J. S., AUCOTT, J. W., LUNEL, T. & HOWARTH, R. J., 1969. The chemical analysis of rock powders by automatic X-ray fluorescence. CHEM. GEOL., 5, 238-254.

LINDGREN, W., 1905. The copper deposits of the Clifton-Morenci district, Arizona. U.S. GEOL. SURV. PROF. PAPER 43, 375pp.

LIOU, J. G., 1974. Stability relations of andradite-quartz in the system Ca-Fe-Si-O-H. AM. MINERALOGIST, 59, 1016-1025.

LLOYD, G. E., FERGUSON, C. C. & READING, K., 1982. A stress-transfer model for the development of extension fracture boudinage. J. STRUCT. GEOL., 4(3), 355-372.

LOBERG, B. E. H., 1980. A Proterozoic subduction zone in southern Sweden. EARTH PLANET. SCI. LETT., 46, 287-294.

LÖFGREN, C., 1979. Do leptites represent Precambrian island arc rocks? LITHOS, 12, 149-165.

LUNDQUIST, T., 1980. The Precambrian of Sweden. SVER. GEOL. UNDERS., C, 768, 1-87.

LUOSTO, U., LANNE, E., HORHONEN, H., GUTERCH, A., GRAD, M., MATERZOK, R., PAJCHEI, J., PERHUC, E. & VLINIEMI, J., 1983. Results of the deep seismic sounding of the Earth's crust on the profile SVEKA. In ' Proc. of the XVIIIth General Assoc. of ESC, Leeds, 23-27.8.82', ed. by Stiller, M.. Potsdam, 1983, pp265-273.

LYDON, J. W., 1981. Contributed discussion in Goldie, R. & Bottrill, T. J., seminar on sea-floor hydrothermal systems. GEOSCIENCE CAN., 8, 93-104.

LYDON, J. W. & JAMIESON, H. E., 1984. The generation of ore-forming hydrothermal solutions in the Troodos ophiolite complex: some hydrodynamic and mineralogical considerations. In Current Research Part A, GEOL. SURV. CAN., PAPER 84-1A, 617-625.

MACGEEHAN, P. J. & MACLEAN, W. H., 1980. An Archaean sub-seafloor geothermal system, 'calc-alkali' trends, and massive sulphide genesis. NATURE, 286, 767-771.

MAGNUSSON, N. H., 1930. Langbans Malmtrakt. SVERIGES GEOL. UNDERSOKNING, GEOL. BESCRIVNING, 23, 116pp.

MAGNUSSON, N. H., 1960. Iron and sulphide ores of central Sweden. INTERNAT. GEOL. CONG., 21ST, Copenhagen 1960, Excursion Guides A26 and C21, 48pp.

MÄKELÄ, K., 1980. Geochemistry and origin of Haveri and Kiipu, Proterozoic strata-bound volcanogenic gold-copper and zinc mineralisations from southwestern Finland. GEOL. SURV. FINLAND BULL. 310, 79pp.

MCDONALD, J. A., 1970. Some effects of deformation on sulphide-rich layers in lead-zinc ore bodies, Mount Isa, Queensland. ECON. GEOL., 65, 273-298.

MERRILL, R. B., ROBERTSON, J. K. & WYLLIE, P. J., 1970. Melting reactions in the systems $NaAlSi_3O_8$-$KAlSi_3O_8$-SiO_2-H_2O to 20 kilobars compared with results for other feldspar-quartz-H_2O and rock-H_2O systems. J. GEOL., 78, 558-569.

METZ, P., 1976. Experimental investigation of the metamorphism of siliceous dolomites, III. CONTRIB. MINERAL. PETROL., 58, 137-148.

MIYASHIRO, A., 1973. Metamorphism and metamorphic belts. London, Allen & Unwin.

MOODY, J. B., MEYER, D. & JENKINS, J. E., 1983. Experimental characterisation of the greenschist/amphibolite boundary in mafic systems. AM. J. SCI., 283(1), 48-92.

MOOKHERJEE, A., 1971. Deformation of pyrite. ECON. GEOL., 66, p200.

MOORE, J. G., PHILLIPS, R. L., GRIGG, R. W., PETERSON, O. W. & SWANSON, D. A., 1973. Flow of lava into the sea, 1969-1971, Kilauea Volcano, Hawaii. GEOL. SOC. AM. BULL., 84, 537-546.

MOORE, J. G., 1975. Mechanisms of formation of pillow lavas. AM. SCIENTIST, 63, 269-277.

MOTTL, M. J. & HOLLAND, H. D., 1978. Chemical exchange during hydrothermal alteration of basalt by seawater - 1. Experimental results for major and minor components of seawater. GEOCHIM. ET COSMOCHIM. ACTA, 42, 1103-1115.

MUECKE, G. K., PRIDE, C. & SARKER, P., 1979. Rare-earth element geochemistry of regional metamorphic rock. In 'Origin and distribution of elements', ed. by Ahrens, L. H., PHYS. CHEM. EARTH, 11, pp449-464.

MUECKE, G. K., WEDEPOHL, K. H. & MEYER, K., 1983. Chemical composition and genetic relations of meta-volcanic rocks from the Rheno-hercynian belt of NW Germany. In 'Intracontinental fold belts: case studies in the Variscan belt of Europe and the Damara belt in Namibia'. Springer-Verlag, Berlin, pp231-256.

MURPHY, J. B. & HYNES, A. J., 1986. Contrasting secondary mobility of Ti, P, Zr, Nb and Y in two metabasaltic suites in the Appalachians. CAN. J. EARTH SCI., 23, 1138-1145.

MYERS, J. S., 1978. Formation of banded gneisses by deformation of igneous rocks. PRECAMB. RES., 6, 43-64.

NEUVONEN, K. J., KORSMANN, K., KOUVO, O. & PAAVOLAN, J., 1981. Paleomagnetism and age relations of the rocks in the Main Sulphide Ore Belt in central Finland. GEOL. SOC. FINLAND BULL. 53, 109-133.

O'HARA, M. J., 1977. Geochemical evolution during fractional crystallisation of a periodically refilled magma chamber. NATURE, 266, 503-507.

O'NIONS, R. K., EVENSEN, N. M. & HAMILTON, P. J., 1979. Geochemical modelling of mantle differentiation and crustal growth. J. GEOPHYS. RES., 84, 6091-6101.

PARK, A. F. & BOWES, D. R., 1981. Metamorphosed and deformed pillows from Losomaki: evidence of subaqueous volcanism in the Outokumpu association, eastern Finland. BULL. GEOL. SOC. FINLAND, 53-2, 135-145.

PARK, A. F., 1983. Nature, affinities and significance of metavolcanic rocks in the Outokumpu assemblage, eastern Finland. BULL. GEOL. SOC. FINLAND, 56, Part 1-2, 25-52.

PARK, A. F. & BOWES, D. R., 1983. Basement-cover relationships during polyphase deformation in the Svecokarelides of the Kaavi District, eastern Finland. TRANS. R. SOC. EDIN. EARTH SCI., 74, 95-118.

PARK, A. F., 1985. Accretion tectonism in the Proterozoic Svecokarelides of the Baltic Shield. GEOLOGY, 13, 725-729.

PARMENTIER, E. M. & SPOONER, E. T. C., 1978. A theoretical study of hydrothermal convection and the origin of the ophiolite sulphide ore deposits of Cyprus. EARTH PLANET. SCI. LETT., 40, 33-44.

PATCHETT, P. J. & KOUVO, O., 1986. Origin of continental crust of 1.9-1.7 Ga age: Nd isotopes and U-Pb zircon ages in the Svecokarelian terrain of south Finland. CONTRIB. MINERAL. PETROL., 92, 1-12.

PATCHETT, P. J., TODT, W. & GORBATSCHEV, R., 1987. Origin of continental crust of 1.9-1.7 Ga age: Nd isotopes in the Svecofennian Orogenic terrains of Sweden. PRECAMB. RES., 35, 145-160.

PATERSON, M. S. & WEISS, L. E., 1968. Folding and boudinage of quartz-rich layers in experimentally deformed phyllite. GEOL. SOC. AM. BULL., 79, 795-812.

PEARCE, J. A. & CANN, J. R., 1973. Tectonic setting of basic volcanic rocks determined using trace element analysis. EARTH PLANET. SCI. LETT., 19, 290-300.

PEARCE, J. A. & NORRY, M. J., 1979. Petrogenetic implications of Ti, Zr, Y and Nb variations in volcanic rocks. CONTRIB. MINERAL. PETROL., 69, 33-47.

PEARCE, J. A., 1983. Role of sub-continental lithosphere in magma genesis at active continental margins. In 'Continental basalts and mantle xenoliths', eds. Hawkesworth, C. J. & Norry, M. J., pp111-138. Shiva Publishing Ltd, Cheshire, 272pp.

PEDERSEN, F. D., 1980. Remobilisation of the massive sulphide ore of the Black Angel mine, central West Greenland. ECON. GEOL., 75, 1022-1041.

PEDERSEN, F. D., 1981. Polyphase deformation of the massive sulphide ore of the Black Angel mine, central west Greenland. MINERAL. DEPOSITA, 16, 157-176.

PEKKARINEN, L. J., 1979. The Karelian formation and their depositional basement in the Kuhtelysvaara-Vartsila area, eastern Finland. GEOL. SURV. FINLAND BULL., 301.

PETERS, T., VALARELLI, J. N., COUTINHO, J.M.V., SOMMERAUER, J., & VON RAUMER, J., 1977. The manganese deposits of Buritirama (Para, Brazil): SCHWEIZER MINERALOG. PETROG. MITT., 57, 313-327

PHARAOH, T. C. & PEARCE, J. A., 1984. Geochemical evidence for the geotectonic setting of Early Proterozoic metavolcanic sequences in Lapland. PRECAMB. RES., 10, 283-309.

PLIMER, I. R., 1984. The mineralogical history of the Broken Hill lode, N.S.W.. AUSTR. J. EARTH SCI., 31, 379-402.

RAMBERG, H., 1955. Natural and experimental boudinage and pinch-and-swell structures. J. GEOL., 63, 512-526.

RAMSAY, J. G., 1967. Folding and fracturing of rocks. McGraw-Hill, New York, N.Y., 568pp.

RAMSAY, J. G. & GRAHAM, R. H., 1970. Strain variation in shear belts. CAN. J. EARTH SCI., 7, 786-813.

REED, J. C. & MORGAN, B. A., 1971. Chemical alteration and spilitisation of the Catoctin greenstones, Shenandoah National Park, Virginia. J. GEOL., 79, 526-548.

RICHARDSON, S. W., 1968. Staurolite stability in a part of the system Fe-Al-Si-O-H. J. PETROL., 9, 467-488.

RICKARD, D. T., 1978. The Svecokarelian anomalous ore lead line. GEOL. FOREN. STOCKHOLM FORH., 100, 19-29.

ROCK , N. M. S. & WATERHOUSE, K., 1986. Value of chemostratigraphical correlation in metamorphic terrains: an illustration from the Shinness and Armadale marbles, Sutherland, Scotland. PROC. GEOL. ASSOC., 97, 347-357.

RODEN, M. F., FREY, F. A. & CLAGUE, D. A., 1984. Geochemistry of tholeiitic and alkalic lavas from the Koolan Range, Oahu, Hawaii: implications for Hawaiian volcanism. EARTH PLANET. SCI. LETT., 69, 141-158.

ROSCOE, W. E., 1975. Experimental deformation of natural chalcopyrite at temperatures up to 300^{o}C over the strain rate range 10^{-2} to 10^{-6} sec^{-1}. ECON. GEOL., 70, 454-472.

SANGSTER, D. F., 1969. The contact metasomatic magnetite deposits of southwestern British Columbia. GEOL. SURV. CAN. BULL. 172, 1-46.

SAUNDERS, A. D. & TARNEY, J., 1984. Geochemical characteristics of basaltic volcanism within back-arc basins. In 'Marginal Basin Geology', eds. Kokelaar, B. P. & Howells, M. F. GEOL. SOC. LOND. SPEC. PUBL. 16, 59-76.

SAUNDERS, A. D., 1987. Oceanic basalts. GEOL. TODAY, 24-26.

SCEAL, J. S. C. & WEAVER, S. D., 1971. Trace element data bearing on the origin of salic rocks from the Quaternary Volcano Paka, Gregory Rift, Kenya. EARTH PLANET. SCI. LETT., 12, 327-331.

SCHIFFMAN, P., SMITH, B. M., VARGA, R. J. & MOORES, E. M., 1987. Geometry, conditions and timing of off-axis hydrothermal metamorphism and ore-deposition in the Solea graben. NATURE, 325, 423-425.

SCHNEIDERHOHN, H., 1949. Die Erzlagerstatten. Stuttgart.

SCHREURS, J., 1984. The amphibolite-granulite facies transition zone in West Uusima, S.W. Finland. A fluid inclusion study. J. METAMORPHIC GEOL., 2, 327-341.

SCHREYER, W., 1965. Metamorpher Ubergang Saxothuringicum-Moldanubikum ostlich Tirschenreuth-Opf., nachgewiesen durch phasen-petrologische Analyse. GEOL. RUNDSCH., 55, 491-508.

SCOTT, K. M. & TAYLOR, G. F., 1982. Eastern Creek Volcanics as the source of copper at the Mammoth Mine, northwest Queensland. BMR, 7, 93-99.

SCOTT, R. B. & HAJASH, A., 1976. Initial submarine alteration of basaltic pillow lavas : a microprobe study. AM. J. SCI., 276, 480-501.

SEDERHOLM, J. J., 1926. On migmatites and associated pre-Cambrian rocks of southwestern Finland. BULL. COMM. GEOL. FINLANDE, 77, 143pp.

SIIKARLA, T., 1967. On the geophysical investigation in the Virtasalmi area. BULL. COMM. GEOL. FINLANDE, 233.

SIMONEN, A., 1953. Stratigraphy and sedimentation of the Svecofennide early Archaean supracrustal rocks in southwestern Finland. BULL. COMM. GEOL. FINLANDE, 160, 64pp.

SIMONEN, A., 1980. The Precambrian in Finland. GEOL. SURV. FINLAND BULL. 304, 58pp.

SIVRAPRAKASH, C., 1981. Petrology of calc-silicate rocks from Kodura, Andhra Pradesh, India. CONTRIB. MINERAL. PETROL., 77, 121-128.

SKIOLD, T. & CLIFF, R. A., 1984. Sm-Nd and U-Pb dating of early Proterozoic mafic-felsic volcanism in northernmost Sweden. PRECAMB. RES., 26, 1-13.

SKIOLD, T., 1987. Aspects of the Proterozoic geochronology of northern Sweden. PRECAMB. RES., 35, 161-167.

SKIRROW, R. & COLEMAN, M. L., 1982. Origin of sulphur and geothermometry of hydrothermal sulphides from the Galapagos Rift, 86^{o}W. NATURE, 299, 142-144.

SLAUGHTER, J., KERRICK, D. M. & WALL, V. J., 1975. Experimental and thermodynamic study of equilibria in the system CaO-MgO-SiO_2-H_2O-CO_2. AM. J. SCI., 275, 143-162.

SMELLIE, J. A. T., 1974. Formation of atoll garnets from the aureole of the Ardara pluton, Co. Donegal, Ireland. MINERAL. MAG., 39, 878-888.

SMIRNOV, V. I., 1976. Skarn deposits. In 'Geology of mineral deposits', ed. by Smirnov, V. I., pp 156-196. Mir, Moscow.

SMITH, R. E., 1968. Redistribution of major elements in the alteration of some basic lavas during burial metamorphism. J. PETROL., 9, 191-219.

SPOONER, E. T. C. & FYFE, W. S., 1973. Sub-seafloor metamorphism, heat and mass transfer. CONTRIB. MINERAL. PETROL., 42, 287-304.

SPOONER, E. T. C., 1977. Hydrodynamic model for the origin of the ophiolitic cupiferous pyrite ore deposits of Cyprus. In 'Volcanic processes in ore genesis'. GEOL. SOC. LOND. SPEC. PUBL. No. 7, 58-71.

SPOONER, E. T. C. & BRAY, C. J., 1977. Hydrothermal fluids of seawater salinity in ophiolitic sulphide ore deposits in Cyprus. NATURE, 266, 808-812.

STEPHANSSON, O., 1974. Stress-induced diffusion during folding. TECTONOPHYS., 22, 233-251.

STEPHENS, M. B., 1982. Spilitization, volcanite composition and magmatic evolution - their bearing on massive sulphide composition and siting in some volcanic terranes. TRANS. INST. MINING METALL., (SECT. B), 91, B200-213.

STRECKHEISEN, A., 1975. To each plutonic rock its proper name. EARTH SCI. REV., 12, 1-33.

SUN, S. S. & NESBITT, R. W., 1977. Chemical heterogeneity of the Archaean mantle, composition of the Earth and mantle evolution. EARTH PLANET. SCI. LETT., 35, 429-448.

SUN, S. S., NESBITT, R. W. & SHARASKIN, A. Y., 1979. Geochemical characteristics of mid-ocean ridge basalts. EARTH PLANET. SCI. LETT., 44, 119-138.

SUVANTO, J., 1983. Virtasalmen Alueen Karsikivijaksoista. Unpub. MSc Thesis, Helsinki University.

SWANSON, D. A., 1973. Pahoehoe flows from the 1969-1971 Mauna Ulu eruption, Kilauea volcano, Hawaii. GEOL. SOC. AM. BULL., 84, 615-626.

SYLVESTER, A. G. & CHRISTIE, J. M., 1968. The origin of crossed-girdly orientations of optic axes in deformed quartzites. J. GEOL., 76, 571-580.

TARNEY, J., SAUNDERS, A. D., WEAVER, S. D., DONNELLAN, N. C. B. & HENDRY, G. L., 1979. Minor-element geochemistry of basalts from Leg 49, North Atlantic Ocean. In Luyendyk, B. P., Cann, J. R. et al., Init. Repts. DSDP, 49. Washington (U.S. Govt. Printing Office), 657-691.

TAYLOR, B. E. & LIOU, T. K., 1978. The low temperature stability of andradite in C-O-H fluids. AM. MINERALOGIST, 63, 378-393.

THIRWALL, M. F. & GRAHAM, A. M. J., 1984. Evolution of high-Ca, high-Sr C-series basalts from Grenada, Lesser Antibes: the effects of intra-crustal contamination. J. GEOL. SOC. LOND., 141, 427-445.

THOMPSON, R. N., 1982. Magmatism of the British Tertiary Volcanic Province. SCOTT. J. GEOL., 18, 49-108.

TILLING, R. I., RHODES, J. M., SPARKS, J. W., LOCKWOOD, J. P. & LIPMAN, P. W., 1987. Disruption of the Mauna Loa magma system by the 1868 Hawaiian earthquake: geochemical evidence. NATURE, , 196-199

TORNEBOHM, A. E., 1875. Geognostisk beskrifning ofver Persbergets grufvefalt. SVERIGES GEOL. UNDERS., C 14, 1-21.

TRACEY, R. J., ROBINSON, P. & THOMPSON, A. B., 1976. Garnet composition and zoning in the determination of temperature and pressure of metamorphism, central Massachusetts. AM. MINERALOGIST, 61, 762-775.

TREUIL, M. & VARET, J., 1973. Criteres volcanologiques, petrologiques et geochimiques de la genese et de la differentiation des magmas basaltiques : exemple de l'Afar. BULL. SOC. GEOL. FR., 15, 506-540.

TUOMINEN, H. V., AARNISALO, J. & SODERHOLM, B., 1973. Tectonic patterns in the Central Baltic Shield. BULL. GEOL. SOC. FINLAND, 45, 205-217.

TURNER, F. J., 1980. Metamorphic Petrology (2nd Edition). McGraw-Hill.

TUTTLE, O. F. & BOWEN, N. L., 1958. Origin of granite in the light of experimental studies in the system $NaAlSi_3O_8$-$KAlSi_3O_8$-SiO_2-H_2O. MEM. GEOL. SOC. AM., 74.

VAASJOKI, M., 1977. Rapakivi granites and other postorogenic rocks in Finland: their age and the lead isotopic composition of certain associated galena mineralisations. GEOL. SURV. FINLAND BULL. 294, 71pp.

VAASJOKI, M., 1981. The lead isotopic composition of some Finnish galenas. GEOL. SURV. FINLAND BULL. 316, 30pp.

VAUCHEZ, A., 1987. The development of discrete shear-zone in a granite: stress, strain and changes in deformation mechanisms. TECTONOPHYS., 133, 137-156.

VERKAEREN, J. & BARTHOLOME, P., 1979. Petrology of the San Leone magnetite skarn deposit (S.W. Sardinia). ECON. GEOL., 74, 53-66.

VIDALE, R., 1969. Metasomatism in a chemical gradient and the formation of calc-silicate bands. AM. J. SCI., 267, 857-874.

VIDALE, R. & HEWITT, D. A., 1973. "Mobile" components in the formation of calc-silicate bands. AM. MIN., 58, 991-997.

VOKES, F. M., 1971. Some aspects of the regional metamorphic mobilization of preexisting sulphide deposits. MIN. DEPOSITA, 6, 122-129.

WARD, P., 1985. Unpubl. PhD thesis entitled "Deposition and Deformation at a lower Proterozoic cratonic margin, South-east Finland". *'

WARD, P., 1987. Early Proterozoic deposition and deformation at the Karelian Craton Margin in southeastern Finland. PRECAMB. RES., 35, 71-93.

WATANABE, T., 1960. Characteristic features of ore deposits found in contactmetamorphic aureoles in Japan. INTERNAT. GEOL. REV. 2, 946-966.

WATSON, J. V., 1964. Conditions in the metamorphic Caledonides during the period of late orogenic cooling. GEOL. MAG., 101, 457-465.

WEAVER, B. L. & TARNEY, J., 1981. Chemical changes during dyke metamorphism in high-grade basement terrains. NATURE, 289, 47-49.

WEAVER, B. L., TARNEY, J., WINDLEY, B. F. & LEAKE, B. E., 1982. Geochemistry and petrogenesis of Archaean metavolcanic amphibolites from Fiskenaesset, S.W. Greenland. GEOCHIM. ET COSMOCHIM. ACTA, 46, 2203-2215.

WEGMAN, C. E., 1932. Note sur le Boudinage. SOC. GEOL. DE FRANCE BULL., 471-491.

WELIN, E., WIKLANDER, U. & KAHR, A. M., 1980. Radiometric dating of a quartz-porphyritic potassium rhyolite at Hallefors, south central Sweden. GEOL. FOREN. STOCKHOLM FORH., 102, 269-272.

WELIN, E., 1987. The depositional evolution of the Svecofennian supracrustal sequence in Finland and Sweden. PRECAMB. RES., 35, 95-113.

*' Glasgow University

WEST, N. G., HENDRY, G. L. & BAILEY, N. T., 1974. The Analysis of Slags from Primary and Secondary Copper Smelting Processes by X-Ray Fluorescence. X-RAY SPECTROMETRY, 3, 78-87.

WHITE, A. J. R., 1959. Scapolite-bearing marbles and calc-silicate rocks from Tungkillo and Milendella, South Australia. GEOL. MAG., 96, 285-305.

WHITE, A. J. R. & CHAPPELL, B. W., 1977. Ultrametamorphism and granitoid genesis. TECTONOPHYS., 43, 7-22.

WHITE, W. M. & PATCHETT, P. J., 1984. Hf-Nd-SR isotopes and incompatible element abundances in island arcs: implications for magma origins and crust-mantle evolution. EARTH PLANET. SCI. LETT., 67, 167-185.

WILSON, J. R. & LEAKE, B. E., 1972. The petrochemistry of the epi-diorites of the Tayvallich Peninsula, North Knapdale, Argyllshire. SCOTT. J. GEOL., 8(3), 215-252.

WILSON, R. A. M., 1959. The geology of the Xeros-Troodos area. CYPRUS GEOL. SURV. MEM. No. 1.

WINKLER, H. G. F., 1979. Petrogenesis of metamorphic rocks (5th Edition). Springer-Verlag, New York.

WOOD, D. A., TARNEY, J., VARET, J., SAUNDERS, A. D., BOUGAULT, H., JORON, J. L., TREUIL, M. & CANN, J. R., 1979. Geochemistry of basalts drilled in the North Atlantic gy IPOD Leg 49: implications for mantle heterogeneity. EARTH PLANET. SCI. LETT., 42, 77-98.

WOOD, D. A., MARSH, N. G., TARNEY, J., JORON, J. L., FRYER, P. & TREUIL, M., 1981. Geochemistry of igneous rocks recovered from a transect across the Mariana Trough, Arc, Fore-Arc, and Trench, Sites 453 through 461, DSDP Leg 60. In: Hussang, D. M., Uyeda, S. et al. (eds.) INIT. RPT. DSDP, 60, 611-645. U.S. Govt. Printing Offics, Washington.

ZACHRISSON, E., 1982. Spilitization, mineralisation and vertical metal zonation at the Stekenjokk strata-bound sulphide deposit, central Scandinavian Caledonides. TRANS. INST. MIN. METAL. BULL. (SECT. B), 91, 192-199.

ZHARIKOV, V. A., 1970. Skarns. INTERNAT. GEOL. REV. 12, 541-559, 619-647, 760-775.

APPENDIX 1

1. Sample collection and preparation

Samples used for geochemistry were mostly collected using a portable diamond drill. This permitted retrieval of fresh rock form flat, glaciated exposures. The cores obtained were c. 2.5 cm in diameter and up to 30 cm long. The top 2 cm in most samples was weathered. It was necessary to remove any contaminants deposited by the steel core sleeves by rubbing the cores down with emery or corundum paper. A few samples were also taken from drill core through Hallinmaki Mine, stored at Outokumpu's Oravikoski Mine.

2. XRF rock analysis for major and trace elements

2.1 Method

Analysis was carried out using a Philips PW1450/20 automatic X-ray fluorescence spectrometer equipped with a 60 position sample changer and on-line SuperBrain microcomputer for data processing.

The major elements were analysed from fused glass discs prepared according to the method of Harvey *et al.* (1973) and using influence factors to correct for remaining absorption - enhancement effects, (Jenkins, 1969; DeJongh, 1973).

In the course of bead preparation it was found that S_2-bearing samples reacted corrosively with platinum crucibles used to retain the silicate melt. However, following the procedure of West *et al.* (1974) this problem was overcome by

the addition of $NaNO_3$ to CuS-rich rock powder. The following ratio was required in the mixture:

0.15g rock powder : 0.30g $NaNO_3$: 1.92g flux.

This also made it necessary to make up a set of standards with this mixture against which these analyses could be compared for recalibration.

For the trace elements, pressed powder pellets were used (Leake et al., 1969), with correction for absorption using the intensity of the incoherently scattered Compton peak (Harvey, 1981, 1982) using the Molybdenum tube.

It should be noted that all samples were duplicated and that the analyses given in Appendix 2 are averaged analyses.

2.2 Results: major elements

i.e. SiO_2, TiO_2, Al_2O_3, Fe^O, MnO, MgO, CaO, Na_2O, P_2O_5.

Total iron (Fe^O) is determined as Fe_2O_3.

The calibration coefficients are established routinely from internal Glasgow standards with periodic checks of accuracy against international standards. Table 1 gives a statistical summary for the major element results.

2.3 Results: trace elements

The following elements were determined:

Ba, Ce, Co, Cr, Cu, Ga, La, Nb, Ni, Pb, Rb, S, Sr, Th, U, Y, Zn, Zr.

All are analysed with the Mo tube except Nb and S which use the Cr tube. Precision, count rate and calibration statistics are

summarised in Table 2. As all the available International standards were used to establish the calibration, no independant check of accuracy of the results has yet been possible.

TABLE 1 Summary statistics : major elements

Element	SiO_2	TiO_2	Al_2O_3	Fe_2O_3	MnO	MgO	CaO	Na_2O	K_2O	P_2O_5
Count rate error %	0.6	0.8	1.0	1.0	3.0	1.5	0.6	0.7	0.6	1.6
Std. error of estimate wt.%	0.54	0.03	0.52	0.15	0.01	0.30	0.09	0.20	0.07	0.01
Calibration lower	8.00	0.00	0.00	0.00	0.00	0.00	0.00	0.00	0.00	0.00
range upper	80.00	3.20	23.00	14.80	0.20	50.00	32.50	5.40	5.00	0.60
Detection limit wt.%	0.086	0.018	0.087	0.045	0.012	0.165	0.006	0.155	0.002	0.018
Accuracy ± wt.% (average deviations of 11 standards)	0.46	0.11	0.36	0.10	0.008	0.13	0.17	0.26	0.09	0.02
Precision c% : G-SL	0.76	1.55	0.75	1.45	11.1	6.47	1.34	4.35	1.03	4.35

TABLE 2 Summary statistics : trace elements

Element	Count rate error %	Std error of estim. ppm.	Upper limit ppm.	Detection limit ppm.	Precision c% G-TH
Zr	0.7	10	300	2.7	1.7
Y	0.9	4	150	1.4	2.4
Sr	0.9	14	800	1.5	0.9
U	4.0	1	100	9.4	55.9
Rb	0.9	9	600	1.7	4.3
Th	3.0	4	400	11.5	20.6
Pb	6.0	9	100	11.6	12.1
Ga	3.0	3	100	2.4	4.1
Zn	2.0	12	1400	1.8	1.6
Cu	1.5	8	400	4.4	10.9
Ni	1.5	12	2500	4.8	14.6
Co	0.5	3	250	3.2	4.9
Cr	1.2	22	3200	1.9	5.9
Ce	2.2	8	500	3.2	2.0
Ba	0.9	10	2500	12.3	2.7
La	2.5	6	250	3.9	6.1
Nb	2.5	4	980	7.3	
S	2.5	75	5000	7.1	

APPENDIX 2

The major and trace element data used in the geochemical analysis of the amphibolites (Section 3, Part 1) and syn-kinematic intrusions (Section 4) are tabulated in this Appendix. The major elements are expressed as weight percentages and the trace elements as ppm. Copper and sulphur are expressed either as ppm or in weight percent.

No H_2O, CO_2 or Fe^{2+}/Fe^{3+} determinations were carried out. However, samples were duplicated and the values listed are averages of these. The errors involved in calculating the mean were within the ranges cited in Appendix 1 for XRF methods of analysis.

Na_2O values are unreliable for those samples where bead preparation using $NaNO_3$ was carried out. There is an asterisk beside these values.

Totals are for the 10 common elements only.

	1	2	3	4	5	6	7
SiO_2 %	51.46	50.68	44.20	40.66	48.54	36.52	40.77
TiO_2	1.79	1.46	1.08	0.54	1.05	1.72	0.91
Al_2O_3	17.53	20.40	13.60	9.29	15.84	14.80	13.16
Fe_{tot}	6.59	10.74	11.20	17.81	11.84	15.63	8.12
MnO	0.05	0.07	0.23	0.40	0.12	0.29	0.26
MgO	4.61	3.46	8.16	3.02	7.75	2.45	5.69
CaO	11.21	9.37	15.38	23.31	10.55	16.54	17.80
Na_2O	0.26	2.32	1.59	1.37	1.37	0.02	1.75
K_2O	0.54	0.66	0.38	0.25	0.68	0.21	0.09
P_2O_5	0.42	0.45	0.13	0.18	0.14	0.28	0.16
TOTAL	94.46	99.61	95.95	96.83	97.88	88.46	88.71
Co ppm	38	31	88	34	53	204	40
Ce	56	41	20	38	32	9	33
Cr	39	160	482	138	247	1460	84
Ba	98	149	112	45	115	78	56
La	31	20	8	24	22	28	17
Zr	219	175	82	113	114	148	104
Y	31	19	18	41	24	88	21
Sr	384	1022	318	81	322	215	274
U	0	1	0	4	1	4	3
Rb	7	9	5	6	7	4	3
Th	3	1	---	2	---	0	2
Pb	3	0	1	---	0	1	1
Ga	21	26	13	12	20	23	19
Zn	37	92	61	62	75	257	98
Cu	474	174	1593	142	137	257	1474
Ni	62	23	201	25	112	552	75
S	1440	1307	1.98%	904	1098	8.49%	2312
Nb	17	9	13	7	10	16	12

	8	9	10	11	12	13	14
SiO_2 %	52.93	40.06	37.28	44.26	44.51	56.70	45.86
TiO_2	1.71	0.70	1.27	1.45	1.22	0.77	1.76
Al_2O_3	17.29	9.87	6.38	12.26	9.36	19.58	14.98
Fe_{tot}	7.80	18.34	21.06	13.50	17.38	5.28	10.79
MnO	0.11	0.35	0.34	0.20	0.30	0.08	0.25
MgO	5.54	3.16	2.83	7.52	4.07	2.54	7.42
CaO	9.24	26.08	25.09	17.83	20.91	6.40	12.80
Na_2O	3.40	0.46	0.07	0.75		5.90	2.66
K_2O	0.59	0.17	0.17	0.28	0.16	1.04	0.78
P_2O_5	0.40	0.05	0.00	0.28	0.00	0.22	0.50
TOTAL	99.01	99.24	94.49	98.33	97.91	98.51	97.80
Co ppm	35	53	101	122	110	13	53
Ce	60	25	34	37	52	52	45
Cr	56	317	194	560	135	13	157
Ba	78	51	16	44	42	514	204
La	22	21	6	19	40	23	15
Zr	181	109	345	153	332	523	167
Y	28	44	92	24	49	24	26
Sr	341	107	42	246	153	817	360
U	1	4	2	1	3	3	3
Rb	6	5	5	4	3	24	9
Th	1	2	5	---	4	1	5
Pb	0	0	0	---	---	0	5
Ga	21	12	13	14	12	24	20
Zn	45	108	214	86	298	55	141
Cu	2967	1406	19834	3285	23071	59	44
Ni	103	58	185	172	176	4	124
S	0.59%	2933	4.32%	2.38%	3.38%	519	3182
Nb	8	9	8	12		16	6

	15	16	17	18	19	20	21
SiO_2 %	48.11	52.64	46.34	49.87		51.44	35.60
TiO_2	2.38	1.69	2.02	1.64		2.22	0.87
Al_2O_3	15.46	15.90	14.08	16.50		15.97	9.37
Fe_{tot}	8.98	3.59	7.56	9.36		6.73	33.94
MnO	0.09	0.13	0.12	0.14		0.11	0.22
MgO	7.58	5.81	8.77	7.70		3.26	6.03
CaO	11.43	13.66	15.63	8.54		14.72	9.44
Na_2O	3.62	3.27	1.82	4.22		2.82	1.34
K_2O	0.59	0.43	0.54	0.82		0.30	0.73
P_2O_5	0.60	0.31	0.52	0.24		0.47	0.21
TOTAL	98.84	97.43	97.40	99.03		98.04	97.75
Co ppm	43	17	52	48	39	20	90
Ce	87	37	125	38	62	62	82
Cr	286	68	315	65	503	38	137
Ba	120	117	126	243	179	114	191
La	34	17	59	10	24	43	79
Zr	258	143	252	72	105	296	114
Y	33	26	28	19	25	38	29
Sr	514	360	312	673	577	328	261
U	1	2	1	0	1	2	3
Rb	6	7	6	13	9	7	14
Th	---	1	3	0	1	5	4
Pb	---	5	---	1	1	3	3
Ga	18	17	15	22	19	26	26
Zn	44	34	55	74	76	35	225
Cu	13	95	72	132	53	25	3394
Ni	100	52	135	90	117	9	145
S	2.08%	101	233	1402	427	173	1.31%
Nb	11	20	12	10	19	20	7

	22	23	24	25	26	27	28
SiO_2 %	46.48	41.87	45.26	49.68	46.31	49.29	
TiO_2	1.54	0.84	1.20	1.58	0.68	1.76	
Al_2O_3	16.56	13.04	13.09	19.19	12.22	15.94	
Fe_{tot}	8.48	16.36	11.51	9.85	11.17	9.90	
MnO	0.23	0.23	0.19	0.06	0.25	0.18	
MgO	4.59	2.61	15.14	3.99	5.93	7.59	
CaO	19.52	21.73	8.25	8.48	19.11	10.39	
Na_2O	0.68	0.00	3.43	4.56	1.89	0.90	
K_2O	0.18	0.27	1.40	0.61	0.22	0.55	
P_2O_5	0.30	0.19	0.23	0.50	0.25	0.45	
TOTAL	98.56	97.14	99.70	98.50	98.03	96.95	
Co ppm	34	79	70	39	44	42	67
Ce	26	49	28	45	39	116	21
Cr	318	133	981	26	60	115	467
Ba	63	37	229	223	33	121	116
La	21	46	44	26	34	32	8
Zr	119	154	105	114	117	190	81
Y	32	39	22	20	14	26	17
Sr	289	243	276	1035	202	613	311
U	3	8	2	0	2	1	1
Rb	6	6	34	12	2	5	5
Th	4	---	0	4	2	4	1
Pb	2	---	2	8	3	0	0
Ga	21	18	16	28	18	18	16
Zn	52	225	64	90	93	58	71
Cu	286	21540	19	207	77	85	967
Ni	96	114	458	18	42	105	176
S	660	3.15%	88	1453	200	193	7772
Nb	12	12	15	8	16	18	12

	29	30	31	32	33	34	35
SiO_2 %	48.70	52.86	46.76	49.88	48.21	47.76	48.52
TiO_2	1.34	1.21	0.57	1.57	1.49	1.72	1.69
Al_2O_3	16.59	16.08	14.82	18.90	19.22	13.85	18.67
Fe_{tot}	8.47	9.16	11.42	9.03	9.06	9.86	11.06
MnO	0.08	0.16	0.16	0.12	0.13	0.10	0.10
MgO	9.00	6.66	7.83	4.02	6.00	6.38	5.64
CaO	10.31	8.04	17.08	8.51	7.43	15.35	7.82
Na_2O	2.61	3.38	0.96	4.85	3.87	2.86	4.72
K_2O	0.70	0.71	0.40	0.72	1.14	0.51	0.50
P_2O_5	0.23	0.29	0.07	0.53	0.40	0.33	0.56
TOTAL	98.03	98.55	100.07	98.13	97.95	98.66	99.28
Co ppm	42	36	61	33	46	43	30
Ce	32	55	2	46	63	42	41
Cr	218	129	517	30	33	483	38
Ba	95	194	91	269	553	144	204
La	13	25	7	9	23	25	11
Zr	139	100	44	39	157	136	122
Y	20	26	14	17	22	26	21
Sr	343	514	207	1039	725	291	1017
U	1	2	3	0	2	1	1
Rb	9	12	7	16	29	5	7
Th	1	2	1	3	---	0	0
Pb	3	2	4	2	---	1	0
Ga	16	23	14	25	23	16	27
Zn	35	90	57	79	65	42	97
Cu	157	155	116	120	114	23	97
Ni	123	95	238	13	44	216	15
S	299	838	83	547	717	98	197
Nb	10	10	6	10	14	12	8

	36	37	38	39	40	41	42
SiO_2 %	58.79	50.36	46.28	51.36	43.99	46.18	46.57
TiO_2	1.12	1.27	1.21	1.48	1.16	1.51	1.85
Al_2O_3	16.82	12.43	12.79	19.88	13.62	12.42	16.56
Fe_{tot}	7.56	10.27	10.55	9.69	11.66	7.42	11.21
MnO	0.08	0.14	0.24	0.15	0.28	0.10	0.14
MgO	3.14	12.34	16.30	3.99	5.86	9.81	6.67
CaO	6.11	11.14	8.73	7.68	21.48	19.25	9.86
Na_2O	4.43	2.65	2.00	4.29	1.56	1.79	4.66
K_2O	0.55	0.62	1.87	0.51	0.11	0.31	0.75
P_2O_5	0.25	0.13	0.26	0.47	0.20	0.30	0.46
TOTAL	98.85	101.35	100.23	99.49	99.92	99.09	98.73
Co ppm	21	62	67	33	35	33	41
Ce	54	18	27	64	20	26	64
Cr	37	1096	910	25	99	566	37
Ba	182	123	241	195	34	62	206
La	18	16	7	19	12	23	28
Zr	254	83	104	274	99	153	291
Y	25	20	22	26	13	25	33
Sr	530	271	169	813	195	246	461
U	2	3	2	2	3	4	1
Rb	9	11	63	12	5	5	9
Th	1	1	---	1	0	---	0
Pb	2	---	---	1	5	0	0
Ga	21	13	12	25	17	14	21
Zn	80	81	55	101	71	53	61
Cu	90	48	10	94	1	757	269
Ni	27	218	412	22	36	168	94
S	538	28	28	466	30	823	1004
Nb	12	9	15	20	14	11	16

	43	44	45	46	47	48	49
SiO_2 %	44.49	47.73	48.28	46.27	47.04	43.58	45.68
TiO_2	1.00	0.73	1.62	1.39	0.96	1.66	2.00
Al_2O_3	14.59	15.49	18.91	15.13	14.73	17.26	13.19
Fe_{tot}	9.16	10.83	9.22	10.82	9.91	8.91	9.14
MnO	0.09	0.10	0.11	0.16	0.12	0.12	0.13
MgO	10.82	10.46	3.97	9.51	9.38	4.53	5.68
CaO	15.55	11.06	8.77	10.48	12.39	19.50	17.64
Na_2O	1.75	2.93	4.48	2.86	2.73	1.63	1.47
K_2O	0.58	0.62	0.48	0.62	0.61	0.20	0.17
P_2O_5	0.18	0.03	0.53	0.28	0.12	0.32	0.27
TOTAL	98.21	99.98	96.37	97.52	97.49	97.71	96.11
Co ppm	38	44	28	40	37	62	66
Ce	13	0	40	16	15	33	73
Cr	400	353	16	366	463	40	17
Ba	85	111	185	132	101	40	84
La	5	3	16	20	7	33	56
Zr	84	47	124	124	77	183	256
Y	16	18	21	24	16	24	43
Sr	213	150	1057	300	287	174	170
U	1	3	2	1	1	1	5
Rb	8	7	6	8	7	6	6
Th	0	---	---	2	---	0	4
Pb	0	---	---	---	---	---	2
Ga	14	15	26	17	14	20	16
Zn	47	46	81	57	43	143	135
Cu	46	6	109	129	40	10127	10426
Ni	146	122	14	159	147	104	116
S	133	45	589	295	177	9770	13104
Nb	11	9	12	10	10	13	15

	50	51	52	53	54	55	56
SiO_2 %	44.39	47.71	64.86	48.03	46.25	44.88	43.15
TiO_2	1.93	2.20	0.51	1.60	1.37	1.80	1.47
Al_2O_3	13.54	14.01	16.65	15.93	12.97	15.79	14.74
Fe_{tot}	10.52	15.88	4.05	11.58	10.17	8.71	12.42
MnO	0.28	0.24	0.04	0.21	0.15	0.14	0.24
MgO	4.89	5.32	1.70	6.68	6.98	4.19	4.66
CaO	22.11	9.24	3.94	8.44	19.96	20.40	21.72
Na_2O	1.11	3.52	5.02	4.03	0.29	0.38	0.00
K_2O	0.09	0.49	1.11	0.60	0.16	0.17	0.39
P_2O_5	0.45	0.52	0.17	0.37	0.32	0.36	0.20
TOTAL	99.31	99.13	96.55	97.47	98.52	96.82	98.99
Co ppm	28	48	5	45	35	36	36
Ce	58	72	92	51	27	40	17
Cr	20	28	3	62	479	322	288
Ba	52	174	704	169	57	61	73
La	34	40	62	31	21	31	17
Zr	254	270	214	143	111	154	106
Y	28	37	4	24	23	27	35
Sr	209	384	752	461	246	289	268
U	3	2	2	1	4	1	2
Rb	5	6	28	7	6	6	10
Th	3	1	3	0	1	2	---
Pb	2	---	1	0	---	---	---
Ga	13	21	19	19	15	18	15
Zn	53	128	48	82	47	28	57
Cu	26	141	22	122	2	11	814
Ni	12	15	6	110	171	115	193
S	51	506	145	653	17	39	940
Nb	14	14	10	14	13	14	7

	57	58	59	60	61	62	63
SiO_2 %	42.21	43.23	49.62	49.23	50.13	55.41	51.12
TiO_2	1.39	1.58	1.38	1.98	2.24	1.01	2.07
Al_2O_3	14.83	15.05	15.06	14.50	14.83	17.26	14.95
Fe_{tot}	11.75	12.51	9.16	7.50	7.48	5.22	6.26
MnO	0.18	0.16	0.12	0.13	0.16	0.11	0.11
MgO	4.18	3.72	5.27	4.47	3.42	5.70	4.16
CaO	21.82	21.45	12.51	16.01	14.72	7.93	14.88
Na_2O	0.62	0.34	3.84	3.30	3.89	3.69	2.42
K_2O	0.44	0.42	0.41	0.19	0.22	0.55	0.36
P_2O_5	0.17	0.25	0.40	0.47	0.50	0.13	0.39
TOTAL	97.59	98.71	97.33	97.78	97.59	97.01	96.72
Co ppm	28	30	30	18	22	26	33
Ce	16	18	42	50	50	19	46
Cr	259	296	245	65	19	40	13
Ba	66	73	116	111	84	107	113
La	15	23	30	37	28	11	29
Zr	105	123	186	238	261	141	265
Y	33	39	29	32	41	16	32
Sr	282	272	325	334	293	370	284
U	4	2	---	1	2	1	2
Rb	18	18	5	4	4	5	9
Th	---	---	2	---	3	---	0
Pb	---	3	---	1	1	0	0
Ga	20	21	18	22	19	19	17
Zn	46	49	31	43	47	31	30
Cu	221	560	49	45	568	80	266
Ni	120	146	99	19	11	77	26
S	459	998	243	174	683	44	1173
Nb	7	9	15	18	20	9	15

	64	67	68	69	70	71	72
SiO_2 %	55.31	48.10	44.85	46.16	48.25	46.38	
TiO_2	0.84	2.05	0.59	0.58	0.58	0.58	
Al_2O_3	15.45	8.02	16.51	15.07	14.41	14.54	
Fe_{tot}	5.00	11.41	10.35	9.90	10.46	9.43	
MnO	0.08	0.23	0.10	0.15	0.16	0.13	
MgO	4.60	7.08	7.64	6.99	7.76	8.63	
CaO	12.86	20.15	16.81	18.94	16.97	16.38	
Na_2O	1.98	1.15	1.78	1.52	1.27	1.58	
K_2O	0.35	0.24	0.46	0.16	0.35	0.33	
P_2O_5	0.17	0.38	0.06	0.09	0.06	0.08	
TOTAL	96.64	98.81	99.15	99.56	100.27	98.16	
Co ppm	14		42	44	51	33	51
Ce	23		1	10	2	6	2
Cr	66		355	433	471	495	471
Ba	99		113	49	62	58	62
La	9		3	5	---	5	---
Zr	190		47	49	43	45	
Y	19		13	14	14	14	
Sr	340		262	243	234	272	
U	4		1	1	1	2	
Rb	7		7	4	5	5	
Th	2		1	2	0	---	
Pb	3		---	3	0	---	
Ga	17		14	11	14	12	
Zn	27		60	60	53	57	
Cu	8		4	59	8	2	
Ni	39		129	203	237	180	
S	14		52	207	28	21	
Nb	14		4	2	6	5	

	73	74	75	76	77	78	84
SiO_2 %	46.64	44.96	48.01	50.13	51.37	45.48	51.40
TiO_2	0.67	0.67	1.26	1.39	0.39	0.72	0.25
Al_2O_3	15.57	13.79	13.09	18.85	16.76	15.14	16.75
Fe_{tot}	11.06	11.46	8.29	8.63	4.03	11.47	4.65
MnO	0.19	0.12	0.13	0.05	0.08	0.18	0.07
MgO	10.19	10.48	6.61	5.00	6.84	10.63	9.32
CaO	10.67	13.33	17.21	8.84	14.37	12.29	10.44
Na_2O	2.16	0.35	2.11	3.90	2.40	2.09	3.29
K_2O	0.44	0.53	0.49	0.53	0.28	0.79	0.42
P_2O_5	0.07	0.03	0.09	0.27	0.00	0.08	0.03
TOTAL	97.66	95.72	97.29	97.59	96.52	98.87	96.62
Co ppm	46	64	41	30	20	50	34
Ce	5	4	32	38	9	0	---
Cr	303	313	56	65	28	296	547
Ba	81	84	144	197	85	93	91
La	12	2	17	14	7	2	0
Zr	41	37	105	154	59	39	52
Y	17	16	24	19	12	18	8
Sr	170	207	313	737	282	175	264
U	0	2	4	1	1	0	2
Rb	6	6	12	8	6	9	9
Th	---	---	0	---	0	2	0
Pb	---	---	2	2	0	10	2
Ga	14	16	15	24	16	12	12
Zn	54	71	72	83	28	73	33
Cu	57	1535	2447	107	28	450	13
Ni	151	123	70	49	94	147	204
S	69	9936	3732	566	58	1725	47
Nb	9	6	12	9	4	4	5

	85	86	87	88	89	90	91
SiO_2 %	53.67	61.75	51.06	58.31	46.75	47.32	53.27
TiO_2	0.73	0.77	0.30	1.04	2.07	1.86	1.22
Al_2O_3	19.12	17.58	18.05	18.19	14.62	15.74	13.07
Fe_{tot}	2.16	5.15	6.24	5.86	13.02	10.49	14.32
MnO	0.05	0.05	0.10	0.08	0.12	0.11	0.17
MgO	5.24	2.00	8.44	2.50	7.74	6.02	4.59
CaO	13.65	4.81	10.31	5.38	10.40	13.34	6.67
Na_2O	4.16	5.38	4.04	5.54	3.77	3.64	3.74
K_2O	0.30	1.23	0.56	1.17	0.89	0.63	0.42
P_2O_5	0.10	0.26	0.03	0.28	0.47	0.40	0.18
TOTAL	99.18	98.98	99.13	98.35	99.85	99.55	97.65
Co ppm		20	29	16	39	31	35
Ce		59	3	48	35	41	20
Cr		18	144	17	201	126	25
Ba		556	124	552	151	102	127
La		24	0	15	18	19	18
Zr		307	46	227	168	170	132
Y		13	9	18	30	26	41
Sr		760	453	751	320	310	196
U		1	0	0	3	2	0
Rb		28	9	27	10	5	5
Th		1	0	3	2	1	---
Pb		5	4	4	0	2	---
Ga		21	16	25	18	20	12
Zn		61	64	76	45	54	107
Cu		58	5	50	23	4	9
Ni		4	135	8	70	53	30
S		67	53	130	63	34	25
Nb		10	4	14	20	13	9

	92	93	94	95	96	97	98
SiO_2 %	52.09	47.54	50.43	49.73	50.05	52.75	41.98
TiO_2	1.28	1.10	1.27	0.30	1.42	1.32	0.47
Al_2O_3	12.94	12.81	13.56	18.15	12.19	12.99	15.75
Fe_{tot}	15.10	10.80	4.80	4.99	17.28	15.68	13.01
MnO	0.22	0.30	0.10	0.10	0.22	0.22	0.18
MgO	4.56	5.67	7.85	7.73	5.06	5.67	5.24
CaO	6.67	17.44	16.86	13.80	7.53	6.61	18.51
Na_2O	3.75	2.72	2.88	2.81	3.43	3.37	1.10
K_2O	0.41	0.19	0.18	0.38	0.29	0.35	0.48
P_2O_5	0.20	0.21	0.15	0.04	0.22	0.19	0.05
TOTAL	97.22	98.78	98.08	98.09	97.69	99.15	99.77
Co ppm	40	53	24	27	42	49	42
Ce	22	28	18	8	28	29	183
Cr	27	41	212	290	30	9	8
Ba	140	64	102	97	109	86	101
La	13	11	13	3	15	18	---
Zr	138	107	101	43	120	124	43
Y	43	37	22	11	44	37	14
Sr	154	181	278	298	194	192	333
U	2	1	1	2	1	2	2
Rb	4	9	4	7	3	5	16
Th	1	---	1	2	---	1	0
Pb	1	2	0	0	---	2	3
Ga	17	18	14	14	16	17	16
Zn	131	148	38	37	113	105	43
Cu	45	259	73	4	261	74	5
Ni	28	44	70	129	26	33	102
S	29	575	164	8	92	39	35
Nb	6	8	15	4	10	5	5

	99	100	101	102	103	104	105
SiO_2 %	51.29	49.58	49.93	50.61	47.92	49.14	52.47
TiO_2	0.91	1.43	1.77	1.21	0.91	1.14	1.77
Al_2O_3	13.40	12.63	13.05	12.34	13.36	12.21	12.43
Fe_{tot}	11.99	17.99	17.81	15.66	10.79	15.91	17.86
MnO	0.20	0.24	0.28	0.17	0.17	0.34	0.23
MgO	7.31	5.19	6.02	5.89	6.12	5.93	5.24
CaO	7.82	7.31	5.48	6.88	15.17	10.39	4.08
Na_2O	4.36	2.83	4.47	3.74	2.76	3.70	4.03
K_2O	0.68	0.32	0.27	0.44	0.55	0.28	0.21
P_2O_5	0.18	0.23	0.38	0.19	0.17	0.15	0.51
TOTAL	98.04	100.75	99.37	97.13	97.92	99.19	98.83
Co ppm	53	54	39	49	35	41	31
Ce	21	13	37	20	11	17	44
Cr	95	26	24	29	66	48	21
Ba	156	119	123	78	228	115	155
La	11	7	21	8	7	9	17
Zr	70	123	176	127	80	91	215
Y	22	45	63	42	21	34	73
Sr	222	155	119	193	298	306	139
U	2	2	2	3	2	1	0
Rb	8	4	3	4	16	3	5
Th	0	---	0	1	---	---	---
Pb	0	0	4	---	0	---	2
Ga	12	17	21	17	15	15	20
Zn	90	124	139	96	105	95	160
Cu	473	218	26	34	88	126	126
Ni	52	30	20	30	39	35	11
S	2637	86	102	28	294	30	759
Nb	8	8	10	9	7	10	9

	106	107	108	109	110	111	112
SiO_2 %	50.59	51.61	46.12	43.45	47.96	48.59	58.24
TiO_2	1.64	0.94	0.83	0.93	0.88	0.90	1.45
Al_2O_3	13.65	17.31	12.10	8.76	12.63	13.54	15.77
Fe_{tot}	16.97	7.58	11.58	11.35	14.50	12.49	12.21
MnO	0.25	0.15	0.19	0.21	0.26	0.17	0.07
MgO	6.69	6.41	6.28	6.44	8.02	8.60	0.54
CaO	5.18	9.57	17.09	23.81	9.83	9.32	3.75
Na_2O	3.83	5.16	1.85	1.27	3.26	3.96	4.14
K_2O	0.18	0.65	0.91	0.15	0.46	0.72	0.67
P_2O_5	0.33	0.15	0.14	0.13	0.16	0.11	0.17
TOTAL	99.22	99.53	97.09	96.50	97.96	98.40	97.01
Co ppm	36	28	45	30	52	42	11
Ce	42	97	18	9	4	9	33
Cr	18	19	67	30	88	82	21
Ba	65	226	294	74	110	175	184
La	14	10	7	7	10	13	21
Zr	164	115	75	95	72	81	150
Y	51	17	22	31	31	20	60
Sr	150	284	240	155	72	200	297
U	0	0	5	1	2	1	1
Rb	4	11	41	6	4	12	16
Th	0	---	1	2	---	0	0
Pb	5	0	3	4	1	---	1
Ga	20	15	14	12	17	15	21
Zn	151	74	116	97	106	109	76
Cu	162	2	236	52	71	8	133
Ni	20	56	36	31	46	38	12
S	225	27	1036	187	16	35	56
Nb	8	9	7	6	5	6	9

	113	114	115	116	117	118	119
SiO_2 %	45.35	47.69	59.44	52.07	52.11	49.09	41.88
TiO_2	1.16	1.12	0.69	1.40	0.93	1.44	1.24
Al_2O_3	16.16	16.40	14.91	16.66	16.28	17.73	17.73
Fe_{tot}	12.59	6.11	6.98	9.85	9.44	9.51	6.27
MnO	0.17	0.11	0.05	0.15	0.15	0.14	0.10
MgO	8.90	2.89	4.34	6.18	8.40	6.25	3.74
CaO	10.53	18.53	4.61	4.96	5.56	8.94	20.88
Na_2O	3.21	2.76	2.76	4.98	4.17	4.41	1.97
K_2O	0.43	0.14	1.76	0.34	0.46	0.24	0.13
P_2O_5	0.24	0.19	0.17	0.22	0.18	0.21	0.22
TOTAL	98.73	95.94	95.71	96.81	97.68	97.96	94.16
Co ppm	59	38	7	34	34	61	62
Ce	13	16	75	29	23	12	7
Cr	546	319	32	117	157	488	593
Ba	134	39	385	145	221	70	49
La	15	15	46	24	9	11	13
Zr	90	92	305	154	147	120	106
Y	19	19	44	25	19	26	22
Sr	156	139	198	330	359	116	179
U	2	3	5	0	1	2	1
Rb	10	7	70	7	9	5	5
Th	0	---	5	2	0	0	2
Pb	1	2	5	2	1	3	0
Ga	17	24	18	18	19	14	20
Zn	115	38	163	99	95	84	42
Cu	10	11	106	34	71	62	21
Ni	279	154	47	60	111	172	241
S	58	158	11947	84	41	764	270
Nb	14	13	18	12	8	11	10

	120	121	122	123	124	125	126
SiO_2 %	53.63	40.14	46.68	47.64	46.44	49.28	39.78
TiO_2	0.77	1.01	2.48	0.93	0.53	1.20	0.98
Al_2O_3	16.07	11.49	15.69	16.33	15.29	9.84	11.63
Fe_{tot}	6.05	7.31	11.29	10.18	11.47	12.81	27.55
MnO	0.12	0.12	0.14	0.18	0.21	0.29	0.21
MgO	2.99	5.60	7.13	6.35	9.15	3.93	4.61
CaO	17.97	24.11	8.62	11.38	10.25	18.52	13.95
Na_2O	1.17	1.97	4.18	3.25	2.69	1.05	2.91
K_2O	0.19	1.01	0.73	0.27	0.91	0.74	0.18
P_2O_5	0.18	0.34	0.64	0.36	0.06	0.41	0.23
TOTAL	99.15	93.10	97.58	96.87	97.00	98.07	101.03
Co ppm		27	47	38	52	31	45
Ce		27	83	31	2	52	219
Cr		132	284	168	162	28	62
Ba		1556	359	80	73	91	88
La		26	40	23	8	23	267
Zr		132	283	84	39	132	111
Y		18	33	23	19	22	48
Sr		266	355	376	105	139	106
U		2	0	1	2	3	3
Rb		19	10	7	27	35	6
Th		---	1	---	1	0	---
Pb		1	---	2	2	0	0
Ga		12	20	19	11	14	13
Zn		55	97	90	59	94	137
Cu		34	126	2	6	37	52
Ni		69	125	96	139	11	36
S	59	71	139	29	25	124	713
Nb	10	9	20	7	5	8	11

	127	128	129	130	131	132	133
SiO_2 %	50.84	52.25	48.40	49.61	47.24	50.54	54.57
TiO_2	0.99	1.21	0.84	1.55	0.51	1.10	1.07
Al_2O_3	14.16	12.54	15.21	16.01	16.25	12.54	18.23
Fe_{tot}	10.12	15.57	10.14	10.72	3.53	13.87	6.81
MnO	0.15	0.17	0.17	0.14	0.05	0.18	0.09
MgO	6.43	5.83	9.43	6.07	1.73	5.17	3.89
CaO	10.24	7.26	10.16	7.78	2.66	11.67	6.63
Na_2O	3.98	3.42	2.88	4.70	4.86	3.15	5.56
K_2O	0.47	0.54	0.50	0.82	0.89	0.56	1.08
P_2O_5	0.21	0.17	0.14	0.25	0.14	0.22	0.40
TOTAL	97.59	98.96	97.87	97.65	97.86	99.00	98.33
Co ppm	42	38	54	34	10	41	19
Ce	30	24	16	29	112	34	55
Cr	137	52	245	57	8	50	24
Ba	143	107	83	459	547	119	558
La	16	8	5	16	79	17	24
Zr	106	138	32	158	344	134	230
Y	24	50	11	24	15	45	18
Sr	219	106	266	295	407	272	710
U	3	0	2	1	3	3	2
Rb	7	8	7	15	41	9	20
Th	1	1	2	0	8	8	1
Pb	---	0	3	3	5	3	2
Ga	16	15	17	18	20	21	25
Zn	90	122	136	75	54	127	75
Cu	219	2	9	36	32	92	54
Ni	65	52	153	82	3	42	31
S	492	39	26	74	18	46	134
Nb	8	8	6	12	11	16	13

	134	135	136	137	138	139	140
SiO_2 %	46.66	44.83	49.76	52.54	73.81	54.58	50.43
TiO_2	1.16	1.25	0.84	1.48	0.19	1.05	1.54
Al_2O_3	15.50	12.86	12.96	14.42	14.62	15.91	12.69
Fe_{tot}	13.71	18.56	10.10	11.55	1.66	8.60	15.17
MnO	0.38	0.26	0.16	0.20	0.05	0.12	0.19
MgO	7.90	7.16	12.25	4.95	0.21	4.62	5.47
CaO	5.47	9.51	9.22	7.90	1.42	7.47	9.24
Na_2O	3.13	2.83	2.66	3.59	5.16	3.80	3.14
K_2O	2.40	1.08	0.22	0.87	1.55	0.63	0.61
P_2O_5	0.28	0.10	0.19	0.33	0.06	0.20	0.30
TOTAL	96.59	98.54	98.36	97.83	98.73	96.98	99.78
Co ppm	59	82	54	33	---		51
Ce	42	18	24	37	65		22
Cr	131	56	532	33	1		36
Ba	425	109	40	131	650		154
La	14	11	9	11	45		---
Zr	132	83	60	152	185		96
Y	22	38	21	27	10		23
Sr	279	148	256	238	276		196
U	1	2	1	3	3		2
Rb	88	11	6	13	34		9
Th	---	4	1	0	5		2
Pb	0	5	3	0	1		4
Ga	16	18	11	17	16		21
Zn	198	183	75	73	42		107
Cu	69	227	116	88	---		121
Ni	97	39	194	35	---		21
S	87	54	19	147	48	49	60
Nb	10	7	10	10	16	9	8

	141	142	143	144	145	146	147
SiO_2 %	56.75	72.67	69.23	53.31	50.55	47.27	50.51
TiO_2	0.61	0.42	0.39	0.82	1.49	1.65	0.69
Al_2O_3	20.61	14.23	15.63	13.05	14.44	13.99	15.86
Fe_{tot}	4.53	2.31	3.73	12.05	13.37	13.12	10.50
MnO	0.05	0.04	0.03	0.15	0.20	0.19	0.17
MgO	1.63	0.56	1.00	4.79	7.06	8.43	7.03
CaO	4.98	4.73	3.69	14.19	6.52	10.74	9.76
Na_2O	5.48	4.17	4.41	1.39	4.34	3.12	3.60
K_2O	2.02	0.50	1.27	0.15	0.32	0.45	0.75
P_2O_5	0.20	0.08	0.13	0.10	0.31	0.53	0.10
TOTAL	96.86	99.71	99.51	100.00	98.60	99.49	98.97
Co ppm	11	3	6	25	43	62	44
Ce	92	90	40	27	23	57	20
Cr	8	2	18	104	46	170	99
Ba	1353	118	510	92	145	138	89
La	50	37	29	6	5	27	7
Zr	355	435	111	63	140	150	66
Y	10	32	6	27	42	32	20
Sr	196	617	314	478	293	141	460
U	2	1	2	2	2	4	0
Rb	66	7	31	7	8	5	7
Th	7	8	2	---	1	1	---
Pb	9	3	4	---	4	3	1
Ga	27	15	19	15	18	15	11
Zn	61	33	49	47	117	136	100
Cu	5	17	18	37	78	30	33
Ni	6	3	10	30	53	125	48
S	97	21	79	99	115	47	55
Nb	13	24	13	6	9	12	8

	148	149	150	151	152	153	154
SiO_2 %	50.11	45.02	46.04	37.43	46.70	51.03	59.99
TiO_2	1.01	1.01	1.96	0.93	0.93	0.90	0.68
Al_2O_3	14.56	13.79	22.36	16.61	12.36	13.69	10.43
Fe_{tot}	10.43	11.37	16.38	10.64	11.77	11.98	14.37
MnO	0.17	0.35	0.12	0.25	0.25	0.19	0.09
MgO	8.39	5.99	8.76	1.87	6.15	7.56	3.23
CaO	8.18	20.02	26.27	30.65	19.24	7.76	5.09
Na_2O	3.56	1.18	1.15	0.58	1.59	3.35	2.61
K_2O	1.58	0.25	0.21	0.07	0.14	0.52	0.41
P_2O_5	0.28	0.17	0.03	0.13	0.18	0.14	0.14
TOTAL	98.27	99.15	123.30	99.16	99.31	97.12	97.04
Co ppm	40	43	71	19	36		19
Ce	42	26	46	34	23		20
Cr	283	34	224	138	88		39
Ba	498	78	95	20	57		69
La	17	---	16	8	11		22
Zr	95	106	285	191			113
Y	20	43	23	77			31
Sr	223	508	127	122			114
U	2	1	2	1			2
Rb	30	12	7	4			10
Th	2	---	0	---			2
Pb	6	3	0	---			3
Ga	15	15	28	20			18
Zn	107	167	303	66			87
Cu	78	9	184	17			36
Ni	41	24	147	28			29
S	218	113	452	43	28		26
Nb	7	1	15	13	14		11

	156	157	158	159	160	161	162
SiO_2 %	52.65	55.64	51.96	46.17	42.74	40.93	72.94
TiO_2	1.31	0.70	0.57	1.20	1.71	2.02	0.13
Al_2O_3	13.09	17.47	16.32	8.77	13.13	11.90	14.03
Fe_{tot}	15.44	6.32	7.46	17.57	12.42	16.15	2.29
MnO	0.17	0.13	0.12	0.37	0.25	0.19	0.04
MgO	5.52	4.17	7.40	3.15	7.44	9.92	0.25
CaO	6.52	6.64	8.80	20.10	19.95	12.10	2.12
Na_2O	3.30	4.82	3.91	1.13	0.84	1.78	4.79
K_2O	0.30	0.79	0.55	0.46	0.30	0.59	2.15
P_2O_5	0.17	0.18	0.11	0.45	0.46	0.29	0.05
TOTAL	98.47	96.86	97.20	99.37	99.24	95.87	98.79
Co ppm	39	19		39	27	83	---
Ce	4	46		46	49	0	43
Cr	80	51		7	320	532	8
Ba	88	164		67	109	105	991
La	6	19		30	32	---	31
Zr	125	258		118	181	49	70
Y	45	39		28	25	18	4
Sr	140	341		102	315	261	416
U	0	2		3	6	0	3
Rb	6	11		21	10	8	24
Th	---	6		3	0	---	5
Pb	---	6		---	4	1	8
Ga	15	16		18	17	14	18
Zn	79	67		146	112	137	36
Cu	19	56		292	27	76	51
Ni	53	58		7	80	290	---
S	47	95		1160	25	384	346
Nb	10	11		11	21	4	6

	163	164	165	166	167	168	169
SiO_2 %	63.75	45.98	50.99	51.56	48.01	50.35	70.36
TiO_2	0.68	1.02	1.21	0.98	0.66	1.47	0.43
Al_2O_3	17.31	12.70	15.04	19.04	14.99	13.74	14.01
Fe_{tot}	6.87	10.48	10.21	9.94	6.53	10.22	3.40
MnO	0.04	0.34	0.13	0.19	0.28	0.16	0.03
MgO	0.95	5.94	7.12	6.26	6.72	7.67	0.95
CaO	4.11	21.38	7.07	6.70	20.17	10.81	1.72
Na_2O	4.84	0.44	4.59	2.87	0.73	3.09	3.24
K_2O	1.22	0.25	0.63	0.56	0.19	0.65	5.12
P_2O_5	0.14	0.15	0.28	0.20	0.10	0.39	0.12
TOTAL	99.91	98.68	97.27	98.30	98.38	98.85	99.38
Co ppm	9	44	49	44	29	41	6
Ce	812	13	43	28	7	19	211
Cr	20	58	217	70	81	95	7
Ba	875	67	153	146	40	49	1284
La	560	1	13	13	1	9	83
Zr	580	84	185	60	56	116	365
Y	16	28	32	18	18	23	21
Sr	528	150	171	299	177	224	247
U	2	1	1	2	2	4	2
Rb	43	11	8	15	6	7	139
Th	47	2	0	2	4	1	23
Pb	6	6	1	6	2	---	12
Ga	26	14	17	20	13	18	17
Zn	77	148	94	108	88	91	63
Cu	14	19	34	38	11	53	9
Ni	12	31	93	28	35	51	4
S	107	21	77	562	26	58	
Nb	8	6	13	8	5	8	

	170	171	172	173	174	175	176
SiO_2 %	44.12	44.54	52.69	49.23	46.10	45.60	48.50
TiO_2	2.40	2.26	0.55	1.70	1.98	2.91	1.10
Al_2O_3	14.18	14.45	14.76	10.14	11.95	8.46	25.15
Fe_{tot}	17.34	17.20	5.51	13.66	13.39	13.76	3.03
MnO	0.18	0.16	0.14	0.26	0.23	0.25	0.08
MgO	5.87	6.65	4.86	7.53	6.55	7.70	1.69
CaO	9.52	8.86	12.80	11.21	14.10	15.94	13.76
Na_2O	2.40	2.65	3.47	1.64	1.74	1.88	3.62
K_2O	0.72	0.68	0.34	0.72	0.82	0.60	0.35
P_2O_5	0.09	0.09	0.21	0.42	0.29	0.38	0.03
TOTAL	96.82	97.48	95.33	96.51	97.15	97.48	97.31
Co ppm	71	87	21	50	47	65	8
Ce	8	13	25	45	25	34	3
Cr	51	52	50	136	34	44	39
Ba	170	193	151	81	120	132	106
La	7	10	15	18	19	19	0
Zr	81	80	69	157	138	165	113
Y	15	16	18	33	27	35	16
Sr	309	310	414	224	338	186	387
U	4	3	1	1	2	0	1
Rb	11	9	5	9	18	10	9
Th	---	2	3	0	4	0	0
Pb	2	2	3	1	3	2	2
Ga	21	19	15	13	19	14	16
Zn	166	139	70	117	107	111	36
Cu	653	491	67	12	42	74	180
Ni	141	148	62	67	30	40	1
S	678	988	88	31	43	216	262
Nb	11	11	9	11	13	14	15

	177	178	179	180	181	182	183
SiO_2 %	51.62	47.22	72.04	50.58	44.12	42.42	42.93
TiO_2	0.62	1.84	0.17	0.66	1.23	1.24	1.52
Al_2O_3	17.96	12.49	14.07	14.76	13.93	12.65	15.10
Fe_{tot}	6.82	13.89	2.17	6.58	11.81	11.95	10.38
MnO	0.16	0.23	0.03	0.18	0.23	0.28	0.16
MgO	6.76	8.02	0.95	7.59	3.28	4.56	3.48
CaO	8.98	9.58	2.02	15.82	24.33	22.55	19.39
Na_2O	4.01	2.50	4.53	2.24		0.84	
K_2O	0.79	0.96	2.74	0.38	0.11	0.08	0.42
P_2O_5	0.13	0.28	0.08	0.10	0.28	0.31	0.33
TOTAL	97.85	97.01	98.80	98.82	99.32	96.84	93.71
Co ppm	38	54		26	46	40	67
Ce	21	33		3	30	35	35
Cr	63	33		92	124	114	28
Ba	219	166		63	42	43	85
La	7	21		92	17	14	20
Zr	64	143	74	63	99	109	191
Y	13	33	7	19	19	23	19
Sr	303	184	398	223	151	197	203
U	0	3	3	0	4	1	3
Rb	12	11	34	5	4	5	16
Th	1	4	4	---	0	2	2
Pb	---	4	8	---	---	6	2
Ga	18	13	17	13	17	17	18
Zn	67	132	41	82	107	135	228
Cu	58	67	11	---	8001	2466	16194
Ni	87	15	4	34	48	36	80
S	38	35	103	23	0.81%	0.60%	2.55%
Nb	9	12	10	8	14	12	12

	184	185	186	187	189	190	191
SiO_2 %	49.64	43.34		43.94	41.08	46.81	41.68
TiO_2	1.80	0.96		1.37	1.65	0.78	1.28
Al_2O_3	13.67	11.75		13.86	13.45	15.42	16.34
Fe_{tot}	6.82	13.23		11.71	14.28	8.53	12.67
MnO	0.14	0.20		0.15	0.14	0.20	0.20
MgO	6.03	3.71		7.18	4.58	7.50	1.92
CaO	15.58	24.15		17.68	18.06	14.06	20.83
Na_2O	2.78				0.10	2.16	0.31
K_2O	0.29	0.14		0.41	0.14	0.38	0.13
P_2O_5	0.54	0.19		0.26	0.36	0.11	0.22
TOTAL	97.29	97.67		96.74	93.84	95.95	95.58
Co ppm	36	44	37	89	142	62	51
Ce	32	44	27	29	47	8	77
Cr	24	28	23	315	48	314	50
Ba	99	32	39	114	71	160	37
La	18	21	9	24	21	4	31
Zr	192	70	100	135	187	50	212
Y	31	17	16	27	36	18	38
Sr	293	167	215	223	273	387	233
U	2	3	4	3	2	0	6
Rb	5	5	5	6	3	5	4
Th	4	3	0	6	3	---	6
Pb	2	1	---	2	1	---	4
Ga	21	16	21	15	15	16	35
Zn	49	100	72	206	264	103	174
Cu	166	5575	2102	11106	26864	5812	14050
Ni	43	70	29	133	236	107	67
S	363	0.59%	0.35%	2.14%	5.45%	1.77%	2.22%
Nb	16	14	8	13	12	7	20

	192	193	194	195	196	197	198
SiO_2 %	44.02	44.68	43.19	48.97	46.46	43.28	51.14
TiO_2	1.31	1.18	1.32	1.87	0.77	1.48	2.06
Al_2O_3	14.25	12.58	12.95	15.99	15.13	13.64	12.89
Fe_{tot}	11.21	12.98	11.46	9.72	10.29	13.37	7.41
MnO	0.17	0.24	0.22	0.11	0.15	0.27	0.11
MgO	5.13	6.32	4.96	7.10	5.60	4.06	5.10
CaO	17.30	20.44	18.53	8.69	19.18	18.56	17.77
Na_2O		0.56	3.69			1.80	
K_2O	0.16	0.12	0.16	0.55	0.16	0.19	0.27
P_2O_5	0.29	0.33	0.23	0.52	0.07	0.31	0.26
TOTAL	93.84	99.43	93.02	97.23	97.81	96.96	98.01
Co ppm	95	43	97	41	78	40	31
Ce	17	21	32	110	0	19	34
Cr	122	111	296	292	291	13	18
Ba	82	42	58	126	50	31	93
La	19	14	17	48	7	10	58
Zr	105	101	87	204	40	118	159
Y	23	20	24	28	16	24	24
Sr	250	172	231	509	237	76	263
U	2	1	3	1	3	3	0
Rb	3	4	5	6	6	5	5
Th	---	1	5	2	3	1	1
Pb	0	3	4	4	0	---	1
Ga	16	13	19	18	15	18	19
Zn	234	101	250	60	180	36	54
Cu	20646	813	25256	131	12047	1941	1616
Ni	101	19	152	81	107	23	75
S	3.23%	0.16%	4.30%	373	2.21%	0.38%	0.30%
Nb	11	12	13	15	7	7	14

	199	200	201	202	203	204	205
SiO_2 %	45.69	44.17	45.92	49.38	49.12	43.75	48.21
TiO_2	0.75	1.42	0.33	0.41	1.28	2.25	0.56
Al_2O_3	12.62	13.14	19.92	19.51	20.68	13.44	13.89
Fe_{tot}	10.11	13.10	6.13	4.36	9.49	14.67	5.71
MnO	0.10	0.23	0.03	0.09	0.10	0.13	0.07
MgO	9.19	5.02	6.74	7.91	3.10	7.87	8.84
CaO	15.90	18.95	12.70	14.24	8.31	10.27	18.65
Na_2O		1.42	3.08	2.96	4.99	0.40	1.04
K_2O	0.76	0.10	0.29	0.31	1.30	1.00	0.18
P_2O_5	0.07	0.32	0.00	0.19	0.45	0.42	0.00
TOTAL	96.19	97.82	95.14	99.36	98.72	94.20	97.15
Co ppm	62	84	76	23	26	64	34
Ce	1	46	4	13	53	43	7
Cr	388	100	188	515	31	26	391
Ba	109	43	83	42	816	157	39
La	25	31	3	0	15	14	9
Zr	48	115	53	47	367	168	45
Y	15	25	8	12	23	32	14
Sr	184	274	319	324	798	221	212
U	1	4	2	0	0	4	3
Rb	17	5	5	4	42	11	4
Th	0	3	---	1	1	3	2
Pb	5	4	1	---	2	0	1
Ga	14	20	16	18	26	20	14
Zn	66	243	40	38	82	105	54
Cu	1667	15929	6190	145	103	2735	779
Ni	172	96	1241	196	16	29	102
S	0.40%	2.61%	1.39%	385	535		1298
Nb	8	13	5	3	15		9

	206	207	208	209	210	211	212
SiO_2 %	42.10	42.80	47.91	37.44	47.70	43.94	46.67
TiO_2	0.92	1.43	0.60	0.45	0.66	0.74	0.69
Al_2O_3	8.03	13.62	14.32	9.45	15.16	14.77	14.93
Fe_{tot}	18.20	12.03	9.83	19.50	6.86	10.61	8.30
MnO	0.36	0.35	0.21	0.40	0.13	0.14	0.12
MgO	3.28	4.65	5.26	1.04	7.63	7.51	8.02
CaO	25.10	18.02	18.99	27.53	20.19	16.55	18.77
Na_2O	1.21	1.29	0.92	0.97	1.65	1.76	1.51
K_2O	0.09	0.15	0.21	0.09	0.12	0.44	0.25
P_2O_5	0.27	0.36	0.46	0.08	0.09	0.07	0.08
TOTAL	99.47	94.70	98.71	96.95	100.19	96.53	99.34
Co ppm	44			14	32	55	34
Ce	65			61	5	---	5
Cr	96			94	392	562	476
Ba	45			---	40	77	65
La	39			43	13	16	9
Zr	104			114	45	49	41
Y	25			56	18	18	17
Sr	86			71	257	227	246
U	3			3	3	1	2
Rb	4			6	5	7	6
Th	5			---	1	---	0
Pb	---			1	---	---	---
Ga	13			11	11	12	11
Zn	87			49	25	45	34
Cu	168			53	2	23	5
Ni	15			17	100	266	164
S	517			268	11	115	36
Nb	9			3	5	5	3

	213	214	215	216	217	218	219
SiO_2 %	51.40	50.22	47.75	51.08	51.81	51.04	51.10
TiO_2	0.43	0.36	2.22	1.16	0.78	2.22	0.65
Al_2O_3	16.23	17.11	14.71	17.71	15.16	15.49	12.87
Fe_{tot}	4.09	5.69	15.23	9.10	7.57	7.03	11.62
MnO	0.11	0.11	0.25	0.15	0.12	0.14	0.23
MgO	7.21	9.40	5.91	6.51	3.67	3.48	3.99
CaO	16.66	9.33	7.56	8.70	12.28	14.74	17.88
Na_2O	3.47	3.21	3.15	4.07	2.22	3.34	0.28
K_2O	0.18	0.88	0.85	0.49	0.43	0.24	0.15
P_2O_5	0.06	0.03	0.40	0.29	0.16	0.52	0.09
TOTAL	99.84	96.34	97.93	99.26	94.20	98.24	98.86
Co ppm	27	38	54	35	49	18	32
Ce	16	13	65	47	74	66	8
Cr	90	225	41	150	138	33	95
Ba	62	216	251	163	177	135	55
La	4	4	24	12	53	43	1
Zr	53	46	228	318	321	236	50
Y	12	10	31	21	37	38	22
Sr	257	354	379	712	350	379	198
U	1	2	---	2	5	4	2
Rb	4	28	11	8	12	4	6
Th	4	4	4	3	3	5	2
Pb	2	3	2	2	5	---	0
Ga	16	13	23	23	26	20	18
Zn	40	49	119	93	90	47	54
Cu	23	32	321	111	10824	107	35
Ni	52	193	28	106	74	23	33
S	29	14	1632	411	1.15%	192	76
Nb	6	3	15	9	13	22	3

	220	221	222	223	224	225	226
SiO_2 %	49.45		46.49	44.85	64.67	48.84	
TiO_2	0.56		0.68	2.14	0.54	0.35	
Al_2O_3	16.11		22.98	14.11	16.53	15.46	
Fe_{tot}	8.33		5.91	15.08	4.21	7.04	
MnO	0.18		0.14	0.24	0.08	0.17	
MgO	7.79		4.20	7.14	2.43	10.34	
CaO	9.93		13.70	9.50	4.02	11.50	
Na_2O	3.68		2.74	2.52	4.30	1.87	
K_2O	0.72		0.82	0.64	1.57	0.46	
P_2O_5	0.11		0.11	0.19	0.17	0.06	
TOTAL	96.86		97.77	96.40	98.52	96.09	
Co ppm	46	53	31	64	12	40	40
Ce	19	7	13	23	43	---	55
Cr	292	285	113	41	10	217	194
Ba	70	83	442	173	583	57	125
La	7	7	2	13	24	---	25
Zr	70	71	55	66	173	32	170
Y	17	15	14	18	5	10	30
Sr	242	234	370	305	434	231	238
U	2	2	4	1	1	1	1
Rb	9	9	13	12	71	11	8
Th	2	0	1	3	3	1	3
Pb	1	2	2	---	5	1	1
Ga	12	13	16	19	20	12	13
Zn	86	87	81	150	62	51	115
Cu	14	8	86	880	31	35	10
Ni	147	146	47	180	7	151	50
S	31	29	269	372	58	44	62
Nb	7	6	9	12	12	5	11

	227	228	229	230	231	232	234
SiO_2 %	46.58	63.05	63.56	49.08	44.27	53.42	47.32
TiO_2	0.92	0.52	0.67	1.05	1.55	1.23	1.51
Al_2O_3	13.31	14.76	16.89	9.92	13.70	12.10	14.86
Fe_{tot}	9.04	5.23	4.69	12.05	15.17	11.97	9.65
MnO	0.24	0.13	0.05	0.22	0.21	0.17	0.14
MgO	5.48	4.03	1.12	6.49	7.25	5.73	8.93
CaO	18.74	5.43	3.18	15.09	11.57	9.18	9.65
Na_2O	2.33	4.72	3.90	1.91	2.50	0.78	3.59
K_2O	0.30	1.11	3.75	0.30	0.53	0.44	0.64
P_2O_5	0.18	0.12	0.19	0.26	0.24	0.16	0.27
TOTAL	97.12	99.10	98.00	96.37	96.94	95.18	96.56
Co ppm	33	21	3	40	66	45	39
Ce	29	38	113	67	38	17	17
Cr	130	76	29	16	52	43	320
Ba	289	265	1599	94	174	178	159
La	5	14	63	29	34	17	10
Zr	94	86	248	256	134	128	
Y	24	22	21	59	37	30	
Sr	200	295	464	203	200	189	
U	5	2	1	1	3	---	
Rb	7	20	93	6	8	7	
Th	4	1	7	3	---	0	
Pb	4	3	17	1	0	4	
Ga	16	17	17	15	17	15	
Zn	115	62	74	91	145	97	
Cu	107	28	13	1364	566	442	
Ni	52	87	10	27	65	43	
S	686	157	176	3285	1.98%	1.46%	57
Nb	8	13	12	16	14	8	13

	235	236	237	238	239	240	241
SiO_2 %	46.62	52.67	51.15	48.61	43.68	52.03	60.54
TiO_2	2.52	1.41	1.15	0.79	1.78	1.08	0.52
Al_2O_3	16.00	17.28	15.86	15.53	15.79	14.34	16.86
Fe_{tot}	11.12	10.03	10.09	9.22	14.84	7.09	5.53
MnO	0.18	0.19	0.13	0.12	0.18	0.20	0.08
MgO	7.02	6.08	6.50	8.81	7.51	4.42	2.61
CaO	8.79	5.15	7.83	9.98	9.66	15.42	4.61
Na_2O	4.37	5.25	3.69	2.96	1.97	2.30	4.52
K_2O	0.74	0.33	0.35	0.67	0.85	0.32	1.51
P_2O_5	0.62	0.22	0.27	0.10	0.06	0.46	0.24
TOTAL	97.98	98.61	97.02	96.79	96.32	97.66	97.02
Co ppm	39	15		41	70	39	21
Ce	49	16		6	16	26	85
Cr	96	101		245	143	202	16
Ba	43	50		104	208	65	814
La	23	15		5	0	8	42
Zr	166	129		40	63	185	395
Y	31	17		18	15	30	31
Sr	309	456		204	270	269	510
U	1	0		1	0	5	1
Rb	4	10		16	11	10	51
Th	1	2		---	0	2	3
Pb	2	2		0	4	4	6
Ga	18	28		15	18	17	22
Zn	76	36		67	151	91	83
Cu	126	89		110	220	37	363
Ni	84	60		110	158	106	39
S	161			68	304	105	1336
Nb	10			1	6	11	11

	242	243	244	245	246	247	248
SiO_2 %	46.74	45.56	58.84	48.68	71.22	50.40	67.69
TiO_2	1.13	1.05	1.24	1.38	0.21	0.91	0.32
Al_2O_3	7.61	13.25	11.62	16.28	13.36	14.16	16.22
Fe_{tot}	13.42	10.67	13.64	10.34	2.07	9.62	2.69
MnO	0.42	0.40	0.10	0.18	0.08	0.20	0.04
MgO	6.17	5.41	2.33	7.22	1.65	7.70	1.50
CaO	20.61	21.65	11.75	8.65	2.96	10.22	3.48
Na_2O	1.07	0.54	0.19	2.78	3.98	3.81	6.30
K_2O	0.10	0.13	0.22	0.51	1.18	0.66	1.04
P_2O_5	0.17	0.16	0.16	0.24	0.08	0.36	0.12
TOTAL	97.44	98.82	100.09	96.26	96.79	98.04	99.40
Co ppm	46	52	15	60	5	51	3
Ce	11	28	37	35	64	38	46
Cr	43	41	25	73	13	171	1
Ba	65	44	94	149	434	189	407
La	17	3	13	9	28	23	25
Zr	102	95	103	50	152	96	237
Y	32	34	33	15	4	25	5
Sr	104	153	296	383	451	336	639
U	5	2	1	3	1	2	1
Rb	6	5	6	7	35	6	25
Th	11	3	---	2	10	1	0
Pb	0	---	0	0	3	4	0
Ga	11	18	15	18	18	19	20
Zn	294	122	73	99	33	89	38
Cu	55	12	71	108	7	253	93
Ni	33	24	13	175	3	177	---
S	389	13	270	69	39	673	163
Nb	10	7	8	9	4	9	8

	249	250	251	252	253	254	255
SiO_2 %	49.08	45.60	51.81	63.63	44.35	48.78	77.00
TiO_2	1.49	1.52	1.04	0.92	2.02	0.19	0.03
Al_2O_3	15.89	16.22	13.57	16.36	13.20	2.51	13.19
Fe_{tot}	10.98	12.92	7.94	4.49	12.24	10.98	0.55
MnO	0.16	0.14	0.17	0.07	0.16	0.20	0.07
MgO	7.21	6.23	5.61	3.11	7.90	14.26	0.74
CaO	9.52	11.12	14.61	6.28	15.62	20.68	1.47
Na_2O	3.16	2.38	2.64	4.04	1.21	0.56	6.16
K_2O	0.46	0.99	0.32	0.44	0.28	0.26	0.62
P_2O_5	0.18	0.30	0.20	0.26	0.28	0.35	0.02
TOTAL	98.13	97.40	97.91	99.60	97.26	98.77	99.85
Co ppm	47	57	34	16	68	62	---
Ce	27	14	43	73	8	22	12
Cr	83	365	92	23	465	354	0
Ba	145	185	117	420	90	27	---
La	9	17	26	23	4	13	6
Zr	58	133	149	397	60	30	109
Y	18	24	25	33	19	13	58
Sr	342	267	295	596	522	37	14
U	0	3	2	2	2	1	13
Rb	6	9	6	19	6	5	20
Th	0	0	1	3	1	3	8
Pb	1	1	0	2	3	0	23
Ga	19	15	17	16	18	6	19
Zn	90	122	78	33	100	104	13
Cu	259	66	35	215	28	1651	---
Ni	152	193	37	34	217	75	---
S	947	219	28	396	113	1825	16
Nb	9	11	14	15	2	4	50

	256	257	258	259	260	261	262
SiO_2 %	50.57	42.44	43.65	42.49	44.07	45.60	45.04
TiO_2	1.24	2.31	0.64	1.37	1.82	1.20	0.99
Al_2O_3	15.30	12.87	13.05	14.17	16.29	13.19	12.26
Fe_{tot}	9.47	18.56	10.95	10.57	15.52	10.15	11.54
MnO	0.11	0.10	0.16	0.17	0.10	0.12	0.17
MgO	5.77	7.08	15.14	5.41	8.17	9.42	6.18
CaO	9.74	9.28	11.00	18.71	9.67	16.12	18.81
Na_2O	3.56	2.68	1.67	0.00	1.43	1.86	0.00
K_2O	0.63	0.37	0.31	0.10	0.41	0.56	0.10
P_2O_5	0.24	0.05	0.00	0.23	0.01	0.23	0.14
TOTAL	96.63	95.74	96.57	93.02	97.49	98.35	95.23
Co ppm	26	59	67	82	59	38	76
Ce	36	---	---	28	---	15	20
Cr	67	71	652	122	72	389	90
Ba	154	100	54	88	109	157	47
La	15	8	5	14	3	18	16
Zr	159	44	30	124	37	108	93
Y	27	11	10	24	10	24	17
Sr	294	362	168	235	366	178	217
U	2	1	1	2	2	0	1
Rb	7	8	10	5	8	7	3
Th	---	0	---	3	---	---	---
Pb	0	3	---	---	---	0	---
Ga	18	19	10	15	21	15	17
Zn	49	104	141	203	102	54	140
Cu	58	599	1	15163	631	72	7581
Ni	55	189	267	107	181	102	91
S	140	967	8	17713	999	763	9843
Nb	11	7	2	12	4	11	6

	263	264	265	266	267	268	269
SiO_2 %	46.01	46.70	48.86	45.80	46.12	47.32	49.76
TiO_2	1.02	0.68	2.04	1.17	0.64	0.98	1.27
Al_2O_3	14.46	15.25	13.54	12.11	14.84	14.14	13.60
Fe_{tot}	8.64	9.67	7.95	12.37	6.79	6.35	14.96
MnO	0.11	0.10	0.09	0.27	0.08	0.09	0.21
MgO	10.24	8.21	5.27	6.12	9.41	9.36	6.26
CaO	14.94	14.23	15.61	22.92	17.62	19.98	7.06
Na_2O	2.60	2.35	0.67	1.10	1.30	0.21	3.63
K_2O	0.53	0.43	0.19	0.12	0.34	0.26	0.45
P_2O_5	0.16	0.07	0.36	0.12	0.01	0.09	0.19
TOTAL	98.89	97.69	94.58	102.10	97.15	98.78	97.39
Co ppm	41	52	24		31	57	
Ce	13	7	39		0	15	
Cr	409	288	18		320	363	
Ba	74	285	139		99	43	
La	3	3	25		11	9	
Zr	84	41	246		38	84	
Y	16	16	3		16	17	
Sr	221	171	286		237	238	
U	---	1	3		1	1	
Rb	7	7	6		4	6	
Th	1	---	1		---	---	
Pb	0	2	1		---	---	
Ga	14	14	16		13	15	
Zn	49	58	43		60	49	
Cu	16	1797	621		1781	1406	
Ni	161	116	11		90	109	
S	36	0.82%	1435		2166	2878	
Nb	7	2	18		3	7	

	270	271	272	273	274	275	276
SiO_2 %	50.26	46.10	48.54	39.50	46.61	48.32	46.59
TiO_2	0.36	1.20	1.23	2.43	0.71	1.51	0.92
Al_2O_3	16.93	12.60	12.94	10.06	15.33	15.36	15.68
Fe_{tot}	5.70	17.18	13.66	20.44	10.83	10.15	6.92
MnO	0.12	0.27	0.14	0.29	0.14	0.14	0.30
MgO	10.49	6.59	8.42	8.36	10.97	8.43	5.78
CaO	10.72	9.12	12.11	10.05	11.47	11.15	19.66
Na_2O	2.88	2.87	2.99	2.03	2.81	3.59	1.24
K_2O	0.57	1.00	0.43	0.98	0.67	0.64	0.18
P_2O_5	0.04	0.19	0.11	0.77	0.08	0.27	0.16
TOTAL	98.07	97.22	100.57	94.91	99.62	99.56	97.43
Co ppm	40		54		55	41	
Ce	10		2		9	23	
Cr	162		344		308	307	
Ba	105		82		77	139	
La	2		3		4	19	
Zr	31		73		35	126	
Y	8		21		17	25	
Sr	276		380		191	168	
U	2		3		2	2	
Rb	12		7		8	10	
Th	3		---		0	0	
Pb	2		---		0	4	
Ga	14		14		13	12	
Zn	40		100		68	55	
Cu	25		24		43	---	
Ni	186		195		162	158	
S	48		33		79		
Nb	6		8		3		

APPENDIX 3

Tabulation of analysis no., rock type, locality and the chemical subgroup of amphibolites.

Abbreviations used for sample localities:

H.M.	Hällinmäki Mine.
T95m	Underground workings: tunnel at 95m depth.
T175m	Underground workings: tunnel at 175m depth.
T370m	Underground workings: tunnel at 370m depth.
S.O.P.	Small open pit.
M.O.P.	Main open pit.
D.H.	Drill hole sample from Hällinmäki Mine.
T.E.	Tunnel entrance to Mine complex.

Analysis No.	Rock type	Locality	Amphibolite Group
1	Amphibolite	H.M. T370m	Group IIIa
2	Syn-D_3 meta-diorite	"	
3	Amphibolite	"	Group IIIa
4	Skarn	"	
5	Amphibolite	"	Group IIIa
6	Skarned amphibolite	"	
7	Amphibolite	"	Group IIIa
8	Syn-D_3 amphibolite	"	
9	Skarn	"	
10	Skarn	"	
11	Amphibolite	"	Group IIIa
12	Skarn	"	
13	Syn-D_3 metadiorite	"	
14	Amphibolite	"	Group IIIa
15	"	"	"
16	"	"	"
17	"	"	"
18	Early-syn-D_1 meta-leucogabbro	"	
19	Syn-D_3 meta-diorite	"	
20	Amphibolite	"	Group IIIa
21	"	"	"
22	"	"	"
23	Skarned amphibolite	"	"
24	Syn-D_2 biotite amphibolite dyke	"	
25	Syn-D_3 metadiorite	"	
26	Skarned amphibolite	"	Group IIIa
27	Amphibolite	"	"
28	Skarned amphibolite	"	
29	Amphibolite	"	
30	Amphibolite	H.M. D.H. R36A	Group IIIa
31	Amphibolite	H.M. M.O.P.	Group IIc
32	Syn-D_3 metadiorite	H.M. D.H. R36A	
33	Syn-D_3 metagabbro	H.M. M.O.P.	
34	Amphibolite	H.M. D.H. R36	Group IIIa

Analysis No.	Rock type	Locality	Amphibolite Group
35	Syn-D_3 metagabbro	H.M. M.O.P.	
36	Amphibolite	H.M. D.H. R36B	Group IIIa
37	Syn-D_3 metagabbro	H.M. M.O.P.	
38	Syn-D_2 biotite amphibolite dyke	"	
39	Syn-D_3 metagabbro	"	
40	Skarned amphibolite	H.M. S.O.P.	
41	Amphibolite	"	Group IIIa
42	Syn-D_3 amphibolite	"	
43	Amphibolite	"	Group IIIa
44	"	"	Group IIc
45	Syn-D_3 meta-leucogabbro	"	
46	Amphibolite	"	Group IIIa
47	"	"	"
48	"	H.M. T.E.	"
49	"	"	"
50	Skarned amphibolite	"	
51	Amphibolite	"	Group IIIa
52	Syn-D_3 meta-granodiorite	"	
53	Amphibolite	"	Group IIIa
54	"	H.M. M.O.P.	"
55	"	"	"
56	Skarned amphibolite	"	
57	"	"	
58	"	"	
59	Amphibolite	"	Group IIIa
60	"	"	"
61	"	"	"
62	"	"	"
63	"	"	"
64	Skarned amphibolite	"	
67	Skarn	H.M. M.O.P.	
68	Amphibolite	"	Group IIc
69	"	"	"
70	"	"	"
71	"	"	"

Analysis No.	Rock type	Locality	Amphibolite Group
72	Amphibolite	H.M. M.O.P.	
73	"	"	Group IIc
74	"	"	Group IIIa
75	"	"	"
76	Syn-D_3 metagabbro	"	
77	Amphibolite	"	Group IIIa
78	"	"	Group IIc
84	Syn-D_2 meta-leucogabbro	"	
85	Syn-D_3 metadiorite	H.M. T.E.	
86	Syn-D_3 granodiorite	"	
87	Skarn	H.M. M.O.P.	
88	Syn-D_2 metadiorite	H.M. T.E.	
89	Syn-D_2 amphibolite	H.M. M.O.P.	
90	Amphibolite	H.M. S.O.P.	Group IIIa
91	"	W of H.M.	Group Ia
92	"	"	"
93	Syn-D_3 amphibolite	H.M. M.O.P.	
94	Amphibolite	"	Group IIIa
95	Pre-syn-D_1 leuco-gabbro	H.M. T.E.	
96	Amphibolite	W of H.M.	Group Ia
97	"	"	"
98	Skarn	Lari-Sahinjoki	
99	Amphibolite	W of H.M.	Group Ib
100	"	"	Group Ia
101	"	"	"
102	"	"	"
103	"	Lari-Sahinjoki	Group Ib
104	"	W of H.M.	Group Ia
105	"	"	"
106	"	"	"
107	"	Lari-Sahinjoki	Group Ib
108	"	"	"
109	Skarn	"	
110	Amphibolite	"	Group Ib
111	"	"	"
112	Skarn	Narila	

Analysis No.	Rock type	Locality	Amphibolite Group
113	Amphibolite	Narila	Group IIIb
114	Skarn	"	
115	Gneiss	"	
116	Amphibolite	"	Group IIIb
117	"	"	"
118	"	"	"
119	Skarn	"	
120	Amphibolite	"	Group IIIb
121	Skarned amphibolite	"	
122	Amphibolite	"	Group IIIb
123	"	N of Virtasalmi	Group IIIc
124	"	"	"
125	"	"	"
126	Skarned amphibolite	"	
127	Amphibolite	"	Group IIIc
128	"	Lari-Sahinjoki	Group Ib
129	Early-syn-D_1 meta-gabbro	Karrankalahti	
130	Amphibolite	E of H.M.	Group IIIc
131	Skarned amphibolite	Karrankalahti	
132	Early-syn-D_1 meta-gabbro	"	
133	Syn-D_2 granodiorite	Hällinmäki Village	
134	Amphibolite	Huutoniemi	Group IIIc
135	Skarn	H.M. M.O.P.	
136	Amphibolite	Karrankalahti	Group IIIc
137	"	"	"
138	Syn-D_2 meta-trondhjemite	Kiviniemi	
139	Syn-D_2 metadiorite	Karrankalahti	
140	Syn-D_3 amphibolite	Kiviniemi	
141	Metagranodiorite	Hällinmäki Village	
142	Syn-D_2 meta-trondhjemite	Virtasalmi Village	
143	Metagranodiorite	Hällinmäki Village	
144	Amphibolite	Kiviniemi	Group IIIb
145	"	Narila	Group Ia
146	"	Kiviniemi	Group IIIc

Analysis No.	Rock type	Locality	Amphibolite Group
147	Amphibolite	Virtasalmi Village	Group IIIc
148	Syn-D_3 biotite amphibolite dyke	Hällinmäki Village	
149	Skarned amphibolite	Karrankalahti	
150	Skarn	Kiviniemi	
151	"	"	
152	Skarned amphibolite	Karrankalahti	
153	Amphibolite	Kurrikamaki	
154	"	"	Group IIIc
156	"	Virtasalmi Village	
157	"	Kiviniemi	Group IIIc
158	"	Virtasalmi Village	
159	"	Karrankalahti	Group IIIc
160	"	Lari	Group IIIa
161	"	Siikalaniemi	Group IId
162	Syn-D_3 metagranite	Hällinmäki Village	
163	Syn-D_3 metagrano-diorite	"	
164	Skarned amphibolite	Virtasalmi Village	
165	Amphibolite	Kiviniemi	Group IIIc
166	Syn-D_2 amphibolite	"	
167	Skarned amphibolite	Kurrikamaki	
168	Amphibolite	Karrankalahti	Group IIIc
169	Syn-D_6 trondhjemite	Kurrikamaki	
170	Metagabbro	Kiviniemi	Group IIb
171	"	"	"
172	Amphibolite	"	Group IIIc
173	"	Matilanlahti	"
174	"	"	
175	Skarned amphibolite	"	
176		Kurrikamaki	
177	Amphibolite	Kiviniemi	Group IIIc
178	"	Matilanlahti	"
179	Metagranite	Hallinmaki Village	
180	Skarned amphibolite	Kurrikamaki	
181	Skarn	H.M. T175m	
182	Amphibolite	"	Group IIIa
183	"	"	"

Analysis No.	Rock type	Locality	Amphibolite Group
184	Amphibolite	H.M. T175m	Group IIIa
185	Skarn	"	
186	"	"	
187	Amphibolite	"	Group IIIa
189	"	"	"
190	"	"	"
191	Skarn	"	
192	Amphibolite	"	Group IIIa
193	Skarn	"	
194	Amphibolite	"	Group IIIa
195	"	"	"
196	"	"	"
197	Skarned amphibolite	"	
198	Amphibolite	"	Group IIIa
199	"	"	"
200	"	"	"
201	"	"	"
202	"	"	"
203	Syn-D_3 metadiorite	"	
204	Amphibolite	"	Group IIIa
205	Skarned amphibolite	"	
206	Skarn	"	
207	Amphibolite	"	
208	Skarned amphibolite	"	
209	"	"	
210	Amphibolite	H.M. M.O.P.	Group IIc
211	"	"	"
212	"	"	"
213	"	H.M. T175m	Group IIIa
214	"	H.M. M.O.P.	Group IIc
215	"	H.M. T.E.	Group IIIa
216	Syn-D_3 metadiorite	H.M. M.O.P.	
217	Skarned amphibolite	"	
218	Syn-D_3 metadiorite	"	
219	Skarned amphibolite	E of H.M.	
220	Amphibolite	Virtasalmi Village	Group IIIc
221	"	"	
222	"	Huutoniemi	Group IIIc

Analysis No.	Rock type	Locality	Amphibolite Group
223	Metagabbro	Karrankalahti	Group IIb
224	Syn-D_2 granodiorite	Joenpolvi	
225	Amphibolite	Virtasalmi Village	Group IIIc
226	"	Karrankalahti	
227	"	Kiviniemi	Group IIIc
228	Syn-D_2 meta-granodiorite	Hallinmaki Village	
229	Syn-D_2 porphyritic metagranodiorite	Uitonsalmi	
230	Skarned amphibolite	Kurrikamaki	
231	Amphibolite	Huutoniemi	
232	"	"	
234	"	Lari-Sahinjoki	Group Ib
235	"	Narila	Group IIIb
236	"	"	"
237	"	"	
238	"	Huutoniemi	Group IIIc
239	Metagabbro	Kiviniemi	Group IIb
240	Amphibolite	"	Group IIIc
241	Syn-D_2 meta-granodiorite	Hällinmäki Village	
242	Skarned amphibolite	Virtasalmi Village	
243	"	"	
244	Metadiorite	H.M.	
245	Syn-D_2 metadiorite	Kiviniemi	
246	Granite gneiss	Joenpolvi	
247	Syn-D_2 metadiorite	Kiviniemi	
248	Syn-D_2 trondhjemite	"	
249	Syn-D_2 amphibolite	"	
250	Amphibolite	"	
251	"	Karrankalahti	Group IIIc
252	Syn-D_2 meta-granodiorite	Kiviniemi	
253	Amphibolite	Keskikangas	Group IId
254	"	H.M. T95m	Group IIIa
255	Syn-D_2 granite	Hällinmäki Village	
256	Amphibolite	Karrankalahti	Group IIIc
257	Metaperidotite	Virtasalmi Village	Group IIa

Analysis No.	Rock type	Locality	Amphibolite Group
258	Metaperidotite	Virtasalmi Village	Group IIa
259	Amphibolite	H.M. T175m	Group IIIa
260	Metaperidotite	Virtasalmi Village	Group IIa
261	Amphibolite	H.M. D.H. R3	Group IIIa
262	"	H.M. T175m	"
263	"	H.M. S.O.P.	"
264	"	H.M. D.H. R3	"
265	"	"	"
266	Skarned amphibolite	H.M. S.O.P.	
267	Amphibolite	H.M. D.H. R3	Group IIIa
268	"	H.M. S.O.P.	"
269	"	Kurrikamaki	
270	"	H.M. T175m	Group IIIa
271	Skarned amphibolite	Virtasalmi Village	
272	Amphibolite	Kiviniemi	Group IId
273	"	Kurrikamaki	
274	"	H.M. T95m	Group IIc
275	"	Lari-Sahinjoki	Group Ib
276	Skarned amphibolite	Virtasalmi Village	

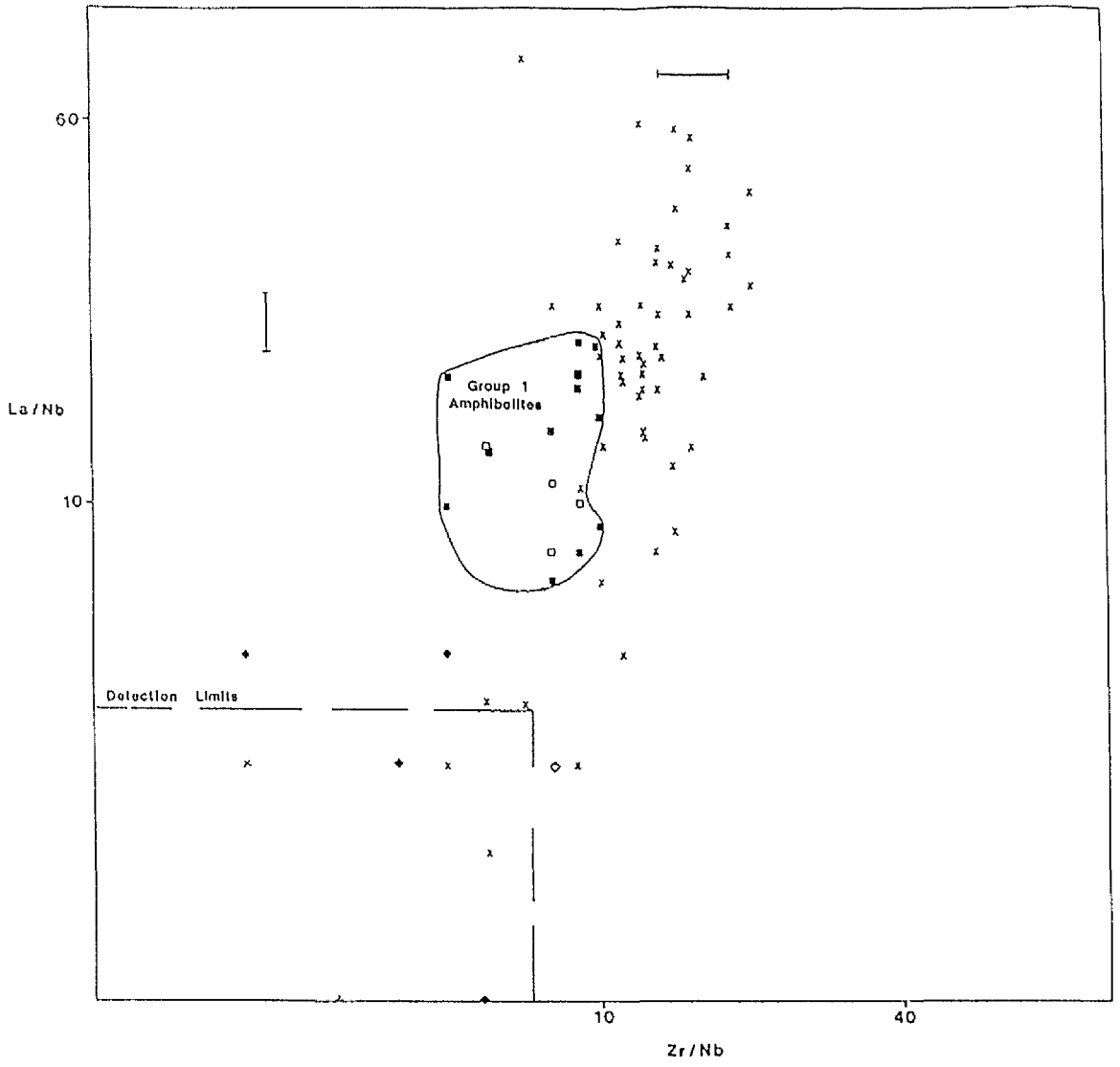

Fig. 3.1.19 Figure 3.1.19 is a plot of La/Nb vs Zr/Nb for Virtasalmi amphibolites. A separation of Group I amphibolites from those of Group III is suggested, pointing to variations in source chemistry.

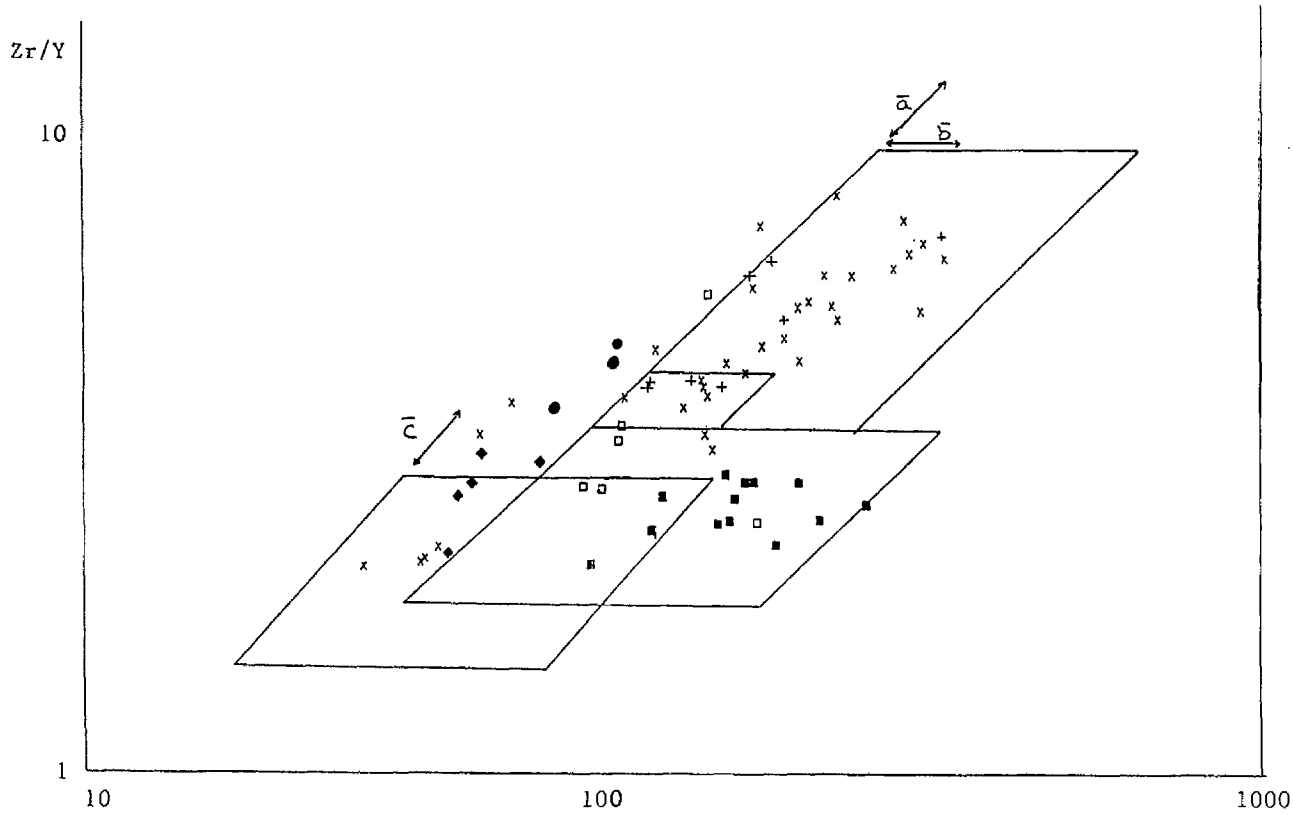

Figure 3.1.18a

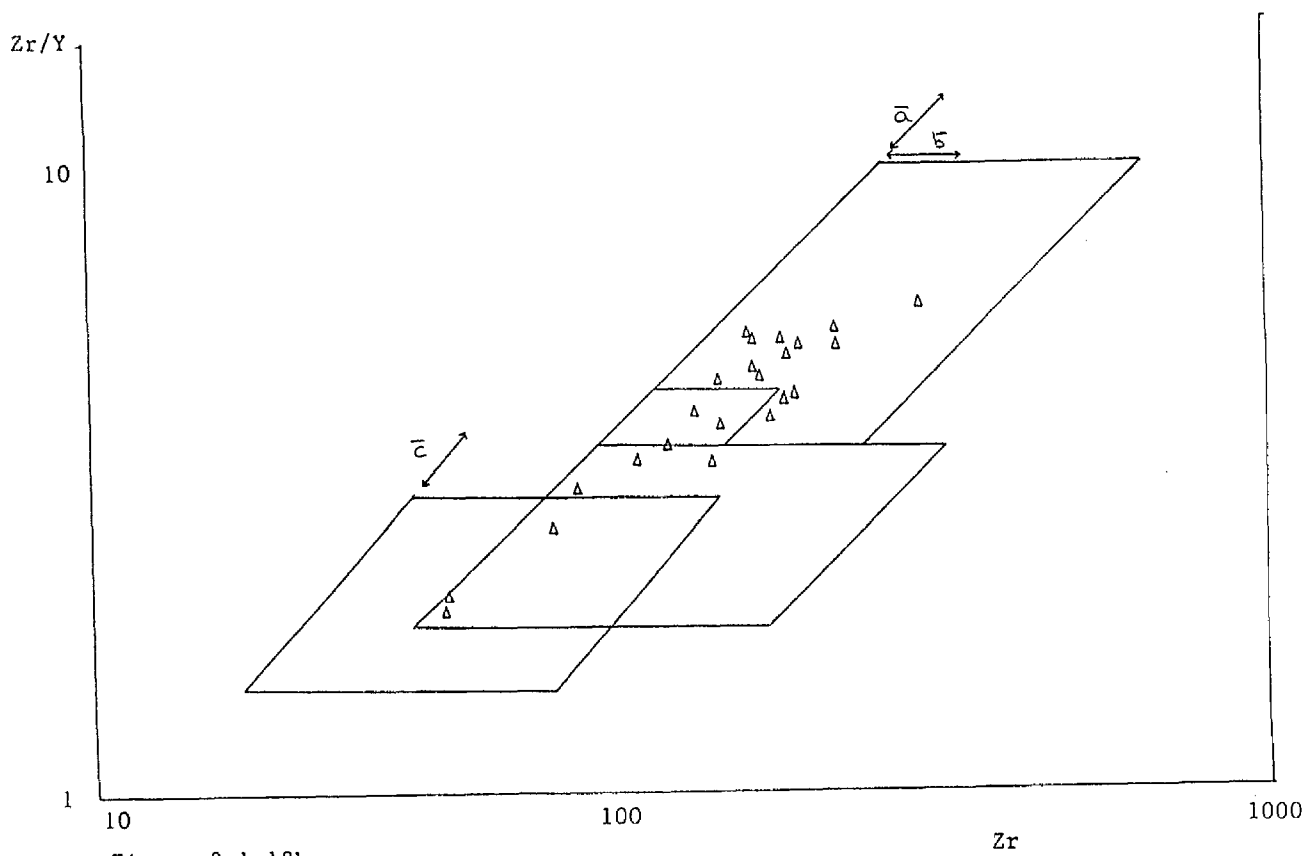

Figure 3.1.18b

Fig. 3.1.18 Figures 3.1.18a and 3.1.18b are log plots of Zr/Y vs Zr for Group I, Group IIb, c and Group IIIa, b amphibolites and Group IIIc amphibolites respectively. The compositional fields are taken from Pearch & Norry (1979) and are as follows:

A - within plate basalts
B - within plate basalts-fast spreading ridge basalts
C - mid-ocean ridge basalts
D - island arc basalts

It is evident from these graphs that Group III amphibolites plot mainly subparallel to vector $\bar{a}$, Group I amphibolites subparallel to vector $\bar{b}$, and Group II amphibolites between vectors $\bar{a}$ and $\bar{c}$.

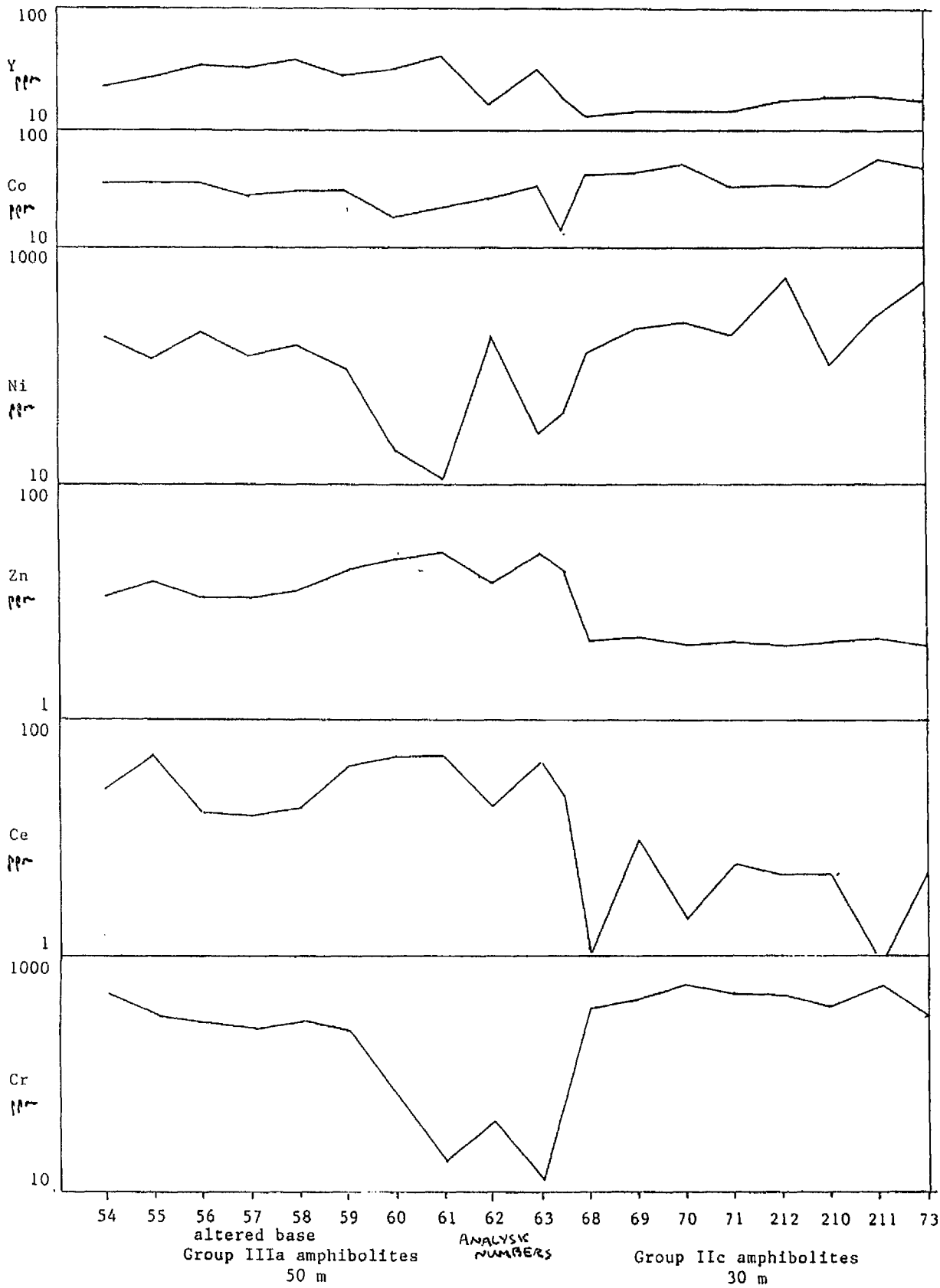
100
Y
ppm
10
100
Co
ppm
10
1000
Ni
ppm
10
100
Zn
ppm
1
100
Ce
ppm
1
1000
Cr
ppm
10
54 55 56 57 58 59 60 61 62 63 68 69 70 71 212 210 211 73
altered base
Group IIIa amphibolites
50 m
ANALYSIS NUMBERS
Group IIc amphibolites
30 m

Figure 3.1.17

Fig. 3.1.17 The chemical variations noted in samples of amphibolites collected from a traverse across the Main Open Pit at Hällinmäki Mine are presented in Figure 3.1.17. Interlayered Group IIc and Group IIIa amphibolites were noted. A 'sawtooth' pattern for some elements e.g. Ni, noted within Group IIIa amphibolites is considered indicative of periodic replenishment of a magma chamber, within an overall trend of increasing fractionation (e.g. Figs. 3.1.1a-d).

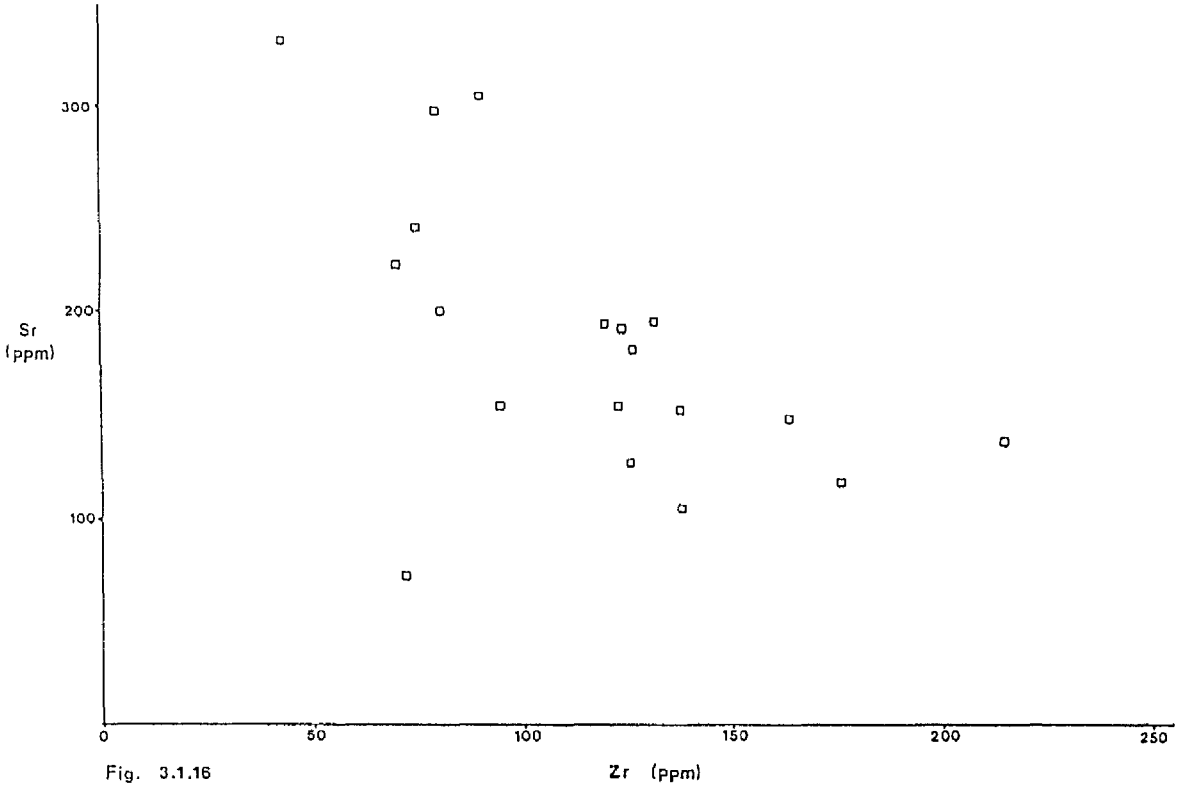

Fig. 3.1.16

Fig. 3.1.16 Figure 3.1.16 is a plot of Sr vs Zr for Group I amphibolites only. A poorly defined trend of decreasing Sr with increasing Zr content is observed.

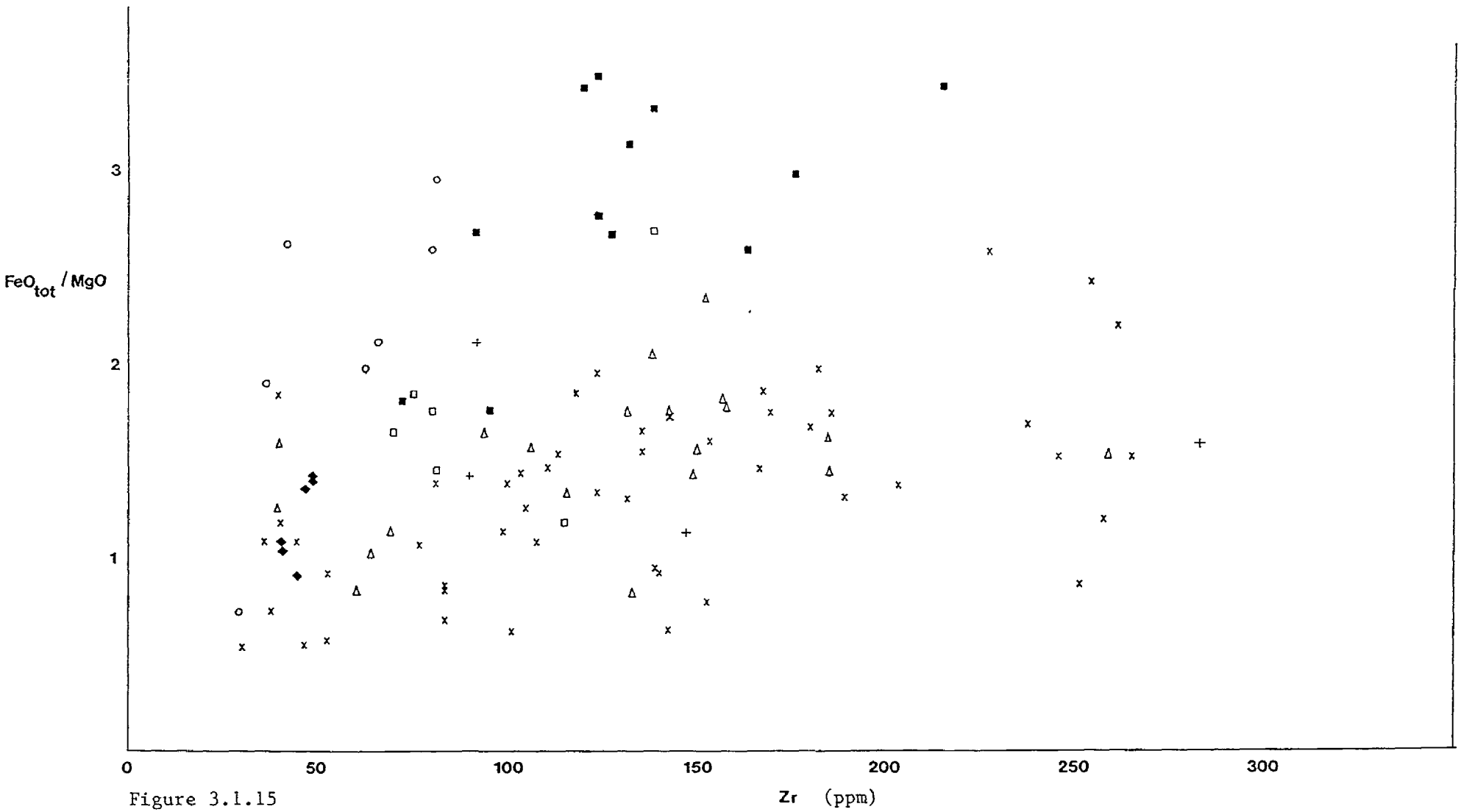

Figure 3.1.15

Fig. 3.1.15 Figure 3.1.15 is a plot of FeO/MgO vs TiO_2 for Virtasalmi amphibolites. Although both FeO and MgO displayed poor linear trends when plotted against Zr, there is a separation in the data which is considered to indicate that Group I (and to a smaller degree, Group II) amphibolites show a greater trend towards iron-enrichment than Group III amphibolites.

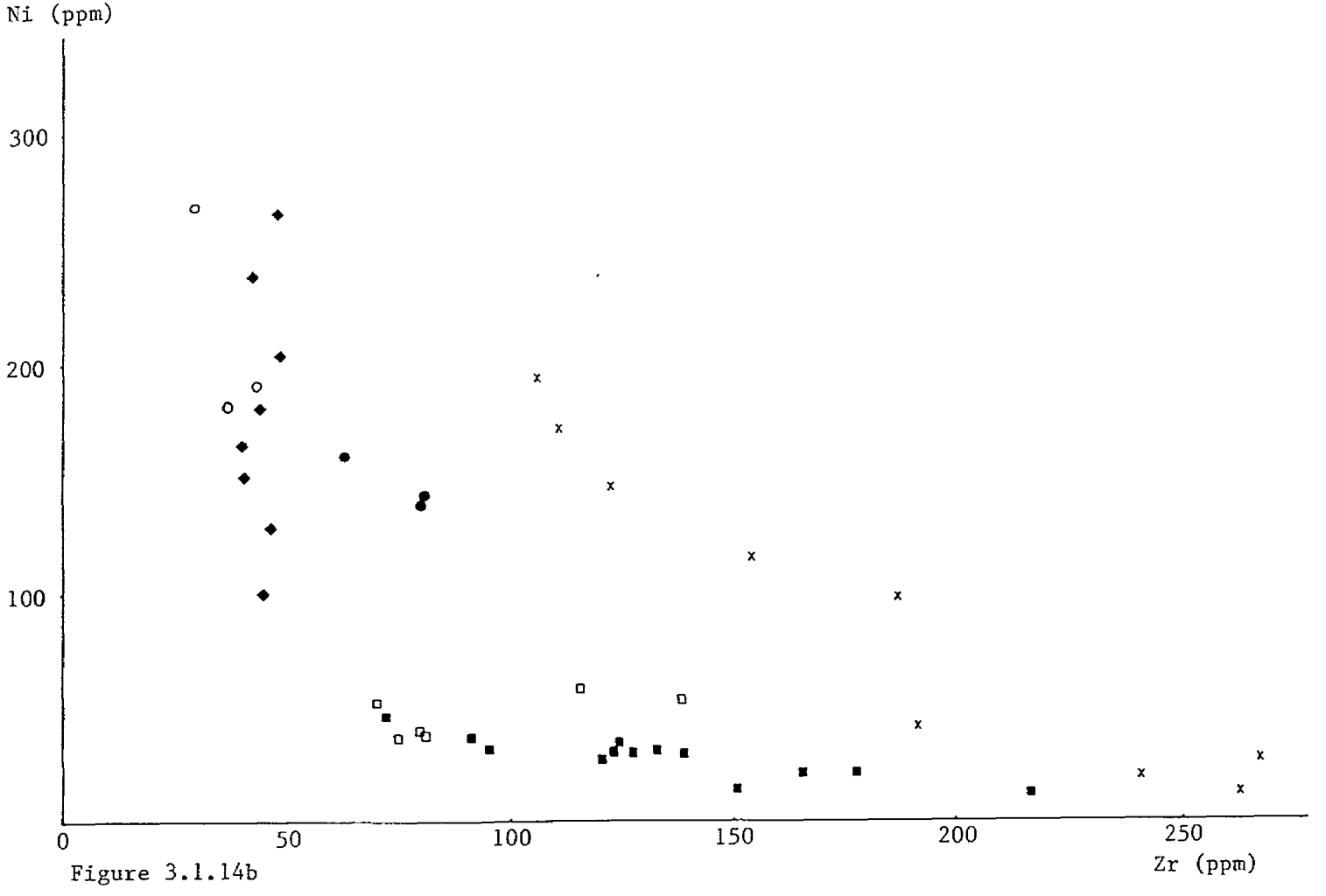

Figure 3.1.14b

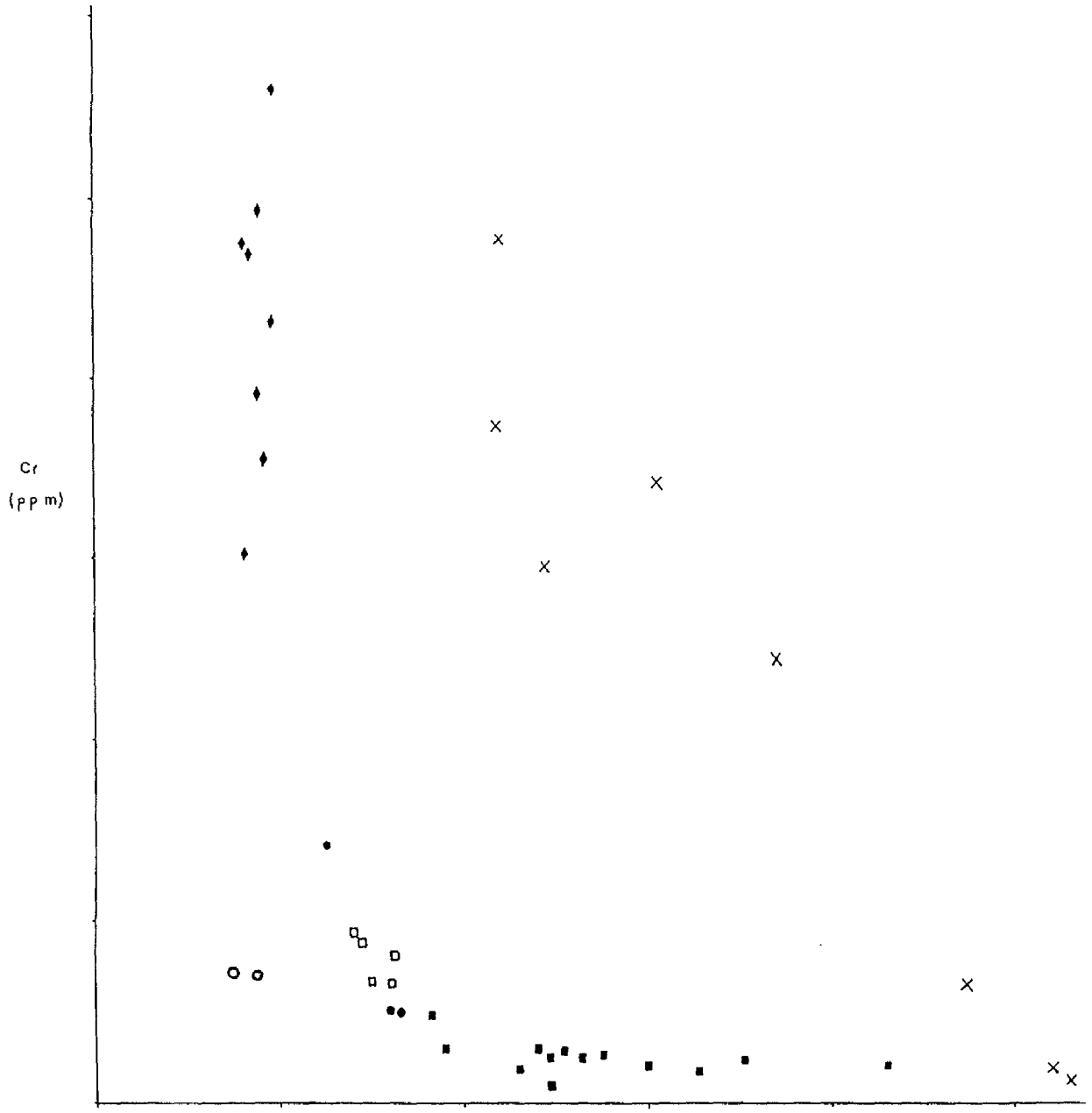

Figure 3.1.14a

Fig. 3.1.14 Figures 3.1.14a and 3.1.14b are plots of Cr and Ni vs Zr respectively for the amphibolites of Group I, Group IIc, Group IIIb and Group IIIa amphibolites, the latter only where collected in a traverse across the main open pit where each unit was sampled from. Distinct linear trends are evident for each group.

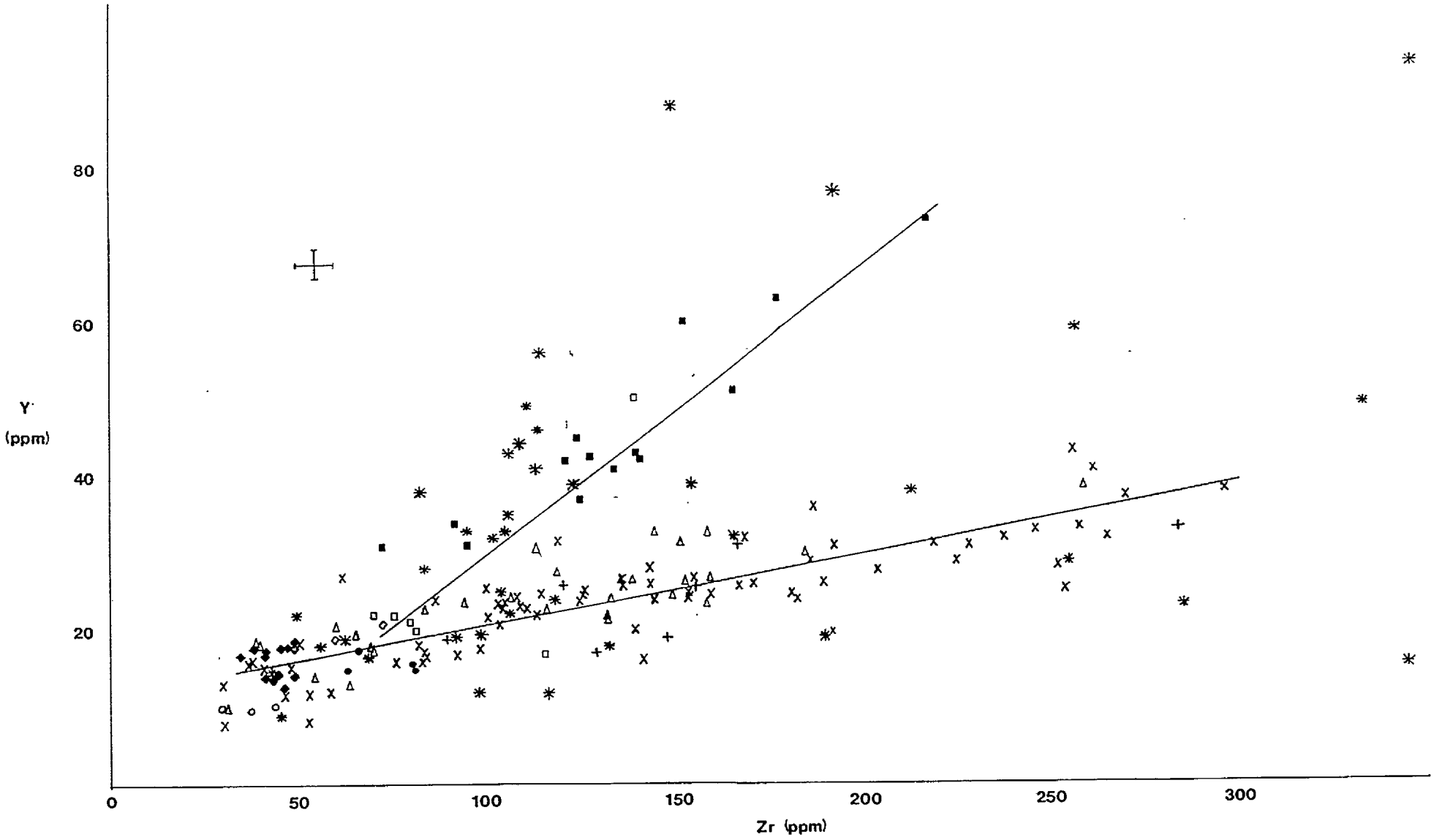

Figure 3.1.13

Fig. 3.1.13 Figure 3.1.13 is a plot of Y vs Zr for Virtasalmi amphibolites and skarns. Two distinct linear trends are recognised in the amphibolites for Groups I and III. The skarns show a more scattered distribution mostly reflecting alteration of amphibolite protoliths.

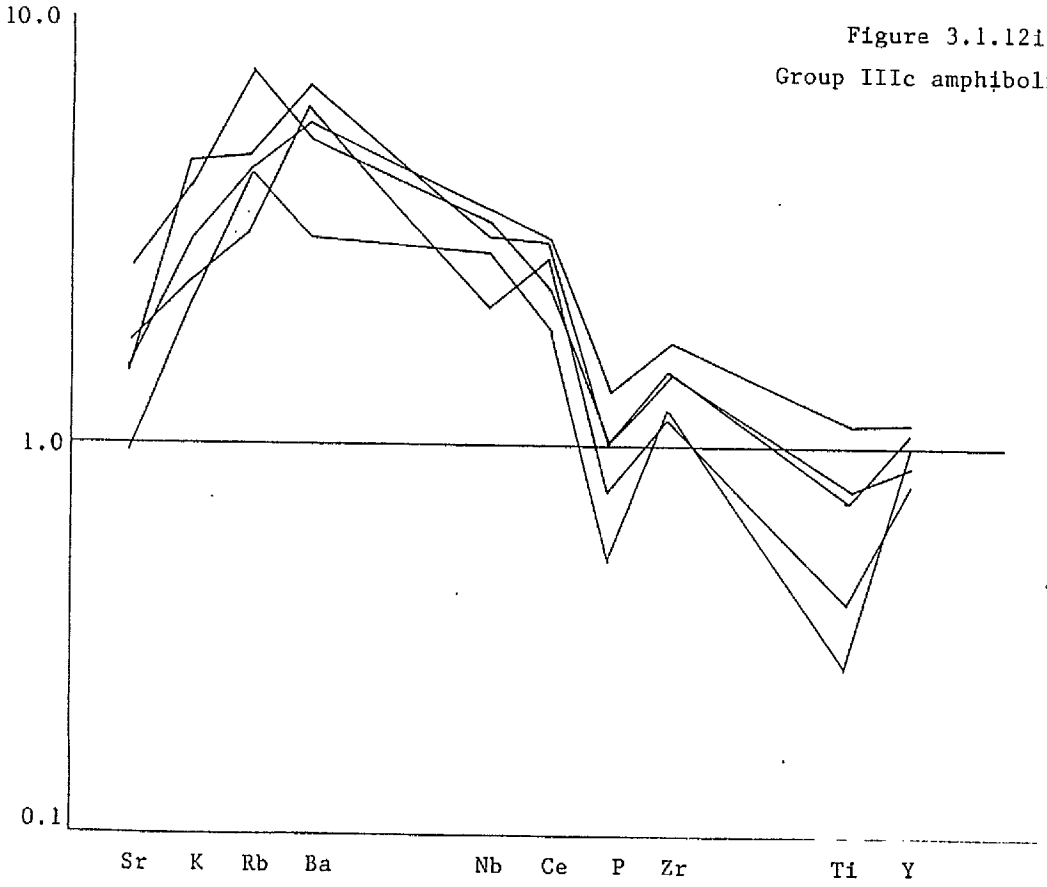

Figure 3.1.12i

Group IIIc amphibolites

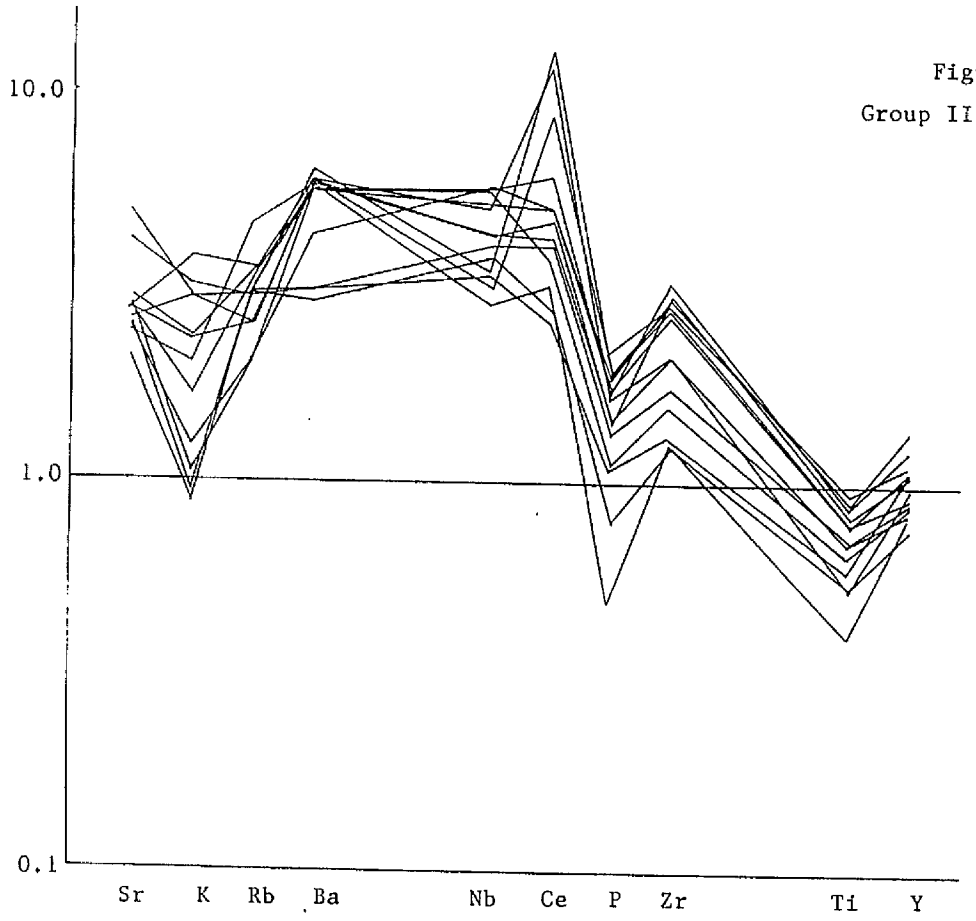

Figure 2.1.12g
Group IIIa amphibolites

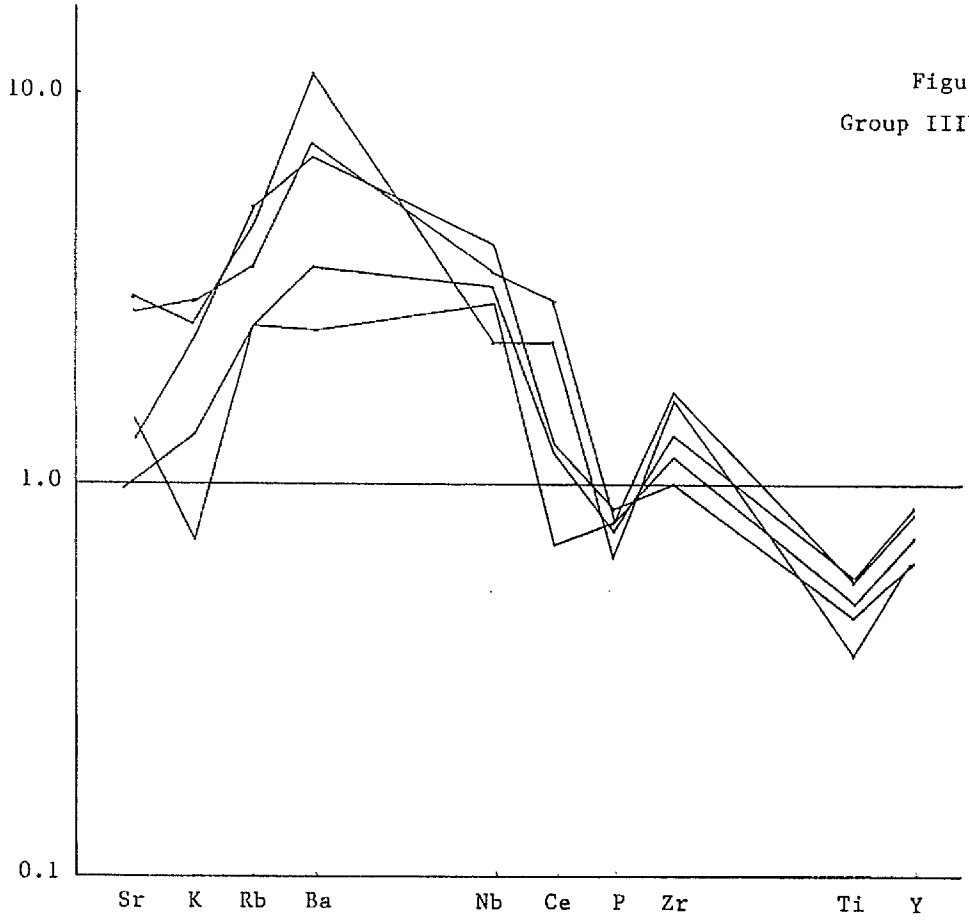

Figure 3.1.12h
Group IIIb amphibolites

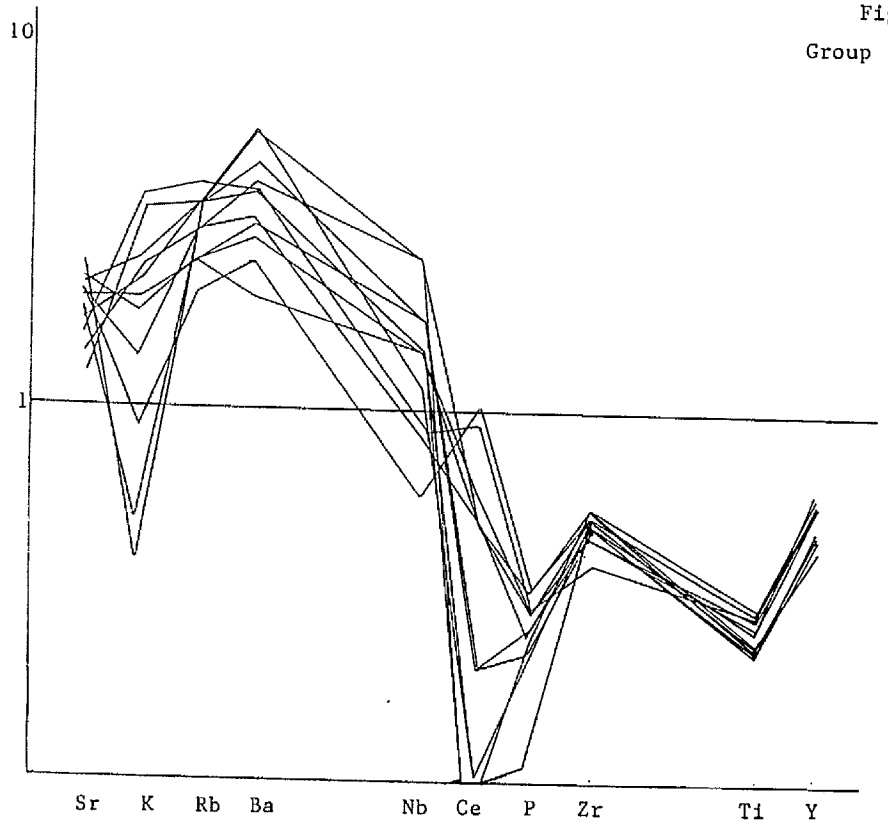

Figure 3.1.12e
Group IIc amphibolites

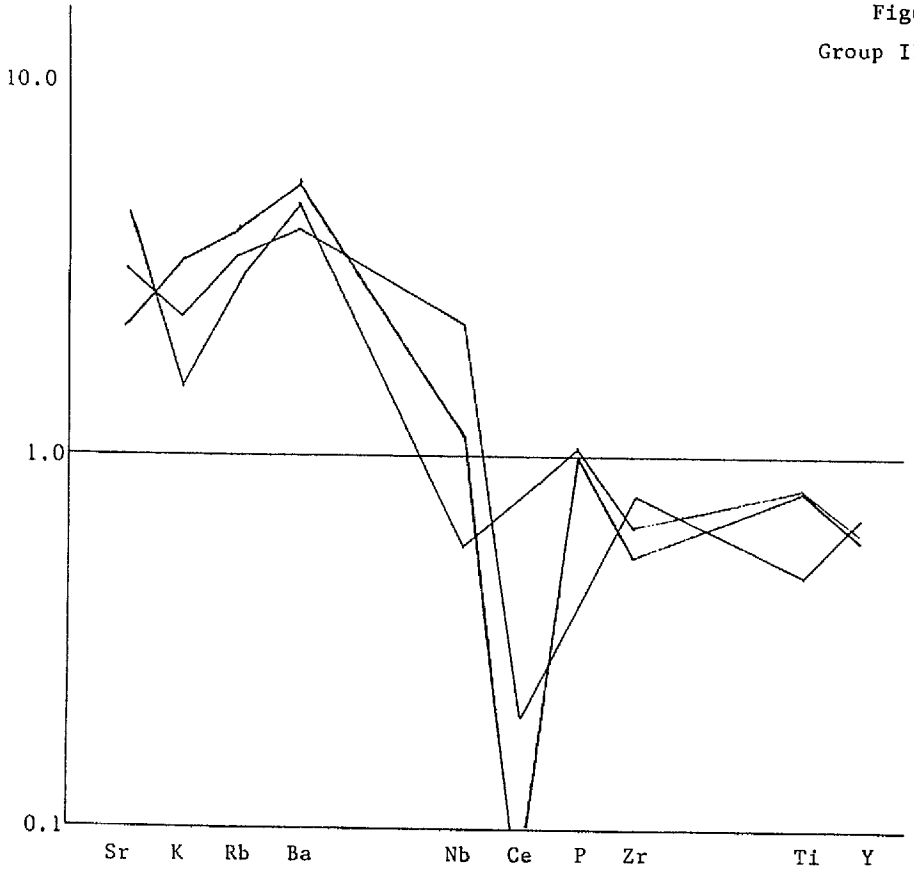

Figure 3.1.12f
Group IId amphibolites

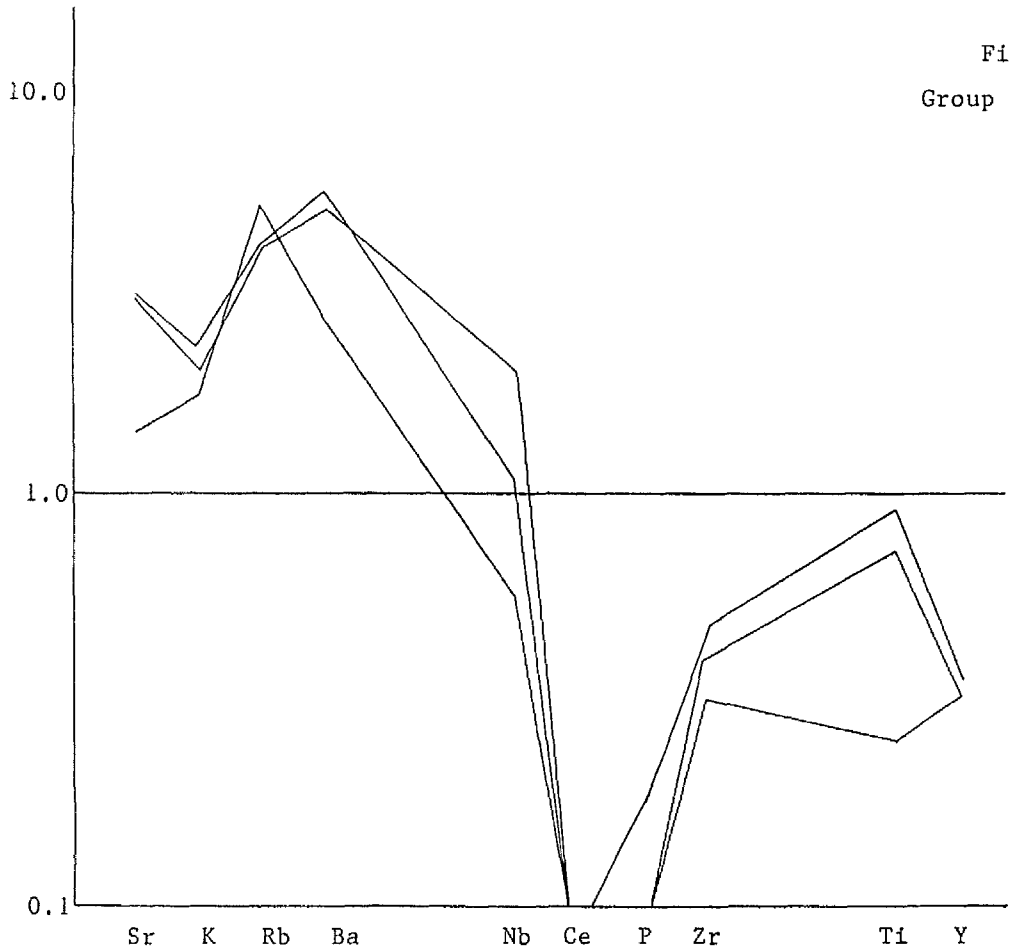

Figure 3.1.12c
Group IIa amphibolites

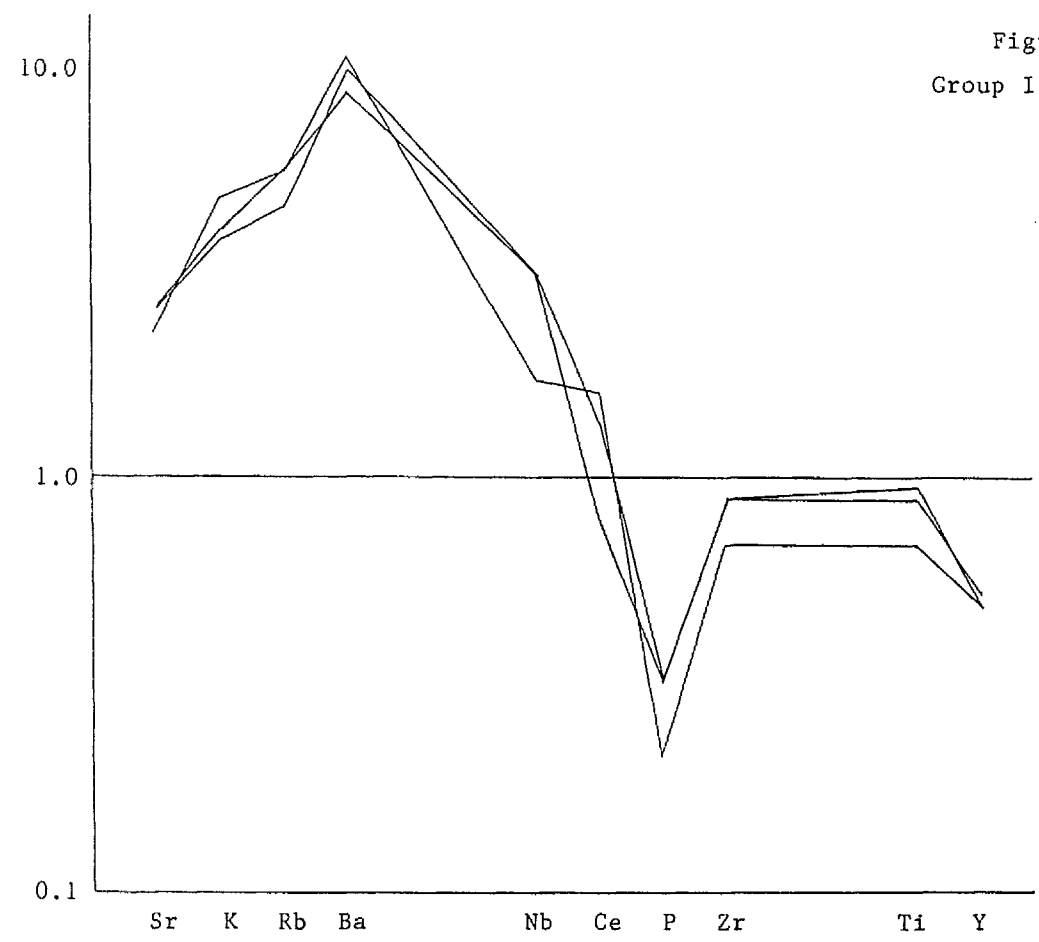

Figure 3.1.12d
Group IIb amphibolites

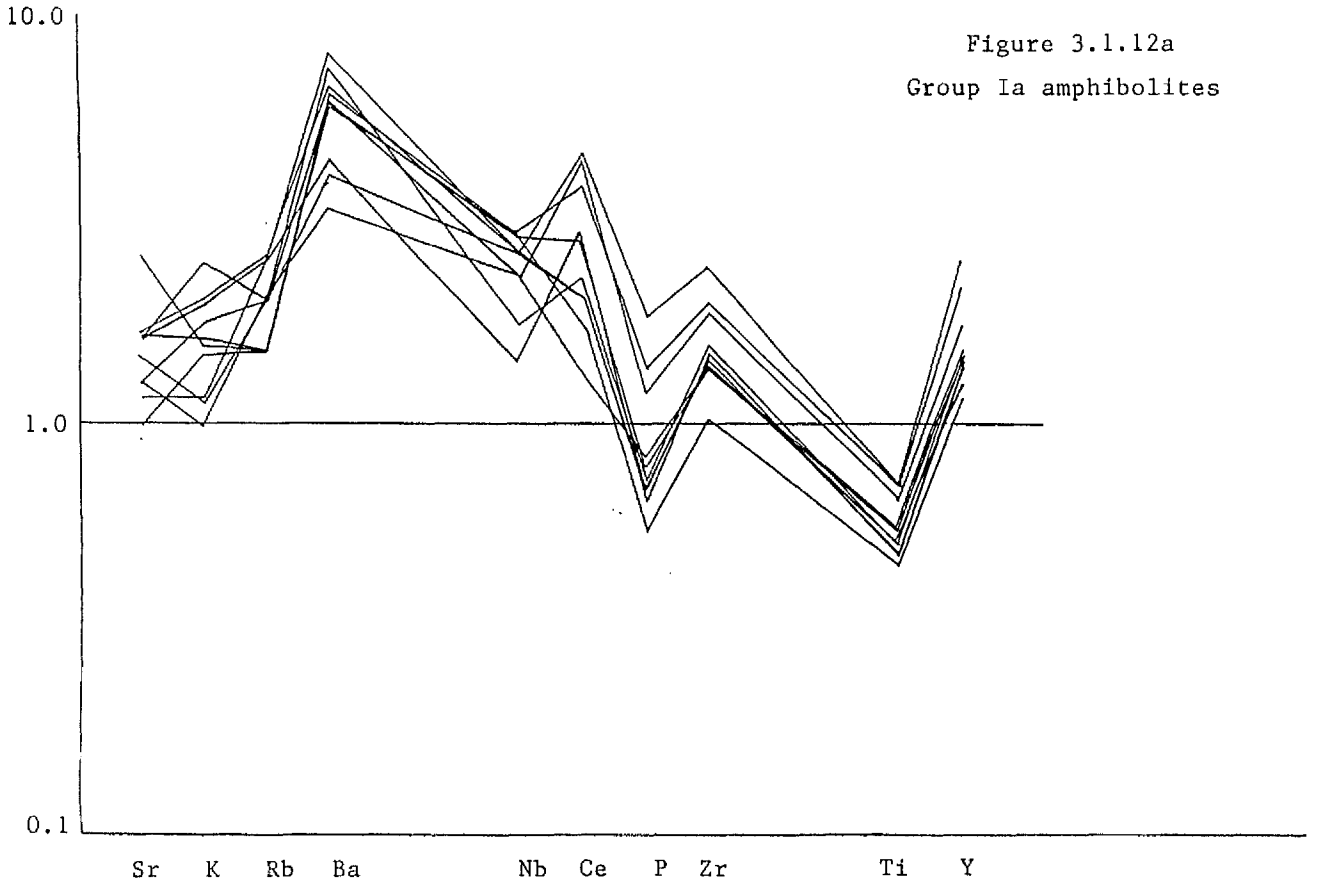

Figure 3.1.12a
Group Ia amphibolites

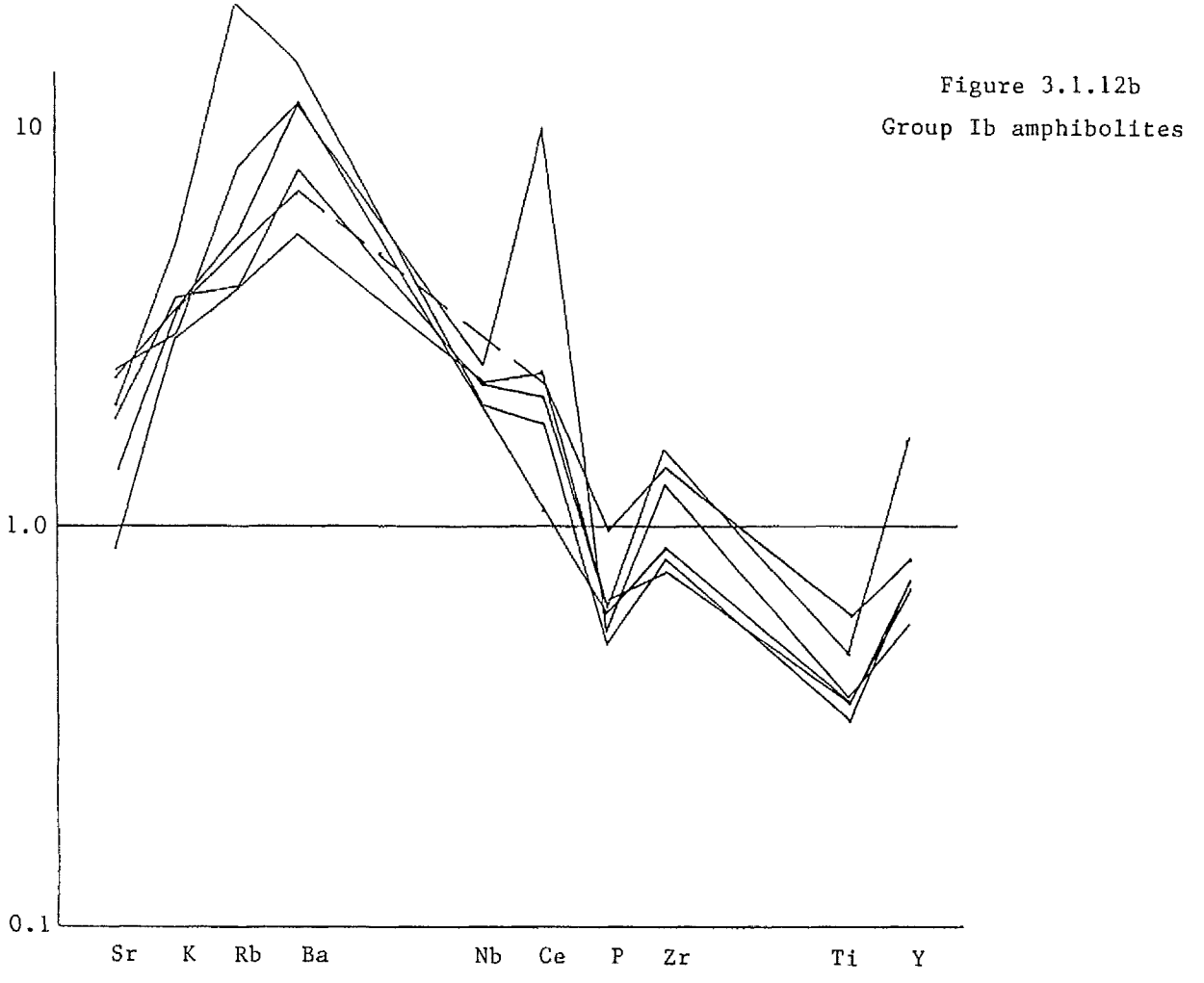

Figure 3.1.12b
Group Ib amphibolites

Fig. 3.1.12 Figures 3.1.12a-i are spidergram plots for the 9 chemically (and petrographically) recognised sub-groups in the amphibolites of the Virtasalmi District.

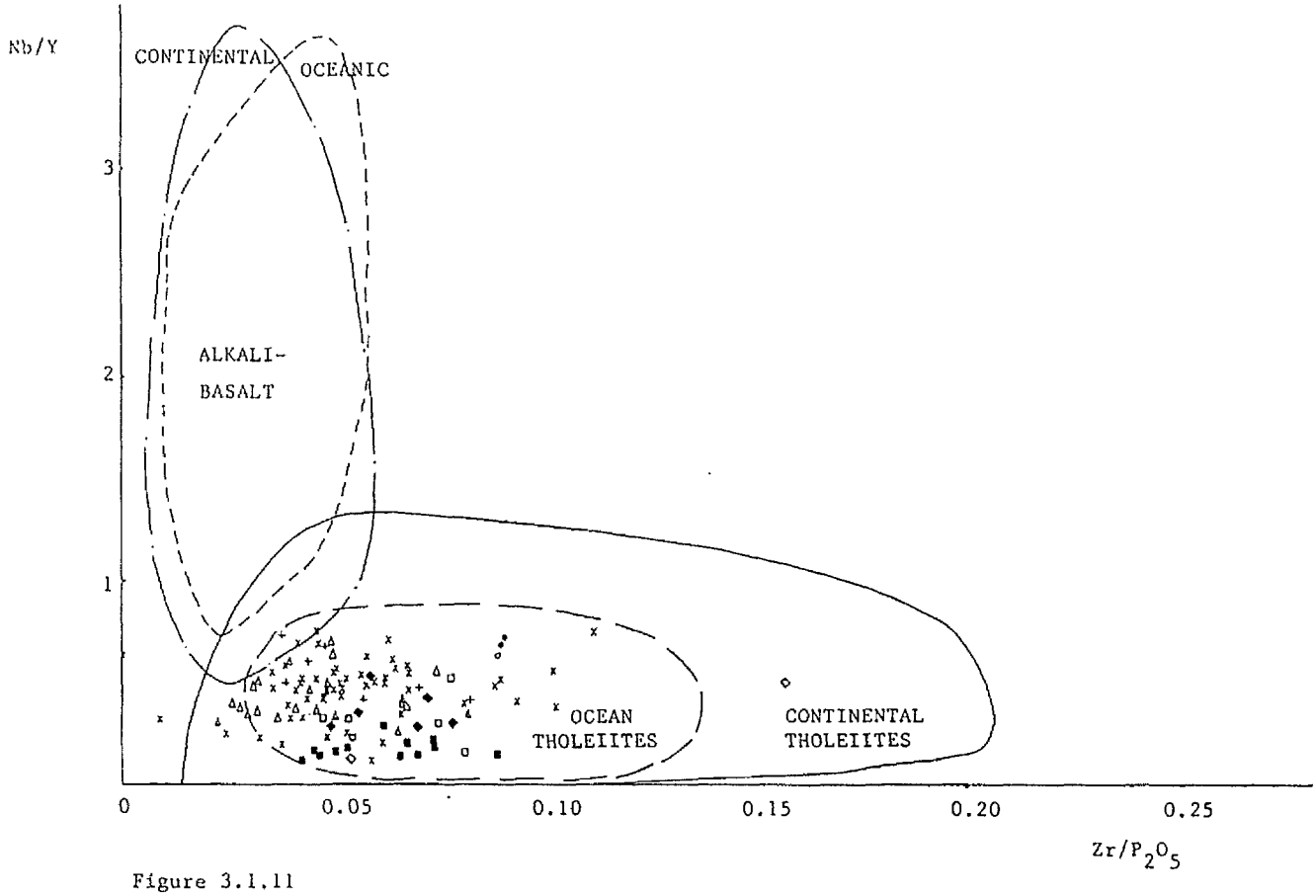

Figure 3.1.11

Fig. 3.1.11 Figure 3.1.11 is a plot of Nb/Y vs Zr/P_2O_5 for Virtasalmi amphibolites. The compositional fields are taken from Floyd & Winchester (1975).

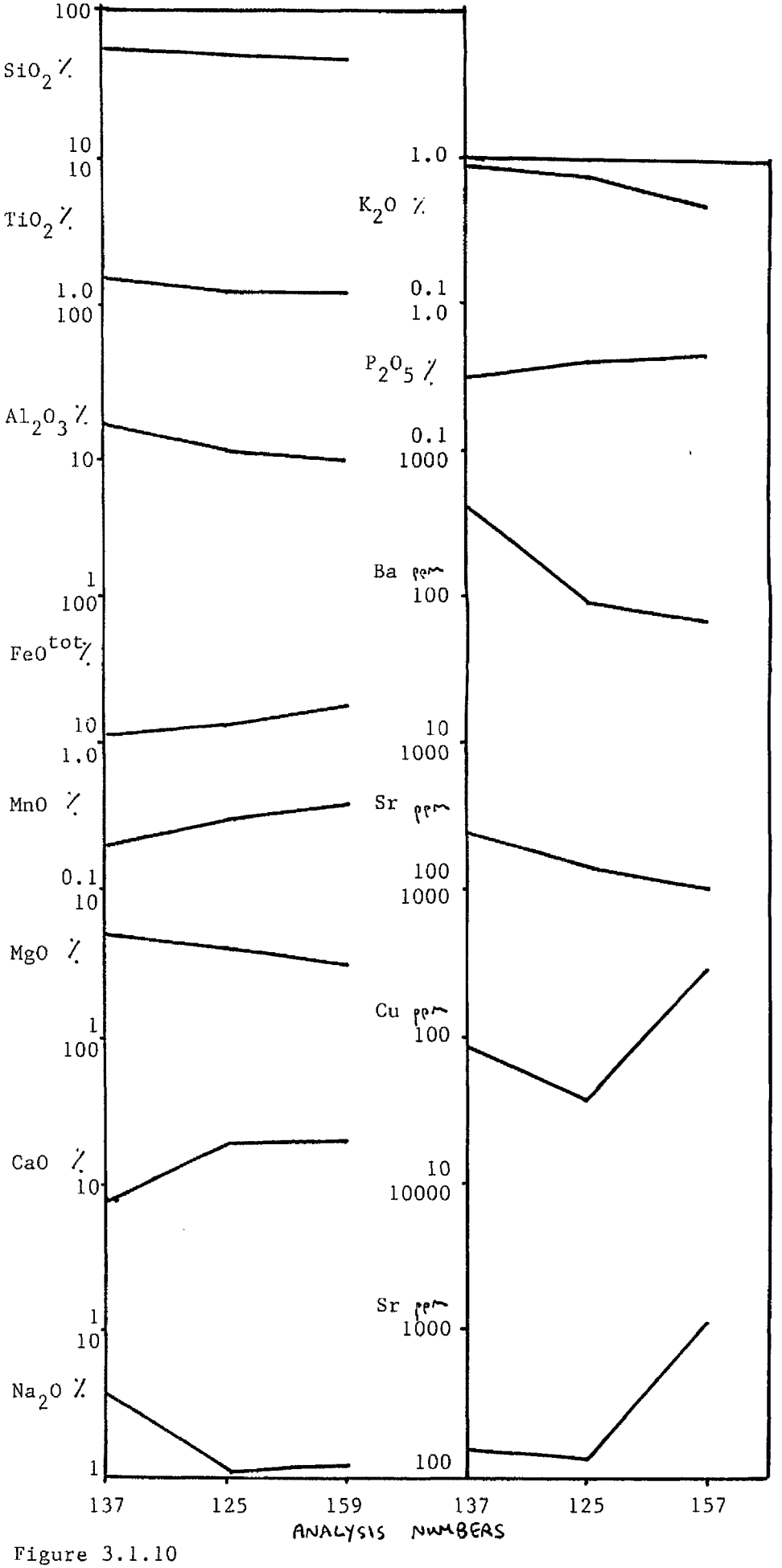
100
SiO2 %
10
10
TiO2 %
1.0
100
Al2O3 %
10
1
100
FeOtot %
10
1.0
MnO %
0.1
10
MgO %
1
100
CaO %
10
1
10
Na2O %
1
1.0
K2O %
0.1
1.0
P2O5 %
0.1
1000
Ba ppm
100
10
1000
Sr ppm
100
1000
Cu ppm
100
10
10000
Sr ppm
1000
100
137
125
159
137
125
157
ANALYSIS NUMBERS

Figure 3.1.10

Fig. 3.1.10 The major and trace element geochemistry for 3 samples collected in a traverse from relatively unaltered amphibolite (Analysis No. 137) to Type II skarn (Analysis No. 159) at the contact with a marble, are presented in Figure 3.1.10. The samples were collected from Karrankalahti.

Figure 3.1.9

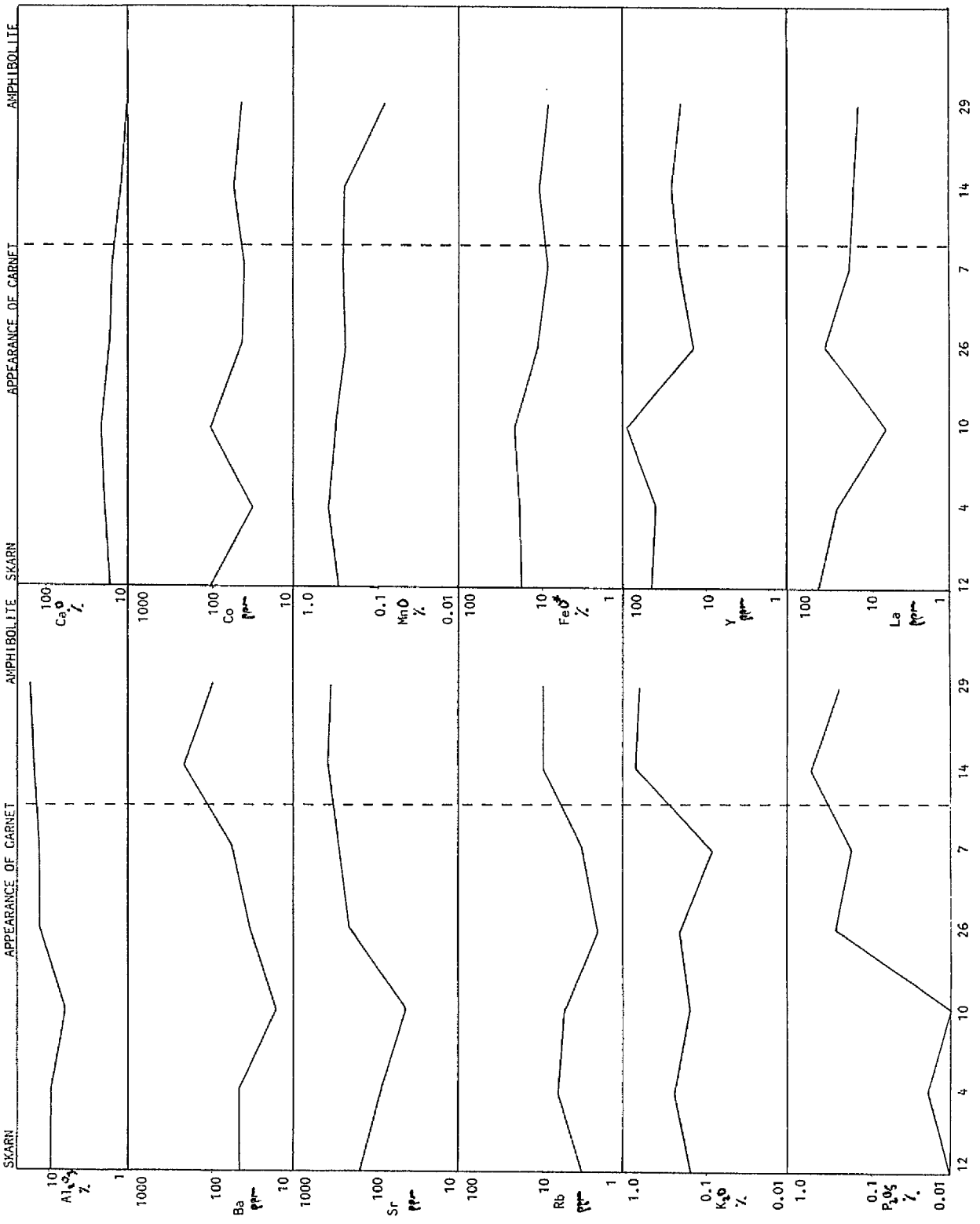
SKARN
APPEARANCE OF GARNET
AMPHIBOLITE
SKARN
APPEARANCE OF GARNET
AMPHIBOLITE
Al2O3 %
Ba ppm
Sr ppm
Rb ppm
K2O %
P2O5 %
CaO %
Co ppm
MnO %
FeO* %
Y ppm
La ppm
12 4 10 26 7 29 14
12 4 10 26 7 29 14
SAMPLE NUMBERS

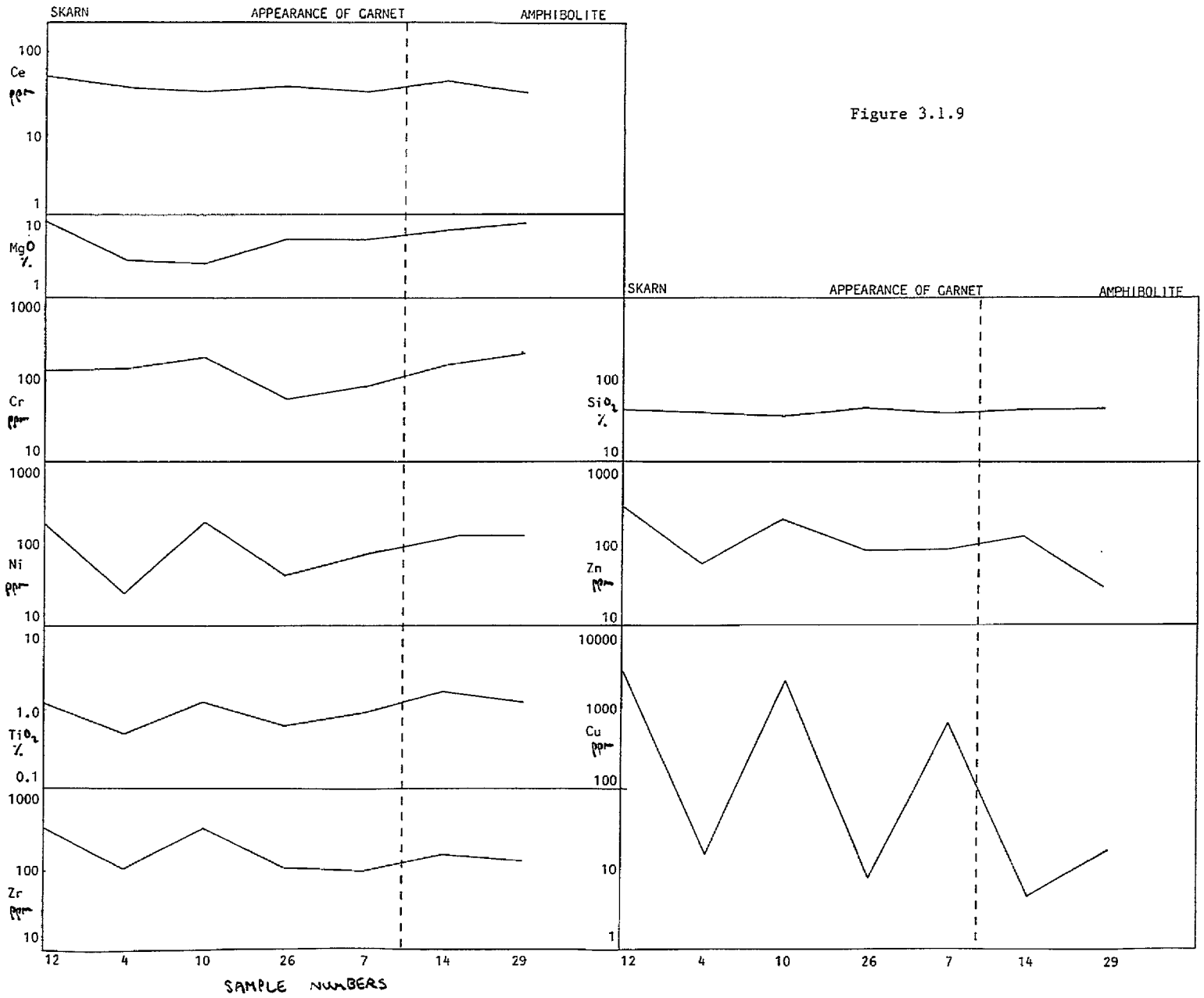
SKARN
APPEARANCE OF GARNET
AMPHIBOLITE
100
Ce
ppm
10
1
10
MgO
%
1
1000
100
Cr
ppm
10
1000
100
Ni
ppm
10
10
1.0
TiO2
%
0.1
1000
100
Zr
ppm
10
SKARN
APPEARANCE OF GARNET
AMPHIBOLITE
100
SiO2
%
10
1000
100
Zn
ppm
10
10000
1000
Cu
ppm
100
10
1
12 4 10 26 7 14 29
12 4 10 26 7 14 29
SAMPLE NUMBERS

Figure 3.1.9

Figure 3.1.9 Schematic plots showing the element variation in a traverse from relatively 'unaltered' amphibolite to a Type V skarn (i.e. from right hand side of each plot to the left hand side) are presented in Figure 3.1.9. The distance between each sample is approximately 2 m. The first appearance of andradite garnet in the traverse is also noted. The samples were collected from T370m, Hällinmäki Mine.

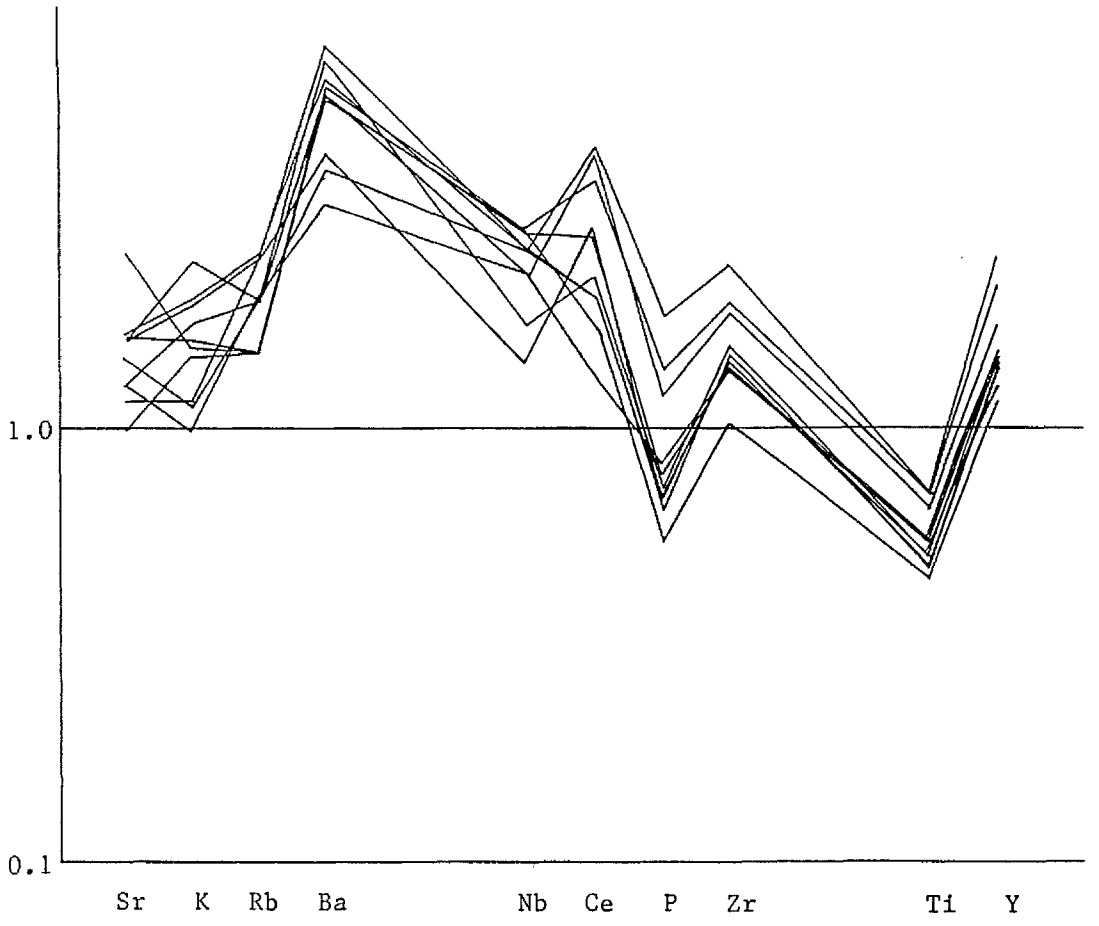

Figure 3.1.8 Group Ia amphibolites

Fig. 3.1.8 Figure 3.1.8 is a spidergram plot for Group Ia amphibolites, west of Hällinmäki Mine. Consistent inter-element ratios, especially for the HFS elements, Zr and Y, suggest original igneous values or ratios are preserved outwith the morphologically identifiable alteratoin haloes around Type III skarn patches.

Figure 3.1.7 The extent of silicification and spilitisation associated with development of Type III skarns is indicated in this photograph by the contrast between dark grey (relatively unaltered) and light grey (altered) rock.
Pillow lavas-lava tubes, Narila.

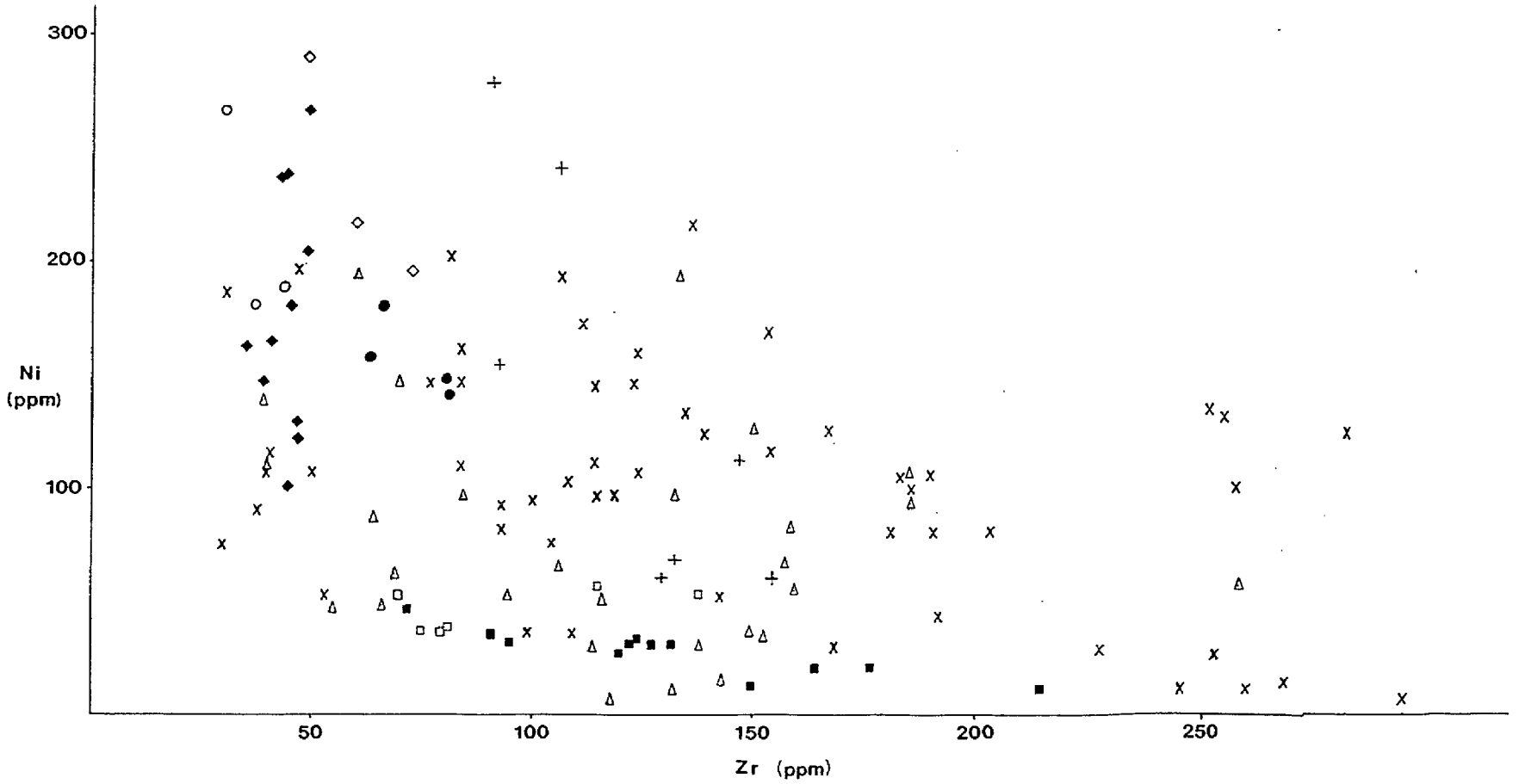

Figure 3.1.6e

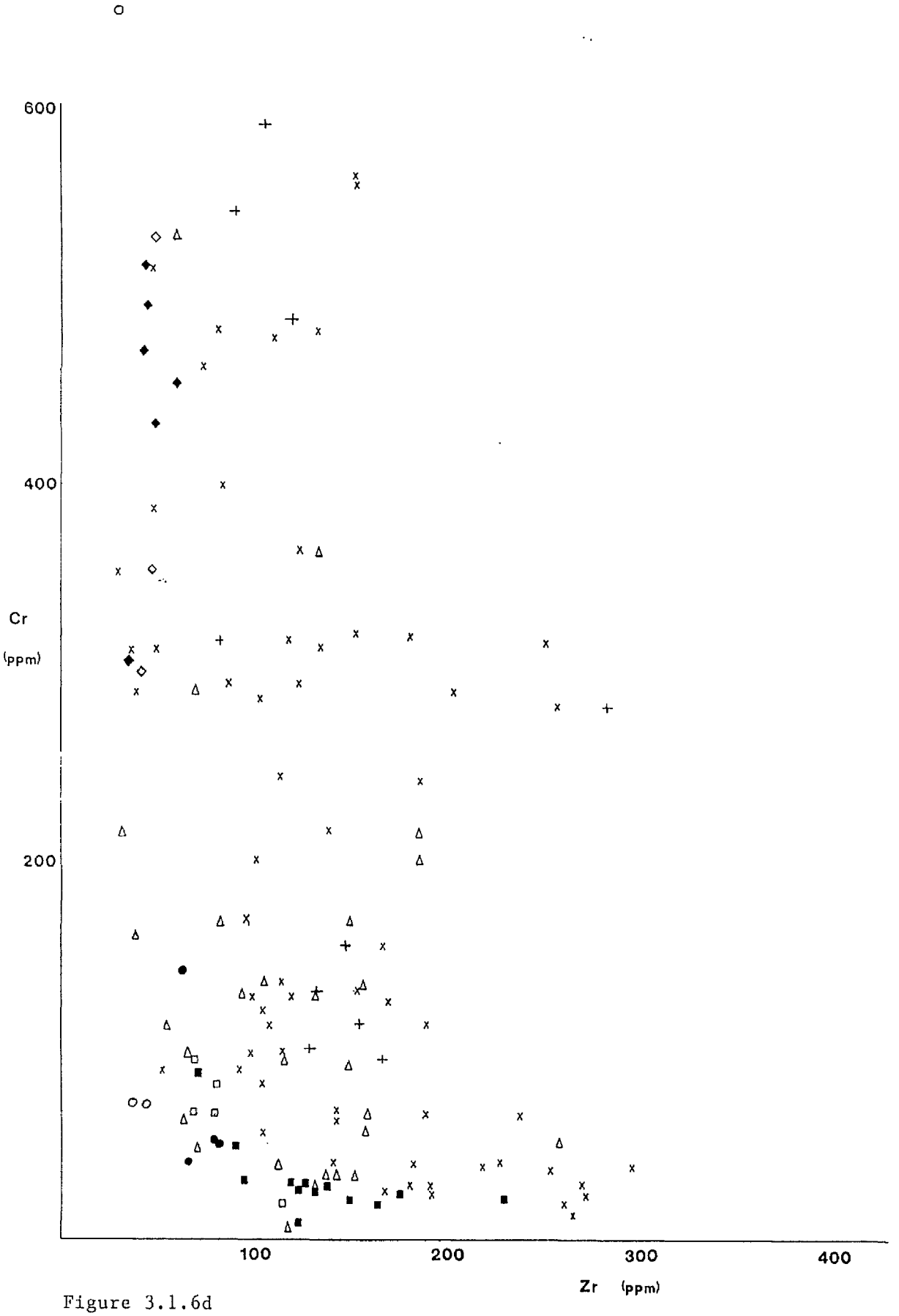

Figure 3.1.6d

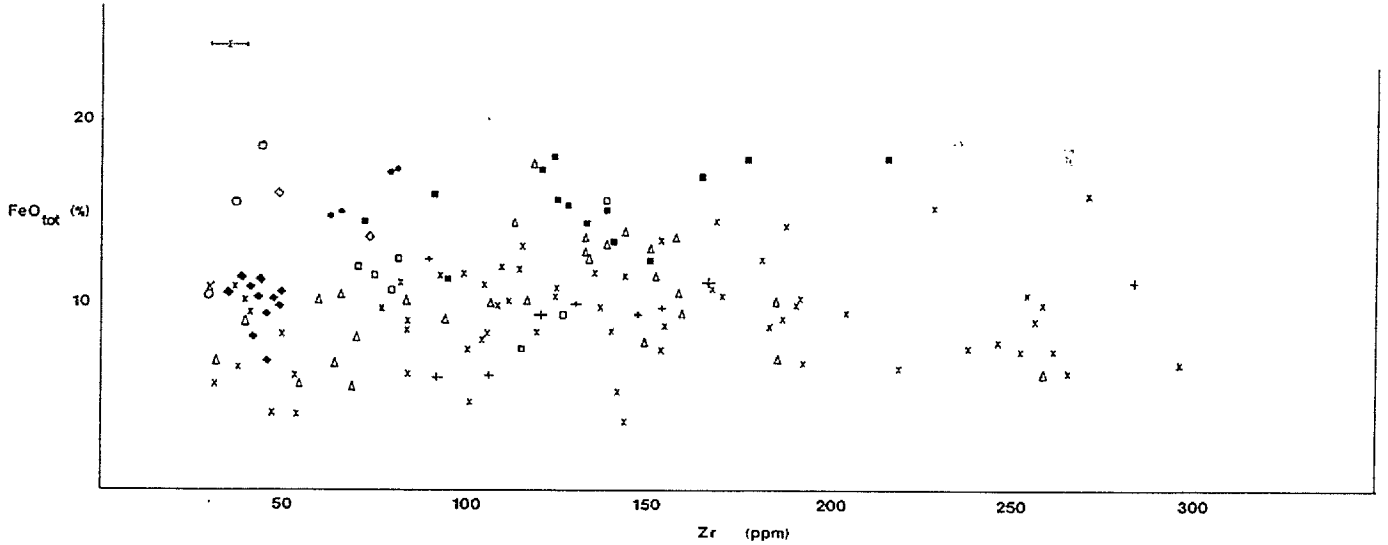

Figure 3.1.6b

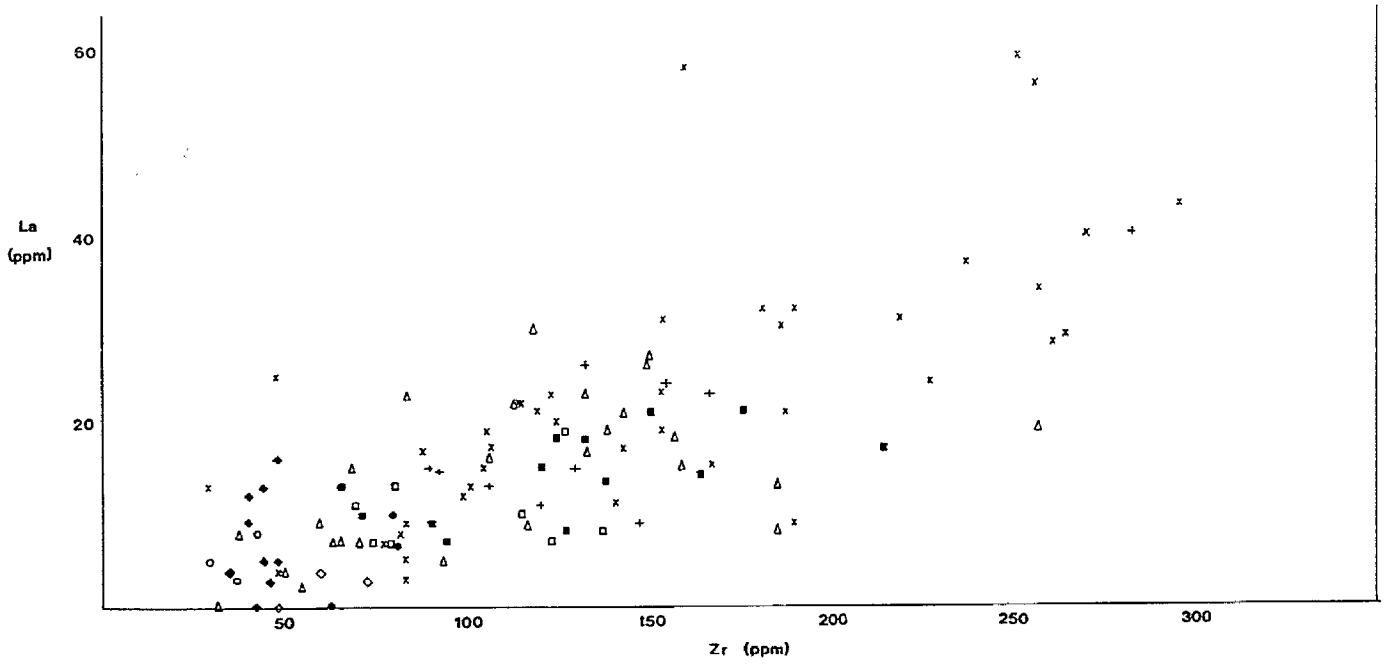

Figure 3.1.6c

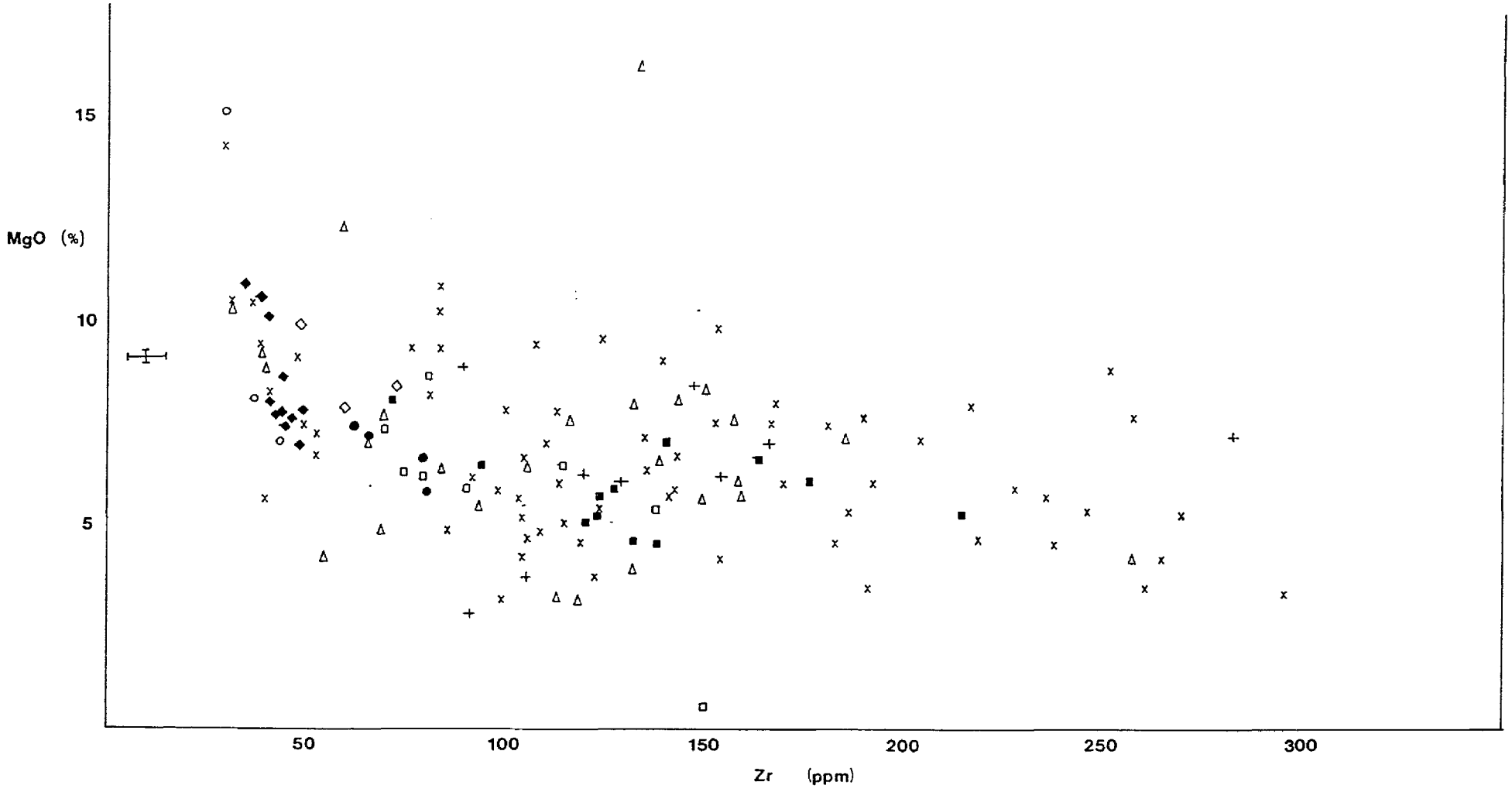

Figure 3.1.6a

Fig. 3.1.6 Figures 3.1.6 are plots of MgO, FeO*, La, Cr and Ni vs Zr respectively. Poorly defined linear trends are observed.

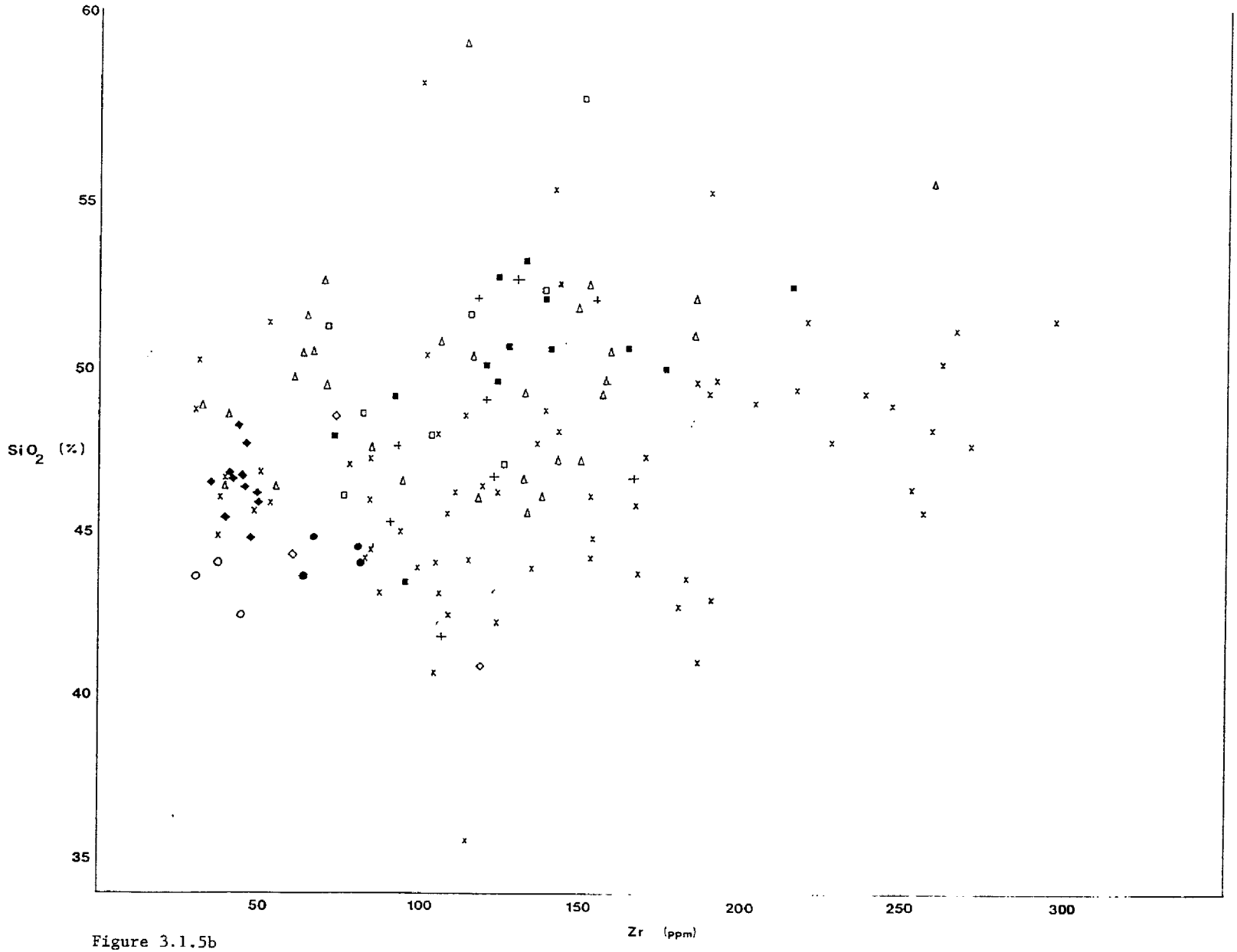

Figure 3.1.5b

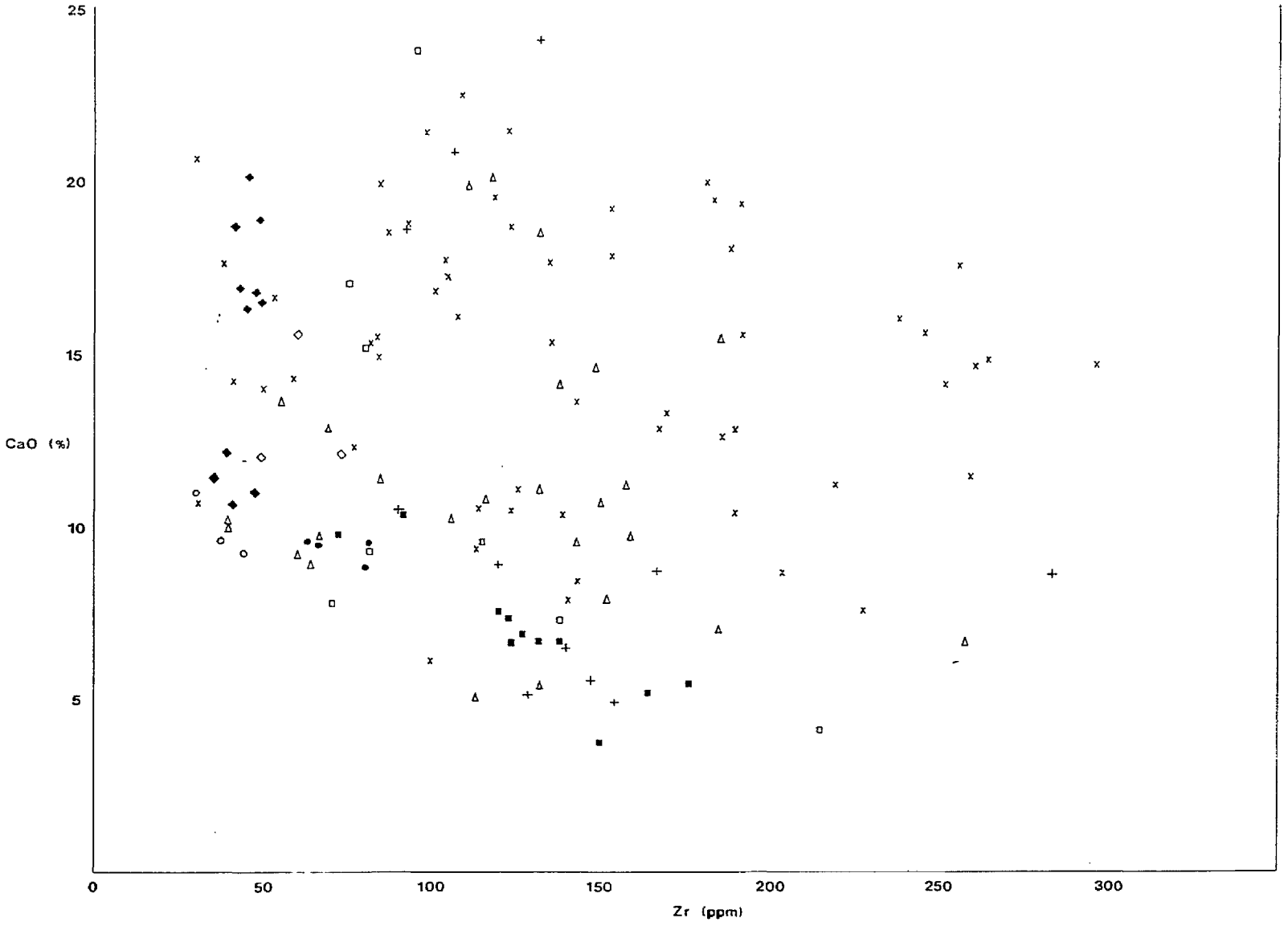

Figure 3.1.5a

Fig. 3.1.5 Figures 3.1.5a,b are plots of CaO and SiO_2 vs Zr respectively for Virtasalmi amphibolites. The scattered distribution is interpreted as indicative of post-crystallisation mobility.

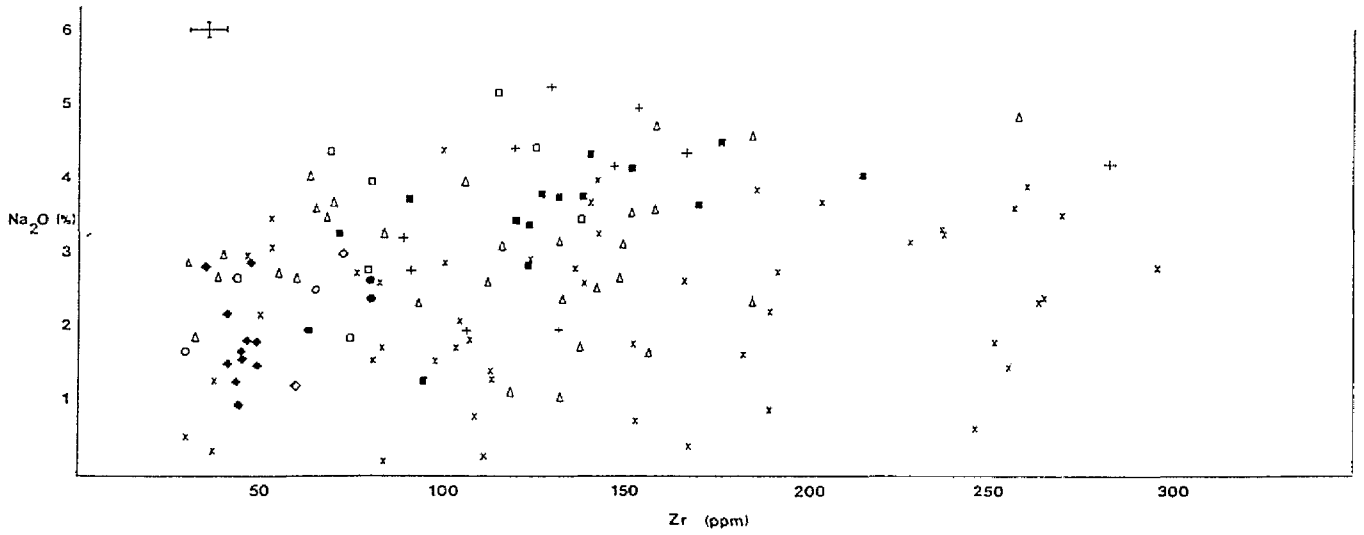

Figure 3.1.4d

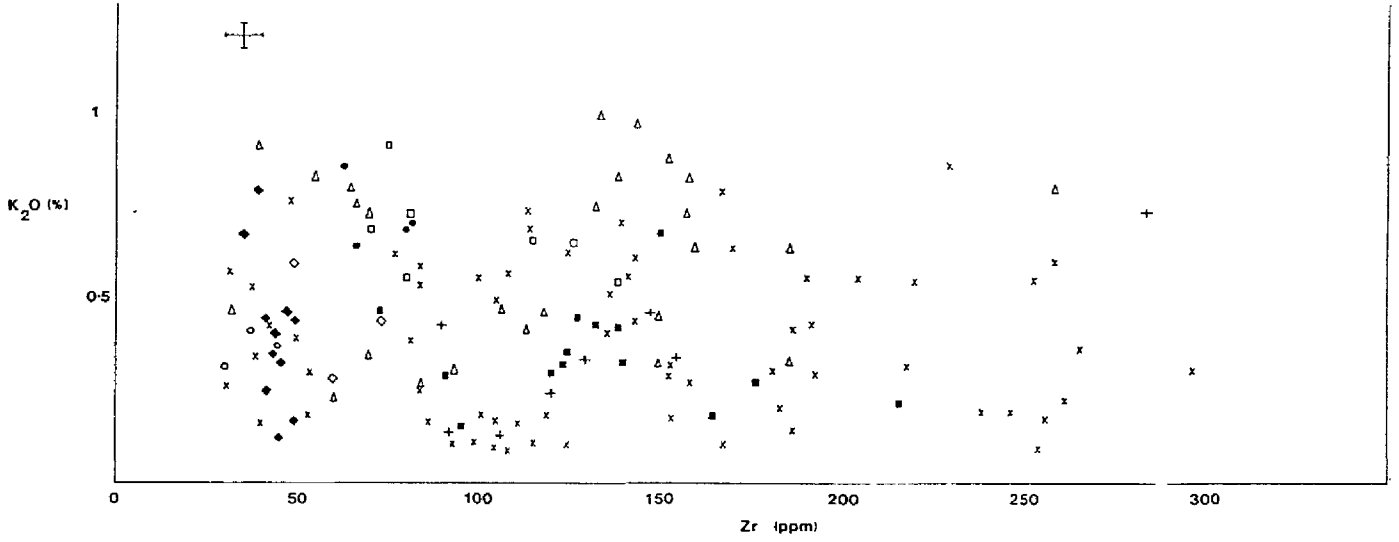

Figure 3.1.4e

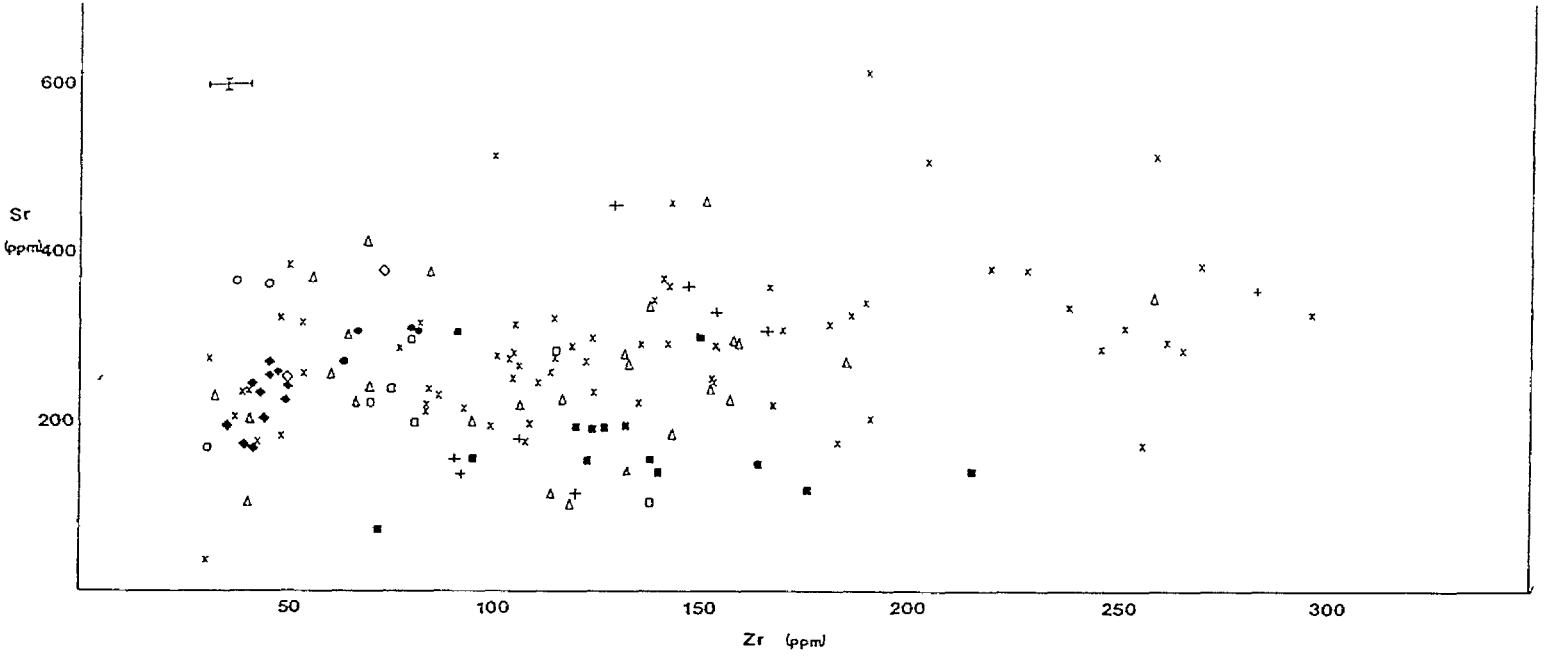

Figure 3.1.4b

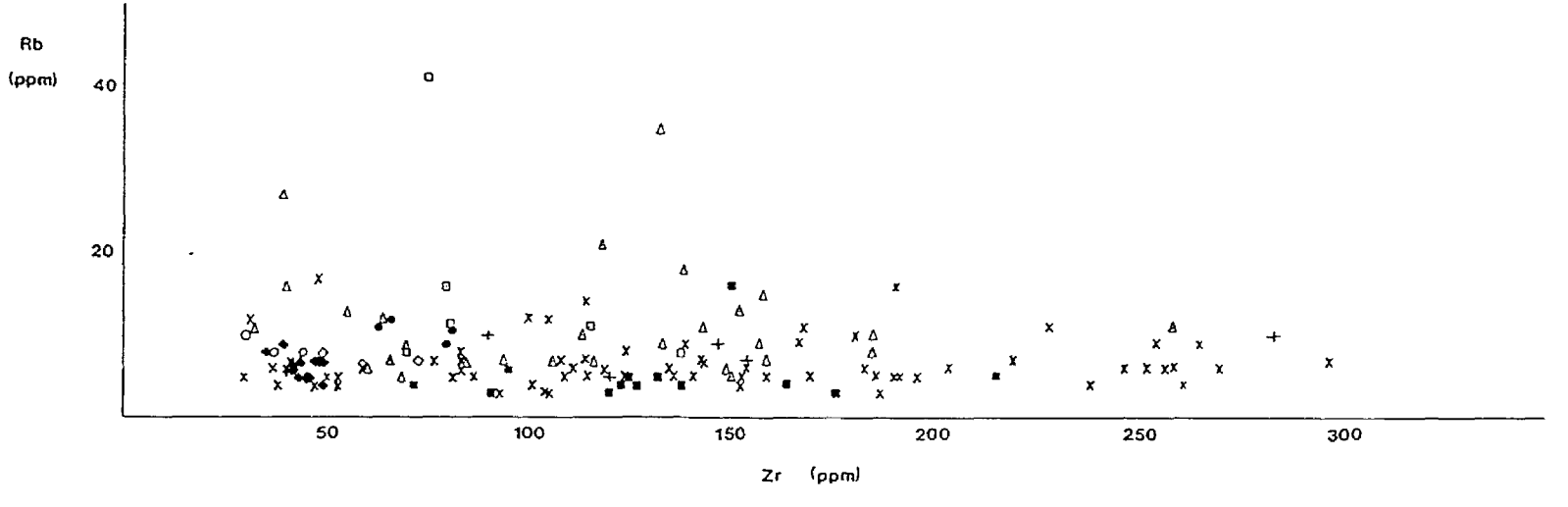

Figure 3.1.4c

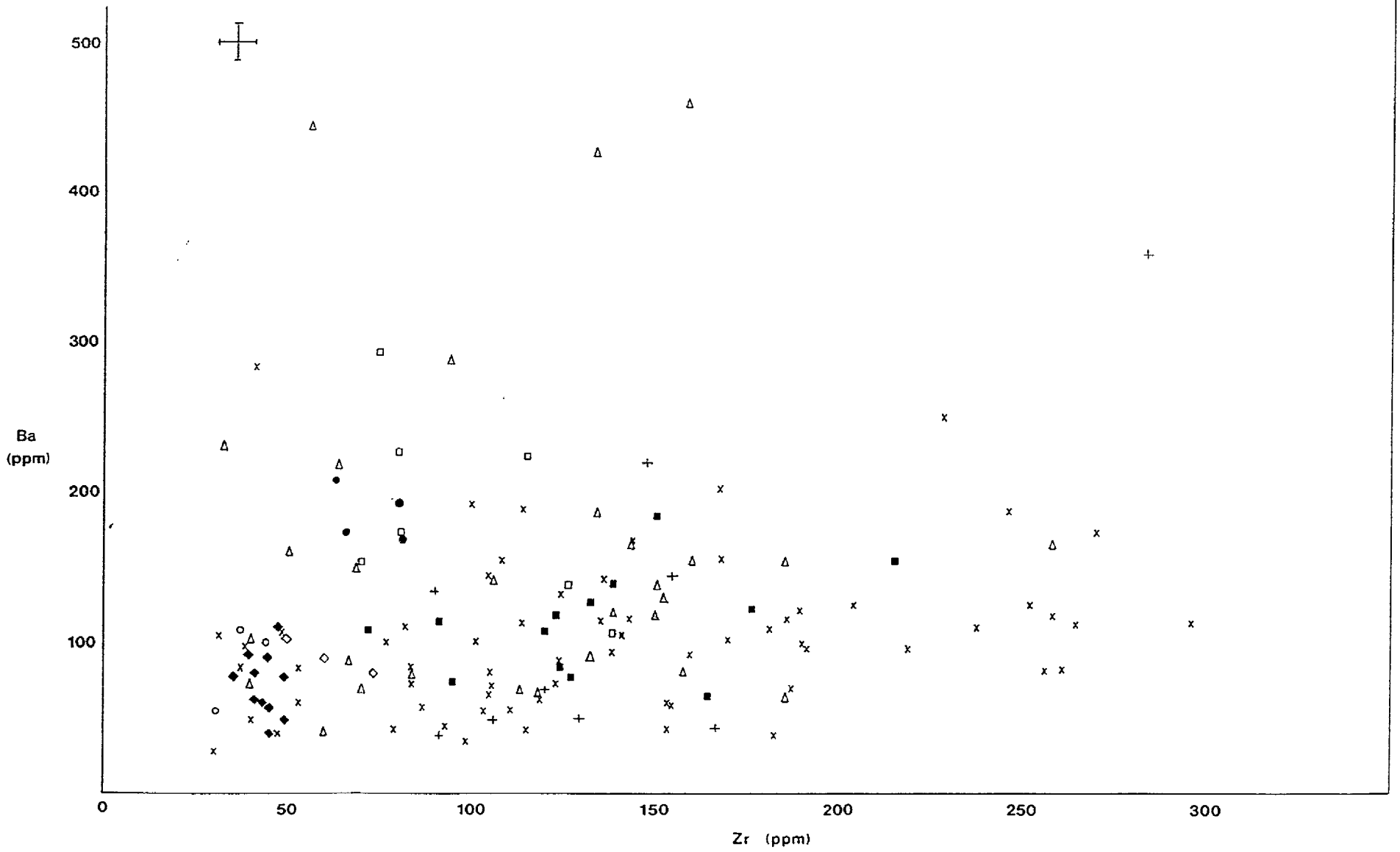

Figure 3.1.4a

Fig. 3.1.4 Figures 3.1.4a-e are plots of Ba, Sr, Rb, Na and K vs Zr respectivley for Virtasalmi amphibolites. The scattered distributions observed in these plots is considered to indicate mobility of the LIL elements during post-crystallisation alteration.

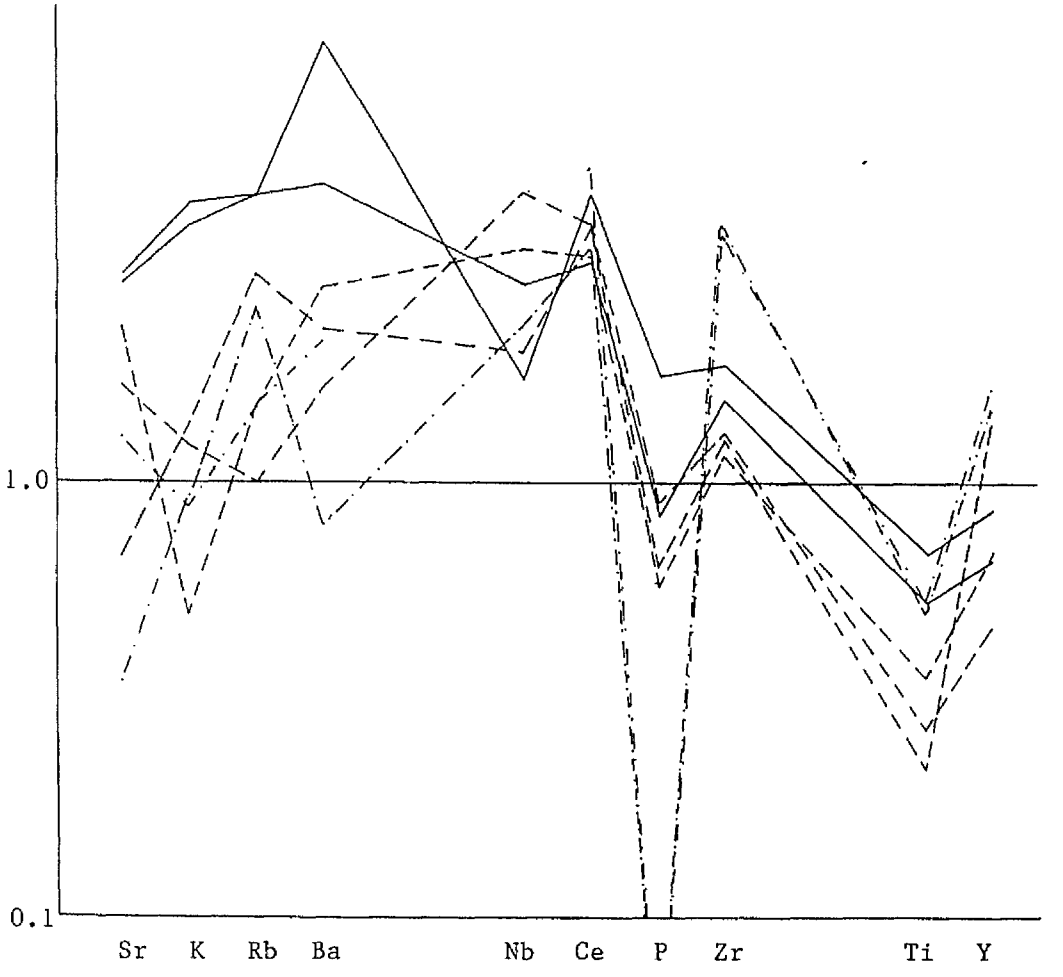

Figure 3.1.3 T370m traverse

Fig. 3.1.3 A spidergram plot of samples collected in a traverse across the irregular and gradational contact from amphibolite to Type V garnet skarn, T370m, Hällinmäki Mine.

KEY: ——— Amphibolite

– – – – Skarned amphibolite

—·—·—·— Skarn

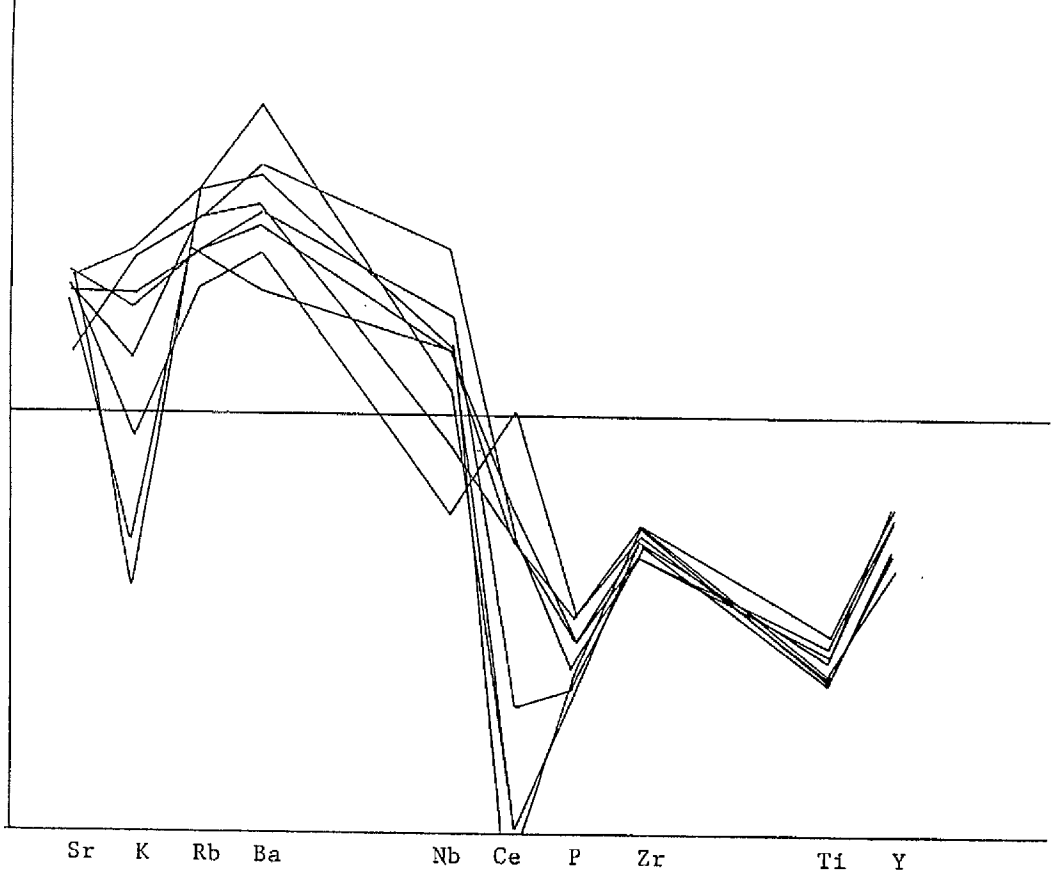

Figure 3.1.2a

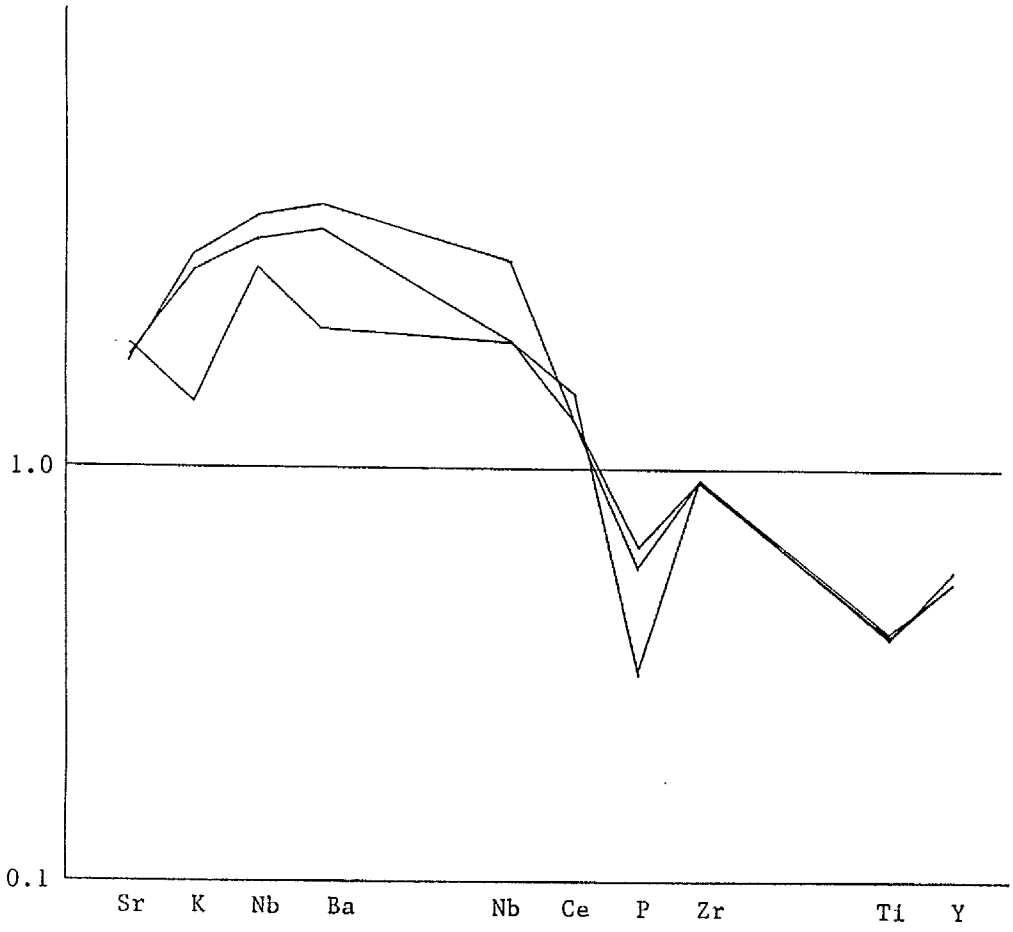

Figure 3.1.2b

Fig. 3.1.2 Figs. 3.1.2a and b are Mid-Ocean Ridge Basalt (MORB)-normalised plots (spidergrams) for a number of analyses samples from two amphibolite lithologies at Hällinmäki Mine.
The ordering of the elements and the normalising values used throughout this section are taken from Pearce (1983).

The MORB-normalising values are as follows:

Ba	20
Rb	2
K	0.15%
Nb	3.5
Ce	10
Sr	120
P	0.12%
Zr	90
Ti	1.5%
Y	30

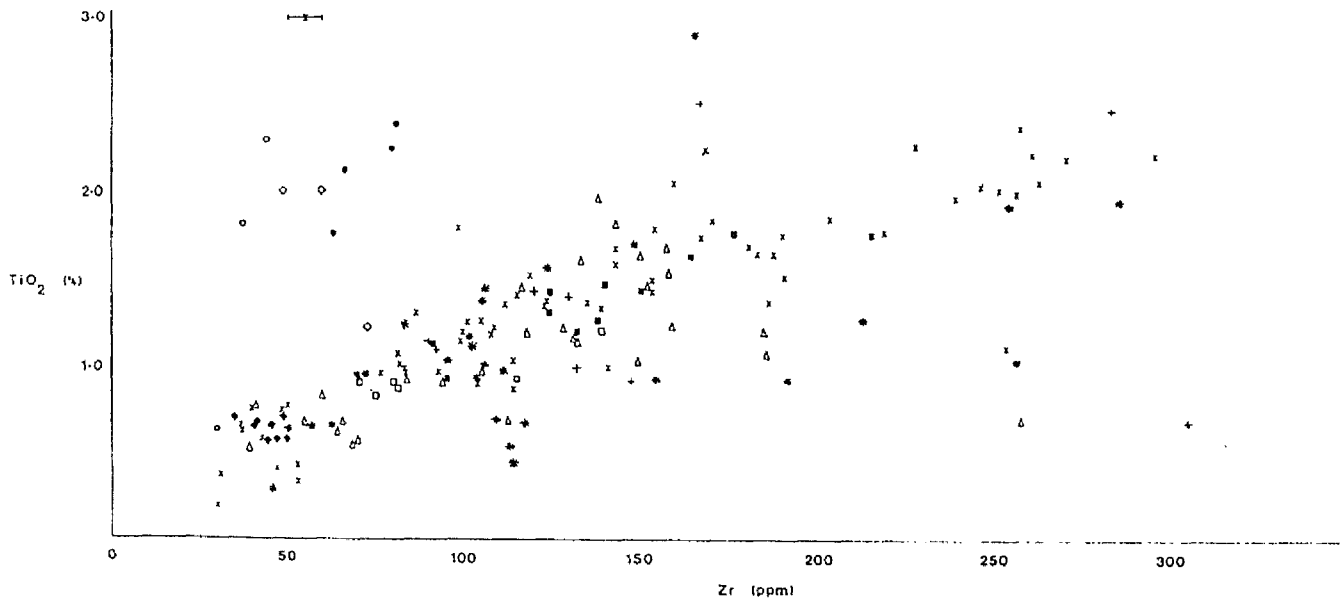

Figure 3.1.1c

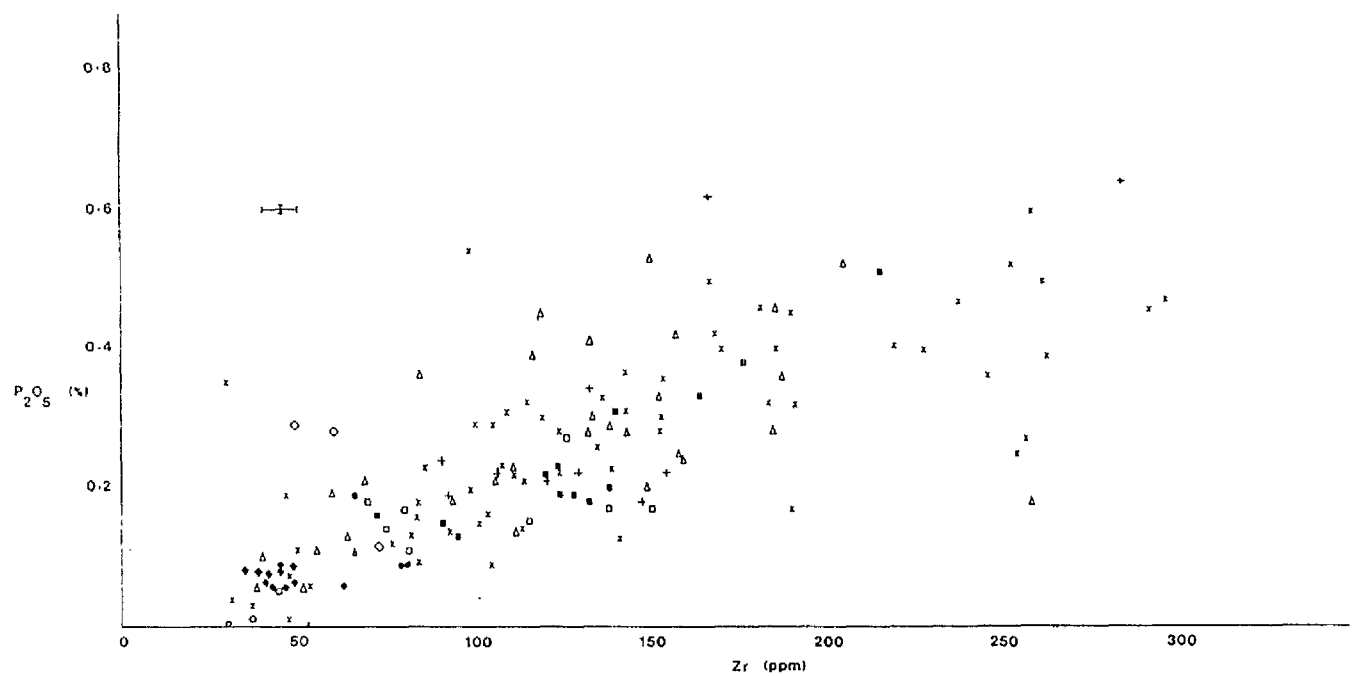

Figure 3.1.1d

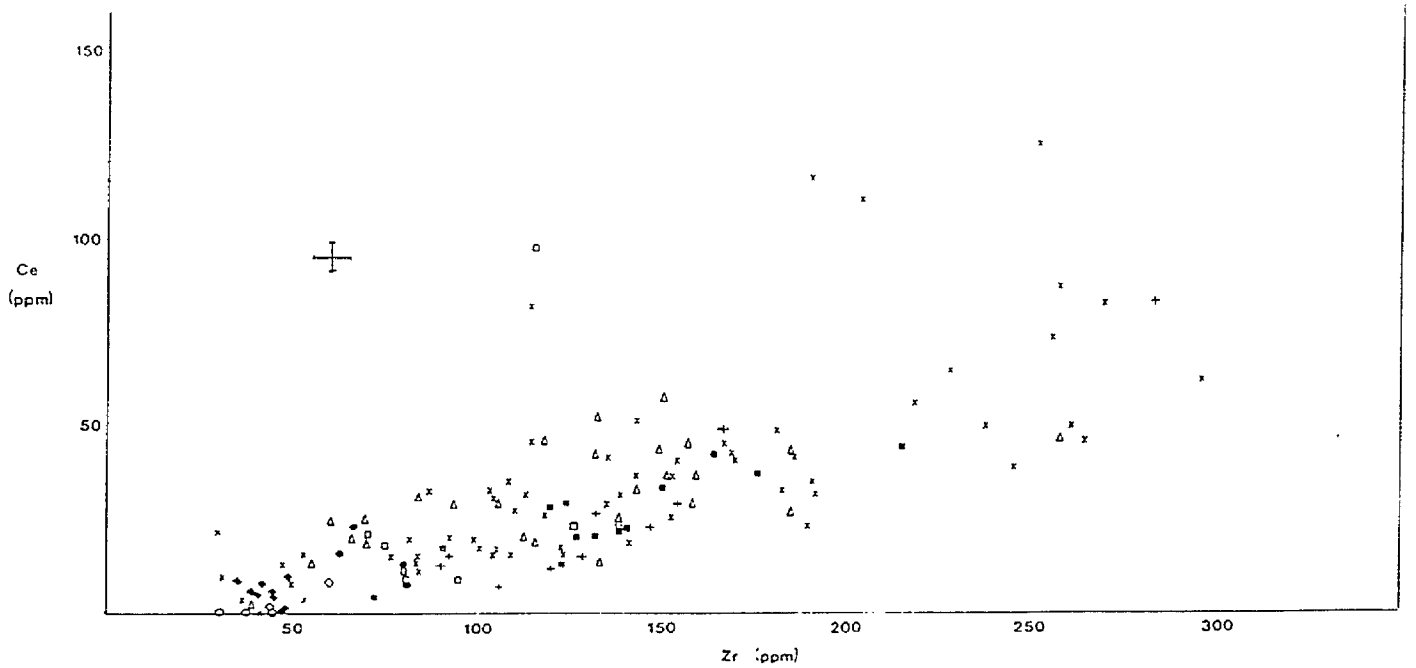

Figure 3.1.1a

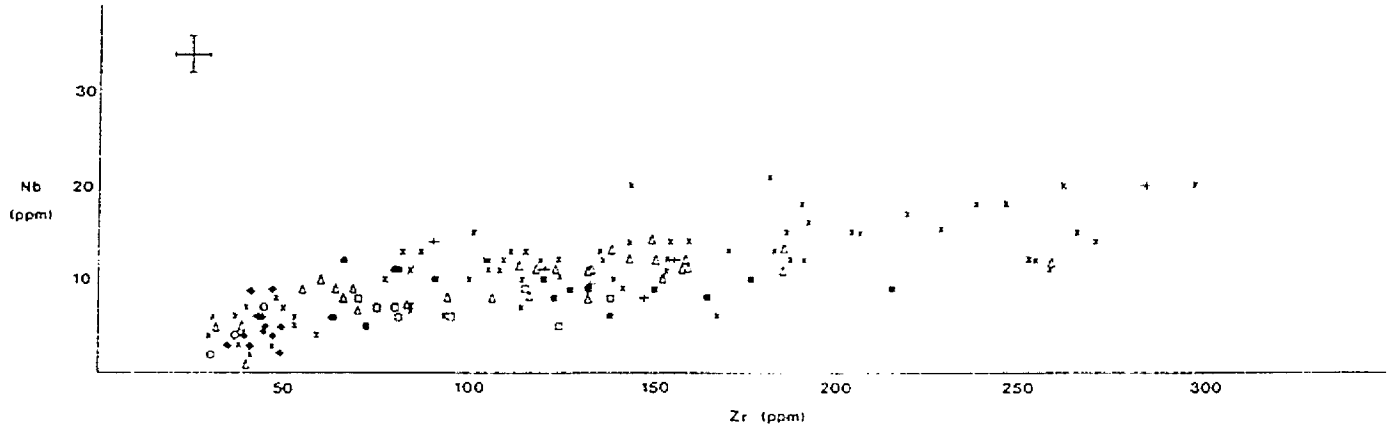

Figure 3.1.1b

Table 3.1.1

	(a)			(b)	
	'unaltered' amphibolite (113)	bleached zone (118)	skarn centre (114)	'unaltered' amphibolite (91)	bleached zone (112)
SiO_2	45.35	49.09	47.69	53.27	58.24
TiO_2	1.16	1.44	1.12	1.22	1.45
Al_2O_3	16.16	17.73	16.40	13.07	15.77
FeO_{tot}	12.59	9.51	6.11	14.32	12.21
MnO	0.17	0.14	0.11	0.17	0.07
MgO	8.90	6.25	2.89	4.59	0.54
CaO	10.53	8.94	18.53	6.67	3.75
Na_2O	3.21	4.41	2.76	3.74	4.14
K_2O	0.43	0.24	0.14	0.42	0.67
P_2O_5	0.24	0.21	0.19	0.18	0.17
Co	59	61	38	35	11
Ce	13	12	16	20	33
Cr	546	488	319	25	21
Ba	134	70	39	127	184
La	15	11	15	18	21
Zr	90	120	92	132	150
Y	19	26	19	41	60
Sr	156	116	139	196	297
U	2	2	3	0	1
Rb	10	5	7	5	16
Th	0	0	-	-	0
Pb	1	3	2	-	1
Ga	17	14	24	12	21
Zn	115	84	38	107	76
Cu	10	62	11	9	133
Ni	279	172	154	30	12
S	58	764	158	25	56
Nb	14	11	13	9	9

Chemical composition of samples from the bleached zones around Type III skarn patches and adjacent 'unaltered' amphibolite from 2 examples near Narila (a) and west of Hällinmäki Mine (b).

Table 3.1.2

Niggli values of Analyses nos. 231 and 232.
Differences between samples are the result of formation of a metamorphic differentiation banding.

	231	232
al	17.76	20.06
fm	48.89	49.36
c	27.27	27.67
alk	6.08	2.92
si	97.39	150.26
k	0.12	0.27
ti	2.56	2.60
mg	0.49	0.49
w	0.00	0.00

Fig. 3.1.1a-d

Figure 3.1.1a-d are plots of Ce, Nb, TiO_2 and P_2O_5 vs Zr for Virtasalmi amphibolites.

The symbols used throughout this section correspond with subdivisions that are demonstrated later in Section 3.1. They are as follows:

- ■ Group Ia amphibolites
- ◘ Group Ib amphibolites
- ○ Group IIa metaperidotites
- ● Group IIb metagabbros
- ♦ Group IIc amphibolites
- ◇ Group IId amphibolites
- × Group IIIa amphibolites
- △ Group IIIb amphibolites
- \+ Group IIIc amphibolites

Other symbols are:

- ✳ Calc-silicate skarns
- ⊢⊣ Error limits at 1 standard deviation

PIEKSÄMÄ

GEOLOGINEN TUTKIMUSLAITOS

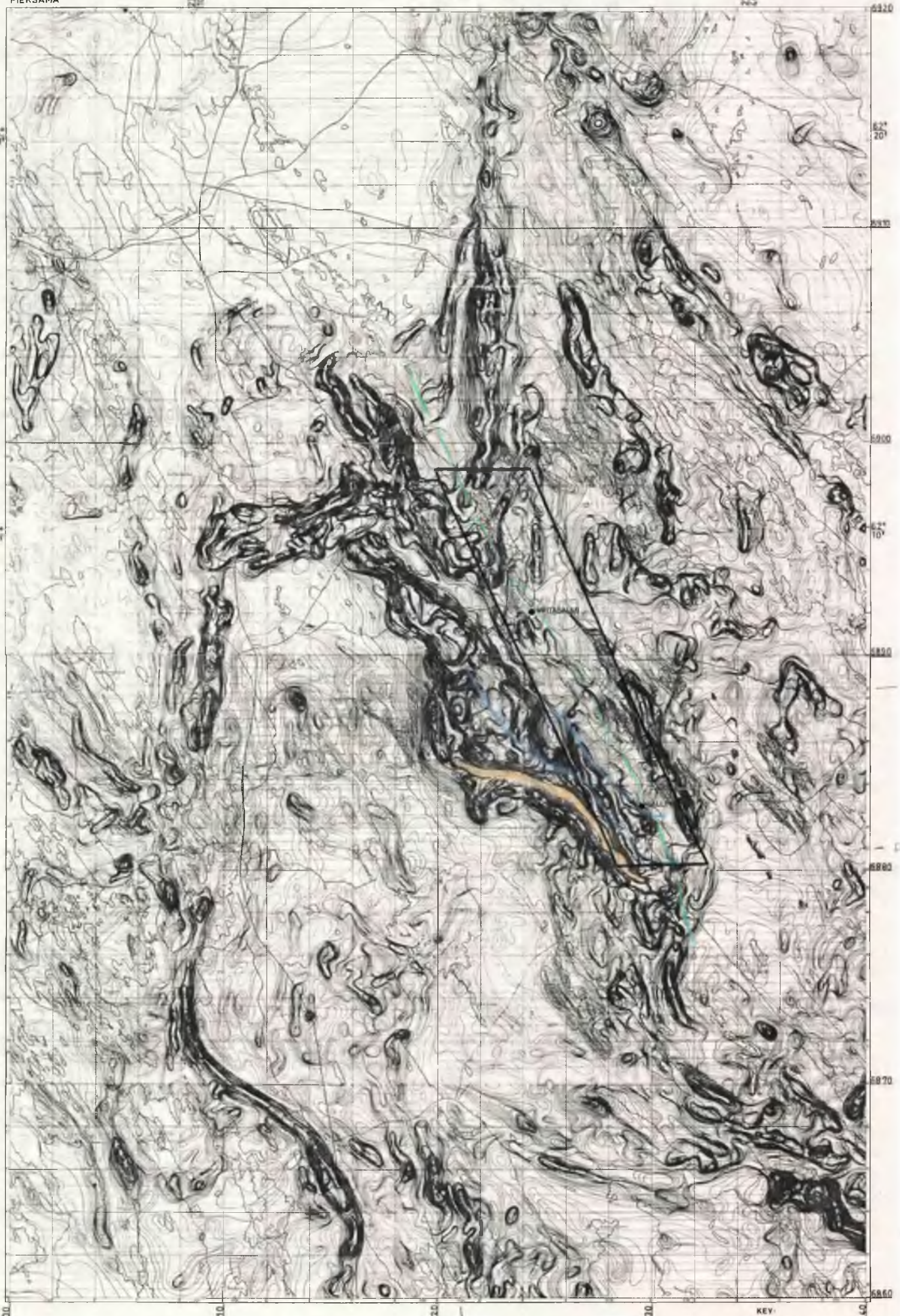

Mittakaava 1:10000

5 km 2,5 0 5 km

MAP 2 : ELECTROMAGNETIC MAP

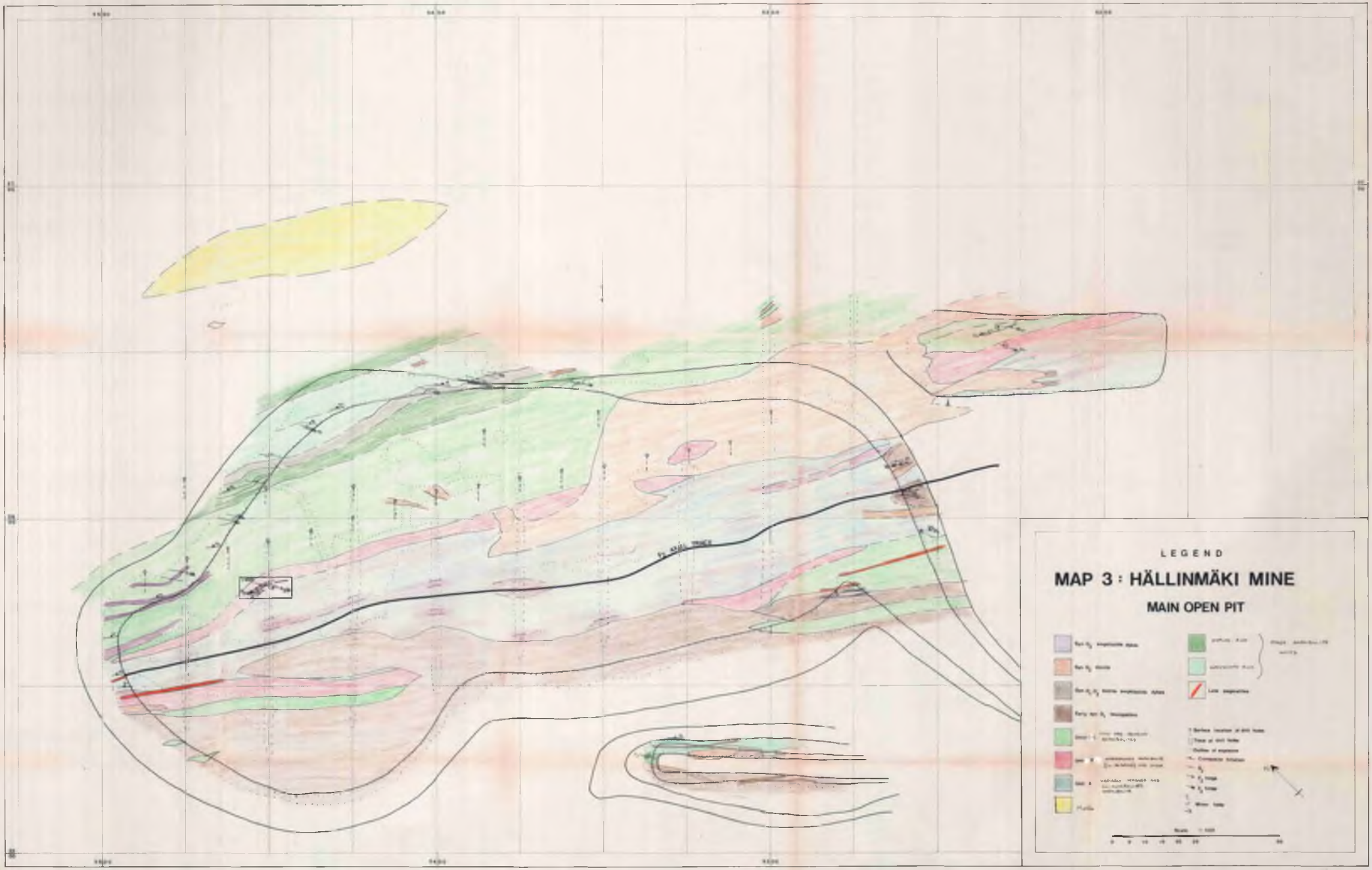
LEGEND
MAP 3 : HÄLLINMÄKI MINE
MAIN OPEN PIT

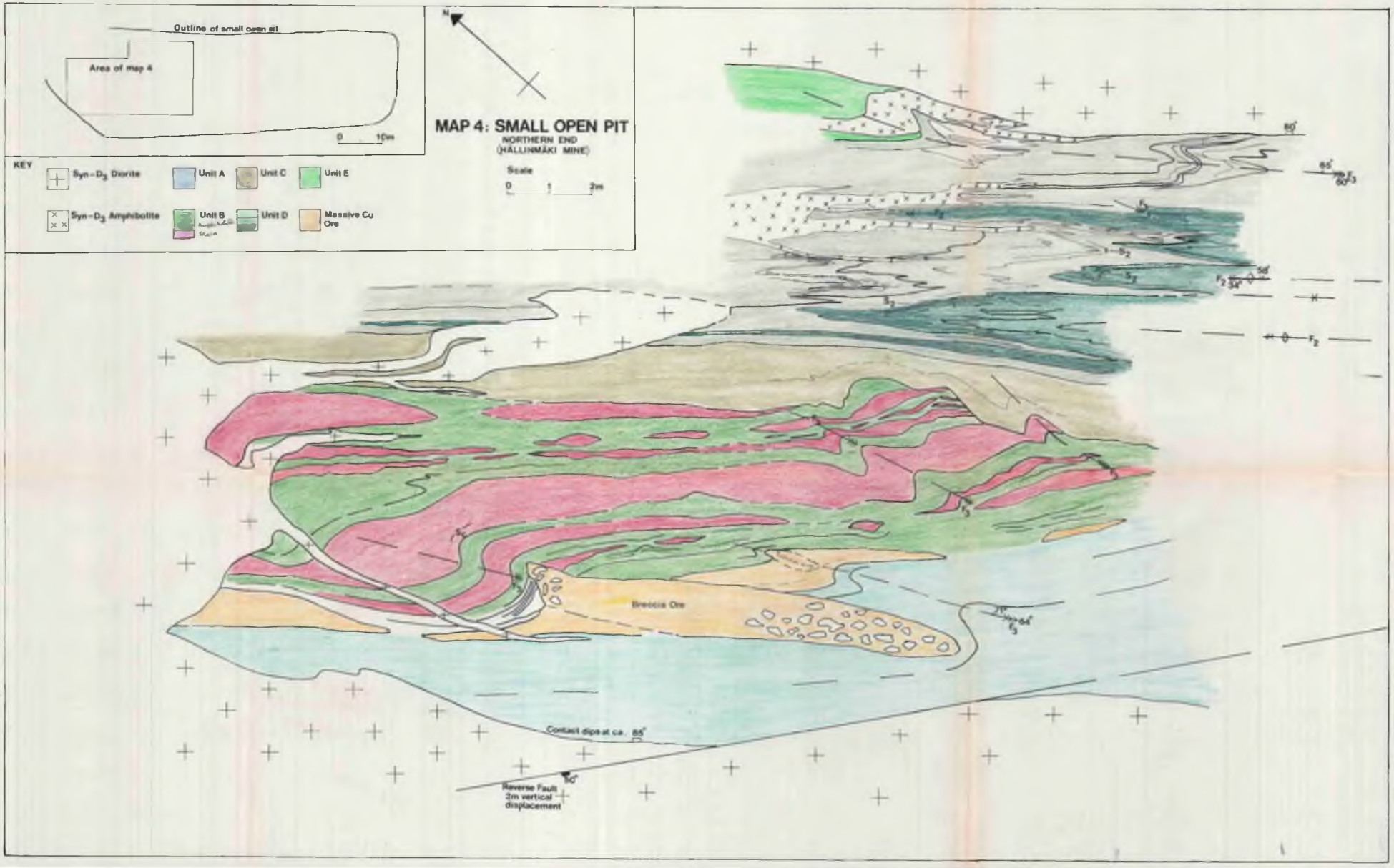
Outline of small open pit
Area of map 4
0 10m
N
MAP 4: SMALL OPEN PIT
NORTHERN END
(HÄLLINMÄKI MINE)
Scale
0 1 2m
KEY
Syn-D_3 Diorite
Unit A
Unit C
Unit E
Syn-D_3 Amphibolite
Unit B
Unit D
Massive Cu Ore
Breccia Ore
Contact dips at ca. 85°
Reverse Fault
2m vertical
displacement

MAP 5 TUNNEL 175 m DEPTH

HALLIMAND MINE

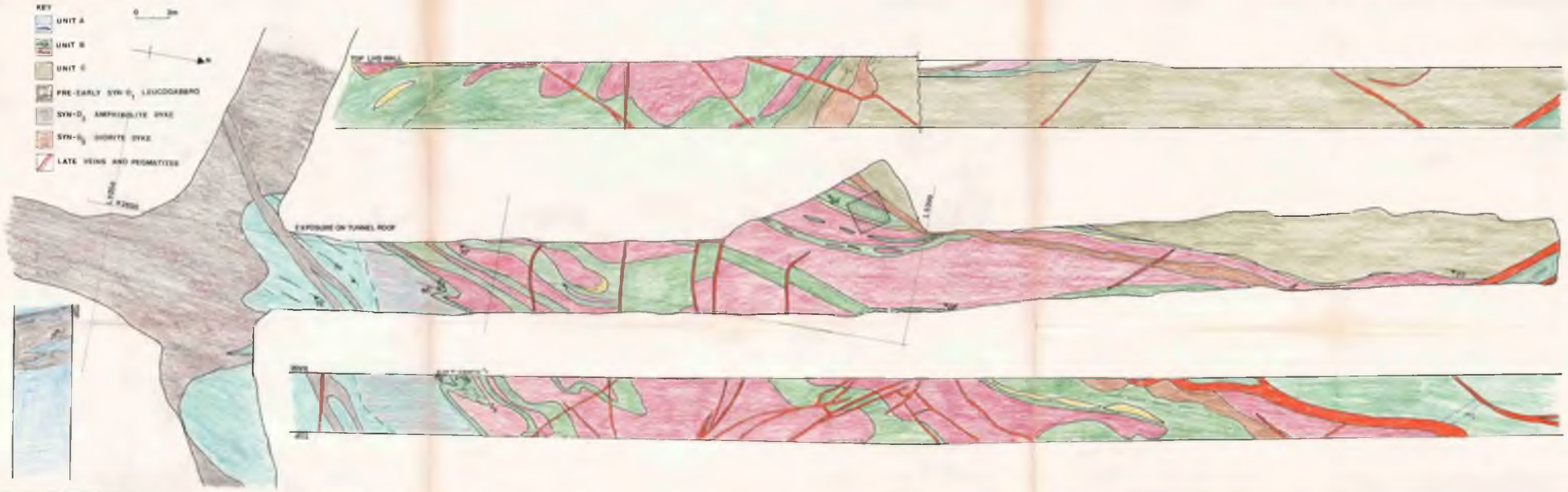

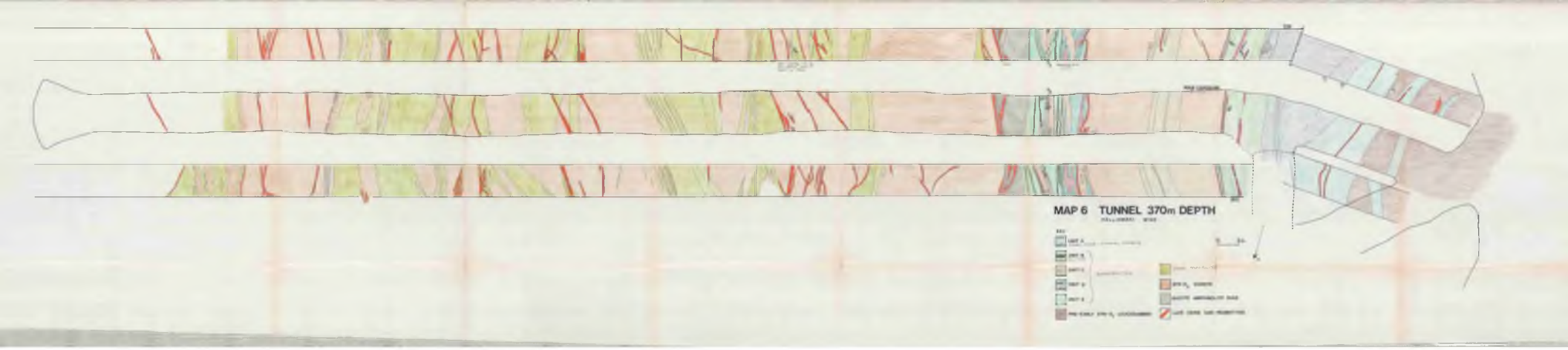
MAP 6 TUNNEL 370m DEPTH

F_2 AXIAL PLANE
173/37NE

HINGE PLUNGES 14° to 029°

FOLD HINGE IS CURVED BY LATER F_3 REFOLDING

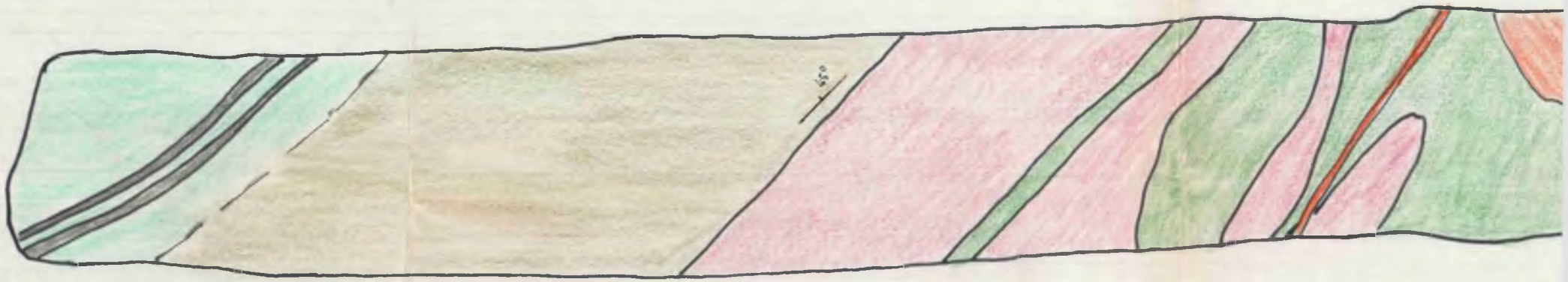

6882

62° 2' 30"

MAP 8 : SAMPLE LOCATIO

The numbers 1 to 276 annotated on this map represent the localities at which sample

for geochemical analysis, the results of which are listed in Appendix 2.

6880

Scale 1: 20,000

1000 500 0 1000

6878

520 522

27° 25'


WEST
EAST
2700
ENCLOSURE 9: MINE CROSS SECTION